METABOLIC REGULATION IN THE DEVELOPMENT OF CARDIOVASCULAR DISEASES

EDITED BY: Xiaoqiang Tang, Md. Shenuarin Bhuiyan and InKyeom Kim
PUBLISHED IN: Frontiers in Cell and Developmental Biology and
Frontiers in Molecular Biosciences

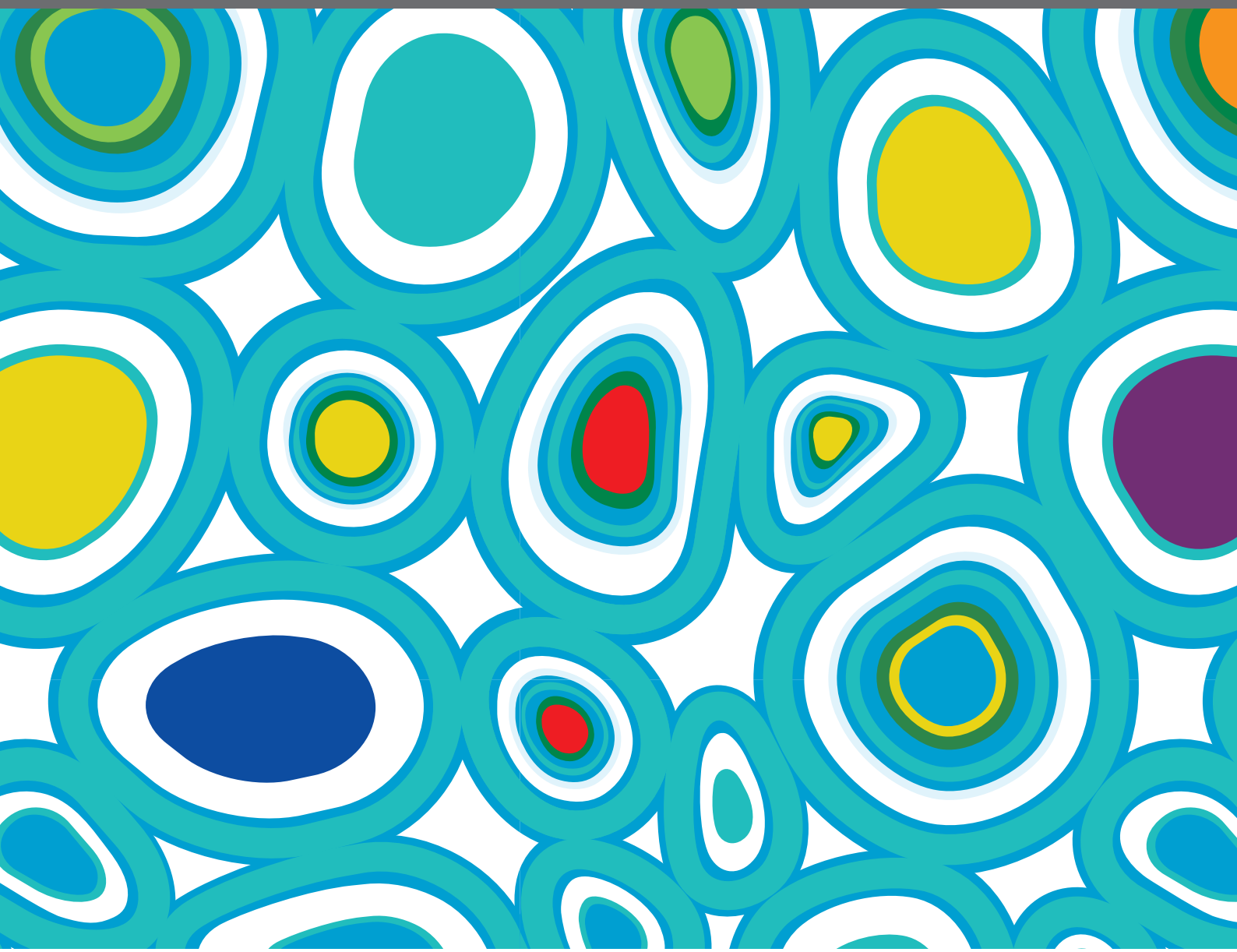

frontiers Research Topics

frontiers

ISSN 1664-8714
ISBN 978-2-88971-813-9
DOI 10.3389/978-2-88971-813-9

About Frontiers

Frontiers is more than just an open-access publisher of scholarly articles: it is a pioneering approach to the world of academia, radically improving the way scholarly research is managed. The grand vision of Frontiers is a world where all people have an equal opportunity to seek, share and generate knowledge. Frontiers provides immediate and permanent online open access to all its publications, but this alone is not enough to realize our grand goals.

Frontiers Journal Series

The Frontiers Journal Series is a multi-tier and interdisciplinary set of open-access, online journals, promising a paradigm shift from the current review, selection and dissemination processes in academic publishing. All Frontiers journals are driven by researchers for researchers; therefore, they constitute a service to the scholarly community. At the same time, the Frontiers Journal Series operates on a revolutionary invention, the tiered publishing system, initially addressing specific communities of scholars, and gradually climbing up to broader public understanding, thus serving the interests of the lay society, too.

Dedication to Quality

Each Frontiers article is a landmark of the highest quality, thanks to genuinely collaborative interactions between authors and review editors, who include some of the world's best academicians. Research must be certified by peers before entering a stream of knowledge that may eventually reach the public - and shape society; therefore, Frontiers only applies the most rigorous and unbiased reviews.
Frontiers revolutionizes research publishing by freely delivering the most outstanding research, evaluated with no bias from both the academic and social point of view. By applying the most advanced information technologies, Frontiers is catapulting scholarly publishing into a new generation.

What are Frontiers Research Topics?

Frontiers Research Topics are very popular trademarks of the Frontiers Journals Series: they are collections of at least ten articles, all centered on a particular subject. With their unique mix of varied contributions from Original Research to Review Articles, Frontiers Research Topics unify the most influential researchers, the latest key findings and historical advances in a hot research area! Find out more on how to host your own Frontiers Research Topic or contribute to one as an author by contacting the Frontiers Editorial Office: frontiersin.org/about/contact

METABOLIC REGULATION IN THE DEVELOPMENT OF CARDIOVASCULAR DISEASES

Topic Editors:
Xiaoqiang Tang, Sichuan University, China
Md. Shenuarin Bhuiyan, Louisiana State University Health Shreveport, United States
InKyeom Kim, Kyungpook National University, South Korea

Citation: Tang, X., Bhuiyan, S., Kim, I., eds. (2021). Metabolic Regulation in the Development of Cardiovascular Diseases. Lausanne: Frontiers Media SA.
doi: 10.3389/978-2-88971-813-9

Table of Contents

frontiers in Cell and Developmental Biology

EDITORIAL
published: 14 October 2021
doi: 10.3389/fcell.2021.768689

Editorial: Metabolic Regulation in the Development of Cardiovascular Diseases

Yimei Ma[1], *Md. Shenuarin Bhuiyan*[2], *InKyeom Kim*[3] *and Xiaoqiang Tang*[1]*

[1] *Key Laboratory of Birth Defects and Related Diseases of Women and Children of Ministry of Education, State Key Laboratory of Biotherapy, Department of Pediatrics, West China Second University Hospital, Sichuan University, Chengdu, China,* [2] *Department of Pathology and Translational Pathobiology, Louisiana State University Health Sciences Center, Shreveport, LA, United States,* [3] *Department of Pharmacology, Cardiovascular Research Institute, BK21 Plus KNU Biomedical Convergence Program, Department of Biomedical Science, School of Medicine, Kyungpook National University, Daegu, South Korea*

Keywords: metabolism, cardiac disease, heart failure, post-translational modification, mitochondria

Editorial on the Research Topic

Metabolic Regulation in the Development of Cardiovascular Diseases

Metabolic syndromes increase the risk of cardiovascular diseases (CVDs) (North and Sinclair, 2012), and metabolic reprogramming can either reverse or rescue the molecular events that lead to CVDs (Chen et al., 2020a). However, the metabolic mechanisms underlying CVDs are not fully understood. We have prepared a special Research Topic. This Research Topic entitled "*Metabolic Regulation in the Development of Cardiovascular Diseases*" received 11 original articles, 7 review articles, and 2 opinion articles. This special issue highlights recent research findings to clarify the relationship between metabolism and CVD.

Metabolic dysregulation and metabolic syndromes are independent risk factors for CVDs (Zhou et al., 2018). Genetic mutations in metabolic enzymes, as well as transcription factors, can cause CVDs (Austin et al., 2019). In this issue, Zhang et al. identify the occurrence of mutations in transcription factor EB (TFEB), which controls lysosomal biogenesis and metabolism (Settembre et al., 2013), as a potential risk factor for acute myocardial infarction. This study detected novel variants of the metabolic regulator, TFEB, that might contribute to the development of acute myocardial infarction. Furthermore, pregnancy-related CVDs, such as arterial dissection, are also affected by metabolic conditions (Wang et al., 2021). Deng et al. emphasized the importance of glycemic control in pregnant women, which could improve the understanding, prevention, and treatment of pregnancy-related arterial dissection.

Genetic mutations, or dysregulation of metabolic enzymes and their regulators, directly alter cell metabolism, intracellular metabolites, and physiological functions of vascular cells such as endothelial cells (ECs) (Tang et al., 2014). Endothelial metabolic homeostasis and reprogramming can regulate endothelial functions, including angiogenesis, inflammation, and barrier maintenance (Tang et al., 2014; Subramanian et al., 2021). Peng et al. provided an overview of the metabolic pathways in ECs under normal and pathological conditions. Their review highlighted the metabolic reprogramming of endothelium as a potential therapeutic approach for controlling CVDs.

Glucose metabolism in ECs is critical for cardiovascular homeostasis and diseases (Dumas et al., 2021). Glucose catabolism is regulated by enzymes such as 6-phosphofructo-2-kinase/fructose-2,6-biphosphatase 3 (PFKFB3), whose dysfunction drives endothelial injury and vascular inflammation (Bartrons et al., 2018). The role of PFKFB3 in non-EC vascular cells remains unclear. In this regard, Poels et al. show that PFKFB3 expression in monocytes is positively correlated with the occurrence of coronary arteries with unstable plaque phenotypes. Inhibition of PFKFB3 reduced the number of late plaques in vulnerable phenotypes

OPEN ACCESS

Edited and reviewed by:
Cecilia Giulivi,
University of California, Davis, United States

***Correspondence:**
Xiaoqiang Tang
tangxiaoqiang@scu.edu.cn;
txiaoqiang@yeah.net
orcid.org/0000-0003-1314-3417

Specialty section:
This article was submitted to Cellular Biochemistry, a section of the journal Frontiers in Cell and Developmental Biology

Received: *01 September 2021*
Accepted: *21 September 2021*
Published: *14 October 2021*

Citation:
Ma Y, Bhuiyan MS, Kim I and Tang X (2021) Editorial: Metabolic Regulation in the Development of Cardiovascular Diseases. Front. Cell Dev. Biol. 9:768689. doi: 10.3389/fcell.2021.768689

and resulted in stable plaque phenotypes. This phenomenon was coupled with a decrease in glycolytic flux in mononuclear cells within the circulating peripheral blood. The study by Tillie et al. also examined the role of myeloid PFKFB3 in atherosclerosis development. Partial knockout of *Pfkfb3* in myeloid cells did not affect the development of atherosclerosis. Thus, further studies are required to dissect the contribution of PFKFB3 in other non-EC vascular cells, such as vascular smooth muscle cells, fibroblasts, and other immune cells, in atherosclerosis.

In addition to metabolic enzymes, their products (metabolites) are critical for organ homeostasis and injury repair (Chen et al., 2021b; Dumas et al., 2021). Zhang et al. discussed the role of endothelium-derived lactate in regulating the metabolic microenvironment in tissue regeneration and CVD. Endothelium-lactate interactions affect the microenvironment *via* multiple routes. Lactate can be produced by ECs during glycolysis and exported *via* its transporters to the extracellular milieu to regulate cells in the microenvironment. Furthermore, lactate can be imported from extracellular blood compartments by ECs to regulate angiogenesis, or transferred transendothelially to the microenvironment to regulate stromal and immune cells. These interactions regulate the cell microenvironment, tissue regeneration, and CVDs. The biochemical mechanisms underlying lactate function remain unknown, although some findings revealed the potential involvement of histone lactylation (Eming et al., 2021).

In addition to pyruvate and lactate, other metabolites also contribute to cardiovascular homeostasis (Li et al., 2019). One such metabolite is epoxyeicosatrienoic acids (EETs), a derivative of arachidonic acid synthesized by cytochrome P450 (Duflot et al., 2014). EETs are rapidly hydrolyzed into less bioactive dihydroxyeicosatrienoic acid (DHET) by soluble epoxide hydrolase (sEH) (Wang et al., 2013). Hamzaoui et al. show that inhibition of sEH inhibits cardiac remodeling, as well as diastolic and systolic dysfunction associated with chronic kidney disease (CKD). Therefore, inhibition of sEH has therapeutic potential for preventing cardiorenal syndrome, which may be regulated by intracellular DHET. Furthermore, metabolites from the gut microbiota are critical regulators of mammalian metabolism and CVDs (Tang et al., 2019). Trimethylamine *N*-oxide (TMAO) is an intestinal microbiome-derived metabolite synthesized from specific food components, such as red meat (Tang et al., 2019). It acts as a risk factor for vascular diseases, such as atherosclerosis (Tang et al., 2019). However, the role of TMAO in cardiac diseases remains unclear. Videja et al. demonstrated that high TMAO levels preserve the production of mitochondrial energy and cardiac function in an experimental model of right ventricular heart failure, thereby suggesting that TMAO promotes effects similar to metabolic preconditioning under specific conditions. This finding is opposite to all other studies published so far on TMAO in CVD (Witkowski et al., 2020).

Mitochondria are essential for maintaining normal cardiomyocyte homeostasis and ensuring healthy heart function (Bonora et al., 2019). Two review papers in this special issue discussed the recent advances regarding mitochondrial biology in CVDs. Xin et al. addressed the function of the mitochondrial fusion protein, mitofusin-2 (MFN2), in regulating mitochondrial morphology, metabolism, calcium homeostasis, and mitochondrial DNA stability in CVDs, and highlighted MFN2 as a therapeutic target for treating CVDs. In addition, Liao et al. discussed the pathways that regulate mitochondrial function in response to mechanical stress during the development of cardiomyopathy and heart failure. One of the central regulators is the Hippo pathway, which plays a pivotal role in heart failure (Wang et al., 2018). The Hippo pathway targets not only mitochondria but also other organelles and pathways (Zhao et al., 2021). Mammalian sterile 20-like kinase 1 (MST1) is a crucial component in the Hippo pathway (Zhao et al., 2021). Feng et al. observed that knockout of *Mst1* inhibited mitochondrial division and reduced left ventricular remodeling in diabetic cardiomyopathy, thereby highlighting the critical role of the Hippo pathway in the regulation of mitochondria and CVDs.

Dysregulation of metabolism can lead to systemic and vascular inflammation, and *vice versa* (Tang et al., 2014). Aging-related chronic inflammation is a hallmark of chronic metabolic disorders, including obesity and type 2 diabetes, contributing to CVDs (Nafisa et al., 2018). Immune cells, especially T cells, accumulate in adipose tissue during aging (Villarroya et al., 2018), and pre-adipose T cells promote aging-related remodeling of adipose tissues (Chen et al., 2021a). Pan et al. compared the differences in adipose tissue morphology and function between young and aged mice, and reported the "whitening" effect of brown adipose tissue (BAT) in old mice. The proportion of T cells in the BAT of old mice was higher, with more aging markers than in those of young mice. Senescent T cells release high levels of interferon-gamma, which inhibits preadipocyte-to-brown adipocyte differentiation. Because BAT is a beneficial factor against CVD (Ruan et al., 2018), further studies are needed to test how T cells in BAT participate in CVD, including cardiac remodeling.

Wu et al. discussed the recent advances regarding the role of CC chemokine receptor-9 (CCR9)/CC motif chemokine 25 (CCL25) in inflammation and CVD. Targeting the CCR9/CCL25 axis pharmacologically can decrease or modulate inflammation. High serum phosphate concentrations are associated with cardiovascular risk in both the general population and patients with CKD (Vervloet et al., 2017). Another review paper, contributed by Zhou et al., discussed the advances in the understanding of phosphate homeostasis in healthy and CKD conditions. The authors highlighted that fibroblast growth factor 23 plays an important role in controlling serum phosphate levels to mitigate phosphate-induced CVD.

The upregulation of endothelin 1 (ET1), a vasoconstrictor factor, contributes to hypertension and organ fibrosis (Tang et al., 2020); however, the mechanism underlying ET1 regulation remains unclear. Xu et al. reported that glycogen synthase kinase 3 (GSK3) and serum response factor (SRF) contributed to angiotensin II-induced ET1 overexpression in ECs. This study highlighted a previously unrecognized mechanism that contributes to the transcriptional regulation of endothelin and could lead to new approaches for CVD interventions targeting the GSK3-SRF axis.

In addition to local inflammation, systemic and local accessibility and bioavailability of gas molecules also regulate cell metabolism (Das et al., 2018). For instance, chronic hypoxia is an essential factor in many CVDs. The main energy fuels of heart are fatty acids. However, under chronic hypoxia, glucose oxidation is downregulated and glycolysis is upregulated (Tang et al., 2017). The mechanisms underlying adaptive cardiac metabolism remain unclear. Su et al. provided a thorough discussion on this topic. They concluded that the heart initiated transcriptional programs to increase the utilization of carbohydrates, rather than fatty acids, to produce ATP. This involves altered mitochondrial structure and function, improved metabolic efficiency, and reduced reactive oxygen species production in hypoxic cardiac tissues. The core participants in hypoxia are hypoxia inducible factors (HIFs) and their modulators, including the HIF-prolyl hydroxylase (PHD) isotypes PDH1, PDH2, and PDH3 (DeBerge et al., 2021). PHD pan-inhibitors have been used to treat anemia in patients with CKD. Similarly, systemic *Phd1* or *Phd2* knockout was found to improve atherosclerosis (Marsch et al., 2016; Rahtu-Korpela et al., 2016). In this issue, Demandt et al. analyzed the roles of PHD3 in hypercholesterolemia using low-density lipoprotein receptor (*Ldlr*) and *Phd3* double knockout mice. The authors found that systemic *Phd3*-deficiency induced adverse lipid profiles and increased hepatocellular volume without altering the development of atherosclerotic plaques, compared to other PHD isotypes. Interestingly, the effect of PHD3 on hypercholesterolemia is opposite to that of PHD1 and 2 (Marsch et al., 2016; Rahtu-Korpela et al., 2016), and to the detrimental effect of PDH3 overexpression on the progression of atherosclerosis in $ApoE^{-/-}$ mice (Liu et al., 2016). Further studies are needed to systematically investigate the multi-dimensional roles of PHDs in hypercholesterolemia and related CVDs such as atherosclerosis.

In addition to HIFs and PHDs, there are other types of hypoxia regulators, such as hypoxia-induced mitogenic factor (HIMF), a member of the resistin-like molecule protein family expressed in mammals (Lin and Johns, 2020). HIMF is involved in numerous physiological processes including mitosis, angiogenesis, inflammation, and vasoconstriction (Lin and Johns, 2020). In addition, HIMF responds to several pathological conditions involving the lungs and the cardiovascular system. In this issue, Lv and Liu discuss the molecular characteristics and pathophysiological effects of HIMF, and highlight the potential clinical implications in CVDs and other diseases. Taken together, there has been remarkable progress in understanding the biology of hypoxia in CVDs. However, currently available drug strategies are still limited and have not been tested in patients with chronic hypoxia-related CVDs.

Considering that CVDs are critically controlled by metabolism and their regulators, metabolism-targeted drugs/interventions are promising strategies for the treatment of CVDs (Tang et al., 2017; Chen et al., 2020b). One drug with such potential is metformin (Kulkarni et al., 2020), a clinical anti-diabetic drug that targets mitochondria and regulates cell metabolism (Foretz et al., 2014). Metformin has the potential to repress cardiovascular aging and diseases (Nafisa et al., 2018); however, the sex-related effects of metformin remain unknown. Zhu et al. investigated the protective effects of metformin on cardiac metabolism and longevity in female mice; however, they found that metformin did not improve cardiac function or longevity in elderly female mice. Although multiple beneficial effects of metformin have been reported in age-related diseases, further systematic evaluation of the sex-related roles of metformin in heart conditions and longevity of older patients should be considered. Additional study of the synergistic effects of metformin with other drugs would also be interesting. Jia et al. investigated the synergistic effects of metformin and atorvastatin on diabetic cardiomyopathy and found the combination to provide better protection against diabetic cardiomyopathy than monotherapy, indicating that drug combinations may achieve greater clinical benefits than the use of a single drug.

In conclusion, the papers published on this Research Topic can potentially improve our understanding of genetic risk factors, metabolic enzymes and metabolites, metabolic inflammation, mitochondrial dynamics, the biology of hypoxia in CVD, and the treatment of cardiovascular diseases.

AUTHOR CONTRIBUTIONS

All authors listed have made a substantial, direct and intellectual contribution to the work, and approved it for publication.

FUNDING

This work was supported by the National Natural Science Foundation of China (grant numbers 81970426 and 81800273); the Young Elite Scientists Sponsorship Program of China Association for Science and Technology (grant number 2018QNRC001); the Scientific and Technological Innovation Talents Program of Sichuan Province (grant number 2020JDRC0017); National Institutes of Health (NIH) grants R01HL145753, R01HL145753-01S1, and R01HL145753-03S1; LSUHSC-S CCDS Finish Line Award, COVID-19 Research Award, and LARC Research Award to MSB; the Basic Science Research Program through the National Research Foundation of Korea (NRF), funded by the Ministry of Education, Science and Technology (NRF-2021R1A2B502001763 and 2021R1A4A1021617); and the Korea Health Technology R&D Project through the Korea Health Industry Development Institute (KHIDI), funded by the Ministry of Health & Welfare, Republic of Korea (HI15C0001). This work was also supported under the framework of international cooperation program managed by the National Research Foundation of Korea (2021K2A9A2A07000135).

ACKNOWLEDGMENTS

We thank all the authors and reviewers who contributed to this Research Topic. The names of the reviewers for each paper have been published, along with the corresponding paper. We apologize to the scientists whose works were not cited because of space limitations. XT expresses his gratitude to Miss Jing Fu (Honghe Primary School) for continuous love and support, and their funny kid Okra (Suyuan) Tang (Golden Apple Kindergarten) for inspiration.

REFERENCES

Austin, K. M., Trembley, M. A., Chandler, S. F., Sanders, S. P., Saffitz, J. E., Abrams, D. J., et al. (2019). Molecular mechanisms of arrhythmogenic cardiomyopathy. *Nat. Rev. Cardiol.* 16, 519–537. doi: 10.1038/s41569-019-0200-7

Bartrons, R., Rodriguez-Garcia, A., Simon-Molas, H., Castano, E., Manzano, A., and Navarro-Sabate, A. (2018). The potential utility of PFKFB3 as a therapeutic target. *Expert Opin. Ther. Targets* 22, 659–674. doi: 10.1080/14728222.2018.1498082

Bonora, M., Wieckowski, M. R., Sinclair, D. A., Kroemer, G., Pinton, P., and Galluzzi, L. (2019). Targeting mitochondria for cardiovascular disorders: therapeutic potential and obstacles. *Nat. Rev. Cardiol.* 16, 33–55. doi: 10.1038/s41569-018-0074-0

Chen, H. J., Meng, T., Gao, P. J., and Ruan, C. C. (2021a). The role of brown adipose tissue dysfunction in the development of cardiovascular disease. *Front. Endocrinol.* 12:652246. doi: 10.3389/fendo.2021.652246

Chen, X.-F., Chen, X., and Tang, X. (2020a). Short-chain fatty acid, acylation and cardiovascular diseases. *Clin. Sci.* 134, 657–676. doi: 10.1042/CS20200128

Chen, X. F., Yan, L. J., Lecube, A., and Tang, X. (2020b). Editorial: diabetes and obesity effects on lung function. *Front. Endocrinol.* 11:462. doi: 10.3389/fendo.2020.00462

Chen, X. F., Ren, S. C., Tang, G., Wu, C., Chen, X., and Tang, X. Q. (2021b). Short-chain fatty acids in blood pressure, friend or foe. *Chin. Med. J.* doi: 10.1097/CM9.0000000000001578

Das, A., Huang, G. X., Bonkowski, M. S., Longchamp, A., Li, C., Schultz, M. B., et al. (2018). Impairment of an endothelial NAD(+)-H(2)S signaling network is a reversible cause of vascular aging. *Cell* 173, 74–89.e20. doi: 10.1016/j.cell.2018.02.008

DeBerge, M., Lantz, C., Dehn, S., Sullivan, D. P., van der Laan, A. M., Niessen, H. W. M., et al. (2021). Hypoxia-inducible factors individually facilitate inflammatory myeloid metabolism and inefficient cardiac repair. *J. Exp. Med.* 218:e20200667. doi: 10.1084/jem.20200667

Duflot, T., Roche, C., Lamoureux, F., Guerrot, D., and Bellien, J. (2014). Design and discovery of soluble epoxide hydrolase inhibitors for the treatment of cardiovascular diseases. *Expert Opin. Drug Discov.* 9, 229–243. doi: 10.1517/17460441.2014.881354

Dumas, S. J., Meta, E., Borri, M., Luo, Y., Li, X., Rabelink, T. J., et al. (2021). Phenotypic diversity and metabolic specialization of renal endothelial cells. *Nat. Rev. Nephrol.* 17, 441–464. doi: 10.1038/s41581-021-00411-9

Eming, S. A., Murray, P. J., and Pearce, E. J. (2021). Metabolic orchestration of the wound healing response. *Cell Metab.* 33, 1726–1743. doi: 10.1016/j.cmet.2021.07.017

Foretz, M., Guigas, B., Bertrand, L., Pollak, M., and Viollet, B. (2014). Metformin: from mechanisms of action to therapies. *Cell Metab.* 20, 953–966. doi: 10.1016/j.cmet.2014.09.018

Kulkarni, A. S., Gubbi, S., and Barzilai, N. (2020). Benefits of metformin in attenuating the hallmarks of aging. *Cell Metab.* 32, 15–30. doi: 10.1016/j.cmet.2020.04.001

Li, X., Sun, X., and Carmeliet, P. (2019). Hallmarks of endothelial cell metabolism in health and disease. *Cell Metab.* 30, 414–433. doi: 10.1016/j.cmet.2019.08.011

Lin, Q., and Johns, R. A. (2020). Resistin family proteins in pulmonary diseases. *Am. J. Physiol. Lung Cell. Mol. Physiol.* 319, L422–L434. doi: 10.1152/ajplung.00040.2020

Liu, H., Xia, Y., Li, B., Pan, J., Lv, M., Wang, X., et al. (2016). Prolyl hydroxylase 3 overexpression accelerates the progression of atherosclerosis in ApoE$^{-/-}$ mice. *Biochem. Biophys. Res. Commun.* 473, 99–106. doi: 10.1016/j.bbrc.2016.03.058

Marsch, E., Demandt, J. A., Theelen, T. L., Tullemans, B. M., Wouters, K., Boon, M. R., et al. (2016). Deficiency of the oxygen sensor prolyl hydroxylase 1 attenuates hypercholesterolaemia, atherosclerosis, and hyperglycaemia. *Eur. Heart J.* 37, 2993–2997. doi: 10.1093/eurheartj/ehw156

Nafisa, A., Gray, S. G., Cao, Y., Wang, T., Xu, S., Wattoo, F. H., et al. (2018). Endothelial function and dysfunction: impact of metformin. *Pharmacol. Ther.* 192, 150–162. doi: 10.1016/j.pharmthera.2018.07.007

North, B. J., and Sinclair, D. A. (2012). The intersection between aging and cardiovascular disease. *Circ. Res.* 110, 1097–1108. doi: 10.1161/CIRCRESAHA.111.246876

Rahtu-Korpela, L., Määttä, J., Dimova, E. Y., Hörkkö, S., Gylling, H., Walkinshaw, G., et al. (2016). Hypoxia-inducible factor prolyl 4-hydroxylase-2 inhibition protects against development of atherosclerosis. *Arterioscler. Thromb. Vasc. Biol.* 36, 608–617. doi: 10.1161/ATVBAHA.115.307136

Ruan, C. C., Kong, L. R., Chen, X. H., Ma, Y., Pan, X. X., Zhang, Z. B., et al. (2018). A(2A) Receptor activation attenuates hypertensive cardiac remodeling via promoting brown adipose tissue-derived FGF21. *Cell Metab.* 28, 476–489.e475. doi: 10.1016/j.cmet.2018.06.013

Settembre, C., Fraldi, A., Medina, D. L., and Ballabio, A. (2013). Signals from the lysosome: a control centre for cellular clearance and energy metabolism. *Nat. Rev. Mol. Cell Biol.* 14, 283–296. doi: 10.1038/nrm3565

Subramanian, A., Becker, L. M., and Carmeliet, P. (2021). Endothelial metabolism going single. *Nat. Metab.* 3, 593–594. doi: 10.1038/s42255-021-00399-3

Tang, W. H. W., Li, D. Y., and Hazen, S. L. (2019). Dietary metabolism, the gut microbiome, and heart failure. *Nat. Rev. Cardiol.* 16, 137–154. doi: 10.1038/s41569-018-0108-7

Tang, X., Chen, X. F., Chen, H. Z., and Liu, D. P. (2017). Mitochondrial sirtuins in cardiometabolic diseases. *Clin. Sci.* 131, 2063–2078. doi: 10.1042/CS20160685

Tang, X., Li, P. H., and Chen, H. Z. (2020). Cardiomyocyte senescence and cellular communications within myocardial microenvironments. *Front. Endocrinol.* 11:280. doi: 10.3389/fendo.2020.00280

Tang, X., Luo, Y. X., Chen, H. Z., and Liu, D. P. (2014). Mitochondria, endothelial cell function, and vascular diseases. *Front. Physiol.* 5:175. doi: 10.3389/fphys.2014.00175

Vervloet, M. G., Sezer, S., Massy, Z. A., Johansson, L., Cozzolino, M., and Fouque, D. (2017). The role of phosphate in kidney disease. *Nat. Rev. Nephrol.* 13, 27–38. doi: 10.1038/nrneph.2016.164

Villarroya, F., Cereijo, R., Villarroya, J., Gavaldà-Navarro, A., and Giralt, M. (2018). Toward an understanding of how immune cells control brown and beige adipobiology. *Cell Metab.* 27, 954–961. doi: 10.1016/j.cmet.2018.04.006

Wang, J., Liu, S., Heallen, T., and Martin, J. F. (2018). The Hippo pathway in the heart: pivotal roles in development, disease, and regeneration. *Nat. Rev. Cardiol.* 15, 672–684. doi: 10.1038/s41569-018-0063-3

Wang, Y. X., Arvizu, M., Rich-Edwards, J. W., Wang, L., Rosner, B., Stuart, J. J., et al. (2021). Hypertensive disorders of pregnancy and subsequent risk of premature mortality. *J. Am. Coll. Cardiol.* 77, 1302–1312. doi: 10.1016/j.jacc.2021.01.018

Wang, Z. H., Davis, B. B., Jiang, D. Q., Zhao, T. T., and Xu, D. Y. (2013). Soluble epoxide hydrolase inhibitors and cardiovascular diseases. *Curr. Vasc. Pharmacol.* 11, 105–111. doi: 10.2174/157016113804547593

Witkowski, M., Weeks, T. L., and Hazen, S. L. (2020). Gut microbiota and cardiovascular disease. *Circ. Res.* 127, 553–570. doi: 10.1161/CIRCRESAHA.120.316242

Zhao, X., Le, T. P., Erhardt, S., Findley, T. O., and Wang, J. (2021). Hippo-yap pathway orchestrates neural crest ontogenesis. *Front. Cell Dev. Biol.* 9:706623. doi: 10.3389/fcell.2021.706623

Zhou, S., Tang, X., and Chen, H.-Z. (2018). Sirtuins and insulin resistance. *Front. Endocrinol.* 9:748. doi: 10.3389/fendo.2018.00748

Conflict of Interest: The authors declare that the research was conducted in the absence of any commercial or financial relationships that could be construed as a potential conflict of interest.

Publisher's Note: All claims expressed in this article are solely those of the authors and do not necessarily represent those of their affiliated organizations, or those of the publisher, the editors and the reviewers. Any product that may be evaluated in this article, or claim that may be made by its manufacturer, is not guaranteed or endorsed by the publisher.

frontiers in Cell and Developmental Biology

ORIGINAL RESEARCH
published: 12 November 2020
doi: 10.3389/fcell.2020.581641

Inhibition of PFKFB3 Hampers the Progression of Atherosclerosis and Promotes Plaque Stability

Kikkie Poels[1†], Johan G. Schnitzler[2†], Farahnaz Waissi[3,4,5], Johannes H. M. Levels[2], Erik S. G. Stroes[2], Mat J. A. P. Daemen[6], Esther Lutgens[1,7,8], Anne-Marije Pennekamp[2], Dominique P. V. De Kleijn[3,4,9], Tom T. P. Seijkens[1‡] and Jeffrey Kroon[2‡]*

[1] Department of Medical Biochemistry, Amsterdam Cardiovascular Sciences, Amsterdam University Medical Centers, University of Amsterdam, Amsterdam, Netherlands, [2] Department of Experimental Vascular Medicine, Amsterdam University Medical Centers, University of Amsterdam, Amsterdam Cardiovascular Sciences, Amsterdam, Netherlands, [3] Division of Surgical Specialties, Department of Vascular Surgery, University Medical Center Utrecht, Utrecht University, Utrecht, Netherlands, [4] Netherlands Heart Institute, Utrecht, Netherlands, [5] Department of Cardiology Amsterdam Cardiovascular Sciences, Amsterdam University Medical Centers, University of Amsterdam, Amsterdam, Netherlands, [6] Department of Pathology, Amsterdam Cardiovascular Sciences (ACS), Amsterdam University Medical Centers, University of Amsterdam, Amsterdam, Netherlands, [7] Institute for Cardiovascular Prevention (IPEK), Ludwig Maximilians University, Munich, Germany, [8] German Center for Cardiovascular Research (DZHK), Partner Site Munich Heart Alliance, Munich, Germany, [9] Department of Vascular Surgery, Netherlands and Netherlands Heart Institute, University Medical Center Utrecht, University Utrecht, Utrecht, Netherlands

OPEN ACCESS

Edited by:
InKyeom Kim,
Kyungpook National University,
South Korea

Reviewed by:
Prasun K. Datta,
Tulane University, United States
Terrence J. Piva,
RMIT University, Australia

***Correspondence:**
Jeffrey Kroon
j.kroon@amsterdamumc.nl

[†]These authors share first authorship

[‡]These authors share senior authorship

Specialty section:
This article was submitted to Cellular Biochemistry, a section of the journal Frontiers in Cell and Developmental Biology

Received: *09 July 2020*
Accepted: *14 October 2020*
Published: *12 November 2020*

Citation:
Poels K, Schnitzler JG, Waissi F, Levels JHM, Stroes ESG, Daemen MJAP, Lutgens E, Pennekamp A-M, De Kleijn DPV, Seijkens TTP and Kroon J (2020) Inhibition of PFKFB3 Hampers the Progression of Atherosclerosis and Promotes Plaque Stability. Front. Cell Dev. Biol. 8:581641. doi: 10.3389/fcell.2020.581641

Aims: 6-phosphofructo-2-kinase/fructose-2,6-biphosphatase (PFKFB)3-mediated glycolysis is pivotal in driving macrophage- and endothelial cell activation and thereby inflammation. Once activated, these cells play a crucial role in the progression of atherosclerosis. Here, we analyzed the expression of PFKFB3 in human atherosclerotic lesions and investigated the therapeutic potential of pharmacological inhibition of PFKFB3 in experimental atherosclerosis by using the glycolytic inhibitor PFK158.

Methods and Results: PFKFB3 expression was higher in vulnerable human atheromatous carotid plaques when compared to stable fibrous plaques and predominantly expressed in plaque macrophages and endothelial cells. Analysis of advanced plaques of human coronary arteries revealed a positive correlation of PFKFB3 expression with necrotic core area. To further investigate the role of PFKFB3 in atherosclerotic disease progression, we treated 6–8 weeks old male *Ldlr*$^{-/-}$ mice. These mice were fed a high cholesterol diet for 13 weeks, of which they were treated for 5 weeks with the glycolytic inhibitor PFK158 to block PFKFB3 activity. The incidence of fibrous cap atheroma (advanced plaques) was reduced in PFK158-treated mice. Plaque phenotype altered markedly as both necrotic core area and intraplaque apoptosis decreased. This coincided with thickening of the fibrous cap and increased plaque stability after PFK158 treatment. Concomitantly, we observed a decrease in glycolysis in peripheral blood mononuclear cells compared to the untreated group, which alludes that changes in the intracellular metabolism of monocyte and macrophages is advantageous for plaque stabilization.

Conclusion: High PFKFB3 expression is associated with vulnerable atheromatous human carotid and coronary plaques. In mice, high PFKFB3 expression is also associated with a vulnerable plaque phenotype, whereas inhibition of PFKFB3 activity leads to plaque stabilization. This data implies that inhibition of inducible glycolysis may reduce inflammation, which has the ability to subsequently attenuate atherogenesis.

Keywords: atherosclerosis, glycolysis, glycolytic inhibition, inflammation, plaque stability

INTRODUCTION

In recent years it has become clear that the development of atherosclerosis coincides with marked metabolic cellular alterations (Ali et al., 2018; Riksen and Stienstra, 2018). Particularly, inflammatory stimuli modify the intracellular metabolism of multiple cell types involved in atherogenesis, such as macrophages and endothelial cells. These cells are highly dependent on glycolysis for their energy metabolism to regulate cellular function (Bekkering et al., 2018; Riksen and Stienstra, 2018; Schnitzler et al., 2020). This induction in glycolysis could already be observed at regions where the endothelium is subjected to disturbed shear stress, making these early lesions susceptible for endothelial activation by lipoproteins, such as low-density lipoprotein (LDL) and lipoprotein(a) [Lp(a)] (Libby, 2012; Schnitzler et al., 2020). Lipid-lowering strategies markedly reduce cardiovascular event rates; however, a residual inflammatory risk remains even after potent lipid-lowering therapy in patients (Ridker, 2016; Stiekema et al., 2019).

Atherogenic stimuli such as Lp(a) have been shown to induce endothelial cell activation through upregulation of key-glycolytic players comprising glucose transporter (GLUT) 1 and hexokinase (Hk) II (Schnitzler et al., 2020). This glycolytic switch relies predominantly on the enzyme 6-phosphofructo-2-kinase/fructose-2,6-biphosphatase (PFKFB3), which serves as a potent source for inducible glycolysis (De Bock et al., 2013; Cantelmo et al., 2016). Conversely, inhibition of PFKFB3 leads to a marked reduction in the lipoprotein-induced inflammatory signature of endothelial cells and immune cells *in vitro*, pointing to a key role for PFKFB3 in the link between glycolysis and inflammation (Tawakol et al., 2015; Schnitzler et al., 2020). In addition, partial glycolytic inhibition in *Apoe*$^{-/-}$ mice via silencing of PFKFB3 results in decreased glycolysis in the arterial wall (Tawakol et al., 2015). However, it is currently not known how glycolytic inhibition affects the progression of atherosclerosis.

In the present study, we analyzed the expression of PFKFB3 in human atherosclerotic lesions and explored the therapeutic potential of pharmacological inhibition of PFKFB3 in experimental atherosclerosis.

MATERIALS AND METHODS

Immunohistochemical Analysis of Human Coronary Plaques

Human coronary artery specimens were obtained after informed written consent of the subjects during autopsies at the Department of Pathology of the Amsterdam University Medical Center (Amsterdam, Netherlands) and immediately fixed in 10% formalin and processed for paraffin embedding. The use of tissue was in agreement with the "Code for Proper Secondary Use of Human Tissue in Netherlands" and was in accordance with the principles as outlined in the Declaration of Helsinki. Based on fibrous cap formation and necrotic core size, specimens were classified as initial or advanced lesion, as described previously (Seijkens et al., 2019). PFKFB3 expression was analyzed by immunohistochemistry. After deparaffinization, slides were blocked for endogenous peroxidase activity in methanol, after which heat induced antigen retrieval was performed. Slides were then covered with 1:100 dilution of rabbit anti-human PFKFB3 antibody (Abcam, AB2617178) for an hour at room temperature. After washing with Tris-Hcl buffered saline (TBS), a secondary goat anti-rabbit biotin labeled antibody (Dako, E0432) was introduced 1:200 to the slides for 30 min, followed by 30 min of incubation with 1:200 ABC-HRP (for DAB) or ABC-AP kit (for Vector blue) (Vector, PK-6100, AK-5000). PFKFB3 was visualized with DAB (Vector SK-4105). For the double stainings, PFKFB3 was visualized with Vector blue (Vector, SK-5300), which was followed by 4% FCS block for 30 min and additional heat induced epitope retrieval. CD68 (mouse anti-human, Abcam, ab201340, 1:100), CD3 (rat anti-human, AbD Serotec, MCA1477, 1:100), αSMA (mouse anti-human, Sigma-Aldrich, F3777, 1:5,000) and CD31 (mouse anti-human, Novus Biologicals, NBP2-15202, 1:100) were used, all for 1 h at RT. Secondary goat anti-mouse biotinylated antibody (Dako, E0433) and rabbit anti-rat biotinylated antibody (Vector, BA-4001) were used at 1:300 for 30 min. Slides were covered in 1:200 ABC-HRP kit (Vector laboratories) for 30 min. Epitopes were visualized with ImmPACT AMEC red (Vector, SK-4285). Analyses of the slides was performed on a Leica DM3000 microscope with a DFC295 camera and further analysis was done with Adobe Photoshop CS6, Image J, and Las 4.1 software (Leica).

Carotid Endarterectomy Specimens From the Athero-Express Biobank

The Athero-Express Biobank study design and plaque processing has been reported previously (Verhoeven et al., 2004,2005). In short, the plaques were randomly selected from patients undergoing a carotid endarterectomy. Percentage of atheroma was estimated by means of visual estimation using Picrosirius red with polarized light in combination with hematoxylin stains. Three groups were considered (n = 10 per group), based on the percentage of atheroma in the plaque being present: fibrous plaques containing < 10% fat; fibro-atheromatous, 10–40%; or

atheromatous, > 40% fat. Next, the cumulative score for plaque vulnerability was determined by scoring macrophage-, collagen-, smooth muscle cell content and intraplaque hemorrhage. This plaque vulnerability index is scored as follows: macrophages: no/minor (0 points), moderate/heavy (1 point); collagen: moderate/heavy (0 points), no/minor (1 point); smooth muscle cells: moderate/heavy (0 points), no/minor (1 point). Intraplaque hemorrhage was scored as absent (0 points) or present (1 point), as previously described (Hellings et al., 2010). Sections were subsequently stained as described previously (Schnitzler et al., 2020). Briefly, plaque sections were dewaxed in xylene and dehydrated in graduated concentration of ethanol (100–70% ethanol). Heat-induced epitope retrieval was performed before blocking the sections for 20 min with 5% BSA in tris-buffered saline (TBS). Next, the sections were incubated for 2 h at room temperature with the following primary antibodies: PFKFB3 rabbit anti-human (Abcam, AB2617178), CD68 (Invitrogen, MA1-80133) and von Willebrand Factor mouse anti-human (Agilent, AB2216702). Next, sections were incubated in the dark at RT with biotinylated secondary antibody: goat anti-rabbit Alexa 488 (Thermo Fisher Scientific, AB 143165), goat anti-mouse Alexa 564 (Thermo Fisher Scientific, AB2536161) and goat anti-mouse Alexa 647 (Thermo Fisher Scientific, AB 2535804). After 1 h incubation, the sections were mounted with DAKO mounting medium containing DAPI (Agilent). A Leica TCS SP8 Confocal laser scanning microscope was used to image the sections and quantification was performed using Leica LAS-X software (Leica Camera, Wetzlar, Germany). All patients provided written informed consent. The Athero-Express study protocol conforms to the Declaration of Helsinki and has been approved by the Institution's ethics committee on research on humans.

Animal Experiments

Male *Ldlr*$^{-/-}$ mice were bred and housed at the local animal facility with normal light/dark cycle and were fed 0.15% cholesterol diet *ad libitum*. At 16 weeks of age mice were injected in the morning 3x/week for 5 weeks with PFK158 (2 mg/kg *ip*) or vehicle control (0.1% DMSO). Mice were euthanized by a single intraperitoneal injection of a cocktail of 30 mg/kg Sedamun (xylazine 20 mg/ml) and 100 mg/kg Anesketin (ketamine, 100 mg/ml) and death was confirmed by heart puncture. All experiments were approved by the Committee for Animal Welfare of the University of Amsterdam, Netherlands (protocol 265-AW-1), and comply to the European Regulations as identified in Directive 2010/63/EU on the protection of laboratory animals.

Lipoprotein Separation by Fast Protein Liquid Chromatography

Blood was obtained by venous or cardiac puncture and collected into ethylenediaminetetraacetic acid (EDTA)-containing tubes. Individual lipoprotein levels were determined by fast-performance liquid chromatography (FPLC) as described previously (Fedoseienko et al., 2018). In short, total cholesterol (TC) and triglyceride (TG) content in the main lipoprotein classes (VLDL, LDL, and HDL) was determined using FPLC. The main system consisted of a PU-980 ternary pump with an LG-980-02 linear degasser and an UV-975 UV/VIS detector (Jasco, Tokyo, Japan). After injection of 30 μl plasma (1:1 diluted with TBS) the lipoproteins were separated using a Superose 6 increase 10/30 column (GE Healthcare Hoevelaken, Netherlands). As eluent TBS pH 7.4 was used at a flow rate of 0.31 ml/min. A second pump (PU-2080i Plus, Jasco, Tokyo Japan) was used for either in-line cholesterol PAP or Triglyceride enzymatic substrate reagent (Sopachem, Ochten, Netherlands) addition at a flowrate of 0.1 ml/min facilitating TC or TC detection. Commercially available lipid plasma standards (low, medium and high) were used for generation of TC or TG calibration curves for the quantitative analysis (SKZL, Nijmegen, Netherlands) of the separated lipoprotein fractions. All calculations performed on the chromatograms were carried out with ChromNav chromatographic software, version 1.0 (Jasco, Tokyo, Japan).

Histology

At the age of 21 weeks, mice were sacrificed and the arterial tree was perfused with PBS and 1% paraformaldehyde. The aortic arch and organs were isolated and fixed in paraformaldehyde. Longitudinal sections of the aortic arch (4 μm) (n = 10/group) and sections of the three valve area in the aortic root (n = 14/group) were stained with hematoxylin and eosin and analyzed for plaque extent and phenotype as previously described (Seijkens et al., 2018). One mouse was excluded from aortic arch analysis due to situs inversus. Necrotic core measurements were only performed in advanced plaques. Intimal xanthoma (IX) was defined by a small lesion consisting of foam cells in which no extracellular lipid accumulation can be detected, pathological intimal thickening (PIT) was defined as a larger lesion that mainly consists of macrophage foam cells, but contains small extracellular lipid pools and the first matrix depositions, a fibrous cap atheroma (FCA) was defined as an advanced atherosclerotic lesion with a clear fibrous cap and necrotic cores (extracellular lipid accumulation, cholesterol crystals and/or calcification; Virmani et al., 2000). Fibrous cap thickness was measured at the thinnest part of each fibrous cap. Immunohistochemistry was performed for MAC3 (BD Pharmingen), alpha smooth muscle actin (Sigma-Aldrich), CD3 (AbD Serotec), CD8 (eBioscience), Ki67 (Abcam) and TUNEL (*in situ* apoptosis detection kit, Roche). The stability index was defined as (% α smooth muscle actin/% necrotic core; Poels et al., 2020). Double immunohistochemical stainings were performed with rabbit anti-mouse PFKFB3 antibody (Abcam, AB2617178) in combination with CD31 (Dianova, Hamburg, Germany), and the previously mentioned MAC3, CD3 and alpha smooth muscle actin. Morphometric analyses were performed on a Leica DM3000 microscope with a DFC 295 camera and Adobe Photoshop CS6, Image J or Las4.0 software (Leica).

Flow Cytometry

Spleen and lymph nodes were homogenized, and blood and spleen samples were subjected to red blood cell lysis. The cells were stained with fluorescently labeled surface

antibodies (CD45, CD3, CD4, CD8, F4/80, Ly6C, Ly6G, MHCI, MHCII, CD44, CD62L, CD19, CD11C, NK1.1; all from BD Biosciences). For intracellular staining, cells were fixed and permeabilized with fixation/permeabilization buffer (eBioscience) and stained with fluorescent antibodies against Foxp3 (BioLegend). Flow cytometric analysis was performed on a BD Canto II (BD Biosciences).

Immunofluorescent Staining of Murine Aortas Using Confocal Microscopy

Abdominal aortas remained intact for *en face* staining with ICAM-1 (Abcam) and VCAM-1 (Abcam) or aortas were dissected until 3–5 mm before the iliac bifurcation to obtain transverse sections. For the latter, aortas were embedded in paraffin for subsequent cutting sections into 10 μm slices for immunofluorescent staining. Next, the transverse sections were stained as described previously (Schnitzler et al., 2020). In summary, the following antibodies were used: ICAM-1 (Abcam), GLUT-1 (Thermo Fisher) and secondary antibody Alexa Fluor 568 for PFKFB3 and Alexa 633 for GLUT1-1 (both Thermo Fisher). HIF1α (R&D systems, MAB1536), GLUT3 (Invitrogen, MA5-32697), and secondary Alexa Fluor 647 for HIF1a and Alexa Fluor 488 for GLUT3 (both Thermo Fisher Scientific). The transverse sections aortas were fixed with DAKO mounting medium containing DAPI (Agilent, Santa Clara, United States). All samples were visualized on a Leica TCS SP8 Confocal laser scanning microscope and quantified using ImageJ.

RNA Isolation, cDNA Synthesis and Real Time Quantitative Polymerase Chain Reaction

Tissues were homogenized and lysed with TriPure (Roche, Basel, Switzerland). RNA was isolated according to the manufacturer's instructions. Briefly, 1 μg of RNA was used for cDNA synthesis with iScript (BioRad, Veenendaal, Netherlands). qPCR was performed using Sybr Green Fast (Bioline Meridian Bioscience, Cincinnati, OH, United States) on a ViiA7 PCR machine (Applied Biosystems, Bleiswijk, Netherlands). Gene expression was normalized to the housekeeping gene *H36B4*. Primer sequences are shown in **Supplementary Table 1**. All gene expression graphs indicate fold change of relative gene expression of which values were normalized to the mean of the control group.

Murine PBMC Isolation and Seahorse Flux Analysis

Murine peripheral blood mononuclear cells (PBMCs) were obtained from whole blood samples through density centrifugation using Lymphoprep (Stemcell Technologies, Koln, Germany; D = 1.077 g/mL) as described in detail previously (Schnitzler et al., 2017). In short, blood was diluted in a 1:1 ratio with PBS enriched with 2 mM EDTA and subsequently added to a layer of Lymphoprep. Next, cells were centrifuged for 20 min at 600× g at RT with slow acceleration and no brake. The PBMC fraction was collected and washed twice with PBS/2 mM EDTA. Next, cells were counted using a Casy Counter (Roche Innovatis Casy TT, Bielefeld, Germany). Next, PBMCs were seeded in 80 μL EGM-2 medium at a density of 50,000 cells per well on XFe96 microplates (Seahorse Bioscience). The cells were incubated in unbuffered DMEM assay medium (Merck) for 1.5 h in a non-CO_2 incubator at 37°C. A Seahorse XFe 96 analyzer (Seahorse Bioscience, Billerica, United States) was used to analyze cellular respiration. Extracellular acidification rates (ECAR) were measured after injecting glucose (10 mM), the mitochondrial/ATP synthase inhibitor oligomycin (1.5 μM), and the glycolysis inhibitor 2-Deoxy-D-glucose (2-DG; 100 mM), to determine glycolysis, glycolytic capacity and glycolytic reserve, respectively. Values were corrected for cell count.

Quantification and Statistical Analysis

Data are presented as the mean ± SEM, unless stated otherwise. To avoid observer bias, the murine and human plaque analysis were blinded. Experiments were assessed with two-tailed Student's *t*-tests, two-tailed Mann Whitney or One-way ANOVA as indicated in the figure legends. Clinical characteristics of patients from the Athero-Express Biobank were compared between the three plaque phenotypically different groups (fibrous, fibro-atheromatous, and atheromatous plaques). Statistical testing for differences between the three group was done by using a One-way ANOVA test for normally distributed data and a Kruskal–Wallis Rank Sum Test for non-normally distributed data [i.e., triglycerides and lipoprotein(a)]. Representative images were selected based on the value closest to the mean value per group. Statistics were performed using Graphpad Prism (v8.0h; La Jolla, CA). The analysis found in the baseline table was performed in R version 3.6.1 (R Foundation, Vienna, Austria). A P-value of < 0.05 was considered statistically significant.

RESULTS

PFKFB3 Expression in Macrophages and Endothelial Cells Correlates With Plaque Instability in Human Atherosclerosis

Carotid plaques were obtained from patients undergoing endarterectomy enrolled in the Athero-Express biobank. Plaques were classified as fibrous plaques (containing < 10% intraplaque fat), fibro-atheromatous (10–40% intraplaque fat) or atheromatous (>40% intraplaque fat; Verhoeven et al., 2004, 2005). Both fibro-atheromatous and atheromatous plaques had an increased plaque vulnerability index (**Table 1**; Verhoeven et al., 2005). Further carotid plaque analysis revealed a marked higher PFKFB3 expression when plaque vulnerability is higher (**Figures 1A,B**). Higher PFKFB3 expression coincides with high number of $CD68^+$ macrophage in atheromatous plaques (**Figures 1A,C**) that positively correlates with PFKFB3 expression (**Figure 1D**). These data imply that mainly macrophages show enhanced PFKFB3 expression in atherosclerotic plaques. In line, human coronary atherosclerotic plaques, histologically classified as fibrous cap atheromata (advanced atherosclerosis) express higher levels

TABLE 1 | Clinical characteristics of included patients of Athero-Express Biobank.

	Fibrous (*n* = 10)	Fibro-Atheromatous (*n* = 10)	Atheromatous (*n* = 10)	*P*-value
Age	73.1 (7.5)	67.7 (8.7)	69.4 (7.4)	0.308
Gender (Male, %)	6 (60.0)	8 (80.0)	8 (80.0)	0.506
Systolic blood pressure, mmHg	148.3 (33.6)	174.7 (45.6)	176.7 (37.3)	0.316
BMI, kg/m^2	26.8 (4.5)	26.0 (2.5)	27.2 (3.8)	0.768
Current smoker (yes, %)	2 (20.0)	4 (40.0)	4 (40.0)	0.549*
Cholesterol lowering medication (yes, %)	9 (90.0)	8 (80.0)	8 (80.0)	0.787
Total cholesterol, mmol/L	3.9 (0.7)	4.3 (0.9)	4.0 (1.3)	0.607
HDL-cholesterol, mmol/L	1.0 (0.3)	1.1 (0.3)	1.0 (0.2)	0.587
LDL-cholesterol, mmol/L	2.0 (0.3)	2.3 (1.0)	2.0 (1.1)	0.709
Triglycerides, mmol/L	1.7 [1.3, 2.5]	1.4 [1.0, 1.8]	1.3 [0.9, 1.8]	0.399
Lipoprotein(a), nmol/L	21.4 [11.1, 44.6]	49.4 [14.0, 121.5]	14.2 [12.2, 47.0]	0.464
Glucose, mmol/L	5.9 (2.1)	6.7 (3.5)	6.8 (3.0)	0.794
Plaque vulnerability index	0.0 (0.0)	1.4 (0.5)	3.8 (0.4)	<0.001

**Chi-Square test, 1-sided. Data are presented as mean (SD), n (%) or median [IQR]. BMI, body-mass index; HDL, high density lipoprotein; LDL, low-density lipoprotein.*

of PFKFB3$^+$ cells when compared with intimal xanthomas or pathological intimal thickenings (initial/intermediate atherosclerosis) (**Figures 1E,F**). PFKFB3 expression positively correlates with necrotic core area (**Figure 1G**), indicating that PFKFB3 expression increases during the progression of atherosclerosis. The majority of PFKFB3$^+$ cells are CD68$^+$ macrophages and PECAM$^+$ endothelial cells (**Figures 1H,I**). Only few CD3$^+$ T cells and α smooth muscle actin (αSMA)$^+$ vascular smooth muscle cells express PFKFB3 (**Figures 1J,K**). A similar expression is observed in murine plaques, where PFKFB3 was also predominantly observed in macrophages (MAC3$^+$) and the endothelium (PECAM$^+$) and to a lesser extend in T-cells (CD3$^+$) and smooth muscle cells (αSMA$^+$) (**Supplementary Figures 1A–D**). Together, these data suggest that PFKFB3 expression increases as plaques become more vulnerable.

PFKFB3 Inhibition Hampers the Progression of Atherosclerosis and Promotes Plaque Stability

To investigate the therapeutic potential of PFKFB3 inhibition on atherosclerosis, 6–8 weeks-old *Ldlr*$^{-/-}$ mice received a high fat diet for 8 weeks and were subsequently treated with the PFKFB3 inhibitor PFK158 for 5 weeks (intraperitoneal administration, 3 times per week, 2 mg/kg) (**Figure 2A**). PFK158 treatment had no effect on bodyweight (**Figure 2B**). To assess the efficacy of PFK158, we examined the metabolic signature of peripheral blood mononuclear cells (PBMCs) of PFK158-treated mice which displayed a significant decrease in glycolysis and their glycolytic capacity (**Figure 2C**). PFK158-treatment had no effect on total plasma cholesterol levels, plasma VLDL-, LDL- and HDL-levels (**Figure 2D**). Immune cell distribution in peripheral blood and lymphoid organs was unaffected by PFK158 treatment (**Supplementary Figures 1E–H**).

While atherosclerotic lesion size in the aortic arch was not affected by PFK158 treatment (**Figures 2E,F**), morphological analysis demonstrated that the aortic arch of PFK158-treated mice contained relatively less FCA (advanced atherosclerotic lesions; **Figure 2G**). This is accompanied by an increase in the incidence of intimal xanthomas (initial atherosclerotic lesions) upon PFK158 treatment (**Figure 2G**), indicating that inhibition of PFKFB3 mitigates progression of atherosclerosis. Interestingly, both the necrotic core area per plaque (**Figure 2H**) and intraplaque apoptosis (**Figure 2I**) were reduced in PFK158-treated mice, whilst the number of CD4$^+$ and CD8$^+$ T cells and proliferating Ki67$^+$ cells remained unaffected (**Supplementary Figures 2A–C**, respectively). In addition, a trend toward increased plaque macrophage content (Mac3$^+$ area) was observed in PFK158 treated mice (**Figure 2J**). Interestingly, PFK158 treatment induced a marked increase in vascular smooth muscle content (αSMA$^+$) (**Figures 2K,L**) and thickening of the fibrous cap (**Figure 2M**). Together this led to a significant rise in stable plaques as shown by an increased plaque stability index (**Figure 2N**). A similar atherosclerotic phenotype was observed in the aortic roots of PFK158 treated mice (**Supplementary Figures 3A–F**). These data indicate that therapeutic inhibition of PFKFB3 inhibits the progression of atherosclerosis and promotes plaque stability.

PFK158 Does Not Affect the Atherosclerotic Phenotype of Endothelium

No differences in ICAM-1 and VCAM-1 expression were observed after PFK158 treatment (**Figure 3A**). Previously, we have shown that GLUT1 protein expression decreases in arterial ECs after PFK158 treatment (Schnitzler et al., 2020); however GLUT1 expression remained unaffected in cross-sections of aortas between groups (**Figure 3B**). Interestingly, after PFK158 treatment we observed a significant downregulation of both GLUT3 (**Figure 3C**) and HIF1α (**Figure 3D**) in the plaques. We furthermore observed a significant positive correlation between HIF1α and Glut3 expression levels (**Figure 3E**), suggesting that HIF1α and GLUT3 levels are regulated via PFKFB3-mediated glycolysis and that increased levels of HIF1α and GLUT3 are associated with

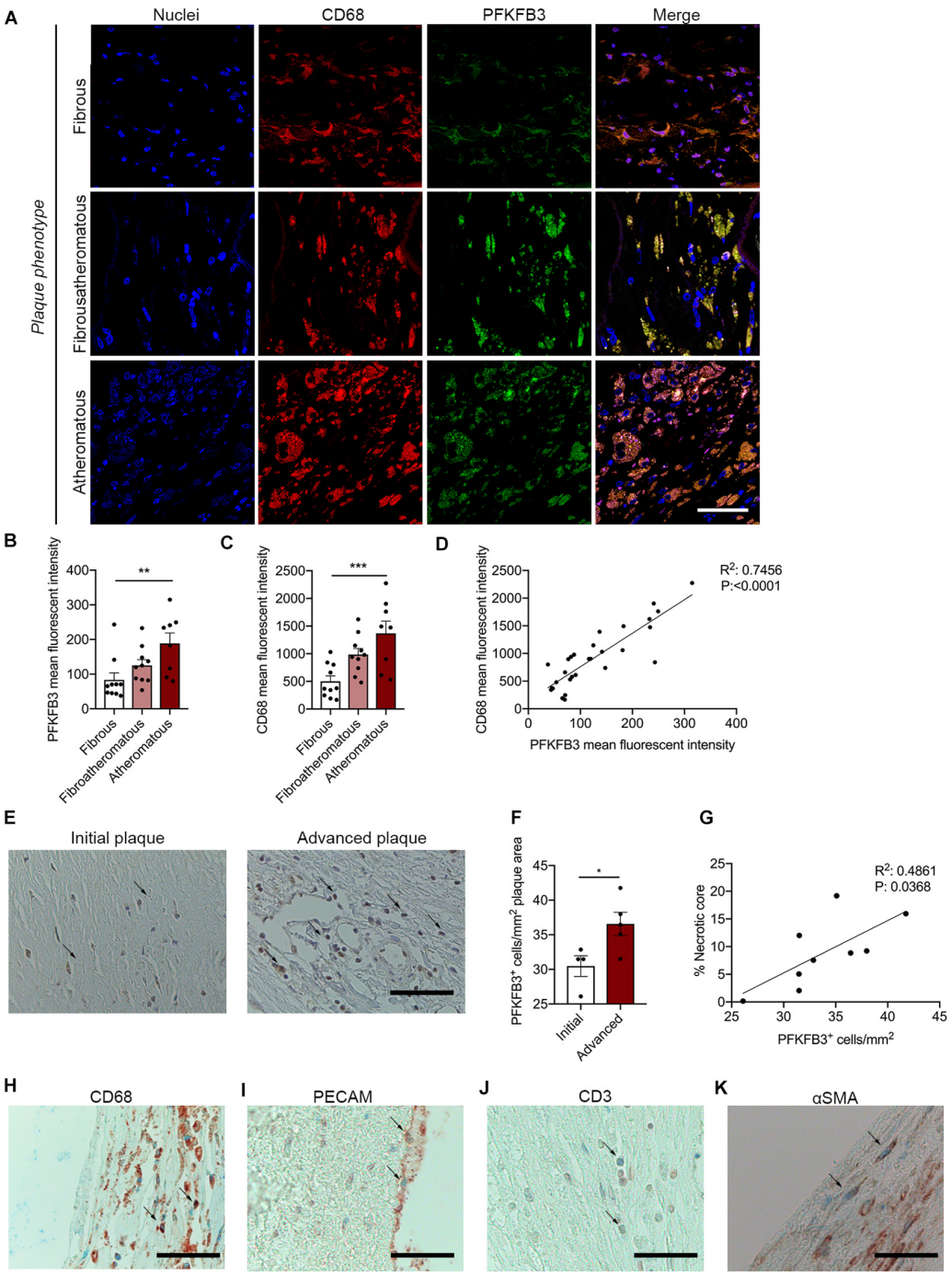

FIGURE 1 | PFKFB3 expression is increased in advanced atherosclerotic plaques and correlates with CD68$^+$ macrophages and necrotic core area. **(A,B)** Increased expression of PFKFB3 (green) in atheromatous plaques compared with fibrous carotid plaques. $n = 10$ for fibrous and fibroatheromatous plaques, $n = 8$ for atheromatous plaques; one-way ANOVA, $P = 0.0078$ for fibrous vs. atheromatous plaques. Scale bar 50 μm. **(A,C)** CD68$^+$ macrophages (red) increased in atheromatous carotid plaques. $n = 10$ for fibrous and fibroatheromatous plaques, $n = 8$ for atheromatous plaques; one-way ANOVA, $P = 0.0008$ for fibrous vs. atheromatous plaques. Scale bar 50 μm **(D)** PFKFB3 expression and CD68 expression correlated significantly. $n = 28$; linear regression analysis, $R^2 = 0.7456$, $P < 0.0001$. **(E)** Human coronary atherosclerotic advanced plaques showed increased PFKFB3 expression compared to initial plaques. $n = 4$ for initial vs. $n = 5$ for advanced plaques; two-tailed unpaired Mann-Whitney, $P = 0.0317$. Scale bar 200 μm. **(F)** PFKFB3 expression positively correlated with necrotic core area. $n = 9$; Linear regression analysis $R^2 = 0.4861$, $P = 0.0368$. **(G)** Immunohistochemistry of PFKFB3$^+$ co-staining with CD68$^+$ macrophages; Scale bar 100 μm, **(H)** PECAM$^+$ endothelial cells; Scale bar 100 μm, **(I)** CD3$^+$ T cells; Scale bar 100 μm, and **(J)** and α smooth muscle actin (αSMA)$^+$ vascular smooth muscle cells **(K)**; Scale bar 100 μm. Data are shown as mean ± standard error of the mean. *$P < 0.05$, **$P \leq 0.005$, ***$P < 0.0005$. PFKFB3, 6-phophofructo-2-kinase/fructose-2,6-biphosphatase 3; PECAM, platelet endothelial cell adhesion molecule; αSMA.

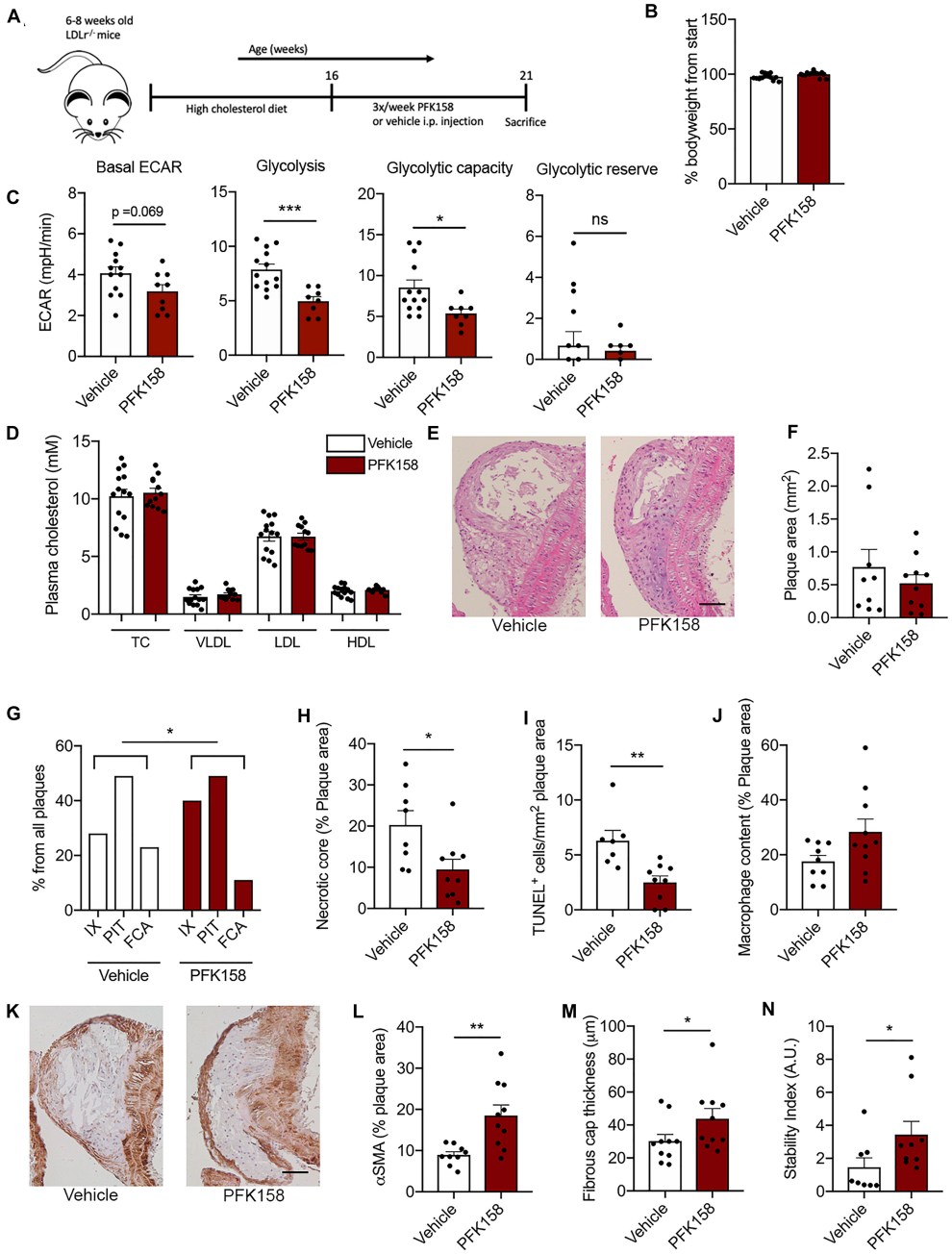

FIGURE 2 | PFK158 hampers the progression of atherosclerosis and increases plaque stability. **(A)** Experimental design: after 8 weeks of 0.15% high cholesterol diet male *Ldlr*$^{-/-}$ mice (*n* = 14/group) were injected 3 times per week with either PFK158 or vehicle for 5 weeks (13 weeks of high fat diet in total). **(B)** PFK158 treatment did not significantly affect bodyweight. **(C)** Analysis of circulating peripheral blood mononuclear cells revealed an increased extracellular acidification rate in vehicle cells (*n* = 13) compared to their PFK158-treated counterparts (*n* = 8) indicating the effectiveness of glycolytic inhibition. Two-tailed unpaired Student's *t*-test *P* = 0.0007. *n* = 10/group. **(D)** Plasma cholesterol levels remained similar between groups. *n* = 14/group **(E,F)** Atherosclerotic lesion area in the aortic arch did not change; scale bar = 50 μm. *n* = 10/group. **(G)** Morphological analysis (Virmani classification) revealed a reduced incidence of FCA in the aortic arch of PFK158 treated mice. The incidence of intimal xanthomas was increased in PFK158-treated mice. Chi-square, *P* = 0.0417. **(H)** Necrotic core area per advanced plaque was reduced in PFK158 treated mice (*n* = 8) vs. vehicle (*n* = 9). Unpaired Student's *t*-test *P* = 0.0205. **(I)** PFK158 treatment (*n* = 9) reduced the number of apoptotic (TUNEL^{+}) cells compared to vehicle (*n* = 7). Two-tailed unpaired Mann-Whitney, *P* = 0.0012. **(J)** A trend toward increased macrophage content was observed in PFK158 treated mice. Two-tailed unpaired Student's *t*-test *P* = 0.0628. **(K,L)** PFK158 increased αSMA content in PFK158 treated mice (*n* = 10) vs. vehicle treated mice (*n* = 9; Two-tailed unpaired Student's *t*-test *P* = 0.0033; scale bar = 50 μm) and **(M)** increased fibrous cap thickness (*n* = 10/group; Two-tailed unpaired Mann-Whitney, *P* = 0.0410). **(N)** which increased the plaque stability index (*n* = 8 for vehicle and *n* = 9 for PFK158 group; Two-tailed unpaired Mann-Whitney, *P* = 0.0464). Data are shown as mean ± standard error of the mean. *$P < 0.05$, **$P < 0.005$, ***$P < 0.0005$. TC, total cholesterol; VLDL, Very low-density lipoprotein; LDL, low-density lipoprotein; HDL, high-density lipoprotein; H&E, hematoxylin and eosin; IX, initial xanthoma; PIT, pathologic intimal thickening; FCA, fibrous cap atheroma; αSMA, α smooth muscle actin; PBMC, peripheral blood mononuclear cell; ECAR, extracellular acidification rate.

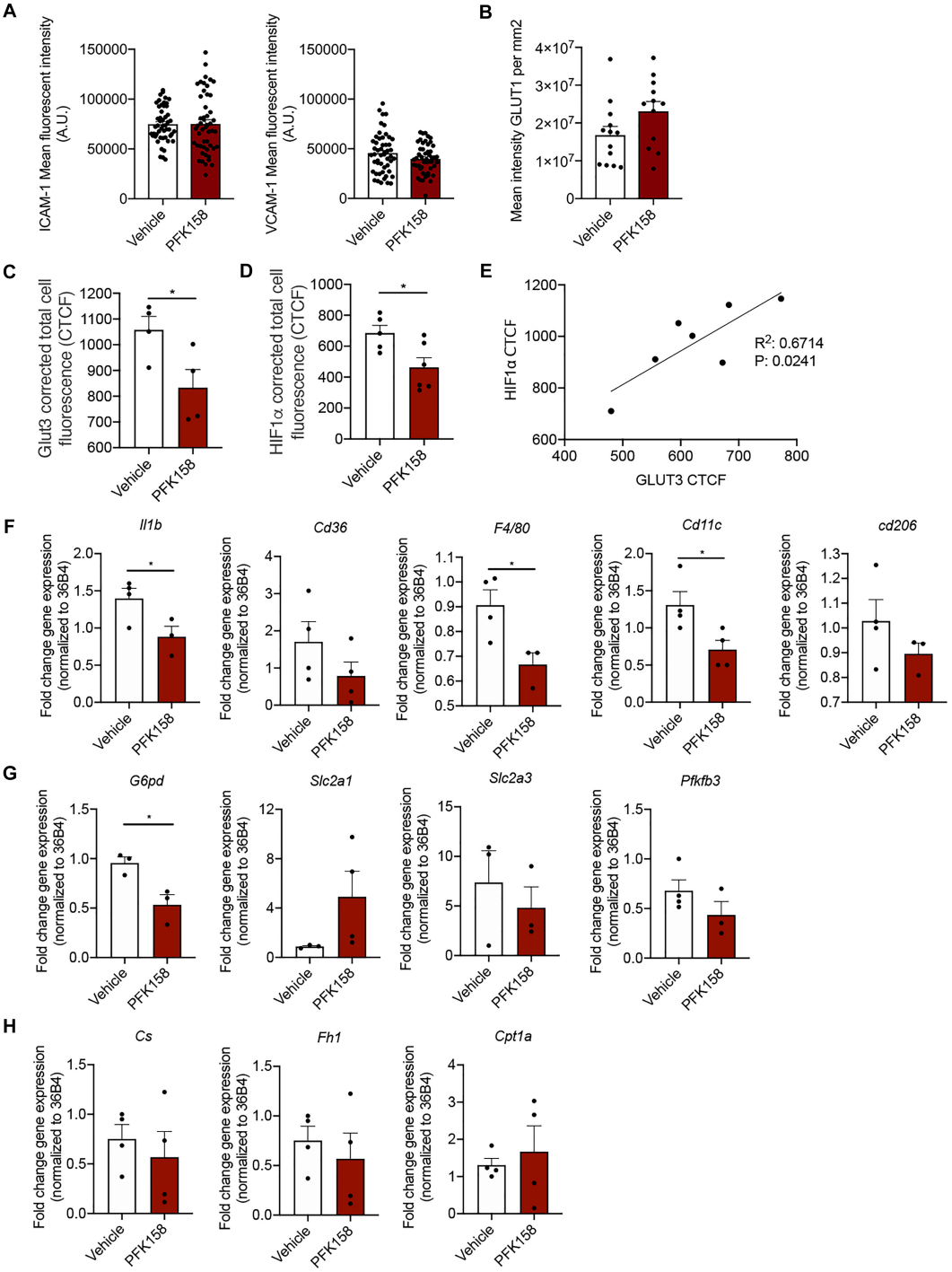

FIGURE 3 | PFK158 alters phenotype of highly vascularized lung tissue but does not affect arterial endothelial phenotype. **(A)** ICAM-1 and VCAM-1 expression per image (n = 50 per group) and **(B)** GLUT1 expression in ECs did not significantly alter between groups (n = 13 for vehicle and n = 12 for PFK158 group). **(C)** GLUT3 expression was significantly decreased after PFK158-treatment (n = 4 for both groups) which coincided with decreased. **(D)** HIF1α levels as well (n = 5 for vehicle and n = 6 for PFK158 group). **(E)** A positive correlation (R^2: 0.6714, P: 0.0241) was observed between HIF1α and GLUT3 expression levels. Homogenates of plaque-containing aortic arches indicated several significantly differentially expressed genes. **(F–H)** Two-tailed unpaired Student's t-test, P = 0.0497 for *Il1*β, P = 0.0239 for *G6pd*, P = 0.0347 for *F4/80*, and P = 0.0348 for *Cd11c* (n = 3–4 per group). Data are shown as mean ± standard error of the mean. *$P < 0.05$. ICAM-1, intercellular adhesion molecule 1; GLUT1, glucose transporter 1, CTCF, corrected total cell fluorescence.

increased plaque stability. Next, homogenates of murine plaque-containing aortic arches indicated that PFK158 treatment did result in a decrease in the gene expression of inflammatory markers *Il1*β and a trend in *Cd36*. Conversely, macrophage marker *F4/80* decreased in the PFK158 group, with a concomitant significant reduction in *Cd11c* and *Cd206*, suggesting a lower content of alternatively activated macrophages (**Figure 3F**). Interestingly, we also observed reduced *G6pd* transcript levels, the first and rate-limiting enzyme in the Pentose Phosphate Pathway (PPP), after PFK158 treatment, whereas *Slc2a1, Slc2a3* and the glycolytic mediator *Pfkfb3* were not altered by PFK158 treatment (**Figure 3G**). Similarly, *Cs, Fh1* involved in the TCA cycle, as well as *Cpt1a*, involved in fatty acid oxidation were not altered by the treatment (**Figure 3H**). In conclusion, these data are indicative of an altered inflammatory profile in the plaques of aortic arches on the level of gene expression after PFK158 treatment.

DISCUSSION

In this study, we reveal for the first time that PFKFB3 expression positively correlates with an unstable plaque phenotype in both carotid and coronary plaques in humans. Targeting PFKFB3 with a low-dose glycolytic inhibitor leads a reduction in advanced plaques with a vulnerable phenotype and an increase in stable plaque phenotype in $Ldlr^{-/-}$ mice, with a concomitant decrease in glycolytic flux in circulating PBMCs. This data may imply an atheroprotective role for glycolytic inhibition.

In humans, increased plaque vulnerability is characterized by a profound inflammatory and glycolytic phenotype (Tomas et al., 2018) as shown by metabolomic analysis on 156 human carotid endarterectomy plaques. They reported that atherosclerotic plaques with a high risk to rupture are recognized by increased glycophorin A (indicative of intraplaque hemorrhage) and a profound glycolytic phenotype (Tomas et al., 2018). Here, we find a positive correlation between PFKFB3 expression and necrotic core area in human coronary plaques and a positive correlation between PFBFB3 and high-risk plaques, mainly attributable to high expression of PFKFB3 in macrophages in both human carotid and coronary plaques (Bekkering et al., 2016). In addition, the increasing vulnerability of carotid plaques is positively associated with an increased prevalence of transient ischemic attack and stroke (Verhoeven et al., 2005). We also substantiate a marked increase in $CD68^{+}$ macrophage content in advanced carotid plaques (Moore et al., 2013; Tomas et al., 2018). Once macrophages are activated, they increase PFKFB3 activity, indicating that inflammation and glycolytic activation are closely intertwined (Tawakol et al., 2015). Conversely, glycolytic inhibition of macrophages using siRNA against PFKFB3 or using 3-[3-pyridinyl]-1-[4-pyridinyl]-2-propen-1-one, a selective inhibitor of PFKFB3, leads to a blockade in macrophage activation (Tawakol et al., 2015). *In vivo,* this translated into decreased ^{18}F-fluorodexyglucose (^{18}F-FDG) uptake in the arterial vessel wall in $Apoe^{-/-}$ mice measured with positron emission tomography/computed tomography (Singh et al., 2016), underscoring attenuated arterial wall inflammation following attenuation of inducible glycolysis in macrophages (Tarkin et al., 2014). In our *Ldlr* knockout mice, we show that the progression of atherosclerosis is attenuated upon PFKFB3 inhibition. Plaques from mice treated with PFK158 displayed less fibrous cap atheromas and increased initial- and intermediate plaques, indicative of reduced formation of advanced plaques (Libby, 2012; Tomas et al., 2018). Thus, PFK158-treated mice displayed an increase in plaque stability index and thickening of the fibrous cap, which can be attributed to enhanced SMC proliferation and/or migration toward the fibrous cap (Allahverdian et al., 2018).

In mice, we showed that targeting PFKFB3, mainly expressed by macrophages and endothelial cell, *in vivo* led to decreased necrotic core area, a phenomenon that could be attributed to the significant loss of apoptotic cells in the PFK158-treated mice compared to the control group. In advanced stages of atherosclerotic plaques, macrophage apoptosis contributes to necrotic core formation, furthermore implying that glycolytic inhibition leads to plaque stabilization (Tabas, 2010; Libby, 2012; Tabas and Bornfeldt, 2016; Gonzalez and Trigatti, 2017).

As plaque progression is dependent on the influx of immune cells, we have investigated the metabolic state of PBMCs. The PBMC fraction comprises monocytes, which are key orchestrators in the development of atherosclerosis (Sotiriou et al., 2006; van der Laan et al., 2014; Nahrendorf and Swirski, 2016; Schnitzler et al., 2019). In patients with severe symptomatic coronary atherosclerosis, monocytes display a distinct glycolytic phenotype by overexpressing hexokinase 2 and PFKFB3 (Bekkering et al., 2016). We corroborated these findings as partial inhibition of PFKFB3 decreased glycolytic flux in PBMCs indicating that these cells were metabolically inhibited which in turn alleviated atherosclerotic burden in mice. However, as PBMCs include a variety of cells, such as monocytes and lymphocytes, it would be interesting to investigate which cell subset plays a predominant role in our model (Kleiveland, 2015).

The other pivotal cell type, the endothelial cells covering the atherosclerotic plaques, did not seem to be affected by glycolytic inhibition as ICAM-1, VCAM-1, and GLUT1 expression did not alter after treatment. This might be a result of treating the mice in this study with a low dose of PFK158, whereas *in vitro* studies used increased concentrations (Schnitzler et al., 2020). Concomitantly, we found increased plaque stability and thickening of the fibrous cap which may be consequences of either a decrease in SMC apoptosis or increased SMC proliferation. Loss of these cells contributes to plaque destabilization once exposed to increased endoplasmic reticulum stress which facilitates apoptosis of SMCs (Myoishi et al., 2007).

In summary, this study demonstrates that intraplaque PFKFB3 levels are associated with plaque stability and glycolytic inhibition leads to a decrease in vulnerable plaque characteristics and increases plaque stabilization. The present study identifies PFKFB3 inhibition as a novel target potentially suitable to further attenuate atherosclerotic development.

DATA AVAILABILITY STATEMENT

The raw data supporting the conclusions of this article will be made available by the authors, without undue reservation.

ETHICS STATEMENT

The animal study was reviewed and approved by the Committee for Animal Welfare of the University of Amsterdam, Netherlands (protocol 265-AW-1), and comply to the European Regulations as identified in Directive 2010/63/EU on the protection of laboratory animals.

AUTHOR CONTRIBUTIONS

JS, KP, TS, and JK conceived and planned the experiments. JS, KP, A-MP, TS, and JK carried out the experiments and data analysis. JS, KP, TS, and JK wrote the manuscript. All authors provided critical feedback and helped shape the research, analysis and manuscript.

FUNDING

This work was supported by the Netherlands Organization for Scientific Research. JK received a VENI grant from ZonMW (91619098). This study was also supported by the Dutch Heart Foundation (Dr. Dekker Physician-in-specialty-training grant to TS). This work was also financially supported by Netherlands CardioVascular Research Initiative: the Dutch Heart Foundation, Dutch Federation of University Medical Centers, Netherlands, Organization for Health Research and Development and the Royal Netherlands Academy of Sciences for the GENIUS-II project "Generating the best evidence-based pharmaceutical targets for atherosclerosis-II" (CVON 2017-20 to ES). Funding was also obtained from the Dutch Heart Foundation, CVON 2017-05 pERSUASIVE and EU 755320 Taxinomisis grant to DDK.

ACKNOWLEDGMENTS

We would like to thank Miranda Versloot, Alinda Schimmel, Myrthe Den Toom, Cindy van Roomen, Linda Beckers and Laurens F. Reeskamp for their technical assistance.

SUPPLEMENTARY MATERIAL

The Supplementary Material for this article can be found online at: https://www.frontiersin.org/articles/10.3389/fcell.2020.581641/full#supplementary-material

REFERENCES

Ali, L., Schnitzler, J. G., and Kroon, J. (2018). Metabolism: the road to inflammation and atherosclerosis. *Curr. Opin. Lipidol.* 29, 474–480. doi: 10.1097/MOL.0000000000000550

Allahverdian, S., Chaabane, C., Boukais, K., Francis, G. A., and Bochaton-Piallat, M.-L. (2018). Smooth muscle cell fate and plasticity in atherosclerosis. *Cardiovasc. Res.* 114, 540–550. doi: 10.1093/cvr/cvy022

Bekkering, S., Arts, R. J. W., Novakovic, B., Kourtzelis, I., van der Heijden, C. D. C. C., Li, Y., et al. (2018). Metabolic induction of trained immunity through the mevalonate pathway. *Cell* 172, 135.e9–146.e9. doi: 10.1016/j.cell.2017.11.025

Bekkering, S., van den Munckhof, I., Nielen, T., Lamfers, E., Dinarello, C., Rutten, J., et al. (2016). Innate immune cell activation and epigenetic remodeling in symptomatic and asymptomatic atherosclerosis in humans in vivo. *Atherosclerosis* 254, 228–236. doi: 10.1016/j.atherosclerosis.2016.10.019

Cantelmo, A. R., Conradi, L.-C., Brajic, A., Goveia, J., Kalucka, J., Pircher, A., et al. (2016). Inhibition of the glycolytic activator PFKFB3 in endothelium induces tumor vessel normalization, impairs metastasis, and improves chemotherapy. *Cancer Cell* 30, 968–985. doi: 10.1016/j.ccell.2016.10.006

De Bock, K., Georgiadou, M., Schoors, S., Kuchnio, A., Wong, B. W., Cantelmo, A. R., et al. (2013). Role of PFKFB3-driven glycolysis in vessel sprouting. *Cell* 154, 651–663. doi: 10.1016/j.cell.2013.06.037

Fedoseienko, A., Wijers, M., Wolters, J. C., Dekker, D., Smit, M., Huijkman, N., et al. (2018). The COMMD family regulates plasma LDL levels and attenuates atherosclerosis through stabilizing the CCC complex in endosomal LDLR Trafficking. *Circ. Res.* 122, 1648–1660. doi: 10.1161/CIRCRESAHA.117.312004

Gonzalez, L., and Trigatti, B. L. (2017). Macrophage apoptosis and necrotic core development in atherosclerosis: a rapidly advancing field with clinical relevance to imaging and therapy. *Can. J. Cardiol.* 33, 303–312. doi: 10.1016/j.cjca.2016.12.010

Hellings, W. E., Peeters, W., Moll, F. L., Piers, S. R. D., van Setten, J., Van der Spek, P. J., et al. (2010). Composition of carotid atherosclerotic plaque is associated with cardiovascular outcome: a prognostic study. *Circulation* 121, 1941–1950. doi: 10.1161/CIRCULATIONAHA.109.887497

Kleiveland, C. R. (2015). "Peripheral blood mononuclear cells," in *The Impact of Food Bioactives on Health*, eds K. Verhoeckx, P. Cotter, I. Lopez-Exposito, C. Kleiveland, T. Lea, A. Mackie, et al. (Cham: Springer), 161–167. doi: 10.1007/978-3-319-16104-4_15

Libby, P. (2012). Inflammation in atherosclerosis. *Arterioscler. Thromb. Vasc. Biol.* 32, 2045–2051. doi: 10.1161/ATVBAHA.108.179705

Moore, K. J., Sheedy, F. J., and Fisher, E. A. (2013). Macrophages in atherosclerosis: a dynamic balance. *Nat. Rev. Immunol.* 13, 709–721. doi: 10.1038/nri3520

Myoishi, M., Hao, H., Minamino, T., Watanabe, K., Nishihira, K., Hatakeyama, K., et al. (2007). Increased endoplasmic reticulum stress in atherosclerotic plaques associated with acute coronary syndrome. *Circulation* 116, 1226–1233. doi: 10.1161/CIRCULATIONAHA.106.682054

Nahrendorf, M., and Swirski, F. K. (2016). Innate immune cells in ischaemic heart disease: does myocardial infarction beget myocardial infarction? *Eur. Heart J.* 37, 868–872. doi: 10.1093/eurheartj/ehv453

Poels, K., van Leent, M. M. T., Reiche, M. E., Kusters, P. J. H., Huveneers, S., de Winther, M. P. J., et al. (2020). Antibody-mediated inhibition of CTLA4 aggravates atherosclerotic plaque inflammation and progression in hyperlipidemic mice. *Cells* 9:1987. doi: 10.3390/cells9091987

Ridker, P. M. (2016). Residual inflammatory risk: addressing the obverse side of the atherosclerosis prevention coin. *Eur. Heart J.* 37, 1720–1722. doi: 10.1093/eurheartj/ehw024

Riksen, N. P., and Stienstra, R. (2018). Metabolism of innate immune cells: impact on atherosclerosis. *Curr. Opin. Lipidol.* 29, 359–367. doi: 10.1097/MOL.0000000000000539

Schnitzler, J. G., Bernelot Moens, S. J., Tiessens, F., Bakker, G. J., Dallinga-Thie, G. M., Groen, A. K., et al. (2017). Nile red quantifier: a novel and quantitative tool to study lipid accumulation in patient-derived circulating monocytes using confocal microscopy. *J. Lipid Res.* 58, 2210–2219. doi: 10.1194/jlr.D073197

Schnitzler, J. G., Dallinga-Thie, G. M., and Kroon, J. (2019). The role of (Modified) lipoproteins in vascular function: a duet between monocytes

and the endothelium. *Curr. Med. Chem.* 26, 1594–1609. doi: 10.2174/0929867325666180316121015

Schnitzler, J. G., Hoogeveen, R. M., Ali, L., Prange, K. H., Waissi, F., van Weeghel, M., et al. (2020). Atherogenic Lipoprotein(a) increases vascular glycolysis, thereby facilitating inflammation and leukocyte extravasation. *Circ. Res*. 126, 1346–1359. doi: 10.1161/circresaha.119.316206

Seijkens, T. T. P., Poels, K., Meiler, S., van Tiel, C. M., Kusters, P. J. H., Reiche, M., et al. (2019). Deficiency of the T cell regulator Casitas B-cell lymphoma-B aggravates atherosclerosis by inducing CD8+ T cell-mediated macrophage death. *Eur. Heart J.* 40, 372–382. doi: 10.1093/eurheartj/ehy714

Seijkens, T. T. P., van Tiel, C. M., Kusters, P. J. H., Atzler, D., Soehnlein, O., Zarzycka, B., et al. (2018). Targeting CD40-Induced TRAF6 signaling in macrophages reduces atherosclerosis. *J. Am. Coll. Cardiol.* 71, 527–542. doi: 10.1016/j.jacc.2017.11.055

Singh, P., Gonzalez-Ramos, S., Mojena, M., Rosales-Mendoza, C. E., Emami, H., Swanson, J., et al. (2016). GM-CSF enhances macrophage glycolytic activity in vitro and improves detection of inflammation in vivo. *J. Nucl. Med.* 57, 1428–1435. doi: 10.2967/jnumed.115.167387

Sotiriou, S. N., Orlova, V. V., Al-Fakhri, N., Ihanus, E., Economopoulou, M., Isermann, B., et al. (2006). Lipoprotein(a) in atherosclerotic plaques recruits inflammatory cells through interaction with Mac-1 integrin. *FASEB J. Off. Publ. Fed. Am. Soc. Exp. Biol.* 20, 559–561. doi: 10.1096/fj.05-4857fje

Stiekema, L. C. A., Stroes, E. S. G., Verweij, S. L., Kassahun, H., Chen, L., Wasserman, S. M., et al. (2019). Persistent arterial wall inflammation in patients with elevated lipoprotein(a) despite strong low-density lipoprotein cholesterol reduction by proprotein convertase subtilisin/kexin type 9 antibody treatment. *Eur. Heart J.* 40, 2775–2781. doi: 10.1093/eurheartj/ehy862

Tabas, I. (2010). Macrophage death and defective inflammation resolution in atherosclerosis. *Nat. Rev. Immunol.* 10, 36–46. doi: 10.1038/nri2675

Tabas, I., and Bornfeldt, K. E. (2016). Macrophage phenotype and function in different stages of atherosclerosis. *Circ. Res.* 118, 653–667. doi: 10.1161/CIRCRESAHA.115.306256

Tarkin, J. M., Joshi, F. R., and Rudd, J. H. F. (2014). PET imaging of inflammation in atherosclerosis. *Nat. Rev. Cardiol.* 11, 443–457. doi: 10.1038/nrcardio.2014.80

Tawakol, A., Singh, P., Mojena, M., Pimentel-Santillana, M., Emami, H., MacNabb, M., et al. (2015). HIF-1alpha and PFKFB3 mediate a tight relationship between proinflammatory activation and anerobic metabolism in atherosclerotic macrophages. *Arterioscler. Thromb. Vasc. Biol.* 35, 1463–1471. doi: 10.1161/ATVBAHA.115.305551

Tomas, L., Edsfeldt, A., Mollet, I. G., Perisic Matic, L., Prehn, C., Adamski, J., et al. (2018). Altered metabolism distinguishes high-risk from stable carotid atherosclerotic plaques. *Eur. Heart J.* 39, 2301–2310. doi: 10.1093/eurheartj/ehy124

van der Laan, A. M., Ter Horst, E. N., Delewi, R., Begieneman, M. P. V., Krijnen, P. A. J., and Hirsch, A. (2014). Monocyte subset accumulation in the human heart following acute myocardial infarction and the role of the spleen as monocyte reservoir. *Eur. Heart J.* 35, 376–385. doi: 10.1093/eurheartj/eht331

Verhoeven, B., Hellings, W. E., Moll, F. L., de Vries, J. P., de Kleijn, D. P. V., and de Bruin, P. (2005). Carotid atherosclerotic plaques in patients with transient ischemic attacks and stroke have unstable characteristics compared with plaques in asymptomatic and amaurosis fugax patients. *J. Vasc. Surg.* 42, 1075–1081. doi: 10.1016/j.jvs.2005.08.009

Verhoeven, B. A. N., Velema, E., Schoneveld, A. H., de Vries, J. P. P. M., de Bruin, P., Seldenrijk, C. A., et al. (2004). Athero-express: differential atherosclerotic plaque expression of mRNA and protein in relation to cardiovascular events and patient characteristics. Rationale and design. *Eur. J. Epidemiol.* 19, 1127–1133. doi: 10.1007/s10564-004-2304-6

Virmani, R., Kolodgie, F. D., Burke, A. P., Farb, A., and Schwartz, S. M. (2000). Lessons from sudden coronary death: a comprehensive morphological classification scheme for atherosclerotic lesions. *Arterioscler. Thromb. Vasc. Biol.* 20, 1262–1275. doi: 10.1161/01.atv.20.5.1262

Conflict of Interest: The authors declare that the research was conducted in the absence of any commercial or financial relationships that could be construed as a potential conflict of interest.

frontiers in Cell and Developmental Biology

ORIGINAL RESEARCH
published: 14 January 2021
doi: 10.3389/fcell.2020.622741

Microbiota-Derived Metabolite Trimethylamine N-Oxide Protects Mitochondrial Energy Metabolism and Cardiac Functionality in a Rat Model of Right Ventricle Heart Failure

Melita Videja[1,2]*, *Reinis Vilskersts*[1,2], *Stanislava Korzh*[1], *Helena Cirule*[1], *Eduards Sevostjanovs*[1], *Maija Dambrova*[1,2] and *Marina Makrecka-Kuka*[1]

[1] Latvian Institute of Organic Synthesis, Riga, Latvia, [2] Faculty of Pharmacy, Riga Stradiņš University, Riga, Latvia

OPEN ACCESS

Edited by:
Md. Shenuarin Bhuiyan,
Louisiana State University Health Shreveport, United States

Reviewed by:
Annamaria Tonazzi,
National Research Council (CNR), Italy
Jyoti Chhibber-Goel,
International Centre for Genetic Engineering and Biotechnology (India), India

***Correspondence:**
Melita Videja
melita.videja@farm.osi.lv

Specialty section:
This article was submitted to Cellular Biochemistry, a section of the journal Frontiers in Cell and Developmental Biology

Received: 29 October 2020
Accepted: 17 December 2020
Published: 14 January 2021

Citation:
Videja M, Vilskersts R, Korzh S, Cirule H, Sevostjanovs E, Dambrova M and Makrecka-Kuka M (2021) Microbiota-Derived Metabolite Trimethylamine N-Oxide Protects Mitochondrial Energy Metabolism and Cardiac Functionality in a Rat Model of Right Ventricle Heart Failure. Front. Cell Dev. Biol. 8:622741. doi: 10.3389/fcell.2020.622741

Aim: Trimethylamine N-oxide (TMAO) is a gut microbiota-derived metabolite synthesized in host organisms from specific food constituents, such as choline, carnitine and betaine. During the last decade, elevated TMAO levels have been proposed as biomarkers to estimate the risk of cardiometabolic diseases. However, there is still no consensus about the role of TMAO in the pathogenesis of cardiovascular disease since regular consumption of TMAO-rich seafood (i.e., a Mediterranean diet) is considered to be beneficial for the primary prevention of cardiovascular events. Therefore, the aim of this study was to investigate the effects of long-term TMAO administration on mitochondrial energy metabolism in an experimental model of right ventricle heart failure.

Methods: TMAO was administered to rats at a dose of 120 mg/kg in their drinking water for 10 weeks. Then, a single subcutaneous injection of monocrotaline (MCT) (60 mg/kg) was administered to induce right ventricular dysfunction, and treatment with TMAO was continued (experimental groups: Control; TMAO; MCT; TMAO+MCT). After 4 weeks, right ventricle functionality was assessed by echocardiography, mitochondrial function and heart failure-related gene and protein expression was determined.

Results: Compared to the control treatment, the administration of TMAO (120 mg/kg) for 14 weeks increased the TMAO concentration in cardiac tissues up to 14 times. MCT treatment led to impaired mitochondrial function and decreased right ventricular functional parameters. Although TMAO treatment itself decreased mitochondrial fatty acid oxidation-dependent respiration, no effect on cardiac functionality was observed. Long-term TMAO administration prevented MCT-impaired mitochondrial energy metabolism by preserving fatty acid oxidation and subsequently decreasing pyruvate metabolism. In the experimental model of right ventricle heart failure, the impact of TMAO on energy metabolism resulted in a tendency to restore right ventricular function, as indicated by echocardiographic parameters and normalized organ-to-body weight indexes. Similarly, the expression of a marker of heart failure severity, brain natriuretic peptide, was substantially increased in the MCT group but tended to be restored to control levels in the TMAO+MCT group.

Conclusion: Elevated TMAO levels preserve mitochondrial energy metabolism and cardiac functionality in an experimental model of right ventricular heart failure, suggesting that under specific conditions TMAO promotes metabolic preconditioning-like effects.

Keywords: trimethylamine N-oxide, right ventricular dysfunction, monocrotaline, mitochondrial function, cardiovascular diseases

INTRODUCTION

Impaired energy metabolism is one of the cornerstones of heart failure pathophysiology (Rosca and Hoppel, 2013). Normally, 60–90% of energy is generated through fatty acid oxidation (FAO) (Lopaschuk et al., 2010; Liepinsh et al., 2014); however, in the early stages of heart failure, a shift from fatty acid oxidation toward glucose utilization is observed and is a mechanism of metabolic adaptation (Ventura-Clapier et al., 2011). Compared to healthy patients, heart failure patients exhibit decreased FAO (Dávila-Román et al., 2002), which correlates with cardiac hypertrophy and reduced ejection fraction (Neglia et al., 2007; Byrne et al., 2016). During the progression of heart failure, overall cardiac oxidative metabolism decreases, resulting in energy starvation (Sabbah, 2020). One of the risk factors that lead to disturbances in energy metabolism and further progression of cardiovascular diseases is unhealthy dietary patterns. For instance, high intake of fat, red meat and processed food, as in Western diet, is shown to damage myocardial oxidative capacity, leading to impaired mitochondrial energy metabolism (Neves et al., 2014). Moreover, dietary choices determine the composition of intestinal microbiota, which further unambiguously affects the host metabolism (Lindsay et al., 2020). It has been shown that chronic heart failure is characterized by substantial alterations in gut microbiome composition and reduced microbial variety (Kummen et al., 2018; Mayerhofer et al., 2020). Previous studies suggest a link between the human gut microbiome and the homeostasis of energy metabolism, however, a clear causal relationship between them remains elusive.

In 2011, in a targeted metabolomics study, trimethylamine N-oxide (TMAO) was identified as a metabolite, which is both microbiota- and diet-derived, and associated with the incidence of adverse cardiovascular outcomes (Wang et al., 2011). TMAO is produced in organisms by gut microbiota during the metabolism of common food constituents, such as carnitine, choline and betaine; this process first leads to the production of trimethylamine (TMA), which is subsequently oxidized by the host liver enzyme group called flavin-containing monooxygenases (Janeiro et al., 2018). High intake of TMAO and its precursor has been shown to promote atherosclerosis and exacerbate cardiovascular risks (Wang et al., 2011; Koeth et al., 2013; Ding et al., 2018). A positive correlation between the circulating levels of TMAO and the severity of metabolic syndrome has been observed (Barrea et al., 2018), and elevated TMAO plasma levels were observed in patients with diabetes (Lever et al., 2014; Dambrova et al., 2016). Moreover, in heart failure patients, increased TMAO concentrations correlate with heart failure severity, as shown by NYHA class (Tang et al., 2014, 2015; Trøseid et al., 2015) and heart failure-associated mortality (Suzuki et al., 2016). Although extensive studies of TMAO in various patient populations clearly demonstrate that TMAO can serve as a biomarker, it remains uncertain whether TMAO is directly involved in the pathogenesis of cardiometabolic diseases (Nowiński and Ufnal, 2018).

Diet supplementation with TMAO or its precursors has been shown to exacerbate cardiac dilation, leading to reduced ejection fraction and increased cardiac fibrosis, in an experimental model of heart failure (Organ et al., 2016). In addition, a reduction of circulating TMAO levels by 3,3-dimethyl-1-butanol or iodomethylcholine resulted in attenuated cardiac remodeling after aortic banding (Organ et al., 2020; Wang et al., 2020). On the other hand, the Mediterranean diet, which is focused on regular consumption of TMAO-rich fish and seafoods (Cho et al., 2017), is inversely correlated with fatal coronary heart disease (He et al., 2004) and is proposed to be a strategy for preventing and reducing the risk of cardiovascular and metabolic diseases (Tørris et al., 2014; Widmer et al., 2015; Estruch et al., 2018). Moreover, it was recently shown that chronic treatment with low-dose TMAO was associated with preserved cardiac hemodynamic parameters in Spontaneously Hypertensive rats and Spontaneously Hypertensive Heart Failure rats (Huc et al., 2018; Gawrys-Kopczynska et al., 2020). Such controversial results raise the question of whether increased availability of TMAO plays detrimental or protective roles in the progression of cardiovascular diseases.

It has been shown that both acute and chronic TMAO treatment can cause disruptions in energy metabolism in the heart by impairing pyruvate and fatty acid metabolism (Makrecka-Kuka et al., 2017). However, there is no evidence that TMAO-induced metabolic alterations result in impaired cardiac functionality. It could be hypothesized that long-term TMAO administration could exert preconditioning-like effects, thus improving cardiovascular outcomes after stress conditions, such as hypoxia, pressure overload and altered energy substrate availability. Thus, the aim of the present study was to investigate the effects of long-term TMAO administration in an experimental rat model of monocrotaline-induced right ventricle heart failure. To mimic the chronic increase in TMAO in plasma and tissues, as observed in cases of regular consumption of seafood, TMAO pretreatment for 10 weeks prior to monocrotaline injection was chosen. The effects of the administration of TMAO on indicators of heart failure severity (cardiac functional parameters, heart failure and hypertrophy-related gene and protein expression) and cardiac mitochondrial energy metabolism were studied.

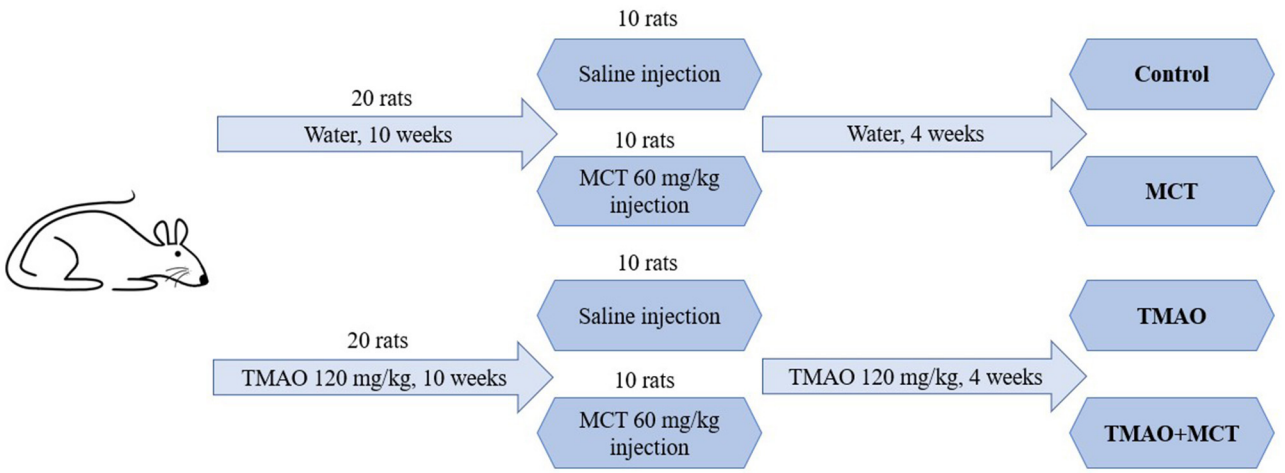

FIGURE 1 | Schematic representation of the study design.

MATERIALS AND METHODS

Experimental Animals

Wistar rats ($n = 40$) weighing 280–380 grams (6–8 weeks old) were obtained from the Laboratory Animal Centre, University of Tartu (Tartu, Estonia) and housed under standard conditions (21–23°C, 12-h light/dark cycle, relative humidity 45–65%) for 2 weeks prior to the start of the experiment. The animals were fed a standard R70 diet (Lantmännen, Stockholm, Sweden) with unlimited access to food and drinking water. All the experimental procedures were performed in accordance with the guidelines reported in the EU Directive 2010/63/EU and in accordance with local laws and policies, and all of the procedures were approved by the Latvian Animal Protection Ethical Committee of the Food and Veterinary Service, Riga, Latvia (Food and Veterinary Service Ethical approval Nr. 105). These studies are reported in accordance with the ARRIVE guidelines (Kilkenny et al., 2010; McGrath et al., 2010). Our previous experiments, in which right ventricular functionality was assessed, indicated that due to interindividual variability, 8–10 animals per group are necessary to obtain significant results; therefore, $n = 10$ per group was chosen. The data from previous experiments in which mitochondrial energy metabolism was studied were subjected to statistical power analysis, and the calculations indicated that the mitochondrial respiration assay requires at least $n = 5$ or 6 per group to produce significant results with a power >0.95.

Experimental Design

The schematic representation of the study design is shown in **Figure 1**. The experimental animals were randomly separated into four groups: control ($n = 10$), TMAO ($n = 10$), MCT (monocrotaline) ($n = 10$) and TMAO+MCT ($n = 10$). One animal in the control group and 2 animals in the other groups died during the experiment due to reasons not related to the experimental protocol and treatment. The samples from these rats were excluded from further analysis; therefore, the final animal count was nine rats in the control group and eight rats in the other groups. The animals in the TMAO group and TMAO+MCT group received TMAO (Alfa Aeser, Kandel, Germany) at a dose of 120 mg/kg in their drinking water daily for 10 weeks. To induce pulmonary hypertension and right ventricular remodeling and dysfunction, a single subcutaneous injection of monocrotaline (MCT) (Sigma-Aldrich, Schnelldorf, Germany) at a dose of 60 mg/kg was administered to the animals in the MCT and TMAO+MCT groups. TMAO treatment was continued in both groups that previously received TMAO until the end of the experiment. The rats were weighed twice a week to monitor their general health condition. Since the time from MCT injection to right ventricular failure onset differs markedly (Hardziyenka et al., 2006), a 4-week time point after the administration of MCT was chosen for the echocardiographic assessment of right ventricle functionality based on our pilot experiments in this model. In addition, invasive direct right ventricular pressure measurement was performed. After the assessment of cardiac functionality, the animals were sacrificed, and cardiac tissue and plasma samples were immediately frozen and stored at −80°C for further analysis. In addition, a mitochondrial functionality study was performed using permeabilized cardiac fibers of the right ventricle.

Echocardiography Assessment and Direct Right Ventricle Blood Pressure Measurement

The rats were anesthetized using 5% isoflurane dissolved in 100% oxygen. After the onset of anesthesia, the concentration of isoflurane was decreased to 2.5%, the experimental animals were placed in a decubitus position, and the chest and upper part of the abdomen were shaved. The animals were connected to a Philips iE33 ultrasonograph (Philips Healthcare, Andover, USA) to record ECG from the II lead. Then, the rat was placed on the left side, and a four-chamber view was recorded from the apical point of view using a Philips (Philips Healthcare, Andover, USA) S12-4 sector array transducer. Right ventricular

(RV) end-diastolic area (RV-EDA) and RV end-systolic area (RV-ESA) were recorded. ECG was used to determine the exact time of RV systole and diastole. Furthermore, RV-EDA and RV-ESA were used to calculate RV fractional area change (RVFAC). The rat was again placed in a decubitus position, and functional parameters of the left ventricle were recorded at the papillary muscle level using a Philips (Philips Healthcare, Andover, USA) linear L15-7io transducer.

After the echocardiographic assessment of ventricular anatomy and functioning, invasive direct right ventricular pressure measurement was performed. The anesthetized rat was intubated using a 16-G intravenous catheter and mechanically ventilated with 2% isoflurane dissolved in 100% oxygen at a tidal volume of 1.5 ml/100 g. The abdominal cavity was opened, and the diaphragm was incised to expose the pleural cavity. The ribs on both sides of the chest were cut to access the heart. An 18-G needle was connected to a pressure transducer (AD Instruments, Sidney, Australia) and inserted into the cavity of the right ventricle through the apex of the heart. The right ventricular pressure was measured until a stable pressure reading was obtained.

Measurement of Organ Mass

To calculate the organ-to-body weight indexes, the heart and lungs were excised and weighed. Then, the right ventricle (excluding the septum) was separated from the heart and weighed.

Measurements of Plasma Biochemical Parameters

To obtain plasma, the blood samples were centrifuged at 1,000 g and 4° for 10 min and then stored at −80°C until further analysis. The levels of triglycerides and total cholesterol in plasma were measured using commercially available kits from Instrumentation Laboratory (Milan, Italy). The level of free fatty acids (NEFA) was measured using a commercially available kit from Wako Chemicals (Neuss, Germany). All measurements were carried out according to the manufacturer's instructions.

Quantification of TMAO in Plasma and Tissue Samples

Determination of the TMAO concentrations in the plasma and heart homogenate samples was performed by ultra-performance liquid chromatography-tandem mass spectrometry (UPLC/MS/MS) using the positive ion electrospray mode as previously described (Dambrova et al., 2013; Grinberga et al., 2015). Briefly, obtained tissues were homogenized with water in OMNI Bead Ruptor 24 (Camlab, Cambridge, United Kingdom) at a w/v ratio of 1:10. The obtained homogenates were centrifuged at 20,000 g for 10 min at 4°C. The supernatants were collected and stored at −80°C until further analysis.

Sample preparation was performed by deproteinization with an acetonitrile–methanol mixture (3:1, v/v). The samples were then vortexed and centrifuged at 15,000 g for 20 min. The supernatant was transferred to UPLC vials and used for UPLC/MS/MS analysis. MassLynx 4.1. software with a QuanLynx 4.1. module (Waters, Milford, USA) was used for data acquisition and processing.

Measurements of Tissue Brain Natriuretic Peptide (BNP)

A Rat BNP 45 ELISA Kit (Abcam, Cambridge, United Kingdom, ab108816) was used to test the levels of makers of congestive heart failure in right ventricular tissue extracts. Extract preparation and analysis were carried out according to the manufacturer's instructions.

Isolation of RNA and qPCR Analysis

Total RNA was isolated from right ventricular tissues using TRI reagent (Sigma, St. Louis, MO, USA) according to the manufacturer's recommended protocol. First-strand cDNA synthesis was performed using the High-Capacity cDNA Reverse Transcription Kit (Applied BiosystemsTM, Foster City, CA, USA) following the manufacturer's instructions. The qPCR mix consisted of SYBR® Green Master Mix (Applied BiosystemsTM, Foster City, CA, USA), synthesized cDNA, and forward and reverse primers specific for VCP, BNP, αMHC, and βMHC. These genes were chosen to characterize heart failure severity and cardiac hypertrophy. The reaction was carried out in an Applied Biosystems Prism 7500 instrument according to the protocol provided by the manufacturer. The relative expression levels of each of the genes of interest were calculated with the ΔΔCt method and were normalized to the expression level of the VCP gene. The primer sequences used for the qPCR analysis are available in **Supplementary Table 1**.

Measurements of Mitochondrial Respiration in Permeabilized Cardiac Fibers

Mitochondrial function was assessed in permeabilized cardiac fibers from the right ventricle that were prepared as previously described (Kuka et al., 2012). The mitochondrial respiration measurements were performed in MiR05 media (110 mM sucrose, 60 mM K-lactobionate, 0.5 mM EGTA, 3 mM $MgCl_2$, 20 mM taurine, 10 mM KH_2PO_4, 20 mM HEPES, pH 7.1, 0.1% BSA essentially free of fatty acids) at 37°C using an Oxygraph-2k (O2k; Oroboros Instruments, Innsbruck, Austria). Mitochondrial functionality measurements were performed using a previously described respirometry protocol (Makrecka-Kuka et al., 2020). Briefly, palmitoylcarnitine (PC) and malate (10 μM and 0.5 mM, respectively) were used to measure FAO-dependent mitochondrial respiration (F(N)-pathway) in a substrate-dependent LEAK (L) state. Then, ADP was added to a concentration of 5 mM to initiate oxidative phosphorylation-dependent respiration (OXPHOS state). Next, pyruvate (5 mM, complex I substrate, N-pathway) was added to reestablish FN-pathway-linked respiration. Succinate (10 mM, complex II substrate, S-pathway) was added to reconstitute convergent FNS-linked respiration. Then, rotenone (0.5 μM, complex I inhibitor) and antimycin A (2.5 μM, complex III inhibitor) were added to determine the S-linked respiration and residual oxygen consumption (ROX), respectively.

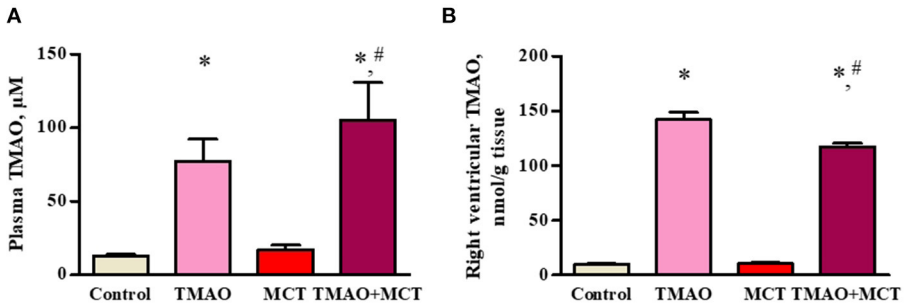

FIGURE 2 | TMAO concentration in plasma **(A)** and right ventricular tissue **(B)** after administration of TMAO at a dose of 120 mg/kg in the drinking water for 14 weeks. The results are presented as the mean ± SEM of 8–9 animals. * Indicates a significant difference from the control group (one-way ANOVA followed by Dunnett's post-test), # indicates a significant difference from the MCT group (unpaired *t*-test), $p < 0.05$.

TABLE 1 | Echocardiographic assessment of right ventricle functionality after administration of TMAO at a dose of 120 mg/kg for 14 weeks in a monocrotaline-induced model of right ventricle heart failure.

	Control	TMAO	MCT	TMAO+MCT
Right ventricular pressure, mmHg	21.9 ± 2	22.7 ± 1.3	33.5 ± 5.3*	26.1 ± 1.8
Right ventricular diastolic area, cm^2	0.37 ± 0.02	0.33 ± 0.02	0.5 ± 0.07	0.4 ± 0.04
Right ventricular systolic area, cm^2	0.2 ± 0.01	0.21 ± 0.02	0.36 ± 0.07*	0.26 ± 0.03
Right ventricular fractional area change, %	46.6 ± 2.6	37 ± 2.8	29.7 ± 4.8*	37 ± 5

*The results are presented as the mean ± SEM of 8–9 animals. *Indicates a significant difference from the control group (one-way ANOVA followed by Dunnett's post-test), $p < 0.05$.*

To determine the contribution of each substrate to the respiration rate, the flux control factor was calculated as follows:

$$1 - \frac{Resp.rate\ before\ the\ addition\ of\ substrate}{Resp.rate\ after\ the\ addition\ of\ substrate}.$$

To determine the mitochondrial mass in the heart, the citrate synthase activity in tissue homogenates was measured spectrophotometrically as previously described (Srere, 1969).

Statistical Analysis

The statistical analysis of the data was performed using GraphPad Prism (GraphPad, Inc., La Jolla, USA) software. All the data are represented as the mean ± standard error of the mean (SEM). Data distribution was determined using Shapiro-Wilk's normality test. The statistical significance of the experimental results was verified by one-way ANOVA followed by Dunnett's multiple comparison test (to compare each experimental group to the control group) following an unpaired *t*-test (to compare the MCT group to the TMAO+MCT group). If the data were not normally distributed, the Kruskal-Wallis test followed by Dunn's multiple comparison test was used. The results were considered statistically significant if the *p*-value was <0.05.

RESULTS

Effects of Long-Term TMAO Administration on Heart Failure Severity

Administration of TMAO at a dose of 120 mg/kg in the drinking water for 14 weeks resulted in a 6-fold increase in the TMAO plasma concentrations (up to 100 µM) in both the TMAO and TMAO+MCT groups (**Figure 2A**). The analysis of the TMAO content in the tissues of the right ventricle revealed that treatment with TMAO resulted in a 14-fold increase in the TMAO tissue content (up to 140 nmol/g tissue) in both groups that received TMAO (**Figure 2B**).

The echocardiographic assessment did not reveal any significant differences in cardiac function between the control and TMAO groups. Administration of TMAO at a dose of 120 mg/kg in the drinking water for 14 weeks did not affect direct right ventricular (RV) pressure, RV systolic and diastolic area or RV fractional area change (**Table 1**) as well as ejection fraction and fractional shortening of the left ventricle (**Supplementary Table 2**). Compared with the control, administration of monocrotaline induced a significant increase (∼50%) in direct right ventricular pressure (**Table 1**). In addition, dilatation of the right ventricle was observed in the hearts of the animals in the MCT group, as indicated by 34 and 83% increases in the RV diastolic and systolic areas, respectively. Subsequently, the right ventricular fractional area change was significantly decreased in the MCT group compared to the control group. Compared to those in the MCT control group, the direct RV pressure measurement was decreased by 22%, the RV diastolic and systolic areas were decreased by up to 27%, and therefore, the RV fractional area change was increased by 25% in the TMAO+MCT group. None of the measured parameters in the TMAO+MCT group were significantly different from those in the control group. Overall, these results indicate that chronically elevated TMAO levels in plasma and cardiac tissue do not affect

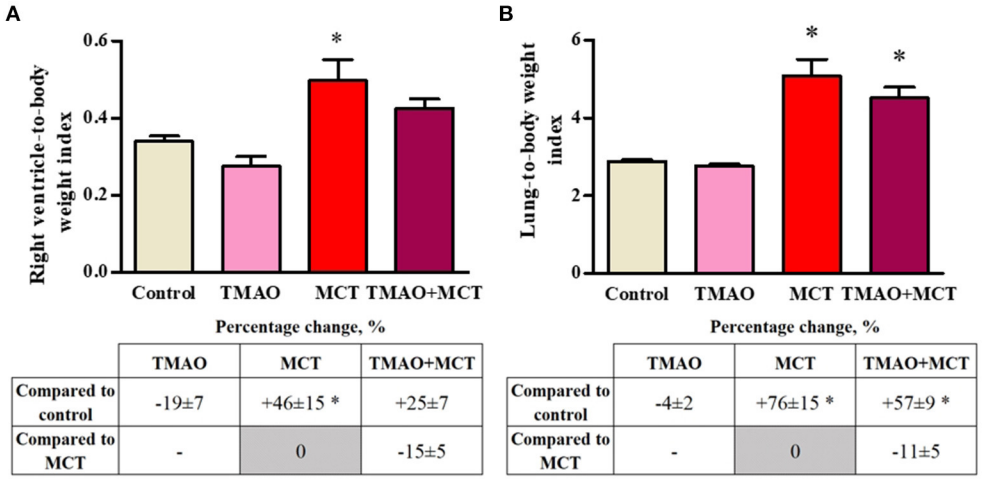

Percentage change, %

	TMAO	MCT	TMAO+MCT
Compared to control	-19±7	+46±15 *	+25±7
Compared to MCT	-	0	-15±5

Percentage change, %

	TMAO	MCT	TMAO+MCT
Compared to control	-4±2	+76±15 *	+57±9 *
Compared to MCT	-	0	-11±5

FIGURE 3 | Changes in the right ventricle-to-body weight **(A)** and lung-to-body weight **(B)** indexes after monocrotaline injection. The results are presented as the mean ± SEM of 8–9 animals. * Indicates a significant difference from the control group (one-way ANOVA followed by Dunnett's post-test), $p < 0.05$.

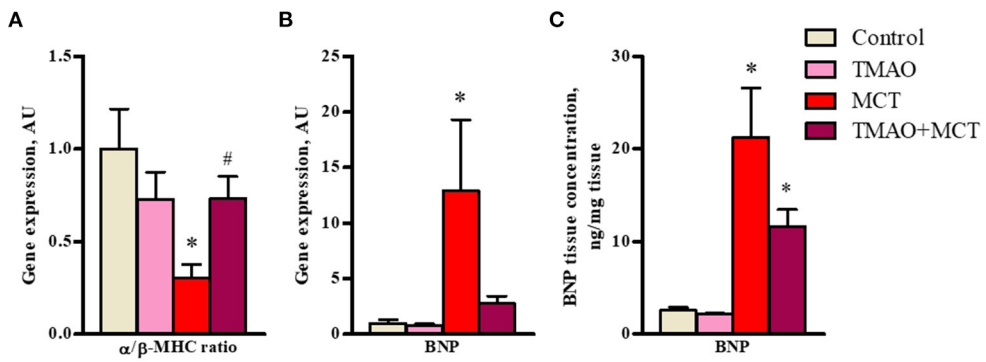

FIGURE 4 | Effect of administration of TMAO at a dose of 120 mg/kg in the drinking water for 14 weeks on heart failure severity-related gene expression **(A,B)** and BNP protein expression **(C)** in right ventricular tissue of a rat model of monocrotaline-induced heart failure. The results are presented as the mean ± SEM of 6–8 animals. * Indicates a significant difference from the control group [one-way ANOVA followed by Dunnett's posttest for **(A)**, Kruskall-Wallis test followed by Dunn's multiple comparison test for **(B)** and **(C)**], # indicates a significant difference from the MCT group (unpaired *t*-test), $p < 0.05$.

cardiac functionality, while long-term TMAO administration preserves myocardial mechanical function in monocrotaline-induced heart failure.

To evaluate MCT-induced cardiac and pulmonary remodeling, the organ mass indexes were calculated. There was no difference in the whole heart-to-body weight index or in the left ventricle-to-body weight index between the experimental groups (**Supplementary Figure 1**). Long-term TMAO administration did not impact either the right ventricle (**Figure 3A**) or lung-to-body weight (**Figure 3B**) indexes. Compared to the control group, the MCT group exhibited increased right ventricle hypertrophy and pulmonary remodeling, as indicated by significant increases in the organ-to-body weight indexes by 46 and 76%, respectively (**Figures 3A,B**). In the TMAO+MCT group, the right ventricle and lung-to-body weight indexes were decreased by 15 and 11%, respectively, compared to those in the MCT group (**Figures 3A,B**) suggesting that long-term TMAO administration can partially prevent monocrotaline-induced organ remodeling and hypertrophy.

In addition, long-term TMAO administration did not cause any significant changes in the expression of genes related to heart failure and hypertrophy (**Figures 4A,B**) or in the protein expression of BNP45 (**Figure 4C**). In the MCT group, a 3-fold decrease in the *α/β-MHC* expression ratio (**Figure 4A**) was observed, indicating a shift in favor of the *β* isoform caused by right ventricle hypertrophy. In addition, the expression of a maker of heart failure severity, *BNP,* was upregulated by 12-fold in the MCT group (**Figure 4B**). Consistent with the gene expression results, BNP45 protein expression in cardiac tissue was significantly increased by 10-fold in the MCT group compared to the control group (**Figure 4C**). In the TMAO+MCT group, the *α/β-MHC* expression ratio was 2-fold higher, suggesting less pronounced cardiac hypertrophy compared to that in the MCT group (**Figure 4A**). The gene and protein expression of BNP was lower in the TMAO+MCT group than in the MCT group (**Figures 4B,C**). Moreover, measurements of total cholesterol, triglycerides and free fatty acids in plasma did not reveal any significant changes between experimental

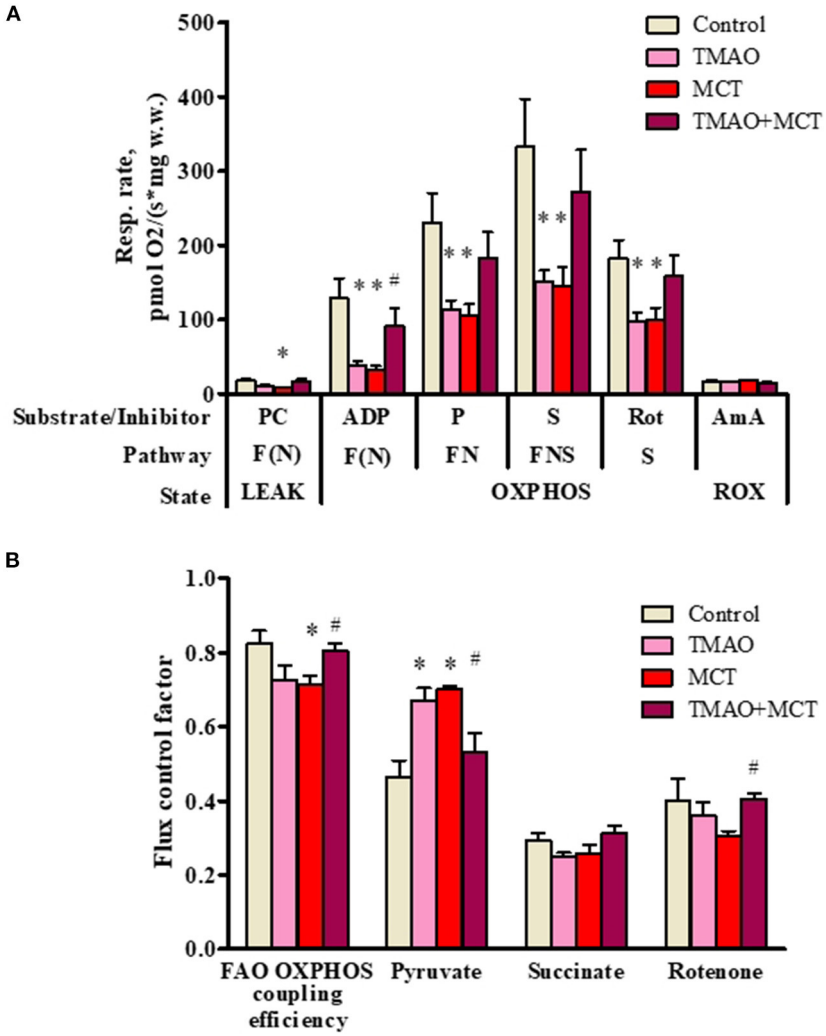

FIGURE 5 | Mitochondrial respiration rate measurements **(A)** and flux control factors **(B)** in right ventricular cardiac fibers using different energy substrates after administration of TMAO at a dose of 120 mg/kg for 14 weeks in a model of monocrotaline-induced right ventricle heart failure. The results are presented as the mean ± SEM of 6 animals. * Indicates a significant difference from the control group (one-way ANOVA followed by Dunnett's post-test), # indicates a significant difference from the MCT group (unpaired *t*-test), $p < 0.05$. Flux control factor, the contribution of each substrate/pathway to the respiration rate; PC, palmitoylcarnitine; ADP, adenosine diphosphate; P, pyruvate; S, succinate; Rot, rotenone; AmA, antimycin A; F, fatty acid oxidation-dependent pathway; N, NADH pathway; LEAK, substrate-dependent state; OXPHOS, oxidative phosphorylation-dependent state; ROX, residual oxygen consumption.

groups (**Supplementary Table 3**), therefore our observed effects of TMAO on cardiac function are independent of plasma lipid profile. Overall, these findings indicate that long-term TMAO administration partially reduced the severity of heart failure induced by monocrotaline administration.

Effects of Long-Term TMAO Administration on Cardiac Mitochondrial Energy Metabolism

To further investigate the effects of long-term TMAO administration on energy metabolism, mitochondrial respiration measurements were performed using permeabilized cardiac fibers prepared from right ventricular tissue samples. Long-term TMAO administration decreased the FAO-dependent respiration rate by 69% in the OXPHOS state (**Figure 5A**), resulting in an 11% decrease in the FAO-dependent OXPHOS coupling efficiency (**Figure 5B**). Although pyruvate metabolism input to overall respiration was increased by ∼44% in the TMAO group, as indicated by Flux control factor analysis (**Figure 5B**), it was not sufficient to restore FN and FNS pathway-linked mitochondrial respiration in the OXPHOS state (**Figure 5A**). In the MCT group, there was a 75% decrease in the FAO-dependent respiration rate in the OXPHOS state (**Figure 5A**) and a subsequent 13% decrease in the FAO-dependent OXPHOS coupling efficiency (**Figure 5B**). Similar to the TMAO group, in the MCT group, pyruvate metabolism input to respiration was increased by 50% (**Figure 5B**), but this increase was not sufficient to restore FN- and FNS-pathway-linked respiration in the OXPHOS state (**Figure 5A**). In contrast to

the TMAO group, in the MCT group, the flux control factor for rotenone was reduced ($p = 0.06$), indicating partial complex I dysfunction (**Figure 5B**). Moreover, in the TMAO+MCT group, mitochondrial energy metabolism was preserved, as shown by normalized respiration rates (**Figure 5A**), preserved FAO-dependent oxidative phosphorylation efficiency and subsequently decreased pyruvate metabolism input (**Figure 5B**). Moreover, measurements of the citrate synthase activity (**Supplementary Figure 2**) in right ventricular tissue showed that there were no differences in mitochondrial mass between the experimental groups. Taken together, the obtained results show that long-term TMAO administration itself induces mitochondrial metabolic preconditioning by causing a switch from fatty acid utilization to pyruvate utilization without affecting electron transfer functionality; moreover, in right ventricle heart failure, TMAO treatment can preserve cardiac mitochondrial energy metabolism.

DISCUSSION

In the present study, we demonstrate the effects of long-term TMAO administration on cardiac mitochondrial energy metabolism and on right ventricular heart failure progression. Although long-term TMAO administration decreases mitochondrial fatty acid oxidation, it has no adverse effects on cardiac mechanical function. However, unexpectedly, long-term TMAO administration results in preserved mitochondrial energy metabolism, leading to reduced heart failure severity and maintained cardiac functionality. Taken together, these results suggest that elevated TMAO concentrations can exert preconditioning-like effects and exhibit cardioprotective properties.

The role of TMAO as a risk factor in the development of cardiovascular diseases is widely debated around the world. It has been shown that even a 100-fold increase in circulating TMAO levels (up to 60 μM) in rats did not affect cardiac functionality (Ufnal et al., 2014). Similarly, no effects on cardiac parameters in mice were observed after 3 weeks of administration of 0.12% TMAO in the chow (Organ et al., 2016). Although the TMAO concentration in target tissues was not determined in previously mentioned studies, it has recently been shown that TMAO at concentrations up to 10 mM does not affect cell viability, mitochondrial membrane potential or ROS production in rat cardiomyocytes (Querio et al., 2019). Our results complement previous findings, reporting the TMAO level reached in cardiac tissue (up to 140 nmol/g tissue) after 14-week administration of TMAO in drinking water and, thus, provide a rationale behind further dose selection strategies in *in vitro* experiments. In our experimental design, TMAO was administered directly (120 mg/kg in their drinking water) and no further metabolization was needed by gut bacteria. However, the possible interindividual variability caused by alterations in gut microbiota composition should be considered if TMAO precursors (i.e., choline or carnitine) were administered during the experiment, since various bacterial genera are able to metabolize different precursors to synthesize TMA (Jameson et al., 2018). It has also been shown that a retroconversion of TMAO to TMA is possible (Hoyles et al., 2017); however, in our study a low variability of TMAO levels in right ventricular tissue was observed, suggesting that gut microbiota composition and TMA/TMAO production capacity was similar in our experimental animals. Moreover, our results demonstrate that a long-term increase in plasma TMAO levels up to 100 μM and a subsequent increase in TMAO levels in cardiac tissue (up to 140 nmol/g tissue) do not affect cardiac function. In addition, recent studies indicated that TMAO administration does not exacerbate the condition of already present stressors (Querio et al., 2019), such as H_2O_2, which is a major contributor to oxidative stress (Nita and Grzybowski, 2016), and doxorubicin, which is known to cause disturbances in cardiac energy substrate metabolism similar to those caused by heart failure (Wu et al., 2016). In our experimental setup, long-term TMAO administration shifted mitochondrial energy substrate utilization from FAO to glucose metabolism, but in contrast to the heart failure group, the TMAO treatment group did not exhibit altered mitochondrial electron transfer system functionality. Since the shift from compensated cardiac hypertrophy to heart failure is preceded by respiratory complex I and II dysfunction (Griffiths et al., 2010), unaltered complex I and complex II function could explain our observations of maintained cardiac functionality even after 14 weeks of TMAO administration, notwithstanding altered energy metabolism. Overall, our findings suggest that despite this metabolic shift, long-term elevations in TMAO levels in plasma and cardiac tissue do not exert detrimental effects on cardiac function.

Previously, increased plasma TMAO levels in experimental models of heart failure led to worsening of cardiac parameters, suggesting that TMAO is a detrimental factor in cardiovascular disease pathophysiology. It has been shown that administration of TMAO and its precursor, choline, exacerbates left ventricle remodeling and cardiac function loss (Organ et al., 2016). Moreover, withdrawal of dietary TMAO even 6 weeks after aortic constriction reversed those changes, indicating an ability of the heart to recover from detrimental changes caused by TMAO (Organ et al., 2020). In addition, a reduction in circulating TMAO levels by 3,3-dimethyl-1-butanol or iodomethylcholine alleviated cardiac hypertrophy and remodeling after aortic banding (Organ et al., 2020; Wang et al., 2020). TMAO-induced impairment in cardiomyocyte contractility and calcium handling (Savi et al., 2018) as well as T-tubule formation (Jin et al., 2020) were suggested as possible mechanisms that may link TMAO to heart failure. In contrast, our results demonstrate that an increase in TMAO levels in plasma and tissues partially prevents the remodeling of the right ventricle and the development of right-sided heart failure. Previously, it has been shown that TMAO treatment reduces cardiac fibrosis and improves cardiac functionality in a model of Spontaneously Hypertensive rats (Huc et al., 2018). Consistent with these findings, our study shows that TMAO administration can partially prevent right ventricular hypertrophy as shown by normalized organ-to-body weight indexes and hypertrophy-related gene expression. Moreover, consistent with our results, protective effects of TMAO were also observed in Spontaneously Hypertensive Heart Failure rats, in which long-term TMAO treatment improved survival and cardiac parameters and lowered plasma NT-proBNP levels (Gawrys-Kopczynska et al., 2020). Similarly, in our study, TMAO

administration preserved right ventricular function, as indicated by normalized direct RV pressure and RV fractional area change; moreover, TMAO decreased the expression of a marker of heart failure severity, BNP, in right ventricular tissue. In addition, a recent study showed that administration of betaine, a common TMAO precursor, attenuated pulmonary artery hypertension (Yang et al., 2018). Interestingly, monocrotaline injection was used to induce pulmonary artery hypertension in the previous study; this is the same method we used in our study to induce right ventricle heart failure. Although ∼100-fold less TMAO is produced from betaine than from choline (Wang et al., 2014), at least to some extent, the observed protective effects of betaine might be explained by increased bioavailability of TMAO. Overall, previous and present observations suggest that long-term TMAO administration can reduce right ventricular remodeling and improve cardiac function in right-sided heart failure. Moreover, our findings also support the hypothesis that a TMAO-rich Mediterranean diet may prevent and reduce the risk of cardiovascular diseases (Estruch et al., 2018).

The protective role of TMAO was previously explained by its ability to reduce endoplasmic reticulum stress (Makhija et al., 2014), oxidative-nitrative stress and the subsequent vascular and diabetic complications (Lupachyk et al., 2013; Fukami et al., 2015). More recently, some protective effects were attributed to the ability of TMAO to increase diuresis and natriuresis (Gawrys-Kopczynska et al., 2020). In addition, our study proposes preserved cardiac energy metabolism as a possible mechanism underlying the observed protective effects of TMAO. The heart is capable of adapting to both physiological and pathological stressors by shifting from FAO as a dominant energy source to more pronounced utilization of glucose (Brown et al., 2017). In physiological states, this shift could be considered a preconditioning strategy, since the heart is thus better prepared for future stress conditions, such as hypoxia, due to higher reliance on more energy-efficient substrates in the case of oxygen deficiency (Karwi et al., 2018). In the present study previously described metabolic shift was observed, when after long-term TMAO administration FAO was decreased, and pyruvate metabolism was subsequently increased without changes in cardiac functionality. It has been previously shown that TMAO decreases FAO with a mechanism not related to inhibition of carnitine palmitoyl transferase 1 (CPT1) (Makrecka-Kuka et al., 2017). Since we did not observe hindered pyruvate metabolism by accumulation of acylcarnitines, which might occur if carnitine/acylcarnitine translocase (CACT) or CPT2 was inhibited (Chegary et al., 2008; Makrecka et al., 2014; Makrecka-Kuka et al., 2020), most likely the decrease in FAO induced by TMAO administration is not related to direct inhibition of CACT or CPT2. Another possible explanation of our observation that TMAO reduces FAO could be that TMAO indirectly inhibits CACT by a nitric oxide (NO)-dependent mechanism (Tonazzi et al., 2017). However, TMAO is not reported to act as NO donor, moreover, it is shown to downregulate NO production *in vitro* (Sun et al., 2016; Chou et al., 2019) and *in vivo* (Li et al., 2017). Thus, it is unlikely that TMAO could cause indirect inhibition of CACT via NO pathway. Overall, an increase in TMAO concentration appears to induce a metabolic shift, possibly through direct inhibition of β-oxidation, toward more efficient substrate metabolism under stress conditions, such as hypoxia, thus ensuring preserved energy metabolism and subsequently improving cardiac function recovery after injury. Taken together, our results suggest that TMAO administration exhibits cardioprotective properties during heart failure by maintaining metabolic flexibility and preserving fatty acid oxidation, both of which are vital strategies to restore cardiac bioenergetic balance (Kolwicz et al., 2012; Karwi et al., 2018). Moreover, our findings demonstrate that long-term consumption of TMAO-rich foods (i.e., Mediterranean diet) might induce metabolic preconditioning-like effects.

In conclusion, our study presents evidence that chronic TMAO administration protects cardiac functionality by preserving mitochondrial energy metabolism in an experimental model of monocrotaline-induced right ventricle heart failure, where TMAO acts as a preconditioning factor. In addition, our results provide a novel insight on the theory, that the role of TMAO in the pathogenesis of cardiometabolic diseases is not limited to either detrimental or protective effects, suggesting that it might actually be dual and depend on specific conditions.

DATA AVAILABILITY STATEMENT

The original contributions presented in the study are included in the article/**Supplementary Materials**, further inquiries can be directed to the corresponding author.

ETHICS STATEMENT

The animal study was reviewed and approved by Latvian Animal Protection Ethical Committee of the Food and Veterinary Service, Riga, Latvia; Food and Veterinary Service Ethical approval Nr. 105.

AUTHOR CONTRIBUTIONS

MV, RV, MD, and MM-K performed planning of the study. MV, RV, SK, HC, and MM-K conducted experiments. MV, RV, SK, and MM-K performed data analysis. ES performed bio-analytical assays and data analysis. MV wrote the manuscript with input from RV, MD, and MM-K. All authors have read and approved the final manuscript.

FUNDING

This study was funded by the Latvian Council of Science project Trimethylamine-N-oxide as a link between unhealthy diet and cardiometabolic risks No. Izp-2018/1-0081, project supervised by MD.

SUPPLEMENTARY MATERIAL

The Supplementary Material for this article can be found online at: https://www.frontiersin.org/articles/10.3389/fcell.2020.622741/full#supplementary-material

REFERENCES

Barrea, L., Annunziata, G., Muscogiuri, G., Di Somma, C., Laudisio, D., Maisto, M., et al. (2018). Trimethylamine-N-oxide (TMAO) as novel potential biomarker of early predictors of metabolic syndrome. *Nutrients* 10, 1–19. doi: 10.3390/nu10121971

Brown, D. A., Perry, J. B., Allen, M. E., Sabbah, H. N., Stauffer, B. L., Shaikh, S. R., et al. (2017). Expert consensus document: mitochondrial function as a therapeutic target in heart failure. *Nat. Rev. Cardiol.* 14, 238–250. doi: 10.1038/nrcardio.2016.203

Byrne, N. J., Levasseur, J., Sung, M. M., Masson, G., Boisvenue, J., Young, M. E., et al. (2016). Normalization of cardiac substrate utilization and left ventricular hypertrophy precede functional recovery in heart failure regression. *Cardiovasc. Res.* 110, 249–257. doi: 10.1093/cvr/cvw051

Chegary, M., te Brinke, H., Doolaard, M., IJlst, L., Wijburg, F. A., Wanders, R. J. A., et al. (2008). Characterization of l-aminocarnitine, an inhibitor of fatty acid oxidation. *Mol. Genet. Metab.* 93, 403–410. doi: 10.1016/j.ymgme.2007.11.001

Cho, C. E., Taesuwan, S., Malysheva, O. V., Bender, E., Tulchinsky, N. F., Yan, J., et al. (2017). Trimethylamine-N-oxide (TMAO) response to animal source foods varies among healthy young men and is influenced by their gut microbiota composition: a randomized controlled trial. *Mol. Nutr. Food Res.* 61, 1–12. doi: 10.1002/mnfr.201600324

Chou, R. H., Chen, C. Y., Chen, I. C., Huang, H. L., Lu, Y. W., Kuo, C. S., et al. (2019). Trimethylamine N-oxide, circulating endothelial progenitor cells, and endothelial function in patients with stable angina. *Sci. Rep.* 9, 1–10. doi: 10.1038/s41598-019-40638-y

Dambrova, M., Latkovskis, G., Kuka, J., Strele, I., Konrade, I., Grinberga, S., et al. (2016). Diabetes is associated with higher trimethylamine N-oxide plasma levels. *Exp. Clin. Endocrinol. Diabetes* 124, 251–256. doi: 10.1055/s-0035-1569330

Dambrova, M., Skapare-makarova, E., Konrade, I., Pugovics, O., Grinberga, S., Tirzite, D., et al. (2013). Meldonium decreases the diet-increased plasma levels of trimethylamine n-oxide, a metabolite associated with atherosclerosis. *J. Clin. Pharmacol.* 53, 1095–1098. doi: 10.1002/jcph.135

Dávila-Román, V. G., Vedala, G., Herrero, P., De Las Fuentes, L., Rogers, J. G., Kelly, D. P., et al. (2002). Altered myocardial fatty acid and glucose metabolism in idiopathic dilated cardiomyopathy. *J. Am. Coll. Cardiol.* 40, 271–277. doi: 10.1016/S0735-1097(02)01967-8

Ding, L., Chang, M., Guo, Y., Zhang, L., Xue, C., Yanagita, T., et al. (2018). Trimethylamine-N-oxide (TMAO)-induced atherosclerosis is associated with bile acid metabolism. *Lipids Health Dis.* 17, 148–154. doi: 10.1186/s12944-018-0939-6

Estruch, R., Ros, E., Salas-Salvadó, J., Covas, M. I., Corella, D., Arós, F., et al. (2018). Primary prevention of cardiovascular disease with a mediterranean diet supplemented with extra-virgin olive oil or nuts. *N. Engl. J. Med.* 378, 1–14. doi: 10.1056/NEJMoa1800389

Fukami, K., Yamagishi, S., Sakai, K., Kaida, Y., Yokoro, M., Ueda, S., et al. (2015). Oral L-carnitine supplementation increases trimethylamine-n-oxide but reduces markers of vascular injury in hemodialysis patients. *J. Cardiovasc. Pharmacol.* 65, 289–295. doi: 10.1097/FJC.0000000000000197. Available online at: https://journals.lww.com/cardiovascularpharm/Fulltext/2015/03000/Oral_L_Carnitine_Supplementation_Increases.12.aspx (accessed December 22, 2020).

Gawrys-Kopczynska, M., Konop, M., Maksymiuk, K., Kraszewska, K., Derzsi, L., Sozanski, K., et al. (2020). TMAO, a seafood-derived molecule, produces diuresis and reduces mortality in heart failure rats. *Elife* 9:e57028. doi: 10.7554/eLife.57028.sa2

Griffiths, E. R., Friehs, I., Scherr, E., Poutias, D., McGowan, F. X., and del Nido, P. J. (2010). Electron transport chain dysfunction in neonatal pressure-overload hypertrophy precedes cardiomyocyte apoptosis independent of oxidative stress. *J. Thorac. Cardiovasc. Surg.* 139, 1609–1617. doi: 10.1016/j.jtcvs.2009.08.060

Grinberga, S., Dambrova, M., Latkovskis, G., Strele, I., Konrade, I., Hartmane, D., et al. (2015). Determination of trimethylamine- N -oxide in combination with l -carnitine and γ -butyrobetaine in human plasma by UPLC/MS/MS. *Biomed. Chromatogr.* 29, 1670–1674. doi: 10.1002/bmc.3477

Hardziyenka, M., Campian, M. E., Rianne de Bruin-Bon, H. A. C. M., Michel, M. C., and Tan, H. L. (2006). Sequence of echocardiographic changes during development of right ventricular failure in rat. *J. Am. Soc. Echocardiogr.* 19, 1272–1279. doi: 10.1016/j.echo.2006.04.036

He, K., Song, Y., Daviglus, M. L., Liu, K., Van Horn, L., Dyer, A. R., et al. (2004). Accumulated evidence on fish consumption and coronary heart disease mortality: a meta-analysis of cohort studies. *Circulation* 109, 2705–2711. doi: 10.1161/01.CIR.0000132503.19410.6B

Hoyles, L., Jiménez-Pranteda, M. L., Chilloux, J., Brial, F., Myridakis, A., Aranias, T., et al. (2017). Metabolic retroconversion of trimethylamine N-oxide and the gut microbiota. *bioRxiv* 6:73. doi: 10.1101/225581

Huc, T., Drapala, A., Gawrys, M., Konop, M., Bielinska, K., Zaorska, E., et al. (2018). Chronic, low-dose TMAO treatment reduces diastolic dysfunction and heart fibrosis in hypertensive rats. *Am. J. Physiol. - Hear. Circ. Physiol.* 315, H1805–H1820. doi: 10.1152/ajpheart.00536.2018

Jameson, E., Quareshy, M., and Chen, Y. (2018). Methodological considerations for the identification of choline and carnitine-degrading bacteria in the gut. *Methods* 149, 42–48. doi: 10.1016/j.ymeth.2018.03.012

Janeiro, M. H., Ramírez, M. J., Milagro, F. I., Martínez, J. A., and Solas, M. (2018). Implication of trimethylamine n-oxide (TMAO) in disease: potential biomarker or new therapeutic target. *Nutrients* 10:1398. doi: 10.3390/nu10101398

Jin, B., Ji, F., Zuo, A., Liu, H., Qi, L., He, Y., et al. (2020). Destructive role of TMAO in T-tubule and excitation-contraction coupling in the adult cardiomyocytes. *Int. Heart J.* 61, 355–363. doi: 10.1536/ihj.19-372

Karwi, Q. G., Uddin, G. M., Ho, K. L., and Lopaschuk, G. D. (2018). Loss of metabolic flexibility in the failing heart. *Front. Cardiovasc. Med.* 5, 1–19. doi: 10.3389/fcvm.2018.00068

Kilkenny, C., Browne, W., Cuthill, I. C., Emerson, M., and Altman, D. G. (2010). Animal research: reporting *in vivo* experiments: the ARRIVE guidelines. *Br. J. Pharmacol.* 160, 1577–1579. doi: 10.1111/j.1476-5381.2010.00872.x

Koeth, R. A., Wang, Z., Levison, B. S., Buffa, J. A., Org, E., Sheehy, B. T., et al. (2013). Intestinal microbiota metabolism of l-carnitine, a nutrient in red meat, promotes atherosclerosis. *Nat. Med.* 19, 576–585. doi: 10.1038/nm.3145

Kolwicz, S. C., Olson, D. P., Marney, L. C., Garcia-Menendez, L., Synovec, R. E., and Tian, R. (2012). Cardiac-specific deletion of acetyl CoA carboxylase 2 prevents metabolic remodeling during pressure-overload hypertrophy. *Circ. Res.* 111, 728–738. doi: 10.1161/CIRCRESAHA.112.268128

Kuka, J., Vilskersts, R., Cirule, H., Makrecka, M., Pugovics, O., Kalvinsh, I., et al. (2012). The cardioprotective effect of mildronate is diminished after co-treatment with l-carnitine. *J. Cardiovasc. Pharmacol. Ther.* 17, 215–222. doi: 10.1177/1074248411419502

Kummen, M., Mayerhofer, C. C. K., Vestad, B., Broch, K., Awoyemi, A., Storm-Larsen, C., et al. (2018). Gut microbiota signature in heart failure defined from profiling of 2 independent cohorts. *J. Am. Coll. Cardiol.* 71, 1184–1186. doi: 10.1016/j.jacc.2017.12.057

Lever, M., George, P. M., Slow, S., Bellamy, D., Young, J. M., Ho, M., et al. (2014). Betaine and trimethylamine-N-oxide as predictors of cardiovascular outcomes show different patterns in diabetes mellitus: an observational study. *PLoS ONE* 9:e0114969. doi: 10.1371/journal.pone.0114969

Li, T., Chen, Y., Gua, C., and Li, X. (2017). Elevated circulating trimethylamine N-oxide levels contribute to endothelial dysfunction in aged rats through vascular inflammation and oxidative stress. *Front. Physiol.* 8:350. doi: 10.3389/fphys.2017.00350

Liepinsh, E., Makrecka, M., Kuka, J., Makarova, E., Vilskersts, R., Cirule, H., et al. (2014). The heart is better protected against myocardial infarction in the fed state compared to the fasted state. *Metab. Clin. Exp.* 63, 127–136. doi: 10.1016/j.metabol.2013.09.014

Lindsay, E. C., Metcalfe, N. B., and Llewellyn, M. S. (2020). The potential role of the gut microbiota in shaping host energetics and metabolic rate. *J. Anim. Ecol.* 89, 2415–2426. doi: 10.1111/1365-2656.13327

Lopaschuk, G. D., Ussher, J. R., Folmes, C. D. L., Jaswal, J. S., and Stanley, W. C. (2010). Myocardial fatty acid metabolism in health and disease. *Physiol. Rev.* 90, 207–258. doi: 10.1152/physrev.00015.2009

Lupachyk, S., Watcho, P., Stavniichuk, R., Shevalye, H., and Obrosova, I. G. (2013). Endoplasmic reticulum stress plays a key role in the pathogenesis of diabetic peripheral neuropathy. *Diabetes* 62, 944–952. doi: 10.2337/db12-0716

Makhija, L., Krishnan, V., Rehman, R., Chakraborty, S., Maity, S., Mabalirajan, U., et al. (2014). Chemical chaperones mitigate experimental asthma by attenuating

endoplasmic reticulum stress. *Am. J. Respir. Cell Mol. Biol.* 50, 923–931. doi: 10.1165/rcmb.2013-0320OC

Makrecka, M., Kuka, J., Volska, K., Antone, U., Sevostjanovs, E., Cirule, H., et al. (2014). Long-chain acylcarnitine content determines the pattern of energy metabolism in cardiac mitochondria. *Mol. Cell. Biochem.* 395, 1–10. doi: 10.1007/s11010-014-2106-3

Makrecka-Kuka, M., Korzh, S., Videja, M., Vilskersts, R., Sevostjanovs, E., Zharkova-Malkova, O., et al. (2020). Inhibition of CPT2 exacerbates cardiac dysfunction and inflammation in experimental endotoxaemia. *J. Cell. Mol. Med.* 24, 11903–11911. doi: 10.1111/jcmm.15809

Makrecka-Kuka, M., Volska, K., Antone, U., Vilskersts, R., Grinberga, S., Bandere, D., et al. (2017). Trimethylamine N-oxide impairs pyruvate and fatty acid oxidation in cardiac mitochondria. *Toxicol. Lett.* 267, 32–38. doi: 10.1016/j.toxlet.2016.12.017

Mayerhofer, C. C. K., Kummen, M., Holm, K., Broch, K., Awoyemi, A., Vestad, B., et al. (2020). Low fibre intake is associated with gut microbiota alterations in chronic heart failure. *ESC Hear. Fail.* 7, 456–466. doi: 10.1002/ehf2.12596

McGrath, J. C., Drummond, G. B., McLachlan, E. M., Kilkenny, C., and Wainwright, C. L. (2010). Editorial: guidelines for reporting experiments involving animals: the ARRIVE guidelines. *Br. J. Pharmacol.* 160, 1573–1576. doi: 10.1111/j.1476-5381.2010.00873.x

Neglia, D., De Caterina, A., Marraccini, P., Natali, A., Ciardetti, M., Vecoli, C., et al. (2007). Impaired myocardial metabolic reserve and substrate selection flexibility during stress in patients with idiopathic dilated cardiomyopathy. *Am. J. Physiol. - Hear. Circ. Physiol.* 293, 3270–3278. doi: 10.1152/ajpheart.00887.2007

Neves, F. A., Cortez, E., Bernardo, A. F., Mattos, A. B. M., Vieira, A. K., de, O., et al. (2014). Heart energy metabolism impairment in Western-diet induced obese mice. *J. Nutr. Biochem.* 25, 50–57. doi: 10.1016/j.jnutbio.2013.08.014

Nita, M., and Grzybowski, A. (2016). The role of the reactive oxygen species and oxidative stress in the pathomechanism of the age-related ocular diseases and other pathologies of the anterior and posterior eye segments in adults. *Oxid. Med. Cell. Longev.* 2016:3164734. doi: 10.1155/2016/3164734

Nowiński, A., and Ufnal, M. (2018). Trimethylamine N-oxide: a harmful, protective or diagnostic marker in lifestyle diseases? *Nutrition* 46, 7–12. doi: 10.1016/j.nut.2017.08.001

Organ, C. L., Li, Z., Sharp, T. E., Polhemus, D. J., Gupta, N., Goodchild, T. T., et al. (2020). Nonlethal inhibition of gut microbial trimethylamine N-oxide production improves cardiac function and remodeling in a murine model of heart failure. *J. Am. Heart Assoc.* 9:e016223. doi: 10.1161/JAHA.119.016223

Organ, C. L., Otsuka, H., Bhushan, S., Wang, Z., Bradley, J., Trivedi, R., et al. (2016). Choline diet and its gut microbe-derived metabolite, trimethylamine N-oxide, exacerbate pressure overload-induced heart failure. *Circ. Hear. Fail.* 9:e002314. doi: 10.1161/CIRCHEARTFAILURE.115.002314

Querio, G., Antoniotti, S., Levi, R., and Gallo, M. P. (2019). Trimethylamine n-oxide does not impact viability, ros production, and mitochondrial membrane potential of adult rat cardiomyocytes. *Int. J. Mol. Sci.* 20:3045. doi: 10.3390/ijms20123045

Rosca, M. G., and Hoppel, C. L. (2013). Mitochondrial dysfunction in heart failure. *Heart Fail. Rev.* 18, 607–622. doi: 10.1007/s10741-012-9340-0

Sabbah, H. N. (2020). Targeting the mitochondria in heart failure: a translational perspective. *JACC Basic Transl. Sci.* 5, 88–106. doi: 10.1016/j.jacbts.2019.07.009

Savi, M., Bocchi, L., Bresciani, L., Falco, A., Quaini, F., Mena, P., et al. (2018). Trimethylamine-N-oxide (TMAO)-induced impairment of cardiomyocyte function and the protective role of urolithin B-glucuronide. *Molecules* 23:e30549. doi: 10.3390/molecules23030549

Srere, P. A. (1969). [1] Citrate synthase. [EC 4.1.3.7. Citrate oxaloacetate-lyase (CoA-acetylating)]. *Methods Enzymol.* 13, 3–11. doi: 10.1016/0076-6879(69)13005-0

Sun, X., Jiao, X., Ma, Y., Liu, Y., Zhang, L., He, Y., et al. (2016). Trimethylamine N-oxide induces inflammation and endothelial dysfunction in human umbilical vein endothelial cells via activating ROS-TXNIP-NLRP3 inflammasome. *Biochem. Biophys. Res. Commun.* 481, 63–70. doi: 10.1016/j.bbrc.2016.11.017

Suzuki, T., Heaney, L. M., Bhandari, S. S., Jones, D. J. L., and Ng, L. L. (2016). Trimethylamine N-oxide and prognosis in acute heart failure. *Heart* 102, 841–848. doi: 10.1136/heartjnl-2015-308826

Tang, W. H. W., Wang, Z., Fan, Y., Levison, B., Hazen, J. E., Donahue, L. M., et al. (2014). Prognostic value of elevated levels of intestinal microbe-generated metabolite trimethylamine-N-oxide in patients with heart failure: refining the gut hypothesis. *J. Am. Coll. Cardiol.* 64, 1908–1914. doi: 10.1016/j.jacc.2014.02.617

Tang, W. H. W., Wang, Z., Shrestha, K., Borowski, A. G., Wu, Y., Troughton, R. W., et al. (2015). Intestinal microbiota-dependent phosphatidylcholine metabolites, diastolic dysfunction, and adverse clinical outcomes in chronic systolic heart failure. *J. Card. Fail.* 21, 91–96. doi: 10.1016/j.cardfail.2014.11.006

Tonazzi, A., Giangregorio, N., Console, L., De Palma, A., and Indiveri, C. (2017). Nitric oxide inhibits the mitochondrial carnitine/acylcarnitine carrier through reversible S-nitrosylation of cysteine 136. *Biochim. Biophys. Acta - Bioenerg.* 1858, 475–482. doi: 10.1016/j.bbabio.2017.04.002

Tørris, C., Molin, M., and Smastuen, M. C. (2014). Fish consumption and its possible preventive role on the development and prevalence of metabolic syndrome-a systematic review. *Diabetol. Metab. Syndr.* 6:112. doi: 10.1186/1758-5996-6-112

Trøseid, M., Ueland, T., Hov, J. R., Svardal, A., Gregersen, I., Dahl, C. P., et al. (2015). Microbiota-dependent metabolite trimethylamine-N-oxide is associated with disease severity and survival of patients with chronic heart failure. *J. Intern. Med.* 277, 717–726. doi: 10.1111/joim.12328

Ufnal, M., Jazwiec, R., Dadlez, M., Drapala, A., Sikora, M., and Skrzypecki, J. (2014). Trimethylamine-N-oxide: a carnitine-derived metabolite that prolongs the hypertensive effect of angiotensin II in rats. *Can. J. Cardiol.* 30, 1700–1705. doi: 10.1016/j.cjca.2014.09.010

Ventura-Clapier, R., Garnier, A., Veksler, V., and Joubert, F. (2011). Bioenergetics of the failing heart. *Biochim. Biophys. Acta - Mol. Cell Res.* 1813, 1360–1372. doi: 10.1016/j.bbamcr.2010.09.006

Wang, G., Kong, B., Shuai, W., Fu, H., Jiang, X., and Huang, H. (2020). 3,3-Dimethyl-1-butanol attenuates cardiac remodeling in pressure overload-induced heart failure mice. *J. Nutr. Biochem.* 78:108341. doi: 10.1016/j.jnutbio.2020.108341

Wang, Z., Klipfell, E., Bennett, B. J., Koeth, R., Levison, B. S., Dugar, B., et al. (2011). Gut flora metabolism of phosphatidylcholine promotes cardiovascular disease. *Nature* 472, 57–65. doi: 10.1038/nature09922

Wang, Z., Tang, W. H. W., Buffa, J. A., Fu, X., Britt, E. B., Koeth, R. A., et al. (2014). Prognostic value of choline and betaine depends on intestinal microbiota-generated metabolite trimethylamine-N-oxide. *Eur. Heart J.* 35, 904–910. doi: 10.1093/eurheartj/ehu002

Widmer, R. J., Flammer, A. J., Lerman, L. O., and Lerman, A. (2015). The Mediterranean diet, its components, and cardiovascular disease. *Am. J. Med.* 128, 229–238. doi: 10.1016/j.amjmed.2014.10.014

Wu, R., Wang, H. L., Yu, H. L., Cui, X. H., Xu, M. T., Xu, X., et al. (2016). Doxorubicin toxicity changes myocardial energy metabolism in rats. *Chem. Biol. Interact.* 244, 149–158. doi: 10.1016/j.cbi.2015.12.010

Yang, J. M., Zhou, R., Zhang, M., Tan, H. R., and Yu, J. Q. (2018). Betaine attenuates monocrotaline-induced pulmonary arterial hypertension in rats via inhibiting inflammatory response. *Molecules* 23, 1–15. doi: 10.3390/molecules23061274

Conflict of Interest: The authors declare that the research was conducted in the absence of any commercial or financial relationships that could be construed as a potential conflict of interest.

frontiers in Cell and Developmental Biology

ORIGINAL RESEARCH
published: 21 January 2021
doi: 10.3389/fcell.2020.628842

Mst1 Knockout Alleviates Mitochondrial Fission and Mitigates Left Ventricular Remodeling in the Development of Diabetic Cardiomyopathy

Xinyu Feng[1†], Shanjie Wang[2†], Xingjun Yang[2†], Jie Lin[2], Wanrong Man[2], Yuan Dong[2], Yan Zhang[2], Zhijing Zhao[2], Haichang Wang[1*] and Dongdong Sun[1*]*

[1] Heart Hospital, Xi'an International Medical Center, Xi'an, China, [2] Department of Cardiology, Xijing Hospital, Fourth Military Medical University, Xi'an, China

OPEN ACCESS

Edited by:
Xiaoqiang Tang,
Sichuan University, China

Reviewed by:
Yi Tan,
University of Louisville, United States
Yifei Li,
Sichuan University, China
Jun Ren,
University of Washington, United States

***Correspondence:**
Dongdong Sun
wintersun3@gmail.com
Haichang Wang
wanghccardio@icloud.com
Zhijing Zhao
zhaozhj@fmmu.edu.cn

[†]These authors have contributed equally to this work

Specialty section:
This article was submitted to Cellular Biochemistry, a section of the journal Frontiers in Cell and Developmental Biology

Received: 13 November 2020
Accepted: 22 December 2020
Published: 21 January 2021

Citation:
Feng X, Wang S, Yang X, Lin J, Man W, Dong Y, Zhang Y, Zhao Z, Wang H and Sun D (2021) Mst1 Knockout Alleviates Mitochondrial Fission and Mitigates Left Ventricular Remodeling in the Development of Diabetic Cardiomyopathy. Front. Cell Dev. Biol. 8:628842. doi: 10.3389/fcell.2020.628842

The disruption of mitochondrial dynamics is responsible for the development of diabetic cardiomyopathy (DCM). However, the mechanisms that regulate the balance of mitochondrial fission and fusion are not well-understood. Wild-type, Mst1 transgenic and Mst1 knockout mice were induced with experimental diabetes by streptozotocin injection. In addition, primary neonatal cardiomyocytes were isolated and cultured to simulate diabetes to explore the mechanisms. Echocardiograms and hemodynamic measurements revealed that Mst1 knockout alleviated left ventricular remodeling and cardiac dysfunction in diabetic mice. Mst1 knockdown significantly decreased the number of TUNEL-positive cardiomyocytes subjected to high-glucose (HG) medium culture. Immunofluorescence study indicated that Mst1 overexpression enhanced, while Mst1 knockdown mitigated mitochondrial fission in DCM. Mst1 participated in the regulation of mitochondrial fission by upregulating the expression of Drp1, activating $Drp1^{S616}$ phosphorylation and $Drp1^{S637}$ dephosphorylation, as well as promoting Drp1 recruitment to the mitochondria. Furthermore, Drp1 knockdown abolished the effects of Mst1 on mitochondrial fission, mitochondrial membrane potential and mitochondrial dysfunction in cardiomyocytes subjected to HG treatment. These results indicated that Mst1 knockout inhibits mitochondrial fission and alleviates left ventricular remodeling thus prevents the development of DCM.

Keywords: Mammalian Sterile 20-like Kinase 1, Mst1, Mitochondrial Fission, Mitochondrial Fusion, Mitochondrial Dysfunction, Diabetic Cardiomyopathy, DCM

INTRODUCTION

The International Diabetes Federation (IDF) highlights that the global prevalence of diabetes has been increasing over recent decades. The prevalence of diabetes was estimated to be 8.8% in 2015 and is predicted to rise to 10.4% in 2040 (Ogurtsova et al., 2017). Diabetes itself is an independent risk factor for cardiovascular disease, and the increased prevalence of diabetes has led to more cases of cardiovascular complications (Adeva-Andany et al., 2019). With the chronic and progressive damage of diabetes, diabetic cardiomyopathy (DCM) which is characterized by early cardiac

diastolic dysfunction, decreased or preserved systolic function and a reduced ejection fraction eventually resulting in heart failure, can be caused (Rubler et al., 1972). It is important to elucidate the mechanism of diabetic cardiomyopathy to reduce the cardiac mortality of diabetic patients.

A universal theory exists across science fields that mitochondria are not static, solitary organelles, but that they constantly undergo shape and number changes due to the mitochondrial dynamics (Williams and Caino, 2018). Mitochondrial dynamics are mainly controlled by the two opposing processes of fission and fusion (Mattie et al., 2019). Dynamin-related protein 1 (DRP1), mitochondrial fission 1 (Fis1), mitochondrial fission factor (MFF) and mitochondrial dynamics proteins (MiD49/MiD51) constitute the core machinery promoting mitochondrial fusion. Mitofusin 1/2 (MFN1/2) and optic atrophy protein 1 (OPA1) achieve fusion of the outer and inner mitochondrial membranes, respectively (van der Bliek et al., 2013). Numerous experiments have observed that hyperglycemia induces mitochondrial fragmentation (Yu et al., 2006, 2011). Dysregulation of mitochondrial dynamics has been hypothesized to contribute to the pathogenic progression of metabolic diseases, including the diabetic complication of DCM (Galloway and Yoon, 2015). However, the molecular mechanisms responsible for mitochondrial dynamics in diabetic stress are not well-understood.

Mammalian sterile 20-like kinase 1 (Mst1) is the core component of the Hippo pathway. It is expressed in various organs and tissues of mammals, especially in cardiomyocytes. The Hippo pathway associated with Mst1 regulates the growth and death of myocardial cells (Yang et al., 2018). We have discussed the role of Mst1 in regulating autophagy and apoptosis in the cardiovascular system, as well as the cardiac function of Mst1 in diabetic mice (Zhang et al., 2016; Wang et al., 2018a). Our previous study demonstrated that the expression of Mst1 increased DCM progression, while other studies showed that mitochondrial fission is increased during DCM progression. Therefore, the purpose of this study was to determine the regulatory effect of Mst1 on mitochondrial fission and fusion of the myocardium under hyperglycemic conditions.

MATERIALS AND METHODS

Animals and Treatment

Mst1 transgenic (Mst1Tg) and Mst1 knockout ($Mst1^{-/-}$) mice (C57BL/6 background) were purchased from K&D gene technology (Wu Han, China). All animals were identified by Western blot and real-time PCR analysis. The present study was performed according to the NIH guidelines on the use of laboratory animals. All protocols were approved by the Institutional Animal Care in the Xi'an International Medical Center. As previously described (Zhang et al., 2016), 8-week old mice (Male, 20–25 g) were intraperitoneally injected with streptozotocin (STZ, 50 mg/kg, dissolved in 100 mmol/L citrate buffers, pH 4.5) for 5 days and fed a high-fat and high-sugar diet to induce a diabetes model, and only those with random blood glucose levels $\geq$16.6 mmol/L twice were labeled having diabetes. Four groups were set as follows: (1) Wild type group (WT, $n = 8$); (2) Diabetes group (DM, $n = 10$); (3) Diabetes + $Mst1^{-/-}$ group (DM+$Mst1^{-/-}$, $n = 11$); (4) Diabetes + Mst1Tg group (DM+Mst1Tg, $n = 9$).

Isolation of Primary Neonatal Mouse Cardiomyocytes

Isolation of primary neonatal mouse cardiomyocytes was described previously (Ehler et al., 2013). Briefly, neonatal mouse hearts were quickly excised and minced into fragments prior to enzymatic digestion with a collagenase/dispase mixture (Invitrogen, USA). After several rounds of digestion, the digested fragments were placed on a sterilized platform to sediment for several minutes, and digested cells in supernatants were pre-placed for 90 min to remove fibroblasts and endothelial cells because of their earlier attachment. Then the residual supernatant with abundant cardiomyocytes was replanted in collagen-coated dishes at $\sim 1.5 \times 10^5$ cells per cm^2. After incubation without being moved for 48 h, the culture medium was refreshed with complete medium.

The Culture of Primary Neonatal Mouse Cardiomyocytes

The culture of primary cardiomyocytes was described previously (Ehler et al., 2013). Briefly, cells were cultured in complete Dulbecco's Modified Eagle's Medium (DMEM, HyClone, USA) with 4,500 mg/L glucose,4 mM L-glutamine, 110 mg/L sodium pyruvate, 1% (v/v) penicillin/streptomycin and 10% (v/v) fetal bovine serum (FBS, Biological Industries). Cells were then placed in an incubator containing 95% air and 5% CO_2 at 37°C. The culture medium was replaced every 2–3 days. For the *in vitro* study, primary cardiomyocytes were treated with low glucose (LG, 5.5 mM/L) and high glucose (HG, 30 mM/L) for 48 h.

Cardiac Function Evaluation

After a three-month duration of the diabetic condition, all mice were carefully anesthetized with 2% isoflurane and fixed on a heating pad (37°C) in a supine position. Cardiac function was evaluated across the thoracic region using 2-D Guided M-mode echocardiography (VisualSonics Vevo 2100, Toronto, ON, Canada) equipped with a 15 MHz linear transducer. Left ventricular end-diastolic diameter (LVEDD) and left ventricular end-systolic diameter (LVESD) were measured on the left ventricular short axis. Left ventricular ejection fraction (LVEF) and left ventricular fraction shortening (LVFS) were calculated by computer algorithms, as described previously. A pressure catheter was used to assess the maximal rate of LV contractility and relaxation with a previously described method (Wang et al., 2018b).

Cell Apoptosis Assay

A terminal deoxynucleotidyl transferased UTP nick end labeling (TUNEL) assay kit (Roche Applied Science, Swiss) was employed to determine myocardial apoptosis following the manufacturer's instructions as previously described (Zhang et al., 2016).

Transmission Electron Microscopy (TEM)

Murine heart tissues were fixed in 2% glutaraldehyde for at least 24 h. Tissues were then immersed in 2% osmium tetroxide and 1% aqueous uranyl acetate, each for 1 h. After being washed with a series of ethanol solutions (50, 70, 90, and 100%), tissues were transferred to propylene oxide, incubated in a 1:1 mixture of propylene oxide and EMbed 812 (Electron Microscopy Sciences) for 1 h and then placed in a 70°C oven to polymerize. Sections (75–80 nm) were cut using a Leica ultramicrotome equipped with a Diatome diamond knife and collected on 200-mesh copper grids. After being post-stained in 5% uranyl acetate for 10 min and in Reynold's lead citrate for 5 min, sections were observed using a 40-120 kV transmission electron microscope (FEI TECNAI G2 Spirit Biotwin, Hong Kong, China). For the *in vitro* study, primary cardiomyocytes were collected by centrifuging at 1,000 rpm for 10 min and fixing them in 100 μL of 2% glutaraldehyde. The subsequent operations were performed as described above (Hu et al., 2017).

Mitochondrial and Cytosolic Protein Extraction

Mitochondrial and cytosolic components were extracted using a Mitochondria Isolation Kit (C3601, C3606, Beyotime). First, cardiomyocytes were well-distributed by Mitochondria Isolation Solution containing PMSF in an ice bath for 15 min. A glass homogenizer was applied to grind the cells followed by centrifugation with 1,000 × g for 10 min at 4°C. The liquid supernatant was shifted to another tube and centrifuged again with 11,000 × g for 10 min. The sediment was blended with Mitochondrial Lysate Solution to obtain mitochondrial proteins. The supernatant was centrifuged with 12,000 × g for 20 min to obtain cytosolic proteins.

Western Blot Analysis

After treatments, murine heart tissues and primary cardiomyocytes were collected, digested and analyzed using a BCA assay (for protein concentration, Thermo Fisher Scientific, USA). Protein samples of each group were separated using SDS-PAGE gels, transferred to the polyvinylidene difluoride membrane (PVDF, Millipore, USA), and then incubated overnight at 4 °C with specific antibodies against Mst1 (1:1,000, Cell Signaling Technology); t-Drp1 (1:1,000, Millipore, USA); p-Drp1^{S616} (1:500, Cell Signaling Technology, USA); p-Drp1^{S637} (1:500, Cell Signaling Technology, USA); Mff (1:1,000, Proteintech, USA); Mid49 (1:500, Proteintech, USA); Mid51 (1:1,000, Proteintech, USA); Fis1 (1:1,000, Proteintech, USA); Mfn1 (1:500, Proteintech, USA); Mfn2 (1:5,000, Abcam, USA); Opa1 (1:2,000, Abcam, USA); caspase-3 (1:1,000, Cell Signaling Technology, USA); cleaved caspase-3 (1:1,000, Cell Signaling Technology, USA) and β-actin (loading control, 1:1,000, Cell Signaling Technology). Then, blots were incubated with horseradish peroxidase (HSP)-conjugated secondary antibody (1:5,000, Proteintech, USA) for 1 h. Finally, blots were scanned and detected by the luminescence method. Band intensity was analyzed using the Image J software (Version 1.45).

Real Time PCR

RNA was extracted with RNeasy mini kit (Qiagen, USA), cDNA was synthesized with a high-capacity cDNA reverse transcription kit (Applied Biosystems, Lithuania). Quantitative real-time PCR was performed using a Power SYBR Green PCR Master Mix (Applied Biosystems, UK). All procedures were performed strictly following the manufacturers' protocols. The primer sequences are as follows: Complex-IV forward CAGGATTCTTCTGAGCGTTCTATCA, Complex-IV reverse AATTCCTGTTGGAGGTCAGCA, NADH dehydrogenase subunit 1 forward ATGGTCAGTCTGTCATGGTGGAAC, NADH dehydrogenase subunit 1 reverse GCATAGCACAAGCAGCGACAAC, GAPDH forward ACGGCAAATTCAACGGCACAGTCA, GAPDH reverse TGGGGGCATCGGCAGAAGG.

Immunofluorescence

For immunostaining, antibodies to Drp1 (1:500, Millipore, USA) and MitoTracker® Red CMXRos (40741ES50,) were used. Cells were grown in a particular vessel for fixed-cell imaging. After treatments, cells were washed twice with PBS and incubated with MitoTracker Red CMXRos for 20 min at 37°C. Cells were fixed in pre-warmed 4% paraformaldehyde for 10 min at 37°C, permeabilized in 0.1% Triton X-100, and all were washed after each step by phosphate-buffered saline. The primary antibodies were incubated for 48 h at 4°C and then conjugated for detection with Alexa fluor 488 anti-goat. The nuclei were dyed with DIPA. Scoring of mitochondrial morphology was performed blind to genotype in triplicates of 100 cells. Imaging was performed with a Plan-Apochromat 63×/1.4 oil objective on a Zeiss LSM 710 confocal microscope driven by Zen 2009 software (Carl Zeiss, Jena, Germany). Images were cropped, globally adjusted for contrast and brightness, and median filtered using ImageJ (National Institutes of Health, Bethesda, MD).

Adenovirus Construction and Transfection

The adenoviruses harboring Drp1 shRNA (Ad-sh-Drp1; MOI: 100); Mst1 shRNA (Ad-sh-Mst1; MOI: 100); Mst1 (Ad-Mst1; MOI: 100); and control vectors (Ad-sh-LacZ and Ad-LacZ; MOI: 100) were purchased from Hanbio Technology, Ltd. (Shanghai, China) and were transduced 4 h after the cardiomyocytes were treated with low (5.5 mM) or high (33 mM) glucose for 48 h.

Determination of Mitochondrial Membrane Potential (MMP)

Primary cardiomyocytes were cultured in disposable confocal dishes. After their corresponding treatments, cells were rinsed with PBS and incubated with 5 μM JC-1 dye (C2006, Beyotime) at 37°C for 20 min. Fluorescent cells were visualized using an Olympus confocal microscope. Cellular mitochondria with normal MMP emitted red fluorescence (J-aggregate), while those with abnormal MMP showed green fluorescence (J-monomer). The mitochondrial membrane potential (MMP) was calculated using Image-Pro-Plus (Version 6.0) as red /green fluorescence.

Mitochondria Biological Function

To assess the functional status of the mitochondria, an ATP bioluminescent assay kit (S0026, Beyotime) was used to detect the ATP level. The tissues were fully homogenized and centrifuged at 12,000 g for 15 min at 4°C. The supernatant was mixed with the corresponding reagent and assessed using a multimode microplate reader equipped with a luminescence luminometer (FLUOstar Omega, BMG Labtech, Germany). Citrate synthase and electron transport chain complex activities (complexes I/II/V) was measured using commercially available kits (Sigma, USA; Cayman, USA) according to the manufacturer's instructions. Data were representative of 4 biological repeats (Wang et al., 2018a).

Statistical Analysis

All data were presented as the mean ± SEM. Differences between specific groups were determined by one-way analysis of variance (ANOVA) followed by Tukey's *post hoc* test (Graph-Pad 4.0, Graph Pad Software, La Jolla, CA, USA). Values with a $P < 0.05$ were considered statistically significant.

RESULTS

Mst1 Inhibition Mitigates Cardiac Dysfunction and Cardiomyocyte Apoptosis in Diabetic Mice

M-mode echocardiograms were used to quantify cardiac function. Representative M-mode echocardiograms were shown in **Figure 1A**. In diabetic mice, decreased LVEF and LVFS and increased LVESD and LVEDD were observed as compared with the WT mice. Mst1 overexpression inhibited, while Mst1 knockout enhanced LVEF and LVFS in mice underwent diabetes insult (**Figures 1B,C**). Mst1 knockout significantly inhibited left ventricular remodeling in diabetic mice, as evidenced by decreased LVESD and LVEDD (**Figures 1D,E**). Hemodynamic measurements also revealed that Mst1 knockout decreased ± LV dp/dt max and alleviated cardiac dysfunction in diabetic mice (**Figures 1F,G**).

Mst1 knockdown significantly decreased the number of TUNEL-positive cardiomyocytes subjected to high-glucose medium culture (**Figures 1H,I**). Furthermore, the ratio of cleaved caspase-3/caspase-3 was also reduced by Mst1 knockdown in cardiomyocytes cultured in high-glucose medium (**Figures 1J,K**). These data indicated that Mst1 deficiency ameliorated the cardiac pathological phenotype of diabetic mice.

Mst1 Knockdown Ameliorates Mitochondrial Fission in the Experimental Diabetic Cardiomyopathy

The dynamic changes in mitochondrial fission and fusion were observed by transmission electron microscopy and confocal imaging. Transmission electron microscopy demonstrated that the mean mitochondrial size was lager, the number of mitochondria was decreased and mitochondrial crista damage was also ameliorated in the Mst1 knockout diabetic mice hearts, as compared with the diabetic mice (**Figures 2A–C**). Mst1 overexpression increased the prevalence of fragmented mitochondria, while Mst1 knockout induced a display of elongated mitochondria in the diabetic mice heart (**Figures 2A–C**). The Mitochondrial Network Analysis (MiNA) toolset, a simple ImageJ macro tool, classified mitochondrial structures as individuals and networks (Valente et al., 2017). MiNA could measure the average lengths of all rods/branches, evaluate the extent of mitochondrial branching and determine the total area in the image (**Figures 2D–G**). Mst1 overexpression decreased the length of rods/branches, the number of branches and the mitochondrial footprint, whereas Mst1 knockdown increased these parameters in cardiomyocytes subjected to high-glucose culture (**Figures 2D–G**). In addition, Mst1 knockout resulted in decreased mtDNA copy number as compared with the DM group. However, the transcript level of mtDNA was not significantly changed in Mst1 overexpression or knockout group (**Figures 2H,I**). Taken together, the above data indicated that Mst1 exacerbates mitochondrial fission and Mst1 knockdown ameliorates mitochondrial fission during DCM.

Mst1 Knockout Decreases Drp1 Expression, Inhibits Drp1^{S616} Phosphorylation and Promotes Drp1^{S637} Phosphorylation in Diabetic Cardiomyopathy

Proteins of the mitochondrial fission machinery include Drp1, Mff, Mid49/51 and Fis1. MfnFN1, Mfn2 and Opa1 are involved consistently in mitochondrial fusion (Otera et al., 2013). Western blot analysis demonstrated that mitochondrial fission related proteins increased and mitochondrial fusion related proteins decreased in DM group compared with WT group (**Figures 3A–L**). Mst1 knockout decreased Drp1 expression, inhibited the phosphorylation of Drp1^{S616} and promoted the phosphorylation of Drp1^{S637}. In contrast, Mst1Tg diabetic mice exhibited increased Drp1 expression, up-regulated phosphorylation of Drp1^{S616} and decreased phosphorylation of Drp1^{S637} (**Figures 3A–D**). Mst1 knockout did not significantly change the expression of MFF, Mid49/51 and FIS1 (**Figures 3E–H**). Furthermore, Mst1 knockout increased Mfn2 levels, while had no role on Mfn1 and Opa1 levels in DCM (**Figures 3I–L**).

Drp1 Knockdown Abolishes the Effects of Mst1 on Mitochondrial Fission in Cardiomyocytes Subjected to High-Glucose Treatment

In cardiomyocytes subjected to high-glucose culture, Mst1 knockdown significantly increased the length of mitochondrial rods/ branches, the number of branches and the mitochondrial footprint. Interestingly, Drp1 knockdown abolished the effects of Mst1 knockdown on the above parameters (**Figures 4A–D**). Consistently, Drp1 knockdown eliminated the role of Mst1 knockdown on the mean size of mitochondria and the number of mitochondria as evaluated by transmission electron microscopy (**Figures 4E–G**). These data indicated that Drp1 may serve as a downstream regulator of Mst1.

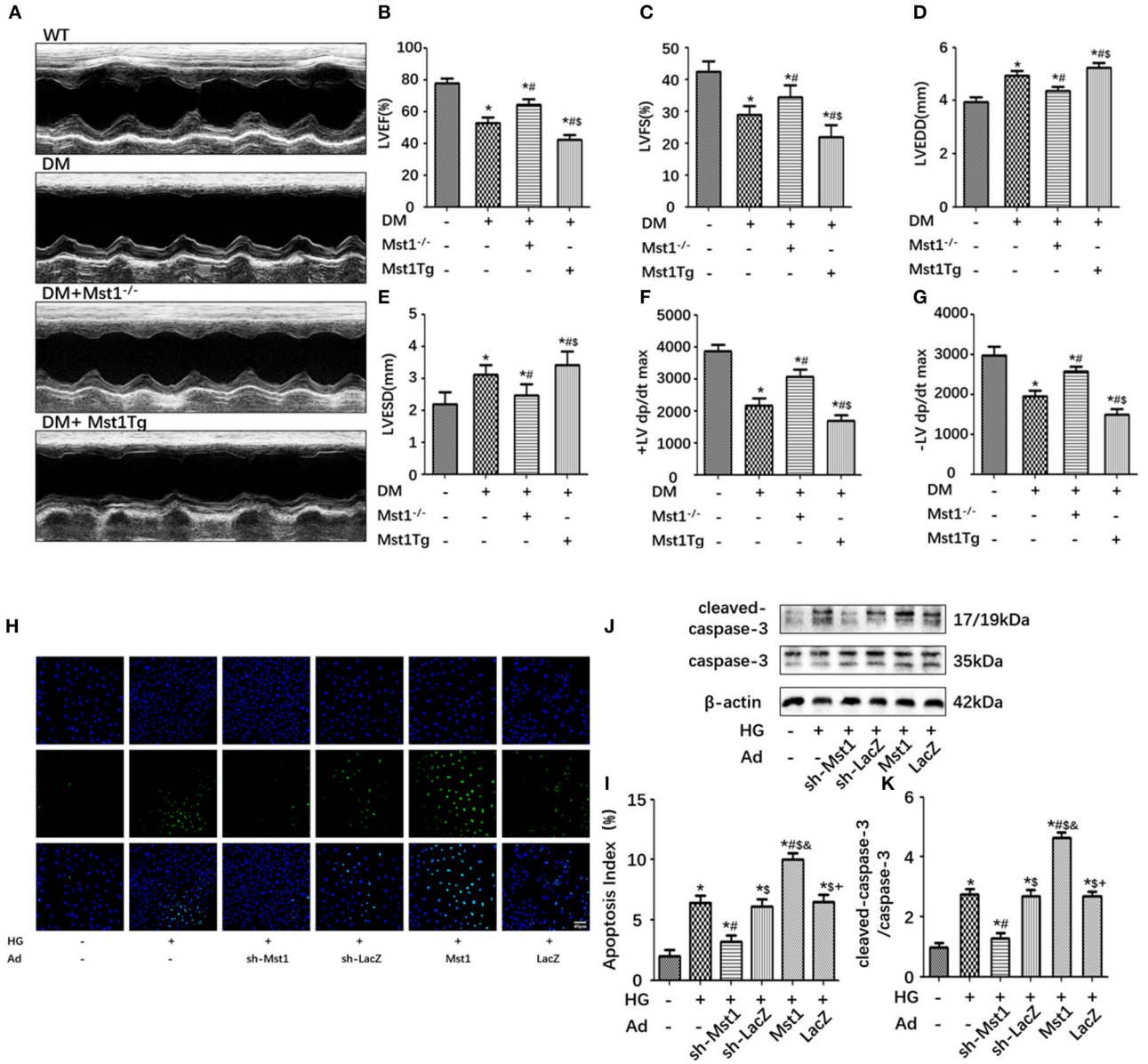

FIGURE 1 | Mst1 inhibition alleviates cardiac dysfunction and cardiomyocyte apoptosis in diabetic mice. **(A)** Representative images of echocardiography. **(B)** Measurements of LVEF (%). **(C)** Measurements of LVFS (%). **(D)** Measurements of LVEDD (mm). **(E)** Measurements of LVESD (mm). **(F)** Hemodynamic evaluation of +LV dp/dt max. **(G)** Hemodynamic evaluation of -LV dp/dt max. The columns and error bars represent the means and SEM. $^{*}P < 0.05$ vs. WT; $^{\#}P < 0.05$ vs. DM; $\$P < 0.05$ vs. DM + Mst1$^{-/-}$. **(H)** Representative images of TUNEL staining in primary cardiomyocytes (scale bar: 40 mm). **(I)** Quantitative analysis of the apoptotic index (percentage of TUNEL-positive nuclei, %). **(J)** Representative western blots showing expression of cleaved-caspase 3, caspase 3 and β-actin (loading control) proteins. **(K)** Quantitative analysis of the ratio of cleaved-caspase 3/caspase 3. The columns and error bars represent the means and SEM. $^{*}P < 0.05$ vs. Con; $^{\#}P < 0.05$ vs. HG; $\$P < 0.05$ vs. HG + Ad-sh-Mst1; and $P < 0.05$ vs. HG + Ad-sh-LacZ; and $+P < 0.05$ vs. HG + Ad-Mst1.

Mst1 Knockdown Inhibits Drp1 Recruitment to the Mitochondria in Cardiomyocytes Under High-Glucose Treatment

Drp1 is largely cytosolic with only 3% of the protein being associated with mitochondria (Smirnova et al., 2001). Drp1 transfer from the cytosol to the mitochondrion was essential for mitochondrial fission (Smirnova et al., 2001; van der Bliek et al., 2013). Immunofluorescence analysis was performed to observe the mitochondrial localization of Drp1. In cardiomyocyts subjected to high-glucose treatment, Drp1 was located increasingly on the mitochondria. Mst1 overexpression increased, while Mst1 knockdown decreased mitochondrial localization of Drp1 (**Figures 5A–D**). By isolating mitochondrial and cytosolic

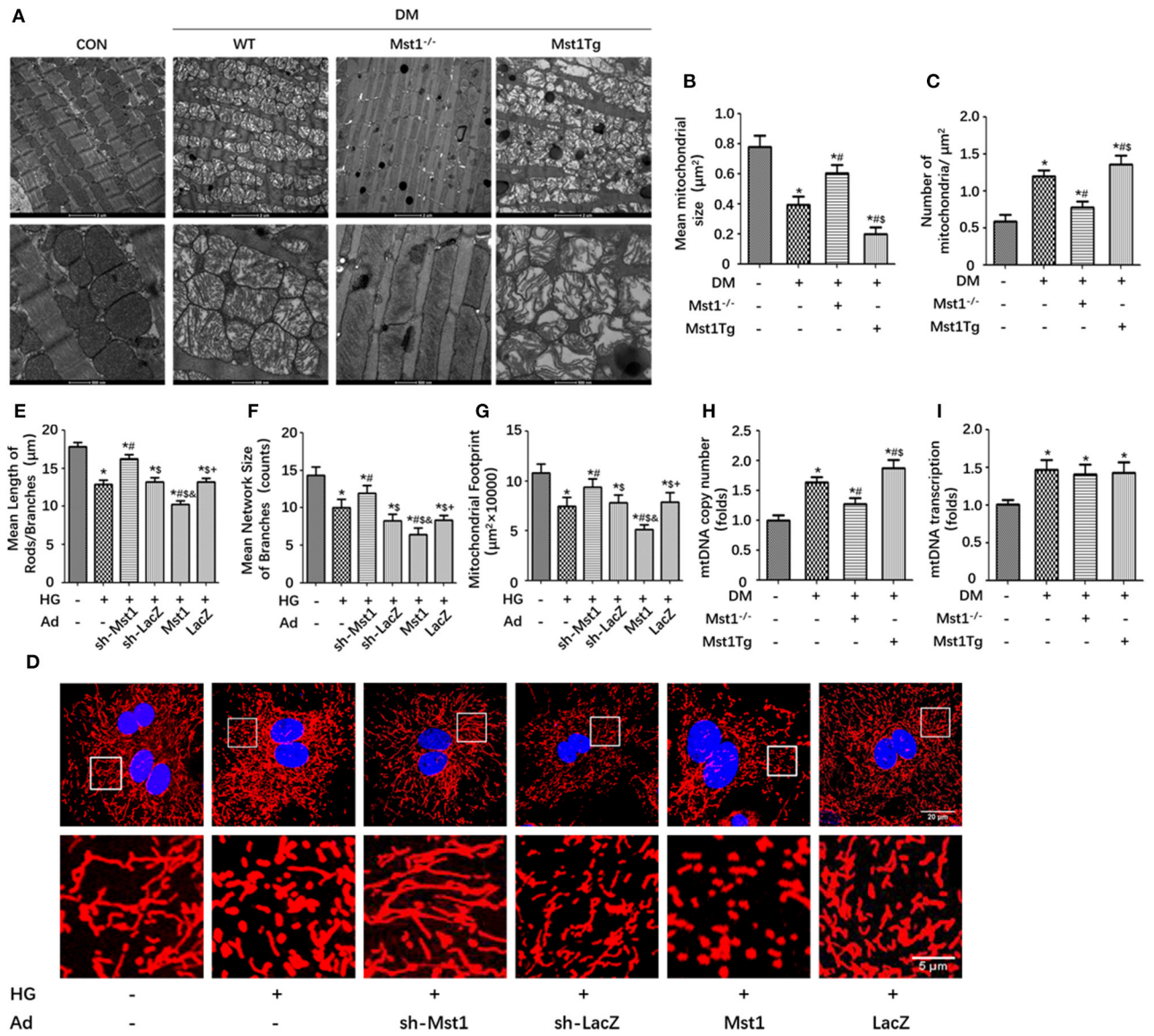

FIGURE 2 | Mst1 participates in the regulation of mitochondrial dynamics. **(A)** Representative images of typical damaged and different sized mitochondria (Scale bars: upper panel 2 μm, lower panel 500 nm). **(B)** Quantitative analysis of the mean mitochondrial size. **(C)** Quantitative analysis of the number of mitochondria per μm^2. The columns and error bars represent the means and SEM. *$P < 0.05$ vs. WT; #$P < 0.05$ vs. DM; \$$P < 0.05$ vs. DM +$Mst1^{-/-}$. **(D)** Representative images of mitochondria (MitoTracker Red) (Scale bars: upper panel 20 μm, lower panel 5 μm). **(E)** Quantitative analysis of the mean length of mitochondria rods/branches. **(F)** Quantitative analysis of the number of branches. **(G)** Quantitative analysis of the mitochondrial footprint. The columns and error bars represent the means and SEM. *$P < 0.05$ vs. Con; #$P < 0.05$ vs. HG; \$$P < 0.05$ vs. HG + Ad-sh-Mst1; and $P < 0.05$ vs. HG + Ad-sh-LacZ; and +$P < 0.05$ vs. HG + Ad-Mst1. **(H)** mtDNA copy number was assessed by complex IV segment. **(I)** The transcript level of mtDNA was assessed by NADH dehydrogenase subunit 1 (ND1). The columns and error bars represent the means and SEM. *$P < 0.05$ vs. WT; #$P < 0.05$ vs. DM; \$$P < 0.05$ vs. DM +$Mst1^{-/-}$.

protein, Mst1 overexpression increased, while Mst1 knockdown reduced both the mitochondrial and cytosolic expression of Drp1 (**Figures 5E–H**). These results indicated that Mst1 triggers mitochondrial fission by promoting Drp1 expression and translocation to the mitochondria under HG treatment.

Drp1 Knockdown Abolishes the Effects of Mst1 on Mitochondrial Membrane Potential and Mitochondrial Dysfunction

Mst1 knockdown increased the mitochondrial membrane potential ($\Delta\Psi m$) in HG treated cardiomyocytes as evidenced by JC-1 fluorescence imaging (**Figures 6A,B**). As expected,

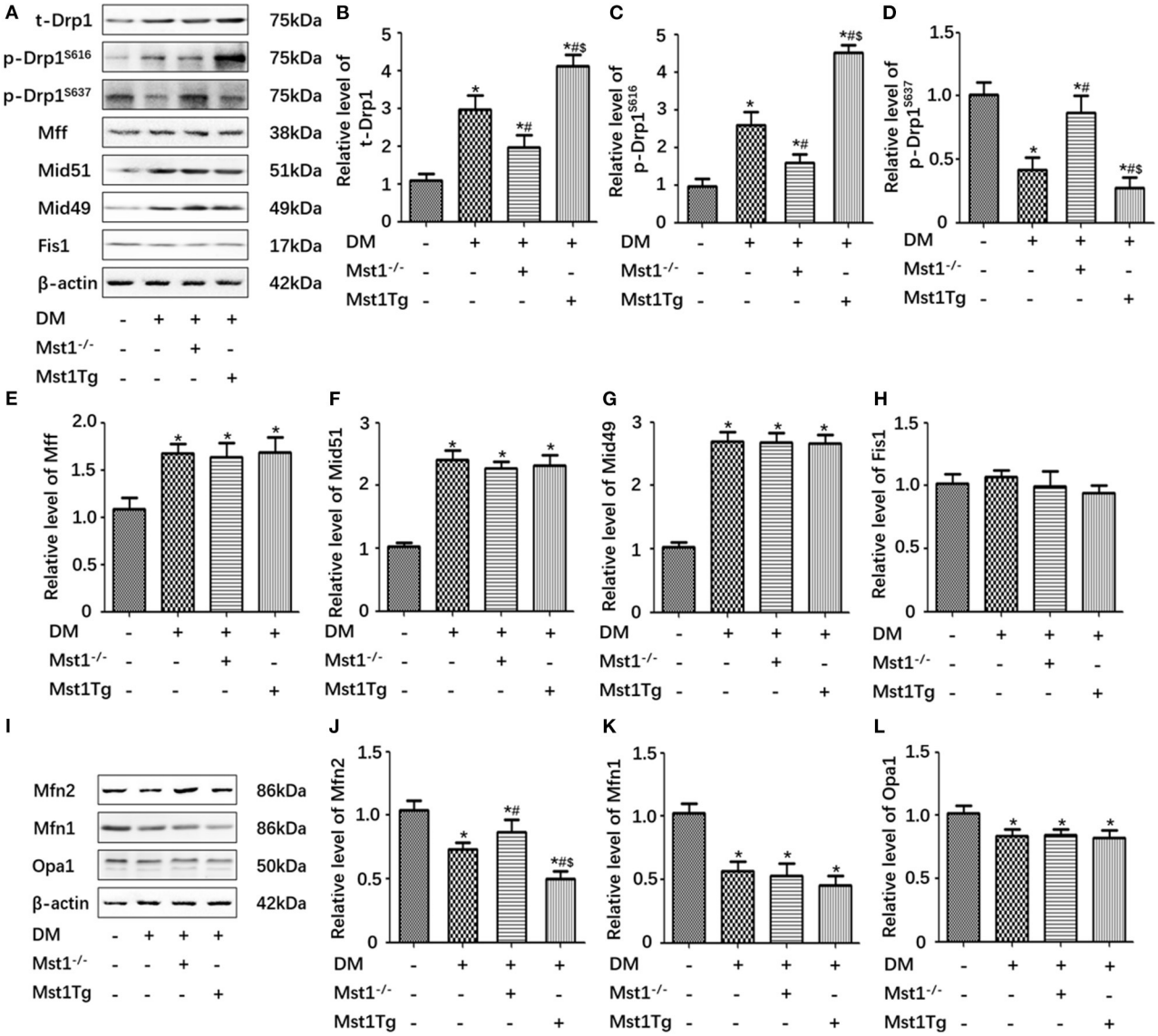

FIGURE 3 | Mst1 knockout decreases Drp1 expression, inhibits Drp1^{S616} phosphorylation and promotes Drp1^{S637} phosphorylation in DCM. **(A)** Protein expression with representative gel blots of t-Drp1, p-Drp1^{S616}, p-Drp1^{S637}, Mff, Mid51, Mid49, Fis1, and β-actin (loading control for Drp1, Mff, Mid51, Mid49 and Fis1). **(B)** Relative level of t-Drp1. **(C)** Relative level of p-Drp1^{S616}. **(D)** Relative level of p-Drp1^{S637}. **(E)** Relative level of Mff. **(F)** Relative level of Mid51. **(G)** Relative level of Mid49. **(H)** Relative level of Fis1. **(I)** Protein expression with representative gel blots of Mfn2, Mfn1, Opa1, and β-actin (loading control for Mfn2, Mfn1, Opa1). **(J)** Relative level of Mfn2. **(K)** Relative level of Mfn1. **(L)** Relative level of Opa1. The columns and error bars represent the means and SEM. *$P < 0.05$ vs. WT; #$P < 0.05$ vs. DM; and \$$P < 0.05$ vs. HG +Mst1$^{-/-}$.

Drp1 knockdown abolished the effects of Mst1 knockdown on mitochondrial membrane potential (**Figures 6A,B**). Mst1 knockdown significantly enhanced mitochondrial ATP content and CS activity in cardiomyocytes underwent HG treatment. Interestingly, Mst1 knockdown did not further increase ATP content or CS activity in cardiomyocytes subjected to Drp1 knockdown (**Figures 6C,D**). Similar results were observed on mitochondrial complex I (Cox I), complex II (Cox II) and complex V (Cox V) enzyme activity (**Figures 6E–G**). These results indicated that Mst1 aggravates mitochondrial functional injury in diabetic hearts via Drp1.

DISCUSSION

Diabetes mellitus describes a group of metabolic disorders characterized by hyperglycemia due to the absolute or relative insufficiency of insulin production or actions caused by a combination of genetic and environmental factors (Alam et al.,

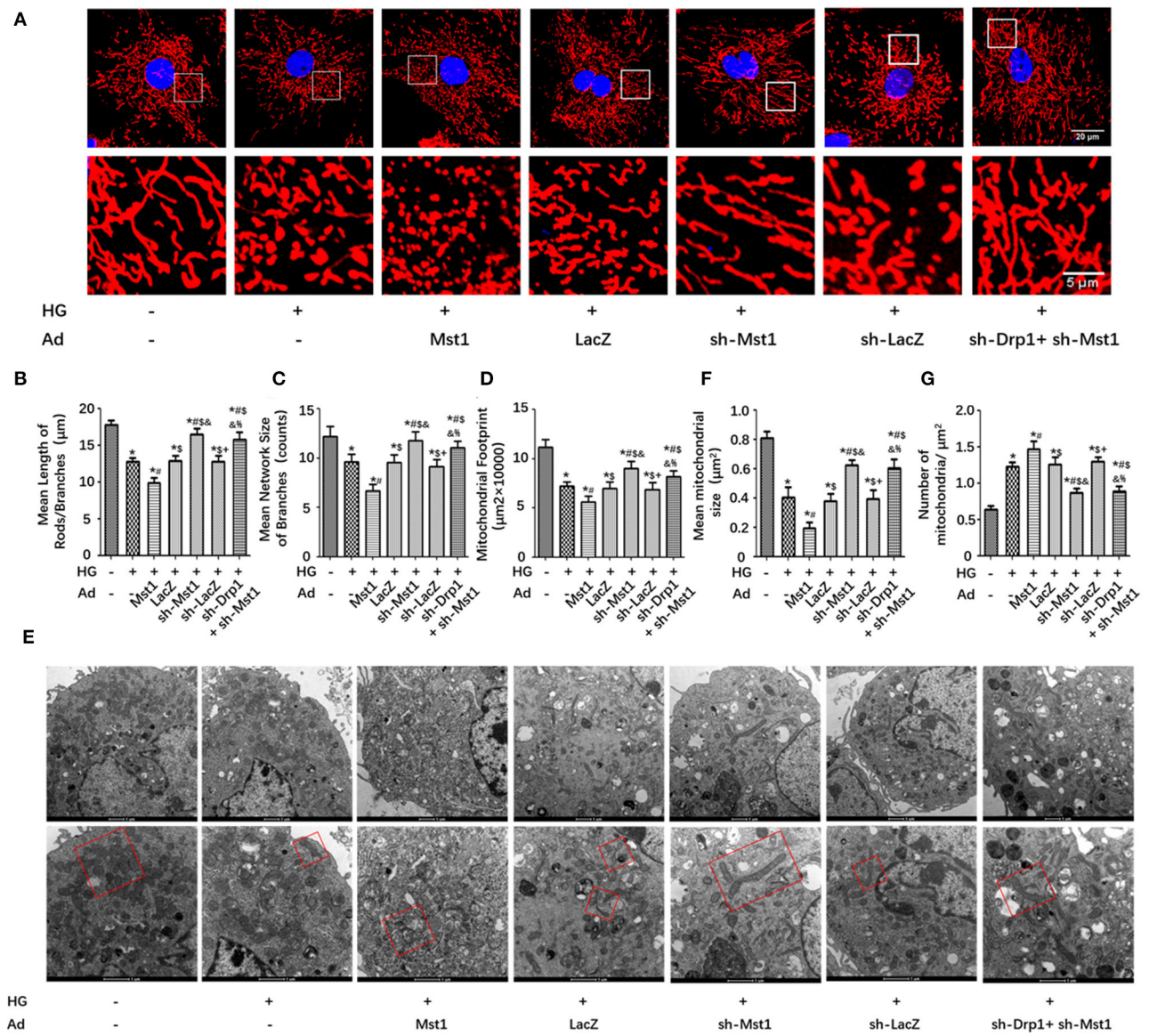

FIGURE 4 | Drp1 knockdown abolishes the effects of Mst1 on mitochondrial fission. **(A)** Representative images of mitochondria (MitoTracker Red) (Scale bars: upper panel 20 μm, lower panel 5 μm). **(B)** Quantitative analysis of the mean length of mitochondria rods/branches. **(C)** Quantitative analysis of the number of branches. **(D)** Quantitative analysis of the mitochondrial footprint. **(E)** Representative images of typical damaged and different sized mitochondria (Scale bars: upper panel 1 μm, lower panel 500 nm). **(F)** Quantitative analysis of the mean mitochondrial size. **(G)** Quantitative analysis of the number of mitochondria per μm^2. The columns and error bars represent the means and SEM. $^*P < 0.05$ vs. Con; $^{\#}P < 0.05$ vs. HG; $\$P < 0.05$ vs. HG + Ad-Mst1; and $P < 0.05$ vs. HG + Ad-LacZ; $+P < 0.05$ vs. HG + Ad-sh- Mst1; and $\%P < 0.05$ vs. HG + Ad-sh- LacZ.

2014; Harreiter and Roden, 2019). Diabetic patients have a higher risk of morbidity and mortality and more documented cases of cardiovascular complications than the general population (Henning, 2018). Diabetic cardiomyopathy (DCM) is manifested as abnormal cardiac structure and function in the absence of ischemic or hypertensive heart disease with diabetes that is due to cardiomyocytes being in a hyperglycemic environment for a long time (Vasquez-Trincado et al., 2016). However, the underlying molecular mechanism of diabetic cardiomyopathy remains unclear. Consistent with our previous study, the present project revealed that Mst1 aggravated the development of DCM (Zhang et al., 2016). Mst1 knockout significantly inhibited left ventricular remodeling, enhanced cardiac function, as well as decreased cardiomyocyte apoptosis in the diabetic heart.

Mitochondrial quality control includes post-translational modification (PTM) of mitochondrial proteins, mitochondrial dynamics (biogenesis, fission, and fusion) and mitochondrial autophagy (mitophagy) (Wu and Ren, 2006; Suliman and

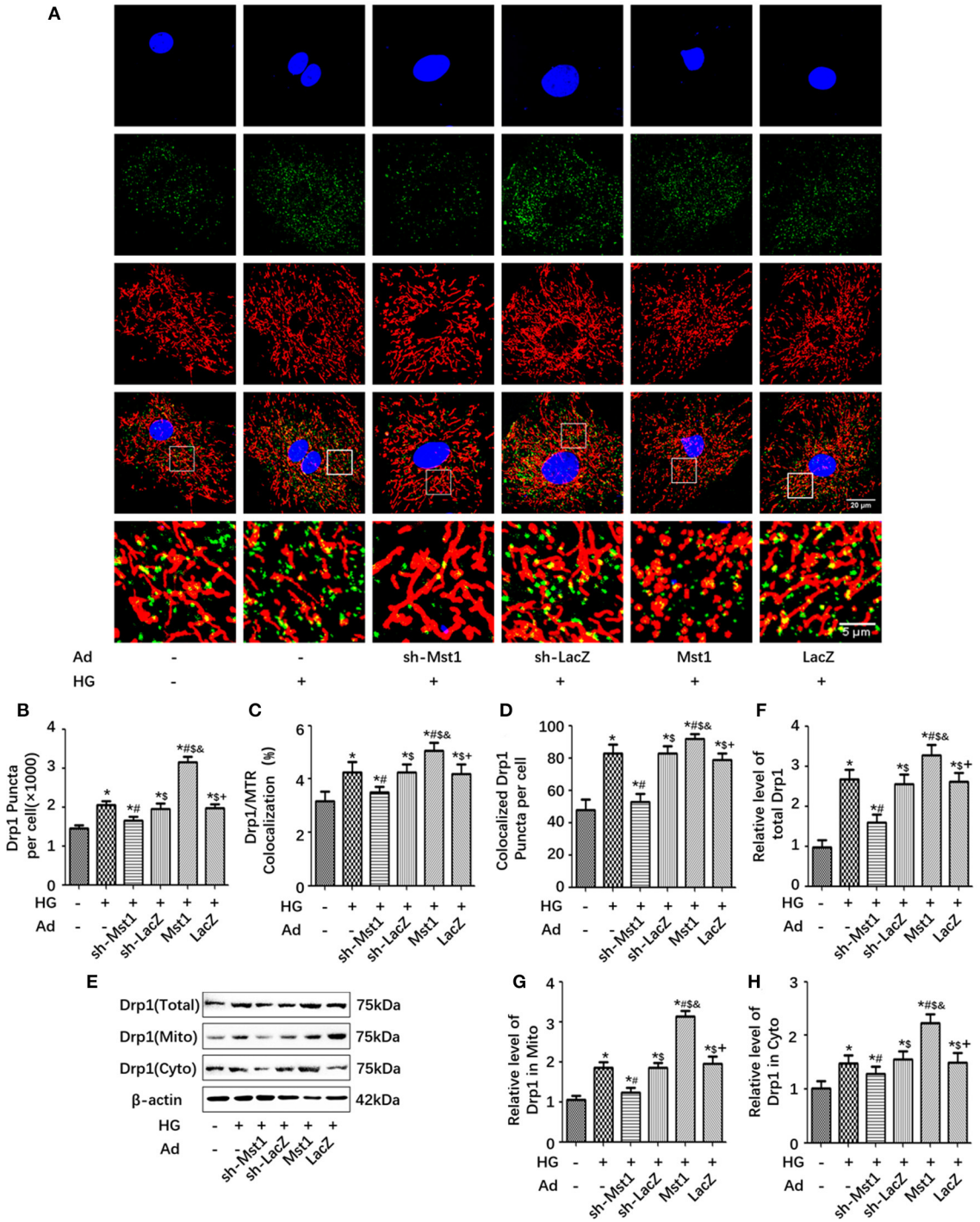

FIGURE 5 | Mst1 knockdown inhibits Drp1 recruitment to the mitochondria. **(A)** Representative colocalization images of Drp1 (Green) and mitochondria (MitoTracker Red) (Scale bars: upper four panels 20 μm, lower panel 5 μm). **(B)** Quantitative analysis of Drp1 puncta per cell. **(C)** Quantitative analysis of Drp1/ MitoTracker Red colocalization. **(D)** Quantitative analysis of colocalized Drp1 Puncta per cell. **(E)** Protein expression with representative gel blots of total Drp1, mitochondrial Drp1 and cytoplasmic Drp1. **(F)** Relative level of total Drp1 **(G)** Relative level of Drp1 in mitochondria. **(H)** Relative level of Drp1 in cytoplasm. The columns and error bars represent the means and SEM. $^{*}P < 0.05$ vs. Con; $^{\#}P < 0.05$ vs. HG; $\$P < 0.05$ vs. HG + Ad-sh-Mst1; and $P < 0.05$ vs. HG + Ad-sh-LacZ; and $+P < 0.05$ vs. HG + Ad-Mst1.

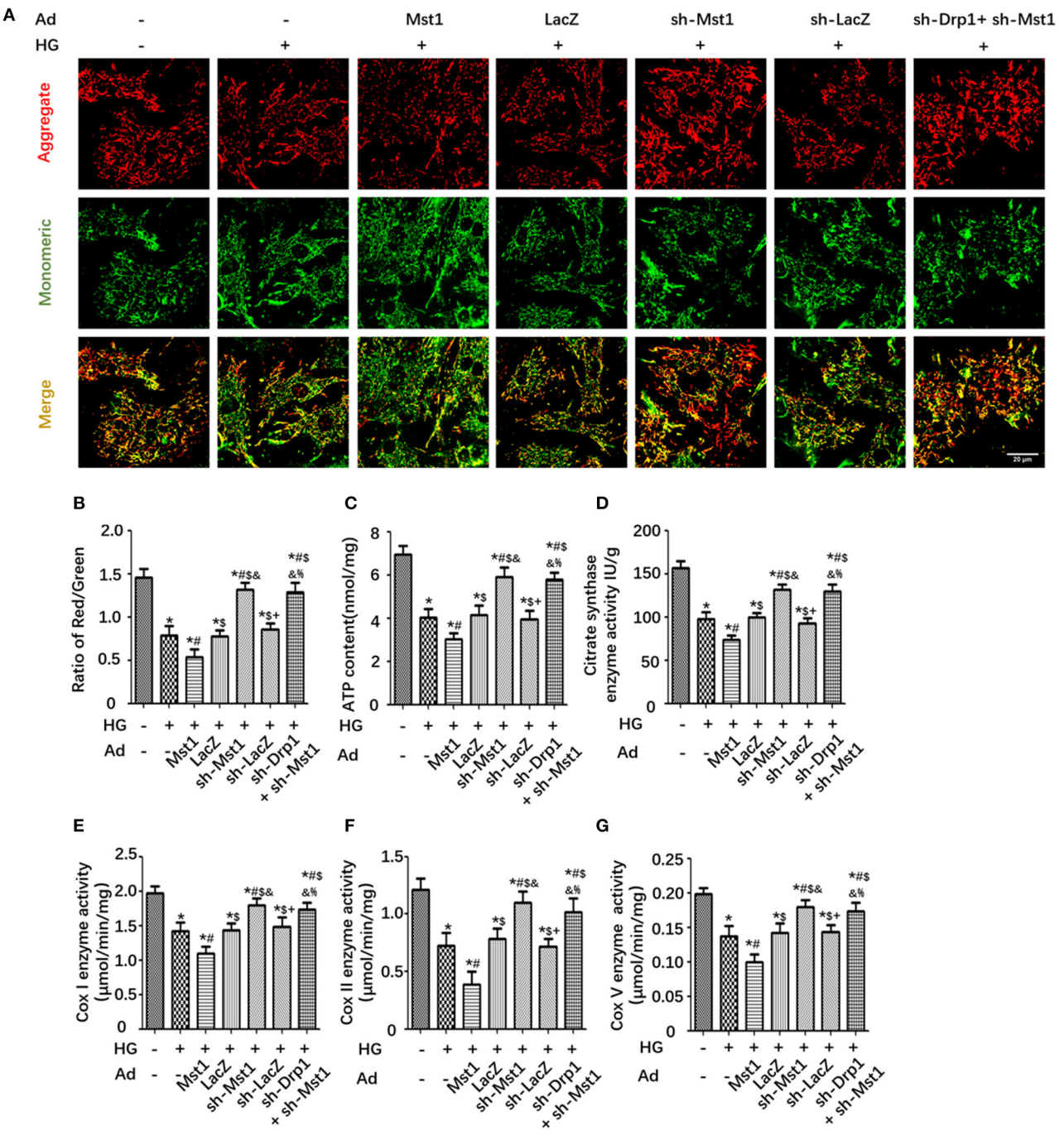

FIGURE 6 | Drp1 knockdown abolishes the effects of Mst1 on mitochondrial membrane potential and mitochondrial dysfunction. **(A)** Representative images of JC-1 fluorescence imaging (Scale bar: 20 μm). **(B)** The ratio of aggregated (Red)/monomeric (Green) JC-1. **(C)** Cellular ATP content. **(D)** Citrate synthase (CS) activity. **(E)** Analysis of Complex I activity (ELISA assay) in primary cardiomyocytes. **(F)** Analysis of Complex II activity (ELISA assay) in primary cardiomyocytes. **(G)** Analysis of Complex V activity (ELISA assay) in primary cardiomyocytes. The columns and error bars represent the means and SEM. $^{*}P < 0.05$ vs. Con; $^{\#}P < 0.05$ vs. HG; $\$P < 0.05$ vs. HG + Ad- Mst1; and $P < 0.05$ vs. HG + Ad-LacZ; $+P < 0.05$ vs. HG + Ad-sh- Mst1; and $\%P < 0.05$ vs. HG + Ad-sh- LacZ.

Piantadosi, 2016; Klimova et al., 2018; Pei et al., 2018). Our previous study demonstrated that Mst1 inhibits Sirt3 expression thus participates in the development of DCM by inhibiting cardiomyocyte mitophagy through inhibiting Parkin-dependent mitophagy (Wang et al., 2018a). Additionally, Mst1 has no effect on mitochondrial biogenesis, which was assessed by PGC-1α, NRF-1 and TFAM expression (Vega et al., 2015; Wang et al., 2018a). There is a large amount of evidence indicating that

mitochondrial fission participates in cardiac metabolic disease (Mishra and Chan, 2016). Here, our work mainly demonstrates that Mst1 is involved in the regulation of mitochondrial fission, which is a crucial factor for exacerbating the mitochondrial dysfunction and cardiac remodeling of DCM mice.

Mitochondrial fission begins with the recruitment of cytoplasmic Drp1 by the adaptor on the mitochondrial membrane protein (MFF, Fis1, and Mid49/51) (Pagliuso et al., 2018). Accumulating evidence indicates that exposure of neonatal cardiomyocytes to sustained, high levels of glucose (35 mm) increased mitochondrial fission, reduced mitochondrial membrane potential ($\Delta\Psi m$) and electron transport chain activity (Yu et al., 2011). Increased mitochondrial Drp1 translocation is a main mediator of mitochondrial fission and may serve as a therapeutic target against high glucose toxicity in DCM (Gawlowski et al., 2012). However, whether mitochondrial fission directly contributes to the cardiac dysfunction associated with diabetic cardiomyopathy is unknown. In the present study, we observed that Mst1 increased the expression and mitochondrial localization of Drp1. This finding indicates that Mst1 triggers mitochondrial fission by promoting Drp1 translocation to the mitochondria.

The effects of Drp1 on mitochondrial fission is regulated by the phosphorylation of two serine residues at the c-terminal guanosine triphosphatase (GTPase) effector domain of Drp1 (Fan et al., 2020). The phosphorylation of Drp1 at S616 activates mitochondrial fission. On the contrary, phosphorylation of Drp1 at S637 inhibits mitochondrial fission. Since Mst1 is a type of serine-threonine kinase comprising 487 amino acids. The present study thus investigated whether Mst1 regulated mitochondrial fission through Drp1 phosphorylation. Interestingly, Mst1 upregulated $Drp1^{S616}$ phosphorylation, inhibited $Drp1^{S637}$ phosphorylation, as well as promoting Drp1 recruitment to the mitochondria. Consistently, Drp1 knockdown eliminated the role of Mst1 knockdown on the mean size of mitochondria and the number of mitochondria as evaluated by transmission electron microscopy. There results further demonstrated that Mst1 is a crucial factor for exacerbating mitochondrial fission and dysfunction by coordinately mediates the phosphorylation of Drp1.

Mfn1 and Mfn2 are well-known mediators of the mitochondrial outer membrane fusion, while Opa1 mediates the fusion of the inner mitochondria membrane (Yang, 2015). It is possible to exchange the contents of two mitochondria so that the defective mitochondrion can regain the necessary components of the respiratory chain and mitochondrial DNA (Wai and Langer, 2016). The crossing and complementation of mitochondrial DNA molecules can also prevent the accumulation of mitochondrial DNA mutations (Chen et al., 2005). In the circumstances of emergency and hunger, mitochondria fuse to meet energy requirements, and the sharing of matrix metabolites maximizes the metabolic efficiency (Mishra and Chan, 2016). Mfn2 is a key protein in mitochondrial morphology (Chandhok et al., 2018; Yu et al., 2018). In the present study, Mst1 also decreased the expression of Mfn2. However, the concrete mechanism of Mfn2 regulation exerted by Mst1 still needs further investigation.

With the progression of diabetic cardiomyopathy, high glucose eventually induces cardiac hypertrophy, fibrosis, increased stiffness and cardiomyocyte loss (Tan et al., 2020). Our previous study indicated that downregulation of Mst1 alleviates cardiac fibrosis but has no effect on cardiac hypertrophy in db/db mice (Xiong et al., 2020). Mst1 serves as an important regulator of the cardiovascular system, playing a unique role in cardiomyocytes, cardiac stem cells/progenitor cells, macrophages, endothelial cells and fibroblasts (Wang et al., 2016; Cheng et al., 2018; Xiong et al., 2020). Mst1 signal pathways are involved in many cardiovascular diseases, including atherosclerosis, myocardial ischemic injury and cardiomyopathy (Yang et al., 2018). Interestingly, the new finding that Mst1 is involved in the regulation of mitochondrial dynamics suggests a possible mechanism in the pathological progression of DCM. Identifying such molecular pathways that control Drp1 alterations in DCM might recover the net balance of continual fission and fusion and provide a new direction for the diagnosis and treatment of DCM.

CONCLUSION

We can conclude from this study that Mst1 aggravates mitochondrial fission, impairs mitochondrial energy metabolism and function, and aggravates cardiac dysfunction in DCM. Whether intervention in mitochondrial dynamics can reverse this damage might warrant further research efforts.

DATA AVAILABILITY STATEMENT

The original contributions presented in the study are included in the article/supplementary materials, further inquiries can be directed to the corresponding authors.

ETHICS STATEMENT

The animal study was reviewed and approved by the Institutional Animal Care in the Xi'an International Medical Center.

AUTHOR CONTRIBUTIONS

DS, HW, and ZZ contributed to conception and design of the study, performed all the experiments, and wrote the manuscript. XF, SW, XY, JL, WM, YD, and YZ performed all cell and animal experiments and collected research data, contributed to analysis and interpretation of data. All authors read and approved the final manuscript.

FUNDING

This work was supported by the National Natural Science Foundation of China (No. 81922008, No. 82070398, No. 81770224), National key research and development plan (2018YFA0107400) and Special support plan of Shaanxi Province.

REFERENCES

Adeva-Andany, M. M., Martinez-Rodriguez, J., Gonzalez-Lucan, M., Fernandez-Fernandez, C., and Castro-Quintela, E. (2019). Insulin resistance is a cardiovascular risk factor in humans. *Diabetes Metab. Syndr.* 13, 1449–1455. doi: 10.1016/j.dsx.2019.02.023

Alam, U., Asghar, O., Azmi, S., and Malik, R. A. (2014). General aspects of diabetes mellitus. *Handb. Clin. Neurol.* 126, 211–222. doi: 10.1016/B978-0-444-53480-4.00015-1

Chandhok, G., Lazarou, M., and Neumann, B. (2018). Structure, function, and regulation of mitofusin-2 in health and disease. *Biol. Rev. Camb. Philos. Soc.* 93, 933–949. doi: 10.1111/brv.12378

Chen, H., Chomyn, A., and Chan, D. C. (2005). Disruption of fusion results in mitochondrial heterogeneity and dysfunction. *J. Biol. Chem.* 280, 26185–26192. doi: 10.1074/jbc.M503062200

Cheng, Z., Zhang, M., Hu, J., Lin, J., Feng, X., Wang, S., et al. (2018). Mst1 knockout enhances cardiomyocyte autophagic flux to alleviate angiotensin II-induced cardiac injury independent of angiotensin II receptors. *J. Mol. Cell. Cardiol.* 125, 117–128. doi: 10.1016/j.yjmcc.2018.08.028

Ehler, E., Moore-Morris, T., and Lange, S. (2013). Isolation and culture of neonatal mouse cardiomyocytes. *J. Vis. Exp.* 79:50154. doi: 10.3791/50154

Fan, H., He, Z., Huang, H., Zhuang, H., Liu, H., Liu, X., et al. (2020). Mitochondrial quality control in cardiomyocytes: a critical role in the progression of cardiovascular diseases. *Front. Physiol.* 11:252. doi: 10.3389/fphys.2020.00252

Galloway, C. A., and Yoon, Y. (2015). Mitochondrial dynamics in diabetic cardiomyopathy. *Antioxid. Redox Signal.* 22, 1545–1562. doi: 10.1089/ars.2015.6293

Gawlowski, T., Suarez, J., Scott, B., Torres-Gonzalez, M., Wang, H., Schwappacher, R., et al. (2012). Modulation of dynamin-related protein 1 (DRP1) function by increased O-linked-beta-N-acetylglucosamine modification (O-GlcNAc) in cardiac myocytes. *J. Biol. Chem.* 287, 30024–30034. doi: 10.1074/jbc.M112.390682

Harreiter, J., and Roden, M. (2019). Diabetes mellitus-Definition, classification, diagnosis, screening and prevention (Update 2019). *Wien Klin Wochenschr* 131(Suppl. 1), 6–15. doi: 10.1007/s00508-019-1450-4

Henning, R. J. (2018). Type-2 diabetes mellitus and cardiovascular disease. *Future Cardiol.* 14, 491–509. doi: 10.2217/fca-2018-0045

Hu, J., Zhang, L., Zhao, Z., Zhang, M., Lin, J., Wang, J., et al. (2017). OSM mitigates post-infarction cardiac remodeling and dysfunction by up-regulating autophagy through Mst1 suppression. *Biochim. Biophys. Acta* 1863, 1951–1961. doi: 10.1016/j.bbadis.2016.11.004

Klimova, N., Long, A., and Kristian, T. (2018). Significance of mitochondrial protein post-translational modifications in pathophysiology of brain injury. *Transl. Stroke Res.* 9, 223–237. doi: 10.1007/s12975-017-0569-8

Mattie, S., Krols, M., and McBride, H. M. (2019). The enigma of an interconnected mitochondrial reticulum: new insights into mitochondrial fusion. *Curr. Opin. Cell Biol.* 59, 159–166. doi: 10.1016/j.ceb.2019.05.004

Mishra, P., and Chan, D. C. (2016). Metabolic regulation of mitochondrial dynamics. *J. Cell Biol.* 212, 379–387. doi: 10.1083/jcb.201511036

Ogurtsova, K., Da, R. F. J., Huang, Y., Linnenkamp, U., Guariguata, L., Cho, N. H., et al. (2017). IDF diabetes atlas: global estimates for the prevalence of diabetes for 2015 and 2040. *Diabetes Res. Clin. Pract.* 128, 40–50. doi: 10.1016/j.diabres.2017.03.024

Otera, H., Ishihara, N., and Mihara, K. (2013). New insights into the function and regulation of mitochondrial fission. *Biochim. Biophys. Acta* 1833, 1256–1268. doi: 10.1016/j.bbamcr.2013.02.002

Pagliuso, A., Cossart, P., and Stavru, F. (2018). The ever-growing complexity of the mitochondrial fission machinery. *Cell. Mol. Life Sci.* 75, 355–374. doi: 10.1007/s00018-017-2603-0

Pei, Z., Deng, Q., Babcock, S. A., He, E. Y., Ren, J., and Zhang, Y. (2018). Inhibition of advanced glycation endproduct (AGE) rescues against streptozotocin-induced diabetic cardiomyopathy: role of autophagy and ER stress. *Toxicol. Lett.* 284, 10–20. doi: 10.1016/j.toxlet.2017.11.018

Rubler, S., Dlugash, J., Yuceoglu, Y. Z., Kumral, T., Branwood, A. W., and Grishman, A. (1972). New type of cardiomyopathy associated with diabetic glomerulosclerosis. *Am. J. Cardiol.* 30:595. doi: 10.1016/0002-9149(72)90595-4

Smirnova, E., Griparic, L., Shurland, D. L., and van der Bliek, A. M. (2001). Dynamin-related protein Drp1 is required for mitochondrial division in mammalian cells. *Mol. Biol. Cell.* 12, 2245–2256. doi: 10.1091/mbc.12.8.2245

Suliman, H. B., and Piantadosi, C. A. (2016). Mitochondrial quality control as a therapeutic target. *Pharmacol. Rev.* 68, 20–48. doi: 10.1124/pr.115.011502

Tan, Y., Zhang, Z., Zheng, C., Wintergerst, K. A., Keller, B. B., and Cai, L. (2020). Mechanisms of diabetic cardiomyopathy and potential therapeutic strategies: preclinical and clinical evidence. *Nat. Rev. Cardiol.* 17, 585–607. doi: 10.1038/s41569-020-0339-2

Valente, A. J., Maddalena, L. A., Robb, E. L., Moradi, F., and Stuart, J. A. (2017). A simple ImageJ macro tool for analyzing mitochondrial network morphology in mammalian cell culture. *Acta Histochem.* 119, 315–326. doi: 10.1016/j.acthis.2017.03.001

van der Bliek, A. M., Shen, Q., and Kawajiri, S. (2013). Mechanisms of mitochondrial fission and fusion. *Csh Perspect. Biol.* 5:a11072. doi: 10.1101/cshperspect.a011072

Vasquez-Trincado, C., Garcia-Carvajal, I., Pennanen, C., Parra, V., Hill, J. A., Rothermel, B. A., et al. (2016). Mitochondrial dynamics, mitophagy and cardiovascular disease. *J. Physiol.* 594, 509–525. doi: 10.1113/JP271301

Vega, R. B., Horton, J. L., and Kelly, D. P. (2015). Maintaining ancient organelles: mitochondrial biogenesis and maturation. *Circ. Res* 116, 1820–1834. doi: 10.1161/CIRCRESAHA.116.305420

Wai, T., and Langer, T. (2016). Mitochondrial dynamics and metabolic regulation. *Trends Endocrinol. Metab.* 27, 105–117. doi: 10.1016/j.tem.2015.12.001

Wang, S., Fan, Y., Feng, X., Sun, C., Shi, Z., Li, T., et al. (2018a). Nicorandil alleviates myocardial injury and post-infarction cardiac remodeling by inhibiting Mst1. *Biochem. Biophys. Res. Commun.* 495, 292–299. doi: 10.1016/j.bbrc.2017.11.041

Wang, S., Zhao, Z., Fan, Y., Zhang, M., Feng, X., Lin, J., et al. (2018b). Mst1 inhibits Sirt3 expression and contributes to diabetic cardiomyopathy through inhibiting parkin-dependent mitophagy. *Biochim. Biophys. Acta Mol. Basis Dis.* 1865, 1905–1914. doi: 10.1016/j.bbadis.2018.04.009

Wang, T., Zhang, L., Hu, J., Duan, Y., Zhang, M., Lin, J., et al. (2016). Mst1 participates in the atherosclerosis progression through macrophage autophagy inhibition and macrophage apoptosis enhancement. *J. Mol. Cell. Cardiol.* 98, 108–116. doi: 10.1016/j.yjmcc.2016.08.002

Williams, M., and Caino, M. C. (2018). Mitochondrial dynamics in type 2 diabetes and cancer. *Front. Endocrinol.* 9:211. doi: 10.3389/fendo.2018.00211

Wu, S., and Ren, J. (2006). Benfotiamine alleviates diabetes-induced cerebral oxidative damage independent of advanced glycation end-product, tissue factor and TNF-alpha. *Neurosci. Lett.* 394, 158–162. doi: 10.1016/j.neulet.2005.10.022

Xiong, Z., Li, Y., Zhao, Z., Zhang, Y., Man, W., Lin, J., et al. (2020). Mst1 knockdown alleviates cardiac lipotoxicity and inhibits the development of diabetic cardiomyopathy in db/db mice. *Biochim Biophys Acta Mol. Basis Dis.* 1866:165806. doi: 10.1016/j.bbadis.2020.165806

Yang, W. Y. (2015). Optogenetic probing of mitochondrial damage responses. *Ann. N. Y. Acad. Sci.* 1350, 48–51. doi: 10.1111/nyas.12818

Yang, Y., Wang, H., Ma, Z., Hu, W., and Sun, D. (2018). Understanding the role of mammalian sterile 20-like kinase 1 (MST1) in cardiovascular disorders. *J. Mol. Cell. Cardiol.* 114, 141–149. doi: 10.1016/j.yjmcc.2017.11.010

Yu, F., Xu, T., Wang, M., Chang, W., Li, P., and Wang, J. (2018). Function and regulation of mitofusin 2 in cardiovascular physiology and pathology. *Eur. J. Cell Biol.* 97, 474–482. doi: 10.1016/j.ejcb.2018.07.003

Yu, T., Jhun, B. S., and Yoon, Y. (2011). High-glucose stimulation increases reactive oxygen species production through the calcium and mitogen-activated protein kinase-mediated activation of mitochondrial fission. *Antioxid. Redox Signal.* 14, 425–437. doi: 10.1089/ars.2010.3284

Yu, T., Robotham, J. L., and Yoon, Y. (2006). Increased production of reactive oxygen species in hyperglycemic conditions requires dynamic change of mitochondrial morphology. *Proc. Natl. Acad. Sci. U.S.A.* 103, 2653–2658. doi: 10.1073/pnas.0511154103

Zhang, M., Zhang, L., Hu, J., Lin, J., Wang, T., Duan, Y., et al. (2016). MST1 coordinately regulates autophagy and apoptosis in diabetic cardiomyopathy in mice. *Diabetologia* 59, 2435–2447. doi: 10.1007/s00125-016-4070-9

Conflict of Interest: The authors declare that the research was conducted in the absence of any commercial or financial relationships that could be construed as a potential conflict of interest.

frontiers in Cell and Developmental Biology

REVIEW
published: 21 January 2021
doi: 10.3389/fcell.2020.625089

Mechanotranduction Pathways in the Regulation of Mitochondrial Homeostasis in Cardiomyocytes

Hongyu Liao[1†], *Yan Qi*[2†], *Yida Ye*[2†], *Peng Yue*[1†], *Donghui Zhang*[2*] *and Yifei Li*[1*]

[1] *Key Laboratory of Birth Defects and Related Diseases of Women and Children of Ministry of Education, Department of Pediatrics, West China Second University Hospital, Sichuan University, Chengdu, China,* [2] *State Key Laboratory of Biocatalysis and Enzyme Engineering, School of Life Science, Hubei University, Wuhan, China*

Mitochondria are one of the most important organelles in cardiomyocytes. Mitochondrial homeostasis is necessary for the maintenance of normal heart function. Mitochondria perform four major biological processes in cardiomyocytes: mitochondrial dynamics, metabolic regulation, Ca^{2+} handling, and redox generation. Additionally, the cardiovascular system is quite sensitive in responding to changes in mechanical stress from internal and external environments. Several mechanotransduction pathways are involved in regulating the physiological and pathophysiological status of cardiomyocytes. Typically, the extracellular matrix generates a stress-loading gradient, which can be sensed by sensors located in cellular membranes, including biophysical and biochemical sensors. In subsequent stages, stress stimulation would regulate the transcription of mitochondrial related genes through intracellular transduction pathways. Emerging evidence reveals that mechanotransduction pathways have greatly impacted the regulation of mitochondrial homeostasis. Excessive mechanical stress loading contributes to impairing mitochondrial function, leading to cardiac disorder. Therefore, the concept of restoring mitochondrial function by shutting down the excessive mechanotransduction pathways is a promising therapeutic strategy for cardiovascular diseases. Recently, viral and non-viral protocols have shown potentials in application of gene therapy. This review examines the biological process of mechanotransduction pathways in regulating mitochondrial function in response to mechanical stress during the development of cardiomyopathy and heart failure. We also summarize gene therapy delivery protocols to explore treatments based on mechanical stress–induced mitochondrial dysfunction, to provide new integrative insights into cardiovascular diseases.

Keywords: mechanotransduction pathway, heart development, cardiac maturation, mitochondrial homeostasis, mitochondrial disorder

OPEN ACCESS

Edited by:
Xiaoqiang Tang,
Sichuan University, China

Reviewed by:
Jia-Hua Qu,
National Institutes of Health (NIH), United States
Ding-Sheng Jiang,
Huazhong University of Science and Technology, China

***Correspondence:**
Donghui Zhang
dongh.zhang@hubu.edu.cn
Yifei Li
liyfwcsh@scu.edu.cn

[†]These authors have contributed equally to this work and share first authorship

Specialty section:
This article was submitted to Cellular Biochemistry, a section of the journal Frontiers in Cell and Developmental Biology

Received: *02 November 2020*
Accepted: *27 November 2020*
Published: *21 January 2021*

Citation:
Liao H, Qi Y, Ye Y, Yue P, Zhang D and Li Y (2021) Mechanotranduction Pathways in the Regulation of Mitochondrial Homeostasis in Cardiomyocytes. Front. Cell Dev. Biol. 8:625089. doi: 10.3389/fcell.2020.625089

INTRODUCTION

The heart is an electromechanical organ that needs to beat thousands of times a day to provide enough blood supplement to the body (Saucerman et al., 2019). Cardiomyocytes (CMs) are subjected to chronic physiological hemodynamics, chamber pressure, tissue shape, and contractile stretch alterations (Barki-Harrington and Rockman, 2003; Linari et al., 2015; Lorenz et al., 2018).

The Frank–Starling law and the Anrep effect describe the exquisite intrinsic mechanisms used by the heart to autoregulate contractile forces to maintain cardiac output under pre-load and afterload (Bluhm et al., 1998; Ait-Mou et al., 2016; Ruan et al., 2016). Throughout heart development, mechanical stress is essential for normal CM proliferation and differentiation during specification and morphogenesis (Miller et al., 2000; Clause et al., 2009; Banerjee et al., 2015). The heart follows a specific course of maturation, which begins from the very first heartbeat after birth, under hyperoxygenated conditions, and leads to the establishment of adult myocardial morphology (Guo and Pu, 2020). During heart development, there are dramatic adaptation switches involving gene expressions and the environment, including rapidly elevated circulating pressure. These changes require the maturation of CMs, which encode the physiological hypertrophy phenomenon (Gholipour and Tabrizi, 2020; Wang L. et al., 2020; Xiang et al., 2020). Following this, optimal levels of mechanical stress are involved in maintaining biological hemostasis and pathological maladaptation occurring in intracellular and extracellular matrix (ECM) remodeling (Kresh and Chopra, 2011; Collins et al., 2014; Dogan et al., 2016; Sessions et al., 2017).

In eukaryotic cells, mitochondria are involved in a large array of metabolic and bioenergetic processes that are vital for cell survival (Kaasik et al., 2004; Brown et al., 2010; Caffarra Malvezzi et al., 2020; Lyra-Leite et al., 2020). Within CMs, mitochondria are one of the most important organelles. Mitochondria are involved in almost all the major biological process of CMs, including supporting cellular morphology, ATP production through the electron transport chain (ETC), regulation of intracellular calcium ion signaling, and balance of reactive oxygen species (ROS) levels (Huss and Kelly, 2005; Koo and Guan, 2018; Fernandez-Caggiano et al., 2020). The mitochondria occupy a large fraction of CM cell volume (35–40%) and supply more than 90% energy of the cells' energy requirements. Over the last decade, we have seen an explosion in our knowledge of the role of mitochondrial dysfunction in human pathologies. This has led to the realization that mitochondria are important for all cell types and are especially important in energy-intensive cells including those of the skeletal and muscle, heart muscle, and neuronal cells. Emerging evidence indicates that mechanotransduction pathways greatly impact the regulation of mitochondrial homeostasis (Iribe et al., 2017). Excessive mechanical stress loading contributes to alterations in mitochondrial homeostasis, leading to cardiac dysfunction (Koo and Guan, 2018). The concept of restoring mitochondrial function by shutting down mechanotransduction pathways presents a potential therapeutic strategy for cardiovascular diseases. Recently, viral and non-viral protocols have shown great promise in regulating gene expression in CMs, highlighting the potential of these cells for gene therapy (Chen et al., 2016; Bezzerides et al., 2019; Wang S. et al., 2020). Herein, this review will highlight the biological processes of mechanotransduction pathways that respond to mechanical stress in CM dysfunction by regulating mitochondrial function.

BIOLOGICAL FUNCTION OF MECHANICAL STRESS IN CMS

Heart development involves (1) specification of cardiac progenitor cells, (2) formation of the linear heart tube, (3) cardiac looping, and (4) formation of the cardiac valve to form a mature beating heart. Normal mechanical stimulation is essential to maintain the normal physiological processes of CMs, including proliferation, differentiation, and maturation. Generally, there are three types of mechanical loading approaches to CMs, including shear stress, cyclic strain, and static stretching. Shear stress is generated by friction at the interface between the blood and the endocardium in the same direction as the blood flow (Lee J. M. et al., 2016). Cyclic strain is referred to the complex tensile and compressive strains with every heartbeat according to systolic and diastolic rhythm (Salameh et al., 2010). Static stretching should be considered as the compressive mechanical loading due to the blood pressure (Saucerman et al., 2019).

The physiological processes of CMs start at the beginning of mesoderm progenitor cell movements. These movements are initiated by a variety of morphogenic signals, including bone morphogenic protein (BMP), through the Wnt/activin/nodal pathway (Pandur, 2005; Murry and Keller, 2008; Ye et al., 2011), Gata-4 (Pu et al., 2004; Zeisberg et al., 2005; He et al., 2014; Akerberg et al., 2019), and the Hedgehog family (Mammoto and Ingber, 2010). Optimal stress force contributes to the maintenance of pluripotency through *Oct-4* expression (Fok and Zandstra, 2005; Earls et al., 2013). More recently, human induced pluripotent stem cells (iPSCs) have been successfully maintained at 6.4 dyn/cm^2 for up to 32 days, with high levels of Oct4, Nanog, and alkaline phosphatase activity (Shafa et al., 2012). The two dominant types of stress during cardiogenesis are fluid shear stress and cyclic strain (Majkut et al., 2014). Even in the early stage of heart development during embryogenesis, influx and efflux of sodium and calcium trigger contractions while tube formation, indicating cyclic strain properties, is occurring (Sylva et al., 2014; Tyser et al., 2016). These are then followed by blood flow–induced pressure and shear stress. The functions of shear stress have been well-documented in endothelial cells. However, the role of shear stress during large parts of cardiomyogenesis remains unknown. In the embryonic stem cell model, *Mef2c* expression was induced under 10 dyn/cm^2 shear stress (Kudo et al., 2000). Other studies indicate that the contributions of CMs, beyond endothelial cellular function, are very limited. Cyclic strain also maintains pluripotency in human embryonic stem cells and initiates the expression of key genes including *NOS-3*, *ET-1*, and *KLF-2* (Groenendijk et al., 2004). These genes regulate the differentiation of cardiac progenitors and illustrate the association between regions of increased differentiation and higher expression levels. Subjecting mouse embryonic CMs to cyclic stretch using an *in vitro* platform revealed that transforming growth factor β (TGF-β) plays a repressive role under these conditions (Banerjee et al., 2015). TGF-β is involved in the formation of hypoplasia of left heart syndrome via SMAD3 (Zeigler et al., 2016). Day 6 mouse embryoid bodies, exposed to 5–10% mechanical strain, have

significantly increased levels of connexin 43 (Cx43) and Nkx2.5 expression (Schmelter et al., 2006; Gwak et al., 2008). Therefore, shear stress has important consequences in vascular network building and might be essential for the developing vasculature, whereas cyclic strain is critical for cardiomyogenesis.

Mechanical stimuli are involved in cellular physical structure formation from the membrane to nucleus. The ECM and cell–cell interaction allow intracellular connections to grow between the nuclear membrane and lamina (Jongsma and Wilders, 2000; Boukens et al., 2009; Delmar and McKenna, 2010). This contributes to isoform switching from lamin-B2 to lamin-A and controls the nucleocytoplasmic shunting of MKL1, a critical factor for cardiac functional maturation (Guo and Zheng, 2013, 2015; Ho et al., 2013; Guo et al., 2014). Cell–cell interaction between CMs involves the desmosome and adherens junction (Austin et al., 2019). This interaction includes *PKP2* (encoding plakophilin 2), *DSG2* (encoding desmoglein 2), *DSC2* (encoding desmocollin 2), *JUP* (junction plakoglobin), and *DSP* (desmoplakin) for desmosome formation and *CDH2* (encoding cadherin 2, also known as N-cadherin) and *CTNNA3* (encoding catenin-α3) for adherens junction formation (van Tintelen and Hauer, 2009; Sato et al., 2011; Saguner et al., 2013; Moncayo-Arlandi and Brugada, 2017; Austin et al., 2019; Kim et al., 2019; Xia et al., 2020). Importantly, mitochondria bind to microtubules and are affected by changes in their mechanotransmission. Ca^{2+} release by mitochondria is the first thing observed under mechanical stress. Iribe et al. demonstrated that stretch caused activation of the respiratory chain to hyperpolarize $\Delta\psi m$, followed by NADPH oxidase (NOX) activation, and increased ROS production (Iribe et al., 2017). Mechanical stress also controls mitochondrial fission and fusion, contributing to the post-natal maturation of mitochondria.

Mechanical stress is generated by circulating pressure and myocardium contraction, but is also related to ECM stiffness (Collins et al., 2014; Chiou et al., 2016; Herum et al., 2017). Moreover, cyclic strain helps to build a normal ECM around CMs by modulating fibroblasts (Saucerman et al., 2019). *In vivo*, paracrine signaling molecules are stimulated by mechanical stress and by targeting cardiac fibroblasts proliferation rates. The heart gradually grows larger and more functional as the body develops and matures (Guo and Pu, 2020). After the proliferation period, only a limited number of CMs have the ability to regenerate, and heart enlargement primarily occurs through CM hypertrophy. To maintain cardiac function and meet the mechanical demands of adapting to tissue stresses due to pressure or volume overload, CMs grow in size by elongating and making the myocardial wall thicker, which is a part of the maturation phase. In addition to shear stress and cyclic strain, static stretching becomes a dominant factor during the maturation phase (Aragona et al., 2013; Hirt et al., 2014; Karbassi et al., 2020). Hypertrophy is achieved by increasing cell volume and polarity and by the arrangement of contractile protein content and mitochondria. Additionally, mechanical loads affect the cytoskeleton or sarcomere to regulate cell shape and arrangement. Cardiac contractile force regulates the distribution of the vinculin (VCL) cytoskeletal protein and activates slingshot protein phosphatase 1 and the CFL actin depolymerizing factor to promote myofilament maturation via F-actin rearrangement (Guo and Pu, 2020). Recent studies showed that CMs from neonatal rats seeded on a collagen (Col)-coated PA gel matrix had an elastic modulus equal to 10 kPa, showing perfect morphological structure (Jacot et al., 2010). However, the sarcomeres of CMs seeded on matrix with an elastic modulus >10 kPa or smaller than 10 kPa were less defined and unaligned and contained stress fibers. Mechanical loads also regulate Ca^{2+} maturation in CMs. Ruan et al. used engineered myocardium under a static stretch of 0.63 ± 0.10 mN/mm^2 and found increased expression of ryanodine receptor 2 and sarcoplasmic reticulum (SR)/endoplasmic reticulum (ER) calcium ATPase 2 (SERCA2) (Ruan et al., 2016). Cyclic mechanical stress during systole and passive stretch during diastole induce CM maturation in cell culture. In the process of myocardial contraction, the amount and duration of calcium ion release regulate the magnitude of contractile force (Zhang et al., 2020). Several studies have shown that the magnitude of the calcium transient and the amount of SR calcium and SERCA2a correlate with the magnitude of force generated in primary cultured neonatal rat CMs. Metabolic changes, including mitochondrial ETC function, morphology, and ROS production, are guided by mechanical stress. CM hypertrophy is also a key parameter of maturation post-natally (Caffarra Malvezzi et al., 2020). Inert polycaprolactone (PCL) planar layers with different cross-linking densities and Young modulus ranging from 1 to 133 MPa (measured by tensile test) have been prepared (Govoni et al., 2013). These PCL layers indicate that differentiation of the CM hypertrophic phenotype is influenced by substrate stiffness and that a more mature phenotype could be obtained with substrate stiffness of around 0.91 ± 0.08 MPa (Forte et al., 2012). The effect of substrate stiffness on the beating rate of CMs was also studied, and it was found that muscle cells beat fastest on substrates that mimic the stiffness of natural tissue. Additionally, the stretching substrate in mechanical stimulation can also promote the proliferation and maturation of functional CM characteristics. Therefore, CM development and maturation involve the physical cues of mechanical stress (**Figure 1**).

MOLECULES INVOLVED IN MECHANOTRANSDUCTION IN CMS

CMs are sensitive to mechanical stress, and responses to mechanical stress culminate in downstream gene transcription alterations. Therefore, the fundamental biological role of mechanotransduction is to transduce physical stimuli to molecular signaling. There are two common types of mechanical sensors within the cellular membranes of CMs, which are known as biophysical and biochemical sensor mediating pathways. The sensors are located in membrane to transduce extracellular stress stimulation into intracellular signals. Generally, the role of the physical sensors is to connect the ECM and cytoskeleton, to reshape actin proteins, and finally change chromosome structure to influence gene transcription. Chemical sensors mainly impact the modification of downstream molecules, to transduce signals into transcription regulation (**Table 1**).

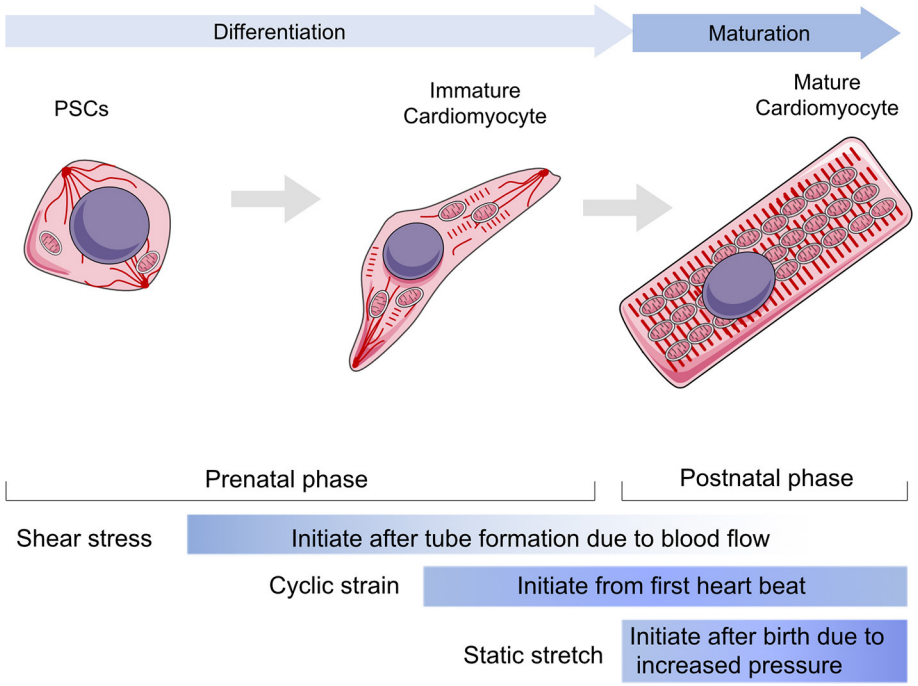

FIGURE 1 | The role of mechanical stress in guiding cardiomyocytes in differentiation and maturation. The differentiation stage is referring the duration from progenitor stem cells to immature cardiomyocytes within prenatal phase, whereas the maturation stage is mainly referring to the post-natal phase to establish a functional cardiomyocyte. The shear stress would be loaded to cardiovascular system since tube formation, but it mainly impacts the early stage of cardiac development and vascular migrations. Cyclic strain influences cardiomyocytes after the heart starts to beat, while contributing to maintain heart function throughout all lifetime. The static stretch is considered to play a major role after birth as the pressure goes up rapidly and becomes the most dominant one following aging. PSCs, progenitor stem cells.

TABLE 1 | Molecules involved in mechanotransduction in CMs.

Mechanotransduction	Function	Components	Signal pathways
Biophysical sensors	Maintain cellular shape, Resist external mechanical force, Link up inner and outer cellular	Integrins, desmosome, adherens junctions	Akt, c-Jun N-terminal kinase, MAPK-ERK-p38
Biochemical sensors	Regular cardiogenesis and hypertrophic cardiomyopathy, maintain heart development under stress, Ca^{2+}-channel regulation, mediating contraction–excitation coupling and heart rhythm	Ras-like small GTP-binding proteins, Ras superfamily including Ras, Rho, Ran, and Rab families	RAS/RAF-dependent MAPK signaling, RhoA signaling RAP-Hippo-YAP pathway

Biophysical Sensors

The sensing of mechanical force and the transduction of the resulting signal are a typical physical process. It is important that CMs resist external mechanical force to maintain their normal cellular shape and initiate crosstalk between inner-cellular and outer-cellular forces (Geiger et al., 2009; Oria et al., 2017). The ECM surrounds the CMs to provide an optimal microenvironment for myocardiogenesis and maturation. Typically, the major structural components of cardiac ECMs include fibrillar Col, fibronectin (FN), glycoproteins, proteoglycans, and glycosaminoglycans (Rienks et al., 2014). Fibroblasts critically contribute to the generation of ECM macromolecules. The architectural meshwork of the ECM also works as a reservoir for cytokines including TGF-β, BMP, platelet-derived growth factor, and connective tissue growth factor (Carè et al., 2007; Gordon and Blobe, 2008; Francisco et al., 2020). The proportion of different Cols (*Col1a1a*, *Col1a2*, and *Col5a1*) and cytokine expression levels contribute to the changes in ECM stiffness observed in healthy and damaged myocardium tissues (Horn and Trafford, 2016). Integrins are the major substrates that connect the ECM to the costamere proteins, establishing a bridge from the extracellular environment to the Z-line located in the sarcomere (Wang et al., 1993). Several integrins, consisting of α and β subunits, are expressed in mammalian cells. α1, α5, α7, and β1 are the most highly expressed subunits in CMs and form α1β1, α5β1, and α7β1 heterodimers,

which are predominantly Col, FN, and laminin-binding receptors (Israeli-Rosenberg et al., 2014). This kind of structure mediates the connection between CMs and the ECM, while the desmosome (including PKP2, DSG2, DSC2, JUP, and DSP) and adherens junctions (including CHD and CTNNA3, which mainly serve as types of cadherins) maintain cell–cell adhesions, which facilitate the binding of desmin to intermediate filaments. Structural proteins on the cell surface bind to filamentous actin (acto–myosin stress fiber and α-actin) and myosin (myosin II), generating intracellular force to target the nuclear membrane (Maniotis et al., 1997; Geiger and Bershadsky, 2002). Thus, cytoskeletal force generation helps to push against the stress from the ECM, inducing a bidirectional balance that maintains normal cellular shape. Increasing force stretches the structural proteins, and once mechanical force exceeds the threshold, activation domains are exposed, recruiting talin to the β subunits of integrins, VCL, paxillin, and FA kinase (FAK). This produces a wide range of intracellular signals, including those of the Akt, c-Jun N-terminal kinase, and MAPK-ERK-p38 pathways (Sun et al., 2019). This biophysical mechanotransduction pathway has been presented simply in **Figure 2**.

Biochemical Sensors

Biochemical sensors are biomechanical stress–sensitive activators that regulate CMs. Ras-like small GTP-binding proteins are the main components of myocardial biochemical sensors. The Ras superfamily, including Ras, Rho, Ran, and Rab families, is involved in cardiovascular diseases. The transition between the GTP- and GDP-bound forms of Ras proteins is accompanied by conformational changes that significantly affect its affinity for downstream signaling molecules (Meng et al., 2018). The activation of the RAS/RAF/MEK/ERK1/2 cascade is essential for cardiogenesis, and RAS/RAF-dependent MAPK signaling induces hypertrophic cardiomyopathy. RhoA signaling activates SRF and Mef2c to maintain heart development under stress. Moreover, a large number of Ras superfamily proteins are involved in Ca^{2+}-channel regulation, mediating contraction–excitation coupling and heart rhythm. Kluge et al. demonstrated that the Rho-family GTPase1, Rnd1, serves as a biomechanical stress–sensitive activator, influencing cell proliferation, and cellular hypertrophy via activation of RhoA-mediated SRF-dependent and -independent signaling pathways (Kluge et al., 2019).

Recently, Meng et al. (2018) demonstrated that Rap2 is a key intracellular signal transducer that controls mechanosensitive cellular activities through Yes-associated protein (YAP) and transcriptional coactivator with PDZ-binding motif (TAZ). Mechanistically, matrix stiffness influences the levels of phosphatidylinositol 4,5-bisphosphate and phosphatidic acid through phospholipase Cγ1 (PLCγ1), leading to Rap2 activation through PDZGEF1 and PDZGEF2. Therefore, Rap2 is a pioneer that converts mechanical signals from physical stress to biochemical molecular activation. Deletion of *RAP2* increases the nuclear localization of YAP and TAZ. However, the functions of Rap2 have not been confirmed in cardiogenesis and maturation, or in cardiomyopathy. The Hippo-YAP/TAZ pathway functions downstream of Rap2 and has been well-studied throughout heart biogenesis, hemostasis, and regeneration. Under normal mechanical stress, activated Hippo pathway proteins, including MAP4K4, MAP4K7, ARHGAP29, LATS1/2, and MOB1/2, phosphorylate YAP/TAZ, confining them to the cytoplasm (Dupont et al., 2011; Aragona et al., 2013). Under excessive mechanical stress, Hippo is deactivated, and YAP/TAZ translocate into the nucleus as co–transcription factors that interact with TEAD1 family proteins to develop transcription complexes (Mosqueira et al., 2014; Totaro et al., 2018). TEAD1 functions in cardiogenesis during the fetal stage of development and regulates the actin cytoskeleton and metabolism in CMs during the adult stage. VGLL4 binds with TEAD1 to regulate YAP function to control downstream genes. When VGLL4 binds to TEAD1, it induces TEAD1 degradation, inhibiting the response to exceeding mechanical stress (Kim et al., 2015; Narimatsu et al., 2015; Chang et al., 2018). The RAP-Hippo-YAP pathway is illustrated in **Figure 3**.

Moreover, the biophysical and biochemical sensors demonstrated several instances of crosstalk in their downstream signals. The biophysical transduction pathways have been studied for several years, and functional molecules have been identified. However, we still have very limited knowledge about biochemical sensors and their functional messengers. The key molecules, YAP/TAZ, are involved in both biophysical and chemical regulation pathways. Therefore, we believe there should be more connection between the two sensor types. However, there is still no evidence that shows how one kind of sensor induced pathway changes when another is knocked out. ECM remodeling is important for the maintenance of CM function. Therefore, it is necessary to understand how biochemical sensors influence the ECM, which is always bound by integrins, to regulating biophysical signaling.

THE COMMON UNDERSTANDING OF MITOCHONDRIAL HOMEOSTASIS IN CMS

Mitochondrial Quality Control

Mitochondria maintain their shape and number through biogenesis, fission, fusion, and mitophagy to ensure normal physiological function. This process is called mitochondrial quality control (MQC). MQC is a complex process that includes three main levels. The first level prevents mitochondrial damage and maintains mitochondrial stability through proteasome activation. The second level maintains the number and shape of mitochondria through mitochondrial biogenesis, fission, and fusion. The third level selectively removes damaged mitochondria and is called mitophagy (Pickles et al., 2018).

Biogenesis and Degradation

Mitochondrial biogenesis is the process through which cells increase their mitochondrial mass. Proliferator-activated receptor γ coactivator 1 (PGC1) is a critical factor in this process. PGC1 activates peroxisome proliferator-activated receptor, which leads to the gain of mitochondrial DNA (mtDNA) content, and promotes the transcription of mitochondrial uncoupling protein 1 (UCP1). This helps CMs adapt to the post-natal environment with a mature ETC utilizing fatty acid.

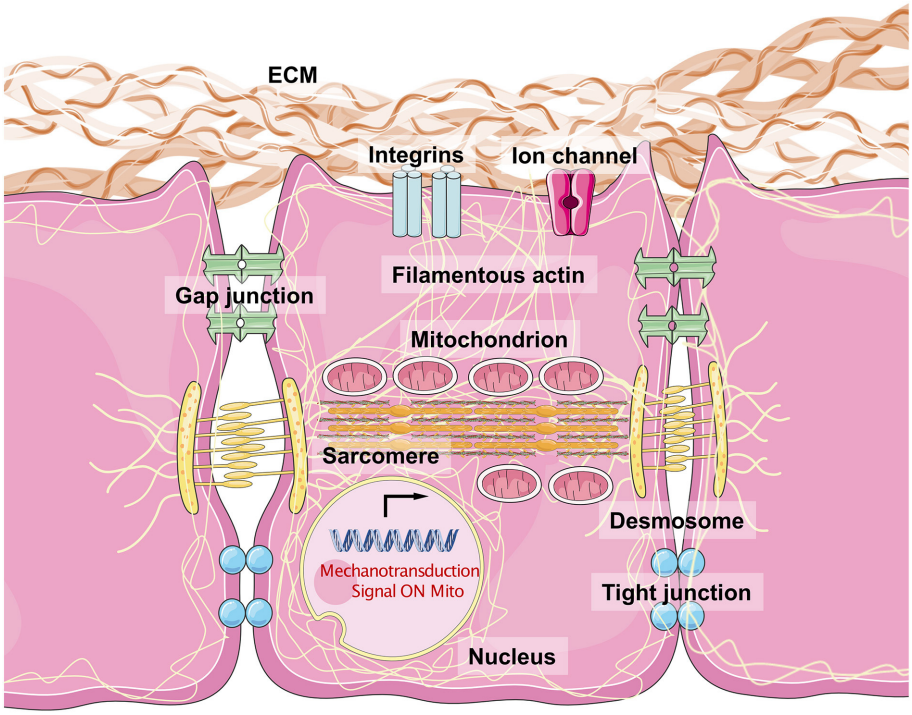

FIGURE 2 | The biophysical sensors of mechanical stress in cardiomyocytes and the intracellular mechanisms. The integrins are considered as the most major biophysical sensors located in cellular membrane of cardiomyocytes. While the desmosome, gap junction, and tight junction also contribute to maintain a cell–cell junction with a physical mechanical contact. Filamentous actin connects all the molecules with mitochondria, sarcomere, and nuclear membrane, especially lamin A/C. The acto–myosin action and myosin II structure make the dominant unit for actin movement. Once the mechanical stress loaded on cell surface, the integrin would phosphorylate FAK and downstream molecules, which force the myosin protein to move along acto–myosin actin, and then change the shapes of mitochondria, sarcomere, and nuclear membrane, regulating related genes expression and mitochondrial function.

PGC-1α expression is regulated by YAP/TAZ, and PGC-1α depletion results in lethal cardiomyopathy. Moreover, PCG-1 interacts with Mfn1/Mfn2 and Drp1. TFAM is another essential factor for mitochondrial biogenesis and is required for mtDNA transcription and mitochondrial self-replication. Zhang and Li demonstrated that the Nkx2.5-driven Tfam knockout leads to total mitochondrial loss in CMs (Zhang et al., 2018).

Mitochondria are divided into four parts by the double-layer membrane structure, the mitochondrial outer membrane, mitochondrial inner membrane, intermembrane space, and matrix. In the mitochondrial outer membrane, the ubiquitin–protease degradation system (UPS) is the main mechanism of maintaining homeostasis. The UPS consists of ubiquitin, ubiquitin initiation enzyme, the 26S proteasome, and deubiquitination enzyme. Ubiquitin initiation enzyme is responsible for activating ubiquitin and target protein binding to form a target protein polyubiquitin chain or to ubiquitinate the degraded protein. Then, ubiquitinated proteins are transported to 26S proteasomes, where they are recognized and degraded (Tsakiri and Trougakos, 2015). The deubiquitination enzyme dissociates ubiquitin from the substrate, allowing ubiquitin recycling (Fang et al., 2010). UPS is involved in abnormal protein degradation and plays an important regulatory role in the cell cycle, signal transduction, DNA damage repair, and cell stress. Impairment of UPS function has been detected in heart tissues of patients with hypertrophic cardiomyopathy and heart failure (Predmore et al., 2010). Conversely, enhancement of cardiac proteasome proteolytic function plays a protective role against the pathophysiology of proteinopathy and ischemia–reperfusion (IR) injury in mice (Li et al., 2011). Furthermore, accumulation of polyubiquitinated substrates has been observed in the heart tissue of patients with cardiac diseases such as cardiomyopathy and heart failure (Nishida and Otsu, 2017).

In the intermembrane space, HTRA2/OMI is thought to function as a protein quality control protease. HTRA2/OMI is an ATP-independent serine protease involved in the regulation of mitochondrial E3 ubiquitin ligase. Lack of HTRA2/OMI leads to mitochondrial dysfunction, mitochondrial morphological changes, and the production of ROS, leading to mtDNA damage. There are two ATPases associated with various cellular activities (AAAs) in the mitochondrial inner membrane. The proteasome complex can recognize misfolded transmembrane protein polypeptide chains and degrade unassembled mitochondrial complex subunits and transmembrane segments (Leonhard et al., 2000). The biochemical and genetic interactions of the RUVBL1 and RUVBL2 AAA family proteins play a novel functional role in symmetry breaking and cardiac development (Hartill et al., 2018). There are two AAA proteins in the

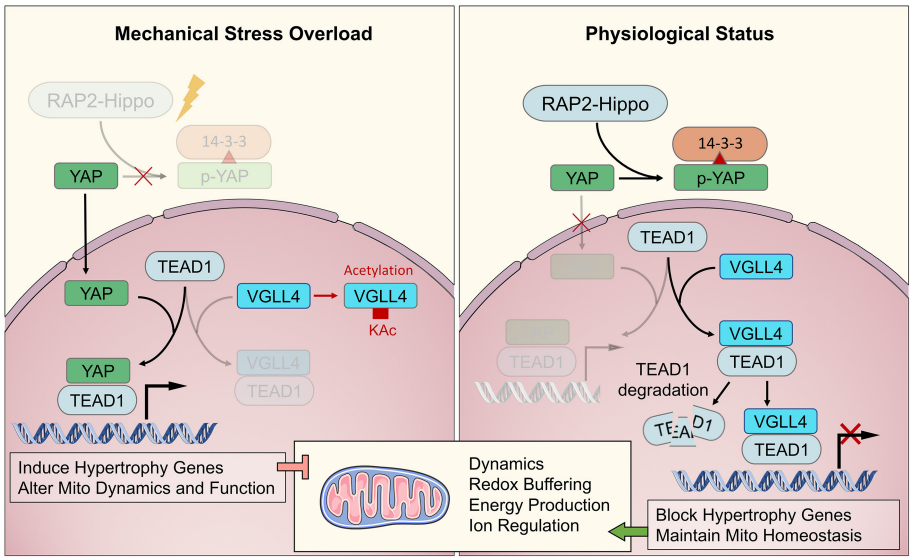

FIGURE 3 | The major biochemical pathway of RAP2-Hippo-YAP in mechanical transduction. The RAP2-Hippo-YAP pathway is the most determined one of biochemical sensor pathway. The overloading pressure would inactivate the RAP2 and then turn off Hippo signaling. Then, the YAP would be dephosphorylated and translocated in to nucleus. VGLL4 demonstrated a competition role with YAP in binding to TEAD1. The exceeding mechanical stress would activate YAP and up-regulated hypertrophic genes, leading to mitochondrial dysfunction in adulthood.

mitochondrial matrix, Lon and ClpXP. Lon is mainly responsible for removing oxidized proteins and preventing oxidative stress damage. ClpXP can degrade proteins that are not bound to molecular chaperones and mediate the mitochondrial unfolded protein reaction (Hammerling and Gustafsson, 2014). Lon is involved in cardiac disorders. Lon is upregulated in hypoxia-induced CMs, and Lon downregulation attenuates hypoxia-induced CM apoptosis through decreased oxidant generation. Lon overexpression stimulates oxidant production and induces apoptosis under normoxic conditions in CMs (Bota and Davies, 2016).

The selective removal of redundant or damaged mitochondria through the process of autophagy is called mitochondrial autophagy or mitophagy. The selective removal of damaged mitochondria is a complex process whose molecular mechanisms involve a variety of proteins, which are mainly classified as Parkin-dependent or Parkin-independent. Parkin-dependent mitophagy is the most dominant mechanism of mitophagy. The transfer of Parkin requires PTEN-induced kinase 1 (PINK1). PINK1 recruits phosphorylated Parkin through its silk/threonine kinase activity and transfers Parkin from the cytoplasm to the mitochondria. Parkin has E3 ubiquitin ligase activity and can mediate the ubiquitination of mitochondrial outer membrane proteins including HKI, VDAC1, and MFN1/2, to initiate mitophagy (Geisler et al., 2010). Parkin-independent regulatory proteins include the BNIP3, NIX, and FUNDC1 mitophagy receptors. FUNDC1 is highly expressed in the heart, interacts with LC3 on autophagosome membranes, and mediates mitochondrial fragmentation and mitophagy under hypoxia (Liu et al., 2012). BNIP3 and NIX are proapoptotic proteins located in the outer membrane of mitochondria and can directly bind with LC3 to induce mitochondrial recruitment into autophagosomes for degradation. In a Parkin knockout fly model, CM mitochondria exhibit dysmorphology, depolarization, and ROS generation. Accumulation of enlarged hollow donut mitochondria with dilated cardiomyopathy was also observed and could be rescued by CM-specific Parkin expression (Bhandari et al., 2014). Furthermore, Parkin deletion led to increased DRP1 levels and simultaneous deficiency of DRP1 and Parkin-exacerbated cardiomyopathy (Kageyama et al., 2014). In 2017, it was reported that resveratrol, known for its antiaging properties, can be used to treat cardiovascular complications related to aging through Parkin and PINK1 activation (Ren et al., 2017). However, mitophagy can be also detrimental. Some findings demonstrate that when CMs undergo IR, ATP production is reduced because of greatly enhanced mitophagy and impaired mitochondrial fission and fusion leading to cell damage (Anzell et al., 2018).

Fission and Fusion

Mitochondrial fission and fusion must exist in balance to maintain mitochondrial integrity, which is critical for heart health. Through mitochondrial fission, the required number of mitochondria can be ensured, irreversible mitochondrial damage can be isolated, and mitochondrial movement and distribution can be promoted. Mitochondrial fission is mainly mediated by dynamin-related protein 1 (DRP1). DRP1 is highly expressed in heart tissues and can be upregulated under stress. Additionally, post-transcriptional SUMOylation and phosphorylation modulate DRP1 function. Mitochondrial fusion involves the joining of normal and damaged mitochondria to replace the materials in damaged mitochondria. This is conducive to material circulation and energy transmission and can protect cells. Mitochondrial fusion is mainly mediated

by mitochondrial fusion proteins, including MFN1 and MFN2, which serve the outer mitochondrial membrane, and optic atrophy 1 (OPA1), which serves the intermitochondrial membrane. MFN1 and MFN2 have amino-terminal conserved GTPase domains and carboxy-terminal coiled helix structures and can bind to the mitochondrial outer membrane and form transhomologous or heterologous oligomeric complexes simultaneously, bringing two mitochondria into close proximity for fusion (Koshiba et al., 2004). Proteins involved in fission and fusion function within a signaling network to maintain mitochondrial homeostasis and play important roles in regulating cardiac response under pathological stress and mechanical stretching, such as during IR, cardiomyopathy, and heart failure (Kuzmicic et al., 2011). For example, DRP1 ablation in adult mouse cardiac myocytes interrupts mitochondrial fission and provokes the mitophagic mitochondrial depletion that contributes to lethal cardiomyopathy (Song et al., 2015a). Deletion of Mfn1/Mfn2 fusion proteins in mouse heart results in abnormal mitochondrial morphology and mitochondrial fragmentation, leading to ventricular wall thickening and an increase in cardiac mass (>30%) accompanied by symptoms of eccentric hypertrophy. Additionally, the Mfn1/Mfn2/Drp1 triple knockout causes mitochondrial heterogeneity and impaired mitophagy (Song et al., 2015b). Moreover, OPA1 helps to maintain the cristae structure and reduce apoptosis.

ATP Production

Mitochondria use fatty acids, glucose, and amino acid metabolites to synthesize ATP through the tricarboxylic acid cycle and oxidative phosphorylation pathways. ATP production through the ETC is the principal function of mitochondria. The ETC is a multisubunit complex in the mitochondrial inner membrane and is an important field of ATP production. The transportation of protons from the matrix to the intermembrane space through complexes I, III, and IV generates energy. The mitochondrial transmembrane potential ($\Delta\psi m$) is essential to maintain the electrochemical proton gradient across the mitochondrial inner membrane and should always remain 150–180 mV negative to the cytosol. ATP produced by mitochondria in myocardial tissue is mainly responsible for myocardial contraction, cellular excitability, and maintenance of calcium homeostasis. McCully et al. found that under myocardial ischemia and other pathological conditions, mitochondrial respiratory chain function is decreased, and ATP synthesis is impaired (McCully et al., 2007). Moreover, in some genetic mitochondrial diseases, the CMs reveal increased basic energy production, but deficient maximal ATP synthesis (Zhang et al., 2018). In turn, ATP synthesis disorder leads to changes in various biochemical and ultrastructure properties of CMs, including calcium accumulation and acidosis in the cytoplasm, mitochondria, and nucleus, as well as large quantities of ROS production, leading to progressive damage of mitochondrial function and decreased CM activity.

Regulation of ROS

Normally, the respiratory chain effectively uses more than 98% of the electrons to synthesize ATP, and 1–2% of the electrons are released outside the mitochondria to produce ROS. ROS are involved in signal transduction and regulation of apoptosis in cell response to stress and risk factors and are broken down by superoxide dismutase (Penna et al., 2009). In pathological conditions, the uncoupling of oxidation and phosphorylation results in a mass release of electrons. Excessive ROS production then leads to oxidation of mtDNA, lipids, and proteins and extensive cell damage. MtDNA is in a state of continuous replication with weak DNA repair abilities, making it vulnerable to oxidative damage. MtDNA damage further stimulates the production of ROS, forming a vicious cycle and aggravating the damage of CMs (Yu and Bennett, 2014; Lee et al., 2017). ROS regulation also plays an important role in heart development, whereas mitochondrial damage would cause ROS accumulation, which induces DNA damage and leads to cell cycle arrest (Zhang et al., 2018).

Ca^{2+} Handling

Mitochondrial Ca^{2+} homeostasis is a result of the dynamic equilibrium between Ca^{2+} influx and efflux. Many factors influence these processes. First, the spatial organization of mitochondria within cells and their tethering with other organelles, especially with the ER, play a pivotal role in mitochondrial Ca^{2+} homeostasis. The estimated area of contact sites between mitochondria and ER accounts for 5–20% of the total mitochondrial surface (Rizzuto et al., 1998). It is broadly considered that these contact sites are very important and are the sites where Ca^{2+} is rapidly transported into the matrix. De Brito and Scorrano identified MFN2 as an essential protein that directly bridges these two organelles, and mitochondria Ca^{2+} uptake is impaired following genetic ablation of MFN2 (de Brito and Scorrano, 2008). Second, the uptake of calcium by mitochondria depends on the MCU (mitochondrial Ca^{2+} uniporter). The electrophysiological characterization and molecular identity of MCU are partially determined. MCU is an inward rectifying channel that is highly Ca^{2+}-selective (Kirichok et al., 2004). Mitochondrial protein MICU1 (mitochondrial Ca^{2+} uptake protein 1), SLC25A23 (solute carrier 25A23), and MCUR1 (mitochondrial calcium uniporter regulator 1) are important regulators of Ca^{2+} uptake (Perocchi et al., 2010; Sancak et al., 2013; Hoffman et al., 2014; Mallilankaraman et al., 2015). A growing number of researchers found that MCU is a key component of a higher-order macromolecular complex that requires further investigation but was named the MCU complex (De Stefani et al., 2015). Furthermore, Ca^{2+} release from mitochondria relies on two different pathways, the $2H^+/Ca^{2+}$ antiporter (mHCX), and the Na^+/Ca^{2+} exchanger (NCLX) (Palty et al., 2010).

MECHANICAL CUES CONTRIBUTE TO THE MAINTENANCE OF MITOCHONDRIAL HOMEOSTASIS

Mechanical Stress Controls MQC

In normal conditions, the mechanisms of MQC mainly consist of proteasome activation, fission and fusion, and

mitophagy. Furthermore, mitochondria exhibit some unique behaviors when cells undergo mechanical stress. In the heart, abnormal mechanical stress is mainly caused by hypertension, ventricular hypertrophy, ECM remodeling, or other types of cardiomyopathy. As rich contents and ATP factories of CMs, mitochondria will show corresponding pathophysiological changes. A study in rats with spontaneous hypertension and left ventricle hypertrophy reported overexpression of proteins related to mitochondrial oxidative phosphorylation and underexpression of the mitochondrial precursor of ATP synthase (Zamorano-León et al., 2010).

The mechanisms of MCQ are also important. Alterations in mitochondrial fission, fusion, and mitophagy are associated with pathological conditions in the heart. DRP1 is an essential protein that mediates mitochondrial fission under stress. Hypertension is usually accompanied by elevated levels of norepinephrine. Using norepinephrine to culture CMs of newborn rats can promote mitochondrial fission. This is because norepinephrine can increase cytoplasmic Ca^{2+} and activate calcineurin to promote DRP1 migration to mitochondria (Pennanen et al., 2014). After DRP1 has been recruited to mitochondria, the phosphorylation of the GTPase effector domain of DRP1 at Ser637 reduces its response to norepinephrine, which causes a further increase in mitochondrial fission (Santel and Frank, 2008). Taken together, these data indicate that mitochondrial fission may be a compensatory mechanism to maintain heart contractility under conditions of exceeding mechanical stress (Lahera et al., 2017). However, mitochondrial fusion is a repressed process under stress. A study demonstrated a decrease in mRNA levels of Mfn1 and Mfn2, which are major proteins mediating fusion in hypertensive and cardiac hypertrophy rats caused by phenylephrine (Fang et al., 2007). Mitophagy is another essential mechanism to maintain MCQ. However, under pressure overload, mitophagy can be maladaptive. Sympathetic, parasympathetic, renin–angiotensin–aldosterone, and antidiuretic hormone systems are involved in blood pressure regulation. And most peptides and hormones in these systems can regulate mitophagy (Gottlieb and Thomas, 2017). For example, the angiotensin receptor blocker valsartan can diminish mitophagy (Zhang et al., 2014). Usually, mitophagy is enhanced in the heart of patients with hypertension, and hemodynamic stress can induce a robust autophagic response in cardiac myocytes (Zhu et al., 2007), which is considered detrimental. Mechanical stress can upregulate *Beclin-1* gene expression, which amplifies the autophagic response to stress and augments pathological remodeling (Zhu et al., 2007). However, the absence of mitophagy is also a type of maladaptation. Temporally controlling cardiac-specific Atg5 deficiency in mice suggested that autophagy plays a beneficial role in the response of the heart to pressure overload and is important for preventing the accumulation of abnormal proteins or damaged organelles (Nakai et al., 2007). Mechanical stress regulates mitophagy to maintain optimal mitochondrial number and health.

Mechanical Transduction Pathways in the ETC

Normal physiological processes of the cell are accompanied by ATP consumption. CMs need a large amount of ATP due to their contraction activity. To make more efficient use of ATP to support CMs, many mitochondria attach to the sarcomere and SR (Pasqualini et al., 2016). This arrangement greatly promotes the transport of intermediate metabolites in nucleotide and oxidative phosphorylation (Auerbach et al., 1997).

In the early stage of mechanical stress, CM structure is intact, energy metabolism is mainly performed by fatty acid as substrate, and sufficient ATP is produced through the ETC to supply normal mechanical CM contraction (Lopaschuk et al., 2010). However, after a longer period of mechanical stress, the mitochondrial structure varies with abnormal MQC, the ETC is impaired, glycolysis and glucose oxidation increase, and the energy supply becomes inadequate. The utilization of energy substrates and changes in energy metabolism, including abnormal mitochondrial function and increased glucose utilization, are phenotypes of myocardial hypertrophy and heart failure (Ventura-Clapier et al., 2004; Stanley et al., 2005).

External mechanical stress activates the integrin signaling pathway mediated by MAPK (de Cavanagh et al., 2009) and Rho-family GTP-binding proteins, and the stress response damages the mitochondrial ETC (Werner and Werb, 2002). Following mechanical stress, the heart gradually loses the ability to produce an adequate ATP supply, leading to heart failure. Mechanical force and cell junctions can regulate RhoA and affect YAP and TAZ by LATS-dependent or independent mechanisms (Zhao et al., 2012). YAP and TAZ can regulate UCP1, Marf, Opa1, and many glutamine-metabolizing enzymes, which are coupled with ATP production (Kashihara and Sadoshima, 2019).

Exceeding Mechanical Loading Induces ROS Accumulation

Exceeding mechanical loading can occur via several methods, including cyclic strain, shear stress, and static stretch. CMs seeded on BioFlex culture plates were placed on a gasketed baseplate and subjected to a vacuum of −5 or −21 kPa using a Flexcell system, low and high tension, and a frequency of 1 Hz to generate cyclic strain. Using these parameters, the system generates a deformation gradient on the membrane, with maximum deformation of 5 and 25% at −5 and −21 kPa, respectively. In this system, short-term mechanical stress results in increased CM contractile force *in vitro*, whereas long-term and transient stimulation leads to structural changes in CMs (Pedrozo et al., 2015). Different stretching amplitudes in neonatal rat ventricular cells cause ERK1/2 phosphorylation, but only high-intensity stretching causes CM apoptosis and JNK phosphorylation. Activation of ERK1/2 and JNK is also accompanied by increased ROS. Single-cell stretch, known as the carbon fiber method, is another simple stretch method for cyclic strain. In brief, a pair of carbon fibers (10 μm in diameter) are attached to either end of a CM using custom-made three-axis hydraulic manipulators, each mounted on separate computer-controlled piezo-electric translators on a custom-made railing system (Pimentel et al., 2001). Another study found that excessive mechanical stress activates RAC1-ROS and leads to ROS accumulation in rat ventricular cells. This accumulation induces apoptosis and activates the downstream p38-MAPK pathway, eventually leading to pathological hypertrophy of the

cell (Aikawa et al., 2001). Experimental analysis showed that mechanical stretching can lead to increased ROS production, cytoskeleton changes, apoptosis, and necrosis (Ulmer and Eschenhagen, 2020). Similar conclusions were reached in studies using rat and human CMs (Fujita and Ishikawa, 2011; Mohamed et al., 2016; Iribe et al., 2017).

Regulation of Ca^{2+} Transit Under Mechanical Stress

Ca^{2+} affects CM contraction and is affected by mechanical stress (Bers, 2008). Ca^{2+} transit is difficult to observe and analyze *in vivo*. Therefore, mechanical stress models established *in vitro* allow for the visualization of Ca^{2+} transit. Cells isolated from human heart failure hearts show a decrease in the amplitude of Ca^{2+} transients with reduced Ca^{2+} removal rates (Lou et al., 2012). *In vitro* mechanical stress largely consists of large amplitude and large force or small amplitude and small force (Kurihara and Komukai, 1995). Axial stretching reduced the total Ca^{2+} load of guinea pig CMs within seconds (Iribe and Kohl, 2008). Another study showed that stretching increased the Ca^{2+} sparks rate of rat CMs through a nitric oxide–mediated pathway after prolonged exposure to mechanical stimulus (Petroff et al., 2001). A study in neonatal mouse CMs showed that the Ca^{2+} signaling pathway is mainly involved in the early stages of stretch-induced apoptosis. Ca^{2+} signaling pathways are located upstream of these known stretch-activated apoptotic events, such as caspase 3/9 activation, mitochondrial membrane potential corruption, and ROS production. Inhibition of intracellular Ca^{2+} can prevent these events (Liao et al., 2003). Additionally, researchers found that Duchenne muscular dystrophy (mdx) is a model of mechanical stress that triggers Ca^{2+} responses in resting dystrophy mdx CMs. Following mechanical stretch, multiple Ca^{2+} influx pathways are activated by stretch-activated channels, resulting in abnormal Ca^{2+} responses in mdx myocytes (Fanchaouy et al., 2009). In a study examining the acute effect of the axial application of single rat CM on the diastolic Ca^{2+} discharge rate, it was found that a rapid but short-term calcium spark was guided through a pathway that required the integrity of the cytoskeleton (Iribe et al., 2009). Within a few minutes of the pressure increasing, Ca^{2+} participated in the accumulation of the Anrep effect through autocrine/paracrine signals induced by stretching (Cingolani et al., 2013). When the stress is chronic, the increased calcium influx activates CaMKII/MEF2 expression and leads to cardiac hypertrophy (Gómez et al., 2013). Prosser et al. (Prosser et al., 2011) demonstrated that heart cell stretching activates NOX2 and leads to ROS generation in a microtubule-dependent manner under healthy conditions. This is known as "X-ROS signaling" and describes a mechanochemical signal induction of ROS-mediated RYRs and SR activation to generate a calcium burst, leading to muscle contraction (Santulli et al., 2018). In diseased CMs of Duchenne muscular dystrophy, "X-ROS signaling" generates arrhythmogenic Ca^{2+} waves (Khairallah et al., 2012). Exceeding mechanical stress conditions imply high concentrations of peroxynitrite, which causes SERCA2a inactivation through nitration. Lokuta et al. revealed that SERCA2a inactivation by nitration might contribute to calcium pump failure (Lokuta et al., 2005).

TARGETING MECHANOTRANSDUCTION PATHWAYS TO RESTORE MITOCHONDRIAL FUNCTION

Exceeding mechanical stress induces the dysfunction of myocardial mitochondria, leading to morphological changes and contractile impairment. Therefore, blocking abnormal mechanotransduction appears to be a valid approach of attenuating such adverse effects. However, this strategy brings a new issue into consideration: How can we block mechanotransduction when normal mechanical stress helps to maintain CM hemostasis? Therapeutic strategies targeting the mechanotransduction pathway should avoid the development and maturation stage, where a lack of mechanical stress would induce myocardium hyperplasia. Besides, the total knockout of any key genes in transduction pathway seems unacceptable. However, it has recently been demonstrated that the deletion of a specific gene in around 30% CMs would achieve the therapeutic goal. Following this, a method called "mosaic" knockout was developed to generate partial knockout CMs using varied dosage of delivery vehicles, including adeno-associated virus (AAV) (Guo et al., 2017; VanDusen et al., 2017). In the past year, the risks associated with AAV usage have been raised. Therefore, instead of generating permanent isogeneic insertions, some non-viral transient gene expression technologies have been developed that alter expression using modified mRNAs, miRNAs, and non-coding RNAs (ncRNAs) (**Figure 4**).

Small Molecular Inhibitors

Recently, many reports have focused on the development of therapeutic compounds and drugs targeting mechanotransduction pathways to restore mitochondrial function in heart disease. For example, apigenin inhibits ROS generation, the loss of mitochondrial membrane potential, and apoptosis through PI3K/AKT signals and mitochondrial Notch1/HES1 signals, protecting H9C2 and rat heart cells from IR injury (Hu et al., 2015; Zhou et al., 2018). Additionally, melatonin promotes OPA-1–mediated mitochondrial fusion by activating YAP, thereby reducing IR-induced mitochondrial apoptosis and cardiac IR injury (Ma and Dong, 2019). Several signaling pathways are involved in cardiac mechanotransduction, and molecules have been targeted to attenuate specific pathways to inhibit or reverse harmful mechanical stress–induced cardiomyopathy. Verteporfin inhibits the interaction between YAP and TEAD1 to deplete the downstream YAP signal. Therefore, verteporfin has therapeutic potential for pressure overload cardiac remodeling.

Non-coding RNAs

In the last 10 years, ncRNAs have been studied worldwide, and several critical ncRNAs with essential biological functions have been identified. Antisense oligonucleotide therapy targeting strategies to modulate gene splicing have been used for

FIGURE 4 | The strategy for gene delivery for CMs therapy. Gene therapy is a promising way to transduce exogenous gene expression. The two most common delivery methods are viral and non-viral vehicles. AAV is the most promising vector to delivery oligonucleotides. However, risk of high dosage of AAV administration limits its clinical practice. Thus, the mosaic genetic editing has been brought to reduce the requirement for AAV to avoid adverse effects. Besides, the non-viral delivery strategy is able to do transit gene expression, which works as an alternation to viral approach. Intramyocardial *in situ* and systematic injections are both able to achieve therapeutic goal.

ncRNA-based gene therapy. While lncRNA mimics have been used to express specific oligonucleotides (Lee J. et al., 2016), lncRNA-Plscr4 overexpression regulates mitochondrial function to attenuate hypertrophic stress by targeting miR-214 in mice-TAC or Ang-II–treated CMs (Lv et al., 2018; Zhang J. et al., 2019; Zhang M. et al., 2019). Additionally, silencing of lncRNA-Uc.323 or overexpression of lncRNA-Ahit could attenuate phenylephrine-induced CM enlargement through the mitochondrial pathway (Liu et al., 2016; Viereck et al., 2016; Yan et al., 2019; Sun et al., 2020).

Gene Editing for Genetic Disorder

CRISPR/Cas9 has rapidly become one of the most popular and important approaches for genome editing because of its simplicity and adaptability. CRISPR/Cas9 and iPSC technology were recently applied to characterize Barth syndrome with mitochondrial abnormalities. The administration of the mitoTEMPO antioxidant to patient-derived iPSC-CMs efficiently regulated mitochondrial ROS production and sarcomere organization to rescue the pathological phenotype of Barth syndrome (Wang et al., 2014). Additionally, AAV technology has been developed to deliver genes to reverse cardiac function and restore mitochondrial function (Wang L. et al., 2020; Wang et al., 2021). AAV and lentivirus are the main viral tools for gene delivery for genetic editing. Diabetic mice induced by intraperitoneal streptozocin injections were randomized for treatment with lentivirus carrying Lin28a siRNA or Lin28a cDNA to knock down or overexpress Lin28a, respectively. Lin28a overexpression significantly decreased RhoA/ROCK signaling to alleviate mitochondria cristae destruction and promote heart function in diabetic mice (Sun et al., 2016). Additionally, Dkk1 adenovirus is transduced by intramyocardial injection, and Dkk1 overexpression aggravates Dox-induced CM apoptosis via the mitochondrial damage pathway (Liang et al., 2019). AAV serotype 9 (AAV-9) Plscr4, lncRNA-Plscr4 overexpression attenuates the hypertrophic response in hyperpressure-loaded CMs (Liu et al., 2020). Non-viral delivery approaches involve liposome- or nanoparticle-mediated oligonucleotide delivery to heart tissue (Ishikawa et al., 2013). Chen et al. showed that modified aYAP mRNA could induce CM regeneration in an IR mouse model, which demonstrated a promising way to induce transit gene expression to achieve gene therapy.

PERSPECTIVES

In summary, biophysical and biochemical sensing pathways establish the fundamental mechanotransduction pathways that impact the regulation of mitochondrial homeostasis. Shear stress, cyclic stretch, and static strain are three major mechanical forces CMs are subjected to. Exceeding mechanical stress impairs mitochondrial function through regulating MQC, ATP production, ROS accumulation, and Ca^{2+} handling, leading to CM hypertrophy and dysfunction. Therefore, restoring mitochondrial function by shutting down the exceeding mechanotransduction pathway is a potential therapeutic strategy for cardiovascular diseases. In this review, we highlighted the biological processes of mechanotransduction pathways in regulating mitochondrial function in response to mechanical stress. We also provided a brief description of gene therapy delivery modes used to deliver treatment based on mechanical stress–induced mitochondrial dysfunction, providing new integrative insights into cardiovascular diseases. According to current evidence provided by this review on mechanotransduction in mitochondrial hemostasis, the future cut edge should be located in the following several perspectives. The first thing is to get better understanding of how biophysical mechanical stresses regulate mitochondrial function, as present studies revealed several molecular signals downstream of integrin-FAK–myosin–laminA/C pathway involved in nuclear mitochondrial genes expression. However, mitochondria are found to bind with F-actin, so that the changes of mitochondria are unclear when faced with the physical stress directly. Second, the biochemical sensor–related signaling is really limited to describe, especially the crosstalk between physical and chemical changes under exceeding mechanical stress. At last, to attenuate the abnormal mechanical stress to restore normal mitochondrial function aiming to reverse CMs' phenotype is a promising way. However, the risks of high dosage of AAV administration need

to be noticed, and modified strategy is urgently required to be induced to reduce the supplement of AAV and achieve the same therapeutic goal at the same time. In generally, there is still a long way to obtain detailed understanding of mechanotransduction pathway in regulating mitochondrial function and to make targeting treatments.

AUTHOR CONTRIBUTIONS

HL and PY were primarily responsible for the Biological function of mechanical stress in cardiomyocytes, Molecules involved in mechanotransduction in CMs, and The common understanding of mitochondrial homeostasis sections, respectively. YQ and YY were primarily responsible for the Mechanical cues contribute to the maintenance of mitochondrial homeostasis, and Targeting mechanotransduction pathways to restore mitochondrial function sections, respectively. DZ and YL contributed equally to organize and edit the article. All authors contributed to the article and approved the submitted version.

FUNDING

All phase of this study was supported by a National Key R&D Program of China (2018YFC1002301) and Natural Science Foundation of China (81700360). The funders had no role in study design, data collection and analysis, decision to publish, or preparation of the manuscript.

REFERENCES

Aikawa, R., Nagai, T., Tanaka, M., Zou, Y., Ishihara, T., Takano, H., et al. (2001). Reactive oxygen species in mechanical stress-induced cardiac hypertrophy. *Biochem. Biophys. Res. Commun*. 289, 901–907. doi: 10.1006/bbrc.2001.6068

Ait-Mou, Y., Hsu, K., Farman, G. P., Kumar, M., Greaser, M. L., Irving, T. C., et al. (2016). Titin strain contributes to the Frank-Starling law of the heart by structural rearrangements of both thin- and thick-filament proteins. *Proc. Natl. Acad. Sci. U.S.A*. 113, 2306–2311. doi: 10.1073/pnas.1516732113

Akerberg, B. N., Gu, F., VanDusen, N. J., Zhang, X., Dong, R., Li, K., et al. (2019). A reference map of murine cardiac transcription factor chromatin occupancy identifies dynamic and conserved enhancers. *Nat. Commun*. 10:4907. doi: 10.1038/s41467-019-12812-3

Anzell, A. R., Maizy, R., Przyklenk, K., and Sanderson, T. H. (2018). Mitochondrial Quality Control and Disease: Insights into Ischemia-Reperfusion Injury. *Mol. Neurobiol*. 55, 2547–2564. doi: 10.1007/s12035-017-0503-9

Aragona, M., Panciera, T., Manfrin, A., Giulitti, S., Michielin, F., Elvassore, N., et al. (2013). A mechanical checkpoint controls multicellular growth through YAP/TAZ regulation by actin-processing factors. *Cell* 154, 1047–1059. doi: 10.1016/j.cell.2013.07.042

Auerbach, D., Rothen-Ruthishauser, B., Bantle, S., Leu, M., Ehler, E., Helfman, D., et al. (1997). Molecular mechanisms of myofibril assembly in heart. *Cell Struct. Funct*. 22, 139–46. doi: 10.1247/csf.22.139

Austin, K. M., Trembley, M. A., Chandler, S. F., Sanders, S. P., Saffitz, J. E., Abrams, D. J., et al. (2019). Molecular mechanisms of arrhythmogenic cardiomyopathy. *Nat. Rev. Cardiol*. 16, 519–537. doi: 10.1038/s41569-019-0200-7

Banerjee, I., Carrion, K., Serrano, R., Dyo, J., Sasik, R., Lund, S., et al. (2015). Cyclic stretch of embryonic cardiomyocytes increases proliferation, growth, and expression while repressing Tgf-Œ≤ signaling. *J. Mol. Cell. Cardiol*. 79, 133–144. doi: 10.1016/j.yjmcc.2014.11.003

Barki-Harrington, L., and Rockman, H. A. (2003). Sensing heart stress. *Nat. Med*. 9, 19–20. doi: 10.1038/nm0103-19

Bers, D. M. (2008). Calcium cycling and signaling in cardiac myocytes. *Annu. Rev. Physiol*. 70, 23–49. doi: 10.1146/annurev.physiol.70.113006.100455

Bezzerides, V. J., Caballero, A., Wang, S., Ai, Y., Hylind, R. J., Lu, F., et al. (2019). Gene therapy for catecholaminergic polymorphic ventricular tachycardia by inhibition of Ca(2+)/calmodulin-dependent kinase II. *Circulation* 140, 405–419. doi: 10.1161/CIRCULATIONAHA.118.038514

Bhandari, P., Song, M., Chen, Y., Burelle, Y., and Dorn, G. W. 2nd. (2014). Mitochondrial contagion induced by parkin deficiency in drosophila hearts and its containment by suppressing mitofusin. *Circ. Res*. 114, 257–265. doi: 10.1161/CIRCRESAHA.114.302734

Bluhm, W. F., Sung, D., Lew, W. Y., Garfinkel, A., and McCulloch, A. D. (1998). Cellular mechanisms for the slow phase of the frank-starling response. *J. Electrocardiol*. 31, 13–22. doi: 10.1016/S0022-0736(98)90273-4

Bota, D. A., and Davies, K. J. (2016). Mitochondrial Lon protease in human disease and aging: including an etiologic classification of Lon-related diseases and disorders. *Free Radical Biol. Med*. 100, 188–198. doi: 10.1016/j.freeradbiomed.2016.06.031

Boukens, B. J., Christoffels, V. M., Coronel, R., and Moorman, A. F. (2009). Developmental basis for electrophysiological heterogeneity in the ventricular and outflow tract myocardium as a substrate for life-threatening ventricular arrhythmias. *Circ. Res*. 104, 19–31. doi: 10.1161/CIRCRESAHA.108.188698

Brown, D. A., Aon, M. A., Frasier, C. R., Sloan, R. C., Maloney, A. H., Anderson, E. J., et al. (2010). Cardiac arrhythmias induced by glutathione oxidation can be inhibited by preventing mitochondrial depolarization. *J. Mol. Cell. Cardiol*. 48, 673–679. doi: 10.1016/j.yjmcc.2009.11.011

Caffarra Malvezzi, C., Cabassi, A., and Miragoli, M. (2020). Mitochondrial mechanosensor in cardiovascular diseases. *Vascular Biol*. 2, R85–R92. doi: 10.1530/VB-20-0002

Carè, A., Catalucci, D., Felicetti, F., Bonci, D., Addario, A., Gallo, P., et al. (2007). MicroRNA-133 controls cardiac hypertrophy. *Nat. Med*. 13, 613–618. doi: 10.1038/nm1582

Chang, L., Azzolin, L., Di Biagio, D., Zanconato, F., Battilana, G., Lucon Xiccato, R., et al. (2018). The SWI/SNF complex is a mechanoregulated inhibitor of YAP and TAZ. *Nature* 563, 265–269. doi: 10.1038/s41586-018-0658-1

Chen, J., Ma, Q., King, J. S., Sun, Y., Xu, B., Zhang, X., et al. (2016). aYAP modRNA reduces cardiac inflammation and hypertrophy in a murine ischemia-reperfusion model. *Life Sci. Alliance* 2020:3. doi: 10.26508/lsa.201900424

Chiou, K. K., Rocks, J. W., Chen, C. Y., Cho, S., Merkus, K. E., Rajaratnam, A., et al. (2016). Mechanical signaling coordinates the embryonic heartbeat. *Proc. Natl. Acad. Sci. U.S.A*. 113, 8939–8944. doi: 10.1073/pnas.1520428113

Cingolani, H. E., Pérez, N. G., Cingolani, O. H., Ennis, I. L. (2013). The anrep effect: 100 years later. *Am J Physiol Heart Circ Physiol*. 304:H175–H82. doi: 10.1152/ajpheart.00508.2012

Clause, K. C., Tinney, J. P., Liu, L. J., Keller, B. B., and Tobita, K. (2009). Engineered early embryonic cardiac tissue increases cardiomyocyte proliferation by cyclic mechanical stretch via p38-MAP kinase phosphorylation. *Tissue Eng. Part A*. 15, 1373–1380. doi: 10.1089/ten.tea.2008.0169

Collins, C., Osborne, L. D., Guilluy, C., Chen, Z., O'Brien, E. T. 3rd, Reader, J. S., et al. (2014). Haemodynamic and extracellular matrix cues regulate the mechanical phenotype and stiffness of aortic endothelial cells. *Nat. Commun*. 5:3984. doi: 10.1038/ncomms4984

de Brito, O. M., and Scorrano, L. (2008). Mitofusin 2 tethers endoplasmic reticulum to mitochondria. *Nature* 456, 605–610. doi: 10.1038/nature07534

de Cavanagh, E. M., Ferder, M., Inserra, F., and Ferder, L. (2009). Angiotensin II, mitochondria, cytoskeletal, and extracellular matrix connections: an integrating viewpoint. *Am. J. Physiol. Heart Circ. Physiol*. 296:H550–H558. doi: 10.1152/ajpheart.01176.2008

De Stefani, D., Patron, M., and Rizzuto, R. (2015). Structure and function of the mitochondrial calcium uniporter complex. *Biochim. Biophys. Acta*. 1853, 2006–2011. doi: 10.1016/j.bbamcr.2015.04.008

Delmar, M., and McKenna, W. J. (2010). The cardiac desmosome and arrhythmogenic cardiomyopathies: from gene to disease. *Circ. Res.* 107, 700–714. doi: 10.1161/CIRCRESAHA.110.223412

Dogan, A., Parmaksz, M., Elßin, A. E., and Elßin, Y. M. (2016). Extracellular matrix and regenerative therapies from the cardiac perspective. *Stem Cell Rev. Rep*. 12, 202–213. doi: 10.1007/s12015-015-9641-5

Dupont, S., Morsut, L., Aragona, M., Enzo, E., Giulitti, S., Cordenonsi, M., et al. (2011). Role of YAP/TAZ in mechanotransduction. *Nature* 474, 179–183. doi: 10.1038/nature10137

Earls, J. K., Jin, S., and Ye, K. (2013). Mechanobiology of human pluripotent stem cells. *Tissue Eng. Part B Rev*. 19, 420–430. doi: 10.1089/ten.teb.2012.0641

Fanchaouy, M., Polakova, E., Jung, C., Ogrodnik, J., Shirokova, N., and Niggli, E. (2009). Pathways of abnormal stress-induced Ca2+ influx into dystrophic mdx cardiomyocytes. *Cell Calcium.* 46, 114–21. doi: 10.1016/j.ceca.2009.06.002

Fang, L., Moore, X. L., Gao, X. M., Dart, A. M., Lim, Y. L., and Du, X. J. (2007). Down-regulation of mitofusin-2 expression in cardiac hypertrophy *in vitro* and *in vivo*. *Life Sci*. 80, 2154–2160. doi: 10.1016/j.lfs.2007.04.003

Fang, Y., Fu, D., and Shen, X. Z. (2010). The potential role of ubiquitin c-terminal hydrolases in oncogenesis. *Biochim. Biophys. Acta*. 1806, 1–6. doi: 10.1016/j.bbcan.2010.03.001

Fernandez-Caggiano, M., Kamynina, A., Francois, A. A., Prysyazhna, O., Eykyn, T. R., Krasemann, S., et al. (2020). Mitochondrial pyruvate carrier abundance mediates pathological cardiac hypertrophy. *Nat. Metab*. 2, 1223–1231. doi: 10.1038/s42255-020-00276-5

Fok, E. Y., and Zandstra, P. W. (2005). Shear-controlled single-step mouse embryonic stem cell expansion and embryoid body-based differentiation. *Stem Cells*. 23, 1333–1342. doi: 10.1634/stemcells.2005-0112

Forte, G., Pagliari, S., Ebara, M., Uto, K., Tam, J. K., Romanazzo, S., et al. (2012). Substrate stiffness modulates gene expression and phenotype in neonatal cardiomyocytes *in vitro*. *Tissue Eng. Part A*. 18, 1837–48. doi: 10.1089/ten.tea.2011.0707

Francisco, J., Zhang, Y., Jeong, J. I., Mizushima, W., Ikeda, S., Ivessa, A., et al. (2020). Blockade of fibroblast YAP attenuates cardiac fibrosis and dysfunction through MRTF-A inhibition. *JACC Basic Transl. Sci.* 5, 931–945. doi: 10.1016/j.jacbts.2020.07.009

Fujita, T., and Ishikawa, Y. (2011). Apoptosis in heart failure. -The role of the beta-adrenergic receptor-mediated signaling pathway and p53-mediated signaling pathway in the apoptosis of cardiomyocytes. *Circ. J.* 75, 1811–8. doi: 10.1253/circj.CJ-11-0025

Geiger, B., and Bershadsky, A. (2002). Exploring the neighborhood: adhesion-coupled cell mechanosensors. *Cell* 110, 139–142. doi: 10.1016/S0092-8674(02)00831-0

Geiger, B., Spatz, J. P., and Bershadsky, A. D. (2009). Environmental sensing through focal adhesions. *Nat. Rev. Mol. Cell Biol.* 10, 21–33. doi: 10.1038/nrm2593

Geisler, S., Holmström, K. M., Skujat, D., Fiesel, F. C., Rothfuss, O. C., Kahle, P. J., et al. (2010). PINK1/Parkin-mediated mitophagy is dependent on VDAC1 and p62/SQSTM1. *Nat. Cell Biol.* 12, 119–131. doi: 10.1038/ncb2012

Gholipour, M., and Tabrizi, A. (2020). The role of hippo signaling pathway in physiological cardiac hypertrophy. *BioImpacts* 10, 251–257. doi: 10.34172/bi.2020.32

Gómez, A. M., Ruiz-Hurtado, G., Benitah, J. P., and Domínguez-Rodríguez, A. (2013). Ca2+ fluxes involvement in gene expression during cardiac hypertrophy. *Curr. Vasc. Pharmacol*. 11, 497–506. doi: 10.2174/1570161111311040013

Gordon, K. J., and Blobe, G. C. (2008). Role of transforming growth factor-beta superfamily signaling pathways in human disease. *Biochim. Biophys. Acta*. 1782, 197–228. doi: 10.1016/j.bbadis.2008.01.006

Gottlieb, R. A., and Thomas, A. (2017). Mitophagy and mitochondrial quality control mechanisms in the heart. *Curr Pathobiol Rep*. 5, 161–169. doi: 10.1007/s40139-017-0133-y

Govoni, M., Muscari, C., Guarnieri, C., and Giordano, E. (2013). Mechanostimulation protocols for cardiac tissue engineering. *Biomed Res. Int*. 2013:918640. doi: 10.1155/2013/918640

Groenendijk, B. C., Hierck, B. P., Gittenberger-De Groot, A. C., and Poelmann, R. E. (2004). Development-related changes in the expression of shear stress responsive genes KLF-2, ET-1, and NOS-3 in the developing cardiovascular system of chicken embryos. *Dev. Dyn.* 230, 57–68. doi: 10.1002/dvdy.20029

Guo, Y., Kim, Y., Shimi, T., Goldman, R. D., and Zheng, Y. (2014). Concentration-dependent lamin assembly and its roles in the localization of other nuclear proteins. *Mol. Biol. Cell*. 25, 1287–1297. doi: 10.1091/mbc.e13-11-0644

Guo, Y., and Pu, W. T. (2020). Cardiomyocyte maturation: new phase in development. *Circ. Res.* 126, 1086–1106. doi: 10.1161/CIRCRESAHA.119.315862

Guo, Y., VanDusen, N. J., Zhang, L., Gu, W., Sethi, I., Guatimosim, S., et al. (2017). Analysis of cardiac myocyte maturation using CASAAV, a platform for rapid dissection of cardiac myocyte gene function *in vivo*. *Circ. Res.* 120, 1874–1888. doi: 10.1161/CIRCRESAHA.116.310283

Guo, Y., and Zheng, Y. (2013). Sculpting the nucleus with dynamic microtubules. *Dev. Cell*. 27, 1–2. doi: 10.1016/j.devcel.2013.09.027

Guo, Y., and Zheng, Y. (2015). Lamins position the nuclear pores and centrosomes by modulating dynein. *Mol. Biol. Cell*. 26, 3379–3389. doi: 10.1091/mbc.E15-07-0482

Gwak, S. J., Bhang, S. H., Kim, I. K., Kim, S. S., Cho, S. W., Jeon, O., et al. (2008). The effect of cyclic strain on embryonic stem cell-derived cardiomyocytes. *Biomaterials* 29, 844–856. doi: 10.1016/j.biomaterials.2007.10.050

Hammerling, B. C., and Gustafsson, Å. B. (2014). Mitochondrial quality control in the myocardium: cooperation between protein degradation and mitophagy. *J. Mol. Cell. Cardiol*. 75, 122–130. doi: 10.1016/j.yjmcc.2014.07.013

Hartill, V. L., van de Hoek, G., Patel, M. P., Little, R., Watson, C. M., Berry, I. R., et al. (2018). DNAAF1 links heart laterality with the AAA+ ATPase RUVBL1 and ciliary intraflagellar transport. *Hum. Mol. Genet*. 27, 529–545. doi: 10.1093/hmg/ddx422

He, A., Gu, F., Hu, Y., Ma, Q., Ye, L. Y., Akiyama, J. A., et al. (2014). Dynamic GATA4 enhancers shape the chromatin landscape central to heart development and disease. *Nat. Commun*. 5:4907. doi: 10.1038/ncomms5907

Herum, K. M., Lunde, I. G., McCulloch, A. D., and Christensen, G. (2017). The soft- and hard-heartedness of cardiac fibroblasts: mechanotransduction signaling pathways in fibrosis of the heart. *J. Clin. Med.* 6:53. doi: 10.3390/jcm6050053

Hirt, M. N., Hansen, A., and Eschenhagen, T. (2014). Cardiac tissue engineering: state of the art. *Circ. Res.* 114, 354–367. doi: 10.1161/CIRCRESAHA.114.300522

Ho, C. Y., Jaalouk, D. E., Vartiainen, M. K., and Lammerding, J. (2013). Lamin A/C and emerin regulate MKL1-SRF activity by modulating actin dynamics. *Nature* 497, 507–511. doi: 10.1038/nature12105

Hoffman, N. E., Chandramoorthy, H. C., Shanmughapriya, S., Zhang, X. Q., Vallem, S., Doonan, P. J., et al. (2014). SLC25A23 augments mitochondrial Ca²? uptake, interacts with MCU, and induces oxidative stress-mediated cell death. *Mol. Biol. Cell*. 25, 936–947. doi: 10.1091/mbc.e13-08-0502

Horn, M. A., and Trafford, A. W. (2016). Aging and the cardiac collagen matrix: novel mediators of fibrotic remodelling. *J. Mol. Cell. Cardiol*. 93, 175–185. doi: 10.1016/j.yjmcc.2015.11.005

Hu, J., Li, Z., Xu, L. T., Sun, A. J., Fu, X. Y., Zhang, L., et al. (2015). Protective effect of apigenin on ischemia/reperfusion injury of the isolated rat heart. *Cardiovasc. Toxicol*. 15, 241–249. doi: 10.1007/s12012-014-9290-y

Huss, J. M., and Kelly, D. P. (2005). Mitochondrial energy metabolism in heart failure: a question of balance. *J. Clin. Invest*. 115, 547–555. doi: 10.1172/JCI24405

Iribe, G., Kaihara, K., Yamaguchi, Y., Nakaya, M., Inoue, R., and Naruse, K. (2017). Mechano-sensitivity of mitochondrial function in mouse cardiac myocytes. *Prog. Biophys. Mol. Biol*. 130, 315–322. doi: 10.1016/j.pbiomolbio.2017.05.015

Iribe, G., and Kohl, P. (2008). Axial stretch enhances sarcoplasmic reticulum Ca2+ leak and cellular Ca2+ reuptake in guinea pig ventricular myocytes: experiments and models. *Prog. Biophys. Mol. Biol*. 97, 298–311. doi: 10.1016/j.pbiomolbio.2008.02.012

Iribe, G., Ward, C. W., Camelliti, P., Bollensdorff, C., Mason, F., Burton, R. A., et al. (2009). Axial stretch of rat single ventricular cardiomyocytes causes an acute and transient increase in Ca2+ spark rate. *Circ. Res*. 104, 787–795. doi: 10.1161/CIRCRESAHA.108.193334

Ishikawa, K., Aguero, J., Naim, C., Fish, K., and Hajjar, R. J. (2013). Percutaneous approaches for efficient cardiac gene delivery. *J. Cardiovasc. Transl. Res*. 6, 649–659. doi: 10.1007/s12265-013-9479-7

Israeli-Rosenberg, S., Manso, A. M., Okada, H., and Ross, R. S. (2014). Integrins and integrin-associated proteins in the cardiac myocyte. *Circ. Res.* 114, 572–586. doi: 10.1161/CIRCRESAHA.114.301275

Jacot, J. G., Kita-Matsuo, H., Wei, K. A., Chen, H. S., Omens, J. H., Mercola, M., et al. (2010). Cardiac myocyte force development during differentiation and maturation. *Ann. N. Y. Acad. Sci.* 1188, 121–127. doi: 10.1111/j.1749-6632.2009.05091.x

Jongsma, H. J., and Wilders, R. (2000). Gap junctions in cardiovascular disease. *Circ. Res.* 86, 1193–1197. doi: 10.1161/01.RES.86.12.1193

Kaasik, A., Joubert, F., Ventura-Clapier, R., and Veksler, V. (2004). A novel mechanism of regulation of cardiac contractility by mitochondrial functional state. *FASEB J.* 18, 1219–1227. doi: 10.1096/fj.04-1508com

Kageyama, Y., Hoshijima, M., Seo, K., Bedja, D., Sysa-Shah, P., Andrabi, S. A., et al. (2014). Parkin-independent mitophagy requires Drp1 and maintains the integrity of mammalian heart and brain. *EMBO J.* 33, 2798–2813. doi: 10.15252/embj.201488658

Karbassi, E., Fenix, A., Marchiano, S., Muraoka, N., Nakamura, K., Yang, X., et al. (2020). Cardiomyocyte maturation: advances in knowledge and implications for regenerative medicine. *Nat. Rev. Cardiol.* 17, 341–359. doi: 10.1038/s41569-019-0331-x

Kashihara, T., and Sadoshima, J. (2019). Role of YAP/TAZ in energy metabolism in the heart. *J. Cardiovasc. Pharmacol.* 74, 483–490. doi: 10.1097/FJC.0000000000000736

Khairallah, R. J., Shi, G., Sbrana, F., Prosser, B. L., Borroto, C., Mazaitis, M. J., et al. (2012). Microtubules underlie dysfunction in duchenne muscular dystrophy. *Sci. Signal.* 5:ra56. doi: 10.1126/scisignal.2002829

Kim, J. C., Pérez-Hernández, M., Alvarado, F. J., Maurya, S. R., Montnach, J., Yin, Y., et al. (2019). Disruption of Ca(2+)(i) homeostasis and connexin 43 hemichannel function in the right ventricle precedes overt arrhythmogenic cardiomyopathy in plakophilin-2-deficient mice. *Circulation* 140, 1015–1030. doi: 10.1161/CIRCULATIONAHA.119.039710

Kim, T., Yang, S. J., Hwang, D., Song, J., Kim, M., Kyum Kim, S., et al. (2015). A basal-like breast cancer-specific role for SRF-IL6 in YAP-induced cancer stemness. *Nat. Commun.* 6:10186. doi: 10.1038/ncomms10186

Kirichok, Y., Krapivinsky, G., and Clapham, D. E. (2004). The mitochondrial calcium uniporter is a highly selective ion channel. *Nature* 427, 360–364. doi: 10.1038/nature02246

Kluge, A., Rangrez, A. Y., Kilian, L. S., Pott, J., Bernt, A., Frauen, R., et al. (2019). Rho-family GTPase 1 (Rnd1) is a biomechanical stress-sensitive activator of cardiomyocyte hypertrophy. *J. Mol. Cell. Cardiol.* 129, 130–143. doi: 10.1016/j.yjmcc.2019.01.028

Koo, J. H., and Guan, K. L. (2018). Interplay between YAP/TAZ and metabolism. *Cell Metab.* 28, 196–206. doi: 10.1016/j.cmet.2018.07.010

Koshiba, T., Detmer, S. A., Kaiser, J. T., Chen, H., McCaffery, J. M., and Chan, D. C. (2004). Structural basis of mitochondrial tethering by mitofusin complexes. *Science* 305, 858–862. doi: 10.1126/science.1099793

Kresh, J. Y., and Chopra, A. (2011). Intercellular and extracellular mechanotransduction in cardiac myocytes. *Pflugers Archiv Eur. J. Physiol.* 462, 75–87. doi: 10.1007/s00424-011-0954-1

Kudo, S., Morigaki, R., Saito, J., Ikeda, M., Oka, K., and Tanishita, K. (2000). Shear-stress effect on mitochondrial membrane potential and albumin uptake in cultured endothelial cells. *Biochem. Biophys. Res. Commun.* 270, 616–621. doi: 10.1006/bbrc.2000.2482

Kurihara, S., and Komukai, K. (1995). Tension-dependent changes of the intracellular Ca2+ transients in ferret ventricular muscles. *J Physiol.* 489(Pt 3), 617–625. doi: 10.1113/jphysiol.1995.sp021077

Kuzmicic, J., Del Campo, A., López-Crisosto, C., Morales, P. E., Pennanen, C., Bravo-Sagua, R., et al. (2011). Mitochondrial dynamics: a potential new therapeutic target for heart failure. *Rev. Esp. Cardiol.* 64, 916–923. doi: 10.1016/j.rec.2011.05.022

Lahera, V., de Las Heras, N., López-Farré, A., Manucha, W., and Ferder, L. (2017). Role of mitochondrial dysfunction in hypertension and obesity. *Curr. Hypertens. Rep.* 19:11. doi: 10.1007/s11906-017-0710-9

Lee, J., Fei, P., Packard, R. R., Kang, H., Xu, H., Baek, K. I., et al. (2016). 4-dimensional light-sheet microscopy to elucidate shear stress modulation of cardiac trabeculation. *J. Clin. Invest.* 126, 1679–90. doi: 10.1172/JCI83496

Lee, J. M., Nobumori, C., Tu, Y., Choi, C., Yang, S. H., Jung, H. J., et al. (2016). Modulation of LMNA splicing as a strategy to treat prelamin A diseases. *J. Clin. Invest.* 126, 1592–1602. doi: 10.1172/JCI85908

Lee, S. R., Kim, N., Noh, Y. H., Xu, Z., Ko, K. S., Rhee, B. D., et al. (2017). Mitochondrial DNA, mitochondrial dysfunction, and cardiac manifestations. *Front. Biosci.* 22, 1177–1194. doi: 10.2741/4541

Leonhard, K., Guiard, B., Pellecchia, G., Tzagoloff, A., Neupert, W., and Langer, T. (2000). Membrane protein degradation by AAA proteases in mitochondria: extraction of substrates from either membrane surface. *Mol. Cell.* 5, 629–638. doi: 10.1016/S1097-2765(00)80242-7

Li, J., Horak, K. M., Su, H., Sanbe, A., Robbins, J., and Wang, X. (2011). Enhancement of proteasomal function protects against cardiac proteinopathy and ischemia/reperfusion injury in mice. *J. Clin. Invest.* 121, 3689–3700. doi: 10.1172/JCI45709

Liang, L., Tu, Y., Lu, J., Wang, P., Guo, Z., Wang, Q., et al. (2019). Dkk1 exacerbates doxorubicin-induced cardiotoxicity by inhibiting the Wnt/β-catenin signaling pathway. *J. Cell Sci.* 132:jcs228478. doi: 10.1242/jcs.228478

Liao, X. D., Tang, A. H., Chen, Q., Jin, H. J., Wu, C. H., Chen, L.-Y., et al. (2003). Role of Ca2+ signaling in initiation of stretch-induced apoptosis in neonatal heart *Cells* 310, 405–411. doi: 10.1016/j.bbrc.2003.09.023

Linari, M., Brunello, E., Reconditi, M., Fusi, L., Caremani, M., Narayanan, T., et al. (2015). Force generation by skeletal muscle is controlled by mechanosensing in myosin filaments. *Nature* 528, 276–279. doi: 10.1038/nature15727

Liu, L., An, X., Li, Z., Song, Y., Li, L., Zuo, S., et al. (2016). The H19 long noncoding RNA is a novel negative regulator of cardiomyocyte hypertrophy. *Cardiovasc. Res.* 111, 56–65. doi: 10.1093/cvr/cvw078

Liu, L., Feng, D., Chen, G., Chen, M., Zheng, Q., Song, P., et al. (2012). Mitochondrial outer-membrane protein FUNDC1 mediates hypoxia-induced mitophagy in mammalian cells. *Nat. Cell Biol.* 14, 177–185. doi: 10.1038/ncb2422

Liu, L., Zhang, D., and Li, Y. (2020). LncRNAs in cardiac hypertrophy: from basic science to clinical application. *J. Cell. Mol. Med.* 24, 11638–11645. doi: 10.1111/jcmm.15819

Lokuta, A. J., Maertz, N. A., Meethal, S. V., Potter, K. T., Kamp, T. J., Valdivia, H. H., et al. (2005). Increased nitration of sarcoplasmic reticulum Ca2+-ATPase in human heart failure. *Circulation* 111, 988–995. doi: 10.1161/01.CIR.0000156461.81529.D7

Lopaschuk, G. D., Ussher, J. R., Folmes, C. D., Jaswal, J. S., and Stanley, W. C. (2010). Myocardial fatty acid metabolism in health and disease. *Physiol. Rev.* 90, 207–258. doi: 10.1152/physrev.00015.2009

Lorenz, L., Axnick, J., Buschmann, T., Henning, C., Urner, S., Fang, S., et al. (2018). Mechanosensing by Œ≤1 integrin induces angiocrine signals for liver growth and survival. *Nature* 562, 128–132. doi: 10.1038/s41586-018-0522-3

Lou, Q., Janardhan, A., and Efimov, I. R. (2012). Remodeling of calcium handling in human heart failure. *Adv. Exp. Med. Biol.* 740, 1145–1174. doi: 10.1007/978-94-007-2888-2_52

Lv, L., Li, T., Li, X., Xu, C., Liu, Q., Jiang, H., et al. (2018). The lncRNA Plscr4 controls cardiac hypertrophy by regulating miR-214. *Mol. Ther. Nucleic Acids* 10, 387–397. doi: 10.1016/j.omtn.2017.12.018

Lyra-Leite, D. M., Petersen, A. P., Ariyasinghe, N. R., Cho, N., and McCain, M. L. (2020). Mitochondrial architecture in cardiac myocytes depends on cell shape and matrix rigidity. *J. Mol. Cell. Cardiol.* 150, 32–43. doi: 10.1016/j.yjmcc.2020.10.004

Ma, S., and Dong, Z. (2019). Melatonin attenuates cardiac reperfusion stress by improving OPA1-related mitochondrial fusion in a yap-hippo pathway-dependent manner. *J. Cardiovasc. Pharmacol.* 73, 27–39. doi: 10.1097/FJC.0000000000000626

Majkut, S., Dingal, P. C., and Discher, D. E. (2014). Stress sensitivity and mechanotransduction during heart development. *Curr. Biol.*. 24, R495–R501. doi: 10.1016/j.cub.2014.04.027

Mallilankaraman, K., Cárdenas, C., Doonan, P. J., Chandramoorthy, H. C., Irrinki, K. M., Golenár, T., et al. (2015). MCUR1 is an essential component of mitochondrial Ca(2+) uptake that regulates cellular metabolism. *Nat. Cell Biol.* 17:953. doi: 10.1038/ncb3202

Mammoto, T., and Ingber, D. E. (2010). Mechanical control of tissue and organ development. *Development* 137, 1407–1420. doi: 10.1242/dev.024166

Maniotis, A. J., Chen, C. S., and Ingber, D. E. (1997). Demonstration of mechanical connections between integrins, cytoskeletal filaments, and nucleoplasm that

stabilize nuclear structure. *Proc. Natl. Acad. Sci. U.S.A.* 94, 849–854. doi: 10.1073/pnas.94.3.849

McCully, J. D., Rousou, A. J., Parker, R. A., and Levitsky, S. (2007). Age- and gender-related differences in mitochondrial oxygen consumption and calcium with cardioplegia and diazoxide. *Ann. Thorac. Surg.* 83, 1102–1109. doi: 10.1016/j.athoracsur.2006.10.059

Meng, Z., Qiu, Y., Lin, K. C., Kumar, A., Placone, J. K., Fang, C., et al. (2018). RAP2 mediates mechanoresponses of the Hippo pathway. *Nature* 560, 655–660. doi: 10.1038/s41586-018-0444-0

Miller, C. E., Donlon, K. J., Toia, L., Wong, C. L., and Chess, P. R. (2000). Cyclic strain induces proliferation of cultured embryonic heart cells. *In Vitro Cell. Dev. Biol. Anim.* 36, 633–639. doi: 10.1290/1071-2690(2000)036<0633:CSIPOC>2.0.CO;2

Mohamed, B. A., Schnelle, M., Khadjeh, S., Lbik, D., Herwig, M., Linke, W. A., et al. (2016). Molecular and structural transition mechanisms in long-term volume overload. *Eur. J. Heart Fail.* 18, 362–371. doi: 10.1002/ejhf.465

Moncayo-Arlandi, J., and Brugada, R. (2017). Unmasking the molecular link between arrhythmogenic cardiomyopathy and Brugada syndrome. *Nat. Rev. Cardiol.* 14, 744–756. doi: 10.1038/nrcardio.2017.103

Mosqueira, D., Pagliari, S., Uto, K., Ebara, M., Romanazzo, S., Escobedo-Lucea, C., et al. (2014). Hippo pathway effectors control cardiac progenitor cell fate by acting as dynamic sensors of substrate mechanics and nanostructure. *ACS Nano* 8, 2033–2047. doi: 10.1021/nn4058984

Murry, C. E., and Keller, G. (2008). Differentiation of embryonic stem cells to clinically relevant populations: lessons from embryonic development. *Cell* 132, 661–680. doi: 10.1016/j.cell.2008.02.008

Nakai, A., Yamaguchi, O., Takeda, T., Higuchi, Y., Hikoso, S., Taniike, M., et al. (2007). The role of autophagy in cardiomyocytes in the basal state and in response to hemodynamic stress. *Nat. Med.* 13, 619–624. doi: 10.1038/nm1574

Narimatsu, M., Samavarchi-Tehrani, P., Varelas, X., and Wrana, J. L. (2015). Distinct polarity cues direct Taz/Yap and TGFbeta receptor localization to differentially control TGFbeta-induced smad signaling. *Dev. Cell.* 32, 652–656. doi: 10.1016/j.devcel.2015.02.019

Nishida, K., and Otsu, K. (2017). Sterile inflammation and degradation systems in heart failure. *Circ. J.* 81, 622–628. doi: 10.1253/circj.CJ-17-0261

Oria, R., Wiegand, T., Escribano, J., Elosegui-Artola, A., Uriarte, J. J., Moreno-Pulido, C., et al. (2017). Force loading explains spatial sensing of ligands by cells. *Nature* 552, 219–224. doi: 10.1038/nature24662

Palty, R., Silverman, W. F., Hershfinkel, M., Caporale, T., Sensi, S. L., Parnis, J., et al. (2010). NCLX is an essential component of mitochondrial Na+/Ca2+ exchange. *Proc. Natl. Acad. Sci. U.S.A.* 107, 436–441. doi: 10.1073/pnas.0908099107

Pandur, P. (2005). What does it take to make a heart? *Biology Cell.* 97, 197–210. doi: 10.1042/BC20040109

Pasqualini, F. S., Nesmith, A. P., Horton, R. E., Sheehy, S. P., and Parker, K. K. (2016). Mechanotransduction and metabolism in cardiomyocyte microdomains. *Biomed Res. Int.* 2016:4081638. doi: 10.1155/2016/4081638

Pedrozo, Z., Criollo, A., Battiprolu, P. K., Morales, C. R., Contreras-Ferrat, A., Fernández, C., et al. (2015). Polycystin-1 is a cardiomyocyte mechanosensor that governs L-type Ca2+ channel protein stability. *Circulation* 131, 2131–2142. doi: 10.1161/CIRCULATIONAHA.114.013537

Penna, C., Mancardi, D., Rastaldo, R., and Pagliaro, P. (2009). Cardioprotection: a radical view free radicals in pre and postconditioning. *Biochim. Biophys. Acta.* 1787, 781–793. doi: 10.1016/j.bbabio.2009.02.008

Pennanen, C., Parra, V., López-Crisosto, C., Morales, P. E., Del Campo, A., Gutierrez, T., et al. (2014). Mitochondrial fission is required for cardiomyocyte hypertrophy mediated by a Ca2+-calcineurin signaling pathway. *J. Cell Sci.* 127, 2659–2671. doi: 10.1242/jcs.139394

Perocchi, F., Gohil, V. M., Girgis, H. S., Bao, X. R., McCombs, J. E., Palmer, A. E., et al. (2010). MICU1 encodes a mitochondrial EF hand protein required for Ca(2+) uptake. *Nature* 467, 291–296. doi: 10.1038/nature09358

Petroff, M. G., Kim, S. H., Pepe, S., Dessy, C., Marban, E., Balligand, J. L., et al. (2001). Endogenous nitric oxide mechanisms mediate the stretch dependence of Ca2+ release in cardiomyocytes. *Nat. Cell Biol.* 3, 867–873. doi: 10.1038/ncb1001-867

Pickles, S., Vigié P., and Youle, R. J. (2018). Mitophagy and quality control mechanisms in mitochondrial maintenance. *Curr. Biol.* 28, R170–r85. doi: 10.1016/j.cub.2018.01.004

Pimentel, D. R., Amin, J. K., Xiao, L., Miller, T., Viereck, J., Oliver-Krasinski, J., et al. (2001). Reactive oxygen species mediate amplitude-dependent hypertrophic and apoptotic responses to mechanical stretch in cardiac myocytes. *Circ. Res.* 89, 453–460. doi: 10.1161/hh1701.096615

Predmore, J. M., Wang, P., Davis, F., Bartolone, S., Westfall, M. V., Dyke, D. B., et al. (2010). Ubiquitin proteasome dysfunction in human hypertrophic and dilated cardiomyopathies. *Circulation.* 121, 997–1004. doi: 10.1161/CIRCULATIONAHA.109.904557

Prosser, B. L., Ward, C. W., and Lederer, W. J. (2011). X-ROS signaling: rapid mechano-chemo transduction in heart. *Science* 333, 1440–1445. doi: 10.1126/science.1202768

Pu, W. T., Ishiwata, T., Juraszek, A. L., Ma, Q., and Izumo, S. (2004). GATA4 is a dosage-sensitive regulator of cardiac morphogenesis. *Dev. Biol.* 275, 235–244. doi: 10.1016/j.ydbio.2004.08.008

Ren, X., Chen, L., Xie, J., Zhang, Z., Dong, G., Liang, J., et al. (2017). Resveratrol ameliorates mitochondrial elongation via Drp1/Parkin/PINK1 signaling in senescent-like cardiomyocytes. *Oxid. Med. Cell. Longev.* 2017:4175353. doi: 10.1155/2017/4175353

Rienks, M., Papageorgiou, A. P., Frangogiannis, N. G., and Heymans, S. (2014). Myocardial extracellular matrix: an ever-changing and diverse entity. *Circ. Res.* 114, 872–888. doi: 10.1161/CIRCRESAHA.114.302533

Rizzuto, R., Pinton, P., Carrington, W., Fay, F. S., Fogarty, K. E., Lifshitz, L. M., et al. (1998). Close contacts with the endoplasmic reticulum as determinants of mitochondrial Ca2+ responses. *Science* 280, 1763–1766. doi: 10.1126/science.280.5370.1763

Ruan, J. L., Tulloch, N. L., Razumova, M. V., Saiget, M., Muskheli, V., Pabon, L., et al. (2016). Mechanical stress conditioning and electrical stimulation promote contractility and force maturation of induced pluripotent stem cell-derived human cardiac tissue. *Circulation* 134, 1557–1567. doi: 10.1161/CIRCULATIONAHA.114.014998

Saguner, A. M., Duru, F., and Brunckhorst, C. B. (2013). Arrhythmogenic right ventricular cardiomyopathy: a challenging disease of the intercalated disc. *Circulation* 128, 1381–1386. doi: 10.1161/CIRCULATIONAHA.112.001009

Salameh, A., Wustmann, A., Karl, S., Blanke, K., Apel, D., Rojas-Gomez, D., et al. (2010). Cyclic mechanical stretch induces cardiomyocyte orientation and polarization of the gap junction protein connexin43. *Circ. Res.* 106, 1592–1602. doi: 10.1161/CIRCRESAHA.109.214429

Sancak, Y., Markhard, A. L., Kitami, T., Kovács-Bogdán, E., Kamer, K. J., Udeshi, N. D., et al. (2013). EMRE is an essential component of the mitochondrial calcium uniporter complex. *Science* 342, 1379–1382. doi: 10.1126/science.1242993

Santel, A., and Frank, S. (2008). Shaping mitochondria: The complex posttranslational regulation of the mitochondrial fission protein DRP1. *IUBMB Life.* 60, 448–455. doi: 10.1002/iub.71

Santulli, G., Lewis, D., des Georges, A., Marks, A. R., and Frank, J. (2018). Ryanodine receptor structure and function in health and disease. *Subcell. Biochem.* 87, 329–352. doi: 10.1007/978-981-10-7757-9_11

Sato, P. Y., Coombs, W., Lin, X., Nekrasova, O., Green, K. J., Isom, L. L., et al. (2011). Interactions between ankyrin-G, plakophilin-2, and connexin43 at the cardiac intercalated disc. *Circ. Res.* 109, 193–201. doi: 10.1161/CIRCRESAHA.111.247023

Saucerman, J. J., Tan, P. M., Buchholz, K. S., McCulloch, A. D., and Omens, J. H. (2019). Mechanical regulation of gene expression in cardiac myocytes and fibroblasts. *Nat. Rev. Cardiol.* 16, 361–378. doi: 10.1038/s41569-019-0155-8

Schmelter, M., Ateghang, B., Helmig, S., Wartenberg, M., and Sauer, H. (2006). Embryonic stem cells utilize reactive oxygen species as transducers of mechanical strain-induced cardiovascular differentiation. *FASEB J.* 20, 1182–1184. doi: 10.1096/fj.05-4723fje

Sessions, A. O., Kaushik, G., Parker, S., Raedschelders, K., Bodmer, R., Van Eyk, J. E., et al. (2017). Extracellular matrix downregulation in the Drosophila heart preserves contractile function and improves lifespan. *Matrix Biol.* 62, 15–27. doi: 10.1016/j.matbio.2016.10.008

Shafa, M., Sjonnesen, K., Yamashita, A., Liu, S., Michalak, M., Kallos, M. S., et al. (2012). Expansion and long-term maintenance of induced pluripotent stem

cells in stirred suspension bioreactors. *J. Tissue Eng. Regen. Med.* 6, 462–472. doi: 10.1002/term.450

Song, M., Gong, G., Burelle, Y., Gustafsson, Å. B., Kitsis, R. N., Matkovich, S. J., et al. (2015a). Interdependence of parkin-mediated mitophagy and mitochondrial fission in adult mouse hearts. *Circ. Res.* 117, 346–351. doi: 10.1161/CIRCRESAHA.117.306859

Song, M., Mihara, K., Chen, Y., Scorrano, L., and Dorn, G. W. 2nd. (2015b). Mitochondrial fission and fusion factors reciprocally orchestrate mitophagic culling in mouse hearts and cultured fibroblasts. *Cell Metab.* 21, 273–286. doi: 10.1016/j.cmet.2014.12.011

Stanley, W. C., Recchia, F. A., and Lopaschuk, G. D. (2005). Myocardial substrate metabolism in the normal and failing heart. *Physiol. Rev.* 85, 1093–1129. doi: 10.1152/physrev.00006.2004

Sun, S., Zhang, M., Lin, J., Hu, J., Zhang, R., Li, C., et al. (2016). Lin28a protects against diabetic cardiomyopathy via the PKA/ROCK2 pathway. *Biochem. Biophys. Res. Commun.* 469, 29–36. doi: 10.1016/j.bbrc.2015.11.065

Sun, Y., Fan, W., Xue, R., Dong, B., Liang, Z., Chen, C., et al. (2020). Transcribed Ultraconserved Regions, Uc.323, ameliorates cardiac hypertrophy by regulating the transcription of CPT1b (carnitine palmitoyl transferase 1b). *Hypertension* 75, 79–90. doi: 10.1161/HYPERTENSIONAHA.119.13173

Sun, Z., Costell, M., and Fässler, R. (2019). Integrin activation by talin, kindlin and mechanical forces. *Nat. Cell Biol.* 21, 25–31. doi: 10.1038/s41556-018-0234-9

Sylva, M., van den Hoff, M. J., and Moorman, A. F. (2014). Development of the human heart. *Am. J. Med. Genetics Part A.* 164a, 1347–1371. doi: 10.1002/ajmg.a.35896

Totaro, A., Panciera, T., and Piccolo, S. (2018). YAP/TAZ upstream signals and downstream responses. *Nat. Cell Biol.* 20, 888–899. doi: 10.1038/s41556-018-0142-z

Tsakiri, E. N., and Trougakos, I. P. (2015). The amazing ubiquitin-proteasome system: structural components and implication in aging. *Int. Rev. Cell Mol. Biol.* 314, 171–237. doi: 10.1016/bs.ircmb.2014.09.002

Tyser, R. C., Miranda, A. M., Chen, C. M., Davidson, S. M., Srinivas, S., and Riley, P. R. (2016). Calcium handling precedes cardiac differentiation to initiate the first heartbeat. *eLife*. 5:e17113. doi: 10.7554/eLife.17113

Ulmer, B. M., and Eschenhagen, T. (2020). Human pluripotent stem cell-derived cardiomyocytes for studying energy metabolism. *Biochim. Biophys. Acta. Mol. Cell. Res.* 1867:118471. doi: 10.1016/j.bbamcr.2019.04.001

van Tintelen, J. P., and Hauer, R. N. (2009). Cardiomyopathies: new test for arrhythmogenic right ventricular cardiomyopathy. *Nat. Rev. Cardiol.* 6, 450–451. doi: 10.1038/nrcardio.2009.97

VanDusen, N. J., Guo, Y., Gu, W., and Pu, W. T. (2017). CASAAV: A CRISPR-based platform for rapid dissection of gene function *in vivo*. *Curr. Protoc. Mol. Biol.* 120:31.11.1–31.11.4. doi: 10.1002/cpmb.46

Ventura-Clapier, R., Garnier, A., and Veksler, V. (2004). Energy metabolism in heart failure. *J Physiol.* 555, 1–13. doi: 10.1113/jphysiol.2003.055095

Viereck, J. K. R., Foinquinos, A., Xiao, K., Avramopoulos, P., Kunz, M., Dittrich, M., et al. (2016). Long noncoding RNA Chast promotes-cardiac remodeling. *Sci. Transl. Med.* 8:326ra22. doi: 10.1126/scitranslmed.aaf1475

Wang, G., McCain, M. L., Yang, L., He, A., Pasqualini, F. S., Agarwal, A., et al. (2014). Modeling the mitochondrial cardiomyopathy of Barth syndrome with induced pluripotent stem cell and heart-on-chip technologies. *Nat. Med.* 20, 616–623. doi: 10.1038/nm.3545

Wang, L., Wang, J., Li, G., and Xiao, J. (2020). Non-coding RNAs in physiological cardiac hypertrophy. *Adv. Exp. Med. Biol.* 1229, 149–161. doi: 10.1007/978-981-15-1671-9_8

Wang, N., Butler, J. P., and Ingber, D. E. (1993). Mechanotransduction across the cell surface and through the cytoskeleton. *Science* 260, 1124–1127. doi: 10.1126/science.7684161

Wang, S., Guo, Y., and Pu, W. T. (2021). AAV gene transfer to the heart. *Methods Mol. Biol.* 2158, 269–280. doi: 10.1007/978-1-0716-0668-1_20

Wang, S., Li, Y., Xu, Y., Ma, Q., Lin, Z., Schlame, M., et al. (2020). AAV gene therapy prevents and reverses heart failure in a murine knockout model of barth syndrome. *Circ. Res.* 126, 1024–1039. doi: 10.1161/CIRCRESAHA.119.315956

Werner, E., and Werb, Z. (2002). Integrins engage mitochondrial function for signal transduction by a mechanism dependent on Rho GTPases. *J. Cell Biol.* 158, 357–368. doi: 10.1083/jcb.200111028

Xia, S., Wang, X., Yue, P., Li, Y., and Zhang, D. (2020). Establishment of induced pluripotent stem cell lines from a family of an ARVC patient receiving heart transplantation in infant age carrying compound heterozygous mutations in DSP gene. *Stem Cell Res.* 48:101977. doi: 10.1016/j.scr.2020.101977

Xiang, K., Qin, Z., Zhang, H., and Liu, X. (2020). Energy metabolism in exercise-induced physiologic cardiac hypertrophy. *Front. Pharmacol.* 11:1133. doi: 10.3389/fphar.2020.01133

Yan, S. M., Li, H., Shu, Q., Wu, W. J., Luo, X. M., and Lu, L. (2019). LncRNA SNHG1 exerts a protective role in cardiomyocytes hypertrophy via targeting miR-15a-5p/HMGA1 axis. *Cell Biol Int.* 44, 1009–1019. doi: 10.1002/cbin.11298

Ye, Z., Zhou, Y., Cai, H., and Tan, W. (2011). Myocardial regeneration: roles of stem cells and hydrogels. *Adv. Drug Deliv. Rev.* 63, 688–697. doi: 10.1016/j.addr.2011.02.007

Yu, E. P., and Bennett, M. R. (2014). Mitochondrial DNA damage and atherosclerosis. *Trends Endocrinol. Metab.* 25, 481–487. doi: 10.1016/j.tem.2014.06.008

Zamorano-León, J. J., Modrego, J., Mateos-Cáceres, P. J., Macaya, C., Martín-Fernández, B., Miana, M., et al. (2010). A proteomic approach to determine changes in proteins involved in the myocardial metabolism in left ventricles of spontaneously hypertensive rats. *Cell. Physiol. Biochem.* 25, 347–358. doi: 10.1159/000276567

Zeigler, A. C., Richardson, W. J., Holmes, J. W., and Saucerman, J. J. (2016). A computational model of cardiac fibroblast signaling predicts context-dependent drivers of myofibroblast differentiation. *J. Mol. Cell. Cardiol.* 94, 72–81. doi: 10.1016/j.yjmcc.2016.03.008

Zeisberg, E. M., Ma, Q., Juraszek, A. L., Moses, K., Schwartz, R. J., Izumo, S., et al. (2005). Morphogenesis of the right ventricle requires myocardial expression of Gata4. *J. Clin. Invest.* 115, 1522–1531. doi: 10.1172/JCI23769

Zhang, D., Li, Y., Heims-Waldron, D., Bezzerides, V., Guatimosim, S., Guo, Y., et al. (2018). Mitochondrial cardiomyopathy caused by elevated reactive oxygen species and impaired cardiomyocyte proliferation. *Circ. Res.* 122, 74–87. doi: 10.1161/CIRCRESAHA.117.311349

Zhang, J., Liang, Y., Huang, X., Guo, X., Liu, Y., Zhong, J., et al. (2019). STAT3-induced upregulation of lncRNA MEG3 regulates the growth of cardiac hypertrophy through miR-361-5p/HDAC9 axis. *Sci. Rep.* 9:460. doi: 10.1038/s41598-018-36369-1

Zhang, M., Jiang, Y., Guo, X., Zhang, B., Wu, J., Sun, J., et al. (2019). Long non-coding RNA cardiac hypertrophy-associated regulator governs cardiac hypertrophy via regulating miR-20b and the downstream PTEN/AKT pathway. *J. Cell. Mol. Med.* 23, 7685–7698. doi: 10.1111/jcmm.14641

Zhang, X., Li, Z. L., Crane, J. A., Jordan, K. L., Pawar, A. S., Textor, S. C., et al. (2014). Valsartan regulates myocardial autophagy and mitochondrial turnover in experimental hypertension. *Hypertension* 64, 87–93. doi: 10.1161/HYPERTENSIONAHA.113.02151

Zhang, Y., Qi, Y., Li, J. J., He, W. J., Gao, X. H., Zhang, Y., et al. (2020). Stretch-induced sarcoplasmic reticulum calcium leak is causatively associated with atrial fibrillation in pressure-overloaded hearts. *Cardiovascular Res.* cvaa163. doi: 10.1093/cvr/cvaa163. [Epub ahead of print].

Zhao, B., Li, L., Wang, L., Wang, C. Y., Yu, J., and Guan, K. L. (2012). Cell detachment activates the Hippo pathway via cytoskeleton reorganization to induce anoikis. *Genes Dev.* 26, 54–68. doi: 10.1101/gad.173435.111

Zhou, Z., Zhang, Y., Lin, L., and Zhou, J. (2018). Apigenin suppresses the apoptosis of H9C2 rat cardiomyocytes subjected to myocardial ischemia-reperfusion injury via upregulation of the PI3K/Akt pathway. *Mol. Med. Rep.* 18, 1560–1570. doi: 10.3892/mmr.2018.9115

Zhu, H., Tannous, P., Johnstone, J. L., Kong, Y., Shelton, J. M., Richardson, J. A., et al. (2007). Cardiac autophagy is a maladaptive response to hemodynamic stress. *J. Clin. Invest.* 117, 1782–1793. doi: 10.1172/JCI27523

Conflict of Interest: The authors declare that the research was conducted in the absence of any commercial or financial relationships that could be construed as a potential conflict of interest.

frontiers in Cell and Developmental Biology

BRIEF RESEARCH REPORT
published: 26 January 2021
doi: 10.3389/fcell.2020.626011

Effect of Metformin on Cardiac Metabolism and Longevity in Aged Female Mice

Xudong Zhu[1†], Weiyan Shen[2†], Zhu Liu[1], Shihao Sheng[3], Wei Xiong[4], Ruikun He[5], Xuguang Zhang[5], Likun Ma[3*] and Zhenyu Ju[2*]*

[1] Key Laboratory of Aging and Cancer Biology of Zhejiang Province, Institute of Ageing Research, Hangzhou Normal University School of Medicine, Hangzhou, China, [2] Key Laboratory of Regenerative Medicine of Ministry of Education, Guangzhou Regenerative Medicine and Health Guangdong Laboratory, Institute of Aging and Regenerative Medicine, Jinan University, Guangzhou, China, [3] Department of Cardiology, the First Affiliated Hospital of USTC, Division of Life Sciences and Medicine, University of Science and Technology of China, Hefei, China, [4] Institute on Aging and Brain Disorders, Division of Life Sciences and Medicine, University of Science and Technology of China, Hefei, China, [5] By-Health Co. Ltd., Guangzhou, China

OPEN ACCESS

Edited by:
Xiaoqiang Tang,
Sichuan University, China

Reviewed by:
Hengyi Xiao,
Sichuan University, China
Yiwei Liu,
Chinese Academy of Medical Sciences and Peking Union Medical College, China

***Correspondence:**
Zhenyu Ju
zhenyuju@163.com
Likun Ma
lkma@ustc.edu.cn
Xuguang Zhang
zhangxg2@by-health.com

[†] These authors share first authorship

Specialty section:
This article was submitted to Cellular Biochemistry, a section of the journal Frontiers in Cell and Developmental Biology

Received: 04 November 2020
Accepted: 09 December 2020
Published: 26 January 2021

Citation:
Zhu X, Shen W, Liu Z, Sheng S, Xiong W, He R, Zhang X, Ma L and Ju Z (2021) Effect of Metformin on Cardiac Metabolism and Longevity in Aged Female Mice. Front. Cell Dev. Biol. 8:626011. doi: 10.3389/fcell.2020.626011

The antidiabetic drug metformin exerts pleiotropic effects on multiple organs, including the cardiovascular system. Evidence has shown that metformin improves healthspan and lifespan in male mice, yet its lifespan lengthening effect in females remains elusive. We herein demonstrated that metformin fails to extend the lifespan in female mice. Compared to 2-month-old young controls, 20-month-old female mice showed a spectrum of degenerative cardiac phenotypes alongside significant alterations in the extracellular matrix composition. Despite lowered reactive oxygen species production, long-term metformin treatment did not improve cardiac function in the aged female mice. In contrast, RNA sequencing analyses demonstrated that metformin treatment elevated the extracellular matrix-related gene while lowering oxidative phosphorylation-related gene expression in the heart. In addition, metformin treatment induced metabolic reprogramming that suppressed mitochondrial respiration but activated glycolysis (i.e., Warburg effect) in cultured primary cardiomyocytes and macrophages, thereby sustaining an inflammatory status and lowering ATP production. These findings suggest the unexpected detrimental effects of metformin on the regulation of cardiac homeostasis and longevity in female mice, reinforcing the significance of comprehensive testing prior to the translation of metformin-based novel therapies.

Keywords: metformin, heart aging, longevity, ECM—extracellular matrix, inflammation, mitochondrion

INTRODUCTION

Cardiac function declines with advancing age, thereby increasing cardiovascular diseases in the geriatric population (Gude et al., 2018). Cardiac degeneration often accompanies the proinflammatory microenvironment and lowers mitochondrial function, the two most common signatures of cardiac aging (Ferrucci and Fabbri, 2018), which is attributed to a dysregulated redox system (Dai et al., 2009), altered cell composition (Spadaccio et al., 2016), aberrant mitochondrial function (Zhu et al., 2019), and (epi-)genetic abnormalities (Zhang et al., 2018). Despite lacking a consensus on the precise mechanisms that lead to degenerative cardiac phenotypes, rejuvenating the aging heart *via* targeting immune response and mitochondrial metabolism holds great promise to attenuate the functional decline.

Metformin (Met) was initially introduced for the treatment of type II diabetes mellitus in 1957, which has been then found salutary in reducing cardiovascular mortality and morbidity (Vasamsetti et al., 2015; Bergmark et al., 2019). The benefit of this old drug in cardiovascular diseases may be attributed to its classical AMPK-dependent metabolic signaling pathways (Nafisa et al., 2018) or anti-inflammatory effect (Cameron et al., 2016) *via* the suppression of NF-kB or attenuation of endothelial dysfunction *via* the inhibition of LOX-1 (Xu et al., 2013) or anti-oxidant effect *via* inhibiting TRAF3IP2 (Valente et al., 2014) and NOX4 (Sato et al., 2016). In contrast, several reports of Met-associated lactic acidosis have been documented, although the incidence is sporadic (Fitzgerald et al., 2009; Defronzo et al., 2016). A study using the myocardial infarction (MI) swine model also suggested no effect in reducing MI size by Met (Techiryan et al., 2018), reinforcing the importance of rigorously checking Met monotherapy or in combination with other medications in large animal models to facilitate the clinical translation. Nonetheless, existing study documented a life-extending effect in male mice receiving Met (Martin-Montalvo et al., 2013), suggesting that Met could be a promising candidate to help realize healthy aging. Data on whether female mice can also benefit from Met's cardioprotective and life-extending effects remain elusive.

To this end, we set to investigate the role of Met treatment in female mice. Despite a lowered reactive oxygen species (ROS) production, long-term Met treatment did not improve cardiac function in the aged female mice. Surprisingly, rather than the life-extending effect, we found a significantly shortened lifespan in aged female mice receiving long-term Met supplementation *vs.* age-matched controls. Our results reinforce the importance of carefully evaluating the Met-based strategies in a context-dependent manner to facilitate the clinical translation of novel cardioprotective therapies.

METHODS

Animals

All procedures involving experimental animals were conducted in full accordance with and as approved by the Animal Care and Use Committee of Hangzhou Normal University. Young (2-month-old) and old (20- to 30-month-old) mice were maintained in a temperature-controlled room (22 ± 1°C) on a 12-h light/dark cycle with *ad libitum* access to food and water.

Chemicals and Antibodies

Metformin hydrochloride was purchased from TargetMol (T0740) or Selleck (S1950). Vinculin (13901), phosphorylated AMPKα (Thr172) (2535), AMPKα antibody (5831), and anti-rabbit IgG (7074) were purchased from Cell Signaling Technology. TRIzol Reagent (15596-018) was purchased from Invitrogen. EvaGreen Supermix (172-5201AP) was purchased from Bio-Rad Laboratories Inc. PrimeScript first-strand cDNA Synthesis Kit (6110A) was purchased from TaKaRa Bio Inc. All other chemicals were purchased from Sigma-Aldrich, unless otherwise stated.

Isolation and Culture of Primary Cells

Primary cardiomyocytes and bone marrow-derived macrophages were isolated and cultured as previously described (Trouplin et al., 2013; Zhu et al., 2019). Dulbecco's modified Eagle's medium (Hyclone) containing 4.5 g/l glucose, penicillin–streptomycin (100 IU/ml to 100 μg/ml), 10% fetal bovine serum (Gibco), and 20 ng/ml GM-CSF was used for cell culture.

RNA Sequencing

The RNAs were isolated from heart tissues using TRI® reagent (Sigma-Aldrich) as per the manufacturers' instructions. Library construction and sequencing were performed in Novogene, China. Briefly, RNA samples for transcriptome analysis were pre-treated with DNase and processed following the Illumina manufacturer's instructions, where magnetic beads with oligo (dT) were used to isolate polyadenylated mRNA (polyA + mRNA) from the total RNA. Fragmentation buffer consisting of divalent cations was added for shearing mRNA to short fragments of 200–700 nucleotides in length. These short fragments were used as templates to synthesize the first-strand cDNA using random hexamer priming. The second-strand cDNA was synthesized using buffer including dNTPs, RNase H, and DNA polymerase I. The products were purified and resolved with QIAquick PCR Purification Kit (Qiagen) and elution buffer for end preparation and tailing A, respectively. Purified cDNA fragments were connected with sequencing adapters and gel-electrophoresed to select suitable fragments for PCR amplification. The Agilent 2100 Bioanalyzer and Applied Biosystems StepOnePlus™ Real-Time PCR System were used in the quantification and analysis of the sample library for quality control. A paired-end cDNA library was constructed and sequenced using Illumina HiSeq™ X Ten at Novogene, China. The sequencing reads were mapped to the mouse reference genome (mm9) using HISAT (Kim et al., 2015). Differentially expressed genes (DEGs) between each genotype were calculated by a standard bioinformatic analysis package, and the hierarchical clustering for DEGs between samples was generated based on DEGs. The RNAseq data have been deposited to Sequence Read Archive under the BioProject number PRJNA681488.

Echocardiography

Cardiac function was evaluated by transthoracic echocardiography (Vevo2100, Visualsonic) in the short-axis view. M-mode images were used for measurement of fractional shortening (FS%) and ejection fraction (EF%) in lightly anesthetized mice (1–2% isoflurane mixed in 100% of oxygen, with the mice placed on a heating table to preserve the physiological body temperature). Heart rate was monitored to maintain the mice at approximately 550 bpm.

Seahorse Cellular Flux Assay

Cells were seeded 48 h before measurement by the XFe96 Seahorse extracellular flux analyzer (Agilent). Cartridges were hydrated by a calibrant for 24 h before measurement in a non-CO_2 incubator at 37°C. The XFe96 Seahorse instrument was utilized following the manufacturer's instructions. The results

were normalized by cell number in each well and analyzed *via* Wave software (version 2.6, Seahorse Bioscience).

Immunoblotting

Total proteins were extracted from ventricular tissues using radioimmunoprecipitation assay buffer (Applygen Technologies Inc., Beijing, China) supplemented with phosphatase and protease inhibitors (TargetMol). Equal amounts of proteins were separated by sodium dodecyl sulfate–polyacrylamide gel electrophoresis and then transferred to polyvinylidene fluoride membranes (Millipore). The membranes were reacted with a primary antibody followed by a secondary antibody. The immunoreactive bands were detected by Immun-Star WesternC chemiluminescence solutions (BioRad).

Endurance Running Test

The mouse exercise tolerance studies were performed as previously described (Zhu et al., 2019). All mice were acclimated to the treadmill system before the running test. The exercise regimen commenced at a speed of 15 m/min, with an inclination of 7°. The mice were considered to be exhausted and removed from the treadmill following the accumulation of 10 or more shocks (0.1 mA) per minute for two consecutive minutes. The electric shock times were registered within a 15-min running period.

Quantitative Polymerase Chain Reaction

The transcriptional expression levels of the targeted genes were assayed by quantitative polymerase chain reaction (qPCR) using the following primer sequences: Nppa-F: 5′-TTCTTCCTC GTCTTGGCCTTT-3′, Nppa-R: 5′-GACCTCATCTTCTAC CGGCATCT-3′, Nppb-F: 5′-CACCGCTGGGAGGTCACT-3′, Nppb-R: 5′-GTGAGGCCTTGGTCCTTCAAGGTCACT-3′, Myh6-F: 5′-GTGACCATAAAGGAGGACCAGG-3′, Myh6-R: 5′-CCCGAGTAGGTATAGATCATCC-3′, Myh7-F: 5′-TTCAT CCGAATCCATTTTGGGG-3′, Myh7-R: 5′-GCATAATCGT AGGGGTTGTTGG-3′, Col1a1-F: 5′-CGAAGGCAACAGTCGC TTCA-3′, Col1a1-R: 5′-GGTCTTGGTGGTTTTGTATTCGA-3′, Col3a1-F: 5′-GAACCTGGTTTCTTCTCACCC-3′, Col3a1-R: 5′-TCATAGGACTGACCAAGGTGG-3′, Ppargc1a1α-F: 5′-AA GTGTGGAACTCTCTGGAACTG-3′, Ppargc1a1α-R: 5′-GGG TTATCTTGGTTGGCTTTATG-3′, Tfam-F: 5′-GGAATGTG GAGCGTGCTAAA-3′, Tfam-R: 5′-GGTAGCTGTTCTGTG GAAAATCG-3′, Atp5b-F: 5′-ACGTCCAGTTCGATGAG GGAT-3′, Atp5b-R: 5′-TTTCTGGCCTCTAACCAAGCC-3′, β-actin-F: 5′-CAGCCTTCCTTCTTGGGTAT-3′, and β-actin-R: 5′-TGGCATAGAGGTCTTTACGG-3′. Total RNA was extracted using Trizol reagent (Life Technologies) according to the manufacturer's instructions. Reverse transcription and qPCR were performed using the PrimeScript first-strand cDNA Synthesis Kit (TaKaRa Bio) and EvaGreen Supermix (Bio-Rad) as per the manufacturers' instructions. The cycle threshold value determined for each RNA was normalized to the β-actin content to indicate the relative RNA level.

Histological Analysis

The hearts were fixed with 4% paraformaldehyde and embedded in paraffin, and 6-μm-thick sections were stained with Masson's trichrome as per the manufacturer's instructions (#GP1032, Servicebio). Images were acquired using a Panoramic automated slide scanner.

Flow Cytometry

ROS levels were analyzed with an LSRFortessa^{TM} cell analyzer (BD Biosciences) as described previously (Zhu et al., 2019).

NAD^+/NADH Ratio Measurement

Left ventricular tissues were freshly excised and snap-frozen for the measurements. NAD^+/NADH ratio was analyzed with a commercial NADH/NAD quantification kit (K337-100; Biovision) as per the manufacturers' instructions.

Statistics

All experimental results are representative of repeated experiments. Statistical analyses were performed using Prism 7 (GraphPad Software Inc.) and Image J software (version 1.48). The data are represented as mean values ± the standard error of the mean. Unpaired Student's *t*-test (two-tailed) was used to compare two normally distributed data sets. Two-way ANOVA was used for seahorse analyses. Survival analyses were performed using the Kaplan–Meier method, and the significance of differences between survival curves was calculated using the log-rank (Mantel–Cox) test. A P value <0.05 was considered to be statistically significant.

All data from these experiments are available from the corresponding author upon reasonable request.

RESULTS

Phenotyping the Age-Associated Cardiac Degeneration in Female Mice

We compared the degenerative cardiac signatures of 2-month old C57BL/6 (young) and 20-month-old (old) female mice with identical breeding conditions. The echocardiographic assessment confirmed a significantly reduced ejection fraction and fraction shortening in old female mice compared to those of young mice (**Figure 1A**). Histological staining also found more cardiac collagen deposition (**Figure 1B**) in the aged females, which coincided with an increased heart weight-to-body weight ratio (**Figure 1C**) and augmented inflammatory gene expression (**Figure 1D**). To evaluate whether these age-related degenerative indices link to impaired exercise capacity, we next examined the 15-min-run tolerance between young and old females. All mice were acclimated to the treadmill system with a gradual increment of running speed (from 7.5, 10, 12.5 to 15 m/min). Young female mice exhibited an excellent exercise capacity such that all were able to run for more than 30 min. In contrast, aged mice could not maintain the speed and struggled to catch up with the set speed, thus experiencing a high frequency of electric shock (**Figure 1E**). These data suggest that 20-month-old female mice have already exhibited phenotypes of age-associated

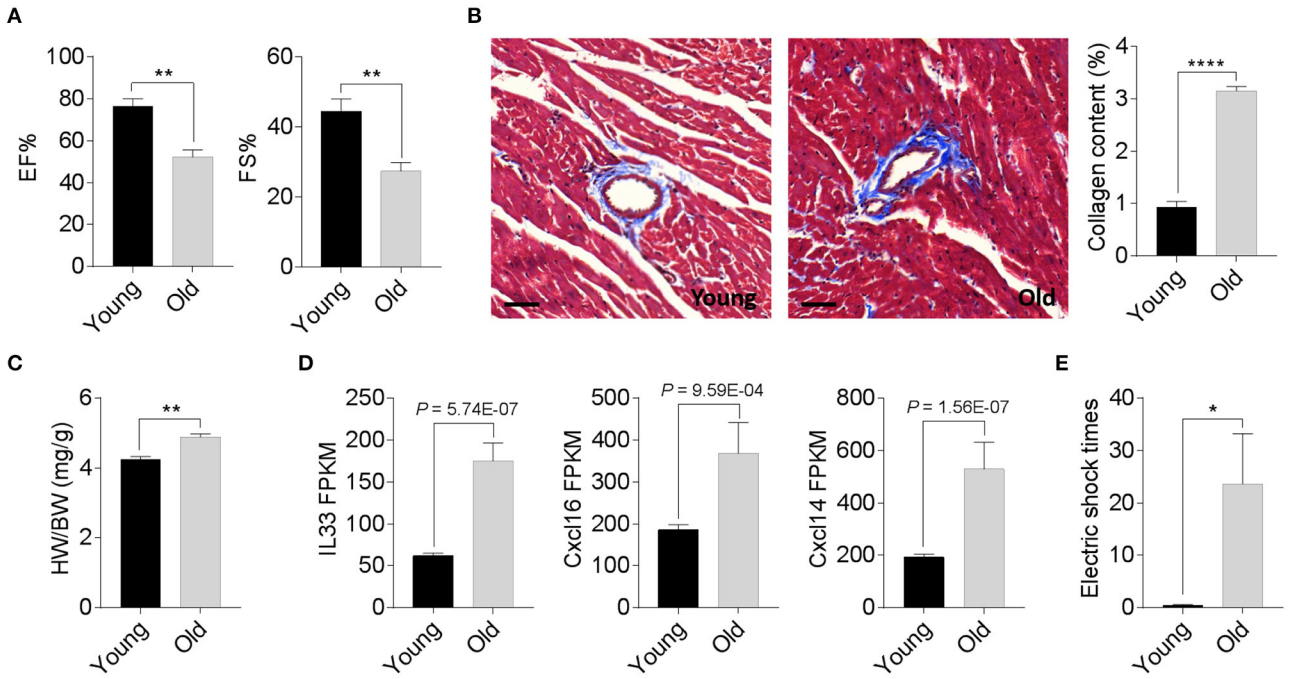

FIGURE 1 | Phenotypic cardiac degeneration in old mice. **(A)** Measurements of ejection fraction (EF%) and fractional shortening (FS%) in 2-month-old and 20-month-old wild-type (WT) female mice; $n = 5$ per group, $^{**}P < 0.01$. **(B)** Representative images of Masson's trichrome staining and collagen content quantification in 2-month-old and 20-month-old WT female hearts; $n = 5$ for each group, bar = 50 μm, $^{****}P < 0.0001$. **(C)** Quantification of heart weight-to-body weight ratio in 2-month-old and 20-month-old WT female mice; $n = 5$ for each group, $^{**}P < 0.01$. **(D)** Relative inflammatory cytokine comparisons between 2-month-old and 20-month-old WT female hearts. Data derived from RNA sequencing analyses, $n = 3$ per genotype. The P values are displayed. FPKM, fragments per kilobase of exon model per million reads mapped. **(E)** Exercise tolerance test in 2-month-old and 20-month-old WT female mice. The mice were subjected to treadmill exercise once a day for four consecutive days; $n = 5$ per genotype, $^{*}P < 0.05$.

cardiac degeneration, although the outer appearance is far from advanced aging.

Late-Life Metformin Treatment Is Detrimental to Female Mice

Previous studies demonstrate that Met is cardioprotective under a pathological condition (Gundewar et al., 2009; El Messaoudi et al., 2013). Besides this, a life-extending effect of Met has been reported in male mice (Martin-Montalvo et al., 2013), prompting an assessment of whether Met could attenuate cardiac aging and likely extend the lifespan in female mice. To this end, we supplemented Met (100 mg/kg/day) or water as vehicle (Veh) to 20-month-old female mice till death (**Figure 2A**) and monitored their body weight and survival. Unexpectedly, a shortened median lifespan (Veh: 852 days *vs.* Met: 839 days, $P < 0.05$; **Figure 2B**) alongside a trend of body weight decrease (**Figure 2C**) at late stage was seen in female mice receiving Met treatment. This Met toxicity to female mice was not due to cardiac oxidative stress since Met treatment lowered the ROS production (**Figure 2D**). However, cardiac stress indices, including Myh7/Myh6, Nppa, and Nppb, were all elevated in the Met group compared to the Veh group (**Figure 2E**), although the ejection fraction and fraction shortening were unchanged between the two cohorts (**Figure 2F**).

Metformin-Treated Mice Exhibit Altered Transcriptomics

To explore the underlying mechanism of Met toxicity, we performed RNA sequencing to compare the transcriptional changes in the old heart with or without Met. Gene set enrichment analysis (GSEA) demonstrated many significantly enriched signaling pathways in the ventricular tissue of old Met mice compared to Veh mice. Gene Ontology (GO) enrichment and Kyoto Encyclopedia of Genes and Genomes (KEGG) enrichment indicated that Met treatment caused a reduction in mitochondrial respiratory genes, concurrent with an increase of extracellular matrix-related genes (**Figures 3A,B**). In line with this, extracellular matrix organization and oxidative phosphorylation topped in GO enrichment and KEGG enrichment, respectively (**Figures 3C,D**). qPCR analyses further validated the RNA sequencing findings as evidenced by augmented collagen synthesis-related genes (*Col1a1* and *Col3a1*; **Figure 3E**) and downregulated mitochondrial-related genes (*Ppargc1a*, *Tfam*, and *Atp5b*; **Figure 3F**). Moreover, Met-treated hearts exhibited a lowered NAD^+/NADH ratio compared to Veh hearts (**Figure 3G**). These data together suggest that Met supplementation to age female mice may cause mitochondrial dysregulation and abnormal collagen biosynthesis.

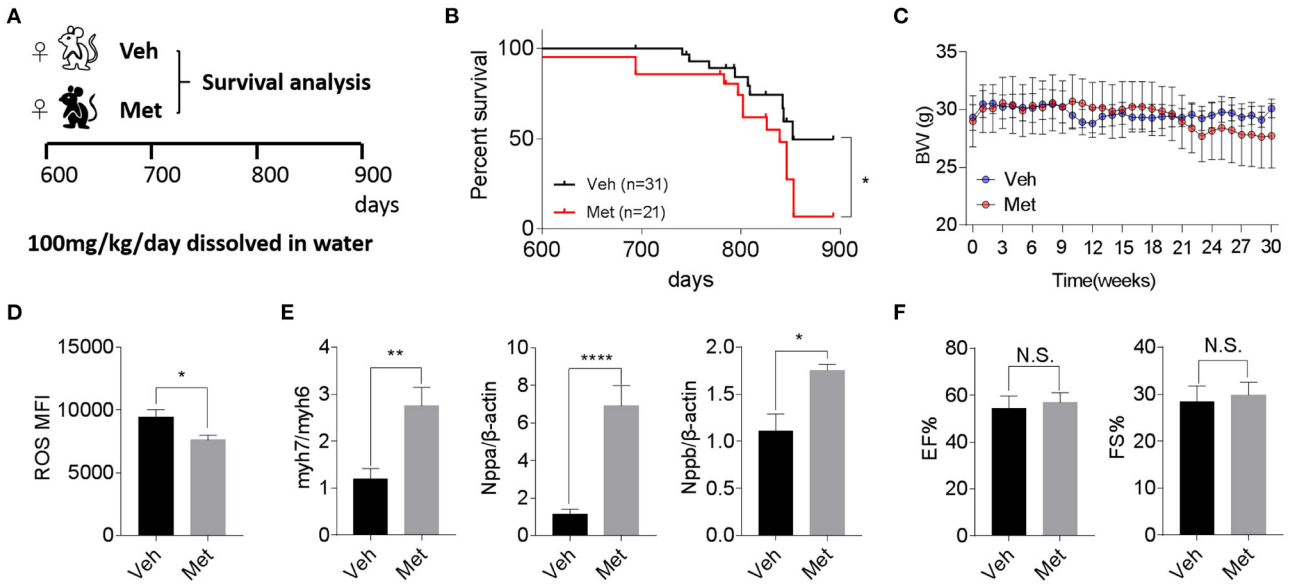

FIGURE 2 | Metformin treatment is not associated with improved cardiac function and longevity in aged female mice. **(A)** The schematic image depicts the experimental procedures. Aged female wild-type (WT) mice were given water (Veh) or metformin (Met) from 600 days onwards (100 mg/kg/day oral gavage till the end of the experiment). **(B)** A shortened lifespan was seen in Met-treated female mice. Kaplan–Meier survival curves with Mantel–Cox test; $n = 31$ for Veh group and $n = 21$ for Met group, $^{*}P < 0.05$. **(C)** Body mass curve comparisons between Veh and Met female mice. The mice were weighed weekly since the start of the metformin treatment. **(D)** The Met-treated mice exhibited a lower reactive oxygen species production *vs.* Veh mice; $n = 8$ for Veh group and $n = 6$ for Met group; $^{*}P < 0.05$. MFI, mean fluorescent intensity. **(E)** Cardiac stress-related gene expression was upregulated in Met-treated old female mice. β-Actin was used to normalize the data; $n = 8$ for Veh group and $n = 4$ for Met group; $^{*}P < 0.05$, $^{**}P < 0.01$, $^{****}P < 0.0001$. **(F)** Measurements of ejection fraction and fractional shortening in old WT female mice with or without metformin treatment; $n = 4$ for Veh group and $n = 3$ for Met group. N.S., not significant.

Metformin Toxicity Causing Metabolic Reprograming Is AMPK Independent

Since several lines of evidence demonstrate that AMPK is central to metformin's effect (Zhou et al., 2001), we assessed AMPK activation in aged hearts *via* detecting AMPKα phosphorylation at Thr172. Consistent with previous findings, the young mice receiving Met activated the phosphorylation of AMPKα at Thr172, thereby increasing the p-AMPK/AMPK ratio (**Figure 4A**). However, the old hearts failed to activate AMPK upon Met treatment (**Figure 4B**), suggesting a possible mechanism that leads to the loss of the life-extending effect in aged females. Moreover, Met incubation drastically inhibits mitochondrial respiration and ATP production, while it increased glycolysis in primary cultured primary cardiomyocytes (**Figures 4C,D**) and bone marrow-derived macrophages (**Figures 4E,F**) from aged female mice. Collectively, these data indicated that metformin induced metabolic reprogramming that suppressed mitochondrial respiration but activated glycolysis (i.e., Warburg effect), thereby sustaining a relatively low-ATP and proinflammatory microenvironment.

DISCUSSION

In this study, we report an unexpected Met toxicity to late-life female mice, where Met treatment fails to extend the lifespan and downregulates mitochondrial respiration. One previous study has documented that early-life Met treatment (starting from 3 months old) extended the lifespan in female SHR mice (Anisimov et al., 2008). A subsequent investigation compared the effects of different Met treatment time windows on the lifespan of female SHR mice (Anisimov et al., 2011). Interestingly, an identical dosage of Met intervention started at an early life (3 months old) increased the mean lifespan by 14%, but the salutary life-extending effect was time-dependently abolished when starting Met treatment at the age of 9 or 15 months (Anisimov et al., 2011). Despite the difference between the WT and SHR female mice, their studies and our current finding indicate that Met's effect on the lifespan is age dependent. In addition, Met was reported to exert various effects primarily in an AMPK-dependent manner, yet we did not detect any change in AMPK phosphorylation, suggesting that the loss of Met-based benefits to aged female mice is possibly AMPK independent.

Although Met was found to extend the healthspan and lifespan in mice through elevating the AMPK activity (Martin-Montalvo et al., 2013), we failed to observe such a lifespan-promoting effect in our experimental setting. This effect is reminiscent of the very recent finding that occurs with Met supplementation in *Caenorhabditis elegans*, where Met caused a lethal ATP exhaustion (Espada et al., 2020). Consistently, we also observed a decreased ATP in Met-treated cardiomyocytes, although the ejection fraction was not changed between the aged Veh and Met mice. Given that ATP decline is often associated with cardiac dysfunction, a possible explanation is that our aged

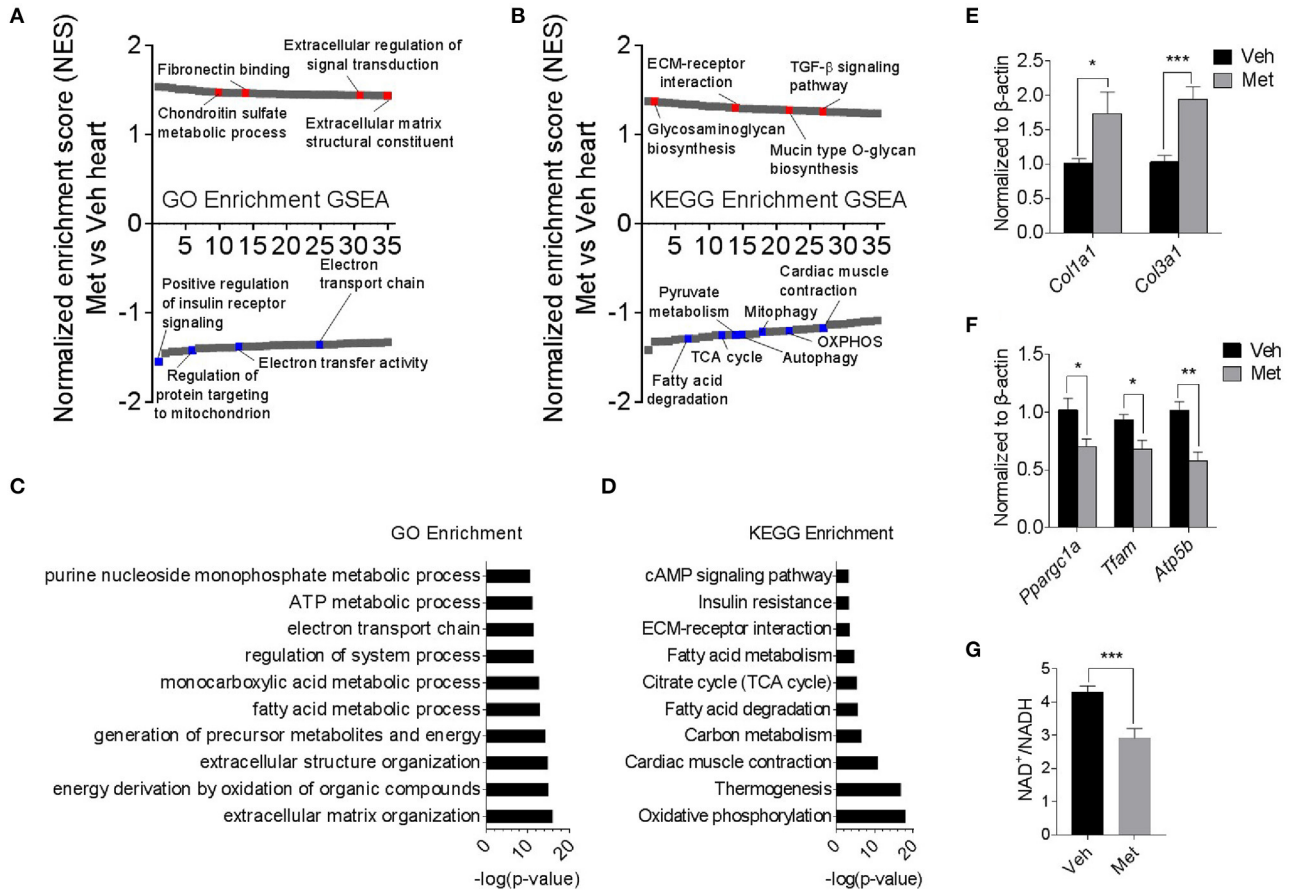

FIGURE 3 | Transcriptomics analyses in old female mice with or without metformin treatment. **(A,B)** Gene set enrichment analysis demonstrated 35 TOP up- and downregulated signaling pathways in the ventricular tissue of old Met mice, compared to Veh mice. Gene Ontology enrichment and Kyoto Encyclopedia of Genes and Genomes enrichment were used for the analysis of RNA sequencing data, respectively. Signaling pathways were ranked on the basis of normalized enrichment scores (NESs); positive and negative NESs indicate down- or upregulation in aged ventricular tissue, respectively. Specific pathways related to cardiac function were highlighted in red and blue. **(C,D)** GO and KEGG enrichment-based pathway analysis of Met and Veh hearts. The results were expressed as -log (*P*-value). **(E,F)** qPCR validation of collagen synthesis-related and mitochondrial-related gene expression in Veh and Met hearts. β-Actin was used to normalize the data; $n = 8$ for Veh group and $n = 4$ for Met group. $^{*}P < 0.05$, $^{**}P < 0.01$, $^{***}P < 0.001$. **(G)** NAD^{+}/NADH ratio was downregulated in Met-treated hearts; $n = 4$ for each group in triplicate. $^{*}P < 0.05$, $^{***}P < 0.001$.

female mice fed Met resembled a mouse model of heart failure with preserved ejection fraction (HFpEF), a most common form of heart failure in patients older than 65 years (Kitzman et al., 2001; Kumar et al., 2019), predominantly females (Wintrich et al., 2020). Indeed decreased ATP with preserved ejection fraction is found in patients of HFpEF. Mitochondrial deficiency of ubiquinol resulting in decreased ATP synthesis has been documented as a possible mechanism for the lowered ATP in HFpEF patients (Pierce et al., 2018). Moreover, cardiac cell types, extracellular matrix (ECM) composition, and detection methods may also affect the EF and ATP readouts. Further investigation is warranted to clarify how these factors may affect the action of Met under different circumstances.

The ECM has been long studied in the regulation of cardiac homeostasis (Bowers et al., 2010). Both structural and non-structural ECM proteins create strength and plasticity that not only provide mechanical scaffolds but also dynamically participate in physiological and pathological signaling. For instance, cardiac ECM proteins accumulate during aging, pressure overload, and myocardial infarction, thereby regulating compensatory remodeling and repair. Conversely, ECM dysregulation promotes the onset of oxidative stress and inflammation, leading to adverse cardiac remodeling and decompensation (Frangogiannis, 2017). We found an increased cardiac ECM deposition during aging, whereas collagen expression was inversely downregulated, which is in agreement with the previous literature (Meschiari et al., 2017), implicating a post-transcriptional regulation of collagen content that exists with age. We further revealed that Met treatment upregulated ECM-related transcripts, concurrent with increased proinflammatory glycolysis in the macrophages. Although we cannot exclude the possibility that abnormal ECM drives immunometabolic reprogramming, Met may disturb the ECM network in the aged heart through

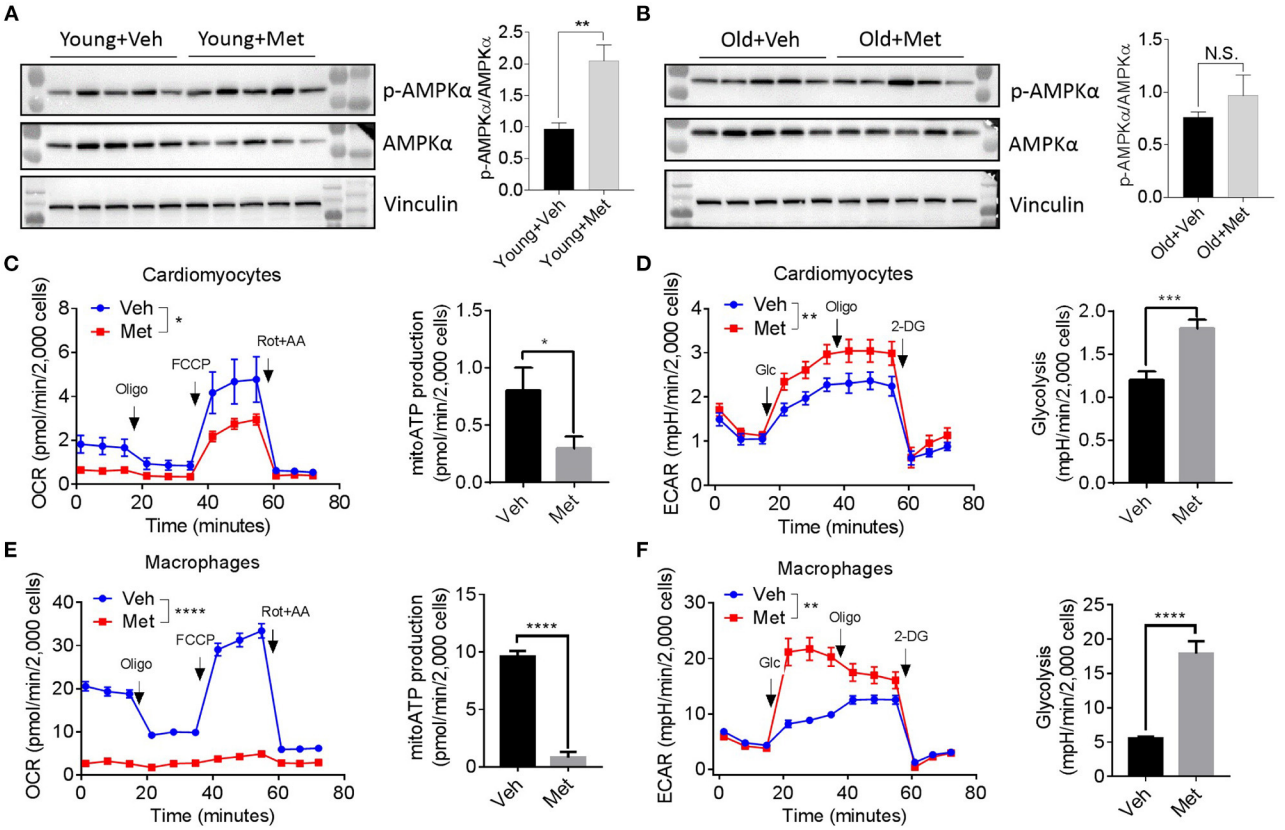

FIGURE 4 | Metformin treatment fails to activate AMPK but triggers metabolic reprogramming. **(A,B)** The effect of activating AMPK *via* metformin was blunted in Met-treatment old hearts. Vinculin was used as loading control. Phosphorylated AMPK (p-AMPKα)/AMPKα ratio indicated the activation status of AMPK; $n = 5$ per group, $^{**}P < 0.01$; N.S., not significant. **(C)** Mitochondrial respiration and mitochondrial ATP (mitoATP) production were measured in primary cardiomyocytes from old Veh or Met mice. Oxygen consumption rates were presented as pmol/min per 2,000 cells; $n = 12$ per group, two-way ANOVA, $^{*}P < 0.05$. **(D)** Non-mitochondrial respiration and glycolytic level were measured in primary cardiomyocytes from old Veh or Met mice. Extracellular acidification rates (ECAR) were presented as mpH/min per 2,000 cells; $n = 10$ per group, two-way ANOVA; $^{**}P < 0.01$, $^{***}P < 0.001$. **(E)** Mitochondrial respiration and mitochondrial ATP production were measured in primary bone marrow-derived macrophages from old Veh or Met mice. Oxygen consumption rates were presented as pmol/min per 2,000 cells; $n = 9$ per group, two-way ANOVA, $^{****}P < 0.0001$. **(F)** Non-mitochondrial respiration and glycolytic level were measured in primary bone marrow-derived macrophages from old Veh or Met mice. ECAR were presented as mpH/min per 2,000 cells; $n = 9$ per group, two-way ANOVA, $^{**}P < 0.01$. Oligo, oligomycin; FCCP, carbonyl cyanide 4-(trifluoromethoxy)phenylhydrazone; Rot, rotenone; AA, antimycin A; Glc, glucose; 2-DG, 2-deoxy-D-glucose.

exacerbating mitochondrial complex I inhibition, thereby activating macrophages (Fontaine, 2018).

There are some limitations to the study. The goal of this study was to investigate whether Met exerts protective effects in myocardial metabolism and longevity in murine models, especially in females. Given the unexpected lifespan-shortening outcome in our current study and a recent worm study (Espada et al., 2020), as well as the marginal benefit of Met treatment in a MI swine model (Techiryan et al., 2018), it is obligatory to perform double-blinded, placebo-controlled clinical trials to extrapolate animal-based findings to human cardiovascular aging/diseases. Besides this, with the limited number of the aging mice cohort, we only tested one dosage at a one-time window. The methods of Met delivery, dosage, intervention time point, and age factors may lead to different consequences. In particular, acute MI causes severe fibrotic scar formation, with patients of renal impairment showing a contraindication to metformin usage due to the increased risk of lactic acidosis. Thus, the effect of Met-mediated ECM remodeling may differ from that in the chronic aging process.

In summary, our data indicated that Met did not improve the cardiac function and lifespan in old female mice. Despite the fact that the multiple salutary effects of Met pave the way to combat aging-related diseases, a systematic evaluation of Met's cardiac and life-extending effect in the late life of individuals should be considered.

DATA AVAILABILITY STATEMENT

The RNAseq data have been deposited to Sequence Read Archive (SRA) under the BioProject number PRJNA681488.

ETHICS STATEMENT

The animal study was reviewed and approved by the Animal Care and Use Committee of Hangzhou Normal University.

AUTHOR CONTRIBUTIONS

XZhu and ZJ initiated the study and developed the concept of the paper. XZhu, LM, and ZJ designed the experiments. XZhu, WS, ZL, SS, RH, and XZha performed experiments. XZhu, WS, ZL, SS, WX, RH, and XZha analyzed and interpreted the data. XZhu, LM, WX, and ZJ wrote the manuscript. All authors contributed to the article and approved the submitted version.

FUNDING

This work was supported by grants from the National Natural Science Foundation of China (91749203, 81525010, and 82030039) and the National Key Research and Development Program of China (2017YFA0103302), Innovative Team Program of Guangzhou Regenerative Medicine and Health Guangdong Laboratory (2018GZR110103002) and the Program for Guangdong Introducing Innovative and Entrepreneurial Teams (2017ZT07S347) to ZJ; the National Natural Science Foundation of China (82071572), the Opening Project of Key Laboratory of Integrative Chinese and Western Medicine for the Diagnosis and Treatment of Circulatory Diseases of Zhejiang Province (2C32003), and the Innovative Talent Support Program of Medical and Health Research Project of Zhejiang Province (2021RC118) to XZhu; the Users with Excellence Program/Project of Hefei Science Center CAS (2019HSC-UE006) to WX.

REFERENCES

Anisimov, V. N., Berstein, L. M., Egormin, P. A., Piskunova, T. S., Popovich, I. G., Zabezhinski, M. A., et al. (2008). Metformin slows down aging and extends life span of female SHR mice. *Cell Cycle* 7, 2769–2773. doi: 10.4161/cc.7.17.6625

Anisimov, V. N., Berstein, L. M., Popovich, I. G., Zabezhinski, M. A., Egormin, P. A., Piskunova, T. S., et al. (2011). If started early in life, metformin treatment increases life span and postpones tumors in female SHR mice. *Aging (Albany NY)* 3, 148–157. doi: 10.18632/aging.100273

Bergmark, B. A., Bhatt, D. L., Mcguire, D. K., Cahn, A., Mosenzon, O., Steg, P. G., et al. (2019). Metformin use and clinical outcomes among patients with diabetes mellitus with or without heart failure or kidney dysfunction: observations from the SAVOR-TIMI 53 trial. *Circulation* 140, 1004–1014. doi: 10.1161/CIRCULATIONAHA.119.040144

Bowers, S. L., Banerjee, I., and Baudino, T. A. (2010). The extracellular matrix: at the center of it all. *J. Mol. Cell Cardiol.* 48, 474–482. doi: 10.1016/j.yjmcc.2009.08.024

Cameron, A. R., Morrison, V. L., Levin, D., Mohan, M., Forteath, C., Beall, C., et al. (2016). Anti-inflammatory effects of metformin irrespective of diabetes status. *Circ. Res.* 119, 652–665. doi: 10.1161/CIRCRESAHA.116.308445

Dai, D. F., Santana, L. F., Vermulst, M., Tomazela, D. M., Emond, M. J., Maccoss, M. J., et al. (2009). Overexpression of catalase targeted to mitochondria attenuates murine cardiac aging. *Circulation* 119, 2789–2797. doi: 10.1161/CIRCULATIONAHA.108.822403

Defronzo, R., Fleming, G. A., Chen, K., and Bicsak, T. A. (2016). Metformin-associated lactic acidosis: current perspectives on causes and risk. *Metabolism* 65, 20–29. doi: 10.1016/j.metabol.2015.10.014

El Messaoudi, S., Rongen, G. A., and Riksen, N. P. (2013). Metformin therapy in diabetes: the role of cardioprotection. *Curr. Atheroscler. Rep.* 15:314. doi: 10.1007/s11883-013-0314-z

Espada, L., Dakhovnik, A., Chaudhari, P., Martirosyan, A., Miek, L., Poliezhaieva, T., et al. (2020). Loss of metabolic plasticity underlies metformin toxicity in aged *Caenorhabditis elegans*. *Nat. Metab.* 2, 1316–1331. doi: 10.1038/s42255-020-00307-1

Ferrucci, L., and Fabbri, E. (2018). Inflammageing: chronic inflammation in ageing, cardiovascular disease, and frailty. *Nat. Rev. Cardiol.* 15, 505–522. doi: 10.1038/s41569-018-0064-2

Fitzgerald, E., Mathieu, S., and Ball, A. (2009). Metformin associated lactic acidosis. *BMJ* 339:b3660. doi: 10.1136/bmj.b3660

Fontaine, E. (2018). Metformin-induced mitochondrial complex I inhibition: facts, uncertainties, and consequences. *Front. Endocrinol. (Lausanne)* 9:753. doi: 10.3389/fendo.2018.00753

Frangogiannis, N. G. (2017). The extracellular matrix in myocardial injury, repair, and remodeling. *J. Clin. Invest.* 127, 1600–1612. doi: 10.1172/JCI87491

Gude, N. A., Broughton, K. M., Firouzi, F., and Sussman, M. A. (2018). Cardiac ageing: extrinsic and intrinsic factors in cellular renewal and senescence. *Nat. Rev. Cardiol.* 15, 523–542. doi: 10.1038/s41569-018-0061-5

Gundewar, S., Calvert, J. W., Jha, S., Toedt-Pingel, I., Ji, S. Y., Nunez, D., et al. (2009). Activation of AMP-activated protein kinase by metformin improves left ventricular function and survival in heart failure. *Circ. Res.* 104, 403–411. doi: 10.1161/CIRCRESAHA.108.190918

Kim, D., Langmead, B., and Salzberg, S. L. (2015). HISAT: a fast spliced aligner with low memory requirements. *Nat. Methods* 12, 357–360. doi: 10.1038/nmeth.3317

Kitzman, D. W., Gardin, J. M., Gottdiener, J. S., Arnold, A., Boineau, R., Aurigemma, G., et al. (2001). Importance of heart failure with preserved systolic function in patients > or = 65 years of age. CHS Research Group. Cardiovascular Health Study. *Am. J. Cardiol.* 87, 413–419. doi: 10.1016/S0002-9149(00)01393-X

Kumar, A. A., Kelly, D. P., and Chirinos, J. A. (2019). Mitochondrial dsfunction in heart failure with preserved ejection fraction. *Circulation* 139, 1435–1450. doi: 10.1161/CIRCULATIONAHA.118.036259

Martin-Montalvo, A., Mercken, E. M., Mitchell, S. J., Palacios, H. H., Mote, P. L., Scheibye-Knudsen, M., et al. (2013). Metformin improves healthspan and lifespan in mice. *Nat. Commun.* 4:2192. doi: 10.1038/ncomms3192

Meschiari, C. A., Ero, O. K., Pan, H., Finkel, T., and Lindsey, M. L. (2017). The impact of aging on cardiac extracellular matrix. *Geroscience* 39, 7–18. doi: 10.1007/s11357-017-9959-9

Nafisa, A., Gray, S. G., Cao, Y., Wang, T., Xu, S., Wattoo, F. H., et al. (2018). Endothelial function and dysfunction: impact of metformin. *Pharmacol. Ther.* 192, 150–162. doi: 10.1016/j.pharmthera.2018.07.007

Pierce, J. D., Mahoney, D. E., Hiebert, J. B., Thimmesch, A. R., Diaz, F. J., Smith, C., et al. (2018). Study protocol, randomized controlled trial: reducing symptom burden in patients with heart failure with preserved ejection fraction using ubiquinol and/or D-ribose. *BMC Cardiovasc. Disord.* 18:57. doi: 10.1186/s12872-018-0796-2

Sato, N., Takasaka, N., Yoshida, M., Tsubouchi, K., Minagawa, S., Araya, J., et al. (2016). Metformin attenuates lung fibrosis development via NOX4 suppression. *Respir. Res.* 17:107. doi: 10.1186/s12931-016-0420-x

Spadaccio, C., Mozetic, P., Nappi, F., Nenna, A., Sutherland, F., Trombetta, M., et al. (2016). Cells and extracellular matrix interplay in cardiac valve disease: because age matters. *Basic Res. Cardiol.* 111:16. doi: 10.1007/s00395-016-0534-9

Techiryan, G., Weil, B. R., Palka, B. A., and Canty, J. M. Jr. (2018). Effect of intracoronary metformin on myocardial infarct size in swine. *Circ. Res.* 123, 986–995. doi: 10.1161/CIRCRESAHA.118.313341

Trouplin, V., Boucherit, N., Gorvel, L., Conti, F., Mottola, G., and Ghigo, E. (2013). Bone marrow-derived macrophage production. *J. Vis. Exp.* e50966. doi: 10.3791/50966

Valente, A. J., Irimpen, A. M., Siebenlist, U., and Chandrasekar, B. (2014). OxLDL induces endothelial dysfunction and death via TRAF3IP2: inhibition by HDL3 and AMPK activators. *Free Radic. Biol. Med.* 70, 117–128. doi: 10.1016/j.freeradbiomed.2014.02.014

Vasamsetti, S. B., Karnewar, S., Kanugula, A. K., Thatipalli, A. R., Kumar, J. M., and Kotamraju, S. (2015). Metformin inhibits monocyte-to-macrophage differentiation via AMPK-mediated inhibition of STAT3 activation: potential role in atherosclerosis. *Diabetes* 64, 2028–2041. doi: 10.2337/db14-1225

Wintrich, J., Kindermann, I., Ukena, C., Selejan, S., Werner, C., Maack, C., et al. (2020). Therapeutic approaches in heart failure with preserved ejection fraction: past, present, and future. *Clin. Res. Cardiol.* 109, 1079–1098. doi: 10.1007/s00392-020-01633-w

Xu, S., Ogura, S., Chen, J., Little, P. J., Moss, J., and Liu, P. (2013). LOX-1 in atherosclerosis: biological functions and pharmacological modifiers. *Cell Mol. Life Sci.* 70, 2859–2872. doi: 10.1007/s00018-012-1194-z

Zhang, W., Song, M., Qu, J., and Liu, G. H. (2018). Epigenetic modifications in cardiovascular aging and diseases. *Circ. Res.* 123, 773–786. doi: 10.1161/CIRCRESAHA.118.312497

Zhou, G., Myers, R., Li, Y., Chen, Y., Shen, X., Fenyk-Melody, J., et al. (2001). Role of AMP-activated protein kinase in mechanism of metformin action. *J. Clin. Invest.* 108, 1167–1174. doi: 10.1172/JCI13505

Zhu, X., Shen, W., Yao, K., Wang, H., Liu, B., Li, T., et al. (2019). Fine-tuning of PGC1alpha expression regulates cardiac function and longevity. *Circ. Res.* 125, 707–719. doi: 10.1161/CIRCRESAHA.119.315529

Conflict of Interest: The authors declare that the research was conducted in the absence of any commercial or financial relationships that could be construed as a potential conflict of interest.

frontiers in Cell and Developmental Biology

REVIEW
published: 02 February 2021
doi: 10.3389/fcell.2021.625524

Adaptive Cardiac Metabolism Under Chronic Hypoxia: Mechanism and Clinical Implications

Zhanhao Su[1], *Yiwei Liu*[2]* *and Hao Zhang*[2]*

[1] State Key Laboratory of Cardiovascular Disease, National Center for Cardiovascular Diseases, Fuwai Hospital, Chinese Academy of Medical Sciences and Peking Union Medical College, Beijing, China, [2] Heart center and Shanghai Institute of Pediatric Congenital Heart Disease, Shanghai Children's Medical Center, National Children's Medical Center, Shanghai Jiaotong University School of Medicine, Shanghai, China

Chronic hypoxia is an essential component in many cardiac diseases. The heart consumes a substantial amount of energy and it is important to maintain the balance of energy supply and demand when oxygen is limited. Previous studies showed that the heart switches from fatty acid to glucose to maintain metabolic efficiency in the adaptation to chronic hypoxia. However, the underlying mechanism of this adaptive cardiac metabolism remains to be fully characterized. Moreover, how the altered cardiac metabolism affects the heart function in patients with chronic hypoxia has not been discussed in the current literature. In this review, we summarized new findings from animal and human studies to illustrate the mechanism underlying the adaptive cardiac metabolism under chronic hypoxia. Clinical focus is given to certain patients that are subject to the impact of chronic hypoxia, and potential treatment strategies that modulate cardiac metabolism and may improve the heart function in these patients are also summarized.

Keywords: cardiac metabolism, chronic hypoxia, metabolic efficiency, heart function, heart failure, HIF-1α

OPEN ACCESS

Edited by:
Xiaoqiang Tang,
Sichuan University, China

Reviewed by:
Yan Zhang,
Peking University, China
Ying Mei Zhang,
Fudan University, China

***Correspondence:**
Hao Zhang
drzhanghao@yahoo.com
Yiwei Liu
jacklyw@foxmail.com

Specialty section:
This article was submitted to Cellular Biochemistry, a section of the journal Frontiers in Cell and Developmental Biology

Received: *03 November 2020*
Accepted: *11 January 2021*
Published: *02 February 2021*

Citation:
Su Z, Liu Y and Zhang H (2021) Adaptive Cardiac Metabolism Under Chronic Hypoxia: Mechanism and Clinical Implications. Front. Cell Dev. Biol. 9:625524. doi: 10.3389/fcell.2021.625524

INTRODUCTION

The human heart is extremely robust in energy metabolism with the highest uptake of oxygen in the body (~0.1 ml O_2/g/min), and requires ~6 kg of ATP per day, which is 15–20 times its own weight (Kolwicz et al., 2013). To sustain the high energetic demand in the heart, continuous supply of sufficient oxygen is needed. However, a variety of cardiac and pulmonary diseases and systemic pathologies can lead to decreased capacity for oxygen transport and exchange, or decreased blood flow, which reduces oxygen supply to the heart and impairs cardiac energetics.

Hypoxia is the result of the imbalance between oxygen supply and oxygen demand. Under chronic hypoxia, the heart is challenged to produce similar amount of ATP with limited O_2 for contractile work to maintain normal heart function. This comes in the issue of cardiac metabolic efficiency, which is important in heart function as impaired metabolic efficiency appears to be a prominent feature in heart failure (Bertero and Maack, 2018). In response to hypoxic stimuli, the heart has evolved a delicate adaptive program to maintain metabolic efficiency, in which glucose becomes preferentially used over fatty acid for ATP production. Although the amount of ATP generated from fatty acids is substantially higher than that of glucose (106 vs. 32 molecules of ATP for per molecule of palmitate or glucose respectively), the oxidation of glucose consumes less oxygen compared to fatty acids, which makes it more oxygen efficient (Darvey, 1998). Therefore,

when glucose utilization is increased, the coupling of glycolysis and glucose oxidation improves cardiac metabolic efficiency and maintains ATP production (Abdurrachim et al., 2015).

In this review, we will focus on characterizing the major features and the underlying mechanism of adaptive cardiac metabolism under chronic hypoxia from recent studies. The role of altered metabolic adaptation in the progression of cardiac dysfunction in patients with chronic hypoxia and potential available treatment strategies are also discussed.

Chronic Hypoxia as a Pathophysiologic Component in Cardiac Diseases

Exposure to chronic hypoxia is a notable feature in high-altitude populations, which constitute ∼7% of the world's population, and their number has been rising considerably by 20% since 1990 (Woolcott et al., 2015). These populations are living in a hypobaric and hypoxic environment, which reduce alveolar oxygen level and subject them to the impact of chronic hypobaric hypoxia (**Figure 1**). From the epidemiologic perspective, hypoxia has major significance as an important risk factor for population health because it is not only the prominent feature in the high-altitude populations, but also involved in the pathophysiology of many cardiac diseases, including ischemic heart disease (IHD), cardiac hypertrophy, hypertension, and heart failure (Abe et al., 2017). In 2019, the prevalent cases of ischemic and hypertensive heart disease were estimated to be 197 million and 18.6 million worldwide, causing a total of 9.14 and 1.16 million deaths respectively (Roth et al., 2020). In these patients, microvascular dysfunction is common and the heart is associated with varying degrees of microvascular obstruction, impaired vascularization and decreased oxygen supply to cardiomyocytes, which causes chronic local hypoxia. In addition, certain congenital heart defects can subject patients to the effect of chronic hypoxia, a condition called cyanotic congenital heart disease (CCHD) (Mahle et al., 2009). In 2019, the number of patients living with congenital heart disease was estimated to be 13 million worldwide (Roth et al., 2020), and nearly 20% of incident congenital heart disease cases in the newborns were CCHD (Zhao et al., 2013).

Chronic hypoxia is also a prominent pathophysiologic feature in some commonly seen pulmonary diseases. For instance, in patients with obstructive sleep apnea (OSA), chronic obstructive pulmonary disease (COPD), or interstitial lung disease (ILD) etc. (Kent et al., 2011; Ryan, 2018), impaired ventilation of air or reduced oxygen diffusion capacity can significantly decrease exchange of oxygen in the lung, which reduces arterial oxygen level. In these pulmonary conditions, COPD and ILD can lead to chronic systemic hypoxia in affected patients, whereas OSA is associated with another type of chronic hypoxia that is characterized by recurrent episodes of hypoxia and reoxygenation, i.e., chronic intermittent hypoxia (CIH). Of note, CIH differs from the continuous exposure to chronic systemic hypoxia as seen in high-altitude populations and CCHD patients. Recent epidemiologic studies suggest that about 10% of the general adult population could suffer from COPD or OSA (McNicholas, 2018), and these conditions are associated with substantially higher risk of cardiovascular co-morbidity and mortality.

Chronic hypoxia has mixed effects on cardiovascular health, whether it is beneficial or detrimental depends on the specific pathophysiologic context and patient risk factors (Savla et al., 2018). In this review, we focus on discussing cardiac metabolism under the context of chronic systemic hypoxia.

Major Features of the Adaptative Cardiac Metabolism Under Chronic Hypoxia

Metabolic Switch of Cardiac Fuels

The human heart is a metabolic omnivore capable to consume all types of available fuels. In the healthy adult human heart, over 95% of ATP are produced from fatty acid and glucose. However, metabolic efficiency differs between these two fuels. Fatty acid has the highest ATP yields on an energy per gram basis, but the oxidation of 1 mol of glucose generates 6.3 high-energy phosphate bonds per mole of O_2, which is 53.7% higher than that of fatty acid (Kessler and Friedman, 1998). In other words, given a certain amount of oxygen, the use of glucose over fatty acid can yield higher quantity of ATP. Therefore, it has been proposed that increased reliance on glucose might improve cardiac metabolic efficiency and maintain ATP production, which is beneficial in the adaptation to chronic hypoxia (Essop, 2007). In humans, the increased reliance on glucose metabolism is a notable feature in high-altitude populations, such as Tibetans, Sherpas in Nepal, and the Andeans, all of whom are subjected to the chronic effect of hypobaric hypoxia. In a study involving these chronically hypoxic populations, positron emission tomographic (PET) and plasma measurements showed enhanced glucose uptake in the myocardium (0.34 vs. 0.20 μmol glucose/g/min) and lower plasma glucose level (4.7 vs. 5.3 μmol/ml) compared to lowlanders, suggesting a true metabolic adaptation against chronic hypoxia in these populations (Holden et al., 1995). Although the authors had not directly measured the myocardial uptake of fatty acid, plasma level of fatty acid was higher in highlanders than lowlanders (0.65 vs. 0.51 μmol/ml), indicating decreased utilization of fatty acid as metabolic fuels in highlanders (Holden et al., 1995).

Increased reliance on glucose is also a notable cardiac metabolic feature in patients with CCHD. Myocardial samples from patients with tetralogy of Fallot (the most common cyanotic heart defect) showed significantly higher lactate concentrations than acyanotic controls (Modi et al., 2004). Recent data on the surgical samples from CCHD patients also found significantly higher levels of glycolytic intermediates, and the measurement of mitochondrial respiration in primary cardiomyocytes isolated from CCHD patients revealed enhanced substrate utilization with glucose (Liu et al., 2020). Collectively, these data suggest that enhanced utilization of glucose as cardiac fuel is a prominent feature in patients with CCHD. Of note, current studies on the metabolic adaptation under chronic hypoxia in humans are mainly of cross-sectional design, whether this adaptive process occurs progressively through multiple stages require further investigations in future longitudinal studies.

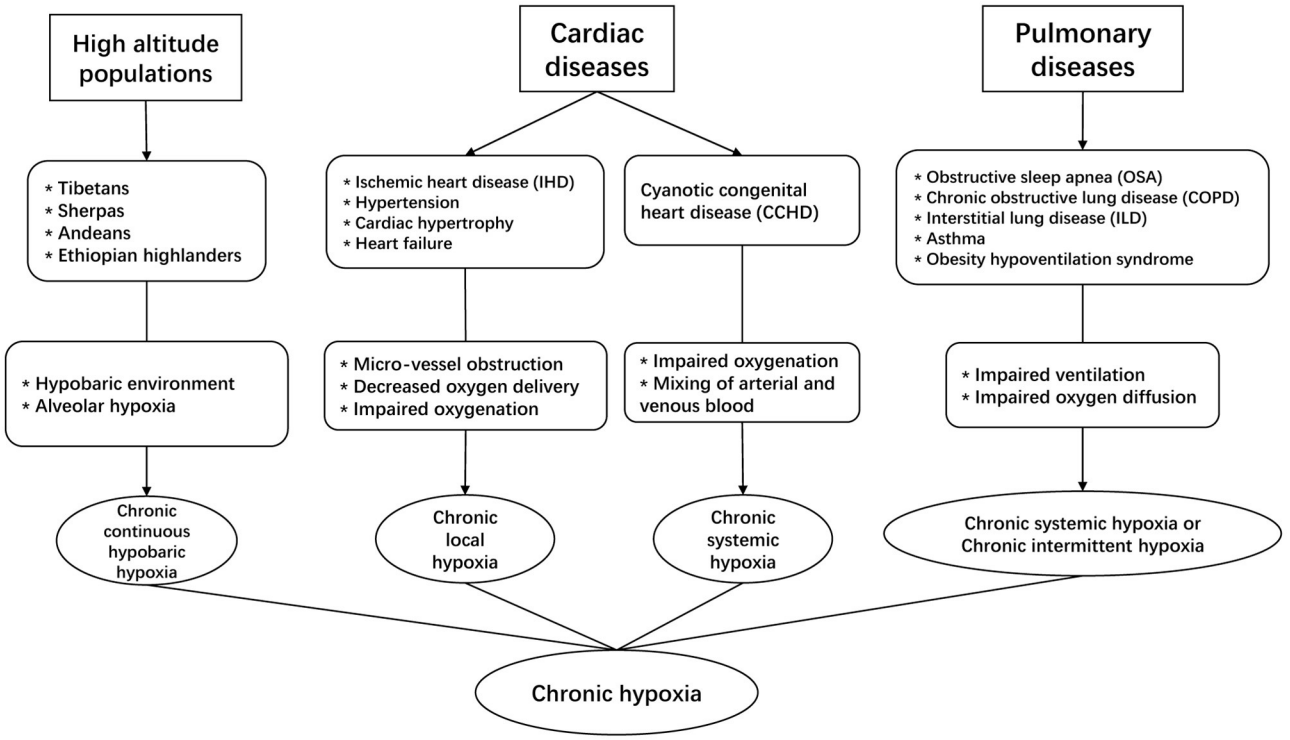

FIGURE 1 | The involvement of chronic hypoxia in different clinical scenarios.

Findings regarding the adaptive cardiac metabolism under chronic hypoxia from human studies corroborate with those from animal studies. In rats exposed to normobaric hypoxia (10% O_2) for 4 weeks, the left ventricle showed increased reliance on pyruvate for energy production, and the maximal mass-specific and mitochondrial-specific respiration as measured by pyruvate increased by 25% (Ferri et al., 2018). The right ventricle showed similar pattern of changes but the difference appeared non-significant between hypoxic and normoxic myocardium (Ferri et al., 2018). In chronically hypoxic rabbits exposed to 10% O_2 for up to 5 weeks, the hearts exhibited enhanced ventricular function and increased capacity for glucose oxidation compared to normoxic counterparts (Ross-Ascuitto et al., 2004). In a piglet model of chronic hypoxia (exposed to 8% O_2 for 4 weeks), the hearts showed elevated baseline glycogen storage levels and increased rates of glycolysis, which conferred protection against ischemic stress (Plunkett et al., 1996). Therefore, various animal models have demonstrated that chronically hypoxic hearts showed increased reliance on carbohydrates for energy production. Notably, a recent study using hyperpolarized ^{13}C-magnetic resonance spectroscopy to non-invasively measure pyruvate metabolism showed that in rats exposed to 3-week hypoxia, the conversion of pyruvate into lactate was comparable between hypoxic hearts and normoxic controls (Le Page et al., 2019), which suggests unchanged cardiac metabolism of pyruvate. Nonetheless, given that exposure to chronic hypoxia is associated with reduced utilization of fatty acid (Cole et al., 2016; Mansor et al., 2016), the unchanged metabolism of pyruvate as reported by this study indeed suggests a relatively increased reliance on carbohydrates for energy production in chronically hypoxic hearts, which corroborates with the conclusions from previous studies (Ross-Ascuitto et al., 2004; Ferri et al., 2018).

In addition to carbohydrates, other metabolic fuels with higher energetic efficiency than fatty acid, such as ketones, could have important roles in the adaptive cardiac metabolism. Ketone bodies consist of β-hydroxybutyrate (β-OHB) and acetoacetate. The oxidation of ketones is comparable to glucose and pyruvate in terms of oxygen efficiency (Ferrannini et al., 2016), which makes it an equally efficient fuel under metabolically stressed conditions. This property is potentially beneficial for cardiac adaptation during periods of nutrient or oxygen scarcity. In chronically hypoxic rats, the plasma concentration of β-OHB was significantly elevated (Mansor et al., 2016). Moreover, in primary cardiomyocytes, the presence of β-OHB improves excitation-contraction coupling under hypoxic environment, suggesting its potential role in the protective response against hypoxia (Klos et al., 2019). However, the effect of ketones on the adaptive cardiac metabolism has not been fully explored in animals nor investigated in human patients. Whether ketone bodies contribute to the adaptive cardiac metabolism under chronic hypoxia warrants further studies.

Adaptive Changes in Cardiac Mitochondria

Cardiac mitochondria comprise approximately one third of the volume of mature cardiomyocytes and they are well-known for the central roles in energy production and the regulation of various important cellular processes (Tian et al., 2019). Chronic hypoxia can induce a series of adaptive structural and functional

changes in cardiac mitochondria. Current studies seem to report different findings due to variations in experimental methodologies and the indicators chosen for measurement. To quantify mitochondrial contents, some studies used the measurement of citrate synthase (CS) activity as the indirect biomarker of mitochondrial content (Larsen et al., 2012). In these studies, the exposure of rats to chronic hypoxia resulted in comparable CS activity in both left and right ventricles with normoxic controls (Heather et al., 2012; Horscroft et al., 2015; Ferri et al., 2018), which suggests little changes in mitochondrial content in the chronically hypoxic myocardium. However, other studies report that in rats exposed to 3-week hypoxia, the ratio of mitochondrial DNA to nuclear DNA was reduced in both ventricles (Nouette-Gaulain et al., 2005), which suggests decreased mitochondrial content. Moreover, morphometric analysis of mitochondria showed that the numerical density significantly increased and the mean volume significantly decreased in both ventricles, indicating an increase in the number of smaller mitochondria (Nouette-Gaulain et al., 2005). The increase in mitochondria number is considered favorable under chronic hypoxia because it can facilitate the mitochondrial transport of oxygen by increasing the surface-to-volume ratio of mitochondria (Nouette-Gaulain et al., 2005).

Mitochondrial oxidative capacity can be altered under chronic hypoxia. These functional changes in cardiac mitochondria should be evaluated in the context of the switch of cardiac fuels. Furthermore, due to diversity in the methodology and the specimens (isolated mitochondria, cells, tissues) to measure mitochondrial oxidation, results from different studies should be interpreted based on the specific methodology and specimen types (Horan et al., 2012). Measurement from bundles of myocardial fibers (non-isolated cardiomyocytes) showed that chronic hypoxia causes a reduction in mitochondrial oxidative capacity as measured with palmitate (Nouette-Gaulain et al., 2005, 2011). The left ventricle showed more rapid declines than right ventricle in mitochondrial oxidative capacity as measured with palmitate, whereas the right ventricle remained relatively unchanged until 3 weeks after exposure to hypoxia (Nouette-Gaulain et al., 2005), suggesting delayed alteration in mitochondrial respiratory chain complexes in the right ventricle. In another study using the similar technique, the measurement of myocardial fibers with pyruvate showed greater mass-specific respiration in the left ventricle (Ferri et al., 2018). The above results are consistent with a recent study, in which primary cardiomyocytes isolated from the left ventricle of hypoxic rats showed an increase in mitochondrial oxidation as measured with pyruvate and decreased mitochondrial oxidation as measured with palmitate (Liu et al., 2020). Some studies involve the isolation of cardiac mitochondria and direct measurement of their respiration. Cardiac mitochondria consist of two anatomically and biochemically distinct subtypes, namely subsarcolemmal mitochondria (SSM) and interfibrillar mitochondria (IFM) (Palmer et al., 1977). In rats exposed to 11% O_2 for 2 weeks, the hypoxic SSM and IFM showed decreased respiration as measured with fatty acid and pyruvate (Heather et al., 2012). These changes were associated with downregulation of complexes I, II and IV of electron transport chain (ETC) in hypoxic SSM and downregulation of TCA cycle enzyme aconitase in IFM, which indicates decreased functional mass within a mitochondrion (Heather et al., 2012). Taken together, current evidence suggests that at the cellular and tissue level, mitochondrial oxidation capacity appeared to increase for pyruvate and decrease for fatty acids, but in the isolated mitochondria, the oxidative capacity appeared to decrease for both fuels. As we discussed earlier, this may be due to smaller size of mitochondria in chronically hypoxic hearts (Nouette-Gaulain et al., 2005).

The adaptive changes in ETC components are important in hypoxic cardiomyocytes. The mitochondria use oxygen to generate ATP, which can produce reactive oxygen species (ROS) during this process (Giordano, 2005). This issue becomes more prominent under hypoxia, as impaired transport of electron to oxygen and mismatch between electron and oxygen could aggravate ROS production (Guzy and Schumacker, 2006). The downregulation of ETC components in hypoxic SSM was accompanied by reductions in ROS production and offered protection against mitochondrial permeability transition pore (MPTP) opening (Heather et al., 2012), which is beneficial for cell survival under chronic hypoxia. Moreover, the uncoupling protein 3 (UCP3) located in the inner membrane of mitochondria was also decreased by chronic hypoxia (Cole et al., 2016), an adaptive change that decreased proton leak and thereby increased mitochondrial efficiency to use oxygen.

The biosynthesis of another important molecule along the ETC, Coenzyme Q10 (CoQ10), can also be affected under chronic hypoxia. CoQ10 is a vitamin-like organic component of ETC and is ubiquitously expressed in different tissues (Zozina et al., 2018). CoQ10 serves as an important electron carrier in the mitochondrial oxidation and also acts as a potent antioxidant to offset the damaging effect from ROS (Zozina et al., 2018). Given its various biological effect, the importance of CoQ10 should not be neglected. In rats exposed to chronic hypoxia for 3 weeks, reduced cardiac expression of cold-inducible RNA binding protein (CIRBP) caused decreased stabilization of the mRNA responsible for the biosynthesis of CoQ10, which could be associated with reduced ATP production, increased cellular apoptosis, and impaired heart function upon acute stress (Liu et al., 2019). These new findings suggest that under certain pathophysiologic conditions, chronically hypoxic hearts could suffer from impaired protective response against external stress due to its unique remodeling changes within the mitochondria.

Adaptive Changes in the High Energy Phosphate System

Chronic hypoxia can induce beneficial adaptive changes in the high energy phosphate system, which is composed of phosphocreatine (PCr) and creatine kinase (CK). This energy buffer system catalyzes the reversible reaction: Phosphocreatine + ADP + H^+ ↔ Creatine + ATP, and it not only serves as an important shuttle for ATP between mitochondria and muscle fibers, but also a buffer between ATP and ADP levels in the cytosol (Guimaraes-Ferreira, 2014). The ratio of phosphocreatine and ATP (PCr/ATP), as measured by ^{31}P Magnetic Resonance Spectroscopy, reflects the energy status of the myocardium.

Lowered PCr/ATP ratio is commonly seen in certain cardiac pathological conditions, such as ischemia and heart failure, and it can also be found under hypoxic condition when the heart preferentially uses glucose for metabolism. In the left ventricle, exposure to chronic hypoxia lowers total CK activity, more specifically for the mitochondrial CK isoform (Novel-Chate et al., 1998). In mice exposed to 3-week chronic hypoxia, the heart had decreased PCr/ATP ratio but higher response of ATP/PCr production to PCr changes (Calmettes et al., 2008; Cole et al., 2016), which indicates improved regulation of the balance between energy demand and energy supply. This beneficial adaptation enables the heart to maintain ATP level to withstand the impact of acute hypoxia (Calmettes et al., 2010). As such, the adaptive change of high energy phosphate system from the exposure to chronic hypoxia confers more metabolic resilience for the heart to tolerate ischemic insult.

In human patients, changes in the high energy phosphate system appeared to be consistent with those from animal studies. In a study involving the *in vivo* measurement of phosphocreatine and ATP in high-land Sherpas (Hochachka et al., 1996), cardiac PCr/ATP ratio was shown about half of that in these individuals compared to low-landers, and this difference remained unchanged even after 1-month de-acclimatization from high-altitude environment. These findings suggest the metabolic remodeling toward higher preference for glucose metabolism and increased glucose contribution to aerobic ATP turnover rates in the Sherpa heart (Hochachka et al., 1996). Interestingly, another study measuring cardiac energetics in patients with CCHD reported a PCr/ATP ratio comparable to controls, except that patients with heart failure had significantly lowered PCr/ATP ratio (Miall-Allen et al., 1996). In another groups of patients with Eisenmenger syndrome, which is associated with chronic hypoxemia, PCr/ATP ratio was reported to be significantly lowered than that in normoxic controls (Bowater et al., 2016). These data indicate that in patients with chronically hypoxic hearts, lowered PCr/ATP ratio could be accompanied by the presence of impaired heart function.

The Mechanism of Adaptive Cardiac Metabolism Under Chronic Hypoxia

The Regulatory Roles of Hif-1α and PKC Proteins

Exposure to chronic hypoxia activates the adaptive cardiac metabolic program through the induction of master regulators. In the myocardium, the physiologic response to hypoxia is mediated by the transcription factors from hypoxia-inducible factor (HIF) family. The biochemical properties and the detailed regulation of Hif-1α by oxygen have been summarized in a previous review (Sousa Fialho et al., 2019). Notably, myocardial expression of Hif-1α mRNA and protein was significantly induced in rats exposed to 10% O_2 for 3 weeks (Jung et al., 2000; Forkel et al., 2004). In patients with cyanotic heart defects, myocardial samples showed elevated HIF-1α protein levels and increased DNA binding activity, which are directly correlated with the degrees of hypoxemia (Qing et al., 2007). The stabilization of HIF-1α protein binds to hypoxia-response element (HRE) and promotes the expression of metabolic genes that facilitate the utilization of glucose and glycolysis, including glucose transporters 1 (GLUT1), hexokinase (HK), phosphofructokinase (PFK), pyruvate dehydrogenase kinase 1 (PDK1), and lactate dehydrogenase (LDHA) (Semenza, 2014). Moreover, increased HIF-1α promotes glycogen synthesis through induction of glycogen synthase 1 (GYS1) (Pescador et al., 2010) and phosphoglucomutase (PGM) (Semenza, 2014) (**Figure 2**).

The role of protein kinase C (PKC) in the metabolic adaptation to chronic hypoxia should be mentioned. PKC isozymes are serine/threonine kinases that regulates the protective response against ischemic injury in the heart (Singh et al., 2017). In chronically hypoxic patients and animals, PKCε is activated along with p38 MAP kinase and JUN kinase pathways (Rafiee et al., 2002), which confers cardio-protection in the myocardium. Moreover, the activation of PKCε inactivates glycogen synthase kinase 3β (GSK3β) through phosphorylation, which results in increased accumulation of HIF-1α in the chronically hypoxic heart (McCarthy et al., 2011). Activation of PKC also confers preference for glucose metabolism, with higher rates of glycolysis and glucose oxidation, as well as increased storage of glycogen (McCarthy et al., 2011).

The Regulators of Fatty Acid and Mitochondrial Metabolism

The activation of HIF-1α signaling pathway is only half the story, because chronic hypoxia is also associated with downregulation of regulators responsible for fatty acid metabolism. During exposure to hypoxia, both peroxisome proliferator-activated receptor-α (PPARα) and peroxisome proliferator-activated receptor-γ coactivator-1α (PGC-1α) are significantly downregulated (Cole et al., 2016; Mansor et al., 2016), which decreases the expression of their target metabolic genes. The PPARα transcriptional regulatory complex is composed of PPARα, retinoid X receptor (RXR) and PGC-1α, which binds to PPAR response element (PPRE) and regulates fatty acid transport and β-oxidation in the heart through targeting the expression of fatty acid transport protein (FATP), carnitine palmitoyl transferase 1 (CPT1), medium-chain acyl-CoA dehydrogenase (MCAD), long-chain acyl-CoA dehydrogenase (LCAD) (Finck and Kelly, 2002). Importantly, the DNA binding activity of PPARα/retinoid X receptor (RXR) could be reduced by elevated HIF-1α level in the hypoxic hearts (Belanger et al., 2007). PPARα can also regulate glucose metabolism through targeting the expression of PDK2 and PDK4 (Cole et al., 2016; Mansor et al., 2016), which inhibits pyruvate dehydrogenase (PDH) activity through phosphorylation and therefore reduces pyruvate flux. In this sense, PPARα is critical for the mechanistic basis of metabolic switch between fatty acid and glucose. Importantly, the role of these metabolic regulators has been confirmed in genetic studies involving high-altitude populations. For instance, the role of PPARα in the metabolic adaptation in humans was confirmed in several genetic studies of Tibetans (Ge et al., 2012) and Sherpas (Horscroft et al., 2017; Kinota et al., 2018). Genetic variants of PPARα in high-altitude inhabitants is associated with lowered capacity for fatty acid oxidation (Murray et al., 2018), indicating that the metabolic

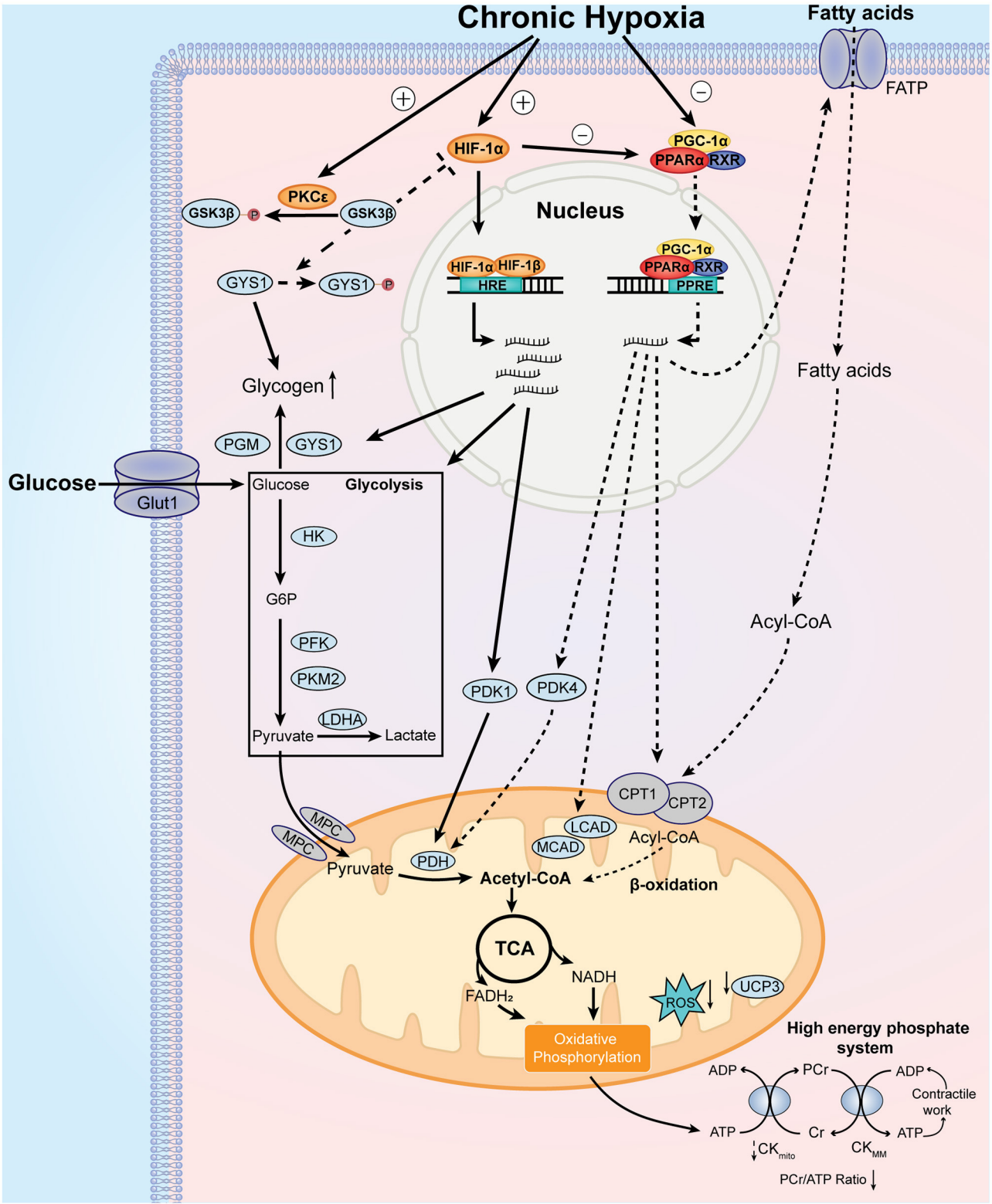

FIGURE 2 | Major features and mechanistic basis of the adaptive cardiac metabolism under chronic hypoxia. Chronic hypoxia leads to increased level and stabilization of HIF-1α, which upregulates the expression of glucose transporter 1 (GLUT1), hexokinase (HK), phosphofructokinase (PFK), pyruvate kinase isozyme M2 (PKM2), lactate dehydrogenase A (LDHA), pyruvate dehydrogenase kinase 1 (PDK1), glycogen synthase 1 (GYS1), and phosphoglucomutase (PGM). These changes lead to increase in glucose uptake, glycolysis, and glycogen synthesis. Additionally, chronic hypoxia decreases PPARα and PGC-1α levels, which decrease fatty acid

(Continued)

FIGURE 2 | uptake and β-oxidation through downregulation of fatty acid transport protein (FATP), carnitine palmitoyl transferase 1 (CPT1), medium chain acyl-CoA dehydrogenase (MCAD), long chain acyl-CoA dehydrogenase (LCAD) and uncoupling protein 3 (UCP3). Decreased UCP3 level is associated with less proton leak and increased mitochondrial efficiency for oxygen utilization. Of note, pyruvate dehydrogenase kinase 4 (PDK4) is reduced by downregulated PPARα, which activates pyruvate dehydrogenase (PDH) activity. Decreased PGC-1α reduces mitochondrial biosynthesis of components of electron transport chain, which reduces the generation of reactive oxygen species (ROS). Moreover, protein kinase C epsilon (PKCε) is activated under chronic hypoxia, which phosphorylates glycogen synthase kinase 3β (GSK3β) and reduces its phosphorylation on HIF-1α and GYS1. As the phosphorylation of HIF-1α and GYS1 leads to inhibition of their activities, activated PKCε promotes HIF-1α signaling and glycogen storage under chronic hypoxia. Collectively, these metabolic changes result in increased reliance on carbohydrates over fatty acids for ATP production. Other notable metabolic features include smaller size of mitochondria and decreased phosphocreatine (PCr)/ATP ratio. See text for further details. MPC, mitochondrial pyruvate carrier.

adaption under chronic hypoxia has genetic basis that occurred over generations. Beneficial genetic variants in HIF pathway was also shown in these highlanders (Bigham and Lee, 2014).

PGC-1α is a potent transcriptional coactivator of PPARα that controls cardiac mitochondrial biogenesis (Dorn and Kelly, 2015). The cardiac expression of PGC-1α can be differentially affected by oxygen level, and also seems to differ by left and right ventricle. In one study, chronic exposure to 3-week hypoxia in rats significantly downregulates the mRNA and protein levels of PGC-1α in both left and right ventricle (Ramjiawan et al., 2013). However, another study showed that in rats exposed to 4-week hypoxia, the expression of PGC-1α showed no difference in the left ventricle but was significantly lowered in the right ventricle (Ferri et al., 2018); the expression of another PGC-related family protein, PGC-1β, was significantly elevated in the left ventricle with increased maximal mitochondrial-specific respiration as measured with pyruvate and malate (Ferri et al., 2018). However, in the myocardium of right ventricle from patients with tetralogy of Fallot, cardiac expression of PGC-1α was significantly elevated and was positively correlated with the severity of cyanosis (Zhu et al., 2010). Other proteins involved in PGC-1α regulation cascade, including nuclear respiratory factors (NRF-1/NRF-2) and estrogen-related receptors (ERRs), are important transcriptional factors implicated in mitochondrial biogenesis and can be differentially regulated by hypoxia (Hochachka and Lutz, 2001; Cunningham et al., 2015), which also contribute to the altered mitochondrial biosynthesis under chronic hypoxia. Hence, current studies provide inconsistent evidence between animal and human studies with regard to the regulators of mitochondrial biosynthesis in chronically hypoxic hearts. A deeper understanding on this topic should warrant more comprehensive evaluation of different regulators in future studies.

The Regulation of PDH Activity Under Chronic Hypoxia

As we mentioned above, the adaptive cardiac metabolism under chronic hypoxia shows increased reliance on carbohydrates for ATP production. The transition from fatty acid to glucose metabolism requires allosteric and transcriptional regulation of key metabolic enzymes that are controlled by HIF-1α, PPARα and PGC-1α. The "Randle cycle" theory proposed in 1960's illustrates the famous 'glucose-fatty acid cycle', in which acetyl-CoA generated from fatty acid metabolism inhibits glucose oxidation, or products of glucose metabolism inhibit the entry of fatty acid into mitochondria for β-oxidation (Hue and Taegtmeyer, 2009). This theory forms the basis of adaptive cardiac metabolism. Of note, PDH is the key enzyme that couples glycolysis and glucose oxidation through catalyzing the oxidative decarboxylation of pyruvate, which generates acetyl-CoA that feeds into Krebs cycle (or tricarboxylic acid cycle, TCA cycle). Cardiac PDH activity is regulated by the reversible phosphorylation by PDK and phosphatases (PDP), with phosphorylation resulting in PDH inhibition (Holness and Sugden, 2003). PDK is critical for controlling PDH activity and it can be allosterically regulated by pyruvate, acetyl-CoA and NADH (Holness and Sugden, 2003). Of note, the major PDK isoforms in the heart (PDK1, 2, 4) differ in the kinetic parameters and regulation, such that PDK1 is proposed to be specialized for short-term control of PDH activity, whereas PDK4 is more involved in the regulation of adaptive responses of PDH in circumstances such as starvation (Bowker-Kinley et al., 1998). Moreover, PDK4 appears to be more responsive to intracellular levels of fatty acid, which makes it an important component of the substrate competition via the glucose-fatty acid cycle (Sugden and Holness, 2006). Hence, studies had proposed that PDK4 is an essential component of the cardiac adaptation to maintain the metabolic homeostasis in response to chronic changes in glucose and lipids (Holness and Sugden, 2003). Therefore, in the context of adaptation to chronic hypoxia, PDK1 (as regulated by HIF-1α) and PDK4 (as regulated by PPARα) seems to be more involved in the regulation of PDH activity (**Figure 3**).

Despite the importance of PDK in the regulation of PDH activity, current studies seemingly reported mixed findings on the relative changes of PDK expression in chronically hypoxic hearts. In the left ventricle, while some studies reported significantly reduced expression of PDK4 (Cole et al., 2016; Mansor et al., 2016), other studies reported unaltered levels of PDK1, 2, and 4 (Heather et al., 2012; Handzlik et al., 2018). An earlier study even reported significantly elevated PDK4 in both left and right ventricles after 14 days of exposure to hypobaric hypoxia (Sharma et al., 2004). Differences in hypoxic models (i.e., length of exposure to hypoxia, the presence of low atmospheric pressure), animal species, and measurement techniques between these studies could be responsible for these mixed results. As we discussed above, chronic hypoxia is associated with elevated myocardial HIF-1α and suppressed PPARα, therefore, it is more plausible that in chronically hypoxic hearts, PDK1 is induced by myocardial HIF-1α, whereas PDK4 level is decreased due to lowered PPARα. In this case, the opposite direction of changes in PDK1 and PDK4 in chronically hypoxic hearts appears to produce opposing regulatory effects on cardiac PDH activity. Importantly, this theory may explain why cardiac PDH activity and pyruvate flux in chronically hypoxic hearts was comparable

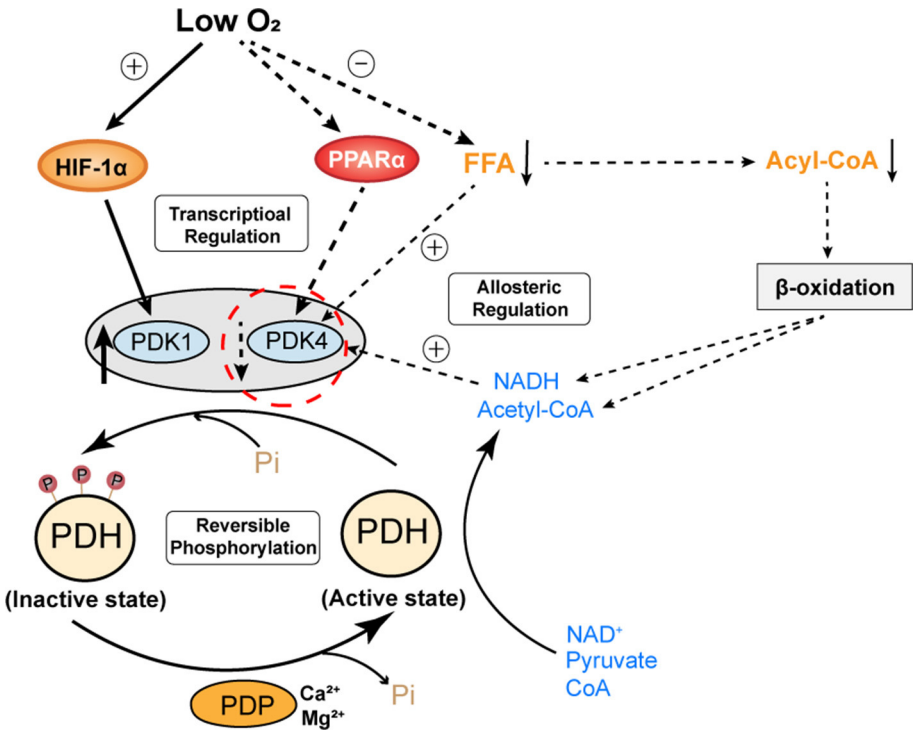

FIGURE 3 | A proposed regulation model of cardiac PDH activity under chronic hypoxia. The activity of PDH is mainly determined by reversible phosphorylation from PDK and PDP. PDK1 is oxygen sensitive and transcriptionally regulated by HIF-1α. PDK4 is nutrient sensitive, its expression is transcriptionally regulated by PPARα and its activity is allosterically regulated by FFA and metabolites (NADH, acetyl-CoA) derived from the oxidation of pyruvate or FFA. Under chronic hypoxia, elevated HIF-1α and decreased PPARα have opposing effects on the expression of PDK1 and PDK4. However, the activity of PDK4 is also affected by decreased levels of fatty acids and metabolites derived from β-oxidation. Hence, PDK4 appears to be more involved in the regulation of PDH activity in the chronically hypoxic heart. Decreased expression and activity of PDK4 reduce the phosphorylation of PDH, which maintains its active state. PDH, pyruvate dehydrogenase; PDK, pyruvate dehydrogenase kinase; PDP, pyruvate dehydrogenase phosphatase; Pi, inorganic phosphate; FFA, free fatty acids; NADH, nicotinamide adenine dinucleotide.

to that in normoxic controls in some animal studies (Handzlik et al., 2018; Le Page et al., 2019). It could also explain why some studies reported that the oxidation of glucose or pyruvate was increased in chronically hypoxic hearts compared to normoxic hearts (Ross-Ascuitto et al., 2004; Ferri et al., 2018). Given these mixed findings, further studies are warranted to confirm the relative changes in the expression level and activity of PDKs in the chronically hypoxic hearts.

Maladaptive Cardiac Metabolism and Cardiac Dysfunction Under Chronic Hypoxia

The flexibility in the switch of metabolic fuels underlies cellular adaption to chronic hypoxia. Current evidence suggests that hearts adapted to chronic hypoxia could maintain ATP production and provide sufficient cardiac work. However, this exquisite energy balance could be perturbed by various factors that are associated with reduced glucose utilization, which decreases cardiac metabolic efficiency. Indeed, decreased cardiac metabolic efficiency has been proposed to impair mitochondrial energetics and increase the risk of heart failure in patients with diabetes (Boudina and Abel, 2006). Here, we illustrate certain scenarios in which maladaptive cardiac metabolism could be associated with the development of cardiac dysfunction under chronic hypoxia.

Despite the critical role of HIF-1α in the adaptive response to chronic hypoxia, it is important to note that the regulation of myocardial HIF-1α could be implicated with signaling pathways other than oxygen sensing, such as insulin signaling pathway. Insulin modulates HIF-1α protein synthesis and activity via phosphatidylinositol-3 kinase (PI3-K) and mitogen-activated protein kinase (MAPK) pathways (Doronzo et al., 2006). Furthermore, insulin signaling pathway promotes the stabilization of HIF-1α complex, thereby inducing HIF-1α target genes (Zelzer et al., 1998). In diabetic hearts, the presence of insulin resistance attenuates the expression of HIF-1α protein, which impairs HIF-1α-mediated signaling and adaptation to hypoxia (Dodd et al., 2018). In rats exposed to prolonged hypoxia (10% O_2), sustained elevation of myocardial Hif-1α regulates the metabolic switch from fatty acid to glucose for ATP production since birth. However, when they enter puberty, the rise of insulin resistance attenuates myocardial expression of Hif-1α and reduces the capacity of the heart to use glucose, which disrupts the adaptive cardiac metabolic program, decreases ATP production and leads to cardiac dysfunction (Liu et al., 2020). As increased insulin resistance could blunt the HIF-1α driven response to hypoxia, this

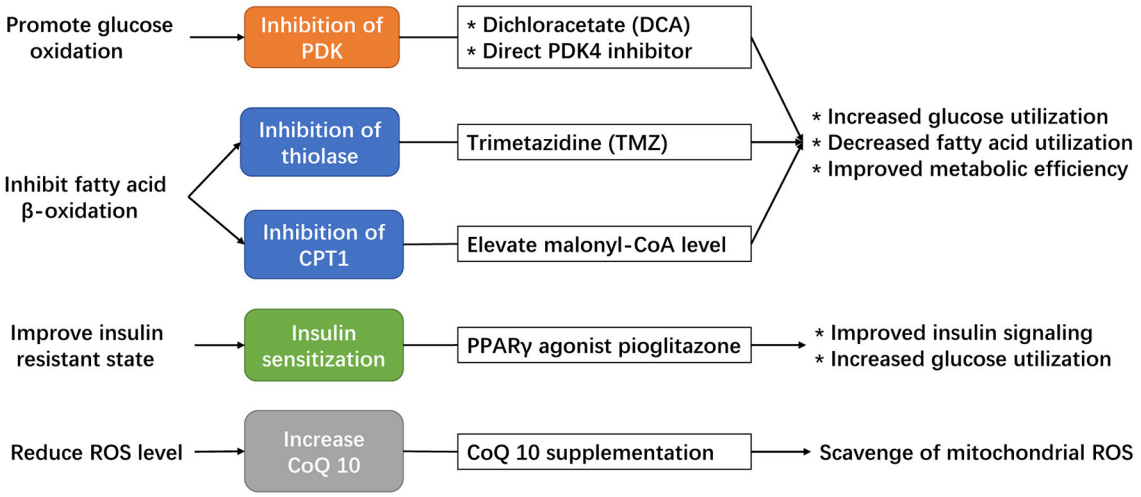

FIGURE 4 | Potential strategies available to modulate the adaptive cardiac metabolism under chronic hypoxia.

may explain a recent finding that children from Tibet had reduced left ventricular function at pubertal age (Qi et al., 2015). In this high-altitude population, increased insulin resistance during puberty might attenuate myocardial HIF-1α signaling, which impairs the adaptive cardiac metabolism under chronic hypoxia.

Insulin resistance can prevent the heart from using glucose effectively. Therefore, insulin resistance is particularly relevant in the chronically hypoxic populations who have increased reliance on glucose metabolism. The presence of metabolic risk factors, including obesity and hyperglycemia, has been noted to be independently associated with left ventricular diastolic dysfunction in high-altitude populations (Zheng et al., 2019). The development of insulin resistance is also commonly observed in patients with chronic hypoxia, such as obstructive sleep apnea (Ip et al., 2002) and cyanotic congenital heart disease (Niwa, 2019). In these patients, the presence of insulin resistance disrupts the utilization of glucose, which impairs cardiac efficiency and alters the adaptive cardiac metabolism under chronic hypoxia. As a result, these patients could be particularly susceptible to cardiac dysfunction and heart failure when metabolic diseases are present. Therefore, early intervention strategies to control metabolic risk factors could translate into cardiovascular benefits for the chronically hypoxic population.

The long-term outcomes of the adaptive cardiac metabolism in persons exposed to the effect of chronic hypoxia remains to be determined. After all, this is not a "physiological" status for the heart because fatty acid is the major metabolic fuel in the normoxic state. As patients become older, newly-developed co-morbidities or the worsening of pre-existing cardiopulmonary diseases could also pre-dispose to heart failure. Future studies are warranted to investigate and dissect the long-term impact of the adaptive cardiac metabolism on heart function in patients with chronic hypoxia.

Potential Strategies to Modulate Adaptive Cardiac Metabolism Under Chronic Hypoxia

As we discussed above, in chronically hypoxic patients, any disruptions in the utilization of glucose, including uptake, degradation, or catabolism, could result in cardiac energy deficit and pre-disposition to cardiac dysfunction. Therefore, potential treatment strategies should increase glucose uptake or target the coupling of glycolysis and glucose oxidation to improve cardiac metabolic efficiency and maintain ATP production for contractile work in this patient population. Currently, the number of potential drug targets is limited. There are several available drugs that can promote glucose metabolism, but none have been tested in patients with chronic hypoxia (**Figure 4**).

The first is dichloroacetate (DCA), a direct inhibitor of PDK enzyme that serves to increase PDH activity. DCA has been shown to improve the coupling of glucose oxidation to glycolysis in hypertrophied hearts (Lydell et al., 2002), which might offer a potential benefit in chronically hypoxic hearts to promote the formation of adaptive metabolism. Indeed, the use of DCA in rat exposed to chronic hypoxia has already been shown to increase cardiac pyruvate flux, which elevates the stockpile of acetyl-carnitine, maintains ATP production, and improves tolerance to acute hypoxic stress (Handzlik et al., 2018). DCA treatment can also decrease oxidative stress and prevent cell death (Kato et al., 2010), which is beneficial in hypoxic cardiomyocytes. However, the half-life of DCA is short (Kim and Chauhan, 2018) and might hinder its clinical translation.

The second available drug is trimetazidine (TMZ), an established antianginal drug that inhibit fatty acid metabolism through inhibition of mitochondrial 3-ketoacyl thiolase and enhance PDH activity to improve the metabolic efficiency in the myocardium (McCarthy et al., 2016). The administration of TMZ in hypoxic cardiomyocytes promotes glucose oxidation and was protective against hypoxia-induced injury (Wei et al.,

2015), however, the effect of TMZ in hypoxic animal models has not been explored. Moreover, clinical studies of TMZ showed mixed results regarding its clinical benefits. In a meta-analysis involving 995 patients with heart failure (Gao et al., 2011), the use of TMZ was associated with significant improvement in left ventricular ejection fraction, end-systolic volume, NYHA classification, as well as protective effect for all-cause mortality, cardiovascular events and hospitalization. However, in a latest clinical trial, the use of TMZ in patients after percutaneous coronary intervention failed to improve the composite endpoint of cardiac death, hospitalization for cardiac events, or angina leading to angiography or changes in antianginal medication (Ferrari et al., 2020). These contradictory results indicate that TMZ might provide clinical benefits in certain patient subgroups, such as those with an established diagnosis of heart failure, but not in other subgroups. Therefore, in patients with chronic hypoxia, those with impaired cardiac function could be the population likely to benefit from using TMZ.

The third option is CPT1 inhibition, which could result in decreased mitochondrial uptake of long-chain fatty acid, reduced β-oxidation, and promotion of glucose oxidation. Although several synthetic CPT1 inhibitors, including oxfenicine, etormoxir and perhexiline, have been developed in the past decades, none of them have made into clinical practice to treat heart failure (Heggermont et al., 2016). Malonyl-CoA is a natural inhibitor of CPT1, and pre-clinical studies had shown that modulation of malonyl-CoA, or more specifically, increasing cardiac malonyl-CoA level or inhibition of malonyl-CoA decarboxylase, can lead to improvement in cardiac function by decreasing fatty acid oxidation and increasing cardiac metabolic efficiency (Fillmore and Lopaschuk, 2014). In this case, indirect inhibition of CPT1 through modulating malonyl-CoA could be a feasible strategy to improve cardiac metabolic efficiency in chronically hypoxic patients.

In recent years, novel strategies are emerging to modulate cardiac metabolism by direct targeting of specific regulators. For instance, direct modulation of cardiac PDK4 activity could offer a potentially feasible strategy to enhance glucose metabolism in chronically hypoxic hearts. A recent study found that conditional cardiac deletion of PDK4 could result in an increase in PDH activity and consequently an increase in glucose relative to fatty-acid oxidation, which was associated with reduced cardiac fibrosis and improved left ventricular function in mice following myocardial infarction (Cardoso et al., 2020). The recent discovery of oral compound that specifically inhibit PDK4 could offer a potential strategy for clinical translation (Lee et al., 2019).

As we had discussed above, insulin resistance and altered insulin signaling could impair the protective HIF-1α pathway in response against chronic hypoxia. Hence, another potentially feasible strategy to maintain the adaptive cardiac metabolism under chronic hypoxia is by improving cardiac insulin sensitivity. Pioglitazone is a potent insulin sensitizer that targets PPARγ signaling to decrease systemic and myocardial insulin resistance (Soccio et al., 2014), with favorable effects on cardiac metabolism (Young, 2003). In animal studies, pioglitazone has been demonstrated to promote myocardial glucose uptake, enhance glucose oxidation, and improve contractile function in isolated hearts of rats with insulin resistance (Golfman et al., 2005). In patients with T2DM, pioglitazone has been shown to improve left ventricular diastolic function and cardiac output (van der Meer et al., 2009; Clarke et al., 2017). A recent study shows that the use of pioglitazone in pubertal hypoxic rats could attenuate insulin resistance and restore the protective cardiac Hif-1α signaling in the hypoxic myocardium, which maintains the adaptive cardiac metabolism and preserves cardiac function (Liu et al., 2020). More animal and human studies should test this strategy in chronically hypoxic patients with increased insulin resistance to preserve adaptive metabolism and reduce the risk of heart failure.

Modulation of CoQ10 biosynthesis, or direct supplementation of CoQ10, should be considered in patients with chronic hypoxia. Although the biological effects of CoQ10 have been reported in various cardiac diseases (Zozina et al., 2018), its biological relevance and clinical benefits are yet to be determined in patients with chronic hypoxia. Given its potent antioxidant effect and involvement in mitochondrial respiration, the addition of CoQ10 in chronically hypoxic patients may improve their adaptive cardiac metabolism and produce clinical benefits. The clinical benefits of CoQ10 has been established in patients with heart failure (Sharma et al., 2016), and it is reasonable to test the effects of CoQ10 on patients with chronic hypoxia in future studies.

CONCLUSIONS

In response to chronic hypoxia, the hearts initiate transcriptional programs to increase reliance on carbohydrates over fatty acid for ATP production, with altered mitochondrial structure and function that improve metabolic efficiency and reduce ROS generation, as well as beneficial changes in glycogen storage and high energy phosphate system. Collectively, the adaptive cardiac program improves the regulation of the balance between energy demand and energy supply when oxygen is limited. Of note, this adaptive program is prone to be disrupted by systemic pathological factors, such as insulin resistance, and it can be complicated with other pathological factors concomitantly seen in patients with chronic hypoxia. The presence of these risk factors can pre-dispose to altered adaptive metabolism and cardiac dysfunction. Currently available pharmacological strategies are limited and none have been tested in patients with chronic hypoxia. Therefore, more investigational studies are needed to unravel the critical features and mechanism for maladaptive cardiac metabolism in these patients.

AUTHOR CONTRIBUTIONS

ZS and YL contributed to the conception of the article. ZS drafted the first manuscript and YL contributed to the revision of the manuscript and graphical design. HZ contributed to the critical revision of the manuscript. HZ and YL obtained funds. All authors approved the submission of the article.

FUNDING

This work was supported by the National Natural Science Foundation of China (81525002, 31971048), Shanghai Outstanding Medical Academic Leader program (2019LJ22), Shanghai Sailing Program (20YF1428700) and Collaborative Innovation Program of Shanghai Municipal Health Commission (2020CXJQ01).

REFERENCES

Abdurrachim, D., Luiken, J. J., Nicolay, K., Glatz, J. F., Prompers, J. J., and Nabben, M. (2015). Good and bad consequences of altered fatty acid metabolism in heart failure: evidence from mouse models. *Cardiovasc. Res*. 106, 194–205. doi: 10.1093/cvr/cvv105

Abe, H., Semba, H., and Takeda, N. (2017). The roles of hypoxia signaling in the pathogenesis of cardiovascular diseases. *J. Atheroscler. Thromb*. 24, 884–894. doi: 10.5551/jat.RV17009

Belanger, A. J., Luo, Z., Vincent, K. A., Akita, G. Y., Cheng, S. H., Gregory, R. J., et al. (2007). Hypoxia-inducible factor 1 mediates hypoxia-induced cardiomyocyte lipid accumulation by reducing the DNA binding activity of peroxisome proliferator-activated receptor alpha/retinoid X receptor. *Biochem. Biophys. Res. Commun*. 364, 567–572. doi: 10.1016/j.bbrc.2007.10.062

Bertero, E., and Maack, C. (2018). Metabolic remodelling in heart failure. *Nat. Rev. Cardiol*. 15, 457–470. doi: 10.1038/s41569-018-0044-6

Bigham, A. W., and Lee, F. S. (2014). Human high-altitude adaptation: forward genetics meets the HIF pathway. *Genes Dev*. 28, 2189–2204. doi: 10.1101/gad.250167.114

Boudina, S., and Abel, E. D. (2006). Mitochondrial uncoupling: a key contributor to reduced cardiac efficiency in diabetes. *Physiology* 21, 250–258. doi: 10.1152/physiol.00008.2006

Bowater, S. E., Weaver, R. A., Beadle, R. M., Frenneaux, M. P., Marshall, J. M., and Clift, P. F. (2016). Assessment of the physiological adaptations to chronic hypoxemia in eisenmenger syndrome. *Congenit. Heart Dis*. 11, 341–347. doi: 10.1111/chd.12373

Bowker-Kinley, M. M., Davis, W. I., Wu, P., Harris, R. A., and Popov, K. M. (1998). Evidence for existence of tissue-specific regulation of the mammalian pyruvate dehydrogenase complex. *Biochem J*. 329(Pt. 1), 191–196. doi: 10.1042/bj3290191

Calmettes, G., Deschodt-Arsac, V., Gouspillou, G., Miraux, S., Muller, B., Franconi, J. M., et al. (2010). Improved energy supply regulation in chronic hypoxic mouse counteracts hypoxia-induced altered cardiac energetics. *PLoS ONE* 5:e9306. doi: 10.1371/journal.pone.0009306

Calmettes, G., Deschodt-Arsac, V., Thiaudiere, E., Muller, B., and Diolez, P. (2008). Modular control analysis of effects of chronic hypoxia on mouse heart. *Am. J. Physiol. Regul. Integr. Comp. Physiol*. 295, R1891–R1897. doi: 10.1152/ajpregu.90548.2008

Cardoso, A. C., Lam, N. T., Savla, J. J., Nakada, Y., Pereira, A. H. M., Elnwasany, A., et al. (2020). Mitochondrial substrate utilization regulates cardiomyocyte cell cycle progression. *Nat Metab*. 2, 167–178. doi: 10.1038/s42255-020-0169-x

Clarke, G. D., Solis-Herrera, C., Molina-Wilkins, M., Martinez, S., Merovci, A., Cersosimo, E., et al. (2017). Pioglitazone improves left ventricular diastolic function in subjects with diabetes. *Diabetes Care* 40, 1530–1536. doi: 10.2337/dc17-0078

Cole, M. A., Abd Jamil, A. H., Heather, L. C., Murray, A. J., Sutton, E. R., Slingo, M., et al. (2016). On the pivotal role of PPARalpha in adaptation of the heart to hypoxia and why fat in the diet increases hypoxic injury. *FASEB J*. 30, 2684–2697. doi: 10.1096/fj.201500094R

Cunningham, K. F., Beeson, G. C., Beeson, C. C., Baicu, C. F., Zile, M. R., and McDermott, P. J. (2015). Estrogen-related receptor alpha (ERRalpha) is required for adaptive increases in PGC-1 isoform expression during electrically stimulated contraction of adult cardiomyocytes in sustained hypoxic conditions. *Int. J. Cardiol*. 187, 393–400. doi: 10.1016/j.ijcard.2015.03.353

Darvey, I. G. (1998). How does the ratio of ATP yield from the complete oxidation of palmitic acid to that of glucose compare with the relative energy contents of fat and carbohydrate? *Biochem. Educ*. 26, 22–23. doi: 10.1016/S0307-4412(97)00046-0

Dodd, M. S., Sousa Fialho, M. D. L., Montes Aparicio, C. N., Kerr, M., Timm, K. N., Griffin, J. L., et al. (2018). Fatty acids prevent hypoxia-inducible factor-1alpha signaling through decreased succinate in diabetes. *JACC Basic Transl. Sci*. 3, 485–498. doi: 10.1016/j.jacbts.2018.04.005

Dorn, G. W. II, Vega, R. B., and Kelly, D. P. (2015). Mitochondrial biogenesis and dynamics in the developing and diseased heart. *Genes Dev*. 29, 1981–1991. doi: 10.1101/gad.269894.115

Doronzo, G., Russo, I., Mattiello, L., Riganti, C., Anfossi, G., and Trovati, M. (2006). Insulin activates hypoxia-inducible factor-1alpha in human and rat vascular smooth muscle cells via phosphatidylinositol-3 kinase and mitogen-activated protein kinase pathways: impairment in insulin resistance owing to defects in insulin signalling. *Diabetologia* 49, 1049–1063. doi: 10.1007/s00125-006-0156-0

Essop, M. F. (2007). Cardiac metabolic adaptations in response to chronic hypoxia. *J Physiol*. 584(Pt. 3), 715–726. doi: 10.1113/jphysiol.2007.143511

Ferrannini, E., Mark, M., and Mayoux, E. (2016). CV protection in the EMPA-REG OUTCOME trial: a "thrifty substrate" hypothesis. *Diabetes Care* 39, 1108–1114. doi: 10.2337/dc16-0330

Ferrari, R., Ford, I., Fox, K., Challeton, J. P., Correges, A., Tendera, M., et al. (2020). Efficacy and safety of trimetazidine after percutaneous coronary intervention (ATPCI): a randomised, double-blind, placebo-controlled trial. *Lancet* 396, 830–838. doi: 10.1016/S0140-6736(20)31790-6

Ferri, A., Panariti, A., Miserocchi, G., Rocchetti, M., Buoli Comani, G., Rivolta, I., et al. (2018). Tissue specificity of mitochondrial adaptations in rats after 4 weeks of normobaric hypoxia. *Eur. J. Appl. Physiol*. 118, 1641–1652. doi: 10.1007/s00421-018-3897-9

Fillmore, N., and Lopaschuk, G. D. (2014). Malonyl CoA: A promising target for the treatment of cardiac disease. *IUBMB Life*. 66, 139–146. doi: 10.1002/iub.1253

Finck, B. N., and Kelly, D. P. (2002). Peroxisome proliferator-activated receptor alpha (PPARalpha) signaling in the gene regulatory control of energy metabolism in the normal and diseased heart. *J. Mol. Cell. Cardiol*. 34, 1249–1257. doi: 10.1016/S0022-2828(02)92061-4

Forkel, J., Chen, X., Wandinger, S., Keser, F., Duschin, A., Schwanke, U., et al. (2004). Responses of chronically hypoxic rat hearts to ischemia: KATP channel blockade does not abolish increased RV tolerance to ischemia. *Am. J. Physiol. Heart Circ. Physiol*. 286, H545–H551. doi: 10.1152/ajpheart.00022.2003

Gao, D., Ning, N., Niu, X., Hao, G., and Meng, Z. (2011). Trimetazidine: a meta-analysis of randomised controlled trials in heart failure. *Heart* 97, 278–286. doi: 10.1136/hrt.2010.208751

Ge, R. L., Simonson, T. S., Cooksey, R. C., Tanna, U., Qin, G., Huff, C. D., et al. (2012). Metabolic insight into mechanisms of high-altitude adaptation in Tibetans. *Mol. Genet. Metab*. 106, 244–247. doi: 10.1016/j.ymgme.2012.03.003

Giordano, F. J. (2005). Oxygen, oxidative stress, hypoxia, and heart failure. *J. Clin. Invest*. 115, 500–508. doi: 10.1172/JCI200524408

Golfman, L. S., Wilson, C. R., Sharma, S., Burgmaier, M., Young, M. E., Guthrie, P. H., et al. (2005). Activation of PPARgamma enhances myocardial glucose oxidation and improves contractile function in isolated working hearts of ZDF rats. *Am. J. Physiol. Endocrinol. Metab*. 289, E328–E336. doi: 10.1152/ajpendo.00055.2005

Guimaraes-Ferreira, L. (2014). Role of the phosphocreatine system on energetic homeostasis in skeletal and cardiac muscles. *Einstein* 12, 126–131. doi: 10.1590/S1679-45082014RB2741

Guzy, R. D., and Schumacker, P. T. (2006). Oxygen sensing by mitochondria at complex III: the paradox of increased reactive oxygen species during hypoxia. *Exp. Physiol*. 91, 807–819. doi: 10.1113/expphysiol.2006.033506

Handzlik, M. K., Constantin-Teodosiu, D., Greenhaff, P. L., and Cole, M. A. (2018). Increasing cardiac pyruvate dehydrogenase flux during chronic hypoxia improves acute hypoxic tolerance. *J. Physiol*. 596, 3357–3369. doi: 10.1113/JP275357

Heather, L. C., Cole, M. A., Tan, J. J., Ambrose, L. J., Pope, S., Abd-Jamil, A. H., et al. (2012). Metabolic adaptation to chronic hypoxia in

cardiac mitochondria. *Basic Res. Cardiol.* 107:268. doi: 10.1007/s00395-012-0268-2

Heggermont, W. A., Papageorgiou, A. P., Heymans, S., and van Bilsen, M. (2016). Metabolic support for the heart: complementary therapy for heart failure? *Eur. J. Heart Fail.* 18, 1420–1429. doi: 10.1002/ejhf.678

Hochachka, P. W., Clark, C. M., Holden, J. E., Stanley, C., Ugurbil, K., and Menon, R. S. (1996). 31P magnetic resonance spectroscopy of the Sherpa heart: a phosphocreatine/adenosine triphosphate signature of metabolic defense against hypobaric hypoxia. *Proc. Natl. Acad. Sci. U.S.A.* 93, 1215–1220. doi: 10.1073/pnas.93.3.1215

Hochachka, P. W., and Lutz, P. L. (2001). Mechanism, origin, and evolution of anoxia tolerance in animals. *Comp. Biochem. Physiol. B Biochem. Mol. Biol.* 130, 435–459. doi: 10.1016/S1096-4959(01)00408-0

Holden, J. E., Stone, C. K., Clark, C. M., Brown, W. D., Nickles, R. J., Stanley, C., et al. (1995). Enhanced cardiac metabolism of plasma glucose in high-altitude natives: adaptation against chronic hypoxia. *J. Appl. Physiol. (1985)* 79, 222–228. doi: 10.1152/jappl.1995.79.1.222

Holness, M. J., and Sugden, M. C. (2003). Regulation of pyruvate dehydrogenase complex activity by reversible phosphorylation. *Biochem Soc Trans.* 31(Pt. 6), 1143–1151. doi: 10.1042/bst0311143

Horan, M. P., Pichaud, N., and Ballard, J. W. (2012). Review: quantifying mitochondrial dysfunction in complex diseases of aging. *J. Gerontol. A Biol. Sci. Med. Sci.* 67, 1022–1035. doi: 10.1093/gerona/glr263

Horscroft, J. A., Burgess, S. L., Hu, Y., and Murray, A. J. (2015). Altered oxygen utilisation in rat left ventricle and soleus after 14 days, but not 2 days, of environmental hypoxia. *PLoS ONE* 10:e0138564. doi: 10.1371/journal.pone.0138564

Horscroft, J. A., Kotwica, A. O., Laner, V., West, J. A., Hennis, P. J., Levett, D. Z. H., et al. (2017). Metabolic basis to sherpa altitude adaptation. *Proc. Natl. Acad. Sci. U.S.A.* 114, 6382–6387. doi: 10.1073/pnas.1700527114

Hue, L., and Taegtmeyer, H. (2009). The randle cycle revisited: a new head for an old hat. *Am. J. Physiol. Endocrinol. Metab.* 297, E578–E591. doi: 10.1152/ajpendo.00093.2009

Ip, M. S., Lam, B., Ng, M. M., Lam, W. K., Tsang, K. W., and Lam, K. S. (2002). Obstructive sleep apnea is independently associated with insulin resistance. *Am. J. Respir. Crit. Care Med.* 165, 670–676. doi: 10.1164/ajrccm.165.5.2103001

Jung, F., Palmer, L. A., Zhou, N., and Johns, R. A. (2000). Hypoxic regulation of inducible nitric oxide synthase via hypoxia inducible factor-1 in cardiac myocytes. *Circ. Res.* 86, 319–325. doi: 10.1161/01.RES.86.3.319

Kato, T., Niizuma, S., Inuzuka, Y., Kawashima, T., Okuda, J., Tamaki, Y., et al. (2010). Analysis of metabolic remodeling in compensated left ventricular hypertrophy and heart failure. *Circ. Heart Fail.* 3, 420–430. doi: 10.1161/CIRCHEARTFAILURE.109.888479

Kent, B. D., Mitchell, P. D., and McNicholas, W. T. (2011). Hypoxemia in patients with COPD: cause, effects, and disease progression. *Int. J. Chron. Obstruct. Pulmon. Dis.* 6, 199–208. doi: 10.2147/COPD.S10611

Kessler, G., and Friedman, J. (1998). Metabolism of fatty acids and glucose. *Circulation* 67(Suppl. 3), 519S−526S. doi: 10.1161/circ.98.13.1350/a

Kim, D. H., and Chauhan, S. (2018). The role of dichloroacetate in improving acute hypoxic tolerance and cardiac function: translation to failing hearts? *J. Physiol.* 596, 2967–2968. doi: 10.1113/JP276217

Kinota, F., Droma, Y., Kobayashi, N., Horiuchi, T., Kitaguchi, Y., Yasuo, M., et al. (2018). The contribution of genetic variants of the peroxisome proliferator-activated receptor-alpha gene to high-altitude hypoxia adaptation in sherpa highlanders. *High Alt. Med. Biol.* doi: 10.1089/ham.2018.0052. [Epub ahead of print].

Klos, M., Morgenstern, S., Hicks, K., Suresh, S., and Devaney, E. J. (2019). The effects of the ketone body beta-hydroxybutyrate on isolated rat ventricular myocyte excitation-contraction coupling. *Arch. Biochem. Biophys.* 662, 143–150. doi: 10.1016/j.abb.2018.11.027

Kolwicz, S. C. Jr., Purohit, S., and Tian, R. (2013). Cardiac metabolism and its interactions with contraction, growth, and survival of cardiomyocytes. *Circ. Res.* 113, 603–616. doi: 10.1161/CIRCRESAHA.113.302095

Larsen, S., Nielsen, J., Hansen, C. N., Nielsen, L. B., Wibrand, F., Stride, N., et al. (2012). Biomarkers of mitochondrial content in skeletal muscle of healthy young human subjects. *J. Physiol.* 590, 3349–3360. doi: 10.1113/jphysiol.2012.230185

Le Page, L. M., Rider, O. J., Lewis, A. J., Noden, V., Kerr, M., Giles, L., et al. (2019). Assessing the effect of hypoxia on cardiac metabolism using hyperpolarized (13) C magnetic resonance spectroscopy. *NMR Biomed.* 32:e4099. doi: 10.1002/nbm.4099

Lee, D., Pagire, H. S., Pagire, S. H., Bae, E. J., Dighe, M., Kim, M., et al. (2019). Discovery of novel pyruvate dehydrogenase kinase 4 inhibitors for potential oral treatment of metabolic diseases. *J. Med. Chem.* 62, 575–588. doi: 10.1021/acs.jmedchem.8b01168

Liu, Y., Luo, Q., Su, Z., Xing, J., Wu, J. Xiang, L., et al. (2020). Suppression of myocardial HIF-1 by pubertal insulin resistance compromises metabolic adaptation and impairs cardiac function in patients with cyanotic congenital heart disease. *European Heart Journal*, 41:ehaa946.2168. doi: 10.1093/ehjci/ehaa946.2168

Liu, Y., Xing, J., Li, Y., Luo, Q., Su, Z., Zhang, X., et al. (2019). Chronic hypoxia-induced Cirbp hypermethylation attenuates hypothermic cardioprotection via down-regulation of ubiquinone biosynthesis. *Sci. Transl. Med.* 11:eaat8406. doi: 10.1126/scitranslmed.aat8406

Lydell, C. P., Chan, A., Wambolt, R. B., Sambandam, N., Parsons, H., Bondy, G. P., et al. (2002). Pyruvate dehydrogenase and the regulation of glucose oxidation in hypertrophied rat hearts. *Cardiovasc. Res.* 53, 841–851. doi: 10.1016/S0008-6363(01)00560-0

Mahle, W. T., Newburger, J. W., Matherne, G. P., Smith, F. C., Hoke, T. R., Koppel, R., et al. (2009). Role of pulse oximetry in examining newborns for congenital heart disease: a scientific statement from the AHA and AAP. *Pediatrics* 124, 823–836. doi: 10.1542/peds.2009-1397

Mansor, L. S., Mehta, K., Aksentijevic, D., Carr, C. A., Lund, T., Cole, M. A., et al. (2016). Increased oxidative metabolism following hypoxia in the type 2 diabetic heart, despite normal hypoxia signalling and metabolic adaptation. *J. Physiol.* 594, 307–320. doi: 10.1113/JP271242

McCarthy, C. P., Mullins, K. V., and Kerins, D. M. (2016). The role of trimetazidine in cardiovascular disease: beyond an anti-anginal agent. *Eur. Heart J. Cardiovasc. Pharmacother.* 2, 266–272. doi: 10.1093/ehjcvp/pvv051

McCarthy, J., Lochner, A., Opie, L. H., Sack, M. N., and Essop, M. F. (2011). PKCepsilon promotes cardiac mitochondrial and metabolic adaptation to chronic hypobaric hypoxia by GSK3beta inhibition. *J. Cell. Physiol.* 226, 2457–2468. doi: 10.1002/jcp.22592

McNicholas, W. T. (2018). Comorbid obstructive sleep apnoea and chronic obstructive pulmonary disease and the risk of cardiovascular disease. *J. Thorac. Dis.* 10(Suppl. 34), S4253–S61. doi: 10.21037/jtd.2018.10.117

Miall-Allen, V. M., Kemp, G. J., Rajagopalan, B., Taylor, D. J., Radda, G. K., and Haworth, S. G. (1996). Magnetic resonance spectroscopy in congenital heart disease. *Heart.* 75, 614–619. doi: 10.1136/hrt.75.6.614

Modi, P., Suleiman, M. S., Reeves, B. C., Pawade, A., Parry, A. J., Angelini, G. D., et al. (2004). Basal metabolic state of hearts of patients with congenital heart disease: the effects of cyanosis, age, and pathology. *Ann. Thorac. Surg.* 78, 1710–1716. doi: 10.1016/j.athoracsur.2004.05.010

Murray, A. J., Montgomery, H. E., Feelisch, M., Grocott, M. P. W., and Martin, D. S. (2018). Metabolic adjustment to high-altitude hypoxia: from genetic signals to physiological implications. *Biochem. Soc. Trans.* 46, 599–607. doi: 10.1042/BST20170502

Niwa, K. (2019). Metabolic syndrome in adult congenital heart disease. *Korean Circ. J.* 49, 691–708. doi: 10.4070/kcj.2019.0187

Nouette-Gaulain, K., Biais, M., Savineau, J. P., Marthan, R., Mazat, J. P., Letellier, T., et al. (2011). Chronic hypoxia-induced alterations in mitochondrial energy metabolism are not reversible in rat heart ventricles. *Can. J. Physiol. Pharmacol.* 89, 58–66. doi: 10.1139/Y10-105

Nouette-Gaulain, K., Malgat, M., Rocher, C., Savineau, J. P., Marthan, R., Mazat, J. P., et al. (2005). Time course of differential mitochondrial energy metabolism adaptation to chronic hypoxia in right and left ventricles. *Cardiovasc. Res.* 66, 132–140. doi: 10.1016/j.cardiores.2004.12.023

Novel-Chate, V., Mateo, P., Saks, V. A., Hoerter, J. A., and Rossi, A. (1998). Chronic exposure of rats to hypoxic environment alters the mechanism of energy transfer in myocardium. *J. Mol. Cell. Cardiol.* 30, 1295–1303. doi: 10.1006/jmcc.1998.0694

Palmer, J. W., Tandler, B., and Hoppel, C. L. (1977). Biochemical properties of subsarcolemmal and interfibrillar mitochondria isolated from rat cardiac muscle. *J. Biol. Chem.* 252, 8731–8739. doi: 10.1016/S0021-9258(19)75283-1

Pescador, N., Villar, D., Cifuentes, D., Garcia-Rocha, M., Ortiz-Barahona, A., Vazquez, S., et al. (2010). Hypoxia promotes glycogen accumulation through hypoxia inducible factor (HIF)-mediated induction of glycogen synthase 1. *PLoS ONE* 5:e9644. doi: 10.1371/journal.pone.0009644

Plunkett, M. D., Hendry, P. J., Anstadt, M. P., Camporesi, E. M., Amato, M. T., St Louis, J. D., et al. (1996). Chronic hypoxia induces adaptive metabolic changes in neonatal myocardium. *J. Thorac. Cardiovasc. Surg.* 112, 8–13. doi: 10.1016/S0022-5223(96)70171-X

Qi, H., Xu, S., Ma, R., Jiang, L., Li, S., Mai, S., et al. (2015). Comparison of echocardiographic parameters in healthy Chinese children born and living at high altitude or at sea-level. *Zhonghua Xin Xue Guan Bing Za Zhi*. 43, 774–781. doi: 10.3760/cma.j.issn.0253-3758.2015.09.006

Qing, M., Gorlach, A., Schumacher, K., Woltje, M., Vazquez-Jimenez, J. F., Hess, J., et al. (2007). The hypoxia-inducible factor HIF-1 promotes intramyocardial expression of VEGF in infants with congenital cardiac defects. *Basic Res. Cardiol.* 102, 224–232. doi: 10.1007/s00395-007-0639-2

Rafiee, P., Shi, Y., Kong, X., Pritchard, K. A. Jr., Tweddell, J. S., Litwin, S. B., et al. (2002). Activation of protein kinases in chronically hypoxic infant human and rabbit hearts: role in cardioprotection. *Circulation* 106, 239–245. doi: 10.1161/01.CIR.0000022018.68965.6D

Ramjiawan, A., Bagchi, R. A., Blant, A., Albak, L., Cavasin, M. A., Horn, T. R., et al. (2013). Roles of histone deacetylation and AMP kinase in regulation of cardiomyocyte PGC-1alpha gene expression in hypoxia. *Am. J. Physiol. Cell Physiol.* 304, C1064–C1072. doi: 10.1152/ajpcell.00262.2012

Ross-Ascuitto, N. T., Joyce, J. J., Hasan, A. Z., and Ascuitto, R. J. (2004). Performance of the chronically hypoxic young rabbit heart. *Pediatr. Cardiol.* 25, 397–405. doi: 10.1007/s00246-003-0429-z

Roth, G. A., Mensah, G. A., Johnson, C. O., Addolorato, G., Ammirati, E., Baddour, L. M., et al. (2020). Global burden of cardiovascular diseases and risk factors, 1990-2019: update from the GBD 2019 study. *J. Am. Coll. Cardiol.* 76, 2982–3021. doi: 10.1016/j.jacc.2020.11.010

Ryan, S. (2018). Mechanisms of cardiovascular disease in obstructive sleep apnoea. *J. Thorac. Dis.* 10(Suppl. 34), S4201–S11. doi: 10.21037/jtd.2018.08.56

Savla, J. J., Levine, B. D., and Sadek, H. A. (2018). The effect of hypoxia on cardiovascular disease: friend or foe? *High Alt. Med. Biol.* 19, 124–130. doi: 10.1089/ham.2018.0044

Semenza, G. L. (2014). Hypoxia-inducible factor 1 and cardiovascular disease. *Annu. Rev. Physiol.* 76, 39–56. doi: 10.1146/annurev-physiol-021113-170322

Sharma, A., Fonarow, G. C., Butler, J., Ezekowitz, J. A., and Felker, G. M. (2016). Coenzyme Q10 and heart failure: a state-of-the-art review. *Circ. Heart Fail.* 9:e002639. doi: 10.1161/CIRCHEARTFAILURE.115.002639

Sharma, S., Taegtmeyer, H., Adrogue, J., Razeghi, P., Sen, S., Ngumbela, K., et al. (2004). Dynamic changes of gene expression in hypoxia-induced right ventricular hypertrophy. *Am. J. Physiol. Heart Circ. Physiol.* 286, H1185–H1192. doi: 10.1152/ajpheart.00916.2003

Singh, R. M., Cummings, E., Pantos, C., and Singh, J. (2017). Protein kinase C and cardiac dysfunction: a review. *Heart Fail. Rev.* 22, 843–859. doi: 10.1007/s10741-017-9634-3

Soccio, R. E., Chen, E. R., and Lazar, M. A. (2014). Thiazolidinediones and the promise of insulin sensitization in type 2 diabetes. *Cell Metab.* 20, 573–591. doi: 10.1016/j.cmet.2014.08.005

Sousa Fialho, M. D. L., Abd Jamil, A. H., Stannard, G. A., and Heather, L. C. (2019). Hypoxia-inducible factor 1 signalling, metabolism and its therapeutic potential in cardiovascular disease. *Biochim. Biophys. Acta Mol. Basis Dis.* 1865, 831–843. doi: 10.1016/j.bbadis.2018.09.024

Sugden, M. C., and Holness, M. J. (2006). Mechanisms underlying regulation of the expression and activities of the mammalian pyruvate dehydrogenase kinases. *Arch. Physiol. Biochem.* 112, 139–149. doi: 10.1080/13813450600935263

Tian, R., Colucci, W. S., Arany, Z., Bachschmid, M. M., Ballinger, S. W., Boudina, S., et al. (2019). Unlocking the secrets of mitochondria in the cardiovascular system: path to a cure in heart failure-A report from the 2018 national heart, lung, and blood institute workshop. *Circulation* 140, 1205–1216. doi: 10.1161/CIRCULATIONAHA.119.040551

van der Meer, R. W., Rijzewijk, L. J., de Jong, H. W., Lamb, H. J., Lubberink, M., Romijn, J. A., et al. (2009). Pioglitazone improves cardiac function and alters myocardial substrate metabolism without affecting cardiac triglyceride accumulation and high-energy phosphate metabolism in patients with well-controlled type 2 diabetes mellitus. *Circulation* 119, 2069–2077. doi: 10.1161/CIRCULATIONAHA.108.803916

Wei, J., Xu, H., Shi, L., Tong, J., and Zhang, J. (2015). Trimetazidine protects cardiomyocytes against hypoxia-induced injury through ameliorates calcium homeostasis. *Chem. Biol. Interact.* 236, 47–56. doi: 10.1016/j.cbi.2015.04.022

Woolcott, O. O., Ader, M., and Bergman, R. N. (2015). Glucose homeostasis during short-term and prolonged exposure to high altitudes. *Endocr. Rev.* 36, 149–173. doi: 10.1210/er.2014-1063

Young, L. H. (2003). Insulin resistance and the effects of thiazolidinediones on cardiac metabolism. *Am. J. Med.* 115(Suppl. 8A), 75S−80S. doi: 10.1016/j.amjmed.2003.09.013

Zelzer, E., Levy, Y., Kahana, C., Shilo, B. Z., Rubinstein, M., and Cohen, B. (1998). Insulin induces transcription of target genes through the hypoxia-inducible factor HIF-1alpha/ARNT. *EMBO J.* 17, 5085–5094. doi: 10.1093/emboj/17.17.5085

Zhao, Q. M., Ma, X. J., Jia, B., and Huang, G. Y. (2013). Prevalence of congenital heart disease at live birth: an accurate assessment by echocardiographic screening. *Acta Paediatrica* 102, 397–402. doi: 10.1111/apa.12170

Zheng, C., Chen, Z., Zhang, L., Wang, X., Dong, Y., Wang, J., et al. (2019). Metabolic risk factors and left ventricular diastolic function in middle-aged chinese living in the Tibetan plateau. *J. Am. Heart Assoc.* 8:e010454. doi: 10.1161/JAHA.118.010454

Zhu, L., Wang, Q., Zhang, L., Fang, Z., Zhao, F., Lv, Z., et al. (2010). Hypoxia induces PGC-1alpha expression and mitochondrial biogenesis in the myocardium of TOF patients. *Cell Res.* 20, 676–687. doi: 10.1038/cr.2010.46

Zozina, V. I., Covantev, S., Goroshko, O. A., Krasnykh, L. M., and Kukes, V. G. (2018). Coenzyme Q10 in cardiovascular and metabolic diseases: current state of the problem. *Curr. Cardiol. Rev.* 14, 164–174. doi: 10.2174/1573403X14666180416115428

Conflict of Interest: The authors declare that the research was conducted in the absence of any commercial or financial relationships that could be construed as a potential conflict of interest.

frontiers in Cell and Developmental Biology

ORIGINAL RESEARCH
published: 16 February 2021
doi: 10.3389/fcell.2021.634900

Combined Administration of Metformin and Atorvastatin Attenuates Diabetic Cardiomyopathy by Inhibiting Inflammation, Apoptosis, and Oxidative Stress in Type 2 Diabetic Mice

Weikun Jia[1†], Tao Bai[2†], Jiang Zeng[3†], Zijing Niu[4†], Daogui Fan[4], Xin Xu[3], Meiling Luo[4], Peijian Wang[5], Qingliang Zou[5] and Xiaozhen Dai[4*]*

[1] Department of Cardiothoracic Surgery, The First Affiliated Hospital of Chengdu Medical College, Chengdu, China, [2] Department of Cardiovascular Center, The First Hospital of Jilin University, Changchun, China, [3] School of Basic Medicine, Chengdu Medical College, Chengdu, China, [4] School of Biosciences and Technology, Chengdu Medical College, Chengdu, China, [5] Department of Cardiology, The First Affiliated Hospital of Chengdu Medical College, Chengdu, China

OPEN ACCESS

Edited by:
Xiaoqiang Tang,
Sichuan University, China

Reviewed by:
LiTai Jin,
Wenzhou Medical University, China
Xiaojing Liu,
Sichuan University, China

***Correspondence:**
Xiaozhen Dai
xiaozhendai2012@163.com
Qingliang Zou
zql-sibs@163.com

[†] These authors have contributed equally to this work

Specialty section:
This article was submitted to Cellular Biochemistry, a section of the journal Frontiers in Cell and Developmental Biology

Received: 29 November 2020
Accepted: 12 January 2021
Published: 16 February 2021

Citation:
Jia W, Bai T, Zeng J, Niu Z, Fan D, Xu X, Luo M, Wang P, Zou Q and Dai X (2021) Combined Administration of Metformin and Atorvastatin Attenuates Diabetic Cardiomyopathy by Inhibiting Inflammation, Apoptosis, and Oxidative Stress in Type 2 Diabetic Mice. Front. Cell Dev. Biol. 9:634900. doi: 10.3389/fcell.2021.634900

Diabetic cardiomyopathy (DCM), a common complication of diabetes mellitus, may eventually leads to irreversible heart failure. Metformin is the cornerstone of diabetes therapy, especially for type 2 diabetes. Statins are widely used to reduce the risk of cardiovascular diseases. In this study, we aimed to investigate whether the combined administration of metformin and atorvastatin could achieve superior protective effects on DCM and to elucidate its molecular mechanism. Here, *db/db* mice (9–10 weeks old) were randomly divided into four groups, including sterile water group (DM), metformin group (MET, 200 mg/kg/day), atorvastatin group (AVS, 10 mg/kg/day), and combination therapy group (MET + AVS). Mice were treated with different drugs via gavage once per day for 3 months. After 3 months of treatment, the pathological changes (inflammation, fibrosis, hypertrophy, and oxidative stress makers) were detected by histopathological techniques, as well as Western blotting. The H9C2 cardiomyocytes were treated with palmitate (PAL) to mimic diabetic condition. The cells were divided into control group, PAL treatment group, MET + PAL treatment group, AVS + PAL treatment group, and MET + AVS + PAL treatment group. The effects of MET and AVS on the cell viability and inflammation of H9C2 cells subjected to PAL condition were evaluated by terminal deoxynucleotidyl transferase-mediated dUTP nick-end labeling (TUNEL) assay, immunofluorescence staining, and Western blotting. Both MET and AVS prevented diabetes-induced fibrosis, hypertrophy, and inflammation. The combination therapy showed superior effects in protecting myocardial tissue against diabetes-induced injury. Mechanistically, the combination therapy significantly inhibited oxidative stress and the expression levels of inflammation-related proteins, e.g., NLRP3, caspase-1, interleukin-1β (IL-1β), Toll-like receptor 4 (TLR4), and P-p65/p65, in both cardiac tissues and H9C2 cells. TUNEL assay showed that the combination therapy significantly attenuated the apoptosis of cardiomyocytes; decreased the expression level of pro-apoptotic-related

proteins, such as cleaved caspase-3 and BAX; and enhanced the expression level of anti-apoptotic protein (Bcl-2). Furthermore, the combination therapy remarkably upregulated the expression levels of 5′-AMP-activated protein kinase (AMPK) and SIRT1. Our findings indicated that the anti-inflammation and anti-apoptosis effects of the combination therapy may be related to activation of AMPK/SIRT1 signaling pathway.

Keywords: metformin, atorvastatin, diabetic cardiomyopathy, inflammation, apoptosis, oxidative stress

INTRODUCTION

Clinical trials showed that the prevalence of myocardial dysfunction in diabetic patients varies from 19 to 26%, and the outcomes associated with myocardial dysfunction are remarkably worse in patients with diabetes than in those without diabetes (Jia et al., 2018). Diabetic cardiomyopathy (DCM) is a descriptive terminology used to define myocardial dysfunctions in the presence of diabetes mellitus (DM) and in the absence of coronary artery disease, valvular heart disease, and other conventional risks for cardiovascular diseases (e.g., hypertension, dyslipidemia, and alcoholism) (Bai et al., 2016). As the prevalence of DM continues to rise, the DCM increases in parallel. Several mechanisms contribute to the development and progression of DCM, including systemic inflammation, mitochondrial dysfunction, myocardial interstitial fibrosis, altered intracellular signaling, autophagy, defective intracellular calcium transport of calcium, enhanced oxidative stress, micro-RNA altercations, and cardiovascular and metabolic disorders (Fang et al., 2015).

At present, several strategies are used to prevent or treat DCM. With respect to the positive effects of exercise and diet control on diabetes, they are also beneficial to prevent DCM. Metformin, a commonly used drug to treat diabetes for over 50 years, is significant to alleviate DCM. The positive effects of metformin on DCM are mainly associated with activation of 5′-AMP-activated protein kinase (AMPK) (Min et al., 2018), thereby, improving cardiac energy metabolism, as well as protecting heart against diabetic conditions. Metformin also influences DCM through modulating cardiac autophagy (Xie et al., 2011) and inhibiting myocardial inflammation (Yang et al., 2019) and coronary microangiopathy (Abdel-Hamid and Firgany, 2018). Statins are effective, lipid-lowering drugs with a satisfactory safety profile that have become the first-line therapy for patients with dyslipidemia and a cornerstone of ischemic cardiovascular prevention. Statins are pleiotropic drugs, inhibiting the biosynthesis of cholesterol, and they possess anti-inflammation and anti-oxidative effects. In previous animal experiments, statins could prevent DCM by alleviating left ventricular dysfunction and inhibiting myocardial fibrosis through anti-apoptosis and anti-inflammation pathways (Abdel-Hamid and Firgany, 2015; Al-Rasheed et al., 2017). Although the above-mentioned outcomes proved significant effects of statins on preventing or treating DCM, it is noteworthy that DCM is triggered by multiple complicated, cross-talked mechanisms. Thus, a single therapeutic strategy may fail, or it only partially prevents or treats DCM; for instance, intensive glucose control in a clinic failed to protect against heart under diabetic conditions (Group, 1998).

In the current study, we presented a combined therapy, metformin plus atorvastatin, for diabetic mice, and we attempted to indicated whether the combined therapy could possess superior protective effects on DCM than administration of a single drug.

MATERIALS AND METHODS

Cell Culture and Interventions

Embryonic rat heart-derived H9C2 cells, purchased from the Shanghai Institute of Biochemistry and Cell Biology (Shanghai, China), were cultured in Dulbecco's modified Eagle's medium (DMEM; Gibco, Rockville, MD, USA), containing 100 U/ml of penicillin, 0.1 mg/ml of streptomycin, 25 mmol/L of D-glucose, and 10% fetal bovine serum (FBS; Gibco). Palmitate was used to treat H9C2 cells to mimic hyperlipidemia of type-2 diabetes. H9C2 cells were exposed palmitate (100 μM, Sigma-Aldrich, St. Louis, MO, USA) with or without metformin (1 mM, Sigma-Aldrich) and atorvastatin (10 μM, Sigma-Aldrich) in the form of single or combined treatment strategies. Palmitate solution was prepared as reported previously (Zhao et al., 2013). Briefly, palmitate was dissolved in 50% ethanol, heated at 70°C for 2 min, and added to 2% fatty acid-free bovine serum albumin (BSA; Sigma-Aldrich) medium as stock solution (2.5 mmol/L). Before use, the stock palmitate solution was gently rotated for 1 h at 37°C and further diluted to the required concentrations for treatment.

Cell Counting Kit-8 Assay

The Cell Counting Kit-8 (CCK-8) assay was performed to evaluate the viability of H9C2 cells. H9C2 cells (1×10^4 cells/well) were seeded into 96-well plates with 100 μl of DMEM and incubated for 24 h. Then, H9C2 cells were exposed to palmitate with or without metformin and atorvastatin for 48 h. After treatment, CCK-8 solution (10 μl/well) was added to the culture medium, and the cells were further incubated for 2 h. Finally, the absorbance value of medium was measured by a microplate enzyme-linked immunosorbent assay reader (Bio-Tek Instruments Inc., Winooski, VT, USA).

Animal Models

Here, 9–10-week-old male *db/db* mice were purchased from the Model Animal Research Center of Nanjing University (Nanjing, China) and maintained under a 12:12-h light–dark cycle. All the animal experiments were approved by the Animal Research Committee of Chengdu Medical College (Chengdu,

China). The mice were randomly assigned to four groups and exposed to the following interventions: vehicle group (DM group, $n = 8$), mice treated with sterilized water; metformin group (MT group, $n = 8$), mice treated with 200 mg/kg/day of metformin; atorvastatin group (AVS group, $n = 8$), mice treated with 10 mg/kg/day of atorvastatin; and atorvastatin/metformin combination group (MT + AVS group, $n = 8$), mice treated with combination of 200 mg/kg/day of metformin and 10 mg/kg/day of atorvastatin. Metformin hydrochloride tablets were purchased from Bristol-Myers Squibb (New York, NY, USA), and atorvastatin calcium was purchased from Pfizer (New York, NY, USA). Both drugs were dissolved in sterilized water and administrated by gastric gavage (orally) once per day for 3 months.

Sample Collection and Preparation

After the last treatment, the body weight of mice was measured, and then, mice were euthanized. Blood sample was collected and processed to separate plasma. Heart tissues of mice were excised and weighed. Samples from the heart were cut. Some sample tissues were fixed in 4% paraformaldehyde and then embedded into paraffin for histological and immunohistochemical assays. Other samples were kept at −80°C for Western blotting.

Biomedical Indicators

In order to assess changes in levels of glucose and lipid in *db/db* mice that received different treatments, the fasting blood glucose (FBG) level was measured using Accu-Chek Active Blood Glucose Test Strips (Roche, Indianapolis, IN, USA), and the levels of total cholesterol (TC) and triglyceride (TG) in plasma were detected according to the instructions presented by Nanjing Jiancheng Bioengineering Institute (Nanjing, China).

Immunohistochemistry and Immunofluorescence Staining

To evaluate the pathologic changes, the paraffin-embedded heart samples were sliced into 3- to 4-mm-thick slices for hematoxylin and eosin (H&E) staining (Sigma-Aldrich). To detect heart fibrosis, tissue sections were stained with Masson's trichrome staining method.

For immunohistochemistry (IHC), tissue sections were dewaxed, hydrated, and then incubated with 1× target retrieval solution (Dako, Carpinteria, CA, USA) for antigen retrieval, followed by 3% hydrogen peroxide and 5% BSA for 30 min. The sections were incubated overnight at 4°C with the following primary antibodies: p-P65 (dilution, 1:500; #ab76302, Abcam, Cambridge, MA, USA), NLRP3 (dilution, 1:500; #ab214185, Abcam), caspase-1 (dilution, 1:500; #ab138483, Abcam), and interleukin-1β (IL-1β) (dilution, 1:300; #sc-12742, Santa Cruz Biotechnology, Dallas, TX, USA). After incubation with the primary antibodies, sections were incubated with secondary antibodies (dilution, 1:500 dilutions) for 1 h at room temperature. Finally, sections were treated with peroxidase substrate DAB (3,3-diaminobenzidine; Vector Laboratories, Burlingame, CA, USA) and counterstained with hematoxylin.

Heart sections were stained using fluorescein isothiocyanate (FITC)-conjugated wheat germ agglutinin (WGA; Invitrogen Inc., Carlsbad, CA, USA) to measure the cross-sectional area of cardiomyocytes. Images were visualized by using a fluorescence microscope (BX63; Olympus, Tokyo, Japan).

Terminal Deoxynucleotidyl Transferase-Mediated dUTP Nick-End Labeling Assay

For apoptosis analysis of H9C2 cells exposed to palmitate, terminal deoxynucleotidyl transferase-mediated dUTP nick-end labeling (TUNEL) assay was performed with One Step TUNEL Apoptosis Assay Kit (Keygen Biotechnology Co. Ltd., Nanjing, China) according to the manufacturer's protocol. Images of TUNEL and DAPI-stained sections were obtained using a fluorescence microscope (BX63; Olympus, Tokyo, Japan). Only TUNEL- and DAPI-positive nuclei were counted as apoptotic nuclei.

Dihydroethidium Fluorescence Staining

Dihydroethidium (DHE) staining (Molecular Probes, Eugene, OR, USA) was carried out to detect the level of reactive oxygen species (ROS) levels in H9C2 cells and frozen heart sections according to the previous description (Dai et al., 2017). To evaluate the levels of ROS in H9C2 cells, H9C2 cells were seeded into 24-well plates and exposed to palmitate with or without metformin and atorvastatin for 48 h. Then, H9C2 cells were twice rinsed with phosphate-buffered saline (PBS) and incubated with 5 μmol/L of DHE for 15 min at 37°C. After that, the fluorescent images of H9C2 cells were captured by a fluorescence microscope (BX63; Olympus, Tokyo, Japan), and the fluorescence intensity was detected by a microplate reader (SpectraMax M3, Molecular Devices Inc., Sunnyvale, CA, USA) under specific wave length conditions (excitation's wavelength = 518 nm; fluorescence's wavelength = 605 nm). The levels of ROS in heart tissues were determined as follows: left ventricles were excised from mice and immediately embedded into optimal cutting temperature (OCT) compound; the tissues were cut into 10-μm-thick sections and then were incubated with DHE (5 μmol/L) in PBS in a dark and humidified container at 37°C for 15 min. Finally, the fluorescence images were observed under a fluorescence microscope.

Mitochondrial Membrane Potential Assay

The mitochondrial membrane potential (MMP) assay was performed using the JC-10 MMP assay kit according to the manufacturer's protocol. Briefly, H9C2 cells (5×10^4 cells/ml) seeded into a 96-well clear bottom black plate (Eppendorf Co., Ltd., Hamburg, Germany) were exposed to palmitate with or without metformin and atorvastatin for 48 h. Following the incubation, JC-10 dye-loading solution (JC-10 and assay buffer A 1:100 v/v) was added (50 μl/well) to H9C2 cells. The plate was kept under dark conditions for 30 min. Afterwards, assay buffer B (50 μl/well) was added, and the fluorescence intensity was measured at 490/525 nm (green) and 540/590 nm (red) by a microplate reader (SpectraMax M3, Molecular Devices, Sunnyvale, CA, USA). The ratio of red/green fluorescence intensity was used to determine the MMP. The decrease in the ratio indicates the depolarization of mitochondrial membrane.

To visualize the protective effects of metformin and atorvastatin on palmitate-mediated loss of MMP, the plate was analyzed under an inverted fluorescence microscope (Model 1X73, Olympus).

Western Blot Assay

Western blot assay was undertaken to detect the protein expression. Heart tissues and harvested cells were lysed in ice-cold radio-immunoprecipitation (RIPA) lysis buffer (Santa Cruz Biotechnology). The protein concentration was determined using a Bradford Protein Assay kit (Bio-Rad Laboratories Inc., Hercules, CA, USA). The total proteins (30 μg per well) were separated on 10% sodium dodecyl sulfate–polyacrylamide gel electrophoresis (SDS-PAGE) and then transferred onto polyvinylidene fluoride (PVDF) membranes (Millipore, Billerica, MA, USA). The membranes were blocked in Tris-buffered saline with 5% non-fat milk and 0.5% BSA for 1 h and then incubated with primary antibodies overnight at 4°C, followed by incubation with the secondary antibodies for 1 h at room temperature after standard washing procedures. The primary antibodies against different target proteins were as follows: TXNIP (dilution, 1:1,000; #14715, Cell Signaling Technology, Danvers, MA, USA), NLRP3 (dilution, 1:1,000; #13158, Cell Signaling Technology), cleaved caspase-3 (dilution, 1:1,000, #9664, Cell Signaling Technology), caspase-1 β-actin (dilution, 1:1,000; #ab138483, Abcam, Cambridge, MA), AMPK (dilution, 1:1,000; #9158, Cell Signaling Technology), p-AMPK (dilution, 1:1,000, #2535, Cell Signaling Technology), SIRT1 (dilution, 1:1,000; #8964, Abcam, Cambridge, MA), Toll-like receptor 4 (TLR4) (dilution, 1:1,000; #sc-2930172, Santa Cruz Biotechnology), Bcl-2 (dilution, 1:1,000; #sc-73822, Santa Cruz Biotechnology), Bax (dilution, 1:1,000; #sc-7480, Santa Cruz Biotechnology), nuclear factor kappa B (NF-κB)-p65 (dilution, 1:1,000; #sc-8008, Santa Cruz Biotechnology), p-NF-κB–p65 (dilution, 1:1,000; #ab76302, Abcam), and β-actin (dilution, 1:3000; Bioss Biotechnology, Beijing, China). All horseradish peroxidase (HRP)-conjugated secondary antibodies were purchased from Bioss Biotechnology (Beijing, China). Blots were visualized with chemiluminescent HRP substrate (Millipore) and quantified with Quantity 5.2 software System (Bio-Rad Laboratories Inc.).

Statistical Analysis

All data were presented as mean ± standard deviation (SD). Statistical analysis was performed using GraphPad Prism version 8.0 software (GraphPad Software Inc., San Jose, CA, USA) with one-way analysis of variance (ANOVA), followed by *post-hoc* multiple comparisons with the Scheffe test. $P < 0.05$ was considered statistically significant.

RESULTS

Combined Administration of Metformin and Atorvastatin Improved the Viability and Survival Ability of H9C2 Cells Exposed to Palmitate

To evaluate the protective effects of metformin and atorvastatin on H9C2 cells exposed to palmitate, we investigated the viability and apoptotic rates by CCK-8 assay and TUNEL staining assay, respectively. As illustrated in **Figure 1A**, CCK-8 assay showed that palmitate significantly decreased the viability of H9C2 cells, both metformin and atorvastatin treatment improved the viability of H9C2 cells exposed to palmitate, and combined treatment of metformin and atorvastatin showed more significant protective efforts.

Furthermore, the apoptotic rate of H9C2 cells exposed to palmitate was determined by TUNEL staining assay (**Figures 1B,C**). The results showed that palmitate significantly increased the apoptosis of H9C2 cells apoptosis; besides, combination of metformin and atorvastatin could inhibit palmitate induced-apoptosis of H9C2 cells; as a result, the combined use of metformin and atorvastatin significantly decreased the apoptotic rate of H9C2 compared with treatment with either one. Subsequently, we evaluated the effects of combined therapy with metformin and atorvastatin on the expression of cleaved caspase-3, an apoptotic marker protein, by Western blot assay (**Figure 1D**). Consistent with the results of TUNEL assay, palmitate significantly increased the expression level of cleaved caspase-3; either metformin or atorvastatin treatment slightly decreased the expression level of cleaved caspase-3; combination treatment with metformin and atorvastatin significantly reduced the expression level of cleaved caspase-3.

Combined Administration of Metformin and Atorvastatin Attenuated Oxidative Stress of H9C2 Cells Exposed to Palmitate

Oxidative stress is considered as an important factor during the evolution of DCM. To determine whether combined therapy with metformin and atorvastatin could protect H9C2 cells against oxidative stress caused by palmitate, we detected the levels of intracellular ROS levels and MMP by DHE staining and JC-10 MMP assays, respectively. Expectedly, the fluorescence intensity in palmitate group was significantly higher than that in control group (**Figure 2A**), indicating that palmitate elevated the level of intracellular oxidative stress. In addition, metformin and atorvastatin reduced the ROS level in H9C2 cells exposed to palmitate, especially combined treatment with metformin and atorvastatin showed more valuable anti-oxidative effects (**Figure 2A**).

Oxidative stress may cause loss of MMP; thus, we further investigated the MMP level by MMP assay using JC-10 staining. JC-10, a cationic dye, could remain inside the healthy mitochondria to form JC-10 aggregate, generating red fluorescence at 590 nm. In unhealthy mitochondria with decreased MMP level, JC-10 exists in cytoplasm as monomers form, generating green fluorescence at 520 nm. As shown in **Figure 2B**, H9C2 cells in control group exhibited high red and low green fluorescence intensities. However, H9C2 cells exposed to palmitate displayed high green fluorescence intensity and low red fluorescence intensity, while treatment with metformin or atorvastatin increased the red fluorescence intensity and reduced green fluorescence intensity. Quantitative analysis of fluorescence intensity showed that palmitate significantly

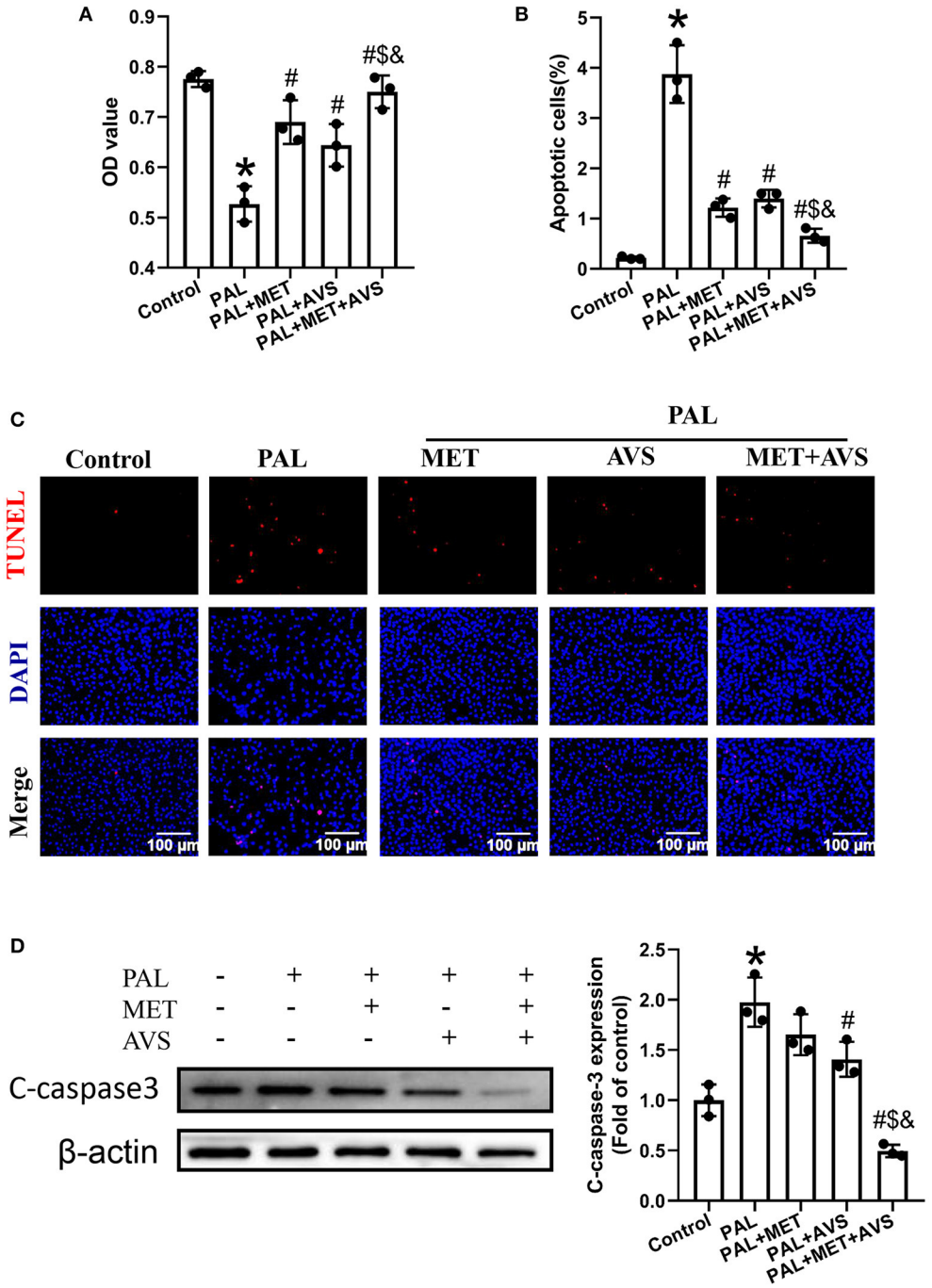

FIGURE 1 | Combination therapy with metformin and atorvastatin improved the viability and survival ability of H9C2 cells exposed to palmitate. H9C2 cells exposed to palmitate (100 μM) with or without metformin (1 mM) or atorvastatin (10 μM) in the form of single or combined administration. **(A)** The cell viability of H9C2 cells exposed to palmitate was determined by Cell Counting Kit-8 (CCK-8) assay. The apoptosis H9C2 exposed to palmitate was detected by terminal deoxynucleotidyl transferase-mediated dUTP nick-end labeling (TUNEL) assay. **(B)** The apoptotic rate was calculated by TUNEL-positive cells. **(C)** The representative pictures of TUNEL staining assay. **(D)** The expression level of cleaved caspase-3 was detected by Western blotting. Three independent experiments were performed for each study. Data were presented as the means ± standard deviation (SD). $^{*}P < 0.05$, vs. control group; $^{\#}P < 0.05$, vs. PAL group; $^{\$}P < 0.05$, vs. PAL + MET group; $^{\&}P < 0.05$, vs. PAL + AVS group. PAL, palmitate group; PAL + MET, metformin treatment group; PAL + AVS, atorvastatin treatment group; PAL + MET + AVS, combination treatment with metformin and atorvastatin group.

decreased the ratio of red/green fluorescence intensity of H9C2 cells, indicating that palmitate caused depolarization of MMP. Either metformin or atorvastatin treatment increased the ratio of red/green fluorescent intensity, and combination treatment with metformin and atorvastatin almost preserved the ratio of red/green fluorescent intensity as the control group (**Figure 2B**).

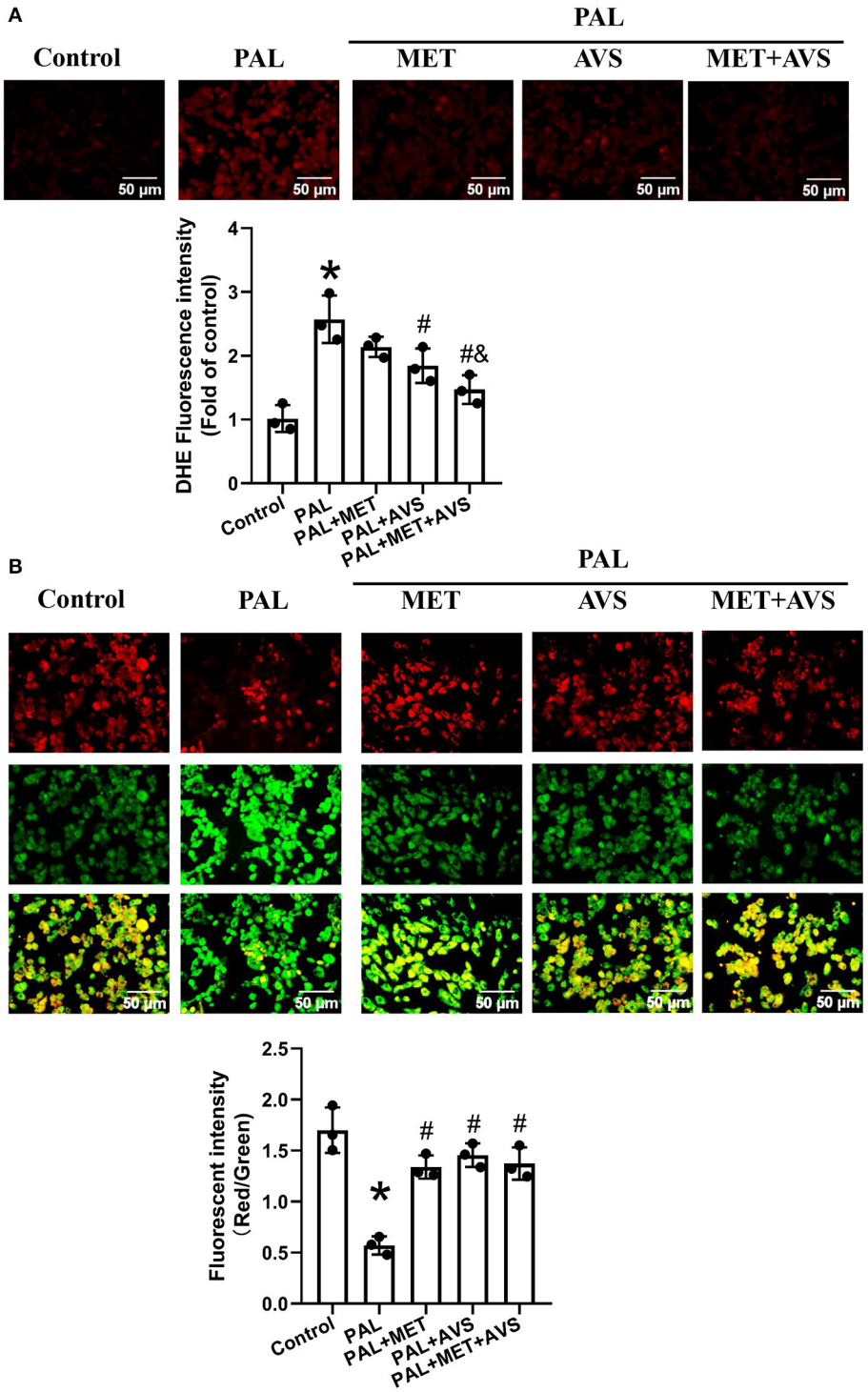

FIGURE 2 | Combined administration of metformin and atorvastatin attenuated oxidative stress of H9C2 cells exposed to palmitate. **(A)** The levels of reactive oxygen species (ROS) in H9C2 cells were detected with dihydroethidium (DHE) staining; the fluorescence images were captured, and the fluorescence intensity was calculated. **(B)** The mitochondrial membrane potential (MMP) of H9C2 cells was determined by JC-10 staining; the MMP was calculated by the ratio of red-to-green fluorescence intensity. Three independent experiments were performed for each study. Data were expressed as means ± standard deviation (SD). $^{*}P < 0.05$, vs. control group; $^{\#}P < 0.05$, vs. PAL group; $^{\$}P < 0.05$, vs. PAL + MET group; $^{\&}P < 0.05$, vs. PAL + AVS group.

Combined Administration of Metformin and Atorvastatin Inhibited NLRP3 Inflammasome in H9C2 Cells Exposed to Palmitate via Toll-Like Receptor 4/NF-κB Signaling Pathway

Hyperlipidemia- and hyperglycemia-induced chronic inflammation has been proposed to contribute to DCM. Especially, NLRP3 inflammasome, expressed abundantly in cardiomyocytes, may play a pivotal role in death of myocardial cell (Luo et al., 2017). The degree of inflammation can determine cell apoptosis by affecting the expression level of caspase-1 (Thawkar and Kaur, 2019). In order to indicate whether metformin and atorvastatin could inhibit NLRP3 inflammasome activation, the expression levels of NLRP3 and its downstream molecules (caspase-1 and IL-1β) were detected by Western

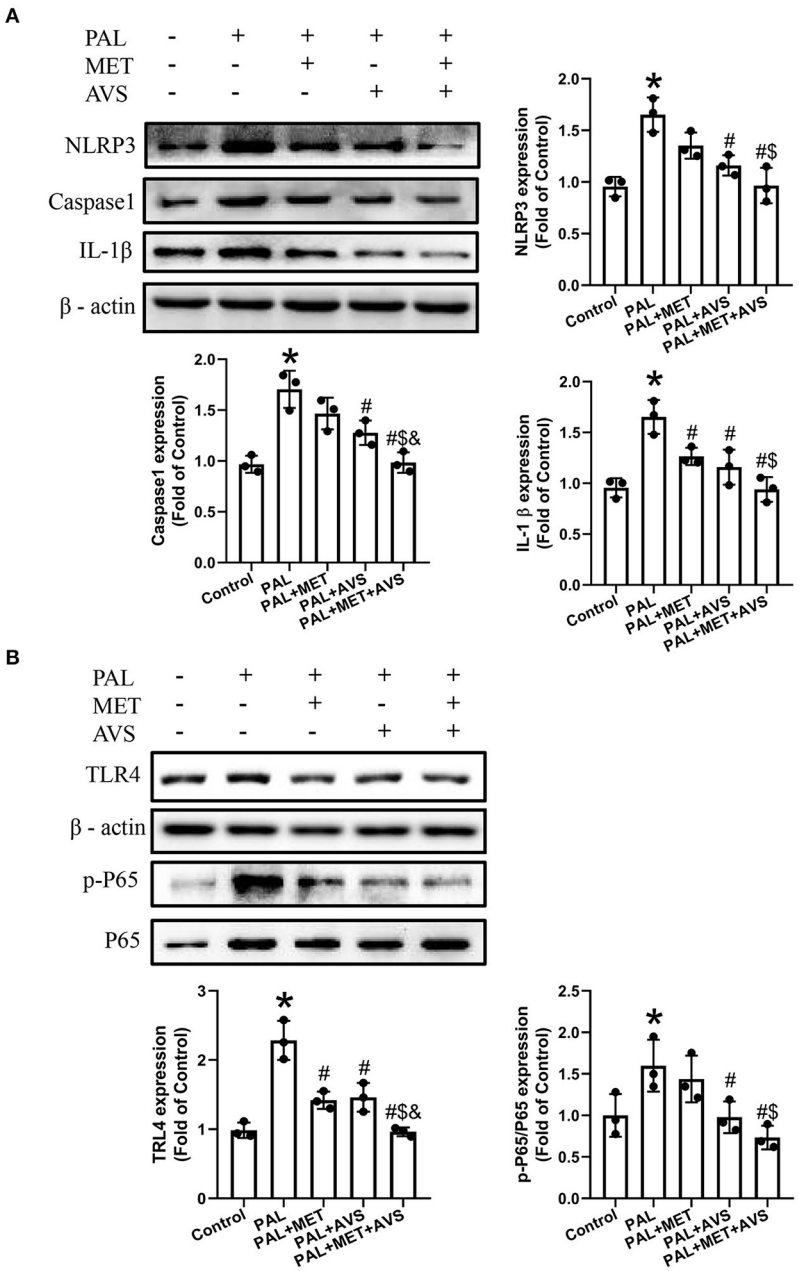

FIGURE 3 | Combined administration of metformin and atorvastatin inhibited NLRP3 inflammasome in H9C2 cells exposed to palmitate via Toll-like receptor 4/nuclear factor kappa B (TLR4/NF-κB) signaling pathway. **(A)** The expression levels of NLRP3 and its downstream molecules (caspase-1 and IL-1β) were detected by Western blot assay. **(B)** The expression levels of TLR4 and NF-κB were detected by Western blot assay. Three independent experiments were performed for each study. Data were presented as the mean ± standard deviation (SD). $^{*}P < 0.05$, vs. control group; $^{\#}P < 0.05$, vs. PAL group; $^{\$}P < 0.05$, vs. PAL + MET group; $^{\&}P < 0.05$, vs. PAL + AVS group.

blot assay. The results revealed that palmitate remarkably increased the expression levels of NLRP3, caspase-1, and IL-1β (**Figure 3A**). Besides, a combined therapy of metformin and atorvastatin treatment significantly inhibited the protein expression as induced by palmitate. Compared with metformin and atorvastatin alone treatment, the combination treatment showed more significant therapeutic effects.

TLR4/NF-κB signaling molecular pathway plays an important role in activation of NLRP3 inflammasome (Tan et al., 2019). To determine whether combined treatment with metformin

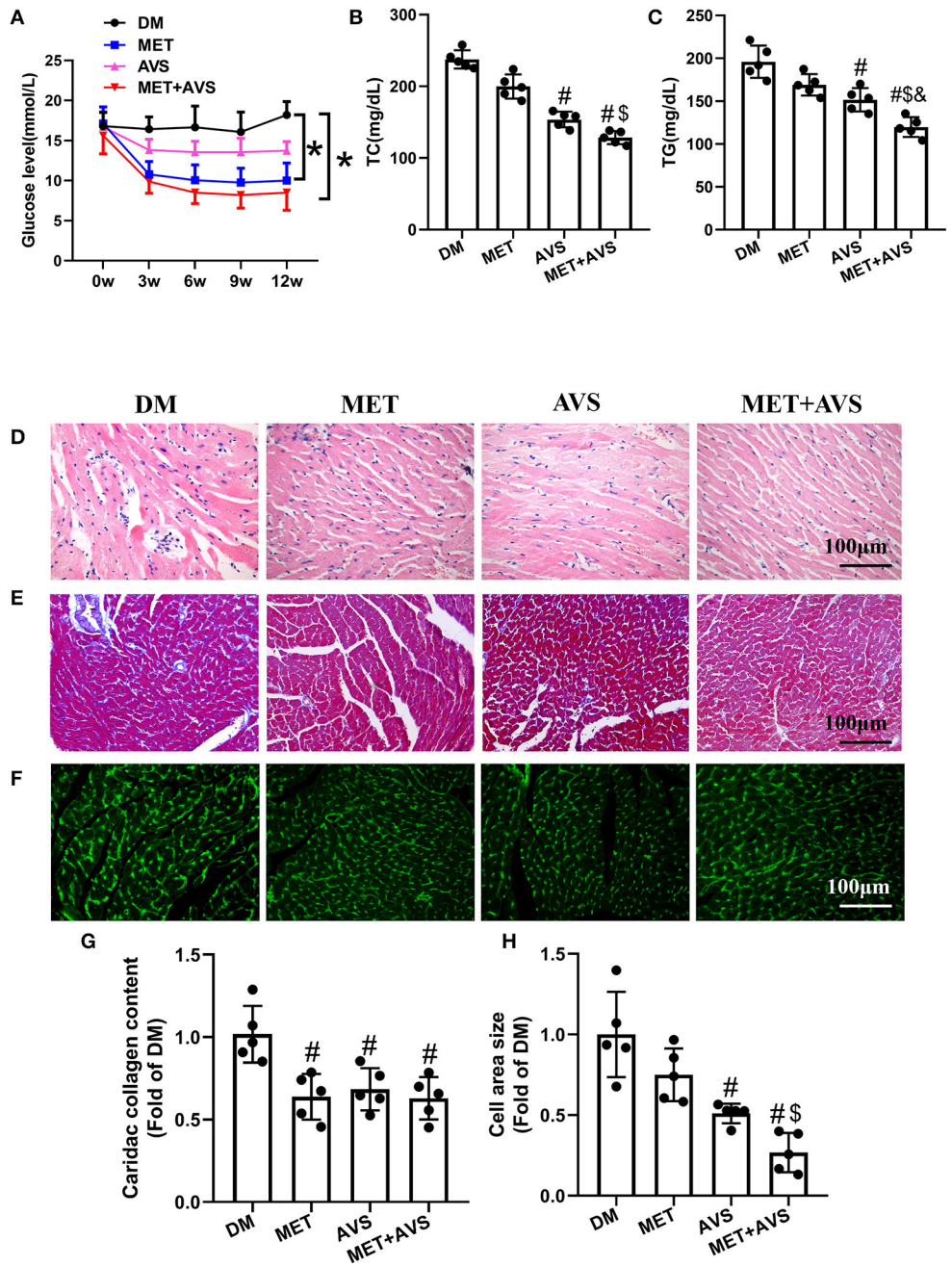

FIGURE 4 | Combined administration of metformin and atorvastatin inhibited cardiac remodeling in *db/db* mice. **(A)** The fasting blood glucose level in *db/db* mice. **(B)** The level of total cholesterol (TC) in plasma. **(C)** The level of triglyceride (TG) in plasma. **(D)** Hematoxylin and eosin (H&E) staining. **(E)** Masson's trichrome staining. **(F)** Heart sections were stained using fluorescein isothiocyanate (FITC)-conjugated wheat germ agglutinin (WGA). **(G)** The quantification of cardiac collagen content. **(H)** The quantification of cross-sectional area of cardiomyocytes. Data are shown as the mean ± standard deviation (SD), $n = 5$. $^{\#}P < 0.05$ vs. DM group; $^{\$}P < 0.05$ vs. MET group; $^{\&}P < 0.05$ vs. AVS group; DM: water treatment group, MET: metformin (200 mg/kg/day) treatment, AVS: atorvastatin group (10 mg/kg/day) treatment, MET + AVS: combination therapy group.

and atorvastatin treatment could inhibit NLRP3 inflammasome via TLR4/NF-κB signaling pathway, we further detected the expression level of TLR4 and NF-κB by Western blot assay. The results showed that the protein expression level of TLR4 and the phosphorylation level of NF-κB p65 were upregulated in H9C2 cells exposed to palmitate, while combined therapy with metformin and atorvastatin treatment remarkably inhibited the increase of the above-mentioned expression levels; consequently, the effects of combination treatment are more significant than either application of metformin or atorvastatin (**Figure 3B**).

Combined Administration of Metformin and Atorvastatin Inhibited Diabetes-Induced Histopathological Changes in *db/db* Mice

As displayed in **Figure 4A**, metformin single-treatment or combined therapy with atorvastatin and metformin significantly reduced FBG level after 3 weeks compared with the DM group, while the FBG level in atorvastatin group was slightly reduced without a significant difference compared with the DM group. Moreover, both metformin and atorvastatin treatment significantly reduced the levels of TC and TG, while the combined therapy showed more significant efforts than a single treatment (**Figures 4B,C**). These results indicated that combined treatment significantly improved the glucose and lipid metabolism.

Heart tissue sections of mice were stained to examine changes in the structure of heart in diabetic mice and to determine whether metformin and atorvastatin could influence the structures. H&E staining showed that the muscle structure has disorder in inflammatory cell infiltration (**Figure 4D**). Metformin combined with atorvastatin could effectively inhibit the morphological changes in heart muscle and decrease inflammatory cell infiltration. We further assessed the effects of

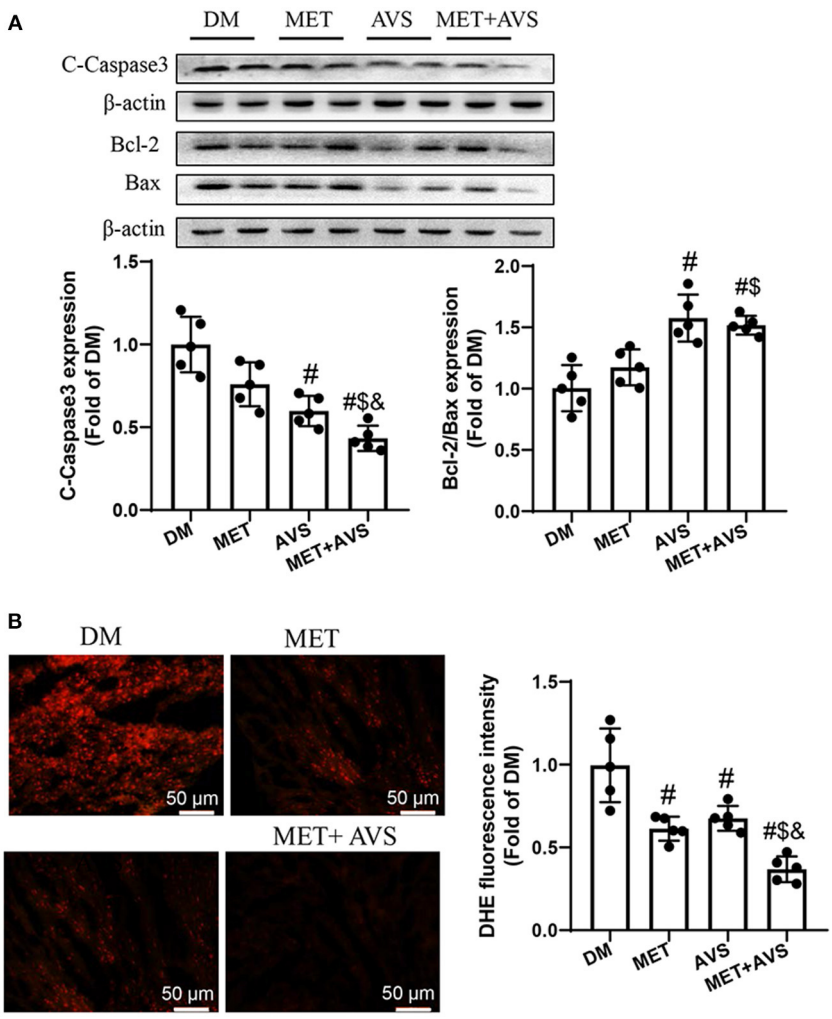

FIGURE 5 | Combined treatment with metformin and atorvastatin inhibited apoptosis of cardiomyocytes and oxidative stress in heart tissues of *db/db* mice. **(A)** The expression levels of cleaved caspase-3, Bcl-2, and Bax were detected by Western blotting. **(B)** Frozen sections of heart were used to evaluate superoxide production by dihydroethidium (DHE) staining. Data were expressed as the mean ± standard deviation (SD), $n = 5$. $^{\#}P < 0.05$ vs. DM group; $^{\$}P < 0.05$ vs. MET group; $^{\&}P < 0.05$ vs. AVS group.

metformin and atorvastatin on myocardial fibrosis by Masson's trichrome staining (**Figures 4E–G**). The results showed that there were more fibrosis fibers in DM group and that both metformin and atorvastatin could inhibit myocardial muscle fibrosis, while combined therapy with metformin and atorvastatin unveiled more significant effects. Moreover, staining of heart sections with FITC-conjugated WGA revealed that the cross-sectional area of cardiomyocytes is larger in DM group, and both metformin and atorvastatin treatment can decrease the cell size (**Figures 4F–H**).

Combined Treatment With Metformin and Atorvastatin Inhibited Apoptosis of Cardiomyocytes and Oxidative Stress in Heart Tissues of *db/db* Mice

The apoptosis of cardiomyocytes is an essential pathological process during the evolution of DCM. We detected the expression levels of apoptotic marker proteins (**Figure 5A**). The results similarly showed that the expression level of cleaved caspase-3 was higher, the ratio of Bcl-2/Bax was lower

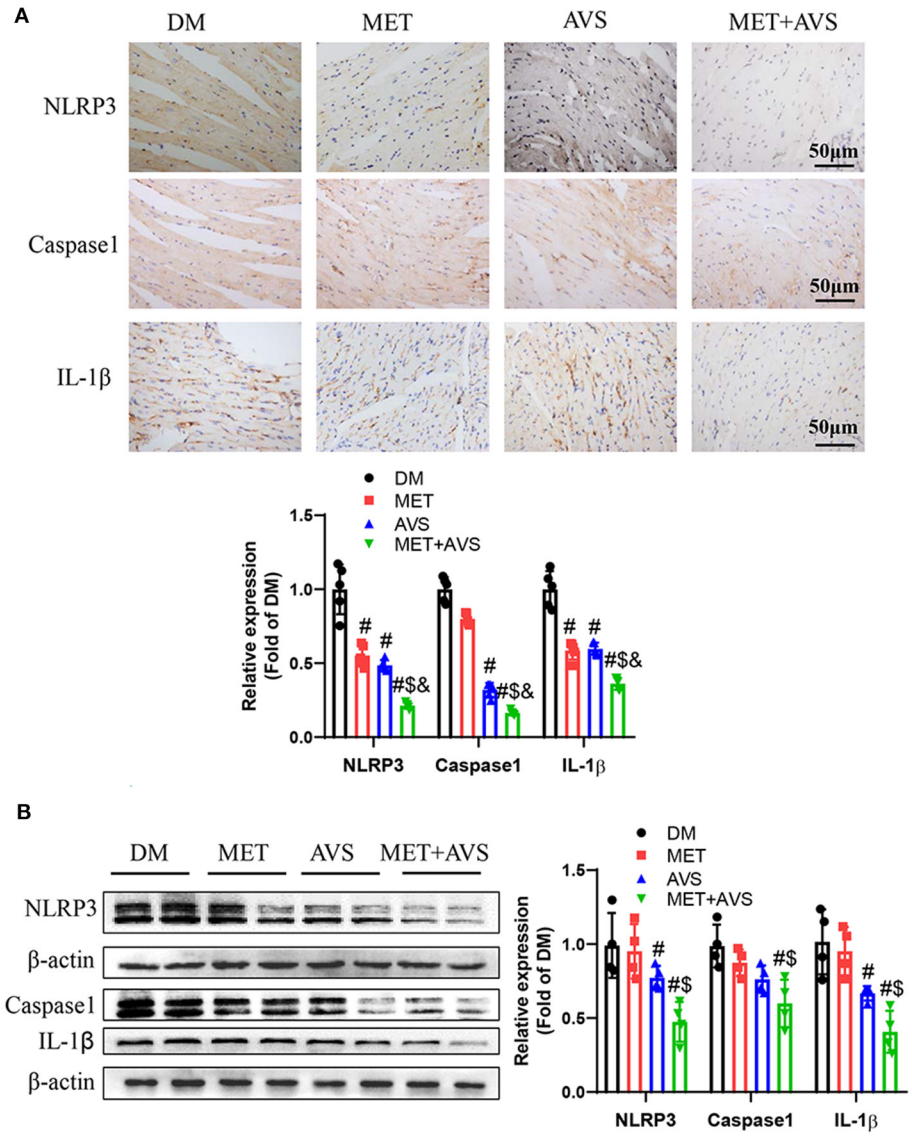

FIGURE 6 | Combined treatment with metformin and atorvastatin inhibited NLRP3 inflammasome in heart tissues from *db/db* mice. **(A)** The expression levels of NLRP3, caspase-1, and IL-1β were detected by immunochemistry staining. **(B)** The expression levels of NLRP3, caspase-1, and IL-1β were detected by Western blot assay. Data were presented as the mean ± standard deviation (SD), $n = 5$. $^{\#}P < 0.05$ vs. DM group; $^{\$}P < 0.05$ vs. MET group; $^{\&}P < 0.05$ vs. AVS group.

in DM group, both metformin and atorvastatin treatment can slightly decrease the expression level of cleaved caspase-3 and increase the ratio of Bcl-2/Bax, and combination treatment could markedly reduce the expression level of cleaved caspase-3 expression and increase the ratio of Bcl-2/Bax. These results demonstrated that combination treatment with metformin and atorvastatin inhibited diabetes-induced cell apoptosis.

We also detected the levels of ROS level in heart tissues stained with DHE staining (**Figure 5B**). The results indicated that the fluorescence intensity was high in DM group, both metformin and atorvastatin treatment decreased the fluorescence intensity, and combination treatment could more significantly decrease the fluorescence intensity. These findings suggested that combination treatment with metformin and atorvastatin could inhibit oxidative stress in heart tissues of diabetes mice.

Combined Treatment With Metformin and Atorvastatin Inhibited Activation of NLRP3 Inflammasome in Heart Tissues of *db/db* Mice

It was revealed that combination treatment with metformin and atorvastatin inhibited activation of NLRP3 inflammasome *in vitro* DCM model. To further confirm the anti-inflammation effects of combined therapy of metformin and atorvastatin,

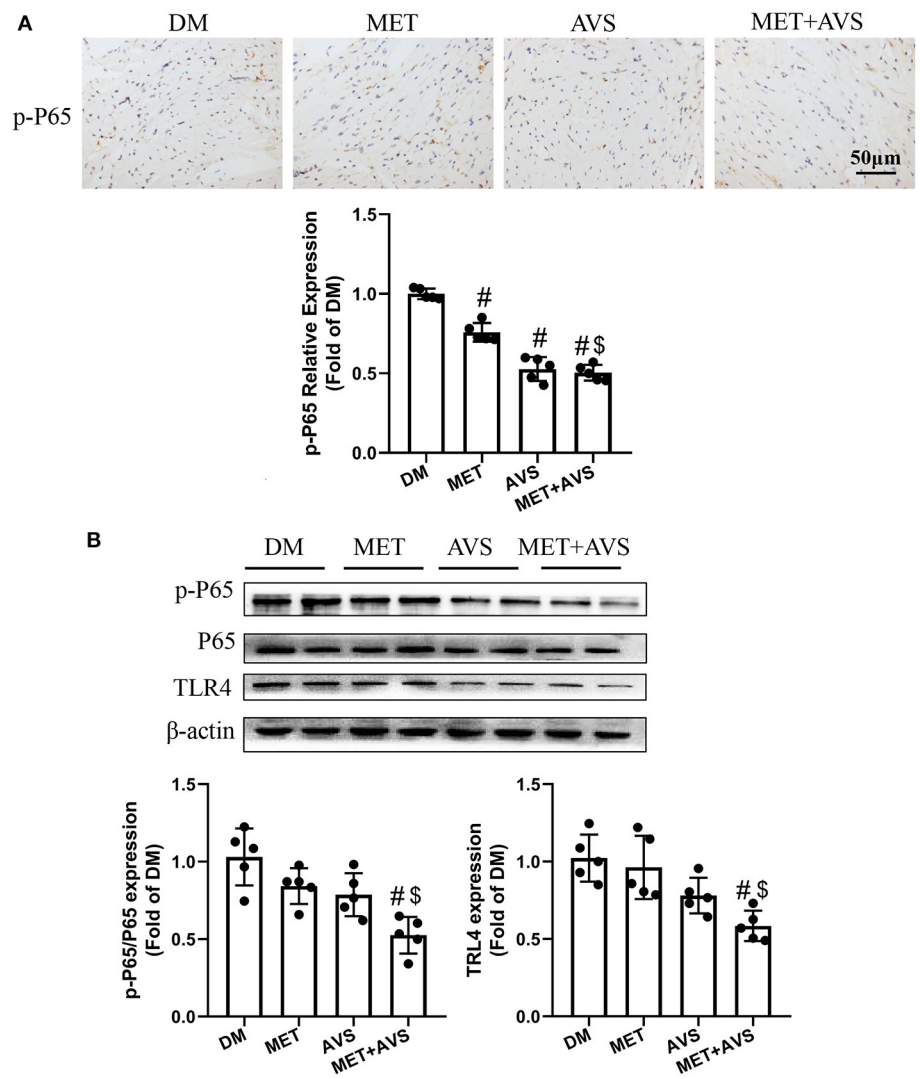

FIGURE 7 | Combined treatment with metformin and atorvastatin inhibited NLRP3 inflammasome in heart tissues via TLR4/NF-κB signaling pathway. **(A)** The phosphorylation level of P65 in heart tissues was detected by immunochemistry staining. **(B)** The expression levels of TLR4 and P65 were detected by Western blot assay. Data are expressed as the mean ± standard deviation (SD), $n = 5$. $^{\#}P < 0.05$ vs. DM group; $^{\$}P < 0.05$ vs. MET group; $^{\&}P < 0.05$ vs. AVS group.

we detected the expression of NLRP3 inflammasome pathway-related proteins by IHC and Western blot assay. As shown in **Figure 6**, both metformin and atorvastatin slightly decreased the expression of NLRP3, caspase-1, and IL-1β, while the combination therapy significantly decreased the expression levels of NLRP3, caspase-1, and IL-1β expression. These results indicated that the combination therapy could inhibit activation of NLRP3 inflammasome.

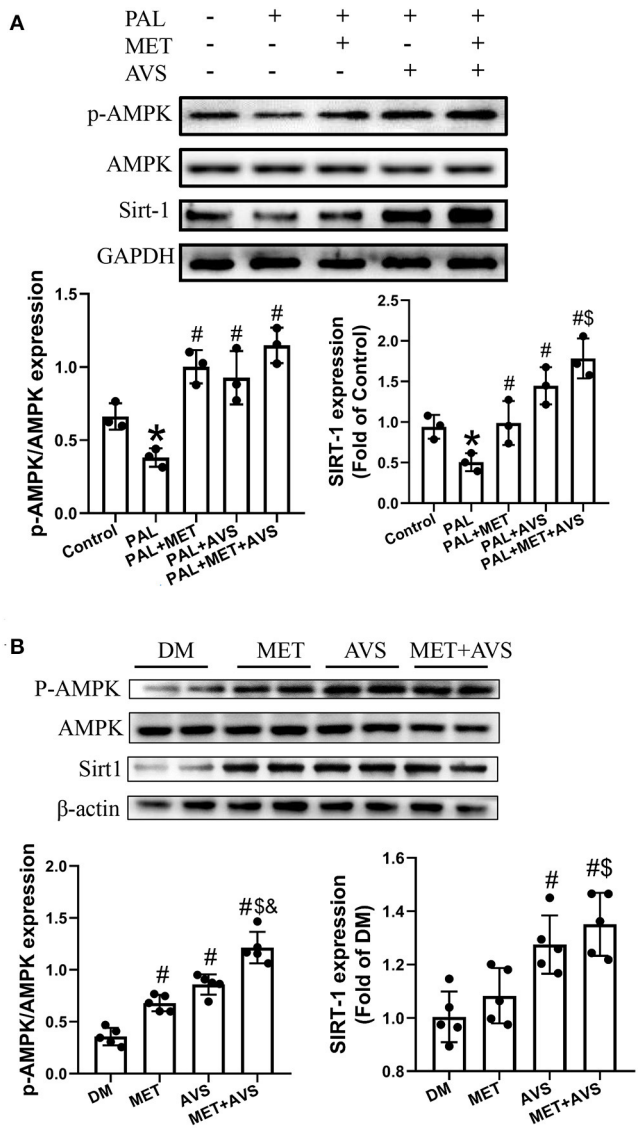

FIGURE 8 | Combined treatment with metformin and atorvastatin activated 5′-AMP-activated protein kinase (AMPK)/SIRT1 signaling pathway. The expression levels of AMPK and SIRT1 in H9C2 cells **(A)** and heart tissues **(B)** were detected by Western blot assay. Three independent experiments were performed for H9C2 cells treatment. In *db/db* mice treatment, $n = 5$ in each group. Data are presented as the mean ± standard deviation (SD). $^{*}P < 0.05$ vs. control group; $^{\#}P < 0.05$ vs. PAL group, or DM group; $^{\$}P < 0.05$ vs. PAL + MET group, or MET group; $^{\&}P < 0.05$ vs. PAL + AVS group, or MET + AVS group.

Furthermore, we identified the expression levels of TLR4 and NF-κB. As shown in **Figure 7A**, the combination therapy significantly reduced the phosphorylation level of P65 in heart tissues. The results of Western blot demonstrated that the expression level of p-P65 was remarkably inhibited by the combination therapy of metformin and atorvastatin (**Figure 7B**). Meanwhile, the expression level of TLR4 was markedly attenuated by the combination therapy.

Combined Treatment With Metformin and Atorvastatin Activated AMPK/SITR1 Signaling Pathway

AMPK and SIRT1 both regulate each other and share several common target molecules. In order to explore whether combination treatment, which improved diabetic cardiomyocytes function, was correlated with the activation of AMPK/SIRT1 signaling pathway, the phosphorylation of AMPK (p-AMPK) and the expression level of SIRT1 in the H9C2 and heart tissues were assessed by Western blot. The results revealed that palmitate significantly decreased the expression level of p-AMPK and SIRT1, while combination treatment inhibited the decreased the expression level of p-AMPK and SIRT1 induced by palmitate (**Figure 8A**). Similarly, the combination therapy elevated the expression levels of p-AMPK and SIRT1 in diabetic heart tissues (**Figure 8B**). The above-mentioned findings suggested that combination treatment with metformin and atorvastatin activated AMPK/SIRT1 signaling pathway.

DISCUSSION

In the present study, we found that the combined use of metformin and atorvastatin achieved superior protective effects on DCM than did single administration of metformin or atorvastatin. The molecular mechanisms contributed to anti-oxidation, anti-inflammation, and anti-apoptosis. The combined use of metformin and atorvastatin may synergistically activate AMPK signaling, which is a pivotal protein in maintaining cellular homeostasis, thereby activating AMPK activator as an effective method to prevent and treat DCM.

At the early stage, the heart only showed transcriptional and metabolic altercations, including enhanced inflammation, oxidative stress, depletion of antioxidant proteins, and changes in energy metabolism. As diabetes continued, the heart showed structural changes, such as myocyte hypertrophy, apoptosis, and collagen deposition in extracellular matrix (ECM), which eventually led to massive cell death, overt cardiac hypertrophy and dilation, remarkable cardiac fibrosis, and diastolic and systolic dysfunction. As cardiac pathology in the early stage appears to be reversible (Lin et al., 2011), we may reverse damages to DCM at the early stage. In the present study, compared with single administration of metformin or atorvastatin, its combined therapy showed superior positive effects on diabetes-induced inflammation and oxidative stress.

In type 2 DM (T2DM), hyperglycemia is also accompanied with hyperlipidemia. Metformin is a widely used drug in the treatment of diabetes, possessing beneficial effects on the

glucose and lipid metabolism. However, statins are a class of drugs that decrease plasma cholesterol levels and are prescribed as first choice to patients suffering from cardiovascular diseases. Previous researches have shown that low-dose (20 mg/day) atorvastatin therapy given to patients with myocardial infarction decreased insulin resistance. In the current study, the results showed that the levels of both glucose and lipid were significantly lower in combination treatment than in a single treatment. However, whether the protective effects of combination treatment are synergic remains elusive. Both metformin and statins have shown regulating glucose and lipid metabolism, whereas they could act on largely parallel pathways (van Stee et al., 2018). Previous studies demonstrated that the combination therapy with metformin and atorvastatin showed positive effects on cardiovascular hypertrophy, which are accompanied with glucose-lowering effects, lipid-lowering effects, and reduced oxidative stress (Matafome et al., 2011; Tousoulis et al., 2011; Kim et al., 2015).

Metformin exerts cardioprotective effects under diabetic conditions through multiple pathways, converging toward the activation of AMPK. A number of scholars pointed out that metformin could inhibit NLRP3 inflammasome by activating the AMPK/mTOR signaling pathway (Yang et al., 2019). SIRT1 is widely expressed in mammalian cells and has been studied in different tissues, including the liver, skeletal muscle, adipose tissue, etc. Its regulation is somewhat less clear than that of AMPK; however, a substantial body of evidence suggests that, similar to AMPK, SIRT1 responds to increases and decreases in nutrient availability. In the current study, we found that the combination therapy with metformin and atorvastatin could activate AMPK/SIRT1 signaling pathway.

Different to metformin, the use of statins in diabetes is a controversial. Although the potential detrimental effects of statin therapy on muscle and liver have been known for a long time, new concerns have emerged regarding the risk of new-onset diabetes (NOM) that often leads to discontinuation of statin discontinuation, non-adherence to therapy, or concerns correlating with initiating statin therapy. It is estimated that a 10–12% increased risk of NOM is be associated with statin therapy (Betteridge and Carmena, 2015). The mechanisms by which statins might lead to the development of NOM were not fully elucidated. The inhibition of 3-hydroxy-3-methylglutaryl coenzyme A reductase activity by statins appears to be a key mechanism (Hao et al., 2007; Han, 2018). However, statins consistently showed a protective role in the setting of DCM due to their roles of anti-inflammation, anti-oxidation, and anti-apoptosis effects (Luo et al., 2014; Carillion et al., 2017). It seems that statins may facilitate the onset of diabetes by impacting peripheral insulin sensitivity and islet β-cell function, while statins can effectively modify the promotive factors promoting DCM, including inflammation and oxidative stress, thereby protecting the heart against diabetic conditions. A recent review suggested that the benefits of statin therapy for diabetes far outweigh any real or perceived risks (Adhyaru and Jacobson, 2018), suggesting that discontinuation of statins for diabetic patients is not recommended.

In conclusion, both metformin and atorvastatin can protect DCM via their anti-inflammation and anti-apoptosis activities, and the combined administration of metformin and atorvastatin resulted in superior protective effects on DCM than a single treatment. We also found that the anti-inflammation and anti-apoptosis effects of combined therapy may be related to activation AMPK/SIRT1 signaling pathway.

DATA AVAILABILITY STATEMENT

The raw data supporting the conclusions of this article will be made available by the authors, without undue reservation.

ETHICS STATEMENT

The animal study was reviewed and approved by Animal Research Committee of Chengdu Medical College.

AUTHOR CONTRIBUTIONS

XD was responsible for project administration and funding acquisition. TB was responsible for project administration and writing of the original draft. QZ, JZ, ZN, and DF performed the experiments and drafted the manuscript. QZ revised the draft and supplied additional materials. XX, ML, and PW collected and analyzed data. All authors read and approved the final manuscript.

FUNDING

This study was supported by the National Natural Science Foundation of China (81770305 and 81900326), Foundation for Distinguished Young Scholars of Sichuan Province (2019JDJQ0042), Sichuan Science and Technology Innovation Miaozi Project (2018071), Innovative Team Project of Chengdu Medical College (CYTD17-01), Fund of Development and Regeneration Key Laboratory of Sichuan Province (SYS18-04), State Undergraduate Innovative Experiment Program (Nos. 201813705007 and 201813705008), Scientific Research Fund of Sichuan Provincial Education Department (18ZA0144), and Key Research and Development Support Plan of Chengdu (2019-yf05-00275-SN).

REFERENCES

Abdel-Hamid, A., and Firgany, A. (2018). Favorable outcomes of metformin on coronary microvasculature in experimental diabetic cardiomyopathy. *J. Mol. Histol.* 49, 639–649. doi: 10.1007/s10735-018-9801-4

Abdel-Hamid, A. A. M., and Firgany, E. D. L. (2015). Atorvastatin alleviates experimental diabetic cardiomyopathy by suppressing apoptosis and oxidative stress. *J. Mol. Histol.* 46, 337–345. doi: 10.1007/s10735-015-9625-4

Adhyaru, B. B., and Jacobson, T. A. (2018). Safety and efficacy of statin therapy. *Nat. Rev. Cardiol.* 15, 757–769. doi: 10.1038/s41569-018-0098-5

Al-Rasheed, N. M., Al-Rasheed, N. M., Hasan, I. H., Al-Amin, M. A., Al-Ajmi, H. N., Mohamad, R. A., et al. (2017). Simvastatin ameliorates diabetic cardiomyopathy by attenuating oxidative stress and inflammation in rats. *Oxid. Med. Cell. Longev*. 2017:1092015. doi: 10.1155/2017/1092015

Bai, T., Wang, F., Mellen, N., Zheng, Y., and Cai, L. (2016). Diabetic cardiomyopathy: role of the E3 ubiquitin ligase. *Ajp Endocrinol. Metabol.* 310:E473. doi: 10.1152/ajpendo.00467.2015

Betteridge, D. J., and Carmena, R. (2015). The diabetogenic action of statins — mechanisms and clinical implications. *Nat. Rev. Endocrinol*. 12, 99–110. doi: 10.1038/nrendo.2015.194

Carillion, A., Feldman, S., Na, N., Biais, M., Carpentier, W., Birenbaum, A., et al. (2017). Atorvastatin reduces β-Adrenergic dysfunction in rats with diabetic cardiomyopathy. *PLoS ONE* 12:E0180103. doi: 10.1371/journal.pone.0180103

Dai, X., Yan, X., Zeng, J., Chen, J., Wang, Y., Chen, J., et al. (2017). Elevating CXCR7 improves angiogenic function of EPCs via Akt/GSK-3beta/Fyn-mediated Nrf2 activation in diabetic limb ischemia. *Circ. Res*. 120, e7–e23. doi: 10.1161/CIRCRESAHA.117.310619

Fang, Z. Y., Prins, J. B., and Marwick, T. H. (2015). Diabetic cardiomyopathy: evidence, mechanisms, and therapeutic implications. *Endocr. Rev*. 25, 543–567. doi: 10.1210/er.2003-0012

Group, U. P. D. S. (1998). Intensive blood-glucose control with sulphonylureas or insulin compared with conventional treatment and risk of complications in patients with type 2 diabetes (UKPDS33). *Lancet* 352, 837–853. doi: 10.1016/S0140-6736(98)07019-6

Han, K. H. (2018). Functional implications of HMG-CoA reductase inhibition on glucose metabolism. *Korean Circ. J*. 48, 951–963. doi: 10.4070/kcj.2018.0307

Hao, M., Head, W. S., Gunawardana, S. C., Hasty, A. H., and Piston, D. W. (2007). Direct effect of cholesterol on insulin secretion: a novel mechanism for pancreatic beta-cell dysfunction. *Diabetes* 56, 2328–2338. doi: 10.2337/db07-0056

Jia, G., Hill, M. A., and Sowers, J. R. (2018). Diabetic cardiomyopathy: an update of mechanisms contributing to this clinical entity. *Circ. Res*. 122, 624–638. doi: 10.1161/CIRCRESAHA.117.311586

Kim, B. H., Han, S., Lee, H., Park, C. H., Chung, Y. M., Shin, K., et al. (2015). Metformin enhances the anti-adipogenic effects of atorvastatin via modulation of STAT3 and TGF-beta/Smad3 signaling. *Biochem. Biophys. Res. Commun*. 456, 173–178. doi: 10.1016/j.bbrc.2014.11.054

Lin, C. H., Kurup, S., Herrero, P., Schechtman, K. B., Eagon, J. C., Klein, S., et al. (2011). Myocardial oxygen consumption change predicts left ventricular relaxation improvement in obese humans after weight loss. *Obesity* 19, 1804–1812. doi: 10.1038/oby.2011.186

Luo, B., Li, B., Wang, W., Liu, X., Liu, X., Xia, Y., et al. (2014). Rosuvastatin alleviates diabetic cardiomyopathy by inhibiting NLRP3 inflammasome and MAPK pathways in a type 2 diabetes rat model. *Cardiovasc. Drugs Ther*. 28, 33–43. doi: 10.1007/s10557-013-6498-1

Luo, F., Guo, Y., Ruan, G. Y., Long, J. K., Zheng, X. L., Xia, Q., et al. (2017). Combined use of metformin and atorvastatin attenuates atherosclerosis in rabbits fed a high-cholesterol diet. *Sci. Rep*. 7:2169. doi: 10.1038/s41598-017-02080-w

Matafome, P., Louro, T., Rodrigues, L., Crisostomo, J., Nunes, E., Amaral, C., et al. (2011). Metformin and atorvastatin combination further protect the liver in type 2 diabetes with hyperlipidaemia. *Diabetes Metab. Res. Rev*. 27, 54–62. doi: 10.1002/dmrr.1157

Min, L., Xiaoying, L., Huijie, Z., and Yan, L. (2018). Molecular mechanisms of metformin for diabetes and cancer treatment. *Front. Physiol*. 9:1039. doi: 10.3389/fphys.2018.01039

Tan, J., Wan, L., Chen, X., Li, X., Hao, X., Li, X., et al. (2019). Conjugated linoleic acid ameliorates high fructose-induced hyperuricemia and renal inflammation in rats via NLRP3 inflammasome and TLR4 signaling pathway. *Mol. Nutr. Food Res.* 63:e1801402. doi: 10.1002/mnfr.201801402

Thawkar, B. S., and Kaur, G. (2019). Inhibitors of NF-kappaB and P2X7/NLRP3/Caspase 1 pathway in microglia: novel therapeutic opportunities in neuroinflammation induced early-stage Alzheimer's disease. *J. Neuroimmunol*. 326, 62–74. doi: 10.1016/j.jneuroim.2018.11.010

Tousoulis, D., Koniari, K., Antoniades, C., Papageorgiou, N., Miliou, A., Noutsou, M., et al. (2011). Combined effects of atorvastatin and metformin on glucose-induced variations of inflammatory process in patients with diabetes mellitus. *Int. J. Cardiol*. 149, 46–49. doi: 10.1016/j.ijcard.2009.11.038

van Stee, M. F., de Graaf, A. A., and Groen, A. K. (2018). Actions of metformin and statins on lipid and glucose metabolism and possible benefit of combination therapy. *Cardiovasc. Diabetol*. 17:94. doi: 10.1186/s12933-018-0738-4

Xie, Z., He, C., and Zou, M. H. (2011). AMP-activated protein kinase modulates cardiac autophagy in diabetic cardiomyopathy. *Autophagy* 7, 1254–1255. doi: 10.4161/auto.7.10.16740

Yang, F., Qin, Y., Wang, Y., Meng, S., Xian, H., Che, H., et al. (2019). Metformin inhibits the NLRP3 inflammasome via AMPK/mTOR-dependent effects in diabetic cardiomyopathy. *Int. J. Biol. Sci.* 15, 1010–1019. doi: 10.7150/ijbs.29680

Zhao, Y., Tan, Y., Xi, S., Li, Y., Li, C., Cui, J., et al. (2013). A novel mechanism by which SDF-1beta protects cardiac cells from palmitate-induced endoplasmic reticulum stress and apoptosis via CXCR7 and AMPK/p38 MAPK-mediated interleukin-6 generation. *Diabetes* 62, 2545–2558. doi: 10.2337/db12-1233

Conflict of Interest: The authors declare that the research was conducted in the absence of any commercial or financial relationships that could be construed as a potential conflict of interest.

frontiers in Cell and Developmental Biology

REVIEW
published: 18 February 2021
doi: 10.3389/fcell.2021.626047

Metabolic Reprogramming of Vascular Endothelial Cells: Basic Research and Clinical Applications

Hanlin Peng[1†], Xiuli Wang[1†], Junbao Du[1,2], Qinghua Cui[2,3], Yaqian Huang[1] and Hongfang Jin[1*]*

[1] Department of Pediatrics, Peking University First Hospital, Beijing, China, [2] Key Laboratory of Molecular Cardiovascular Sciences, Ministry of Education, Beijing, China, [3] Department of Biomedical Informatics, Centre for Non-coding RNA Medicine, School of Basic Medical Sciences, Peking University, Beijing, China

OPEN ACCESS

Edited by:
Xiaoqiang Tang,
Sichuan University, China

Reviewed by:
Ding Ai,
Tianjin Medical University, China
Hou-Zao Chen,
Chinese Academy of Medical Sciences and Peking Union Medical College, China

***Correspondence:**
Yaqian Huang
yaqianhuang@126.com
Hongfang Jin
jinhongfang@bjmu.edu.cn;
jinhongfang51@126.com

[†] These authors have contributed equally to this work

Specialty section:
This article was submitted to Cellular Biochemistry, a section of the journal Frontiers in Cell and Developmental Biology

Received: 04 November 2020
Accepted: 26 January 2021
Published: 18 February 2021

Citation:
Peng H, Wang X, Du J, Cui Q, Huang Y and Jin H (2021) Metabolic Reprogramming of Vascular Endothelial Cells: Basic Research and Clinical Applications. Front. Cell Dev. Biol. 9:626047. doi: 10.3389/fcell.2021.626047

Vascular endothelial cells (VECs) build a barrier separating the blood from the vascular wall. The vascular endothelium is the largest endocrine organ, and is well-known for its crucial role in the regulation of vascular function. The initial response to endothelial cell injury can lead to the activation of VECs. However, excessive activation leads to metabolic pathway disruption, VEC dysfunction, and angiogenesis. The pathways related to VEC metabolic reprogramming recently have been considered as key modulators of VEC function in processes such as angiogenesis, inflammation, and barrier maintenance. In this review, we focus on the changes of VEC metabolism under physiological and pathophysiological conditions.

Keywords: energy metabolism, metabolic reprogramming, endothelial cell dysfunction, glycolysis, mitochondrial oxidation

Vascular endothelium has a variety of physiological functions, for instance, serving as a barrier between blood and tissues and acting as an endocrine organ in the body (Krüger-Genge et al., 2019). Indeed, vascular endothelial cells (VECs) can synthesize and release various endothelial-derived vasoactive factors to regulate blood flow, coagulation, and fibrinolytic balance. VEC activation is defined as stimulus-induced quantitative changes in the expression of specific genes (Pober, 1988), and excessive activation causes endothelial cell dysfunction or unnecessary angiogenesis. VEC activation and dysfunction are characteristics of atherosclerosis, diabetes, obesity, and aging (Theodorou and Boon, 2018). And in the development of atherosclerosis, VEC activation and dysfunction in vulnerable areas of arterial vessels are among the earliest changes that can be detected (Davignon and Ganz, 2004). Moreover, tumor neovascularization is characterized by a highly disordered vascular network and the generation of new blood vessels. Despite in-depth studies of cellular metabolism, the metabolic properties of VECs have only recently been a focus of research (Eelen et al., 2018). It is found that changes in VEC metabolism lead to endothelial cell dysfunction and are closely related with the pathogenesis of many diseases such as atherosclerosis, diabetic angiopathy, pulmonary hypertension, etc. (Pober et al., 2009). Based on these findings, VEC metabolism is becoming a new therapeutic target for various diseases. Nevertheless, the relationship between VEC metabolism and the pathogenesis of vascular dysfunction and remodeling remains incompletely understood. Overall, in this review, we briefly summarize the current understanding of the metabolic changes in dysfunctional VECs, provide a detailed overview of the metabolic pathways activated under normal and pathological conditions, in order to identify potential therapeutic targets on the VEC metabolic reprogramming.

VEC METABOLISM UNDER NORMAL PHYSIOLOGICAL CONDITION

Theoretically, since VECs are exposed to oxygen from the bloodstream, they are expected to produce adenosine triphosphate (ATP) through oxidative phosphorylation (OXPHOS) for energy-yielding. Nevertheless, due to the relatively low mitochondrial content of VECs, energy production is still mainly dependent of glycolysis which yields more than 85% of ATP under normal physiological condition (De Bock et al., 2013b). Conversely, glucose-derived pyruvate enters the mitochondria to participate in the metabolism of glucose via the tricarboxylic acid cycle (TCA), resulting in the production of ATP, which is less than 1% (De Bock et al., 2013b). Although the glycolysis-derived ATP by per mole glucose is low, ATP generated from glycolysis in a short time period is more quickly than that from OXPHOS in the presence of an unrestricted amount of glucose (Eelen et al., 2015), because VECs have a higher glycolytic rate than many other healthy cell types (De Bock et al., 2013b). VEC aerobic glycolysis also has the following advantages over other processes: (1) a reduction of reactive oxygen species (ROS) produced by OXPHOS; (2) the ability to maximize oxygen transfer to cells surrounding the blood vessel; (3) the ability to adapt to hypoxic environments, and (4) the production of lactate, which can promote angiogenesis (Eelen et al., 2015).

Another advantage of glycolysis is the possible shunt of glucose to side branches, including the hexosamine biosynthesis pathway (HBP), pentose phosphate pathway (PPP), and polyol pathway (PP) for biomacromolecule synthesis. Of all the glucose utilized by VECs, only 1–3% enters the PPP under physiological condition (De Bock et al., 2013a). The PPP leads to the generation of nicotinamide adenine dinucleotide phosphate (NADPH) and ribose-5-phosphate (R5P). NADPH can convert oxidized glutathione (GSSG) to glutathione (GSH) and maintain the internal redox balance. And R5P can be used to synthesize nucleotides (De Bock et al., 2013a). On the other hand, although the role of the HBP in VECs *in vivo* is not clear, *N*-acetylglucosamine produced by this pathway is an essential substance for *N*-glycosylation and *O*-glycosylation and may be the key to the glycosylation of angiogenic proteins (Luo et al., 2008). Finally, when the amount of glucose exceeds the capacity of glycolysis, glucose enters the PP, where glucose is catalyzed to sorbitol by aldose reductase (AR), and later is converted to fructose. Since AR requires NADPH to provide reducing power, PP activation consumes NADPH, thus leading to the accumulation of ROS (De Bock et al., 2013a).

In addition to glucose, fatty acids (FAs) are another energy source for VECs. FAs can be converted into acetyl-CoA, and the latter can be used to generate reducing power and produce ATP in the mitochondria. However, the VEC mitochondria serve as a signaling switching station such as mitochondrial calcium signaling, ROS generation from electron transport chain and NO production catalyzed by eNOS, rather than power factories (Davidson, 2010; Groschner et al., 2012). Therefore, fatty acid oxidation (FAO) occurring in the mitochondria may not contribute substantially to total ATP production in VECs. Though mitochondrial is not that important for providing energy, the disturbed mitochondrial dynamics contributes to VEC dysfunction and the development of vascular diseases (Tang et al., 2014). Kalucka et al. found that FAO in the silence ECs is important for maintaining redox homeostasis and EC functions (Kalucka et al., 2018), while FAO in proliferative ECs is also indispensable for *de novo* dNTP synthesis (Schoors et al., 2015).

To date, the metabolism of amino acid in VECs is not well studied except for arginine and glutamine metabolism. Nitric oxide (NO), a crucial modulator of VEC function, is generated from arginine by endothelial nitric oxide synthase (eNOS) (Tousoulis et al., 2012). Interestingly, the conversion of glutamine into glucosamine inhibits the activity of the oxidative PPP (oxPPP), thereby leading to the reduction of NADPH (an important cofactor for eNOS) and inhibiting the production of endothelial NO (Wu et al., 2001). Moreover, glutamine-derived glutamate can be the substrate to be used in the other non-essential amino acids production. It also acts as a supplementary carbon source in the TCA cycle for ATP production after further metabolized into α-ketoglutarate (Kim B. et al., 2017).

In summary, the main energy sources of VECs is derived from glucose glycolysis, whereas FAO and glutamine oxidation are generally thought to supplement the TCA cycle via OXPHOS (**Figure 1**). When the rate of glycolysis decreases, the energy provided by the oxidative metabolism of glucose, FAs, and amino acids might alternatively increase for supporting the VEC activity (Krutzfeldt et al., 1990).

METABOLIC REPROGRAMMING IN DYSFUNCTIONAL VECS

Many factors can activate VECs, such as lipopolysaccharide (LPS), interleukin 1 (IL-1) and tumor necrosis factor (TNF-α) (Magnuson et al., 1989). After activation, VEC metabolism is disordered, represented by the increased glycolysis, and increased expression level and activity of fatty acid synthase (FAS) (Pan et al., 2009; De Bock et al., 2013b; Feng et al., 2017; Singh et al., 2017; Li et al., 2019b). These enhance the proliferation, migration and inflammation of VECs, leading to VEC dysfunction and vascular diseases. In the next paragraphs, we will review in detail the metabolic changes and VEC dysfunction.

Metabolic Reprogramming and VEC Migration

VECs migrate to an anoxic microenvironment in the tumor angiogenesis development. The energy supporting the above process is mainly derived from VEC anaerobic metabolism. Therefore, the migrated VECs are highly dependent of glycolysis compared with silence VECs. In VECs, glycolysis normally occurs in the perinuclear cytoplasm; however, once these cells begin to migrate, glycolysis also takes place in lamellipodia and filopodia to promote the rapid production of ATP needed for migration (De Bock et al., 2013b). Glucose-6-phosphate dehydrogenase (G6PD) is the rate-limiting enzyme of PPP, and the overexpression of G6PD will stimulate VEC migration due to the increase in NO and NADPH production (Pan et al.,

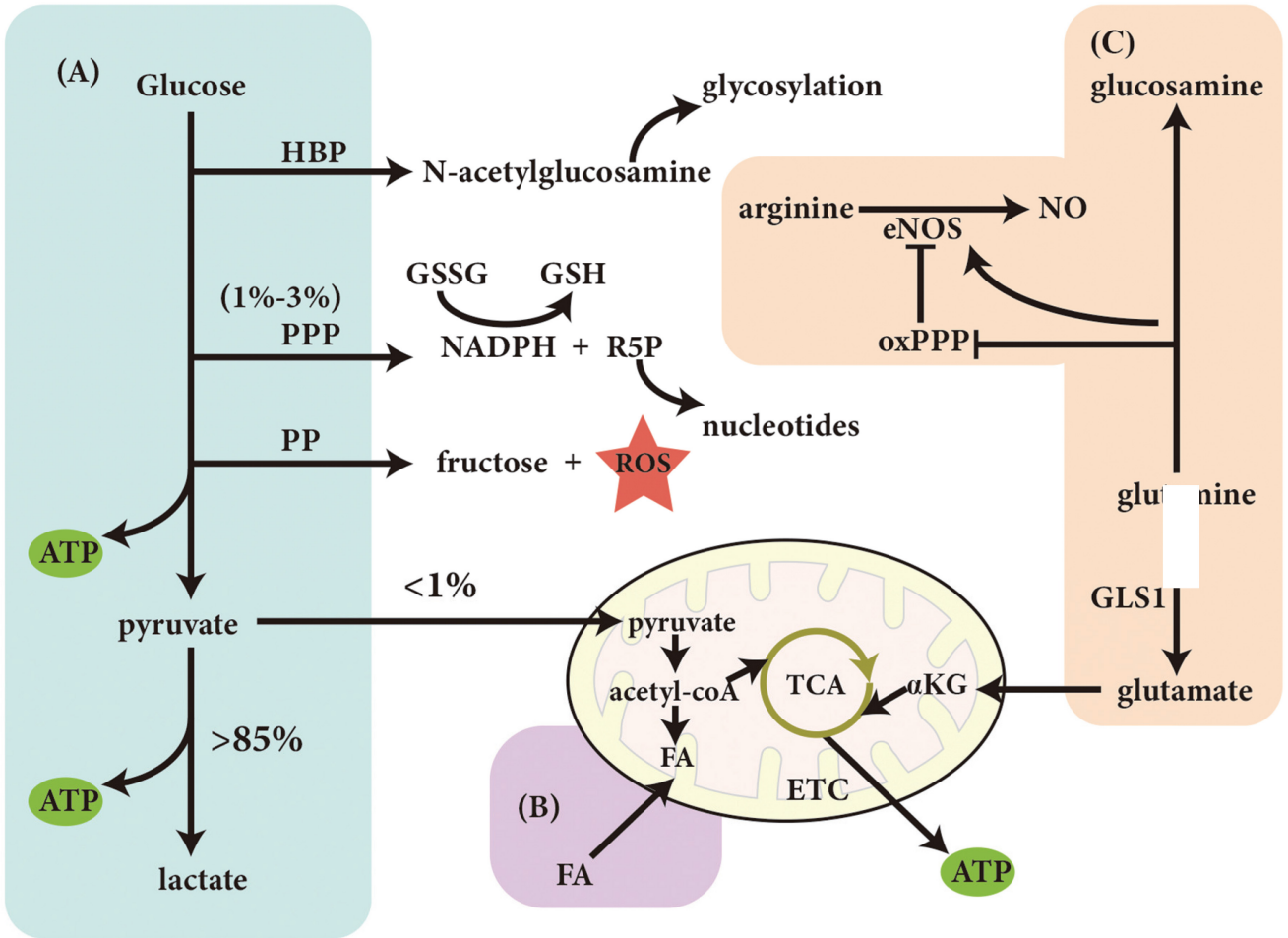

FIGURE 1 | Vascular endothelial cell metabolism under normal physiological conditions. Metabolism of **(A)** glucose, **(B)** fatty acid, **(C)** amino acid. ATP, adenosine triphosphate; HBP, hexosamine biosynthesis pathway; PPP, pentose phosphate pathway; PP, polyol pathway; GSH, glutathione; GSSG, oxidized glutathione; NADPH, nicotinamide adenine dinucleotide phosphate; R5P, ribose-5-phosphate; ETC, electron transport chain; TCA, tricarboxylic acid cycle; FA, fatty acid; eNOS, endothelial nitric oxide synthase; oxPPP, oxidized PPP; GLS1, glutaminase 1, αKG: α-ketoglutarate.

2009). Conversely, an increased glucosamine concentration leads to protein glycosylation and inhibits the migration of VECs (Li et al., 2019b).

Metabolic Reprogramming and VEC Inflammation

The metabolic changes of inflammatory VECs are mainly characterized by increased glycolysis. The study showed that mechanical low shear stress activated hypoxia-inducible factor 1α (HIF-1α) in cultured VECs via activating the nuclear factor-κB (NF-κB) pathway and promoting the expression of deubiquitinating enzyme cezanne. HIF-1α promotes the production of inflammatory factors in VECs by increasing the expression of the glycolysis-related regulators hexokinase 2 (HK2), enolase 2 (ENO2), glucose transporter 1 (GLUT1), fructose-2,6-biphosphatase 3 (PFKFB3) and extracellular acidification rate (ECAR, a direct marker of glycolysis) (Feng et al., 2017).

Metabolic Reprogramming and VEC Proliferation

Studies have found that multiple steps in FA metabolism, such as FA synthesis, FA transport and FAO, are all involved in the proliferation of VECs. Firstly, the expression and activity of FAS are increased in hypoxic human pulmonary artery endothelial cells (HPAECs), while the inhibition of FAS leads to the reduced HPAEC proliferation (Singh et al., 2017). Secondly, VEC proliferation is associated with the expression of fatty acid transporters (FATPs) and fatty acid binding proteins (FABPs). For instance, the silencing of *FABP4* inhibited the VEC proliferation *in vitro* (Elmasri et al., 2012). Also, the downregulation of carnitine palmitoyl transferase 1A (CPT1A) expression, a rate-limiting enzyme in the metabolism of FA, or *CPT1A* knockout was also found to inhibit the proliferation of VECs (Schoors et al., 2015). The above results indicate that fatty acid metabolism plays a significant role in controlling VEC proliferation. However, the detailed mechanisms need further studies.

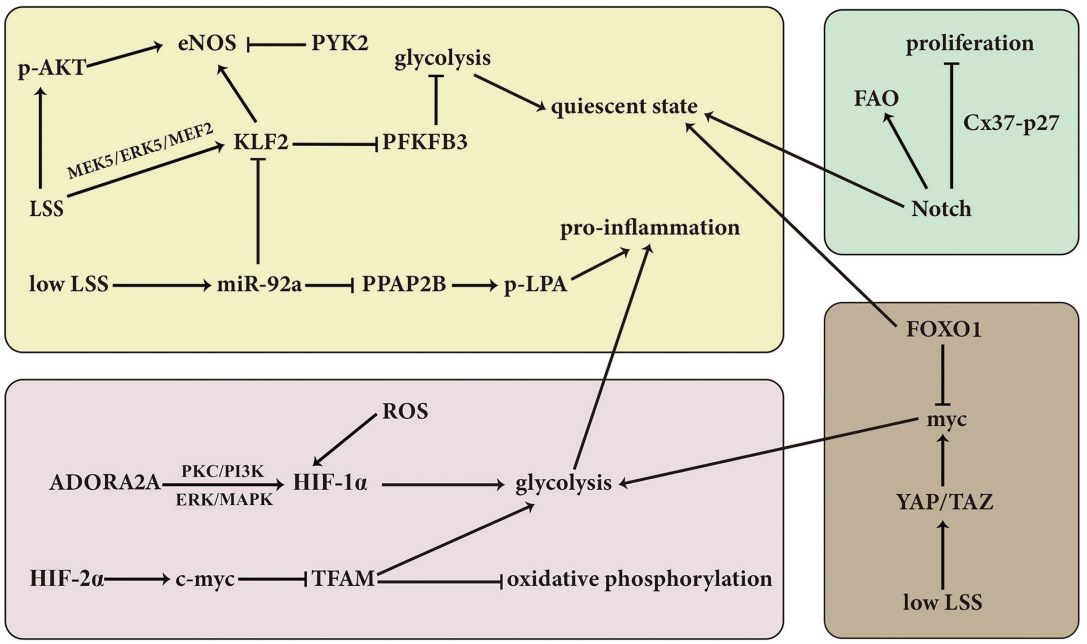

FIGURE 2 | Overview of the molecular mechanisms and signaling pathways involved in the regulation of VEC. LSS, laminar shear stress; KLF2, Kruppel-like factor 2; PFKFB3, fructose-2,6-biphosphatase 3; PPAP2B, phosphatidic acid phosphatase type 2B; LPA, lysophosphatidic acid; AKT, protein kinase B; eNOS, endothelial nitric oxide synthase; PYK2, proline-rich tyrosine kinase 2; ROS, reactive oxygen species; HIF-1α, hypoxia inducible factor-1α; PKC, protein kinase C; ADORA2A, adenosine A2a receptor; FOXO1, forkhead box O1; FAO, fatty acid oxidation; YAP, Yes-associated protein; TAZ, transcriptional coactivator with PDZ-binding motif; p, phosphorylation.

The proliferation of VECs also depends on glutamine metabolism. Indeed, genetic deletion or pharmacological inhibition of glutaminase1(GLS1) inhibits the proliferation of VECs (Kim B. et al., 2017). Asparagine synthetase (ASNS) is an enzyme which is responsible for the generation of asparagine from nitrogen (glutamine-derived) and aspartic acid. Huang et al. found that the silencing of *ASNS* inhibited the proliferation of VECs (Huang et al., 2017).

MOLECULAR MECHANISMS AND SIGNALING PATHWAYS INVOLVED IN THE REGULATION OF VEC METABOLISM

Various signaling pathways are involved in the regulation of VEC metabolism to respond quickly to changes under environmental conditions (**Figure 2**; Li et al., 2019c).

Laminar shear stress (LSS) is mainly transduced via the activation of a mechanical signal transduction pathway triggering a certain response of VECs to the external environment; at the same time, LSS can also affect VEC metabolism. It is reported that the expression of transcriptional factor Kruppel like factor 2 (KLF2) is induced in the LSS-treated VECs via the activation of MEK5/ERK5/MEF2 signaling pathway (Parmar et al., 2006). Subsequently, a great number of genes controlling endothelial energy metabolism, thrombosis/hemostasis, inflammation, vascular tone, and vessel development/remodeling are regulated by the LSS-induced KLF2 pathway (SenBanerjee et al., 2004; Parmar et al., 2006). For example, PFKFB3 is a key glycolytic enzyme. It was found that LSS-upregulated KLF2 reduced glucose uptake and glycolysis by inhibiting the activity of the *PFKFB3* promoter, then decreased the flux of glycolysis and maintained VECs at a resting state (Dekker et al., 2002; Doddaballapur et al., 2015). On the other hand, under normal condition, phosphatidic acid phosphatase type 2B (PPAP2B) dephosphorylates lysophosphatidic acid (LPA) to prevent it from binding to its receptor LPAR1 and then inhibits VEC inflammation. While, low LSS leads to the increased miR-92a and decreased KLF2, which inhibits the expression of PPAP2B in VECs, and then induces the VEC inflammation (Wu et al., 2011, 2015). Another key point in the response to LSS is the activity of eNOS. ECs possess special membrane organelle cilia, which is responsible for sensing the LSS and thus controlling the production of NO (Nauli et al., 2008). However, the underlying mechanisms by which LSS regulates the activity of eNOS are quite sophisticated. For example, LSS-induced phosphorylation of AKT and increased expression of KLF2 can activate and promote the expression of eNOS, respectively, but upregulation of proline-rich tyrosine kinase 2(PYK2) leads to opposite result (Zhou et al., 2014).

Like KLF2, SIRT3 also regulates the metabolic shift between mitochondrial oxidation and glycolysis, targeting on the PFKFB3. It was found that SIRT3 KO-EC exhibited a reduction of glycolysis and an elevation in mitochondrial oxidation and ROS

formation, accompanying with the downregulated expression of PFKFB3 and upregulated acetylation of PFKFB3. The abovementioned EC metabolic shift was regarded to contribute to an impaired angiogenesis, reduced coronary flow reserve and diastolic dysfunction in SIRT3 KO mice (He et al., 2017).

Some studies have suggested that hypoxia signaling also participates in the regulation of VEC metabolism. For example, the upregulation of pyruvate dehydrogenase kinase 1(PDK1) induced by HIF-1 in the disturbed flow-activated ECs results in the phosphorylation and inactivation of pyruvate dehydrogenase (PDH), then blocks the conversion from pyruvate to acetyl-CoA catalyzed by PDH, and finally suppresses the TCA cycle. At the same time, the increased glucose transporter and glycolytic enzyme genes such as GLUT1, lactate dehydrogenase A (LDHA) and HK-2 due to the activation of HIF-1 pathway are also involved in the disturbed flow-activated EC metabolic reprogramming and inflammation (Prabhakar and Semenza, 2012; Wu et al., 2017). Moreover, in hypoxic pulmonary artery ECs, HIF-2α inhibits mitochondrial transcription factor A (TFAM) by downregulating the expression of c-myc, and thus leads to the suppression of mitochondrial gene expression and the decrease in oxidative phosphorylation (Zarrabi et al., 2017). Regarding the mechanism responsible for the activation of HIF signaling, NAD(P)H Oxidase-4 (NOX4)-derived ROS is found to be required for the disturbed flow-activated HIF-1 pathway and subsequently increased glycolysis and decreased mitochondrial respiration (Wu et al., 2017). Besides, protein kinase C (PKC) and PI3K signaling are also involved in the hypoxia-induced HIF-1α activation and reinforced glycolysis in hypoxic VECs (Paik et al., 2017). Except for the above signaling pathways, adenosine A2a receptor (ADORA2A) in hypoxic VECs can enhance HIF-1α protein synthesis via ERK/MAPK and PI3K/Akt pathways and therefore promote glycolytic enzyme expression, glycolytic flux, EC proliferation, and angiogenesis (Liu et al., 2017).

The activation of Notch signaling pathway is necessary for maintaining the quiescent state of VECs. Kalucka et al. found that the treatment with Notch pathway stimulator Dll4 in the proliferating ECs induced a significant quiescence of ECs represented by the fact that the treated ECs became less proliferative and more in G0 phase. Simultaneously, the transcriptome results showed that the expression of genes related with glycolysis, TCA cycle, nucleotide synthesis, and purine/pyrimidine synthesis were decreased while the expression of genes controlling FAO was increased (Kalucka et al., 2018). Furthermore, it was found that Notch signaling led to the increased FAO flux, which was utilized for redox homeostasis through the generation of NADPH in quiescent VECs. The abovementioned effect of Notch signaling was mediated by the upregulation of CPTA1 (Kalucka et al., 2018). Moreover, Notch signaling is activated in the fluid shear stress-induced EC quiescence model, in which Cx37-p27 serve as the downstream of Notch signaling to promote the EC cell cycle arrest (Fang et al., 2017).

Similarly, forkhead box O1 (FOXO1) also is an important switch bridging the EC growth status and metabolic activities (Wilhelm et al., 2016). FOXO1 is found to decrease glycolysis, reduce mitochondrial respiration, inhibit EC proliferation and sprouting angiogenesis, and thereby maintain the EC in a quiescence status. EC-specific deletion of FOXO1, however, results in an uncontrolled EC proliferation, vessel hyperplasia and enlargement. Furthermore, it is found that the constitutive activation of FOXO1 reduces the myc expression, promotes myc degradation, and increases the expression of the negative regulators of myc MXI1. Considering that myc is a strong driver of glycolysis, mitochondrial metabolism, and cell growth, the antagonization of myc might mediate the pro-quiescence effect of FOXO1. FOXO1/myc acts a novel metabolic gatekeeper for switching the EC proliferation to quiescence (Wilhelm et al., 2016). On the contrary, endothelial Yes-associated protein/transcriptional coactivator with PDZ-binding motif complex (YAP/TAZ) promotes the formation and maturation of brain vessel in mice by upregulating myc-drive glycolysis, mitochondrial oxidative phosphorylation and EC proliferation (Kim J. et al., 2017). Low LSS activates YAP/TAZ by enhancing the activity of c-Jun N-terminal kinase (Wang et al., 2016), and the activation of integrin α5β1 and c-Abl induced by low LSS can upregulate the nuclear translocation of YAP by phosphorylating YAP at Y357 (Li et al., 2019a). Additionally, the RAF-MEK-ERK pathway activates glutaminolysis in VECs to support the metabolic requirements of highly proliferative VECs (Guo et al., 2016).

VEC METABOLISM UNDER PATHOLOGICAL CONDITION

Under normal physiological conditions, the main energy source of VECs comes from glycolysis. However, the increased activity of glycolytic-related enzymes after VEC activation can trigger the pro-inflammatory pathway, contributing to the progress of vascular injury diseases like atherosclerosis. Conversely, when the activity of glycolysis-related enzymes is reduced, resulting in stagnated glycolysis, intermediate products accumulate and can be metabolized via other pathways. The consequent generation of a great number of oxidative substances, the generation of advanced glycation end product (AGE), and eNOS uncoupling can lead to diabetic angiopathy. Furthermore, VECs frequently show a high glycolytic phenotype while retaining functional mitochondria during tumor neovascularization. Finally, metabolic reprogramming of VECs is also involved in the pathogenesis of hypertension and pulmonary arterial hypertension (**Figure 3**). In the following paragraphs, we shall review in further detail the abnormal VEC metabolism and its significance under pathophysiological conditions.

VEC Metabolism in Atherosclerosis

One of the most crucial factors for the initiation of VEC activation is disturbed blood flow dynamics (Davignon and Ganz, 2004). The disturbed blood flow mainly leads to the metabolic changes of VEC glycolysis. As mentioned in the above text, the expression of transcription factor KLF2 is upregulated by high LSS, resulting in decreased glycolysis and mitochondrial respiration by inhibiting the promoter of

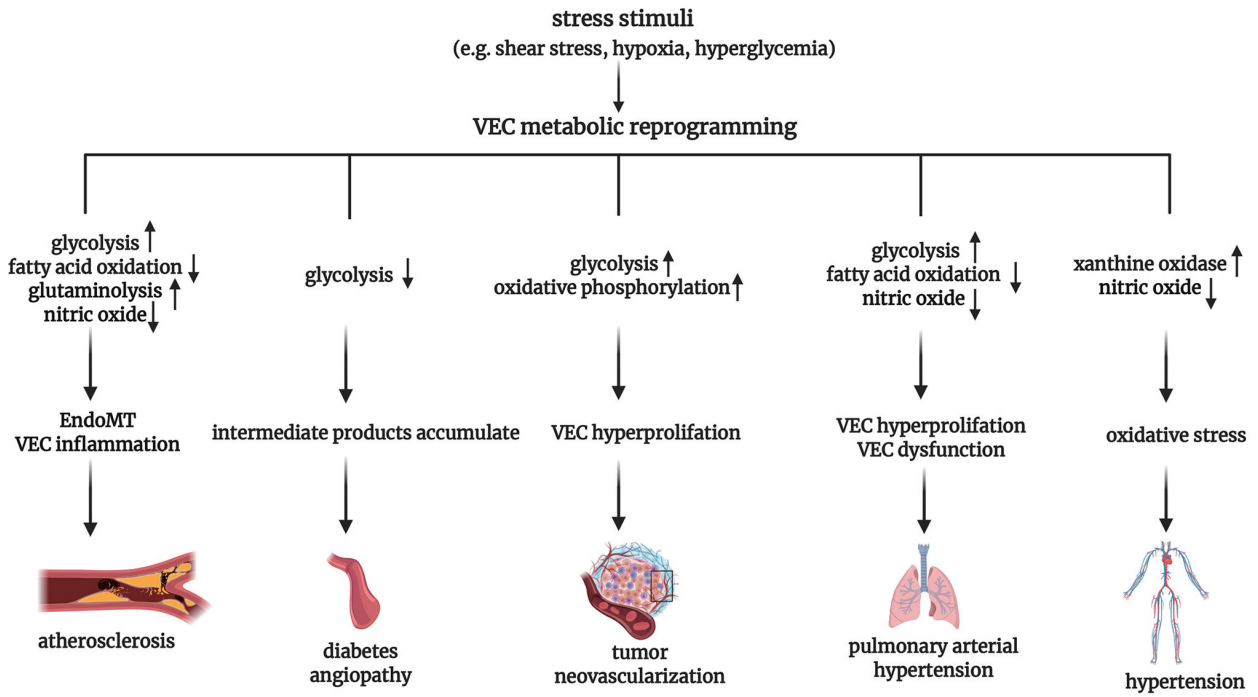

FIGURE 3 | Overview of vascular endothelial cell metabolic reprogramming in the pathogenesis of vascular diseases. VEC, vascular endothelial cell; EndoMT, endothelial-to-mesenchymal transition.

PFKFB3 (Doddaballapur et al., 2015). As a result, KLF2 is thought to be a key transcriptional switch point regulating the quiescent and activated states of VECs. On the other hand, VECs in the atherosclerotic region of the vascular system are disrupted by low LSS. Under low LSS, the activation of NF-κB induces elevated HIF-1α mRNA and increased the expression of cezanne, a ubiquitin-editing enzyme preventing the HIF-1α protein degradation, thus stabilizing HIF-1α. And then, HIF-1α promotes the proliferation and inflammation of VECs by activating glycolytic genes HK2, ENO2, and PFKFB3 to upregulate glycolysis, resulting in the initiation of atherosclerosis (Feng et al., 2017).

Endothelial-to-mesenchymal transition (EndoMT) is an important pathological basis of atherosclerotic lesions. These VEC-derived mesenchymal cells can cause the instability of plaque by enhancing the expression and activity of collagen-matrix metalloproteinase (Evrard et al., 2016). Xiong et al. demonstrated a metabolic mechanism responsible for EndoMT targeting on the FAO-controlled acetyl-CoA. It was found that the induction of EndoMT was associated with a reduction in FAO demonstrated by a decrease in acetyl-CoA levels and a fall in the expression of CPT1A, the enzyme that played rate-limiting and obligate roles in FAO. The downregulation of CPT1A expression in ECs promoted the EndoMT, while the increase in acetyl-CoA levels by supplementing acetate inhibited the SMAD2 activation and EndoMT program in cytokine-stimulated ECs. Those abovementioned results suggest the causal relationship between the reduction of FAO in the ECs and EndoMT, and provide a novel metabolic therapeutic choice for EndoMT-related diseases such as atherosclerosis (Xiong et al., 2018).

It has been proved that the pro-inflammatory YAP/TAZ signaling promotes the glutaminolysis of VECs, suggesting that glutamine has an atherogenic effect (Bertero et al., 2016). Glutamine deficiency can lead to the increased endoplasmic reticulum stress, impaired TCA, inhibition of mTOR signaling and subsequently reduced protein synthesis (Huang et al., 2017). Moreover, glutamate can be converted to neurotransmitter gamma aminobutyric acid (GABA), an anti-inflammatory mediator, in HAECs and HUVECs, and therefore glutamine deficiency may reduce the GABA level and its anti-inflammatory effect (Sen et al., 2016). In atherosclerosis, VECs also show disruption in metabolic pathways related to NO production. In the endothelium, NO-mediated vasodilation is required for vascular homeostasis and the inhibition of important events that promote atherosclerosis, including platelet aggregation, and smooth muscle cells migration (Kawashima, 2004). Consistently, one of the early features of atherosclerosis is eNOS uncoupling, resulting in an imbalance between anti-atherosclerotic NO and pro-atherosclerotic peroxides (Pircher et al., 2016).

VEC Metabolism in Diabetic Angiopathy

As a key metabolic characteristic of diabetes, hyperglycemia is found to be closely correlated with the alterations of

VEC metabolism, VEC dysfunction and consequent diabetic angiopathy. A significantly increased production of ROS and reactive nitrogen species (RNS) is an important change of diabetic VEC metabolism (Goveia et al., 2014). Hyperglycemia leads to an increased ROS level in VEC mainly by three mechanisms: (1) an obviously increased expression and activity of NAD(P)H oxidase protein subunits (p22phox, p67phox, and p47phox), which was observed in the veins and arteries of diabetic patients (Guzik et al., 2002). The NADPH-derived ROS production is associated with the downregulation of 8-oxoguanine glycosylase and subsequent activation of PKC in high glucose-treated HUVECs (Xie et al., 2020); (2) xanthine oxidase (XO) inhibitor allopurinol can prevent hyperglycemia-induced generation of ROS, which indicates that XO may be the major contributor of ROS (Eleftheriadis et al., 2018); (3) uncoupled eNOS can induce the increase of oxidative stress in diabetic mice (Sasaki et al., 2008). Besides, hyperglycemia results in an increase in cAMP, and then through the cAMP-dependent PKA, G6PD is phosphorylated and its activity is inhibited. As a result, the entry of glucose into PPP is reduced, leading to the subsequent decreased NADPH and increased ROS (Zhang et al., 2000). Moreover, when exposed to high glucose, the expression of fission proteins fission-1 (Fis1) and dynamin-related protein-1 (Drp1) in the VEC mitochondrial is enhanced and leads to the increase in the mitochondrial fission and an impaired autophagy of mitochondrial. And then the altered mitochondrial dynamics results in an increase of ROS generation, an inhibition of eNOS activation, and the loss of NO bioavailability (Shenouda et al., 2011).

Excess ROS production in diabetic VECs can activate poly-adenosine diphosphate ribose polymerase 1 (PARP-1), which mediates the ribosylation of poly-ADP, thereby inactivating the key glycolytic enzyme glyceraldehyde triphosphate dehydrogenase (GAPDH), whose activity plays a vital role in the maintenance of glycolytic flux (Du et al., 2003). As a result, the inhibited GAPDH leads to the stalled glycolysis. Excess glucose that cannot be metabolized due to the stalled glycolysis enters the PP and is converted to sorbitol at the cost of NADPH by AR, thereby leading to an increase in ROS. Sorbitol is then switched to fructose and highly active 3-deoxyglucose (3DG), promoting the formation of AGEs (Goveia et al., 2014). And the accumulated glycolysis intermediates then turn to three abnormal metabolic pathways as follows. (1) Glycolytic-derived fructose 6-phosphate can produce fructose-6-phosphate (F6P) via 6-phosphate fructosyl amide transferase; and the accumulated F6P is then mainly metabolized through the HBP, which produces the important precursor of glycosylation, uracil-*N*-acetylglucosamine diphosphate (UDP-GlcNAc) (Brownlee, 2001). Although glycosylation is an important process for the physiological function of VECs, hyperglycemic-induced protein glycosylation may inhibit angiogenesis (Luo et al., 2008). (2) The intermediates of glycolysis glyceraldehyde 3-phosphate (G3P) and dihydroxyacetone phosphate (DHAP) are transferred to the methylglyoxal pathway, which further boosts the production of AGEs (Goveia et al., 2014). Moreover, G3P and DHAP contribute to the diacylglycerol *de novo* synthesis, and subsequent PKC activation causes vascular abnormalities (Das Evcimen and King, 2007). (3) In theory, the accumulated glucose-6-phosphate (G6P) can enter the glucuronate cycle, but there is a lack of comprehensive research on the glucuronate cycle in diabetic VECs (Eelen et al., 2018).

VEC Metabolism in Tumor Neovascularization

The vessels in tumor are highly abnormal, and mainly characterized by VEC hyperproliferation. The switch of VECs from the quiescent state to the proliferative and migratory state during tumor neovascularization is closely related with the VEC metabolic reprogramming. VECs in tumors show a greater dependence on glycolysis to produce ATP than healthy VECs, mainly manifested as increased expression levels of associated genes, such as the glucose transporter *GLUT1* and the glycolytic activator *PFKFB3*, and thus exhibit a high glycolytic phenotype. The upregulation of PFKFB3 in the tumor depends on hypoxia, pro-inflammatory cytokines, or hormone signaling in the microenvironment (Zecchin et al., 2017). In addition, PPP and the serine biosynthetic pathway, which are utilized for the synthesis of nucleotide and biomass, are more highly activated in tumor VECs than in healthy VECs (Rohlenova et al., 2018).

Both tumor and healthy VECs retain functional mitochondria. The active OXPHOS increases the flexibility of using other substrates for energy generation, and provides metabolites for the synthesis of biomass to support cell proliferation. Studies revealed that the death of proliferating tumor VECs caused by mitochondrial respiratory inhibition is more than that of quiescent VECs, which indicated that functional OXPHOS may be quite important for the proliferating tumor VECs (Rohlenova et al., 2018). The role of mitochondria in tumor endothelial cells deserves further study.

VEC Metabolism in Pulmonary Arterial Hypertension

The high proliferation and dysfunction of VECs are main characteristics of pulmonary arterial hypertension (PAH) (Yu and Chan, 2017). The excessive proliferation of VECs in PAH depends on an increased glycolysis flux and a decreased oxygen consumption related to the upregulation of HIF-1α (Tuder et al., 2012). Moreover, bone morphogenetic protein receptor type 2 (*BMPR2*) is an important human PAH pathogenic gene (Majka et al., 2011). The expression of a BMPR2 mutant protein in human lung VECs contributes to the progress of PAH mainly by subsequent metabolic changes in VECs: (1) upregulated expression of glycolysis-related enzymes; (2) depressed carnitine metabolism and fatty acid oxidation;, and (3) decreased TCA cycle intermediates (Fessel et al., 2012). In addition, the increase in isocitrate dehydrogenase (IDH)-1 and IDH-2 activity observed in *BPMR2*-mutated VECs is identical with the increased serum IDH activity of PAH patients (Fessel et al., 2012).

Another characteristic of PAH is the decrease of NO content in VECs, which may be related to the following two aspects: (1) the decrease in antioxidant manganese superoxide dismutase (MnSOD) in mitochondria since MnSOD increases the biological activity of NO by scavenging the superoxide anion (Fijalkowska et al., 2010); and (2) the high expression level of arginase II, which competes with eNOS for the substrate arginine, thus leading to the subsequent decreased production of NO (Xu et al., 2004).

VEC Metabolism in Hypertension

In addition to the above EC metabolic changes, the abnormal purine catabolism in VECs is involved in the EC dysfunction in the development of hypertension. Xanthine oxidoreductase (XOR) catalyzes the oxidation of hypoxanthine to xanthine, and then xanthine to uric acid (UA). XOR exists in two different forms: xanthine dehydrogenase (XD) and XO (Maruhashi et al., 2018). The differences between XD and XO include the following aspects: (1) XD is the main enzyme found in normal tissues, but its activity is low, and XO dominates in tissues with injury and ischemia (Schmitz and Brand, 2016). (2) They use different electron acceptors. NAD^+ is preferentially used in the XD catalyzed-reaction, in which a stable reaction product NADH is generated; while molecular oxygen is preferentially used in the XO catalyzed-reaction, resulting the generation of superoxide anion and hydrogen peroxide (Maruhashi et al., 2018).

Compared with Wistar-Kyoto rat, XO activity was increased in VECs of spontaneously hypertensive rat (SHR), which was related with an elevation of arteriolar tone (Vila et al., 2019). Besides ROS generated from XO catalyzed-reaction, the concomitant product UA is regarded to be closely related with EC dysfunction and hypertension. Correspondingly, UA-lowering drugs have a significant anti-hypertensive effect via protecting EC in the basic experiment and clinical trials (Otani et al., 2018; Yang et al., 2018). The proposed mechanisms responsible for UA-related EC dysfunction involved the followings: (1) the impairment NO production and bioavailability. UA inhibited phosphorylation of eNOS and production of NO via PI3K/Akt pathway (Choi et al., 2014). Also, UA suppressed NO release and reacted directly with NO in an irreversible manner leading to NO depletion (Kang et al., 2005; Gersch et al., 2008). (2) the pro-inflammatory effect. UA treatment in VECs upregulated the mRNA expression, protein and release of inflammatory mediator C-reactive protein via p38 and ERK pathway (Kang et al., 2005). (3) the impaired mitochondrial function. UA-treated human aortic ECs exhibited the reduction mitochondrial mass and ATP production, the decrease in aconitase-2 activity and expression of enoyl CoA hydratase-1 (Sánchez-Lozada et al., 2012). (4) the induction of EC phenotype transition. UA-induced EndoMT in HUVECs via ROS generation and glycocalyx shedding (Ko et al., 2019). (5) The inhibition of EC proliferation and migration (Gersch et al., 2008). However, it is worth noticing that UA is also an antioxidant. Its main properties include scavenging hydroxyl free radicals, superoxide anions, peroxynitrite and preventing lipid peroxidation (Amaro et al., 2019).

KEY INSIGHTS AND THERAPEUTIC PERSPECTIVE

In summary, VECs mostly remain quiescent, but can be activated by various physiological and pathological stimuli. In general, VECs show significant metabolic changes during activation, resulting in further VEC dysfunction and development of cardiovascular disease, diabetic angiopathy, and tumor angiogenesis. For example, the activation and dysfunction of VECs in vulnerable areas of arterial blood vessels can be easily detected in the development of atherosclerosis (Davignon and Ganz, 2004), accompanied by unique metabolic reprogramming of VECs (Goveia et al., 2014). Moreover, vascular dysfunction caused by VEC metabolic changes initiates the development of diabetic angiopathy and contributes to the pathogenesis of vascular complications (Shi and Vanhoutte, 2017). In addition to vascular growth factors, VEC metabolism also plays a significant role in tumor neovascularization (Rohlenova et al., 2018). The abovementioned studies indicate that VEC metabolism might be a possible therapeutic target of vasculature related diseases.

At present, one of the important strategies targeting VEC metabolism is the development of anti-angiogenic drugs (Lopes-Coelho et al., 2020). PFKFB3 is an important enzyme in glycolysis, and participates in the synthesis of ATP and biological macromolecules. Initial study has demonstrated that the inhibition of the gene *PFKFB3* may reduce the formation of vessels under physiological condition (De Bock et al., 2013b). Notably, anti-glycolysis therapy with the PFKFB3 blocker 3-(3-pyridinyl)-1-(4-pyridinyl)-2-propen-1-one(3PO) can reduce glycolysis and pathological angiogenesis (Schoors et al., 2014), and a phase 1 clinical trial of the 3PO derivative PFK158 for the treatment of solid malignant tumor has been carried out (Li et al., 2019b). Therapy targeting PFKFB3 is safe because it temporarily inhibits only a branch of glycolysis and does not harm other healthy tissues that depend on glycolysis for their energy production (Schoors et al., 2014). Besides, Schoonjans et al. have demonstrated that PDK inhibitor dichloroacetate (DCA) and GLS1 inhibitor Bis-2-(5-phenylacetamido-1,3,4-thiadiazol-2-yl) ethyl sulfide (BPTES) affect tumor angiogenesis by lowering glycolysis and glutamate production, respectively, in HUVECs (Schoonjans et al., 2020). The silence of CPT1 in VECs can lead to the proliferation of VECs. As a result, it suggests that the pharmacological blockade of CPT1, such as etomoxir, may be used for the treatment of pathological angiogenesis by lowering FAO (Schoors et al., 2015). Further strategies to recover abnormal metabolism, decrease ROS production, and enhance the clearance of ROS, seem to be able to help counteracting diabetic vascular disease initiated by VEC dysfunction. However, clinical antioxidants have not been successfully applied to treat diabetic complication, to some extent (Ceriello et al., 2016). Therefore, new therapeutic targets are a continued focus of research related to vascular complications in diabetes. Nonetheless, VEC-based metabolic targeted therapies for atherosclerosis had not been developed to date.

As our understanding of VEC metabolism improves, new treatment options may continue to emerge. The detailed characterization of VEC metabolism under normal

and pathophysiological conditions, direct metabolic flux measurements, and more comprehensive metabolomics analyses may provide future treatment targets for a wide range of pathologies related to abnormal vascular development.

AUTHOR CONTRIBUTIONS

HP sorted out, reviewed, and analyzed the literatures, drew the diagrams, and wrote the manuscript. XW sorted out, reviewed, and analyzed the literatures and revised the manuscript. HJ devised the concept. JD, QC, YH, and HJ supervised the writing. All authors revised and approved the final version of the manuscript.

FUNDING

This research was funded by the National Natural Science Foundation of China (81970424 and 81921001) and Beijing Natural Science Foundation (7171010, 7191012, and 7182168).

REFERENCES

Amaro, S., Jiménez-Altayó, F., and Chamorro, Á (2019). Uric acid therapy for vasculoprotection in acute ischemic stroke. *Brain. Circ.* 5, 55–61. doi: 10.4103/bc.bc_1_19

Bertero, T., Oldham, W. M., Cottrill, K. A., Pisano, S., Vanderpool, R. R., Yu, Q., et al. (2016). Vascular stiffness mechanoactivates YAP/TAZ-dependent glutaminolysis to drive pulmonary hypertension. *J. Clin. Invest.* 126, 3313–3335. doi: 10.1172/JCI86387

Brownlee, M. (2001). Biochemistry and molecular cell biology of diabetic complications. *Nature* 414, 813–820. doi: 10.1038/414813a

Ceriello, A., Testa, R., and Genovese, S. (2016). Clinical implications of oxidative stress and potential role of natural antioxidants in diabetic vascular complications. *Nutr. Metab. Cardiovasc. Dis.* 26, 285–292. doi: 10.1016/j.numecd.2016.01.006

Choi, Y. J., Yoon, Y., Lee, K. Y., Hien, T. T., Kang, K. W., Kim, K. C., et al. (2014). Uric acid induces endothelial dysfunction by vascular insulin resistance associated with the impairment of nitric oxide synthesis. *FASEB. J.* 28, 3197–3204. doi: 10.1096/fj.13-247148

Das Evcimen, N., and King, G. L. (2007). The role of protein kinase C activation and the vascular complications of diabetes. *Pharmacol. Res.* 55, 498–510. doi: 10.1016/j.phrs.2007.04.016

Davidson, S. M. (2010). Endothelial mitochondria and heart disease. *Cardiovasc. Res.* 88, 58–66. doi: 10.1093/cvr/cvq195

Davignon, J., and Ganz, P. (2004). Role of endothelial dysfunction in atherosclerosis. *Circulation* 109, III27–III32. doi: 10.1161/01.CIR.0000131515.03336.f8

De Bock, K., Georgiadou, M., and Carmeliet, P. (2013a). Role of endothelial cell metabolism in vessel sprouting. *Cell Metab.* 18, 634–647. doi: 10.1016/j.cmet.2013.08.001

De Bock, K., Georgiadou, M., Schoors, S., Kuchnio, A., Wong, B. W., Cantelmo, A. R., et al. (2013b). Role of PFKFB3-driven glycolysis in vessel sprouting. *Cell* 154, 651–663. doi: 10.1016/j.cell.2013.06.037

Dekker, R. J., van Soest, S., Fontijn, R. D., Salamanca, S., de Groot, P. G., VanBavel, E., et al. (2002). Prolonged fluid shear stress induces a distinct set of endothelial cell genes, most specifically lung Krüppel-like factor (KLF2). *Blood* 100, 1689–1698. doi: 10.1182/blood-2002-01-0046

Doddaballapur, A., Michalik, K. M., Manavski, Y., Lucas, T., Houtkooper, R. H., You, X., et al. (2015). Laminar shear stress inhibits endothelial cell metabolism via KLF2-mediated repression of PFKFB3. *Arterioscler. Thromb. Vasc. Biol.* 35, 137–145. doi: 10.1161/ATVBAHA.114.304277

Du, X., Matsumura, T., Edelstein, D., Rossetti, L., Zsengellér, Z., Szabó, C., et al. (2003). Inhibition of GAPDH activity by poly(ADP-ribose) polymerase activates three major pathways of hyperglycemic damage in endothelial cells. *J. Clin. Invest.* 112, 1049–1057. doi: 10.1172/jci200318127

Eelen, G., de Zeeuw, P., Simons, M., and Carmeliet, P. (2015). Endothelial cell metabolism in normal and diseased vasculature. *Circ. Res.* 116, 1231–1244. doi: 10.1161/CIRCRESAHA.116.302855

Eelen, G., de Zeeuw, P., Treps, L., Harjes, U., Wong, B. W., and Carmeliet, P. (2018). Endothelial cell metabolism. *Physiol. Rev.* 98, 3–58. doi: 10.1152/physrev.00001.2017

Eleftheriadis, T., Pissas, G., Antoniadi, G., Liakopoulos, V., and Stefanidis, I. (2018). Allopurinol protects human glomerular endothelial cells from high glucose-induced reactive oxygen species generation, p53 overexpression and endothelial dysfunction. *Int. Urol. Nephrol.* 50, 179–186. doi: 10.1007/s11255-017-1733-5

Elmasri, H., Ghelfi, E., Yu, C. W., Traphagen, S., Cernadas, M., Cao, H. M., et al. (2012). Endothelial cell-fatty acid binding protein 4 promotes angiogenesis: role of stem cell factor/c-kit pathway. *Angiogenesis* 15, 457–468. doi: 10.1007/s10456-012-9274-0

Evrard, S. M., Lecce, L., Michelis, K. C., Nomura-Kitabayashi, A., Pandey, G., Purushothaman, K. R., et al. (2016). Endothelial to mesenchymal transition is common in atherosclerotic lesions and is associated with plaque instability. *Nat. Commun.* 7:11853. doi: 10.1038/ncomms11853

Fang, J. S., Coon, B. G., Gillis, N., Chen, Z., Qiu, J., Chittenden, T. W., et al. (2017). Shear-induced Notch-Cx37-p27 axis arrests endothelial cell cycle to enable arterial specification. *Nat. Commun.* 8:2149. doi: 10.1038/s41467-017-01742-7

Feng, S., Bowden, N., Fragiadaki, M., Souilhol, C., Hsiao, S., Mahmoud, M., et al. (2017). Mechanical activation of hypoxia-inducible factor 1alpha drives endothelial dysfunction at atheroprone sites. *Arterioscler. Thromb. Vasc. Biol.* 37, 2087–2101. doi: 10.1161/ATVBAHA.117.309249

Fessel, J. P., Hamid, R., Wittmann, B. M., Robinson, L. J., Blackwell, T., Tada, Y., et al. (2012). Metabolomic analysis of bone morphogenetic protein receptor type 2 mutations in human pulmonary endothelium reveals widespread metabolic reprogramming. *Pulm. Circ.* 2, 201–213. doi: 10.4103/2045-8932.97606

Fijalkowska, I., Xu, W., Comhair, S. A., Janocha, A. J., Mavrakis, L. A., Krishnamachary, B., et al. (2010). Hypoxia inducible-factor1alpha regulates the metabolic shift of pulmonary hypertensive endothelial cells. *Am. J. Pathol.* 176, 1130–1138. doi: 10.2353/ajpath.2010.090832

Gersch, C., Palii, S. P., Kim, K. M., Angerhofer, A., Johnson, R. J., and Henderson, G. N. (2008). Inactivation of nitric oxide by uric acid. *Nucleosides. Nucleotides. Nucleic Acids* 27, 967–978. doi: 10.1080/15257770802257952

Goveia, J., Stapor, P., and Carmeliet, P. (2014). Principles of targeting endothelial cell metabolism to treat angiogenesis and endothelial cell dysfunction in disease. *EMBO Mol. Med.* 6, 1105–1120. doi: 10.15252/emmm.201404156

Groschner, L. N., Waldeck-Weiermair, M., Malli, R., and Graier, W. F. (2012). Endothelial mitochondria–less respiration, more integration. *Pflugers Arch.* 464, 63–76. doi: 10.1007/s00424-012-1085-z

Guo, Y., Deng, Y., Li, X., Ning, Y., Lin, X., Guo, S., et al. (2016). Glutaminolysis was induced by TGF-beta1 through PP2Ac regulated Raf-MEK-ERK signaling in endothelial cells. *PLoS One* 11:e0162658. doi: 10.1371/journal.pone.0162658

Guzik, T. J., Mussa, S., Gastaldi, D., Sadowski, J., Ratnatunga, C., Pillai, R., et al. (2002). Mechanisms of increased vascular superoxide production in human diabetes mellitus: role of NAD(P)H oxidase and endothelial nitric oxide synthase. *Circulation* 105, 1656–1662. doi: 10.1161/01.cir.0000012748.58444.08

He, X., Zeng, H., Chen, S. T., Roman, R. J., Aschner, J. L., Didion, S., et al. (2017). Endothelial specific SIRT3 deletion impairs glycolysis and angiogenesis and causes diastolic dysfunction. *J. Mol. Cell Cardiol.* 112, 104–113. doi: 10.1016/j.yjmcc.2017.09.007

Huang, H., Vandekeere, S., Kalucka, J., Bierhansl, L., Zecchin, A., Brüning, U., et al. (2017). Role of glutamine and interlinked asparagine metabolism in vessel formation. *EMBO J.* 36, 2334–2352. doi: 10.15252/embj.201695518

Kalucka, J., Bierhansl, L., Conchinha, N. V., Missiaen, R., Elia, I., Bruning, U., et al. (2018). Quiescent endothelial cells upregulate fatty acid beta-oxidation

for vasculoprotection via redox homeostasis. *Cell Metab.* 28, 881.e13–894.e13. doi: 10.1016/j.cmet.2018.07.016

Kang, D. H., Park, S. K., Lee, I. K., and Johnson, R. J. (2005). Uric acid-induced C-reactive protein expression: implication on cell proliferation and nitric oxide production of human vascular cells. *J. Am. Soc. Nephrol.* 16, 3553–3562. doi: 10.1681/asn.2005050572

Kawashima, S. (2004). Malfunction of vascular control in lifestyle-related diseases: endothelial nitric oxide (NO) synthase/NO system in atherosclerosis. *J. Pharmacol. Sci.* 96, 411–419. doi: 10.1254/jphs.fmj04006x6

Kim, B., Li, J., Jang, C., and Arany, Z. (2017). Glutamine fuels proliferation but not migration of endothelial cells. *EMBO J.* 36, 2321–2333. doi: 10.15252/embj.201796436

Kim, J., Kim, Y. H., Kim, J., Park, D. Y., Bae, H., Lee, D. H., et al. (2017). YAP/TAZ regulates sprouting angiogenesis and vascular barrier maturation. *J. Clin. Invest.* 127, 3441–3461. doi: 10.1172/jci93825

Ko, J., Kang, H. J., Kim, D. A., Kim, M. J., Ryu, E. S., Lee, S., et al. (2019). Uric acid induced the phenotype transition of vascular endothelial cells via induction of oxidative stress and glycocalyx shedding. *FASEB. J.* 33, 13334–13345. doi: 10.1096/fj.201901148R

Krüger-Genge, A., Blocki, A., Franke, R. P., and Jung, F. (2019). Vascular endothelial cell biology: an update. *Int. J. Mol. Sci.* 20:4411. doi: 10.3390/ijms20184411

Krutzfeldt, A., Spahr, R., Mertens, S., Siegmund, B., and Piper, H. M. (1990). Metabolism of exogenous substrates by coronary endothelial cells in culture. *J. Mol. Cell Cardiol.* 22, 1393–1404. doi: 10.1016/0022-2828(90)90984-a

Li, B., He, J., Lv, H., Liu, Y., Lv, X., Zhang, C., et al. (2019a). c-Abl regulates YAPY357 phosphorylation to activate endothelial atherogenic responses to disturbed flow. *J. Clin. Invest.* 129, 1167–1179. doi: 10.1172/jci122440

Li, X., Kumar, A., and Carmeliet, P. (2019b). Metabolic pathways fueling the endothelial cell drive. *Annu. Rev. Physiol.* 81, 483–503. doi: 10.1146/annurev-physiol-020518-114731

Li, X., Sun, X., and Carmeliet, P. (2019c). Hallmarks of endothelial cell metabolism in health and disease. *Cell Metab.* 30, 414–433. doi: 10.1016/j.cmet.2019.08.011

Liu, Z., Yan, S., Wang, J., Xu, Y., Wang, Y., Zhang, S., et al. (2017). Endothelial adenosine A2a receptor-mediated glycolysis is essential for pathological retinal angiogenesis. *Nat. Commun.* 8:584. doi: 10.1038/s41467-017-00551-2

Lopes-Coelho, F., Martins, F., and Serpa, J. (2020). Endothelial cells (ECs) metabolism: a valuable piece to disentangle cancer biology. *Adv. Exp. Med. Biol.* 1219, 143–159. doi: 10.1007/978-3-030-34025-4_8

Luo, B., Soesanto, Y., and McClain, D. A. (2008). Protein modification by O-linked GlcNAc reduces angiogenesis by inhibiting Akt activity in endothelial cells. *Arterioscler. Thromb. Vasc. Biol.* 28, 651–657. doi: 10.1161/ATVBAHA.107.159533

Magnuson, D. K., Maier, R. V., and Pohlman, T. H. (1989). Protein kinase C: a potential pathway of endothelial cell activation by endotoxin, tumor necrosis factor, and interleukin-1. *Surgery* 106, 216–222. discussion 222-213,

Majka, S., Hagen, M., Blackwell, T., Harral, J., Johnson, J. A., Gendron, R., et al. (2011). Physiologic and molecular consequences of endothelial Bmpr2 mutation. *Respir. Res.* 12:84. doi: 10.1186/1465-9921-12-84

Maruhashi, T., Hisatome, I., Kihara, Y., and Higashi, Y. (2018). Hyperuricemia and endothelial function: from molecular background to clinical perspectives. *Atherosclerosis* 278, 226–231. doi: 10.1016/j.atherosclerosis.2018.10.007

Nauli, S. M., Kawanabe, Y., Kaminski, J. J., Pearce, W. J., Ingber, D. E., and Zhou, J. (2008). Endothelial cilia are fluid shear sensors that regulate calcium signaling and nitric oxide production through polycystin-1. *Circulation* 117, 1161–1171. doi: 10.1161/circulationaha.107.710111

Otani, N., Toyoda, S., Sakuma, M., Hayashi, K., Ouchi, M., Fujita, T., et al. (2018). Effects of uric acid on vascular endothelial function from bedside to bench. *Hypertens Res.* 41, 923–931. doi: 10.1038/s41440-018-0095-4

Paik, J. Y., Jung, K. H., Lee, J. H., Park, J. W., and Lee, K. H. (2017). Reactive oxygen species-driven HIF1alpha triggers accelerated glycolysis in endothelial cells exposed to low oxygen tension. *Nucl. Med. Biol.* 45, 8–14. doi: 10.1016/j.nucmedbio.2016.10.006

Pan, S., World, C. J., Kovacs, C. J., and Berk, B. C. (2009). Glucose 6-phosphate dehydrogenase is regulated through c-Src-mediated tyrosine phosphorylation in endothelial cells. *Arterioscler. Thromb. Vasc. Biol.* 29, 895–901. doi: 10.1161/ATVBAHA.109.184812

Parmar, K. M., Larman, H. B., Dai, G., Zhang, Y., Wang, E. T., Moorthy, S. N., et al. (2006). Integration of flow-dependent endothelial phenotypes by Kruppel-like factor 2. *J. Clin. Invest.* 116, 49–58. doi: 10.1172/jci24787

Pircher, A., Treps, L., Bodrug, N., and Carmeliet, P. (2016). Endothelial cell metabolism: a novel player in atherosclerosis? Basic principles and therapeutic opportunities. *Atherosclerosis* 253, 247–257. doi: 10.1016/j.atherosclerosis.2016.08.011

Pober, J. S. (1988). Warner-Lambert/Parke-Davis award lecture. Cytokine-mediated activation of vascular endothelium. Physiology and pathology. *Am. J. Pathol.* 133, 426–433.

Pober, J. S., Min, W., and Bradley, J. R. (2009). Mechanisms of endothelial dysfunction, injury, and death. *Annu. Rev. Pathol.* 4, 71–95. doi: 10.1146/annurev.pathol.4.110807.092155

Prabhakar, N. R., and Semenza, G. L. (2012). Adaptive and maladaptive cardiorespiratory responses to continuous and intermittent hypoxia mediated by hypoxia-inducible factors 1 and 2. *Physiol. Rev.* 92, 967–1003. doi: 10.1152/physrev.00030.2011

Rohlenova, K., Veys, K., Miranda-Santos, I., De Bock, K., and Carmeliet, P. (2018). Endothelial cell metabolism in health and disease. *Trends Cell Biol.* 28, 224–236. doi: 10.1016/j.tcb.2017.10.010

Sánchez-Lozada, L. G., Lanaspa, M. A., Cristóbal-García, M., García-Arroyo, F., Soto, V., Cruz-Robles, D., et al. (2012). Uric acid-induced endothelial dysfunction is associated with mitochondrial alterations and decreased intracellular ATP concentrations. *Nephron. Exp. Nephrol.* 121, e71–e78. doi: 10.1159/000345509

Sasaki, N., Yamashita, T., Takaya, T., Shinohara, M., Shiraki, R., Takeda, M., et al. (2008). Augmentation of vascular remodeling by uncoupled endothelial nitric oxide synthase in a mouse model of diabetes mellitus. *Arterioscler. Thromb. Vasc. Biol.* 28, 1068–1076. doi: 10.1161/atvbaha.107.160754

Schmitz, B., and Brand, S. M. (2016). Uric acid and essential hypertension: the endothelial connection. *J. Hypertens* 34, 2138–2139. doi: 10.1097/hjh.0000000000001109

Schoonjans, C. A., Mathieu, B., Joudiou, N., Zampieri, L. X., Brusa, D., Sonveaux, P., et al. (2020). Targeting endothelial cell metabolism by inhibition of pyruvate dehydrogenase kinase and glutaminase-1. *J. Clin. Med.* 9:3308. doi: 10.3390/jcm9103308

Schoors, S., Bruning, U., Missiaen, R., Queiroz, K. C. S., Borgers, G., Elia, I., et al. (2015). Fatty acid carbon is essential for dNTP synthesis in endothelial cells. *Nature* 526, 192–197. doi: 10.1038/nature14624

Schoors, S., De Bock, K., Cantelmo, A. R., Georgiadou, M., Ghesquiere, B., Cauwenberghs, S., et al. (2014). Partial and transient reduction of glycolysis by PFKFB3 blockade reduces pathological angiogenesis. *Cell Metab.* 19, 37–48. doi: 10.1016/j.cmet.2013.11.008

Sen, S., Roy, S., Bandyopadhyay, G., Scott, B., Xiao, D., Ramadoss, S., et al. (2016). γ-aminobutyric acid is synthesized and released by the endothelium: potential implications. *Circ. Res.* 119, 621–634. doi: 10.1161/CIRCRESAHA.116.308645

SenBanerjee, S., Lin, Z., Atkins, G. B., Greif, D. M., Rao, R. M., Kumar, A., et al. (2004). KLF2 Is a novel transcriptional regulator of endothelial proinflammatory activation. *J. Exp. Med.* 199, 1305–1315. doi: 10.1084/jem.20031132

Shenouda, S. M., Widlansky, M. E., Chen, K., Xu, G., Holbrook, M., Tabit, C. E., et al. (2011). Altered mitochondrial dynamics contributes to endothelial dysfunction in diabetes mellitus. *Circulation* 124, 444–453. doi: 10.1161/CIRCULATIONAHA.110.014506

Shi, Y., and Vanhoutte, P. M. (2017). Macro- and microvascular endothelial dysfunction in diabetes. *J. Diabetes* 9, 434–449. doi: 10.1111/1753-0407.12521

Singh, N., Singh, H., Jagavelu, K., Wahajuddin, M., and Hanif, K. (2017). Fatty acid synthase modulates proliferation, metabolic functions and angiogenesis in hypoxic pulmonary artery endothelial cells. *Eur. J. Pharmacol.* 815, 462–469. doi: 10.1016/j.ejphar.2017.09.042

Tang, X., Luo, Y. X., Chen, H. Z., and Liu, D. P. (2014). Mitochondria, endothelial cell function, and vascular diseases. *Front. Physiol.* 5:175. doi: 10.3389/fphys.2014.00175

Theodorou, K., and Boon, R. A. (2018). Endothelial cell metabolism in atherosclerosis. *Front. Cell Dev. Biol.* 6:82. doi: 10.3389/fcell.2018.00082

Tousoulis, D., Kampoli, A. M., Tentolouris, C., Papageorgiou, N., and Stefanadis, C. (2012). The role of nitric oxide on endothelial function. *Curr. Vasc. Pharmacol.* 10, 4–18. doi: 10.2174/157016112798829760

Tuder, R. M., Davis, L. A., and Graham, B. B. (2012). Targeting energetic metabolism: a new frontier in the pathogenesis and treatment of pulmonary hypertension. *Am. J. Respir. Crit. Care Med.* 185, 260–266. doi: 10.1164/rccm.201108-1536PP

Vila, E., Solé, M., Masip, N., Puertas-Umbert, L., Amaro, S., Dantas, A. P., et al. (2019). Uric acid treatment after stroke modulates the Krüppel-like factor 2-VEGF-A axis to protect brain endothelial cell functions: impact of hypertension. *Biochem. Pharmacol.* 164, 115–128. doi: 10.1016/j.bcp.2019.04.002

Wang, L., Luo, J. Y., Li, B., Tian, X. Y., Chen, L. J., Huang, Y., et al. (2016). Integrin-YAP/TAZ-JNK cascade mediates atheroprotective effect of unidirectional shear flow. *Nature* 540, 579–582. doi: 10.1038/nature20602

Wilhelm, K., Happel, K., Eelen, G., Schoors, S., Oellerich, M. F., Lim, R., et al. (2016). FOXO1 couples metabolic activity and growth state in the vascular endothelium. *Nature* 529, 216–220. doi: 10.1038/nature16498

Wu, C. Q., Huang, R. T., Kuo, C. H., Kumar, S., Kim, C. W., Lin, Y. C., et al. (2015). Mechanosensitive PPAP2B regulates endothelial responses to atherorelevant hemodynamic forces. *Circ. Res.* 117, E41–E53. doi: 10.1161/Circresaha.117.306457

Wu, D., Huang, R. T., Hamanaka, R. B., Krause, M., Oh, M. J., Kuo, C. H., et al. (2017). HIF-1α is required for disturbed flow-induced metabolic reprogramming in human and porcine vascular endothelium. *eLife* 6:e25217. doi: 10.7554/eLife.25217

Wu, G. Y., Haynes, T. E., Li, H., Yan, W., and Meininger, C. J. (2001). Glutamine metabolism to glucosamine is necessary for glutamine inhibition of endothelial nitric oxide synthesis. *Biochem. J.* 353, 245–252. doi: 10.1042/0264-6021:3530245

Wu, W., Xiao, H., Laguna-Fernandez, A., Villarreal, G. Jr., Wang, K. C., Geary, G. G., et al. (2011). Flow-dependent regulation of kruppel-like factor 2 is mediated by microRNA-92a. *Circulation* 124, 633–641. doi: 10.1161/circulationaha.110.005108

Xie, X., Chen, Y., Liu, J., Zhang, W., Zhang, X., Zha, L., et al. (2020). High glucose induced endothelial cell reactive oxygen species via OGG1/PKC/NADPH oxidase pathway. *Life Sci.* 256:117886. doi: 10.1016/j.lfs.2020.117886

Xiong, J., Kawagishi, H., Yan, Y., Liu, J., Wells, Q. S., Edmunds, L. R., et al. (2018). A metabolic basis for endothelial-to-mesenchymal transition. *Mol. Cell* 69, 689.e7–698.e7. doi: 10.1016/j.molcel.2018.01.010

Xu, W. L., Kaneko, F. T., Zheng, S., Comhair, S. A. A., Janocha, A. J., Goggans, T., et al. (2004). Increased arginase II and decreased NO synthesis in endothelial cells of patients with pulmonary arterial hypertension. *FASEB J.* 18, 1746–1748. doi: 10.1096/fj.04-2317fje

Yang, H., Bai, W., Gao, L., Jiang, J., Tang, Y., Niu, Y., et al. (2018). Mangiferin alleviates hypertension induced by hyperuricemia via increasing nitric oxide releases. *J. Pharmacol. Sci.* 137, 154–161. doi: 10.1016/j.jphs.2018.05.008

Yu, Q., and Chan, S. Y. (2017). Mitochondrial and metabolic drivers of pulmonary vascular endothelial dysfunction in pulmonary hypertension. *Adv. Exp. Med. Biol.* 967, 373–383. doi: 10.1007/978-3-319-63245-2_24

Zarrabi, A. J., Kao, D., Nguyen, D. T., Loscalzo, J., and Handy, D. E. (2017). Hypoxia-induced suppression of c-Myc by HIF-2alpha in human pulmonary endothelial cells attenuates TFAM expression. *Cell Signal.* 38, 230–237. doi: 10.1016/j.cellsig.2017.07.008

Zecchin, A., Kalucka, J., Dubois, C., and Carmeliet, P. (2017). How endothelial cells adapt their metabolism to form vessels in tumors. *Front. Immunol.* 8:1750. doi: 10.3389/fimmu.2017.01750

Zhang, Z., Apse, K., Pang, J., and Stanton, R. C. (2000). High glucose inhibits glucose-6-phosphate dehydrogenase via cAMP in aortic endothelial cells. *J. Biol. Chem.* 275, 40042–40047. doi: 10.1074/jbc.M007505200

Zhou, J., Li, Y. S., and Chien, S. (2014). Shear stress-initiated signaling and its regulation of endothelial function. *Arterioscler. Thromb. Vasc. Biol.* 34, 2191–2198. doi: 10.1161/Atvbaha.114.303422

Conflict of Interest: The authors declare that the research was conducted in the absence of any commercial or financial relationships that could be construed as a potential conflict of interest.

frontiers in Cell and Developmental Biology

ORIGINAL RESEARCH
published: 25 February 2021
doi: 10.3389/fcell.2021.630279

TFEB Gene Promoter Variants Effect on Gene Expression in Acute Myocardial Infarction

*Jie Zhang[1], Yexin Zhang[1], Xiaohui He[1], Shuai Wang[1], Shuchao Pang[2,3,4] and Bo Yan[2,3,4]**

[1] Department of Medicine, Shandong University School of Medicine, Jinan, China, [2] Shandong Provincial Key Laboratory of Cardiac Disease Diagnosis and Treatment, Affiliated Hospital of Jining Medical University, Jining Medical University, Jining, China, [3] The Center for Molecular Genetics of Cardiovascular Diseases, Affiliated Hospital of Jining Medical University, Jining Medical University, Jining, China, [4] Shandong Provincial Sino-US Cooperation Research Center for Translational Medicine, Affiliated Hospital of Jining Medical University, Jining Medical University, Jining, China

Autophagy is involved in many physiological processes. Transcription factor EB (TFEB) is a master regulator of autophagy and coordinates the expression of autophagic proteins, lysosomal hydrolases, and lysosomal membrane proteins. Though autophagy has been implicated in several human diseases, little is known regarding TFEB gene expression and regulation in the process. Since dysfunctional autophagy plays critical roles in acute myocardial infarction (AMI), dysregulated TFEB gene expression may be associated with AMI by regulating autophagy. In this study, the TFEB gene promoter was genetically and functionally analyzed in AMI patients (n = 352) and ethnic-matched controls (n = 337). A total of fifteen regulatory variants of the TFEB gene, including eight single-nucleotide polymorphisms (SNPs), were identified in this population. Among these, six regulatory variants [g.41737274T>C (rs533895008), g.41737144A>G, g.41736987C > T (rs760293138), g.41736806C > T (rs748537297), g.41736635T > C (rs975050638), and g.41736544C > T] were only identified in AMI patients. These regulatory variants significantly altered the transcriptional activity of the TFEB gene promoter. Further electrophoretic mobility shift assay revealed that three of the variants evidently affected the binding of transcription factors. Therefore, this study identified novel TFEB gene regulatory variants which affect the gene expression. These TFEB gene regulatory variants may contribute to AMI development as a rare risk factor.

Keywords: acute myocardial infarction, autophagy, TFEB, promoter, genetics

OPEN ACCESS

Edited by:
Xiaoqiang Tang,
Sichuan University, China

Reviewed by:
Shuquan Rao,
Southwest Jiaotong University, China
Qiong Gao,
University of Michigan, United States

***Correspondence:**
Bo Yan
yanbo@mail.jnmc.edu.cn

Specialty section:
This article was submitted to Cellular Biochemistry, a section of the journal Frontiers in Cell and Developmental Biology

Received: *17 November 2020*
Accepted: *26 January 2021*
Published: *25 February 2021*

Citation:
Zhang J, Zhang Y, He X, Wang S, Pang S and Yan B (2021) TFEB Gene Promoter Variants Effect on Gene Expression in Acute Myocardial Infarction. Front. Cell Dev. Biol. 9:630279. doi: 10.3389/fcell.2021.630279

INTRODUCTION

Autophagy is one of the major digestive systems in cells. There are three subtypes of autophagy, macroautophagy, microautophagy, and chaperone-mediated autophagy. Macroautophagy (hereafter referred to as autophagy) degrades cytoplasmic macromolecules and organelles by delivering them to lysosomes. Autophagy has been involved in many physiological processes, including lipid metabolism and inflammation. Dysfunctional autophagy has been implicated in a wide range of human diseases, including cardiovascular diseases (Gatica et al., 2015; Bravo-San Pedro et al., 2017). However, the genetic causes for autophagic dysfunction and underlying molecular mechanisms remain largely unknown.

Transcription factor EB (TFEB) belongs to the MiT-TFE family of basic helix–loop–helix leucine–zipper transcription factors, which include TFEB, TFE3, TFEC, and microphthalmia-associated transcription factor (MITF). TFEB regulates several cellular processes, including lysosome biogenesis, cellular energy homeostasis, autophagy, mitochondrial turnover, innate immune response, and inflammation. Many studies have demonstrated that TFEB has been involved in the co-regulation between lysosome, autophagy, and lipid metabolism (Sardiello et al., 2009; Settembre et al., 2011, 2013; Settembre and Ballabio, 2014; Napolitano and Ballabio, 2016; Brady et al., 2018). At the transcriptional level, TFEB functions as a master regulator of autophagy and coordinates the expression of lysosomal hydrolases, lysosomal membrane proteins, and autophagy proteins. TFEB binds to CLEAR (coordinated lysosomal expression and regulation) motif, a 10 base E-box-like sequence (GTCACGTGAC), within the promoters of the autophagic and lysosomal genes (Sardiello et al., 2009; Bajaj et al., 2019).

Recent studies suggest that TFEB also controls vascular development by regulating the proliferation of endothelial cells (Doronzo et al., 2019). Overexpression of the TFEB gene in endothelial cells in mice increases angiogenesis and improves blood flow recovery after ischemic injury (Fan et al., 2018). Animal experiments show that TFEB inhibits endothelial cell inflammation and reduces atherosclerosis (Lu et al., 2017; Song et al., 2019). Thus, altered TFEB level may contribute to cardiovascular diseases. In this study, we first identified regulatory variants in the TFEB gene promoter in patients with acute myocardial infarction (AMI) and then functionally analyzed the effect of the variants on TFEB gene expression. Furthermore, the molecular mechanisms by which the regulatory variants effect TFEB gene expression were also explored.

MATERIALS AND METHODS

Study Participants

AMI patients (n = 352; male 267 and female 85) were recruited from the Division of Cardiology, Affiliated Hospital of Jining Medical University (Jining, Shandong, China) during the period from March 2015 to June 2017. AMI patients were diagnosed according to clinical manifestations, electrocardiograms, elevated biochemical markers of myocardial necrosis, or coronary angioplasty. Ethnically matched controls (n = 337; male 167 and female 170) were recruited from Physical Examination in the same hospital during the same time period. The controls with a familial history of CAD and other heart diseases were excluded. This study was conducted in accordance with the Declaration of Helsinki (1964). The study protocol was approved by the Human Ethics Committee of the Affiliated Hospital of Jining Medical University. Written informed consent was obtained from all participants.

Direct DNA Sequencing

Fasting venous blood was collected, and peripheral leukocytes were isolated with the Human Leukocyte Isolation system (Haoyang Biological Products Technology Co., Ltd., Tianjin, China). Genomic DNAs were extracted with the QIAamp DNA Mini kit (Qiagen, Inc., Valencia, CA, United States). The promoter region of the human TFEB gene were generated with PCR and directly sequenced. Two overlapped DNA fragments, 705 bp (−1312 ∼ −608 bp) and 801 bp (−657 bp ∼ +144 bp), were overlapped, covering the TFEB gene promoter region. The PCR primers were designed using the human TFEB genomic sequence (National Center for Biotechnology Information GenBank accession no. NC_000006.12). PCR products were directly and bi-directionally sequenced on a 3500XL genetic analyzer (Thermo Fisher Scientific, Inc., Waltham, MA, United States) by Sangon Biotech Co., Ltd. (Shanghai, China). DNA sequences were then compared with the wild-type TFEB gene promoter using the DNAMAN program (Version 5.2.2, Lynnon BioSoft, Quebec, Canada), and regulatory variants including single-nucleotide polymorphisms (SNPs) were identified. Wild and variant TFEB gene promoters were analyzed using TRANSFAC and JASPAR programs to predict the binding sites for the transcription factor affected by regulatory variants.

Functional Analysis of Regulatory Variants by Dual-Luciferase Reporter Assay

Wild-type and variant TFEB gene promoters (1386, −1309 ∼ +77 bp) were generated by PCR, which were then inserted into the KpnI and HindIII sites of a luciferase reporter vector (pGL3-basic, Promega Corporation, Madison, WI, United States) to generate expression constructs. The designated expression constructs were transiently transfected into cultured HEK-293 [CRL-1573; American Type Culture Collection, Manassas, VA, United States (ATCC), Manassas, VA, United States] and H9c2 cells (rat cardiomyocyte line; CRL-1446; ATCC), and dual-luciferase activity was examined using Dual-Luciferase® Reporter Assay on a Glomax 20/20 luminometer (Promega Corporation, Madison, WI, United States). TFEB gene promoter activity was expressed as the ratio of luciferase activity over Renilla luciferase activity. Activity of the wild-type TFEB gene promoter was set as 100%, and the activity of the variant TFEB gene promoter was calculated. Transfection experiments were repeated three times independently, in triplicate.

Prediction of Binding Sites for Transcription Factors

The TFEB gene promoter was analyzed using TRANSFAC and JASPAR programs to predict whether regulatory variants identified in AMI patients change the putative binding sites for transcription factors.

Electrophoretic Mobility Shift Assay

To examine the effects of TFEB gene regulatory variants on the binding sites for transcription factors, electrophoretic mobility shift assay (EMSA) was conducted using the LightShift® Chemiluminescent EMSA kit (Thermo Fisher Scientific, Inc., Waltham, MA, United States). Biotinylated double-stranded oligonucleotides (30 bp) containing regulatory variants were used as probes. Nuclear extracts from HEK-293 and H9c2

cells were prepared using NE-PER® Nuclear and Cytoplasmic Extraction Reagent kit (Thermo Fisher Scientific, Inc., Waltham, MA, United States). Protein concentrations were determined using the Bradford protein assay. DNA-protein binding reactions were conducted for 20 min at room temperature with equal amounts of probes (0.2 pMol) and nuclear extracts (3.0 μg). The reaction mixtures were subsequently separated on a 6% polyacrylamide gel and transferred onto a nylon membrane (Thermo Fisher Scientific, Inc., Waltham, MA, United States). The oligonucleotides were cross-linked to the membrane using the UV Stratalinker 1800 (Stratagene; Agilent Technologies, Inc., Santa Clara, CA, United States) and were detected by chemiluminescence using the LightShift® Chemiluminescent EMSA kit (Thermo Fisher Scientific, Inc., Waltham, MA, United States).

Statistical Analysis

Quantitative data are expressed as the means ± standard error of the mean and were analyzed by student *t*-test using two-way analysis of variance followed by Dunnett test. The frequency of regulatory variants was compared between AMI patients and controls with χ^2 test using SPSS v22.0 software (SPSS, Inc., Chicago, IL, United States). $P < 0.05$ was considered as statistically significant.

RESULTS

Clinical and Biochemical Characteristics

This study included 689 participants, including 352 AMI patients and 337 controls. Clinical and biochemical characteristics are summarized in **Table 1**. Age, body mass index (BMI), triglyceride (TG), total cholesterol (TC), high-density lipoprotein cholesterol (HDL), and low-density lipoprotein cholesterol (LDL) were expressed as mean ± standard deviation. The prevalence of traditional risk factors including male sex, hypertension, diabetes, and smoking was significantly higher in AMI patients compared to controls ($P < 0.01$). TG, TC, HDL, and LDL levels in AMI patients were significantly lower compared to controls ($P < 0.01$), probably due to application of lowering-lipid medicines in AMI patients. In addition, there was no significant difference of BMI between AMI patients and controls ($P > 0.05$).

TABLE 1 | Clinical and biochemical characteristics of AMI patients and controls†.

	Controls (*n* = 337)	AMI (*n* = 352)	*P*-value
Age (years, mean ± SD)	51.25 ± 12.28	61.29 ± 12.01	<0.01
Male (*n*, %)	167 (49.55%)	267 (75.85%)	<0.01
Hypertension (*n*, %)	63 (18.69%)	122 (34.66%)	<0.01
Diabetes (*n*, %)	12 (3.56%)	68 (19.32%)	<0.01
Smoking (*n*, %)	24 (7.12%)	189 (53.69%)	<0.01
BMI (kg/M^2)	25.12 ± 3.51	25.02 ± 3.73	0.783
TG (mmol/L)	1.74 ± 0.98	1.32 ± 1.00	<0.01
TC (mmol/L)	4.88 ± 0.92	4.32 ± 1.13	<0.01
HDL (mmol/L)	1.24 ± 0.25	1.10 ± 0.26	<0.01
LDL (mmol/L)	2.95 ± 0.85	2.62 ± 0.84	<0.01

BMI, body mass index; TG, triglyceride; TC, total cholesterol; HDL, high-density lipoprotein cholesterol; LDL, low-density lipoprotein cholesterol. †quantitative data including age, BMI, TG, TC, HDL, and LDL were expressed as M ± SD.

Identified Regulatory Variants in the TFEB Gene Promoter

A total of fifteen regulatory variants of TFEB gene were identified in this study population, including eight SNPs and seven novel variants. Frequency and locations of the regulatory variants are presented in **Figure 1A** and summarized in **Table 2**. Two novel heterozygous variants (g.41737144A > G and g.41736544C > T) and four SNPs [g.41737274T > C (rs533895008), g.41736987C > T (rs760293138), g.41736806C > T (rs748537297), and g.41736635T > C (rs975050638)] were only identified in six male AMI patients (**Figure 1B**). All the six cases were male, and the age was from 52 to 81 years old. Clinically, four AMI cases suffered from acute inferior myocardial infarction, and two from acute anterior myocardial infarction. Three of the six AMI cases are accompanied with hypertension. Four of the six AMI cases had history of smoking. None of the six cases had diabetes. In addition, the clinical and biochemical parameters of the six AMI cases are listed on **Table 3**.

Altered Activity of the TFEB Gene Promoter by Regulatory Variants

The effect of the regulatory variants on the transcriptional activity of the TFEB gene promoter was analyzed with a luciferase reporter gene assay. We focused on the regulatory variants identified in AMI patients. The seven regulatory variants only identified in controls or both AMI patients and controls were used as internal controls. Expression constructs containing wild-type and variant TFEB gene promoters pGL3-WT (wild type), pGL3-41377451G, pGL3-41737274C, pGL3-41737144G, pGL3-41737034A, pGL3-41737034C, pGL3-41737005A, pGL3-41736987T, pGL3-41736981G, pGL3-41736806T, pGL3-41736635C, pGL3-41736544T, pGL3-41736407T, and pGL3-41736218G, were transfected into HEK-293 and H9c2 cells. The dual-luciferase activities were measured, and relative activity of wild-type and variant TFEB gene promoters was examined.

In HEK-293 cells, two regulatory variants (g.41737144A > G and g.41736544C > T) and three SNPs [g.41737274T > C (rs533895008), g.41736806C > T (rs748537297), and g.41736635T > C (rs975050638)] significantly increased the transcriptional activity of the TFEB gene promoter ($P < 0.01$). The SNP [g.41736987C > T (rs760293138)] significantly decreased the transcriptional activity of the TFEB gene promoter ($P < 0.01$). These results indicated that the regulatory variants identified in AMI patients altered the transcriptional activity of the TFEB gene promoter. In contrast, the regulatory variants only identified in controls [g.41737451T > G, g.41737005G > A (rs149166358), g.41736981A > G, g.41736407C > T, and g.41736218T > G] or both AMI patients and controls [g.41737034G > C (rs73733015) and g.41737034G > A

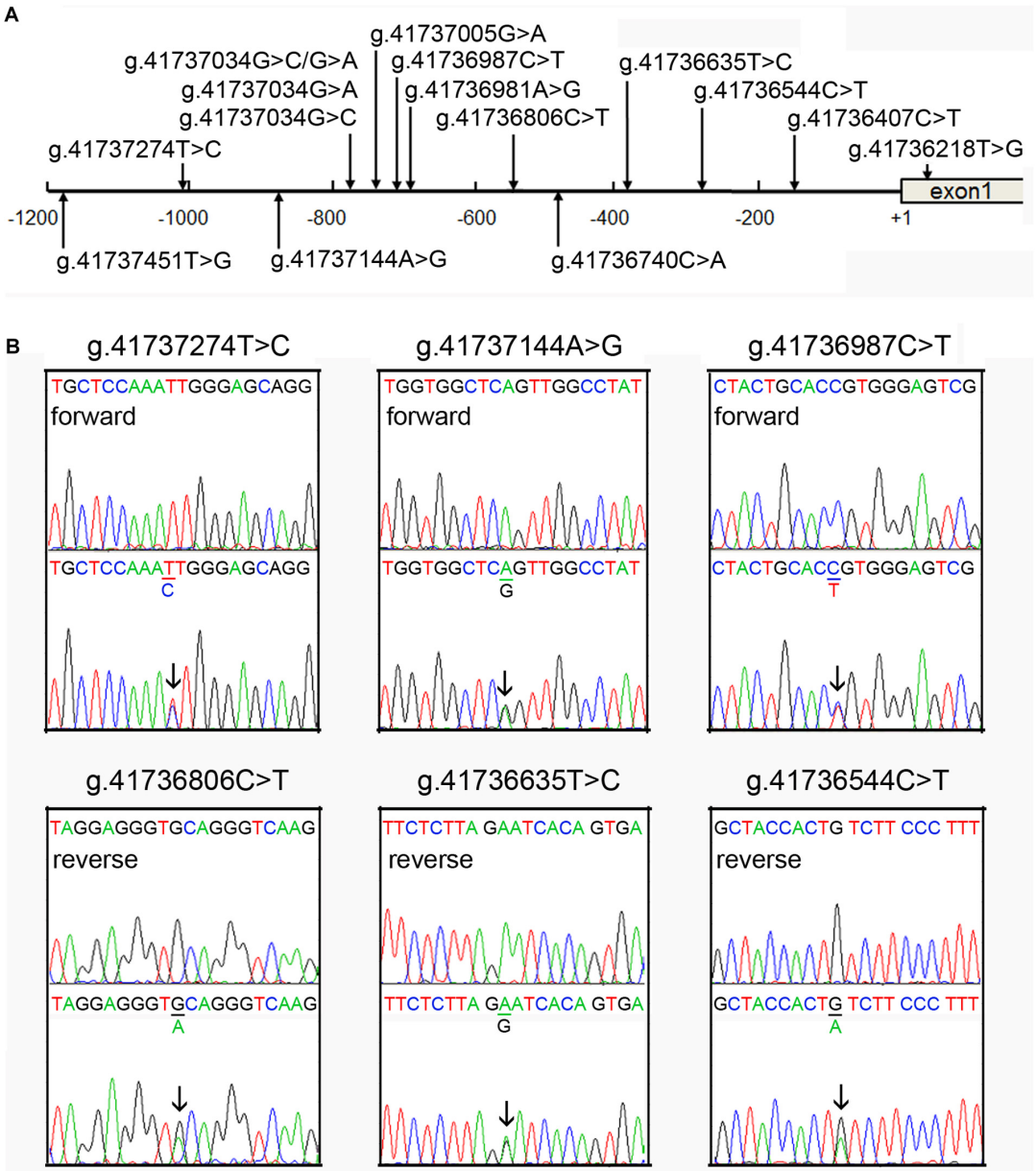

FIGURE 1 | Identified regulatory variants of TFEB gene. **(A)** Locations of the regulatory variants in the TFEB gene promoter. The numbers represent the genomic DNA sequences of the human TFEB gene (Genbank accession number NC_000006.12). The transcription start site is at the position of 41736259 (+1) in the first exon. **(B)** Sequencing chromatograms of the regulatory variants identified in AMI patients. Sequence orientations are marked. Top panels show wild-type and bottom heterozygous DNA sequences. Arrows indicate the heterozygous variant.

(rs73733015)] did not alter the transcriptional activity of the TFEB gene promoter ($P > 0.05$) (**Figure 2**).

As human cardiomyocyte cell lines are currently not available, the H9c2 rat cardiomyocyte cell line was used. Similar results to that in HEK-293 cells were obtained in H9c2 cells. Two variants (g.41737144A > G and g.41736544C > T) and three SNPs [g.41737274T > C (rs533895008), g.41736806C > T (rs748537297), and g.41736635T > C (rs975050638)] significantly increased the transcriptional activity of the TFEB gene promoter ($P < 0.01$), and the SNP [g.41736987C > T (rs760293138)] significantly decreased the transcriptional activity of the TFEB gene promoter ($P < 0.01$) (**Figure 2**).

Regulatory Variant-Affected Binding Sites of Transcription Factors

The binding sites for transcription factors were predicted to be changed by regulatory variants identified in AMI patients. SNP [g.41737274T > C (rs533895008)] may abolish putative binding sites for YB1 (Y-box binding protein 1), MEF2C (myocyte

TABLE 2 | Regulatory variants of TFEB gene in AMI patients and controls.

Regulatory variants	Genotypes	Location†	Controls (*n* = 337)	AMI (*n* = 352)	*P*-value
g.41737451T > G	TG	−1192 bp	1	0	–
g.41737274T > C (rs533895008)	TC	−1015 bp	0	1	–
g.41737144A > G	AG	−885 bp	0	1	–
g.41737034G > C (rs73733015)	GG	−775 bp	209	196	0.239
	GC		111	136	
	CC		17	20	
g.41737034G > A (rs73733015)	GA	−775 bp	1	1	1
g.41737034G > C/G > A (rs73733015)	CA	−775 bp	1	0	–
g.41737005G > A (rs149166358)	GA	−746 bp	1	0	–
g.41736987C > T (rs760293138)	CT	−728 bp	0	1	–
g.41736981A > G	AG	−722 bp	1	0	–
g.41736806C > T (rs748537297)	CT	−547 bp	0	1	–
g.41736740C > A	CA	−481 bp	1	1	1
g.41736635T > C (rs975050638)	TC	−376 bp	0	1	–
g.41736544C > T	CT	−285 bp	0	1	–
g.41736407C > T	CT	−148 bp	1	0	–
g.41736218T > G	TG	+42 bp	1	0	–

†, *variants are located upstream (–) to the transcription start site of TFEB gene at 41736259 (NC_000006.12).*

TABLE 3 | Clinical and biochemical characteristics of the AMI patients carrying TFEB gene regulatory variants.

Patient no.	Regulatory variant	Sex	Age (years)	TG (mmol/L)	TC (mmol/L)	HDL (mmol/L)	LDL (mmol/L)
1	g.41737274T > C (rs533895008)	M	56	0.84	5.20	1.41	3.20
2	g.41737144A > G	M	66	1.38	3.60	0.80	2.40
3	g.41736987C > T	M	62	1.26	2.83	1.38	2.30
4	g.41736806C > T	M	81	0.94	3.02	1.28	1.60
5	g.41736635T > C (rs975050638)	M	63	1.79	3.99	0.85	2.60
6	g.41736544C > T	M	52	1.36	5.25	0.93	3.60

enhancer factor 2C), and MEF2D, and create putative binding sites for MYB (MYB proto-oncogene and transcription factor) and TFCP2 (transcription factor CP2 and also known as LBP1). Variant (g.41737144A > G) may modify the binding site for MYB and the DNA-binding complex of BRCA1 and USF2. The SNP [g.41736987C > T (rs760293138)] may modify the binding sites for SOX18, ZNF75D (zinc finger factor 75D), and ZNF143 factors. SNP [g.41736806C > T (rs748537297)] may abolish the binding sites for SMAD5 (SMAD family member 5), HSF4 (heat shock transcription factor 4), and KLF8 (kruppel-like factor 8), create a germ cell-specific transcription factor ALF-binding site, and modify a KLF6 (kruppel-like factor 6, also known as CPBP) site. SNP [g.41736635T > C (rs975050638)] may abolish a C-MAF (MAF bZIP transcription factor) site, create a RHOXF1 (Rhox homeobox family member 1) site, and modify the binding sites for GATA factors. Variant (g.41736544C > T) may abolish the binding sites for SMAD2 (SMAD family member 2) and P300 and create the binding sites for GATA factors.

Transcription Factor Binding as Determined by EMSA

To experimentally investigate whether regulatory variants affected the binding of transcription factors, EMSA was performed with wild-type or variant oligonucleotides (30 bp). The regulatory variants identified in AMI patients were examined. Biotinylated oligonucleotides for the EMSA are shown in **Table 4**. As shown in **Figure 3**, the SNP [g.41737274T > C (rs533895008)] abolish the binding of a transcription factor and created a binding site for a new transcription factor. One variant (g.41737144A > G and one SNP [g.41736987C > T (rs760293138)] markedly enhanced the binding of an unknown transcription factor in HEK-293 and H9c2 cells. The affected transcription factor, which acted as a transcriptional activator, requires further identification. The variant (g.41736544C > T) did not affect the binding of transcription factors. Similarly, the effects of other two SNPs [g.41736806C > T (rs748537297) and g.41736635T > C (rs975050638)] on the binding of transcription factors were not detected (data not shown).

DISCUSSION

To date, many genome-wide association studies have identified a great number of genetic loci for CAD and AMI. However, the collective genetic loci could explain only <10% of cases (Assimes and Roberts, 2016; McPherson and Tybjaerg-Hansen, 2016). Recent studies have suggested that low-frequency and rare genetic variants may confer susceptibility to cardiovascular diseases (Wain, 2014; Sazonovs and Barrett, 2018). Altered

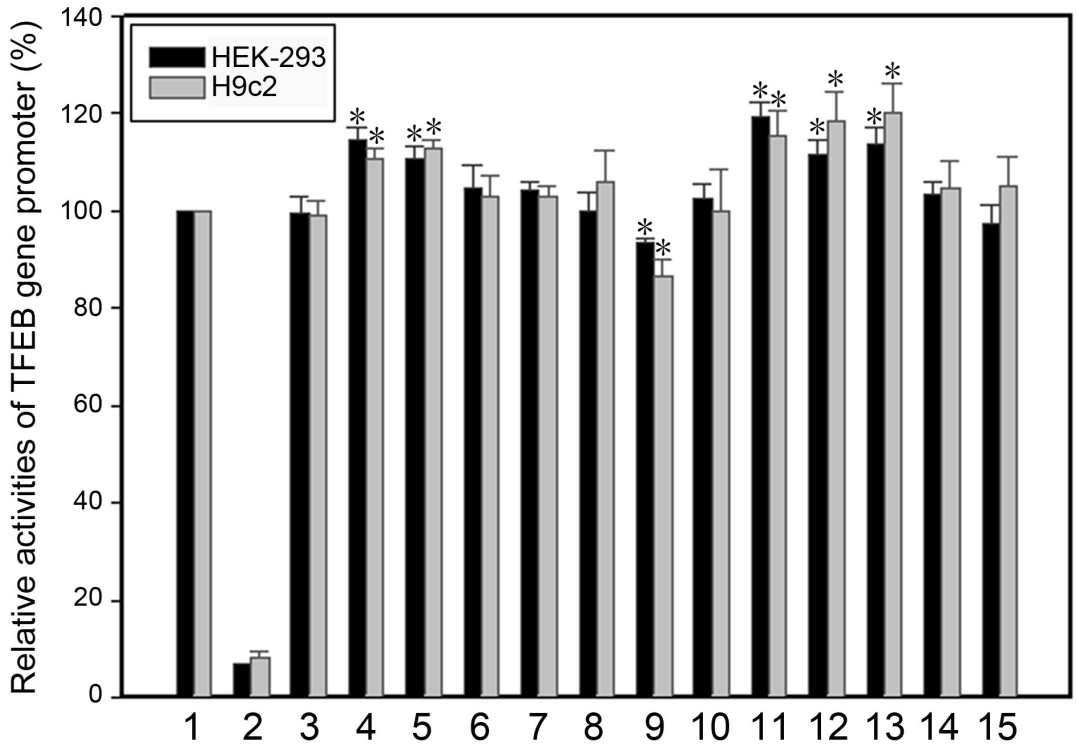

FIGURE 2 | Relative transcriptional activity of wild-type and variant TFEB gene promoters in HEK-293 cells and H9c2 cells. Black bars indicate HEK-293 cells and gray bars H9c2 cells. Empty vector pGL3-basic was used as a negative control. Transcriptional activity of the wild-type TFEB gene promoter was designed as 100%. The relative activity of variant TFEB gene promoters was calculated. Lanes 1, pGL3-WT; 2, pGL3-basic; 3, pGL3-41377451G; 4, pGL3-41737274C; 5, pGL3-41737144G; 6, pGL3-41737034A; 7, pGL3-41737034C; 8, pGL3-41737005A; 9, pGL3-41736987T; 10, pGL3-41736981G; 11, pGL3-41736806T; 12, pGL3-41736635C; 13, pGL3-41736544T; 14, pGL3-41736407T; 15, pGL3-41736218G. WT, wild type. *, $P < 0.01$.

TABLE 4 | The double-stranded biotinylated oligonucleotides for the EMSA.

Variants	Oligonucleotide sequences	Locations
g.41737274T > C	5′-CTGATCTGCTCCAAA (**T/C**)TGGGAGCAGGAGGG-3′	41737289
g.41737144A > G	5′-CTGCTCTGGTGGCTC (**A/G**)GTTGGCCTATGAGC-3′	41737159
g.41736987C > T	5′-CAACGGCTACTGCAC (**C/T**)GTGGGAGTCGAGCC-3′	41737002
g.41736806C > T	5′-TTCCTCTTGACCCTG (**C/T**)ACCCTCCTAGGGCA-3′	41736821
g.41736635T > C	5′-GTGGGTCACTGTGAT (**T/C**)CTAAGAGAAATGGG-3′	41736650
g.41736544C > T	5′-CCTGGAAAGGGAAGA (**C/T**)AGTGGTAGCGCCAT-3′	41736559

TFEB gene expression and subsequent dysfunctional autophagic-lysosomal system have been implicated in human diseases, including cardiovascular diseases (Kuiper et al., 2003; Shen and Mizushima, 2014; Perera et al., 2015; Martini-Stoica et al., 2016). However, TFEB gene expression and regulation have not been characterized in detail. Few mutations or genetic variants in TFEB gene have been reported. In this study, we identified fifteen regulatory variants in the TFEB gene promoter. Among these, six regulatory variants including four SNPs of TFEB gene were identified in AMI patients, which significantly altered the transcriptional activity of the TFEB gene promoter. Three of the regulatory variants evidently affected the binding of unknown transcription factors. In our study population (n = 689), TFEB gene regulatory variants were identified in AMI patients with a collective frequency of 0.9% (6/689). Therefore, these TFEB gene regulatory variants may contribute to AMI development as a rare risk factor. In our future work, the effect of downstream autophagic and lysosomal genes of TFEB on AMI will be further explored.

The human TFEB gene has been localized to chromosome 6p21.1. TFEB recognizes the CLEAR motif within its target genes (Carr and Sharp, 1990; Bajaj et al., 2019). TFEB-null mice die at the embryonic stage due to defective placental vascularization (Steingrímsson et al., 1998). Conditional disruption or transgenic mouse models reveal that TFEB has specialized functions in different tissues (Pastore et al., 2016; Perera and Zoncu, 2016; Mansueto et al., 2017; Sergin et al., 2017; Fan et al., 2018). There are five transcript variants of TFEB, and variant two encodes the longest-isoform, promoter region of which was analyzed in this study. To date, the promoter of the human TFEB gene has not been characterized in details. A proximal TFEB gene promoter of 1,600 bp has been reported for its transcriptional activity (Erlich et al., 2018). In human endothelial cells, paternally expressed gene 3 (PEG3) is an upstream transcriptional regulator

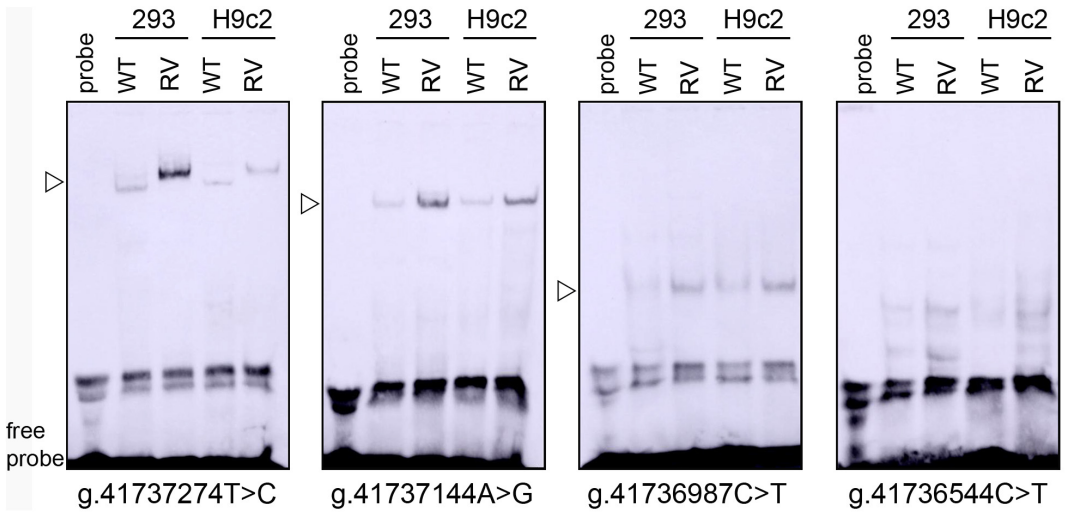

FIGURE 3 | EMSA of biotin-labeled oligonucleotide-containing regulatory variants with nuclear extracts of HEK-293 (293) and H9c2 cells. Free probe was marked at the bottom. The affected binding for an unknown transcription factor was marked with an open arrow. WT, wild type. RV, regulatory variants.

of the TFEB gene (Neill et al., 2017). There are numerous CLEAR sequences in the TFEB gene promoter, indicating that TFEB regulates its own expression in an autoregulatory loop (Settembre et al., 2013; Nabar and Kehrl, 2017). In response to starvation, TFEB upregulation activates its own transcription, indicating a positive feedback loop that regulates cellular lipid metabolism (Settembre et al., 2013). In this study, we analyzed the proximal promoter of the TFEB gene. The regulatory variants were identified, all of which did not interrupt any CLEAR motif in the TFEB gene promoter. Combined with transcriptional activity assay and EMSA results, SNP [g.41737274T > C (rs533895008)] may create a binding site for a transcription activator. The variants (g.41737144A > G and g.41736544C > T) may enhance the binding of a transcription activator. SNP [g.41736987C > T (rs760293138)] may enhance the binding of a transcription repressor. These transcription factors need to be further identified and investigated.

Under normal conditions, TFEB is located in the cytoplasm. The subcellular localization and activity of TFEB are regulated by its phosphorylation state. TFEB phosphorylation is mediated by several kinases, including mammalian target of rapamycin complex 1 (mTORC1), extracellular signal–regulated kinase 2 (ERK2), glycogen synthase kinase-3β (GSK-3β), and AKT (protein kinase B) (Martina et al., 2012; Settembre et al., 2012; Li et al., 2016; Napolitano and Ballabio, 2016; Palmieri et al., 2017; Vega-Rubin-de-Celis et al., 2017; Puertollano et al., 2018). Protein phosphatase 2A stimulates activation of TFEB by dephosphorylation in response to oxidative stress (Martina and Puertollano, 2018). Phosphorylated TFEB is retained in the cytoplasm, whereas dephosphorylated TFEB translocates to the nucleus to induce the transcription of its target genes. A great number of TFEB direct genes have been identified, which represent essential components of the CLEAR gene network (Palmieri et al., 2011; Perera and Zoncu, 2016). TFEB promotes the gene expression of the autophagy and lysosomes and regulates the lysosomal biogenesis, autophagy, lysosomal proteostasis, lysosomal exocytosis, and lysosomal positioning (Medina et al., 2011; Song et al., 2013; Napolitano and Ballabio, 2016; Perera and Zoncu, 2016; Willett et al., 2017). Moreover, TFEB and TFE3 cooperate in regulating the expression of proinflammatory cytokine genes, controlling the adaptive response of whole-body energy metabolism, and modulating the cellular response to endoplasmic reticulum stress (Martina et al., 2016; Pastore et al., 2016, 2017). Therefore, upregulation or downregulation of TFEB gene expression may lead to dysfunctional autophagy.

Accumulating studies have demonstrated that a window of optimal autophagic activity is critical to the maintenance of cardiovascular homeostasis and function. Excessive or insufficient levels of autophagic flux can each contribute to the pathogenesis of cardiovascular diseases, including AMI (Gatica et al., 2015; Lavandero et al., 2015; Bravo-San Pedro et al., 2017). TFEB is differentially activated in human diseases. In Danon disease, TFEB and downstream targets are activated. Conversely, TFEB is inhibited and an autophagy is blocked in glycogen storage disease type II (Nascimbeni et al., 2017). In this study, the six TFEB gene regulatory variants may lead to TFEB gene upregulation or downregulation, both of which could result in subsequent autophagic dysfunction, contributing to AMI development as a rare risk factor.

In conclusion, fifteen regulatory variants in the TFEB gene promoter were identified in this study, and seven were novel. Among these, six functional regulatory variants in the TFEB gene promoter were identified in AMI patients. Functional analysis revealed that these genetic variants significantly altered the transcriptional activity of the TFEB gene by changing the binding site of unknown transcription factors. These TFEB gene regulatory variants may contribute to AMI development as a rare risk factor. Further studies are needed to investigate these unknown transcription factors and related mechanisms.

DATA AVAILABILITY STATEMENT

The raw data supporting the conclusions of this article will be made available by the authors, without undue reservation.

ETHICS STATEMENT

The studies involving human participants were reviewed and approved by the Human Ethics Committee of the Affiliated Hospital of Jining Medical University. The patients/participants provided their written informed consent to participate in this study.

AUTHOR CONTRIBUTIONS

JZ and BY conceived and designed the experiments and wrote the manuscript. JZ, YZ, XH, and SW performed the experiments. JZ and SP analyzed the data. All authors have read and agreed to the published version of the manuscript.

FUNDING

This research was funded Shandong Taishan Scholar Program, China, grant number tshw201502063.

REFERENCES

Assimes, T. L., and Roberts, R. (2016). Genetics: implications for prevention and management of coronary artery disease. *J. Am. Coll. Cardiol.* 68, 2797–2818. doi: 10.1016/j.jacc.2016.10.039

Bajaj, L., Lotfi, P., Pal, R., Ronza, A. D., Sharma, J., and Sardiello, M. (2019). Lysosome biogenesis in health and disease. *J. Neurochem.* 148, 573–589. doi: 10.1111/jnc.14564

Brady, O. A., Martina, J. A., and Puertollano, R. (2018). Emerging roles for TFEB in the immune response and inflammation. *Autophagy* 14, 181–189. doi: 10.1080/15548627.2017.1313943

Bravo-San Pedro, J. M., Kroemer, G., and Galluzzi, L. (2017). Autophagy and mitophagy in cardiovascular disease. *Circ. Res.* 120, 1812–1824. doi: 10.1161/CIRCRESAHA.117.311082

Carr, C. S., and Sharp, P. A. (1990). A helix-loop-helix protein related to the immunoglobulin E box-binding proteins. *Mol. Cell Biol.* 10, 4384–4388. doi: 10.1128/MCB.10.8.4384

Doronzo, G., Astanina, E., Corà, D., Chiabotto, G., Comunanza, V., Noghero, A., et al. (2019). TFEB controls vascular development by regulating the proliferation of endothelial cells. *EMBO J.* 38:e98250. doi: 10.15252/embj.201798250

Erlich, A. T., Brownlee, D. M., Beyfuss, K., and Hood, D. A. (2018). Exercise induces TFEB expression and activity in skeletal muscle in a PGC-1α-dependent manner. *Am. J. Physiol. Cell Physiol.* 314, C62–C72. doi: 10.1152/ajpcell.00162.2017

Fan, Y., Lu, H., Liang, W., Garcia-Barrio, M. T., Guo, Y., Zhang, J., et al. (2018). Endothelial TFEB (Transcription Factor EB) positively regulates postischemic angiogenesis. *Circ. Res.* 122, 945–957. doi: 10.1161/CIRCRESAHA.118.312672

Gatica, D., Chiong, M., Lavandero, S., and Klionsky, D. J. (2015). Molecular mechanisms of autophagy in the cardiovascular system. *Circ. Res.* 116, 456–467. doi: 10.1161/CIRCRESAHA.114.303788

Kuiper, R. P., Schepens, M., Thijssen, J., van Asseldonk, M., van den Berg, E., Bridge, J., et al. (2003). Upregulation of the transcription factor TFEB in t(6;11)(p21;q13)-positive renal cell carcinomas due to promoter substitution. *Hum. Mol. Genet.* 12, 1661–1669. doi: 10.1093/hmg/ddg178

Lavandero, S., Chiong, M., Rothermel, B. A., and Hill, J. A. (2015). Autophagy in cardiovascular biology. *J. Clin. Invest.* 125, 55–64. doi: 10.1172/JCI73943

Li, Y., Xu, M., Ding, X., Yan, C., Song, Z., Chen, L., et al. (2016). Protein kinase C controls lysosome biogenesis independently of mTORC1. *Nat. Cell Biol.* 18, 1065–1077. doi: 10.1038/ncb3407

Lu, H., Fan, Y., Qiao, C., Liang, W., Hu, W., Zhu, T., et al. (2017). TFEB inhibits endothelial cell inflammation and reduces atherosclerosis. *Sci Signal.* 10:eaah4214. doi: 10.1126/scisignal.aah4214

Mansueto, G., Armani, A., Viscomi, C., D'Orsi, L., De Cegli, R., Polishchuk, E. V., et al. (2017). Transcription factor EB controls metabolic flexibility during exercise. *Cell Metab.* 25, 182–196. doi: 10.1016/j.cmet.2016.11.003

Martina, J. A., Chen, Y., Gucek, M., and Puertollano, R. (2012). MTORC1 functions as a transcriptional regulator of autophagy by preventing nuclear transport of TFEB. *Autophagy* 8, 903–914. doi: 10.4161/auto.19653

Martina, J. A., Diab, H. I., Brady, O. A., and Puertollano, R. (2016). TFEB and TFE3 are novel components of the integrated stress response. *EMBO J.* 35, 479–495. doi: 10.15252/embj.201593428

Martina, J. A., and Puertollano, R. (2018). Protein phosphatase 2A stimulates activation of TFEB and TFE3 transcription factors in response to oxidative stress. *J. Biol. Chem.* 293, 12525–12534. doi: 10.1074/jbc.RA118.003471

Martini-Stoica, H., Xu, Y., Ballabio, A., and Zheng, H. (2016). The autophagy-lysosomal pathway in neurodegeneration: a TFEB perspective. *Trends Neurosci.* 39, 221–234. doi: 10.1016/j.tins.2016.02.002

McPherson, R., and Tybjaerg-Hansen, A. (2016). Genetics of coronary artery disease. *Circ. Res.* 118, 564–578. doi: 10.1161/CIRCRESAHA.115.306566

Medina, D. L., Fraldi, A., Bouche, V., Annunziata, F., Mansueto, G., Spampanato, C., et al. (2011). Transcriptional activation of lysosomal exocytosis promotes cellular clearance. *Dev. Cell* 21, 421–430. doi: 10.1016/j.devcel.2011.07.016

Nabar, N. R., and Kehrl, J. H. (2017). The transcription factor EB links cellular stress to the immune response. *Yale J. Biol. Med.* 90, 301–315.

Napolitano, G., and Ballabio, A. (2016). TFEB at a glance. *J. Cell Sci.* 129, 2475–2481. doi: 10.1242/jcs.146365

Nascimbeni, A. C., Fanin, M., Angelini, C., and Sandri, M. (2017). Autophagy dysregulation in danon disease. *Cell Death Dis.* 8:e2565. doi: 10.1038/cddis.2016.475

Neill, T., Sharpe, C., Owens, R. T., and Iozzo, R. V. (2017). Decorin-evoked paternally expressed gene 3 (PEG3) is an upstream regulator of the transcription factor EB (TFEB) in endothelial cell autophagy. *J. Biol. Chem.* 292, 16211–16220. doi: 10.1074/jbc.M116.769950

Palmieri, M., Impey, S., Kang, H., di Ronza, A., Pelz, C., Sardiello, M., et al. (2011). Characterization of the CLEAR network reveals an integrated control of cellular clearance pathways. *Hum. Mol. Genet.* 20, 3852–3866. doi: 10.1093/hmg/ddr306

Palmieri, M., Pal, R., Nelvagal, H. R., Lotfi, P., Stinnett, G. R., Seymour, M. L., et al. (2017). mTORC1-independent TFEB activation via Akt inhibition promotes cellular clearance in neurodegenerative storage diseases. *Nat. Commun.* 8:14338. doi: 10.1038/ncomms14338

Pastore, N., Brady, O. A., Diab, H. I., Martina, J. A., Sun, L., Huynh, T., et al. (2016). TFEB and TFE3 cooperate in the regulation of the innate immune response in activated macrophages. *Autophagy* 12, 1240–1258. doi: 10.1080/15548627.2016.1179405

Pastore, N., Vainshtein, A., Klisch, T. J., Armani, A., Huynh, T., Herz, N. J., et al. (2017). TFE3 regulates whole-body energy metabolism in cooperation with TFEB. *EMBO Mol. Med.* 9, 605–621. doi: 10.15252/emmm.201607204

Perera, R. M., Stoykova, S., Nicolay, B. N., Ross, K. N., Fitamant, J., Boukhali, M., et al. (2015). Transcriptional control of autophagy-lysosome function drives pancreatic cancer metabolism. *Nature* 524, 361–365. doi: 10.1038/nature14587

Perera, R. M., and Zoncu, R. (2016). The lysosome as a regulatory hub. *Annu. Rev. Cell Dev. Biol.* 32, 223–253. doi: 10.1146/annurev-cellbio-111315-125125

Puertollano, R., Ferguson, S. M., Brugarolas, J., and Ballabio, A. (2018). The complex relationship between TFEB transcription factor phosphorylation and subcellular localization. *EMBO J.* 37:e98804. doi: 10.15252/embj.201798804

Sardiello, M., Palmieri, M., di Ronza, A., Medina, D. L., Valenza, M., Gennarino, V. A., et al. (2009). A gene network regulating lysosomal biogenesis and function. *Science* 325, 473–477. doi: 10.1126/science.1174447

Sazonovs, A., and Barrett, J. C. (2018). Rare-variant studies to complement genome-wide association studies. *Annu. Rev. Genomics Hum. Genet.* 19, 97–112. doi: 10.1146/annurev-genom-083117-021641

Sergin, I., Evans, T. D., Zhang, X., Bhattacharya, S., Stokes, C. J., Song, E., et al. (2017). Exploiting macrophage autophagy-lysosomal biogenesis as a therapy for atherosclerosis. *Nat. Commun.* 8:15750. doi: 10.1038/ncomms15750

Settembre, C., and Ballabio, A. (2014). Lysosome: regulator of lipid degradation pathways. *Trends Cell Biol.* 24, 743–750. doi: 10.1016/j.tcb.2014.06.006

Settembre, C., De Cegli, R., Mansueto, G., Saha, P. K., Vetrini, F., Visvikis, O., et al. (2013). TFEB controls cellular lipid metabolism through a starvation-induced autoregulatory loop. *Nat. Cell Biol.* 15, 647–658. doi: 10.1038/ncb2718

Settembre, C., Di Malta, C., Polito, V. A., Garcia Arencibia, M., Vetrini, F., Erdin, S., et al. (2011). TFEB links autophagy to lysosomal biogenesis. *Science* 332, 1429–1433. doi: 10.1126/science.1204592

Settembre, C., Zoncu, R., Medina, D. L., Vetrini, F., Erdin, S., Erdin, S., et al. (2012). A lysosome-to-nucleus signalling mechanism senses and regulates the lysosome via mTOR and TFEB. *EMBO J.* 31, 1095–1108. doi: 10.1038/emboj.2012.32

Shen, H. M., and Mizushima, N. (2014). At the end of the autophagic road: an emerging understanding of lysosomal functions in autophagy. *Trends Biochem. Sci.* 39, 61–71. doi: 10.1016/j.tibs.2013.12.001

Song, W., Wang, F., Savini, M., Ake, A., di Ronza, A., Sardiello, M., et al. (2013). TFEB regulates lysosomal proteostasis. *Hum. Mol. Genet.* 22, 1994–2009. doi: 10.1093/hmg/ddt052

Song, W., Zhang, C. L., Gou, L., He, L., Gong, Y. Y., Qu, D., et al. (2019). Endothelial TFEB (Transcription Factor EB) Restrains IKK (IκB Kinase)-p65 pathway to attenuate vascular inflammation in diabetic db/db mice. *Arterioscler. Thromb. Vasc. Biol.* 39, 719–730. doi: 10.1161/ATVBAHA.119.312316

Steingrímsson, E., Tessarollo, L., Reid, S. W., Jenkins, N. A., and Copeland, N. G. (1998). The bHLH-Zip transcription factor Tfeb is essential for placental vascularization. *Development* 125, 4607–4616.

Vega-Rubin-de-Celis, S., Peña-Llopis, S., Konda, M., and Brugarolas, J. (2017). Multistep regulation of TFEB by MTORC1. *Autophagy* 13, 464–472. doi: 10.1080/15548627.2016.1271514

Wain, L. V. (2014). Rare variants and cardiovascular disease. *Brief. Funct. Genomics* 13, 384–391. doi: 10.1093/bfgp/elu010

Willett, R., Martina, J. A., Zewe, J. P., Wills, R., Hammond, G. R. V., and Puertollano, R. (2017). TFEB regulates lysosomal positioning by modulating TMEM55B expression and JIP4 recruitment to lysosomes. *Nat. Commun.* 8:1580. doi: 10.1038/s41467-017-01871-z

Conflict of Interest: The authors declare that the research was conducted in the absence of any commercial or financial relationships that could be construed as a potential conflict of interest.

frontiers in Cell and Developmental Biology

REVIEW
published: 04 March 2021
doi: 10.3389/fcell.2021.644363

Hyperphosphatemia and Cardiovascular Disease

Chao Zhou[1], Zhengyu Shi[1], Nan Ouyang[2] and Xiongzhong Ruan[3,4]**

[1] Department of Cardiology, The First Affiliated Hospital of Chongqing Medical University, Chongqing, China, [2] Department of Nephrology, The First Affiliated Hospital of Chongqing Medical University, Chongqing, China, [3] John Moorhead Research Laboratory, Centre for Nephrology, University College London (UCL) Medical School, London, United Kingdom, [4] Centre for Lipid Research and Key Laboratory of Molecular Biology for Infectious Diseases (Ministry of Education), Institute for Viral Hepatitis, Department of Infectious Diseases, The Second Affiliated Hospital, Chongqing Medical University, Chongqing, China

Hyperphosphatemia or even serum phosphate levels within the "normal laboratory range" are highly associated with increased cardiovascular disease risk and mortality in the general population and patients suffering from chronic kidney disease (CKD). As the kidney function declines, serum phosphate levels rise and subsequently induce the development of hypertension, vascular calcification, cardiac valvular calcification, atherosclerosis, left ventricular hypertrophy and myocardial fibrosis by distinct mechanisms. Therefore, phosphate is considered as a promising therapeutic target to improve the cardiovascular outcome in CKD patients. The current therapeutic strategies are based on dietary and pharmacological reduction of serum phosphate levels to prevent hyperphosphatemia in CKD patients. Large randomized clinical trials with hard endpoints are urgently needed to establish a causal relationship between phosphate excess and cardiovascular disease (CVD) and to determine if lowering serum phosphate constitutes an effective intervention for the prevention and treatment of CVD.

Keywords: phosphate, cardiovascular disease, vascular calcification, cardiac valvular calcification, atherosclerosis, left ventricular hypertrophy, myocardial fibrosis, hypertension

OPEN ACCESS

Edited by:
Xiaoqiang Tang,
Sichuan University, China

Reviewed by:
Dongdong Sun,
Xijing Hospital, Fourth Military Medical University, China
Xiaozhen Dai,
Chengdu Medical College, China

****Correspondence:***
Nan Ouyang
ouyangnan930@hotmail.com
Xiongzhong Ruan
x.ruan@ucl.ac.uk

Specialty section:
This article was submitted to Cellular Biochemistry, a section of the journal Frontiers in Cell and Developmental Biology

Received: *21 December 2020*
Accepted: *08 February 2021*
Published: *04 March 2021*

Citation:
Zhou C, Shi Z, Ouyang N and Ruan X (2021) Hyperphosphatemia and Cardiovascular Disease. Front. Cell Dev. Biol. 9:644363. doi: 10.3389/fcell.2021.644363

INTRODUCTION

High serum phosphate concentrations associate with cardiovascular disease (CVD) risk in both the general population and chronic kidney disease (CKD) patients (Lim et al., 2015; Reiss et al., 2018). Serum phosphate levels are tightly regulated in healthy individuals through several mechanisms including dietary absorption, bone flux and renal excretion. Hyperphosphatemia occurs due to a decreasing glomerular filtration rate (GFR) and is known to induce hypertension, vascular calcification, cardiac valvular calcification, atherosclerosis, left ventricular hypertrophy, and myocardial fibrosis (Chronic Kidney, Disease Prognosis, Consortium, Matsushita et al., 2010; Sarnak et al., 2019). In this review, we summarize the current knowledge of the roles of phosphate homeostasis in health and CKD conditions, as well as the contribution of phosphate to CVD. Moreover, we discuss therapeutic strategies for lowering serum phosphate level and how this affects the cardiovascular outcome of CKD patients.

BIOLOGICAL CHARACTERISTICS OF PHOSPHATE

Phosphorus is an essential element of the human body. Organic phosphorus mainly exists in nucleic acid, phospholipid and high-energy phosphate compounds (Michigami et al., 2018). Phosphorus is one of the basic components of human genetic material nucleic acid, participating in genetic metabolism, growth, and development (Kornberg, 1979). The phospholipid is the main lipid component on the cell membrane, maintaining the integrity and permeability of membrane (Tero et al., 2017). High energy phosphate compounds such as adenosine triphosphate (ATP) are key substances of energy metabolism (Müller et al., 2017). Inorganic phosphorus exists in the form of inorganic phosphate ion H2PO4- or HPO42-. In the physiological pH state, 80% inorganic phosphate ion in the serum is HPO42- and 20% is H2PO4-. About 10% inorganic phosphorus exists in serum as soluble phosphate, which participates in the phosphorylation and dephosphorylation of various signal transduction proteins. Phosphate buffering also participates in the regulation of acid-base balance *in vivo*. A total of 90% inorganic phosphorus exists in bones and teeth in insoluble hydroxyapatite, forming the skeleton of the body. The body contains about 600–900 g phosphorus, accounting for about 1% of body weight. Serum phosphorus refers to the concentration of serum inorganic phosphate, which is 3–4.5 mg/dL in normal adults. Hyperphosphatemia is defined as plasma phosphate >4.5 mg/dL due to disease or excessive intake. Excessive phosphate content not only causes hypocalcemia, hyperparathyroidism and metabolic bone disease but also is closely related to adverse cardiovascular outcomes (Angelova et al., 2016; Chande and Bergwitz, 2018).

METABOLIC REGULATION OF PHOSPHATE

The organs involved in phosphate regulation include intestine, bone, kidney, and parathyroid gland. The daily intake of dietary phosphate is about 1.0–1.5 g, which is absorbed by the intestinal epithelial cell type II sodium-dependent phosphate co-transporter (Npt)-2a, 2b, and 2c (Masuda et al., 2020). The phosphate absorbed from the intestine is mainly excreted through the kidney. About 80% of the phosphate is reabsorbed through Npt- 2a and 2c in the proximal renal tubular epithelium (Michigami et al., 2018). The key endocrine hormonal regulators of phosphate metabolism include fibroblast growth factor-23 (FGF-23), 1,25-dihydroxyvitamin D (calcitriol), and parathyroid hormone (PTH). FGF-23 is the first discovered bone-derived endocrine hormone, contains a 32 kd peptide chain of 251 amino acids and belongs to the FGF superfamily. Phosphate excess can directly or indirectly stimulate osteoblasts to secrete FGF-23, which regulates phosphate metabolism by affecting the activity of Npt-2 (Sabbagh et al., 2009). FGF homologous receptors (FGFR), including FGFR 1-4, mainly bind to FGF-23 and its co-receptor α-Klotho, effectively activating FGFR 1c to form FGF-23- FGFR 1-α-Klotho ternary complex, lead to activation of mitogen-activated protein kinase (MAPK) pathway, and result in inhibition of Npt-2a and 2c in phosphorus reabsorption in renal tubular epithelial cells. It can also inhibit renal 1α-hydroxylase, reducing the serum calcitriol mediated increment of blood phosphate. Calcitriol receptor is mainly expressed in the small intestine, bone, kidney, and parathyroid gland. Its physiological effect is to increase blood phosphate and calcium. In the small intestine, calcitriol increases the absorption of phosphate by up-regulating the activity of Npt-2 in intestinal epithelial cells (Takashi and Fukumoto, 2020a). Binding of phosphorus to the calcium-sensitive receptor (CaSR) on parathyroid cells stimulates parathyroid hormone (PTH) secretion (Centeno et al., 2019). The target organs of PTH are mainly kidney and bone, and its net effect is to increase blood calcium and reduce blood phosphate. PTH promotes the reabsorption of Ca^{2+} by distal convoluted tubules and collecting ducts, reducing calcium excretion. On the other hand, PTH inhibits the reabsorption of phosphorus in proximal and distal tubules by blocking Npt-2a and 2c, promoting phosphorus excretion and reducing blood phosphate. PTH also activates 1α- hydroxylase in mitochondria of proximal renal tubular cells and facilitates the formation of calcitriol, which indirectly promotes the absorption of calcium and phosphate by intestinal epithelial cells. Moreover, PTH activates osteoclast, enhances its osteolytic effect and releases calcium and phosphorus. In osteoblasts, the binding of PTH to PTH-related protein receptor (PPR) 1 promotes FGF-23 secretion by activating protein kinase A (PKA) and Wnt signaling (Chande and Bergwitz, 2018). In addition, serum iron, erythropoietin (EPO) and insulin-like growth factor-1 (IGF-1) are also involved in the regulation of phosphate. Iron deficiency may promote FGF-23 synthesis through transcriptional regulation of hypoxia-inducible factor (HIF) 1α (Tan et al., 2017). EPO can induce the expression of FGF-23 mRNA in bone marrow erythroid cells (van Vuren et al., 2020). IGF-1 inhibits transcription factor FoxO1 of FGF-23 through phosphatidylinositol 3-kinase (PI3K)/Akt pathway, and negatively regulates FGF-23 (Bär et al., 2018).

THE ROLE OF PHOSPHATE IN CVD

High serum phosphate level is independently associated with increased cardiovascular mortality in CKD patients by contributing to the development of CVD via distinct mechanisms (**Table 1**). Thus, phosphate is considered as a therapeutic target to improve CKD-associated CVD morbidity, and a detailed understanding of the molecular insight of hyperphosphatemia in the development of CVD is essential to explore effective therapeutic strategies.

Hypertension

An increasing number of publications has revealed a detrimental role of inorganic phosphate in promoting hypertension in otherwise healthy individuals. Cross-sectional studies in patients with end-stage renal disease showed that the presence of hyperphosphatemia was significantly associated with high blood pressure (Mendes et al., 2017). Hyperphosphatemia was associated with a blunted decline in nocturnal blood

TABLE 1 | Cardiovascular pathomechanisms of hyperphosphatemia.

CVD	Underlying mechanisms
Hypertension	• Activation of SNS (Mizuno et al., 2016)
	• Increasing renin expression leading to increased circulating angiotensin levels (Bozic et al., 2014)
	• Acute impairment of endothelium-dependent vasodilation (Six et al., 2014)
	• Increase endothelin-1 production via up-regulation of aortic endothelin converting enzyme-1 expression (Olmos et al., 2017)
	• Down-regulating α-klotho expression in the kidney (Hu et al., 2015)
	• Deterioration in renal function (Da et al., 2015; Yoon et al., 2017)
Vascular calcification	• Up-regulate the expression of pit (Shobeiri et al., 2014)
	• Up-regulate osteogenic transcription of VSMCs (Singh et al., 2019; Voelkl et al., 2019; Bao et al., 2020; Chang et al., 2020; Takashi and Fukumoto, 2020b)
	• Pro-inflammatory cytokines (Voelkl et al., 2019; Alesutan et al., 2020)
	• Apoptosis and autophagy (Shroff et al., 2008; Liu et al., 2017; Ciceri et al., 2019; Voelkl et al., 2019)
	• Reduction of fetuin-A (Voelkl et al., 2019)
	• Remodeling of extracellular matrix (Voelkl et al., 2019)
	• Oxidative stress (Voelkl et al., 2019)
	• α-klotho deficiency (Singh et al., 2019)
Cardiac valve calcification	• Activation of NF-κB-AKT/ERK pathway (Li et al., 2017; Shuvy et al., 2019; Zhou et al., 2020)
	• Increased expression of pit-1 (Husseini et al., 2013)
Atherosclerosis	• Reduction of eNOS and promotes ROS in endothelial (Stevens et al., 2017; Roumeliotis et al., 2020)
	• Increase of FGF-23 and α-klotho deficiency (Hu and Moe, 2012; Mencke et al., 2015; Richter et al., 2016; Verkaik et al., 2018)
	• Endothelial cell apoptosis (Roumeliotis et al., 2020)
	• FGF-23 related dyslipidemia (Ellam and Chico, 2012)
	• Reduction of calcitriol promoting ox-LDL uptake in macrophages (Oh et al., 2009)
LVH and VF	• α-klotho independent binding of FGF-23 with FGFR4 (Faul et al., 2011; Grabner et al., 2015; Leifheit-Nestler et al., 2016)
	• Ca^{2+} dependent cardiomyocyte hypertrophy (Ca^{2+}-CAMK II-IP3 pathway) (Mhatre et al., 2018)
	• FGF-23 induced ROS and RAAS (Böckmann et al., 2019; Dong et al., 2019)

pressure in hypertensive patients without CKD (Wang et al., 2018). A large prospective observational study in more than 9,000 hypertensive patients showed that elevated baseline serum phosphate is associated with poor blood pressure control over 5 years of follow-up (Patel et al., 2015). Administration of neutral NaPi (each 1 mM Na contains 0.55 mM of Pi) at the dose approximately 30 mmol of Pi per day for 11 weeks induced a significant increase in 24- h ambulatory blood pressure by 4/3 mmHg when compared to the control group treated with equivalent amounts of sodium as NaCl in combination with phosphate binder lanthanum carbonate to reduce phosphate absorption (Mohammad et al., 2018). This prospective randomized study has established a more definitive blood pressure-raising effect of inorganic phosphate in healthy young adults without hypertension or an antihypertensive drug treatment.

Animal experimental data indicate that dietary phosphate excess engages multiple mechanisms that promote hypertension. In the normotensive Sprague Dawley (SD) rats fed with a high phosphate diet (HPD) for 12 weeks, consumption of HPD induced hypertension and tachycardia in the resting condition and augments cardiovascular and sympathetic responses during muscle contraction (Mizuno et al., 2016). This result implicates that short-term dietary phosphate loading is able to transform the autonomic regulation of blood pressure in normotensive rats to the phenotype observed in hypertensive rats. The mechanisms underlying sympathetic activation induced by dietary phosphate loading are unknown. Other than the activation of the sympathetic nervous system, HPD was shown to increase renin expression, resulting in increased circulating angiotensin levels in healthy rats (Bozic et al., 2014). Acute impairment in endothelium-dependent vasodilation will happen when aortic rings are exposed to culture media with high phosphate milieu (Six et al., 2014). Increases in endothelin-1 production via upregulation of aortic endothelin-converting enzyme-1 protein expression has been demonstrated in one study in aortic endothelial cell culture upon exposure to high extracellular phosphate condition (Olmos et al., 2017). HPD has also been shown to downregulate klotho expression in the kidneys and reduce soluble klotho levels in the serum of mice (Hu et al., 2015). CKD is one of the major risk factors for the development of hypertension, and deterioration in renal function constitutes another potential mechanism by which dietary phosphate excess promotes hypertension (Da et al., 2015; Yoon et al., 2017). Large randomized clinical trials are needed to confirm the findings in animal experiments, and the results may lead to a new paradigm in preventing hypertension in the population at high risk for progression to hypertension.

Vascular Calcification

The risk of cardiovascular death in patients with CKD stage 3a-4 is increased by 2–3 times, and the most common impairment is vascular calcification (VC) (Takashi and Fukumoto, 2020a). To date, there is no epidemiological data with a large sample to show the incidence of VC in CKD. Adeney et al. analyzed 439 patients with moderate to severe CKD and found that the incidence of calcification in the coronary artery and descending aorta increased by 21 and 33%, respectively, with the increase of blood phosphate every 1 mg/dL (Sarnak et al., 2019). The prospective cohort study, CRIC, included 1,123 patients with mild to moderate CKD (EGFR 20–70 ml/min/1.73 m^2), and demonstrated that serum phosphate > 3.9 mg/dL was significantly associated with coronary artery calcification (Mendes et al., 2017; Bundy et al., 2018). Shang et al. (2017) selected 70 peritoneal dialysis patients without coronary artery calcification as the research objects, followed up for at least 3 years, and revealed that hyperphosphatemia was an independent risk factor for coronary artery calcification in dialysis patients. Two large cohort studies showed that serum phosphate > 3.9 mg/dL was independently

associated with coronary artery calcification, even in the normal range (Patel et al., 2015). These clinical studies provide evidence that high phosphate might be a causal factor in the development of vascular calcification in CKD patients.

High phosphate is thought to contribute to the development of vascular calcification by inducing the formation of osteoblast-like cells from vascular smooth muscle cells (Cozzolino et al., 2019). Bao et al. stimulated mice with high phosphate and showed that aortic rings in high phosphate group were obviously calcified by calcium staining (Chang et al., 2020). The perception of extracellular phosphate in vascular smooth muscle is mediated by type III sodium-dependent phosphate co-transporters Pit1 and Pit2, and high phosphate up-regulates the expression of Pit in vascular smooth muscle cells (Shobeiri et al., 2014). Experimental studies indicated that activation of GK1/NF-κB, SGK1/NF-κB, Wnt/β-Catenin signaling, up-regulating osteogenic transcription factors Runx2, Msx2, Sox9 and osterix are classic mechanisms of osteogenic differentiation of vascular smooth muscle cells, among which Runx2 plays a decisive role (Voelkl et al., 2019). Pro-inflammatory cytokines are a class of endogenous peptides mainly produced by immune cells, including interleukin (IL) -1β, tumor necrosis factor (TNF) –α, IL-6. *In vitro* studies showed that IL-1β and TNF-α could stimulate the intracellular NF-κB signaling, and IL-6 activates BMP-2-wnt/β-Catenin pathway to induce the calcification of vascular smooth muscle cells (Voelkl et al., 2019; Alesutan et al., 2020). Increased FGF-23 levels and pro-inflammatory cytokines were found in patients with hyperphosphatemia (Mendoza et al., 2017). A previous prospective study, including 3,879 CKD stage 2–4 patients, indicated that FGF-23 was positively correlated with pro-inflammatory cytokines such as IL-6, CRP, and TNF-α, but there was no experiment to confirm the causal relationship between FGF-23 and pro-inflammatory cytokines (Mendoza et al., 2012). Recent studies have found that GAS5/miR-26-5p/PTEN, FGFR1c-MEK/ERK-GALNT3 pathway and α-Klotho deficiency are also important mechanisms of vascular calcification. Chang et al. showed that high phosphate stimulation downregulated the expression of a long-chain non-coding RNA (IncRNA) growth specific inhibitor GAS5 in human aortic smooth muscle cells, which weakened the inhibition of small nucleolar RNA miR-26b-5p, and thereby its downstream target protein PTEN. PTEN is a protein/lipid phosphatase, which stimulates the osteogenic differentiation of mesenchymal cells by increasing the expression of Runx2 (Bao et al., 2020; Chang et al., 2020). Takashi et al. found that high phosphate binding to FGFR1c activates downstream extracellular regulated protein kinase MEK/ERK phosphorylation and promotes the expression of osteogenic related proteins. Meanwhile, it also promotes the expression of FGF-23 post-transcriptional modified gene peptide *N*-acetylgalactosamine transferase 3 (GALNT3), which inhibited FGF-23 cleavage at multiple glycosylation sites (Takashi and Fukumoto, 2020b). Singh et al. (2019) found that aortic balloon calcification was aggravated and the expression of osteogenic proteins such as matrix metalloproteinase (MMP) 9 and 13 was up-regulated in klotho gene knockout animal models. In addition, high phosphate induces apoptosis of osteoblast-like cells by up-regulating GAS6/AXL, and releases calcium-containing apoptotic bodies (Shroff et al., 2008; Voelkl et al., 2019). Iron citrate inhibits the progression of vascular calcification through anti-apoptosis (Ciceri et al., 2019). Apoptosis is related to autophagy, and high phosphate promotes the expression of autophagy-related protein beclin-1 through the pAMPK-ULK1 pathway (Liu et al., 2017). Other mechanisms include reduction of fetuin-A (a circulating protein that inhibits calcification), remodeling of extracellular matrix and degradation of elastin, oxidative stress, lead to the progression of calcification (Singh et al., 2019; Voelkl et al., 2019).

Altogether, the clinical and experimental data emphasize that high phosphate levels may contribute to vascular calcification not only in CKD patients but also in the general population. This shows the importance of controlled serum phosphate levels and underlines that phosphate represents promising therapeutic targets in preventing vascular calcification in CKD patients.

Valve Calcification

Valve calcification describes pathological depositions of calcium–phosphate salts on the cardiac valves. Increasing evidence has shown that mineral metabolism disorder is an important factor in promoting valve calcification (Rattazzi et al., 2013; Massera et al., 2020). The level of FGF-23 was positively correlated with the occurrence of mitral annular calcification (Bortnick et al., 2016). In another study of 6,814 CKD patients followed-up to 2.3 years, Bortnick et al. (2019) found that for every 18.5 pg/mL increase in FGF-23, the annual mitral valve calcification score measured by CT increased by 2.83 Au. The incidence of the aortic valve and mitral valve calcification increased by 25 and 62% for every 1 mg/dL increase in blood phosphate in a cohort of 439 patients with moderate CKD (Adeney et al., 2009). For every 0.5 mg/dL increase in blood phosphate, the risk of aortic valve ring calcification increases by 1.2 times (Linefsky et al., 2011). The level of blood phosphate was positively correlated with the morbidity of aortic valve calcification, and the average blood phosphate level of 3 mg/dL or more could significantly increase the risk of aortic valve calcification in another cohort of 938 subjects with clinical manifestations of chronic CVD and CKD (Hisamatsu et al., 2018).

NF-κB/Akt/ERK signaling pathway may play an important role in the high phosphate induced valve calcification. The aortic valve calcification in the HPD group was significantly higher than that in the non-phosphate control groups in the uremic rat model; Akt and ERK in the calcified valve were significantly increased; and the osteogenic transcription gene Runx-2 was overexpressed (Shuvy et al., 2019). Pit1 promotes the transfer of serum phosphate into valve interstitial cells, which is the premise of high phosphate induced valve calcification. Husseini et al. (2013) found that the expression of Pit 1 in the calcified aortic valve of human was significantly higher than that of the control group. When exposed human aortic valve interstitial cells to high phosphate medium, Runx2 will transfer from cytoplasm to nucleus, and hydrogen sulfide can reduce calcification by inhibiting Runx2 accumulation in the nucleus (Sikura et al., 2020). The osteogenic related protein Runx2 was overexpressed in the osteogenic human aortic valve stromal cells, and curcumin could suppress Runx2 gene

expression by inhibiting the NF-κ B/Akt/ERK signaling pathway (Shuvy et al., 2019; Zhou et al., 2020). The expression of Runx2 was dependent on Akt and ERK phosphorylation in human aortic valve stromal cells stimulated by high phosphate (Li et al., 2017). Thus, to our current knowledge, cardiac valve calcification may share common pathogenesis with vascular calcification resulting from hyperphosphatemia in CKD patients.

Atherosclerosis

Increasing retrospective studies have found that phosphate can promote the occurrence of atherosclerosis in coronary and peripheral arteries. A cohort study involving 7,553 subjects with near normal renal function (EGFR > 60 ml/min/1.73 m^2) found a positive correlation between high phosphate and coronary artery atherosclerosis (Shin et al., 2012). In another study, 6,329 subjects without clinical manifestations of CKD and coronary artery disease were divided into four groups (≤3.0, 3.1 – 3.3, 3.4 – 3.7, ≥3.8 mg/dL) according to blood phosphate level, and multivariate regression analysis showed that the increase of blood phosphates level indicated the increased risk of coronary atherosclerosis (Park et al., 2020). Multiple linear regression analysis also showed that FGF-23 could increase the risk of carotid atherosclerotic plaque, which reflects systemic peripheral atherosclerosis (Rodríguez-Ortiz et al., 2020). Tuzun et al. (2018) included 54 pregnant women with gestational diabetes mellitus (GDM) and 33 healthy pregnant women, and using color to predict the degree of atherosclerosis, it was found that FGF-23 in GDM group was significantly higher than that in the control group, and the increase of FGF-23 was positively correlated with doppler ultrasound evaluated carotid intima-media thickness. In addition, FGF-23 could increase the recognition rate of the Framingham risk score for carotid atherosclerosis (Hu et al., 2017). There are gender differences in high phosphate induced atherosclerosis. Analysis of 1,687 CKD stage 3–5 non-dialysis patients from the NEFRONA study showed that phosphate levels within the normal range associated with an increased risk of subclinical atheromatosis in men, whereas this risk only increased with serum levels over the normal range in women (Martín et al., 2015). This study suggested that recommended serum phosphate levels could be different for male than for female CKD patients.

At present, the pro-atherogenic mechanism of phosphate excess has not been clarified, and it is considered that endothelial dysfunction caused by high phosphate may be the main reason for promoting lipid infiltration and atherogenesis (Hsu et al., 2010; Scialla and Wolf, 2014; Tripepi et al., 2015; Richter et al., 2016). Endothelial cell injury is the first step of atherogenesis, and endothelial nitric oxide synthase (eNOS) plays an important role in promoting endothelial dysfunction. When human peripheral vascular endothelial cells continuously exposed to high phosphate environment, the production of eNOS was significantly reduced (Ellam and Chico, 2012). High phosphate promotes reactive oxygen (ROS) production, leading to the reduction of tetrahydrobiopterin, a cofactor of eNOS coupling, and the decreasing of eNOS uncoupling nitric oxide (NO) synthesis (Roumeliotis et al., 2020). FGF-23 and Klotho also play an important role in endothelial dysfunction induced by high phosphate. When injecting FGF-23 into normal mice, the endothelium-dependent cardiac and peripheral microvascular relaxation induced by acetylcholine decreased, and the microvascular relaxation ability was restored after injection of FGF-23 antibody (Verkaik et al., 2018). FGF-23/FGFR1/klotho pathway was involved in the regulation of NO synthesis. FGF-23 combined with FGFR1 stimulated the secretion of soluble Klotho, activated Akt phosphorylation, promoted NO synthesis, up-regulated the expression of antioxidant enzymes SOD2 and CAT, and alleviated the inhibition of ROS on NO synthesis (Richter et al., 2016). CKD patients are in klotho deficiency (Hu and Moe, 2012; Mencke et al., 2015), and their NO synthesis is reduced. High phosphate also promotes endothelial cell apoptosis by activating DAXX/ERK pathway and MAPK pathway (Roumeliotis et al., 2020). FGF-23 is associated with dyslipidemia and may also promote atherosclerosis. Cohort studies have found that FGF-23 is negatively correlated with high-density lipoprotein and lipoprotein a, and positively correlated with triglycerides (Ellam and Chico, 2012). Calcitriol could inhibit the uptake of oxidized low-density lipoprotein by macrophages in diabetic patients and suppress the formation of foam cells (Oh et al., 2009). The reduction of calcitriol synthesis in hyperphosphatemia can promote the formation of foam cells. However, Shiota et al. (2011) reported significantly reduced atherosclerotic plaques under high phosphate stimulation, and the researchers attributed the underlying mechanism to the reduction of monocyte activity and the apoptosis of macrophages. This study is independent of endothelial dysfunction, and the results are still controversial.

Left Ventricular Hypertrophy (LVH) and Myocardial Fibrosis

Studies have found that high phosphate can cause LVH, myocardial fibrosis, and increase the risk of cardiovascular death through the paracrine effect of FGF-23 (Courbebaisse and Lanske, 2018; Leifheit-Nestler and Haffner, 2018; Wang and Shapiro, 2019). The prevalence of LVH is about 40% in early-stage CKD patients and 75–80% in end-stage kidney disease patients (Vogt et al., 2019). It was found that serum phosphate > 5 mg/dL was significantly correlated with the increase of left ventricular mass index (Gallieni and Pedone, 2013). Serum level of FGF-23 was positively correlated with left ventricular mass (Kestenbaum et al., 2014). In CHS study including 2,255 subjects over 65 years old, after adjusting for demographic, cardiac and renal related risk factors, FGF-23 can be used as an independent risk factor for LVH, and the left ventricular weight increases by 6.71 g for every doubling of FGF-23 (Jovanovich et al., 2013). After adding the FGF-23 inhibitor bone matrix acidic protein DMP1 into the CKD mice, the left ventricular wall thickness in the DMP1 group was significantly reduced compared with that in the CKD group (Dussold et al., 2019).

Fibroblast growth factor-23 induced LVH mainly through the klotho independent bindings of FGF-23 with FGFR4, activating the phospholipase S γ (PLS γ)/calcineurin-dependent nuclear factor of activated T cells (NFAT) signaling pathway (Faul et al., 2011; Grabner et al., 2015). Myocardial biopsy analysis on 24 patients who died of CKD indicated that 67% of them

had LVH, which was characterized by significantly expressed FGFR4, NFAT, and klotho deficiency compared with the control group (Leifheit-Nestler et al., 2016). FGF-23 and Ang II share a common mechanism in the Ca^{2+} dependent cardiomyocyte hypertrophy. In neonatal rat ventricular myocytes, FGF-23 stimulates the expression of Ang II, and Ang II induces intracellular Ca^{2+} regulated Ca^{2+}/calmodulin dependent protein kinase II (CAMKII)- histone deacetylase 4 (HDAC4) activation via inositol 1,4,5-triphosphate (IP3), promoting myocardial hypertrophy (Mhatre et al., 2018). Using myocardial magnetic resonance (CMR) to detect extracellular volume (ECV) to measure the degree of cardiac fibrosis, it was found that FGF-23 was significantly positively correlated with ECV (Roy et al., 2020). A total of 39 of 51 patients with rheumatic heart disease had persistent atrial fibrillation, the expressions of FGF-23 and FGFR4 were increased in patients with atrial fibrillation, which were positively correlated with atrial fibrosis. It was speculated that FGF-23/FGFR4 pathway may play an important role in promoting atrial fibrillation by atrial fibrosis (Dong et al., 2018). FGF-23 combined with FGFR4 produced ROS, activated downstream STAT3 and Smad3 proteins, and stimulated expression of matrix metalloprotein-2 (MMP-2) in myocardial tissue of patients with atrial fibrillation, leading to myocardial fibrosis (Dong et al., 2019). Renin-angiotensin aldosterone system (RAAS) related genes were significantly expressed in a uremic rat model and positively correlated with left ventricular fibrosis. In neonatal rat ventricular myocytes, FGF-23 can induce the expression of RAAS gene and transforming growth factor – β (TGF-β), and the expression of TGF-β can be reduced by RAAS inhibitor, which indicates that FGF-23 may promote myocardial fibrosis by activating local RAAS (Böckmann et al., 2019). Current studies provide evidence that hyperphosphatemia contributes to the development of LVH. Future work has to be clarified whether phosphate can induce cardiac hypertrophy directly or only indirectly. Possible indirect mechanisms such as the phosphate mediated elevation of FGF23 or development of hypertension may contribute to the development of LVH in CKD patients.

Interventions for Phosphate Excess

According to current knowledge, hyperphosphatemia contributes to the development of various CVD. Multidimensional phosphate-lowering therapeutic strategies targeting serum phosphate by restricting diet uptake or intestinal absorption and promoting renal excretion are pursued.

Dietary Phosphate Restriction

Inorganic phosphate is commonly used as a flavor enhancer or preservative in the processed food, and organic phosphate naturally exists in foods rich in animal protein. Restriction of dietary phosphate intake is the elemental strategy to lower serum phosphate level. A low protein diet reduces serum FGF-23 and phosphate levels in non-dialysis and dialysis CKD patients (Shinaberger et al., 2008; Iorio et al., 2012), and the restricted consumption of inorganic phosphate additives attenuates serum phosphate levels in ESRD patients (Sullivan et al., 2009; de Fornasari and Sens, 2017). Moreover, plant-based diet usually reduced FGF23 levels but not serum phosphate levels compared with a meat-based diet (Moe et al., 2009, 2011; Scialla et al., 2012). The KDOQI guidelines recommend adjusting dietary phosphate intake to maintain serum phosphate levels in the normal range in adults with CKD 3-5D, and in adults with CKD 1-5D or post-transplantation (Ikizler et al., 2020). However, the reduction of total protein intake was associated with increased mortality, and a general restriction of protein uptake is not a suitable therapeutic strategy to reduce serum phosphate (Shinaberger et al., 2008).

The uptake of phosphate depends not only on the amount of phosphate but also on the source. The bioavailability increases from organic plant phosphate to organic animal phosphate and additives of the food industry (Noori et al., 2010). A prospective, observational study of 224 maintenance hemodialysis (MHD) patients reported that higher dietary phosphorus intake and higher dietary phosphorus to protein ratios are each associated with increased death risk in MHD patients, even after adjustments for serum phosphorus, phosphate binders and their types, and dietary protein, energy, and potassium intakes (Noori et al., 2010; Ikizler et al., 2020). The lasted KDOQI guidelines suggested that it is reasonable to consider the bioavailability of phosphate sources (e.g., animal, vegetable, additives), the ratio of phosphate (mg) to protein (g) in food should be 10–12 mg/g to maintain the balance of protein and phosphate in CKD patients when prescribing phosphate restrictive diet (Tsai et al., 2019; Ikizler et al., 2020). Reduced consumption of processed food with flavor enhancer or preservative might show beneficial clinical outcomes. Future studies need to explore if restricted phosphate uptake improves the general and cardiovascular outcome in CKD patients.

Phosphate Binder

Phosphate binders inhibit gastrointestinal absorption of phosphate by the formation of chelating phosphate. Non-calcium phosphate binder reduces serum phosphate level but does not increase serum calcium, which potentially benefits cardiovascular. The representative drugs include sevelamer carbonate, lanthanum carbonate and iron citrate (Kalantar-Zadeh et al., 2010., Ruospo et al., 2018). Sevelamer carbonate is an anion exchange resin, which binds to phosphate in the proximal small intestine, and is similar to iron citrate in reducing serum phosphate levels and the intact FGF-23 peptide chain (St. Peter et al., 2017; Block et al., 2019a). Lanthanum carbonate dissociates in gastric acid and combines with phosphate by ionic bond to form hydrophobic compounds, which reduce serum phosphate levels and the carboxyl terminal FGF-23. Long-term intake of lanthanum has toxic side effects on liver, bone and nervous system (Liabeuf et al., 2017). A meta-analysis of 4,622 patients in 11 RCT studies showed that non-calcium phosphate binders reduced all-cause mortality by 22% and significantly reduced coronary artery calcification (Gonzalez-Parra et al., 2011). A small sample study showed that pulse wave velocity (PWV), an indicator of cardiovascular events, was significantly reduced in patients with low vascular calcification score and normal blood phosphate after 8 weeks of sevelamer

hydrochloride treatment (Jamal et al., 2013). Sevelamer also has the effect of lowering blood lipid and stabilizing plaque, and significantly reduces the atherosclerotic plaque of thoracic aorta in uremic animal model with atherosclerosis (de Krijger et al., 2019). Compared with nicotinamide drugs, sevelamer reduces the low molecular endotoxin in uremic patients and reduces the chronic inflammatory reaction (Phan et al., 2005). The data from a meta-analysis included 77 studies involving 12,562 patients with CKD, showing that sevelamer significantly reduced all-cause mortality by 61% and lanthanum carbonate by 21% when compared with calcium-containing phosphate binder (Lenglet et al., 2019). Iron citrate decomposes ferric ion (Fe^{3+}) and combines with phosphate. Recent studies indicate beneficial effects of ferric citrate treatment for CKD patients (Palmer et al., 2016; Block et al., 2019a,b). Besides reducing blood phosphate and inhibiting FGF-23 secretion, iron citrate increases serum iron reserve and improves anemia (Francis et al., 2019). As shown by Francis et al., ferric citrate also improves the renal and cardiac function in the Col4a3 knockout mouse model of progressive CKD. Treatment with ferric citrate reduced blood urea nitrogen levels and albuminuria, showed less renal interstitial fibrosis and tubular atrophy, and attenuated cardiac dysfunctions than Col4a3 knockout control mice. Finally, ferric citrate slowed the progression of CKD and improved the survival of CKD mice (Francis et al., 2019). If the findings of this animal study can be confirmed by clinical trials, ferric citrate and other non-calcium-phosphate binder represent promising drugs to improve cardiac and kidney function in CKD patients.

In contrast, calcium-containing phosphate binders did not lower or even increased serum FGF23 levels and promoted the progression of vascular calcification (Oliveira et al., 2010; Block et al., 2012; Jamal et al., 2013). Hence, calcium-containing phosphate binders like calcium acetate are rather inappropriate to treat CKD patients. Clinical trials analyzing the actual cardiac outcome of a phosphate binder therapy in CKD patients are still lacking.

Other Approaches

Phosphate binders inhibited the absorption of phosphate, but also up-regulated the active phosphate transporter Npt-2b in the intestine (Isakova et al., 2015). Nicotinamide, the metabolite of vitamin B3, could reduce phosphate by inhibiting the intestinal phosphate transporter Npt-2b, which is a second-line drug for phosphate lowering treatment (Ren et al., 2020). It has been reported that nicotinamide can reduce phosphate by 12–34% in end-stage CKD dialysis patients (Vogt et al., 2019). In CKD patients on dialysis, nicotinamide might have beneficial clinical outcomes owing to the reduction of serum FGF23 and phosphate levels. However, the combination of phosphate binder and nicotinamide did not significantly reduce the levels of serum phosphate and FGF-23 in a randomized, placebo-controlled studies including 205 3b/4 CKD patients during a long-term follow-up of 12 months (Ix et al., 2019). Future studies have to consider new approaches for the long-term control of FGF23 and phosphate levels in non-dialysis CKD patients.

High serum phosphate and low serum magnesium levels correlated with an accelerated CKD progression during a median follow-up of 44 months in CKD patients (Sakaguchi et al., 2015). The cardiovascular mortality risk reduced with increasing magnesium levels in hemodialysis patients with hyperphosphatemia (Sakaguchi et al., 2014). Magnesium can inhibit the deposition of hydroxyapatite and osteogenic differentiation to prevent phosphate induced vascular calcification (Massy and Drüeke, 2015; Braake et al., 2019; Nakagawa et al., 2020). Therefore, magnesium supplementation might be a promising strategy to reduce hyperphosphatemia-associated cardiovascular risk in CKD patients. A small RCT study recruited 125 CKD stage 3–4 patients with risk factors for coronary artery calcification and followed-up for 2 years, the results showed that magnesium oxide group significantly improved vascular calcification in patients with basal coronary calcification score > 400 (Sakaguchi et al., 2019a,b). However, treatment with magnesium oxide did not influence serum phosphate levels and FGF-23 levels were not measured in this study. An animal study indicated the relevance of low magnesium diet with lower serum FGF-23 levels (Sakaguchi et al., 2019a), but FGF-23 levels were reduced after administration of calcium acetate/magnesium carbonate for 25 weeks in CALMAG study (Covic et al., 2013). There is no study report the direct connection between magnesium and CVD outcomes. Future studies should investigate if magnesium supplementation can reduce the cardiovascular mortality in CKD patients.

Promoting phosphate excretion might be another approach to control serum phosphate levels. NaPi-2b knockout uremic mice exhibit lower serum phosphate levels than wild uremic littermates (Schiavi et al., 2012). NaPi-2a inhibitor increased the excretion of phosphate in a dose-dependent manner and reduced serum phosphate levels in both healthy and uremic mice (Thomas et al., 2019). Future clinical studies will have to investigate the outcome of NaPi-2a and 2b inhibition in CKD patients. It is also conceivable that a combined treatment, which inhibits both intestinal absorption and renal reabsorption, could have the most beneficial effect for CKD patients.

CONCLUSION

Hyperphosphatemia participates in the occurrence and development of a variety of cardiovascular diseases, as an important risk factor for the excessively increased cardiovascular mortality, especially in CKD population. FGF-23 plays a key role in controlling serum phosphate levels to attenuate phosphate-induced CVD. In the future, the therapeutic strategies of hyperphosphatemia need to take FGF-23 as an important target besides direct dephosphorization. The clinical compliance of dietary phosphate restriction is poor, and nutrition education should be strengthened. In different degrees of hyperphosphatemia, there is no clear definition to the target range of dephosphorization with long-term cardiovascular benefits. Promising therapeutic strategies beside dietary phosphate restriction, phosphate binders or other approaches

targeting both phosphate and FGF-23 need to be further explored by large randomized clinical trials with hard endpoints to establish a causal relationship between phosphate excess and CVD, and to determine if lowering serum phosphate constitutes an effective intervention for prevention and treatment of CVD.

AUTHOR CONTRIBUTIONS

CZ, NO, and ZS contributed to the collection of the reference and drafted the manuscript. CZ, NO, and XR revised the manuscript. All authors contributed to the article and approved the submitted version.

FUNDING

This work was supported by National Key R&D Program of China (2018YFC1312700), National Natural Science Foundation of China (Nos. 81500341 and 32030054), Chongqing Science and Technology Commission (Nos. cstc2018jcyjAX0134, cstc2020jcyj-msxmX0304, and cstc2020jcyj-msxmX0152) and Moorhead Trust.

REFERENCES

Adeney, K. L., Siscovick, D. S., Ix, J. H., Seliger, S. L., Shlipak, M. G., Jenny, N. S., et al. (2009). Association of serum phosphate with vascular and valvular calcification in moderate CKD. *J. Am. Soc. Nephrol.* 20, 381–387. doi: 10.1681/ASN.2008040349

Alesutan, I., Luong, T. T. D., Schelski, N., Masyout, J., Hille, S., Schneider, M. P., et al. (2020). Circulating uromodulin inhibits vascular calcification by interfering with pro-inflammatory cytokine signaling. *Cardiovasc. Res.* doi: 10.1093/cvr/cvaa081 Online ahead of print.

Angelova, P. R., Baev, A. Y., Berezhnov, A. V., and Abramov, A. Y. (2016). Role of inorganic polyphosphate in mammalian cells: from signal transduction and mitochondrial metabolism to cell death. *Biochem. Soc. Trans.* 44, 40–45. doi: 10.1042/BST20150223

Bao, S., Guo, Y., Diao, Z., Guo, W., and Liu, W. (2020). Genome-wide identification of lncRNAs and mRNAs differentially expressed in human vascular smooth muscle cells stimulated by high phosphorus. *Ren. Fail* 42, 437–446. doi: 10.1080/0886022X.2020.1758722

Bär, L., Feger, M., Fajol, A., Klotz, L. O., Zeng, S., Lang, F., et al. (2018). Insulin suppresses the production of fibroblast growth factor 23 (FGF23). *Proc. Natl. Acad. Sci. U S A.* 115, 5804–5809. doi: 10.1073/pnas.1800160115

Block, G. A., Block, M. S., Smits, G., Mehta, R., Isakova, T., Wolf, M., et al. (2019b). A pilot randomized trial of ferric citrate coordination complex for the treatment of advanced CKD. *J. Am. Soc. Nephrol.* 30, 1495–1504. doi: 10.1681/ASN.2018101016

Block, G. A., Pergola, P. E., Fishbane, S., Martins, J. G., LeWinter, R. D., Uhlig, K., et al. (2019a). Effect of ferric citrate on serum phosphate and fibroblast growth factor 23 among patients with nondialysis-dependent chronic kidney disease: path analyses. *Nephrol. Dial. Transplant.* 34, 1115–1124. doi: 10.1093/ndt/gfy318

Block, G. A., Wheeler, D. C., Persky, M. S., Kestenbaum, B., Ketteler, M., Spiegel, D. M., et al. (2012). Effects of phosphate binders in moderate CKD. *J. Am. Soc. Nephrol.* 23, 1407–1415. doi: 10.1681/ASN.2012030223

Böckmann, I., Lischka, J., Richter, B., Deppe, J., Rahn, A., Fischer, D. C., et al. (2019). FGF23-Mediated activation of local RAAS promotes cardiac hypertrophy and fibrosis. *Int. J. Mol. Sci.* 20:4634. doi: 10.3390/ijms20184634

Bortnick, A. E., Bartz, T. M., Ix, J. H., Chonchol, M., Reiner, A., Cushman, M., et al. (2016). Association of inflammatory, lipid and mineral markers with cardiac calcification in older adults. *Heart* 102, 1826–1834. doi: 10.1136/heartjnl-2016-309404

Bortnick, A. E., Xu, S., Kim, R. S., Kestenbaum, B., Ix, J. H., Jenny, N. S., et al. (2019). Biomarkers of mineral metabolism and progression of aortic valve and mitral annular calcification: the multi-ethnic study of atherosclerosis. *Atherosclerosis* 285, 79–86. doi: 10.1016/j.atherosclerosis.2019.04.215

Bozic, M., Panizo, S., Sevilla, M. A., Riera, M., Soler, M. J., Pascual, J., et al. (2014). High phosphate diet increases arterial blood pressure via a parathyroid hormone mediated increase of renin. *J. Hypertens.* 32, 1822–1832. doi: 10.1097/HJH.0000000000000261

Braake, A. D. T., Smit, A. E., Bos, C., van Herwaarden, A. E., Alkema, W., van Essen, H. W., et al. (2019). Magnesium prevents vascular calcification in Klotho deficiency. *Kidney Int.* 97, 487–501. doi: 10.1016/j.kint.2019.09.034

Bundy, J. D., Chen, J., Yang, W., Budoff, M., Go, A. S., Grunwald, J. E., et al. (2018). Risk factors for progression of coronary artery calcification in patients with chronic kidney disease: the CRIC study. *Atherosclerosis* 271, 53–60. doi: 10.1016/j.atherosclerosis.2018.02.009

Centeno, P. P., Herberger, A., Mun, H. C., Tu, C., Nemeth, E. F., Chang, W., et al. (2019). Phosphate acts directly on the calcium-sensing receptor to stimulate parathyroid hormone secretion. *Nat. Commun.* 10:4693. doi: 10.1038/s41467-019-12399-9

Chande, S., and Bergwitz, C. (2018). Role of phosphate sensing in bone and mineral metabolism. *Nat. Rev. Endocrinol.* 14, 637–655. doi: 10.1038/s41574-018-0076-3

Chang, Z., Yan, G., Zheng, J., and Liu, Z. (2020). The lncRNA GAS5 inhibits the osteogenic differentiation and calcification of human vascular smooth muscle cells. *Calcif. Tissue Int.* 107, 86–95. doi: 10.1007/s00223-020-00696-1

Chronic Kidney, Disease Prognosis, Consortium, Matsushita, K., van der Velde, M., Astor, B. C., et al. (2010). Association of estimated glomerular filtration rate and albuminuria with all-cause and cardiovascular mortality in general population cohorts: a collaborative meta-analysis. *Lancet* 375, 2073–2081. doi: 10.1016/S0140-6736(10)60674-5

Ciceri, P., Falleni, M., Tosi, D., Martinelli, C., Cannizzo, S., Marchetti, G., et al. (2019). Therapeutic effect of iron citrate in blocking calcium deposition in high pi-calcified VSMC: role of autophagy and apoptosis. *Int. J. Mol. Sci.* 20:5925. doi: 10.3390/ijms20235925

Courbebaisse, M., and Lanske, B. (2018). Biology of fibroblast growth factor 23: from physiology to pathology. *Cold Spring Harb. Perspect. Med.* 8:a031260. doi: 10.1101/cshperspect.a031260

Covic, A., Passlick-Deetjen, J., Kroczak, M., Büschges-Seraphin, B., Ghenu, A., Ponce, P., et al. (2013). A comparison of calcium acetate/magnesium carbonate and sevelamer-hydrochloride effects on fibroblast growth factor-23 and bone markers: post hoc evaluation from a controlled, randomized study. *Nephrol. Dial. Transplan.* 28, 2383–2392. doi: 10.1093/ndt/gft203

Cozzolino, M., Ciceri, P., Galassi, A., Mangano, M., Carugo, S., Capelli, I., et al. (2019). The key role of phosphate on vascular calcification. *Toxins (Basel)* 11:213. doi: 10.3390/toxins11040213

Da, J., Xie, X., Wolf, M., Disthabanchong, S., Wang, J., Zha, Y., et al. (2015). Serum phosphorus and progression of CKD and mortality: a meta-analysis of cohort studies. *Am. J. Kidney Di* 66, 258–265. doi: 10.1053/j.ajkd.2015.01.009

de Fornasari, M. L. L., and Sens, Y. A. D. S. (2017). Replacing phosphorus-containing food additives with foods without additives reduces phosphatemia in end-stage renal disease patients: a randomized clinical trial. *J. Ren. Nutr.* 27, 97–105. doi: 10.1053/j.jrn.2016.08.009

de Krijger, A. B., van Ittersum, F. J., Hoekstra, T., Wee, P. M. T., and Vervloet, M. G. (2019). Short-term effects of sevelamer-carbonate on fibroblast growth factor 23 and pulse wave velocity in patients with normophosphataemic chronic kidney disease Stage 3. *Clin. Kidney J.* 12, 678–685. doi: 10.1093/ckj/sfz027

Dong, Q., Li, S., Wang, W., Han, L., Xia, Z., Wu, Y., et al. (2019). FGF23 regulates atrial fibrosis in atrial fibrillation by mediating the STAT3 and SMAD3 pathways. *J. Cell. Physiol.* 234, 19502–19510. doi: 10.1002/jcp.28548

Dong, Q. B., Tang, Y. H., Wang, W. X., Wu, Y. B., Han, L., Li, J. X., et al. (2018). Relationship between FGF23/FGFR4 expression in atrial tissue and atrial fibrosis in patients with atrial fibrillation. *Zhonghua Yi Xue Za Zhi* 98, 1003–1007. doi: 10.3760/cma.j.issn.0376-2491.2018.13.010

Dussold, C., Gerber, C., White, S., Wang, X., Qi, L., Francis, C., et al. (2019). DMP1 prevents osteocyte alterations, FGF23 elevation and left ventricular hypertrophy

in mice with chronic kidney disease. *Bone Res.* 7:12. doi: 10.1038/s41413-019-0051-1

Ellam, T. J., and Chico, T. J. A. (2012). Phosphate: the new cholesterol? the role of the phosphate axis in non-uremic vascular disease. *Atherosclerosis* 220, 310–318. doi: 10.1016/j.atherosclerosis.2011.09.002

Faul, C., Amaral, A. P., Oskouei, B., Hu, M. C., Sloan, A., Isakova, T., et al. (2011). FGF23 induces left ventricular hypertrophy. *J. Clin. Invest.* 121, 4393–4408. doi: 10.1172/JCI46122

Francis, C., Courbon, G., Gerber, C., Neuburg, S., Wang, X., Dussold, C., et al. (2019). Ferric citrate reduces fibroblast growth factor 23 levels and improves renal and cardiac function in a mouse model of chronic kidney disease. *Kidney Int.* 96, 1346–1358. doi: 10.1016/j.kint.2019.07.026

Gallieni, M., and Pedone, M. (2013). Left ventricular hypertrophy and serum phosphate in peritoneal dialysis patients. *Kidney Int.* 84:850. doi: 10.1038/ki.2013.259

Gonzalez-Parra, E., Gonzalez-Casaus, M. L., Galán, A., Martinez-Calero, A., Navas, V., Rodriguez, M., et al. (2011). Lanthanum carbonate reduces FGF23 in chronic kidney disease Stage 3 patients. *Nephrol. Dial. Transplant.* 26, 2567–2571. doi: 10.1093/ndt/gfr144

Grabner, A., Amaral, A. P., Schramm, K., Singh, S., Sloan, A., Yanucil, C., et al. (2015). Activation of cardiac fibroblast growth factor receptor 4 causes left ventricular hypertrophy. *Cell Metab.* 22, 1020–1032. doi: 10.1016/j.cmet.2015.09.002

Hisamatsu, T., Miura, K., Fujiyoshi, A., Kadota, A., Miyagawa, N., Satoh, A., et al. (2018). Serum magnesium, phosphorus, and calcium levels and subclinical calcific aortic valve disease: a population-based study. *Atherosclerosis* 273, 145–152. doi: 10.1016/j.atherosclerosis.2018.03.035

Hsu, Y. J., Hsu, S. C., Huang, S. M., Lee, H. S., Lin, S. H., Tsai, C. S., et al. (2010). Hyperphosphatemia induces protective autophagy in endothelial cells through the inhibition of Akt/mTOR signaling. *J. Vasc. Surg.* 62, 210–221.e2. doi: 10.1016/j.jvs.2014.02.040

Hu, M. C., and Moe, O. W. (2012). Klotho as a potential biomarker and therapy for acute kidney injury. *Nat. Rev. Nephrol.* 423–429. doi: 10.1038/nrneph.2012.92

Hu, M. C., Shi, M., Cho, H. J., Adams-Huet, B., Paek, J., Hill, K., et al. (2015). Klotho and phosphate are modulators of pathologic uremic cardiac remodeling. *J. Am. Soc. Nephrol.* 26, 1290–1302. doi: 10.1681/ASN.2014050465

Hu, X., Ma, X., Luo, Y., Xu, Y., Xiong, Q., Pan, X., et al. (2017). Contribution of fibroblast growth factor 23 to Framingham risk score for identifying subclinical atherosclerosis in Chinese men. *Nutr. Metab. Cardiovasc. Dis.* 27, 147–153. doi: 10.1016/j.numecd.2016.11.009

Husseini, D. E., Boulanger, M. C., Fournier, D., Mahmut, A., Bossé, Y., Pibarot, P., et al. (2013). High expression of the Pi-transporter SLC20A1/Pit1 in calcific aortic valve disease promotes mineralization through regulation of Akt-1. *PLoS One* 8:e53393. doi: 10.1371/journal.pone.0053393

Ikizler, T. A., Burrowes, J. D., Byham-Gray, L. D., Campbell, K. L., Carrero, J. J., Chan, W., et al. (2020). KDOQI clinical practice guideline for nutrition in CKD: 2020 update. *Am. J. Kidney Dis.* 76, S1–S107. doi: 10.1053/j.ajkd.2020.05.006

Iorio, B. D., Micco, L. D., Torraca, S., Sirico, M. L., Russo, L., Pota, A., et al. (2012). Acute effects of very-low-protein diet on FGF23 levels: a randomized study. *Clin. J. Am. Soc. Nephrol.* 7, 581–587. doi: 10.2215/CJN.07640711

Isakova, T., Ix, J. H., Sprague, S. M., Raphael, K. L., Fried, L., Gassman, J. J., et al. (2015). Rationale and approaches to phosphate and fibroblast growth factor 23 reduction in CKD. *J. Am. Soc. Nephrol.* 26, 2328–2339. doi: 10.1681/ASN.2015020117

Ix, J. H., Isakova, T., Larive, B., Raphael, K. L., Raj, D. S., Cheung, A. K., et al. (2019). Effects of nicotinamide and lanthanum carbonate on serum phosphate and fibroblast growth factor-23 in CKD: the combine trial. *J. Am. Soc. Nephrol.* 30, 1096–1108. doi: 10.1681/ASN.2018101058

Jamal, S. A., Vandermeer, B., Raggi, P., Mendelssohn, D. C., Chatterley, T., Dorgan, M., et al. (2013). Effect of calcium-based versus non-calcium-based phosphate binders on mortality in patients with chronic kidney disease: an updated systematic review and meta-analysis. *Lancet* 382, 1268–1277. doi: 10.1016/S0140-6736(13)60897-1

Jovanovich, A., Ix, J. H., Gottdiener, J., McFann, K., Katz, R., Kestenbaum, B., et al. (2013). Fibroblast growth factor 23, left ventricular mass, and left ventricular hypertrophy in community-dwelling older adults. *Atherosclerosis* 231, 114–119. doi: 10.1016/j.atherosclerosis.2013.09.002

Kalantar-Zadeh, K., Gutekunst, L., Mehrotra, R., Kovesdy, C. P., Bross, R., Shinaberger, C. S., et al. (2010). Understanding sources of dietary phosphorus in the treatment of patients with chronic kidney disease. *Clin. J. Am. Soc. Nephrol.* 5, 519–530. doi: 10.2215/CJN.06080809

Kestenbaum, B., Sachs, M. C., Hoofnagle, A. N., Siscovick, D. S., Ix, J. H., Robinson-Cohen, C., et al. (2014). Fibroblast growth factor-23 and cardiovascular disease in the general population: the multi-ethnic study of atherosclerosis. *Circ. Heart Fail* 7, 409–417. doi: 10.1161/CIRCHEARTFAILURE.113.000952

Kornberg, A. (1979). The enzymatic replication of DNA. *CRC Crit. Rev. Biochem.* 7, 23–43. doi: 10.3109/10409237909102568

Leifheit-Nestler, M., and Haffner, D. (2018). Paracrine effects of FGF23 on the heart. *Front. Endocrinol. (Lausanne)* 9:278. doi: 10.3389/fendo.2018.00278

Leifheit-Nestler, M., Siemer, R. G., Flasbart, K., Richter, B., Kirchhoff, F., Ziegler, W. H., et al. (2016). Induction of cardiac FGF23/FGFR4 expression is associated with left ventricular hypertrophy in patients with chronic kidney disease. *Nephrol. Dial. Transplant.* 31, 1088–1099. doi: 10.1093/ndt/gfv421

Lenglet, A., Fabresse, N., Taupin, M., Gomila, C., Liabeuf, S., Kamel, S., et al. (2019). Does the administration of sevelamer or nicotinamide modify uremic toxins or endotoxemia in chronic hemodialysis patients? *Drugs* 79, 855–862. doi: 10.1007/s40265-019-01118-9

Li, F., Yao, Q., Ao, L., Cleveland, J. C. Jr., Dong, N., Fullerton, D. A., et al. (2017). Klotho suppresses high phosphate-induced osteogenic responses in human aortic valve interstitial cells through inhibition of Sox9. *J. Mol. Med. (Berl)* 95, 739–751. doi: 10.1007/s00109-017-1527-3

Liabeuf, S., Ryckelynck, J. P., Esper, N. E., Ureña, P., Combe, C., Dussol, B., et al. (2017). Randomized clinical trial of sevelamer carbonate on serum klotho and fibroblast growth factor 23 in CKD. *Clin. J. Am. Soc. Nephrol.* 12, 1930–1940. doi: 10.2215/CJN.03030317

Lim, C. C., Teo, B. W., Ong, P. G., Cheung, C. Y., Lim, S. C., Chow, K. Y., et al. (2015). Chronic kidney disease, cardiovascular disease and mortality: a prospective cohort study in a multi-ethnic Asian population. *Eur. J. Prev. Cardiol.* 22, 1018–1026. doi: 10.1177/2047487314536873

Linefsky, J. P., O'Brien, K. D., Katz, R., de Boer, I. H. B., Barasch, E., Jenny, N. S., et al. (2011). Association of serum phosphate levels with aortic valve sclerosis and annular calcification: the cardiovascular health study. *J. Am. Coll. Cardiol.* 58, 291–297. doi: 10.1016/j.jacc.2010.11.073

Liu, K. L., Lin, K. H., Tamilselvi, S., Chen, W. K., Shen, C. Y., Chen, R. J., et al. (2017). Elevated phosphate levels trigger autophagy-mediated cellular apoptosis in H9c2 cardiomyoblasts. *Cardiorenal. Med.* 8, 31–40. doi: 10.1159/000479010

Martín, M., Valls, J., Betriu, A., Fernández, E., and Valdivielso, J. M. (2015). Association of serum phosphorus with subclinical atherosclerosis in chronic kidney disease. sex makes a difference. *Atherosclerosis* 241, 264–270. doi: 10.1016/j.atherosclerosis.2015.02.048

Massera, D., Kizer, J. R., and Dweck, M. R. (2020). Mechanisms of mitral annular calcification. *Trends Cardiovasc. Med.* 30, 289–295. doi: 10.1016/j.tcm.2019.07.011

Massy, Z. A., and Drüeke, T. B. (2015). Magnesium and cardiovascular complications of chronic kidney disease. *Nat. Rev. Nephrol.* 11, 432–442.

Masuda, M., Yamamoto, H., Takei, Y., Nakahashi, O., Adachi, Y., Ohnishi, K., et al. (2020). All-trans retinoic acid reduces the transcriptional regulation of intestinal sodium-dependent phosphate co-transporter gene (Npt2b). *Biochem. J.* 477, 817–831. doi: 10.1042/BCJ20190716

Mencke, R., Harms, G., Mirković, K., Struik, J., Ark, J. V., Loon, E. V., et al. (2015). Membrane-bound Klotho is not expressed endogenously in healthy or uraemic human vascular tissue. *Cardiovasc. Res.* 108, 220–231. doi: 10.1093/cvr/cvv187

Mendes, M., Resende, L., Teixeira, A., Correia, J., and Silva, G. (2017). Blood pressure and phosphate level in diabetic and non-diabetic kidney disease: results of the cross-sectional "Low Clearance Consultation" study. *Porto Biomed. J.* 2, 301–305. doi: 10.1016/j.pbj.2017.02.005

Mendoza, J. M., Isakova, T., Cai, X., Bayes, L. Y., Faul, C., Scialla, J. J., et al. (2017). Inflammation and elevated levels of fibroblast growth factor 23 are independent risk factors for death in chronic kidney disease. *Kidney Int.* 91, 711–719. doi: 10.1016/j.kint.2016.10.021

Mendoza, J. M., Isakova, T., Ricardo, A. C., Xie, H., Navaneethan, S. D., Anderson, A. H., et al. (2012). Fibroblast growth factor 23 and Inflammation in CKD. *Clin. J. Am. Soc. Nephrol.* 7, 1155–1162. doi: 10.2215/CJN.13281211

Mhatre, K. N., Wakula, P., Klein, O., Bisping, E., Völkl, J., Pieske, B., et al. (2018). Crosstalk between FGF23- and angiotensin II-mediated Ca 2+ signaling in

pathological cardiac hypertrophy. *Cell Mol. Life. Sci.* 75, 4403–4416. doi: 10.1007/s00018-018-2885-x

Michigami, T., Kawai, M., Yamazaki, M., and Ozono, K. (2018). Phosphate as a Signaling molecule and its sensing mechanism. *Physiol. Rev.* 98, 2317–2348. doi: 10.1152/physrev.00022.2017

Mizuno, M., Mitchell, J. H., Crawford, S., Huang, C. L., Maalouf, N., Hu, M. C., et al. (2016). High dietary phosphate intake induces hypertension and augments exercise pressor reflex function in rats. *Am. J. Physiol. Regul. Integr. Comp. Physiol.* 311, R39–R48. doi: 10.1152/ajpregu.00124.2016

Moe, S. M., Chen, N. X., Seifert, M. F., Sinders, R. M., Duan, D., Chen, X., et al. (2009). A rat model of chronic kidney disease-mineral bone disorder. *Kidney Int.* 75, 176–184. doi: 10.1038/ki.2008.456

Moe, S. M., Zidehsarai, M. P., Chambers, M. A., Jackman, L. A., Radcliffe, J. S., Trevino, L. L., et al. (2011). Vegetarian compared with meat dietary protein source and phosphorus homeostasis in chronic kidney disease. *Clin. J. Am. Soc. Nephrol.* 6, 257–264. doi: 10.2215/CJN.05040610

Mohammad, J., Scanni, R., Bestmann, L., Henry, N., Hulter, H. N., and Krapf, R. (2018). A controlled increase in dietary phosphate elevates bp in healthy human subjects. *J. Am. Soc. Nephrol.* 29, 2089–2098. doi: 10.1681/ASN.2017121254

Müller, W. E. G., Wang, S., Neufurth, M., Kokkinopoulou, M., Feng, Q., Schröder, H. C., et al. (2017). Polyphosphate as a donor of high-energy phosphate for the synthesis of ADP and ATP. *J. Cell Sci.* 130, 2747–2756. doi: 10.1242/jcs.204941

Nakagawa, Y., Komaba, H., and Fukagawa, M. (2020). Magnesium as a Janus-faced inhibitor of calcification. *Kidney Int.* 97, 448–450. doi: 10.1016/j.kint.2019.11.035

Noori, N., Kalantar-Zadeh, K., Kovesdy, C. P., Bross, R., Benner, D., and Kopple, J. D. (2010). Association of dietary phosphorus intake and phosphorus to protein ratio with mortality in hemodialysis patients. *Clin. J. Am. Soc. Nephrol.* 5, 683–692. doi: 10.2215/CJN.08601209

Oh, J., Weng, S., Felton, S. K., Bhandare, S., Riek, A., Butler, B., et al. (2009). 1,25(OH)2 vitamin d inhibits foam cell formation and suppresses macrophage cholesterol uptake in patients with type 2 diabetes mellitus. *Circulation* 120, 687–698. doi: 10.1161/CIRCULATIONAHA.109.856070

Oliveira, R. B., Cancela, A. L. E., Graciolli, F. G., Reis, L. M. D., Draibe, S. A., Cuppari, L., et al. (2010). Early control of PTH and FGF23 in normophosphatemic CKD patients: a new target in CKD-MBD therapy? *Clin. J. Am. Soc. Nephrol.* 5, 286–291. doi: 10.2215/CJN.05420709

Olmos, G., Martínez-Miguel, P., Alcalde-Estevez, E., Medrano, D., Sosa, P., Rodríguez-Mañas, L., et al. (2017). Hyperphosphatemia induces senescence in human endothelial cells by increasing endothelin-1 production. *Aging Cell* 16, 1300–1312. doi: 10.1111/acel.12664

Palmer, S. C., Gardner, S., Tonelli, M., Mavridis, D., Johnson, D. W., Craig, J. C., et al. (2016). Phosphate-Binding agents in adults with CKD: a network meta-analysis of randomized trials. *Am. J. Kidney Di* 68, 691–702. doi: 10.1053/j.ajkd.2016.05.015

Park, K. S., Lee, Y., Park, G. M., Park, J. H., Kim, Y. G., Yang, D. H., et al. (2020). Association between serum phosphorus and subclinical coronary atherosclerosis in asymptomatic Korean individuals without kidney dysfunction. *Am. J. Clin. Nutr.* 112, 66–73. doi: 10.1093/ajcn/nqaa091

Patel, R. K., Jeemon, P., Stevens, K. K., Mccallum, L., Hastie, C. E., Schneider, A., et al. (2015). Association between serum phosphate and calcium, long-term blood pressure, and mortality in treated hypertensive adults. *J. Hypertens.* 33, 2046–2053. doi: 10.1097/HJH.0000000000000659

Phan, O., Ivanovski, O., Nguyen-Khoa, T., Mothu, N., Angulo, J., Westenfeld, R., et al. (2005). Sevelamer prevents uremia-enhanced atherosclerosis progression in apolipoprotein E-deficient mice. *Circulation* 112, 2875–2882. doi: 10.1161/CIRCULATIONAHA105.541854

Rattazzi, M., Bertacco, E., Vecchio, A. D., Puato, M., Faggin, E., and Pauletto, P. (2013). Aortic valve calcification in chronic kidney disease. *Nephrol. Dial. Transplan.* 28, 2968–2976. doi: 10.1093/ndt/gft310

Reiss, A. B., Miyawaki, N., Moon, J., Kasselman, L. J., Iryna Voloshyna, I., D'Avino, R. Jr., et al. (2018). CKD, arterial calcification, atherosclerosis and bone health: inter-relationships and controversies. *Atherosclerosis* 278, 49–59. doi: 10.1016/j.atherosclerosis.2018.08.046

Ren, Z. Z., Yan, J. K., Pan, C., Liu, Y. L., Wen, H. Y., Yang, X., et al. (2020). Supplemental nicotinamide dose-dependently regulates body phosphorus excretion via altering type II sodium-phosphate co-transporter expressions in laying hens. *J. Nutr.* 150, 2070–2076. doi: 10.1093/jn/nxaa148

Richter, B., Haller, J., Haffner, D., and Leifheit-Nestler, M. (2016). Klotho modulates FGF23-mediated NO synthesis and oxidative stress in human coronary artery endothelial cells. *Pflugers. Arch.* 468, 1621–1635. doi: 10.1007/s00424-016-1858-x

Rodríguez-Ortiz, M. E., Alcalá-Díaz, J. F., Canalejo, A., Torres-Peña, J. D., Gómez-Delgado, F., Muñoz-Castañeda, J. R., et al. (2020). Fibroblast growth factor 23 predicts carotid atherosclerosis in individuals without kidney disease. the cordioprev study. *Eur. J. Int. Med.* 74, 79–85. doi: 10.1016/j.ejim.2019.12.008

Roumeliotis, S., Mallamaci, F., and Zoccali, C. (2020). Endothelial dysfunction in chronic kidney disease, from biology to clinical outcomes: a 2020 update. *J. Clin. Med.* 9:2359. doi: 10.3390/jcm9082359

Roy, C., Lejeune, S., Slimani, A., de Meester, C., As, S. A. A., Rousseau, M. F., et al. (2020). Fibroblast growth factor 23: a biomarker of fibrosis and prognosis in heart failure with preserved ejection fraction. *ESC Heart Fail* 7, 2494–2507. doi: 10.1002/ehf2.12816

Ruospo, M., Palmer, S. C., Natale, P., Craig, J. C., Vecchio, M., Elder, G. J., et al. (2018). Phosphate binders for preventing and treating chronic kidney disease-mineral and bone disorder (CKD-MBD). *Cochrane Database. Syst. Rev.* 8:CD006023. doi: 10.1002/14651858.CD006023.pub3

Sabbagh, Y., O'Brien, S. P., Song, W., Boulanger, J. H., Stockmann, A., Arbeeny, C., et al. (2009). Intestinal npt2b plays a major role in phosphate absorption and homeostasis. *J. Am. Soc. Nephrol.* 20, 2348–2358. doi: 10.1681/ASN.2009050559

Sakaguchi, Y., Fujii, N., Shoji, T., Hayashi, T., Rakugi, H., Iseki, K., et al. (2014). Magnesium modifies the cardiovascular mortality risk associated with hyperphosphatemia in patients undergoing hemodialysis: a cohort study. *PLoS One* 9:e116273. doi: 10.1371/journal.pone.0116273

Sakaguchi, Y., Hamano, T., Matsui, I., Oka, T., Yamaguchi, S., Kubota, K., et al. (2019a). Low magnesium diet aggravates phosphate-induced kidney injury. *Nephrol. Dial. Transplant.* 34, 1310–1319. doi: 10.1093/ndt/gfy358

Sakaguchi, Y., Hamano, T., Obi, Y., Monden, C., Oka, T., Yamaguchi, S., et al. (2019b). A randomized trial of magnesium oxide and oral carbon adsorbent for coronary artery calcification in predialysis CKD. *J. Am. Soc. Nephrol.* 30, 1073–1085. doi: 10.1681/ASN.2018111150

Sakaguchi, Y., Iwatani, H., Hamano, T., Tomida, K., Kawabata, H., Kusunoki, Y., et al. (2015). Magnesium modifies the association between serum phosphate and the risk of progression to end-stage kidney disease in patients with non-diabetic chronic kidney disease. *Kidney Int.* 88, 833–842. doi: 10.1038/ki.2015.165

Sarnak, M. J., Amann, K., Bangalore, S., Cavalcante, J. L., Charytan, D. M., Craig, J. C., et al. (2019). Chronic kidney disease and coronary artery disease: JACC state-of-the-art review. *J. Am. Coll. Cardiol.* 74, 1823–1838. doi: 10.1016/j.jacc.2019.08.1017

Schiavi, S. C., Tang, W., Bracken, C., O'Brien, S. P., Song, W., Boulanger, J., et al. (2012). Npt2b deletion attenuates hyperphosphatemia associated with CKD. *J. Am. Soc. Nephrol.* 23, 1691–1700. doi: 10.1681/ASN.2011121213

Scialla, J. J., Appel, L. J., Wolf, M., Yang, W., Zhang, X., Sozio, S. M., et al. (2012). Plant protein intake is associated with fibroblast growth factor 23 and serum bicarbonate levels in patients with chronic kidney disease: the chronic renal insufficiency cohort study. *J. Ren. Nutr.* 22, 379–388.e1. doi: 10.1053/j.jrn.2012.01.026

Scialla, J. J., and Wolf, M. (2014). Roles of phosphate and fibroblast growth factor 23 in cardiovascular disease. *Nat. Rev. Nephrol.* 10, 268–278. doi: 10.1038/nrneph.2014.49

Shang, D., Xie, Q., Shang, B., Zhang, M., You, L., Hao, C. M., et al. (2017). Hyperphosphatemia and hs-CRP initiate the coronary artery calcification in peritoneal dialysis patients. *Biomed. Res. Int.* 2017:2520510. doi: 10.1155/2017/2520510

Shin, S., Kim, K. J., Chang, H. J., Cho, I., Kim, Y. J., Choi, B. W., et al. (2012). Impact of serum calcium and phosphate on coronary atherosclerosis detected by cardiac computed tomography. *Eur. Heart J.* 33, 2873–2881. doi: 10.1093/eurheartj/ehs152

Shinaberger, C. S., Greenland, S., Kopple, J. D., Wyck, D. V., Mehrotra, R., Kovesdy, C. P., et al. (2008). Is controlling phosphorus by decreasing dietary protein intake beneficial or harmful in persons with chronic kidney disease? *Am. J. Clin. Nutr.* 88, 1511–1518. doi: 10.3945/ajcn.2008.26665

Shiota, A., Taketani, Y., Maekawa, Y., Yasutomo, K., Sata, M., Sakai, T., et al. (2011). High phosphate diet reduces atherosclerosis formation in apolipoprotein E-deficient mice. *J. Clin. Biochem. Nutr.* 49, 109–114. doi: 10.3164/jcbn.10-150

Shobeiri, N., Adams, M. A., and Holden, R. M. (2014). Phosphate: an old bone molecule but new cardiovascular risk factor. *Br. J. Clin. Pharmacol.* 77, 39–54. doi: 10.1111/bcp.12117

Shroff, R. C., McNair, R., Figg, N., Skepper, J. N., Schurgers, L., Gupta, A., et al. (2008). Dialysis accelerates medial vascular calcification in part by triggering smooth muscle cell apoptosis. *Circulation* 118, 1748–1757. doi: 10.1161/CIRCULATIONAHA.108.783738

Shuvy, M., Abedat, S., Eliaz, R., Abu-Rmeileh, I., Abu-Snieneh, A., Ben-Dov, I. Z., et al. (2019). Hyperphosphatemia is required for initiation but not propagation of kidney failure-induced calcific aortic valve disease. *Am. J. Physiol. Heart Circ. Physiol.* 317, H695–H704. doi: 10.1152/ajpheart.00765.2018

Sikura, K. E., Potor, L., Szerafin, T., Oros, M., Nagy, P., Méhes, G., et al. (2020). Hydrogen sulfide inhibits calcification of heart valves; implications for calcific aortic valve disease. *Br. J. Pharmacol.* 177, 793–809. doi: 10.1111/bph.14691

Singh, A. P., Sosa, M. X., Fang, J., Shanmukhappa, S. K., Hubaud, A., Fawcett, C. H., et al. (2019). αKlotho regulates age-associated vascular calcification and lifespan in zebrafish. *Cell Rep.* 28, 2767–2776.e5. doi: 10.1016/j.celrep.2019.08.013

Six, I., Okazaki, H., Gross, P., Cagnard, J., Boudot, C., Maizel, J., et al. (2014). Direct, acute effects of Klotho and FGF23 on vascular smooth muscle and endothelium. *PLoS One* 9:e93423. doi: 10.1371/journal.pone.0093423

St. Peter, W. L., Wazny, L. D., Weinhandl, E., Cardone, K. E., and Hudson, J. Q. (2017). A review of phosphate binders in chronic kidney disease: incremental progress or just higher costs? *Drugs* 77, 1155–1186. doi: 10.1007/s40265-017-0758-5

Stevens, K. K., Denby, L., Patel, R. K., Mark, P. B., Kettlewell, S., Smith, G. L., et al. (2017). Deleterious effects of phosphate on vascular and endothelial function via disruption to the nitric oxide pathway. *Nephrol. Dial. Transplant.* 32, 1617–1627. doi: 10.1093/ndt/gfw252

Sullivan, C., Sayre, S. S., Leon, J. B., Machekano, R., Love, T. E., Porter, D., et al. (2009). Effect of food additives on hyperphosphatemia among patients with end-stage renal disease: a randomized controlled trial. *JAMA* 301, 629–635. doi: 10.1001/jama.2009.96

Takashi, Y., and Fukumoto, S. (2020a). Fibroblast growth factor receptor as a potential candidate for phosphate sensing. *Curr. Opin. Nephrol. Hypertens* 29, 446–452. doi: 10.1097/MNH.0000000000000618

Takashi, Y., and Fukumoto, S. (2020b). Phosphate-sensing and regulatory mechanism of FGF23 production. *J. Endocrinol. Invest.* 43, 877–883. doi: 10.1007/s40618-020-01205-9

Tan, S. J., Satake, S., Smith, E. R., Toussaint, N. D., Hewitson, T. D., and Holt, S. G. (2017). Parenteral iron polymaltose changes i:c-terminal FGF23 ratios in iron deficiency, but not in dialysis patients. *Eur. J. Clin. Nutr.* 71, 180–184. doi: 10.1038/ejcn.2016.217

Tero, R., Fukumoto, K., Motegi, T., Yoshida, M., Niwano, M., and Hirano-Iwata, A. (2017). Formation of cell membrane component domains in artificial lipid bilayer. *Sci. Rep.* 7:17905. doi: 10.1038/s41598-017-18242-9

Thomas, L., Xue, J., Murali, S. K., Fenton, R. A., Rieg, J. A. D., and Rieg, T. (2019). Pharmacological Npt2a inhibition causes phosphaturia and reduces plasma phosphate in mice with normal and reduced kidney function. *J. Am. Soc. Nephrol.* 30, 2128–2139. doi: 10.1681/ASN.2018121250

Tripepi, G., Kollerits, B., Leonardis, D., Yilmaz, M. I., Postorino, M., Fliser, D., et al. (2015). Competitive interaction between fibroblast growth factor 23 and asymmetric dimethylarginine in patients with CKD. *J. Am. Soc. Nephrol.* 26, 935–944. doi: 10.1681/ASN.2013121355

Tsai, W. C., Wu, H. Y., Peng, Y. S., Hsu, S. P., Chiu, Y. L., Yang, J. Y., et al. (2019). Short-Term effects of very-low-phosphate and low-phosphate diets on fibroblast growth factor 23 in hemodialysis patients: a randomized crossover trial. *Clin. J. Am. Soc. Nephrol.* 14, 1475–1483. doi: 10.2215/CJN.04250419

Tuzun, D., Oguz, A., Aydin, M. N., Kurutas, E. B., Ercan, O., Sahin, M., et al. (2018). Is FGF-23 an early indicator of atherosclerosis and cardiac dysfunction in patients with gestational diabetes? *Arch. Endocrinol. Metab.* 62, 506–513. doi: 10.20945/2359-3997000000070

van Vuren, A. J., Eisenga, M. F., van Straaten, S., Glenthøj, A., Gaillard, C. A. J. M., Bakker, S. J. L., et al. (2020). Interplay of erythropoietin, fibroblast growth factor 23, and erythroferrone in patients with hereditary hemolytic anemia. *Blood Adv.* 4, 1678–1682. doi: 10.1182/bloodadvances.2020001595

Verkaik, M., Juni, R. P., van Loon, E. P. M., van Poelgeest, E. M., Kwekkeboom, R. F. J., Gam, Z., et al. (2018). FGF23 impairs peripheral microvascular function in renal failure. *Am. J. Physiol. Heart Circ. Physiol.* 315, H1414–H1424. doi: 10.1152/ajpheart.00272.2018

Voelkl, J., Lang, F., Eckardt, K. U., Amann, K., Kuro-O, M., Pasch, A., et al. (2019). Signaling pathways involved in vascular smooth muscle cell calcification during hyperphosphatemia. *Cell Mol. Life. Sci.* 76, 2077–2091. doi: 10.1007/s00018-019-03054-z

Vogt, I., Haffner, D., and Leifheit-Nestler, M. (2019). FGF23 and phosphate-cardiovascular toxins in CKD. *Toxins (Basel)* 11:647. doi: 10.3390/toxins11110647

Wang, Q., Cui, Y., Yogendranath, P., and Wang, N. (2018). Blood pressure and heart rate variability are linked with hyperphosphatemia in chronic kidney disease patients. *Chronobiol. Int.* 35, 1329–1334. doi: 10.1080/07420528.2018.1486850

Wang, X., and Shapiro, J. I. (2019). Evolving concepts in the pathogenesis of uraemic cardiomyopathy. *Nat. Rev. Nephrol.* 15, 159–175. doi: 10.1038/s41581-018-0101-8

Yoon, C. Y., Park, J. T., Jhee, J. H., Noh, J., Kee, Y. K., Seo, C., et al. (2017). High dietary phosphorus density is a risk factor for incident chronic kidney disease development in diabetic subjects: a community-based prospective cohort study. *Am. J. Clin. Nutr.* 106, 311–321. doi: 10.3945/ajcn.116.151654

Zhou, T., Wang, Y., Liu, M., Huang, Y., Shi, J., Dong, N., et al. (2020). Curcumin inhibits calcification of human aortic valve interstitial cells by interfering NF-κB, AKT, and ERK pathways. *Phytother. Res.* 34, 2074–2081. doi: 10.1002/ptr.6674

Conflict of Interest: The authors declare that the research was conducted in the absence of any commercial or financial relationships that could be construed as a potential conflict of interest.

frontiers in Cell and Developmental Biology

ORIGINAL RESEARCH
published: 04 March 2021
doi: 10.3389/fcell.2021.637424

Senescent T Cell Induces Brown Adipose Tissue "Whitening" *Via* Secreting IFN-γ

Xiao-Xi Pan[1†], Kang-Li Yao[2†], Yong-Feng Yang[3], Qian Ge[1], Run Zhang[2], Ping-Jin Gao[1], Cheng-Chao Ruan[3] and Fang Wu[2]**

[1] Department of Cardiovascular Medicine, State Key Laboratory of Medical Genomics, Shanghai Key Laboratory of Hypertension, Department of Hypertension, Ruijin Hospital and Shanghai Institute of Hypertension, Shanghai Jiao Tong University School of Medicine, Shanghai, China, [2] Department of Geriatrics, Ruijin Hospital, Shanghai Jiao Tong University School of Medicine, Shanghai, China, [3] Department of Physiology and Pathophysiology, School of Basic Medical Sciences, Shanghai Key Laboratory of Bioactive Small Molecules, Fudan University, Shanghai, China

OPEN ACCESS

Edited by:
Xiaoqiang Tang,
Sichuan University, China

Reviewed by:
Xinran Ma,
East China Normal University, China
Xifeng Lu,
Shenzhen University, China

***Correspondence:**
Cheng-Chao Ruan
ruancc@fudan.edu.cn;
ruancc@sina.com
Fang Wu
wufangrjh@163.com

[†]These authors have contributed equally to this work and share first authorship

Specialty section:
This article was submitted to Cellular Biochemistry, a section of the journal Frontiers in Cell and Developmental Biology

Received: 03 December 2020
Accepted: 29 January 2021
Published: 04 March 2021

Citation:
Pan X-X, Yao K-L, Yang Y-F, Ge Q, Zhang R, Gao P-J, Ruan C-C and Wu F (2021) Senescent T Cell Induces Brown Adipose Tissue "Whitening" Via Secreting IFN-γ. Front. Cell Dev. Biol. 9:637424. doi: 10.3389/fcell.2021.637424

Aging-associated chronic inflammation is a key contributing factor to a cluster of chronic metabolic disorders, such as cardiovascular disease, obesity, and type 2 diabetes. Immune cells particularly T cells accumulate in adipose tissue with advancing age, and there exists a cross talk between T cell and preadipocyte, contributing to age-related adipose tissue remodeling. Here, we compared the difference in morphology and function of adipose tissue between young (3-month-old) and old (18-month-old) mice and showed the phenomenon of brown adipose tissue (BAT) "whitening" in old mice. Flow cytometry analysis suggested an increased proportion of T cells in BAT of old mice comparing with the young and exhibited senescent characteristics. We take advantage of coculture system to demonstrate directly that senescent T cells inhibited brown adipocyte differentiation of preadipocytes in adipose tissue. Mechanistically, both *in vitro* and *in vivo* studies suggested that senescent T cells produced and released a higher level of IFN-γ, which plays a critical role in inhibition of preadipocyte-to-brown adipocyte differentiation. Taken together, the data indicate that senescent T cell-derived IFN-γ is a key regulator in brown adipocyte differentiation.

Keywords: senescence, T cell, adipose tissue, preadipocyte, brown adipocyte differentiation, IFN-γ

INTRODUCTION

Advancing age is a major risk factor for chronic metabolic diseases, including cardiovascular disease and type 2 diabetes (Partridge et al., 2018). It has become evident that adipose tissue plays an endocrine function, not merely an energy reservoir pool, and exerts a fundamental influence on metabolic regulation (Oikonomou and Antoniades, 2019; Scheja and Heeren, 2019). Adipose tissue is classified as white adipose tissue (WAT) and brown adipose tissue (BAT). BAT has been considered a key for thermogenesis to maintaining body temperature, while WAT stores and releases lipids and is involved in promoting inflammation (Bartelt and Heeren, 2014; van Eenige et al., 2018). Extensive studies have indicated that WAT could obtain multilocular lipid droplet morphology and expression of BAT-specific genes such as Ucp1, Pparg, and Pgc1a in response to various stimuli (Harms and Seale, 2013). In the contrast, BAT "whitening" refers to acquisition of white adipocyte characteristics with enlarged lipid droplets and loss of normal

structure and function of brown adipocyte (Shimizu et al., 2014). Age-related alteration in adipose tissues is manifested on the distribution and composition, as well as a decline in adipose tissue quality and function.

Adipose tissue is composed mainly of adipocytes that interact with other non-adipocyte cells including pre-adipocytes or progenitor cells, endothelial cells, macrophages, and lymphocytes, all of which perform a series of functions for adipose tissue homeostasis (Hafidi et al., 2019). Aging is closely associated with a low-grade systemic inflammation, and innate and adaptive immune systems are influenced by aging. Macrophages, T cells, and other immune cells accumulate with advancing age. Among these, T cells are most susceptible to the detrimental effects of aging and tend to polarize to a proinflammatory phenotype, producing high level of IFN-γ, tumor necrosis factor α (TNF-α), IL-6, and so on (Zanni et al., 2003; Garg et al., 2014; Kalathookunnel Antony et al., 2018). Immune cells infiltrated in adipose tissue have been implicated as either positive or negative regulators in adipogenesis (Brestoff et al., 2015; Lee et al., 2015; Wang and Seale, 2016). Emerging evidence suggests that T cells might participate in regulating differentiation of pre-adipocytes (Wu et al., 2007; Park et al., 2019). However, little attention has been given to contribution of senescent T cells to adipogenic differentiation.

In the present study, we investigated whether T cell senescence in adipose tissue contributed to adipose tissue dysfunction, resulting in age-related metabolic disorders. We verified the BAT whitening in old mice accompanied with increased proportion of T cells. We provided the direct evidence that senescent T cells inhibited the brown adipocyte differentiation of preadipocytes, and white adipocytes formation promoted T cell secreting inflammatory cytokines in turn. Impressively, the inhibitory effect of senescent T cells on BAT whitening was attenuated by blocking IFN-γ. Overall, our findings suggested that senescent T lymphocytes play a negative role in regulation of brown adipocyte formation as well as inflammatory response of adipose tissue *via* secreting inflammatory cytokines, particularly IFN-γ.

MATERIALS AND METHODS

Animals

Wild-type (WT) male mice including young (3-month-old) and old (18-month old) mice, as well as RAG1−/− mice (t004753) were obtained from Model Animal Research Center of Nanjing University (GemPharmatech, Jiangsu, China). All mice were on C57BL/6J background. All animal experiments were approved by institutional guidelines established by the Committee of Ethics on Animal Experiments of Shanghai Jiao Tong University School of Medicine.

Histological Analysis

In order to perform hematoxylin-eosin (H&E) staining, paraformaldehyde-fixed adipose tissues were embedded in paraffin and then cut into 5-μm transverse sections. For immunofluorescence staining, sections were boiled in sodium citrate buffer to retrieve antigen and blocked with 5% bovine serum albumin. Then the sections were then incubated with primary antibodies at 4°C overnight, and incubated with the respective fluorochrome-conjugated secondary antibodies, followed by nuclear staining with 4,6-diamidino-2-phenylindole (DAPI). Images were observed with the Carl Zeiss Axio Imager M2 microscope (Carl Zeiss Corporation, Germany).

Flow Cytometry Analysis

Adipose tissues including interscapular brown adipose tissue (BAT), subcutaneous adipose tissue (SAT), or epididymal visceral adipose tissue (VAT) were isolated from young or old WT mice and cut into small pieces, which digested with collagenase solution (2 mg/ml collagenase type II in RPMI 1,640 medium) at 37°C for 30 min. The samples were filtered with 40 μM strainers and centrifuged at 450 × *g* for 5 min at 4°C. Samples were analyzed for specific surface and intracellular markers by Beckman CytoFLEX (Beckman Coulter, United States). Antibodies used for staining were as follows: Fixable Viability Dye-APC-eFlour780 (65-0865-14, eBioscience), CD45-Violet 510 (103138, BioLegend), CD3e-Violet 605 (100351, BioLegend), IFN-γ-APC (17-7311-81, eBioscience), CD28-PE (12-0281-82, eBioscience), CD44-APC-eFlour780 (47-0441-82, eBioscience), and CD62L-eFlour450 (48-0621-80, eBioscience).

Cell Culture and Differentiation

Stromal vascular fraction (SVF) cells isolated from BAT or SAT of WT mice were maintained in pre-adipocyte medium (DMEM/F12, 10% FBS and 1% penicillin/streptomycin) at 37°C with 5% CO_2. SVF cells at 80% confluences were transferred into brown adipocyte (BA) differentiation medium or white adipocyte (WA) differentiation medium and extended for 8 days until adipocyte formation as previously described (Pan et al., 2019). Splenic $CD3^+$ T cells isolated by negative selection kit (8804-6820-74, eBioscience) from young or old mice were cultured in complete medium (RPMI1640 with 10% FBS and 1% penicillin–streptomycin) and activated by anti-CD3 antibody (2 μg/ml) (16-0031-85, eBioscience) and anti-CD28 antibody (1 μg/ml) (16-0281-85; eBioscience).

To investigate whether T cells could regulate adipogenic differentiation of SVF cells, SVF cells were cocultured with $CD3^+$ T cells of young and old mice, respectively. After coculture for 8 days, T cells and differentiated SVF cells were collected, respectively, for further analysis. To block IFN-γ, IFN-γ-neutralizing antibody (10 μg/ml) was added to cultured media at the beginning of cocultivation.

Western Blotting Analysis

Total protein was extracted from adipose tissues or cultured cells, using RIPA lysis buffer with protease inhibitors cocktail (Selleck). Protein lysates were resolved by SDS-PAGE and transferred onto PVDF membranes. Membranes were then incubated with primary antibodies, including anti-UCP-1 (Abcam, ab23841), anti-perilipin (Abcam, ab61682), anti-APN (R&D, AF1119), anti-PPARγ (Santa Cruz, sc-7273), anti-PGC1α (Santa Cruz, sc-13067), and β-actin for normalization. Subsequently,

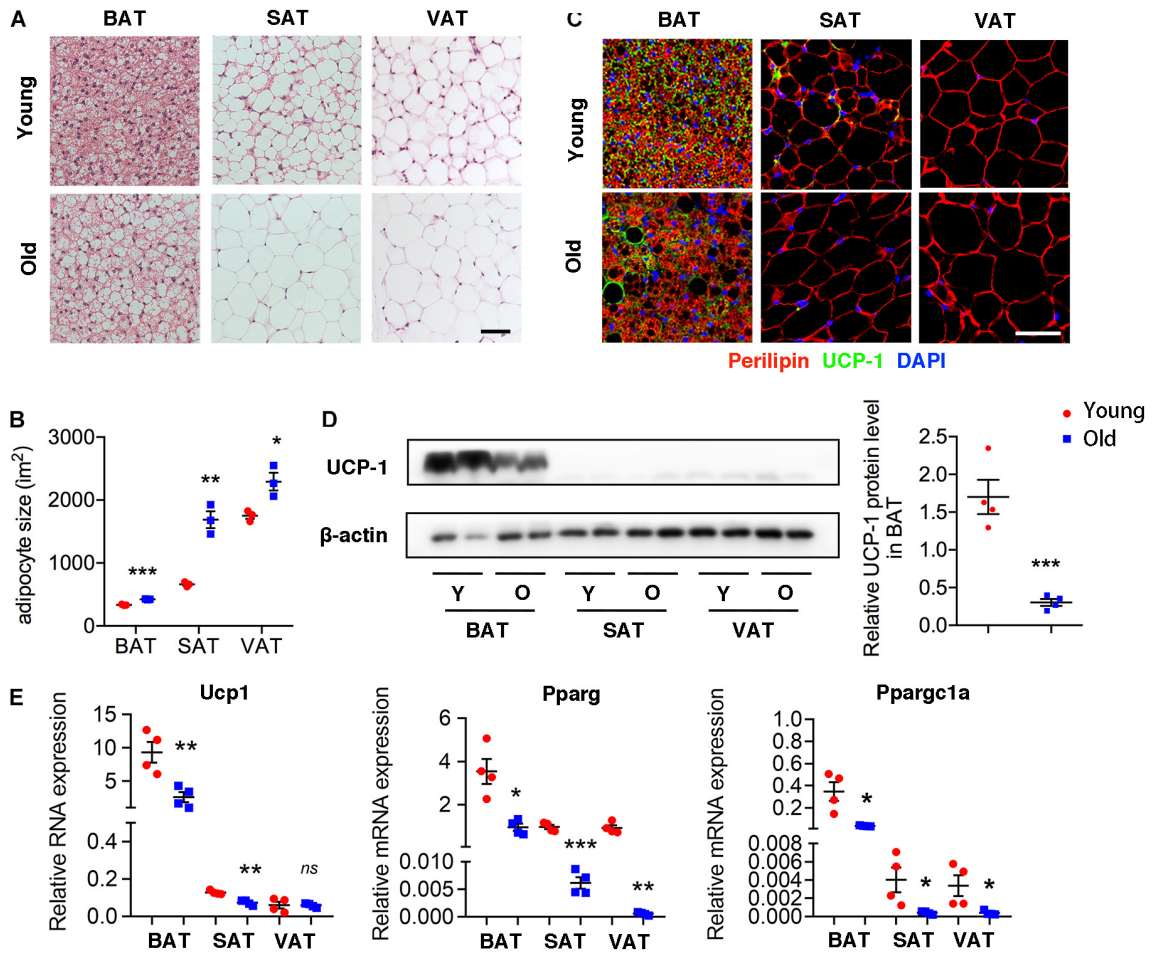

FIGURE 1 | Aging induced brown adipose tissue whitening. **(A)** Representative H&E-stained sections of BAT, SAT, and VAT of young and old mice. **(B)** The quantitative analysis of adipocyte size. **(C)** Representative immunofluorescence of perilipin and UCP-1 in adipose tissues from young and old mice. 4′,6-Diamidino-2-phenylindole (DAPI) was used to detect nucleus. **(D)** Representative Western blot for UCP-1 expression in adipose tissues and their quantitation. **(E)** qRT-PCR analysis of mRNA expression levels of Ucp1, Pparg, and Ppargc1a in adipose tissues. Scale bar, 50 μm. $^{*}P < 0.05$; $^{**}P < 0.01$; $^{***}P < 0.001$ vs. young mice, $n = 4$ per group.

incubation with HRP-conjugated antibodies, and then protein signals were detected with electrochemiluminescence (ECL) detection reagents.

Quantitative Real-Time Polymerase Chain Reaction

Total RNA from adipose tissues or cultured cells was extracted with Trizol (Invitrogen) followed by reverse transcription with 1 μg total RNA according to the manufacturer's protocol. Quantitative real-time polymerase chain reaction (qRT–PCR) were performed with SYBR qPCR Master Mix (Vazyme, China) on ABI PRISM 7900 machine (Applied Biosystems). β-Actin was used as the standard reference. The data were calculated using the 2-ΔΔCT method. Sequences of primers were as follows. mβ-Actin: forward: 5′-CTA AGG CCA ACC GTG AAA AGA T-3′, reverse: 5′-GGG ACA GCA CAG CCT GGA T-3′; Ucp1: forward: 5′-AGG CTT CCA GTA CCA TTA GGT-3′, reverse: 5′-CTG AGT GAG GCA AAG CTG ATT T-3′; Pparg: forward: 5′-TTA GAT GAC AGT GAC TTG GC-3′, reverse: 5′-TCT TCT GGA GCA CCT TGG-3′; Ppargc1a: forward: 5′-GAA GTG GTG TAG CGA CCA ATC-3′, reverse: 5′-AAT GAG GGC AAT CCG TCT TCA-3′; Plin1: forward:5′-GTG CAA TGC CTA TGA GAA GGG TGT AC-3′, reverse: 5′-GTA GAG ATG GTG CCC TTC AGT TCA GA-3′; Adipoq: forward: 5′-GAT GGC AGA GAT GGC ACT CC-3′, reverse: 5′-CTT GCC AGT GCT GCC GTC AT-3′; Ifng: forward: 5′-ATC TGG AGG AAC TGG CAA AA-3′, reverse: 5′-TTC AAG ACT TCA AAG AGT CTG AGG-3′; Il10: forward: 5′-TGG ACA ACA TAC TGC TAA CCG-3′, reverse: 5′-GGA TCA TTT CCG ATA AGG CT-3′; Il6: forward: 5′-TGT GCA ATG GCA ATT CTG AT-3′, reverse: 5′-GGT ACT CCA GAA GAC CAG AGG A -3′.

Statistical Analysis

Results were presented as mean ± SEM and analyzed using Prism (Graph Pad Software). Statistical comparison of data between two groups was tested by unpaired two-tailed Student's

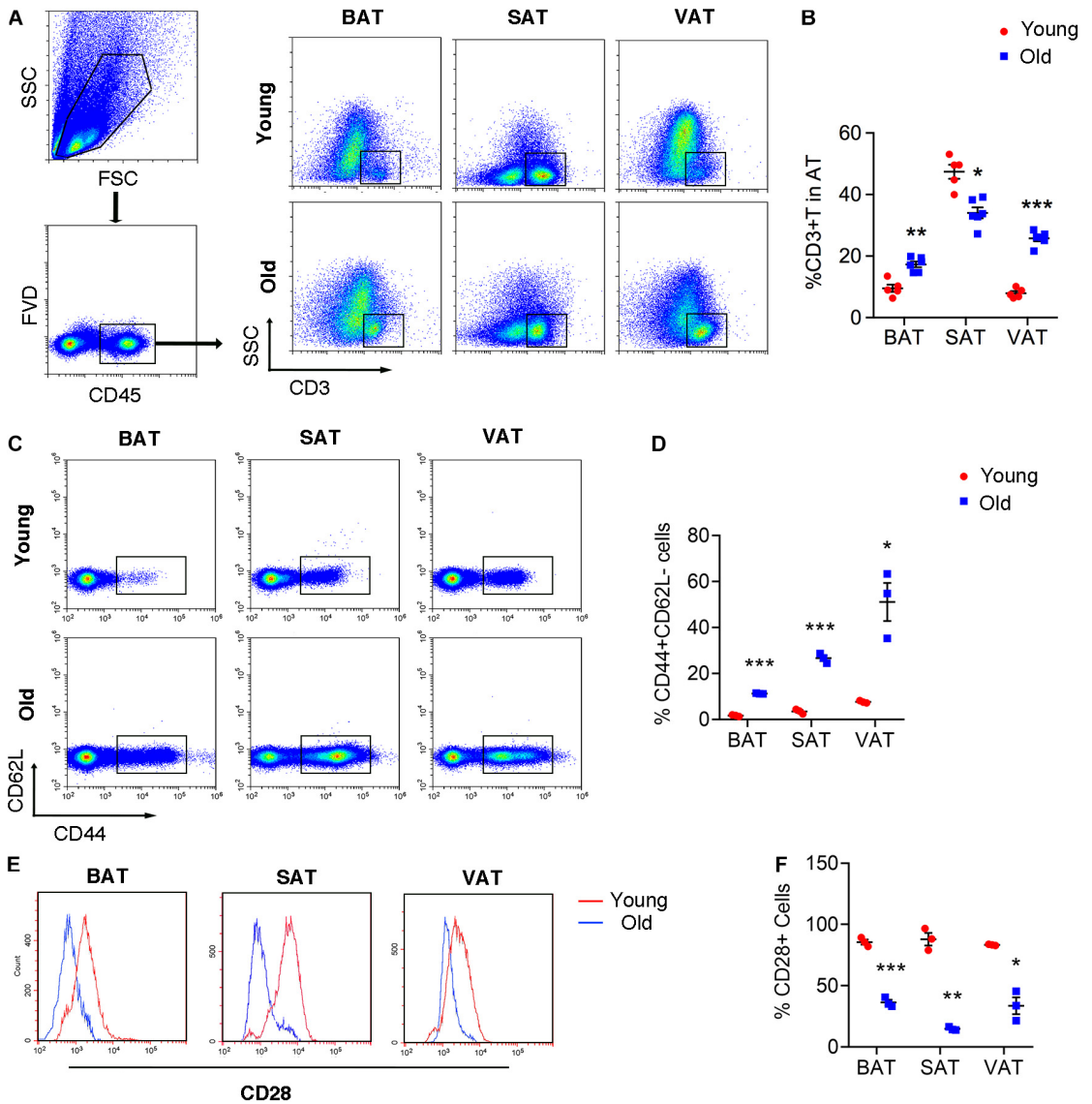

FIGURE 2 | T cell senescence in various adipose tissues of old mice. **(A,B)** Flow cytometric analysis of $CD45^{+}CD3^{+}$ T cells in AT of young and old mice and their quantitation. **(C,D)** Representative flow cytometric analysis of CD44 subsets in T cells isolated from adipose tissue and their quantification. **(E,F)** Representative flow cytometry of $CD28^{+}$ T cells in adipose tissue from young or old mice and their quantification. $^{*}P < 0.05$; $^{**}P < 0.01$; $^{***}P < 0.001$ vs. young mice, $n = 3{\sim}6$ per group.

t test. The value of $P < 0.05$ was considered to be statistically significant.

RESULTS

Aging Induces Brown Adipose Tissue "Whitening" in Adipose Tissue in the Whole Body

H&E staining of different adipose tissue showed dramatically differences in size and characterization. The size of adipocytes in old mice was significantly larger than those in young mice, including BAT, SAT, and VAT. Furthermore, brown adipocytes contained multilocular lipid droplets in BAT of young mice, while adipocytes in aged mice tended to have larger locular lipid droplets, a morphology more similar to a white adipocyte relative to those in young mice (**Figures 1A,B**). More importantly, UCP-1 expression fundamentally decreased in BAT of old mice comparing with that in young mice. Moreover, UCP-1 was weakly detected in the SAT of young mice, whereas it was not detected in old mice (**Figure 1C**). Western blot and qRT-PCR analysis also demonstrated that a lower level of UCP-1 both in BAT of old mice than that in young mice (**Figures 1D,E**). qRT-PCR analysis further indicated that genes involved in brown adipocyte formation, such as Pparg and

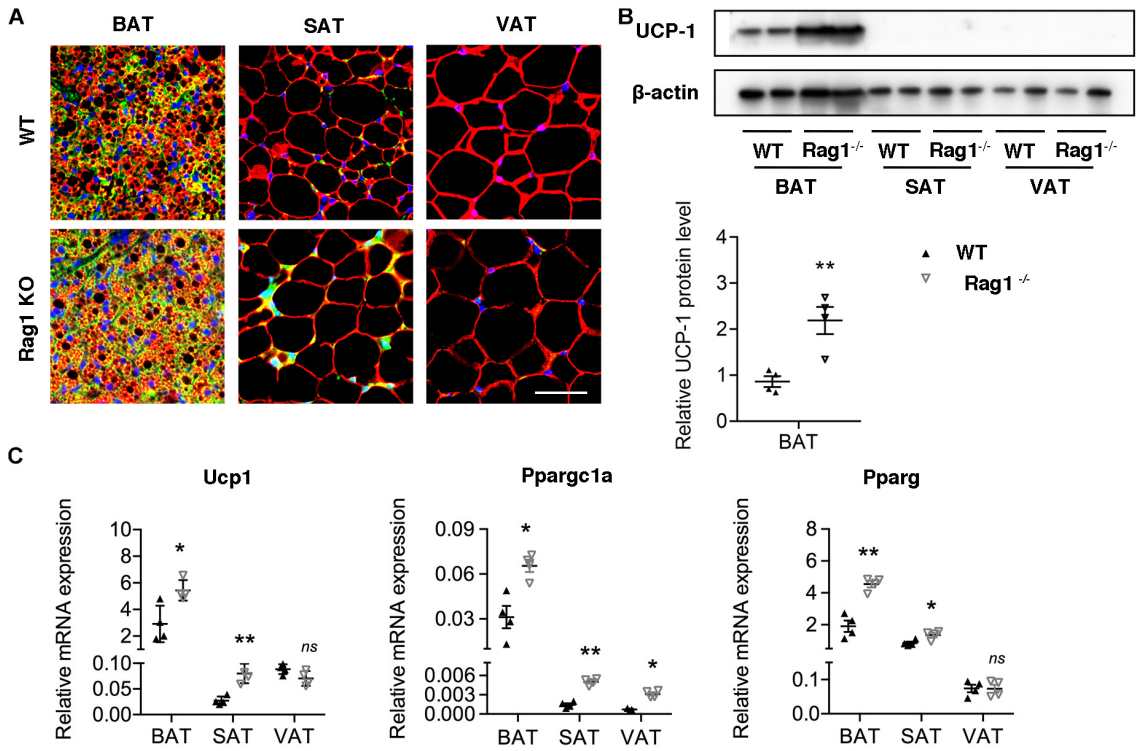

FIGURE 3 | T cell deficiency promoted brown adipocyte formation. **(A)** Representative immunofluorescence of perilipin (red) and UCP-1 (green) in adipose tissues from WT and RAG1 KO mice. **(B)** Representative Western blot and quantitation for UCP-1 in BAT, SAT, and VAT of WT and Rag1 KO mice. **(C)** qRT-PCR analysis of relative mRNA expression of Ucp1, Pparg, and Ppargc1a in AT of WT and Rag1 KO mice. $^{*}P < 0.05$; $^{**}P < 0.01$ vs. WT mice, $n = 4$ per group.

Ppargc1a decreased in these adipose tissues of old mice. All of those indicated that aging inhibited brown adipocyte formation, resulting in BAT whitening.

Infiltration of Senescent T Cell in Adipose Tissue of Old Mice

Given the emerging evidence of immune cells involved in the adipocyte thermogenesis, we firstly detected T cell infiltration in the adipose tissue during aging. Flow cytometric analysis revealed the two- to threefold amount of T cells in BAT and VAT of old mice than those in young mice. However, the proportion of T cells decreased in SAT of old mice (**Figures 2A,B**). More importantly, T cell isolated from adipose tissue of old mice, regardless of BAT, SAT, or VAT, exhibiting senescent features, including loss of CD28 and expansion of $CD44^{+}CD62L^{-}$ memory T cells (**Figures 2C–F**).

Considering the probable function of T cells in regulation of brown adipocyte formation, we assessed brown adipocyte-associated protein and mRNA expression in adipose tissues at different location in age- and weight-matched WT and Rag1 KO male mice that lack T and B cells. UCP-1 expression of both protein and mRNA were found to be higher in BAT of Rag1 KO mice, which was suggestive of an increased proportion of brown adipocytes (**Figures 3A–C**). Consistent with this, gene expression profiling revealed a higher level of Ppargc1a and Pparg, both of which are critical for brown adipocyte differentiation, indicating that T cells may participate in regulation of brown adipocyte differentiation or adipocyte browning (**Figure 3C**).

Senescent T Cell Inhibits Brown Adipocytes Differentiation of SVF Cells

To further investigate the role of senescent T cells in preadipocyte-to-brown adipocyte differentiation, SVF cells from BAT were cocultured with young or senescent T cells, respectively, through Transwell system. In addition, these SVF cells were differentiated toward brown adipocytes or white adipocytes, respectively. Interestingly, SVF cells cocultured with senescent T cells exhibited a significant decrease of brown adipocyte formation comparing with that with young T cells. Both young and senescent T cells seem to inhibit preadipocyte-to-white adipocyte differentiation, but there was no significant difference between two groups (**Figures 4A,B**). This trend was further confirmed by the protein levels of UCP-1 as well as mRNA expression. Quantitatively, old T cell dramatically suppressed expression of UCP-1 and perilipin protein in SVF cells (**Figures 4C,D**). Likewise, qRT-PCR data showed that senescent T cells inhibited expression of genes involved in brown adipogenic differentiation, including Ucp1, Pparg, and Ppargc1a. In addition, Plin1 and Adipoq were decreased in SVF with senescent T cells (**Figures 4E,F**). In line with BAT-preadipocyte differentiation, senescent T cells impaired SAT preadipocytes

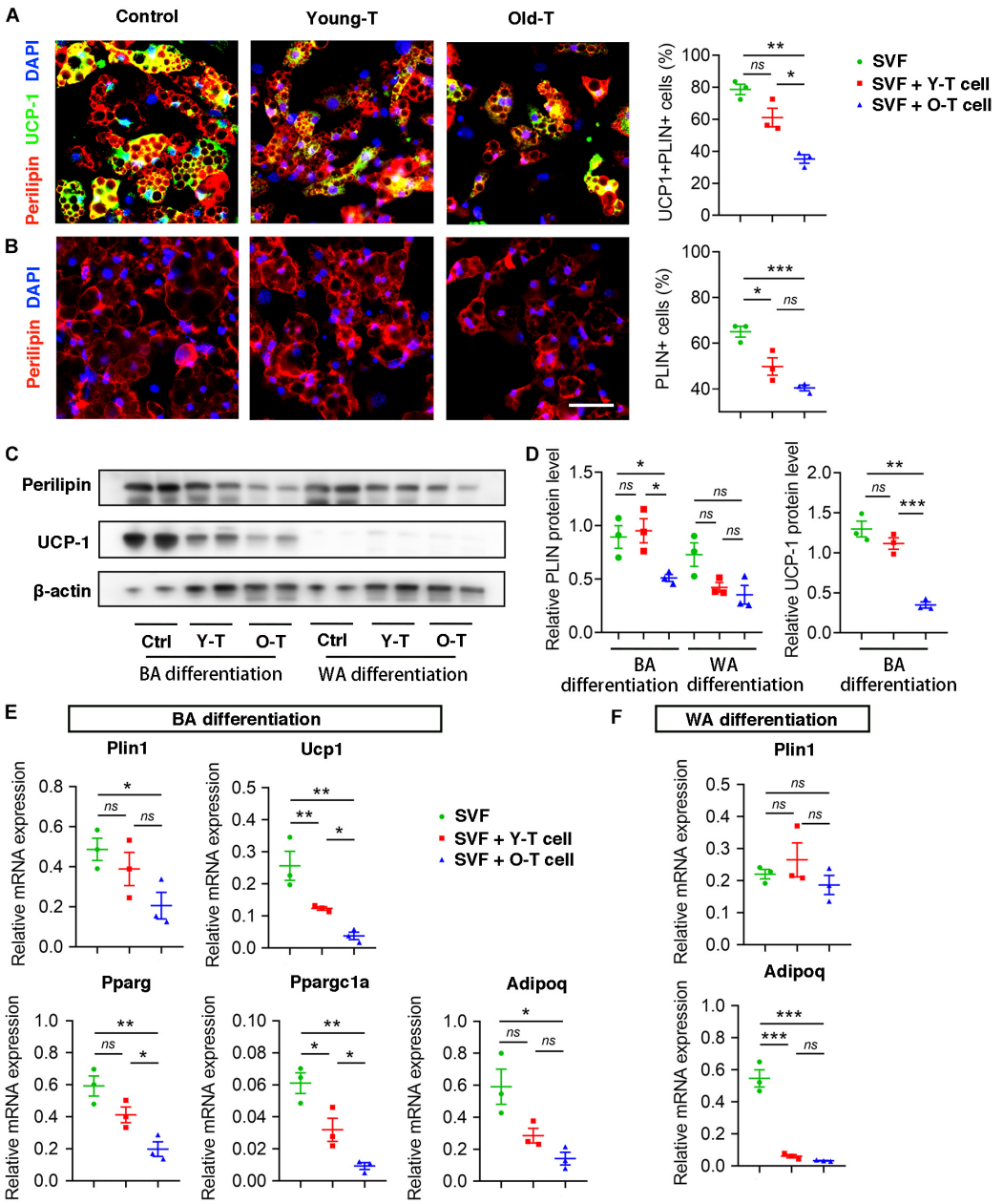

FIGURE 4 | Senescent T cells inhibited brown adipogenic differentiation of SVF cells. **(A,B)** The adipogenic differentiation was determined by costaining of perilipin and UCP-1, and their quantitative analysis. Scale bar, 50 μm. **(C,D)** Representative western blot and quantitation for relative UCP-1 and perilipin (PLIN) protein levels. **(E,F)** qRT-PCR analysis of relative mRNA expression of Plin1, Ucp1, Pparg, and Ppargc1a and Adipoq in SVF cells under BA differentiation **(E)** and WA differentiation **(F)**. $^{*}P < 0.05$; $^{**}P < 0.01$; $^{***}P < 0.001$, $n = 3$ independent experiments.

to differentiate toward brown adipocytes and white adipocytes (**Supplementary Figure 1**).

Senescent T Cell-Derived IFN-γ Involved in Regulation of Brown Adipogenic Differentiation

To explore the underlying mechanism that senescent T cells inhibit pre-adipocyte-to-brown adipocyte differentiation, our previous studies had demonstrated that senescent T cells secret a higher level of IFN-γ than young T cells (Pan et al., 2020). Thus, we detected inflammatory gene expression, including Ifng, Il10, and Il6 in varying adipose tissues of young and old mice. Expression of Ifng was significantly increased in BAT, SAT, as well as VAT of old mice, compared with adipose tissue of young mice. However, Il10 expression was enhanced in SAT whereas being decreased in VAT of old mice compared with the young ones. In addition, there were no significant differences in Il6 expression

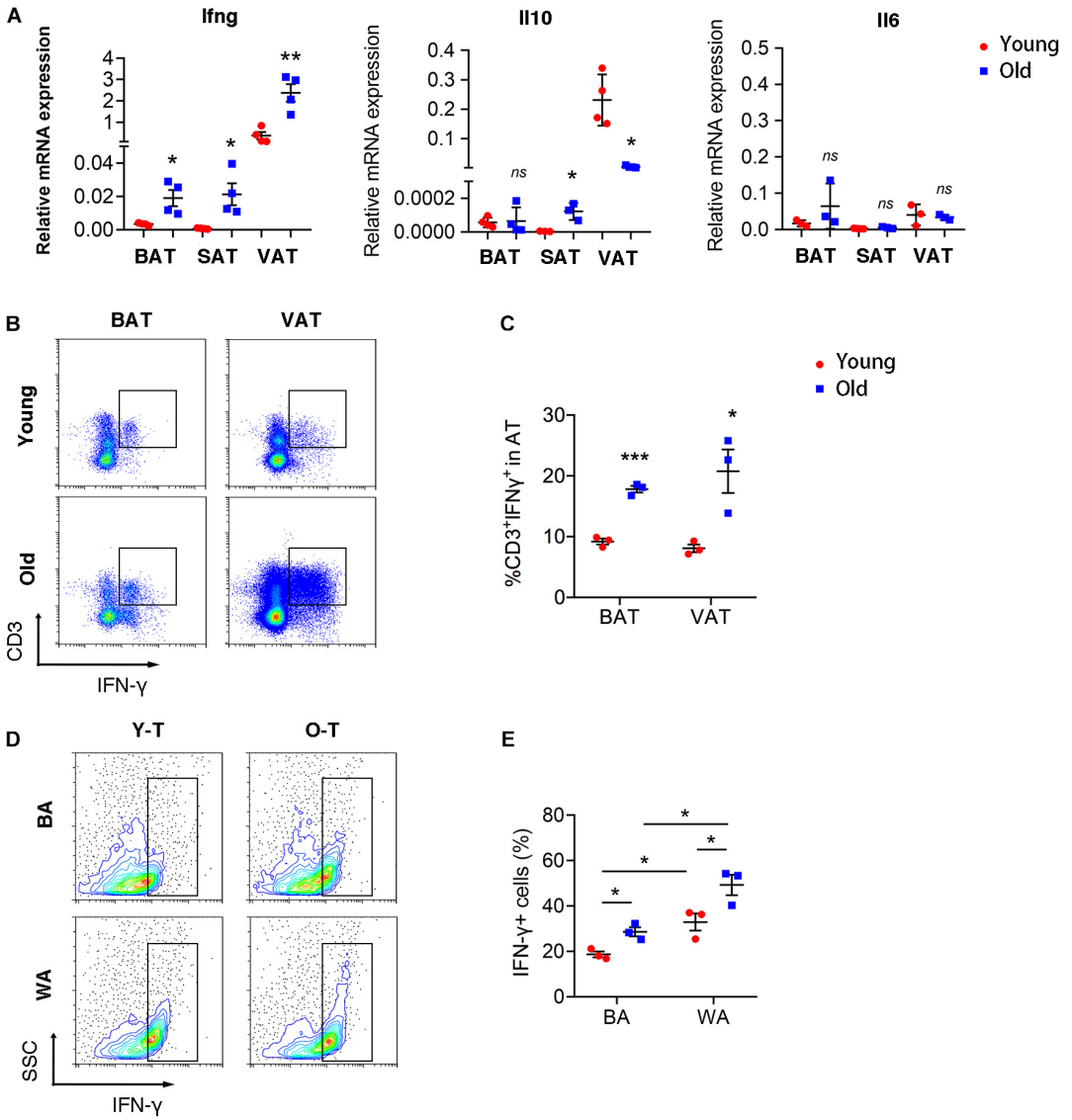

FIGURE 5 | T cell-derived IFN-γ was increased in adipose tissues of old mice. **(A)** qRT-PCR analysis of mRNA expression level of Ifng, Il10, and Il6 in adipose tissue. **(B,C)** Flow cytometric analysis of $CD3^{+}IFN\text{-}\gamma^{+}$ in BAT and VAT of young and old mice. $^{*}P < 0.05$; $^{**}P < 0.01$; $^{***}P < 0.001$ vs. young mice, $n = 3$ per group. **(D,E)** The production of IFN-γ in T cells cocultured with SVF cells under adipogenic differentiation. $^{*}P < 0.05$, $n = 3$ independent experiments.

between young and old mice (**Figure 5A**). As shown in **Figure 5B**, the percentage of IFN-γ^{+} T cells was substantially higher in BAT and VAT of old mice than those in young mice (**Figures 5B,C**). Notably, both young and senescent T cells that cocultured with SVF cells under white adipocyte differentiation produced a higher level of IFN-γ than cells under brown adipogenic differentiation. Furthermore, senescent T cells secreted more IFN-γ than young T cells (**Figures 5D,E**).

To identify the potential role for IFN-γ in brown adipogenic differentiation of SVF cells from BAT, we administrated IFN-γ-neutralizing antibody to block the adverse effect of IFN-γ on adipogenic differentiation. Remarkably, blockade of IFN-γ rescued the brown adipogenic differentiation capacity of SVF cells cocultured with senescent T cells (**Figures 6A,B**). Furthermore, there was no significant difference in preadipocyte-to-brown adipocyte differentiation between SVF cells without the presence of T cells under treatment of IFN-γ-neutralizing antibody or PBS (**Supplementary Figure 2**). In addition, protein level of perilipin and UCP-1 in SVF cells with senescent T cells significantly increased after treatment of IFN-γ-neutralizing antibody, accompanied by an increase in PGC-1α and PPAR-γ expression (**Figures 6C,D**). In keeping with this, genes associated with brown adipogenic differentiation, including Ucp1, Pparg, and Ppargc1a were significantly upregulated under anti-IFN-γ treatment both in young and senescence groups (**Figure 6E**). In addition, brown adipocyte differentiation potential of SAT preadipocyte inhibited by senescent T cell was improved by administration of IFN-γ-neutralizing antibody

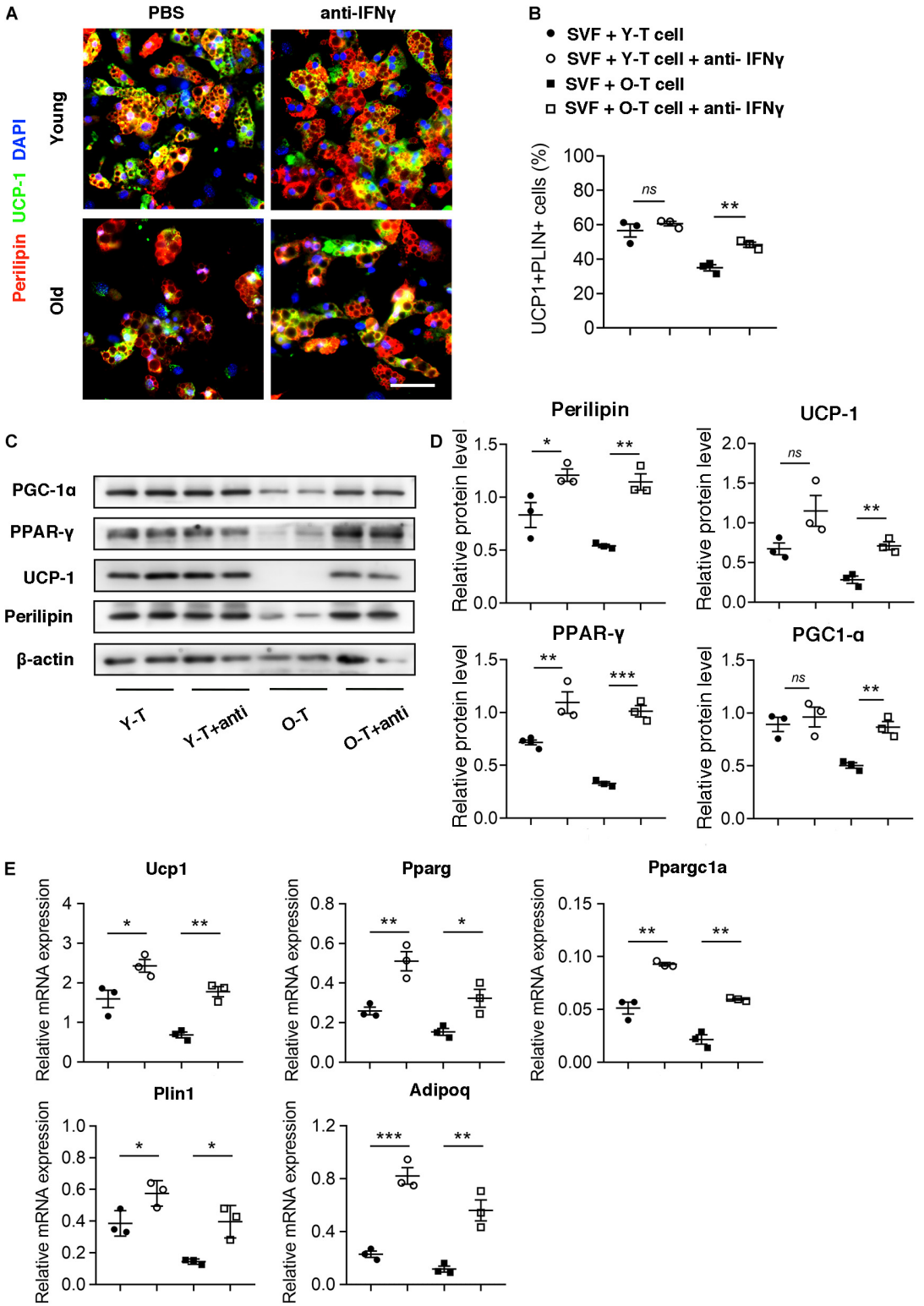

FIGURE 6 | Blockade of IFN-γ rescued the brown adipogenic differentiation potential of SVF cells cocultured with senescent T cells. **(A)** The adipogenic differentiation was determined by costaining of perilipin and UCP-1. Scale bar, 50 μm. **(B)** The quantitative analysis of immunofluorescence. **(C,D)** Representative western blot and their quantitation. **(E)** The adipogenic differentiation was determined by qPCR of specific markers. $^{*}P < 0.05$; $^{**}P < 0.01$; $^{***}P < 0.001$, $n = 3$ independent experiments.

(**Supplementary Figure 3**). These provided direct evidence that T cell-derived IFN-γ plays an important role in inhibiting brown adipocyte differentiation during aging.

DISCUSSION

The increasing population of elderlies combined with obesity, especially expansion of visceral fat mainly composed of white adipocytes results in an alarming rise in cardiometabolic disorders (Martyniak and Masternak, 2017). Adipose tissue remodeling during the aging process is a common phenomenon, and it remains unclear how this maladaptive process is developing. Adipose tissue is composed of several different cellular populations, which varies depending on the location and metabolic status of an organism. Our prior studies has demonstrated that there are distinct cellular components in perivascular stromal cells between young and old mice, and aging influence the potential of stromal cells from perivascular adipose tissue (Pan et al., 2019). Furthermore, adipocyte browning capacity under cold exposure was impaired in the context of aging (Pan et al., 2018). Herein, we further unveil the pivotal role of T cells in age-induced decline of brown adipocyte differentiation.

Adipose tissue is in a constant flux with changing cellular populations, and it plays an important role in the regulation of inflammatory status during aging. Inflammation is believed to closely associate with the metabolic diseases (Hotamisligil, 2006). Mounting evidence emphasizes the importance of immune cells, especially T cells in adipose tissue inflammation (McLaughlin et al., 2014, 2017; Han et al., 2017). Many similarities in chronic inflammation in adipose tissue have been identified between obesity and aging, such as an increase number of $CD4^+$ or $CD8^+$ T cells and a decreased amount of iNK T cells. Moreover, immune cells tend to have proinflammatory phenotypes (Martyniak and Masternak, 2017; Kalathookunnel Antony et al., 2018). A number of studies have clearly demonstrated that T cells in adipose tissue play a role in obesity-associated inflammation. Winer et al. (2009) indicated that lymphocyte-deficient RAG-1 KO mice developed a greater degree of metabolic disorder after 8 weeks of high fat diet, and $CD4^+$ (but not $CD8^+$) T cell adoptive transfer to RAG1 KO mice reversed weight gain and insulin resistance. On the other hand, $CD8^+$ T cells in obese epididymal adipose tissue were significantly increased and preceded the recruitment and activation of adipose tissue macrophages, which lead to the propagation of adipose inflammation (Nishimura et al., 2009). In addition, prior studies show a preferential increase and accumulation of $CD153^+PD\text{-}1^+CD44^{hi}CD4^+$ T cell population in VAT of diet-induced obese mice, which suggests a possible link between visceral adiposity and immune aging (Shirakawa et al., 2016). Given the importance of T cell in diet-induced visceral obesity, it is possible that T cell senescence could influence adipose tissue during the aging process. Our data demonstrate that T cells accumulate in BAT and VAT during aging, but SAT exhibited opposite trends of T cell infiltration. Aging leads to adipose tissue redistribution, including a general increase in visceral fat but a reduction in subcutaneous fat (Ponti et al., 2019), which might result in deposition of collagen instead of immune cells, preadipocyte, and other cells in SAT. Although the amount of T cells is decreased in SAT, T cells isolated from three types of adipose tissue in aged mice present senescent features, such as loss of CD28 and increased proportion of $CD44^+CD62L^-$ effector memory T cells and secrete a higher level of proinflammatory factor such as IFN-γ, which provides a clue that function of T cell rather than quantity of cells exerts a profound influence on adipocyte differentiation.

Both aging and obesity can result in adipose tissue remodeling, along with a decline of its function, predisposing humans to development of metabolic disorder and cardiovascular diseases (Neeland et al., 2018; Marcelin et al., 2019). However, age-induced dysfunction of adipose tissue may be distinct from obese-related malfunction of adipose tissues. In the aging process, redistribution of adipose tissue toward visceral or ectopic sites, such as skeletal muscle and epicardium, has a causal or correlative relation with metabolic and cardiovascular diseases. It has been demonstrated that pre-adipocytes or progenitor cells exist in adipose tissue and can differentiate into brown adipocytes or white adipocytes under a specific condition (Berry et al., 2016; Pyrina et al., 2020). This process is disturbed with senescence. Our data showed that adipocytes in BAT of old mice exhibited a characteristic more similar to white adipocyte, which was termed as BAT "whitening." Low-grade chronic inflammation persists in adipose tissue of aged population and chronic inflammation-induced adipose tissue dysfunction might attribute to impaired brown adipogenic

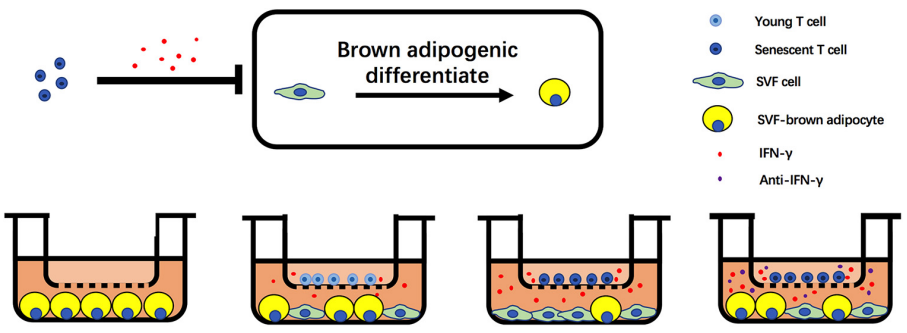

FIGURE 7 | Schematic illustration of adverse effect of T cells on brown adipogenic differentiation of SVF cells regulated by IFN-γ.

differentiation. Emerging evidence suggests the novel role for T lymphocytes in regulating brown adipocyte formation *via* secreting cytokines. $CD8^+$ T cell deficiency enhanced beige adipogenesis in the SAT of Rag1 KO mice, which is mediated by secreted factors such as IFN-γ (Moysidou et al., 2018). iNK T cells remove hypertrophic and proinflammatory adipocytes and induce differentiation of adipocyte progenitor cells, contributing to maintenance of adipose tissue homeostasis (Park et al., 2019). In the present study, accumulation of senescent T cells in BAT of aged mice might lead to a dysfunction in progenitor cell differentiation and then cause adipocytes taking on the appearance of a white adipocyte rather than a brown adipocyte. *In vitro* experiment further provided direct evidence that senescent T cells inhibited brown adipocyte differentiation of pre-adipocytes from both BAT and SAT. Cytokine within adipose tissue is a major mediator of adipose tissue homeostasis and originates from several cell types including adipocytes, pre-adipocytes, as well as immune cells (Coppack, 2001). It has been reported that M1 macrophages impair adipogenesis of 3T3-L1 preadipocytes *via* producing TNF-α (Nisoli et al., 2000; Cawthorn et al., 2007). In contrast, ILC2-derived IL-13 and eosinophil-derived IL-4 together stimulates the expansion of adipocyte progenitor cells and browning of SAT, leading to increase energy expenditure (Brestoff et al., 2015; Lee et al., 2015). Herein, we demonstrated that T cell-derived IFN-γ acted directly on pre-adipocyte to inhibit its brown adipocyte differentiation *via* downregulation of PPARγ expression that is a prime inducer of adipocyte differentiation. Activation of PPARγ is necessary for brown adipocyte differentiation of preadipocyte, and PGC-1α as coactivator of PPARγ also is a key regulator in brown adipogenesis. Of note, blockade of IFN-γ successfully rescued the brown adipocyte differentiation of preadipocyte cocultured with T cells and upregulated level of PPARγ expression. In addition, IFN-γ-neutralizing antibody had no effect on differentiation of preadipocyte to brown adipocyte without the presence of the T cell. These suggested that IFN-γ is the cause for senescent T cell-induced inhibition on BA differentiation of preadipocytes.

In summary, we unveil the critical role of senescent T cell in regulation of aging-induced BAT "whitening." Notably, an increase of senescent T cell accumulation in BAT of aged mice and a higher level of IFN-γ from senescent T cells inhibit the brown adipogenic differentiation of pre-adipocyte, contributing to adipose tissue remodeling in the elderlies. Notwithstanding the complexity of aging-associated alteration in adipose tissue, these data indicate that targeting T cell-derived IFN-γ might be a potential alternative to treat age-related metabolic disorders (**Figure 7**).

DATA AVAILABILITY STATEMENT

The original contributions presented in the study are included in the article/**Supplementary Material**, further inquiries can be directed to the corresponding authors.

ETHICS STATEMENT

The animal study was reviewed and approved by the Ethics Committee of Animal Experiments of Shanghai Jiao Tong University School of Medicine.

AUTHOR CONTRIBUTIONS

C-CR, FW, and X-XP designed the study and wrote the manuscript. K-LY and Y-FY conducted *in vivo* studies. K-LY and RZ performed *in vitro* studies. X-XP and QG performed statistical analyses with assistance from P-JG. All authors contributed to the article and approved the submitted version.

FUNDING

This work was supported by the National Natural Science Foundation of China (81922004, 81770495, 82030006, 81870180, and 81700433), the Natural Science Foundation of Shanghai, China (19JC1414600), and the National Key R&D Program of China (2018YFC2002100 and 2018YFC2002101).

SUPPLEMENTARY MATERIAL

The Supplementary Material for this article can be found online at: https://www.frontiersin.org/articles/10.3389/fcell.2021.637424/full#supplementary-material

REFERENCES

Bartelt, A., and Heeren, J. (2014). Adipose tissue browning and metabolic health. *Nat. Rev. Endocrinol.* 10, 24–36. doi: 10.1038/nrendo.2013.204

Berry, D. C., Jiang, Y., and Graff, J. M. (2016). Emerging roles of adipose progenitor cells in tissue development, homeostasis, expansion and thermogenesis. *Trends Endocrinol. Metab.* 27, 574–585. doi: 10.1016/j.tem.2016.05.001

Brestoff, J. R., Kim, B. S., Saenz, S. A., Stine, R. R., Monticelli, L. A., Sonnenberg, G. F., et al. (2015). Group 2 innate lymphoid cells promote beiging of white adipose tissue and limit obesity. *Nature* 519, 242–246. doi: 10.1038/nature14115

Cawthorn, W. P., Heyd, F., Hegyi, K., and Sethi, J. K. (2007). Tumour necrosis factor-alpha inhibits adipogenesis via a beta-catenin/TCF4(TCF7L2)-dependent pathway. *Cell Death Differ.* 14, 1361–1373. doi: 10.1038/sj.cdd.4402127

Coppack, S. W. (2001). Pro-inflammatory cytokines and adipose tissue. *Proc. Nutr. Soc.* 60, 349–356. doi: 10.1079/PNS2001110

Garg, S. K., Delaney, C., Shi, H., and Yung, R. (2014). Changes in adipose tissue macrophages and T cells during aging. *Crit. Rev. Immunol.* 34, 1–14. doi: 10.1615/CritRevImmunol.2013006833

Hafidi, M. E., Buelna-Chontal, M., Sanchez-Munoz, F., and Carbo, R. (2019). Adipogenesis: a necessary but harmful strategy. *Int. J. Mol. Sci.* 20:3657. doi: 10.3390/ijms20153657

Han, S. J., Glatman Zaretsky, A., Andrade-Oliveira, V., Collins, N., Dzutsev, A., Shaik, J., et al. (2017). White adipose tissue is a reservoir for memory T cells and promotes protective memory responses to infection. *Immunity* 47, 1154–1168.e1156. doi: 10.1016/j.immuni.2017.11.009

Harms, M., and Seale, P. (2013). Brown and beige fat: development, function and therapeutic potential. *Nat. Med.* 19, 1252–1263. doi: 10.1038/nm.3361

Hotamisligil, G. S. (2006). Inflammation and metabolic disorders. *Nature* 444, 860–867. doi: 10.1038/nature05485

Kalathookunnel Antony, A., Lian, Z., and Wu, H. (2018). T cells in adipose tissue in aging. *Front. Immunol.* 9:2945. doi: 10.3389/fimmu.2018.02945

Lee, M. W., Odegaard, J. I., Mukundan, L., Qiu, Y., Molofsky, A. B., Nussbaum, J. C., et al. (2015). Activated type 2 innate lymphoid cells regulate beige fat biogenesis. *Cell* 160, 74–87. doi: 10.1016/j.cell.2014.12.011

Marcelin, G., Silveira, A. L. M., Martins, L. B., Ferreira, A. V., and Clement, K. (2019). Deciphering the cellular interplays underlying obesity-induced adipose tissue fibrosis. *J. Clin. Invest.* 129, 4032–4040. doi: 10.1172/JCI129192

Martyniak, K., and Masternak, M. M. (2017). Changes in adipose tissue cellular composition during obesity and aging as a cause of metabolic dysregulation. *Exp. Gerontol.* 94, 59–63. doi: 10.1016/j.exger.2016.12.007

McLaughlin, T., Ackerman, S. E., Shen, L., and Engleman, E. (2017). Role of innate and adaptive immunity in obesity-associated metabolic disease. *J. Clin. Invest.* 127, 5–13. doi: 10.1172/JCI88876

McLaughlin, T., Liu, L. F., Lamendola, C., Shen, L., Morton, J., Rivas, H., et al. (2014). T-cell profile in adipose tissue is associated with insulin resistance and systemic inflammation in humans. *Arterioscler. Thromb Vasc. Biol.* 34, 2637–2643. doi: 10.1161/ATVBAHA.114.304636

Moysidou, M., Karaliota, S., Kodela, E., Salagianni, M., Koutmani, Y., Katsouda, A., et al. (2018). CD8+ T cells in beige adipogenesis and energy homeostasis. *JCI Insight* 3:e95456. doi: 10.1172/jci.insight.95456

Neeland, I. J., Poirier, P., and Despres, J. P. (2018). Cardiovascular and metabolic heterogeneity of obesity: clinical challenges and implications for management. *Circulation* 137, 1391–1406. doi: 10.1161/CIRCULATIONAHA.117.029617

Nishimura, S., Manabe, I., Nagasaki, M., Eto, K., Yamashita, H., Ohsugi, M., et al. (2009). CD8+ effector T cells contribute to macrophage recruitment and adipose tissue inflammation in obesity. *Nat. Med.* 15, 914–920. doi: 10.1038/nm.1964

Nisoli, E., Briscini, L., Giordano, A., Tonello, C., Wiesbrock, S. M., Uysal, K. T., et al. (2000). Tumor necrosis factor alpha mediates apoptosis of brown adipocytes and defective brown adipocyte function in obesity. *Proc. Natl. Acad. Sci. U.S.A.* 97, 8033–8038. doi: 10.1073/pnas.97.14.8033

Oikonomou, E. K., and Antoniades, C. (2019). The role of adipose tissue in cardiovascular health and disease. *Nat. Rev. Cardiol.* 16, 83–99. doi: 10.1038/s41569-018-0097-6

Pan, X. X., Cao, J. M., Cai, F., Ruan, C. C., Wu, F., and Gao, P. J. (2018). Loss of miR-146b-3p inhibits perivascular adipocyte browning with cold exposure during aging. *Cardiovasc. Drugs Ther.* 32, 511–518. doi: 10.1007/s10557-018-6814-x

Pan, X. X., Ruan, C. C., Liu, X. Y., Kong, L. R., Ma, Y., Wu, Q. H., et al. (2019). Perivascular adipose tissue-derived stromal cells contribute to vascular remodeling during aging. *Aging Cell* 18:e12969. doi: 10.1111/acel.12969

Pan, X. X., Wu, F., Chen, X. H., Chen, D. R., Chen, H. J., Kong, L. R., et al. (2020). T cell senescence accelerates Angiotensin II-induced target organ damage. *Cardiovasc. Res.* 117, 271–283. doi: 10.1093/cvr/cvaa032

Park, J., Huh, J. Y., Oh, J., Kim, J. I., Han, S. M., Shin, K. C., et al. (2019). Activation of invariant natural killer T cells stimulates adipose tissue remodeling via adipocyte death and birth in obesity. *Genes Dev.* 33, 1657–1672. doi: 10.1101/gad.329557.119

Partridge, L., Deelen, J., and Slagboom, P. E. (2018). Facing up to the global challenges of ageing. *Nature* 561, 45–56. doi: 10.1038/s41586-018-0457-8

Ponti, F., Santoro, A., Mercatelli, D., Gasperini, C., Conte, M., Martucci, M., et al. (2019). Aging and imaging assessment of body composition: from fat to facts. *Front. Endocrinol. (Lausanne)* 10:861. doi: 10.3389/fendo.2019.00861

Pyrina, I., Chung, K. J., Michailidou, Z., Koutsilieris, M., Chavakis, T., and Chatzigeorgiou, A. (2020). Fate of adipose progenitor cells in obesity-related chronic inflammation. *Front. Cell Dev. Biol.* 8:644. doi: 10.3389/fcell.2020.00644

Scheja, L., and Heeren, J. (2019). The endocrine function of adipose tissues in health and cardiometabolic disease. *Nat. Rev. Endocrinol.* 15, 507–524. doi: 10.1038/s41574-019-0230-6

Shimizu, I., Aprahamian, T., Kikuchi, R., Shimizu, A., Papanicolaou, K. N., MacLauchlan, S., et al. (2014). Vascular rarefaction mediates whitening of brown fat in obesity. *J. Clin. Invest.* 124, 2099–2112. doi: 10.1172/JCI71643

Shirakawa, K., Yan, X., Shinmura, K., Endo, J., Kataoka, M., Katsumata, Y., et al. (2016). Obesity accelerates T cell senescence in murine visceral adipose tissue. *J. Clin. Invest.* 126, 4626–4639. doi: 10.1172/JCI88606

van Eenige, R., van der Stelt, M., Rensen, P. C. N., and Kooijman, S. (2018). Regulation of adipose tissue metabolism by the endocannabinoid system. *Trends Endocrinol. Metab.* 29, 326–337. doi: 10.1016/j.tem.2018.03.001

Wang, W., and Seale, P. (2016). Control of brown and beige fat development. *Nat. Rev. Mol. Cell Biol.* 17, 691–702. doi: 10.1038/nrm.2016.96

Winer, S., Chan, Y., Paltser, G., Truong, D., Tsui, H., Bahrami, J., et al. (2009). Normalization of obesity-associated insulin resistance through immunotherapy. *Nat. Med.* 15, 921–929. doi: 10.1038/nm.2001

Wu, H., Ghosh, S., Perrard, X. D., Feng, L., Garcia, G. E., Perrard, J. L., et al. (2007). T-cell accumulation and regulated on activation, normal T cell expressed and secreted upregulation in adipose tissue in obesity. *Circulation* 115, 1029–1038. doi: 10.1161/CIRCULATIONAHA.106.638379

Zanni, F., Vescovini, R., Biasini, C., Fagnoni, F., Zanlari, L., Telera, A., et al. (2003). Marked increase with age of type 1 cytokines within memory and effector/cytotoxic CD8+ T cells in humans: a contribution to understand the relationship between inflammation and immunosenescence. *Exp. Gerontol.* 38, 981–987. doi: 10.1016/S0531-5565(03)00160-8

Conflict of Interest: The authors declare that the research was conducted in the absence of any commercial or financial relationships that could be construed as a potential conflict of interest.

frontiers in Molecular Biosciences

ORIGINAL RESEARCH
published: 11 March 2021
doi: 10.3389/fmolb.2020.604042

Soluble Epoxide Hydrolase Inhibition Prevents Experimental Type 4 Cardiorenal Syndrome

Mouad Hamzaoui[1,2], Clothilde Roche[1], David Coquerel[1], Thomas Duflot[1,3], Valery Brunel[4], Paul Mulder[1], Vincent Richard[1], Jérémy Bellien[1,3] and Dominique Guerrot[1,2]*

[1]Normandie University, UNIROUEN, INSERM U1096, FHU REMOD-VHF, Rouen, France, [2]Nephrology Department, Rouen University Hospital, Rouen, France, [3]Pharmacology Department, Rouen University Hospital, Rouen, France, [4]Biochemistry Department, Rouen University Hospital, Rouen, France

Objectives: Cardiovascular diseases (CVD) remain the leading cause of morbimortality in patients with chronic kidney disease (CKD). The aim of this study was to assess the cardiovascular impact of the pharmacological inhibition of soluble epoxide hydrolase (sEH), which metabolizes the endothelium-derived vasodilatory and anti-inflammatory epoxyeicosatrienoic acids (EETs) to dihydroxyeicosatrienoic acid (DHETs), in the 5/6 nephrectomy (Nx) mouse model.

Methods and Results: Compared to sham-operated mice, there was decrease in EET-to-DHET ratio 3 months after surgery in vehicle-treated Nx mice but not in mice treated with the sEH inhibitor *t*-AUCB. Nx induced an increase in plasma creatinine and in urine albumin-to-creatinine ratio as well as the development of kidney histological lesions, all of which were not modified by *t*-AUCB. In addition, *t*-AUCB did not oppose Nx-induced blood pressure increase. However, *t*-AUCB prevented the development of cardiac hypertrophy and fibrosis induced by Nx, as well as normalized the echocardiographic indices of diastolic and systolic function. Moreover, the reduction in endothelium-dependent flow-mediated dilatation of isolated mesenteric arteries induced by Nx was blunted by *t*-AUCB without change in endothelium-independent dilatation to sodium nitroprusside.

Conclusion: Inhibition of sEH reduces the cardiac remodelling, and the diastolic and systolic dysfunctions associated with CKD. These beneficial effects may be mediated by the prevention of endothelial dysfunction, independent from kidney preservation and antihypertensor effect. Thus, inhibition of sEH holds a therapeutic potential in preventing type 4 cardiorenal syndrome.

Keywords: cardiorenal syndrome, heart failure, endothelial (dys)function, chronic kidney disease, epoxyeicosatrienoic acid

OPEN ACCESS

Edited by:
InKyeom Kim,
Kyungpook National University, South Korea

Reviewed by:
Ira Kurtz,
University of California, United States
John D Imig,
Medical College of Wisconsin, United States

****Correspondence:***
Mouad Hamzaoui
mouad.hamzaoui@gmail.com

Specialty section:
This article was submitted to Cellular Biochemistry, a section of the journal Frontiers in Molecular Biosciences

Received: *08 September 2020*
Accepted: *14 December 2020*
Published: *11 March 2021*

Citation:
Hamzaoui M, Roche C, Coquerel D, Duflot T, Brunel V, Mulder P, Richard V, Bellien J and Guerrot D (2021) Soluble Epoxide Hydrolase Inhibition Prevents Experimental Type 4 Cardiorenal Syndrome. Front. Mol. Biosci. 7:604042. doi: 10.3389/fmolb.2020.604042

INTRODUCTION

Chronic kidney disease (CKD) is an important health care problem with a worldwide prevalence around 13% (Hill et al., 2016). CKD is an independent risk factor for cardiovascular (CV) diseases and CV events are the first cause of death in this population (Hatamizadeh et al., 2013). The association between CKD and the occurrence of chronic heart disease has been named uremic

cardiopathy or type 4 cardiorenal syndrome (Zannad Faiez and Rossignol Patrick, 2018). In this setting, the crosstalk between the diseased kidney and heart is not fully understood. The pathophysiology of type 4 cardiorenal syndrome is predominantly mediated by reciprocal hemodynamic effects, neurohormonal activation, inflammation, anaemia, disturbances in the hydro electrolytic balance and abnormalities of the bone-mineral axis (Kovesdy and Quarles, 2013; Kovesdy and Quarles, 2016; Ter Maaten et al., 2016; Rangaswami et al., 2019). Fibroblast growth factor-23 (FGF-23), secreted by osteocytes, regulates phosphate and vitamin D homeostasis and its plasma concentration rises as the kidney function declines. Several studies have shown that higher levels of FGF-23 are associated with a higher risk of death (Scialla et al., 2014; Charytan et al., 2015).In spite of significant breakthroughs in our understanding and treatment of the CV disease associated with CKD, mortality remains high and identifying new therapeutic targets is of critical importance.

Epoxyeicosatrienoic acids (EETs) are arachidonic acid derivatives synthesized by cytochrome P450 (CYP450) epoxygenases (Wang Z. H. et al., 2013; Duflot et al., 2014). EETs are endothelium-derived hyperpolarizing factors with potent antihypertensive, anti-inflammatory and anti-proliferative properties. They are rapidly hydrated into the less active dihydroxyeicosatrienoic acids (DHETs), by an enzyme called soluble epoxide hydrolase (sEH). Thus, inhibition of sEH appears as an interesting pharmacological approach to increase the bioavailability of EETs in various pathological conditions in particular cardiovascular diseases (Wang Z. H. et al., 2013; Duflot et al., 2014). sEH inhibitors were shown to reduce hypertension and endothelial damage in angiotensin II-dependent models (Imig et al., 2002; Gao et al., 2011) and to prevent cardiac dysfunction and remodelling in experimental heart failure (Merabet et al., 2012). In human, genetic polymorphisms of *EPHX2,* which encodes sEH, could either increase hydrolase activity which is associated with a higher occurrence of ischemic cardiac events (Lee et al., 2006), or decrease its activity associated with higher endothelium-dependant dilatation in resistance arteries (Lee et al., 2011), strengthening the interest of inhibiting sEH in cardiovascular diseases. At the renal level, the beneficial impact of sEH has been reported in several works (Liu, 2018) but not all (Jung et al., 2010), and no study has evaluated the interest of this strategy in type 4 cardiorenal syndrome.

In this study we analysed the impact of sEH inhibition on the CV consequences induced by 5/6 nephrectomy (5/6 Nx) in mice, a classical model of CKD.

MATERIAL AND METHODS

Animals and Treatments

All experiments were carried out in 129/Sv male mice, aged 8 weeks and weighing between 20 and 26 g (January laboratory, Genest Isle), in accordance with the standards and ethical rules (CENOMEXA C2EA-54). The surgical procedures were performed by a single experienced operator in order to ensure reproducibility. Briefly, surgical procedure consisted in ligation of the upper branch of the left kidney artery, followed by a cauterization of the lower pole of the left kidney, leading to 2/3 of non-functioning left kidney. One week later, the right kidney was removed, inducing 5/6 Nx. One week after removal of the right kidney, 5/6 Nx mice were randomized into two groups to receive either the sEH inhibitor *trans*-4-[4-(3-adamantan-1-yl-ureido)-cyclohexyloxy]-benzoic acid (*t*-AUCB: 15 mg/L in drinking water after dilution in 15-ml PEG 400) or vehicle (PEG 400) until sacrifice. A third group of sham-operated mice (surgical laparotomy) served as controls.

Blood and Urine Analyses

One month after surgery, 100 µL retro-orbital blood samples were collected in anesthetized animals (isoflurane: 1.5%) to quantify plasma creatinine by enzymatic method. At sacrifice, blood samples were collected allowing to measure plasma creatinine, soluble vascular cell adhesion molecule 1 (sVCAM-1) and fibroblast growth factor-23 (FGF-23) were assessed by enzyme-linked immunosorbent assays (ab100750, Abcam and EZMFGF23–43K, EMD Millipore respectively). In addition, the plasma levels of 14,15-EET, the preferential substrate of sEH, its metabolite 14,15-DHET, and the pro-inflammatory hydroxyeicosatetraenoic acids (5-HETE, 12-HETE and 15-HETE), derived from the lipoxygenase (LOX) metabolites of arachidonic acid, were quantified by LC-MS/MS using a previously published method (Duflot et al., 2017; Duflot et al., 2019). The ratio of 14,15-DHET-to-14,15-EET was used as an index of sEH activity.

24-h urine was collected 1 and 3 months after surgical procedure using metabolic cages. Urine albumin and aldosterone were measured at 3 months using enzyme-linked immunosorbent assays (ab108792 and ab136933, respectively; Abcam, Paris, France). Na^+ excretion was quantified using standard procedure.

Systolic Blood Pressure

Non-invasive measurements of systolic blood pressure were performed by tail cuff plethysmography (CODA, Kent Scientific Corporation) 1 and 3 months after surgery. These measurements were performed in conscious and trained mice and consisted in two series of 10 cycles of measurements for each animal.

Cardiac Function

In mice anesthetized with isoflurane (1.5–2%), left ventricular end-diastolic and end-systolic diameters (LVEDD and LVESD, respectively) were assessed 1 and 3 months after surgery, using a Vivid seven ultrasound device (GE medical). The heart was imaged in the two-dimensional mode in the parasternal short-axis view. Ejection fraction (EF) was calculated from the LV cross-sectional area as EF(%) = ((LVDA – LVSA)/LVDA) x 100 where LVDA and LVSA are LV diastolic and systolic area, estimated from LVEDD and LVESD. In addition, a pulsed Doppler of the LV outflow was performed to obtain heart rate (HR). Doppler measurements were made at the tip of the mitral leaflets for diastolic filling profiles in the apical four-chamber

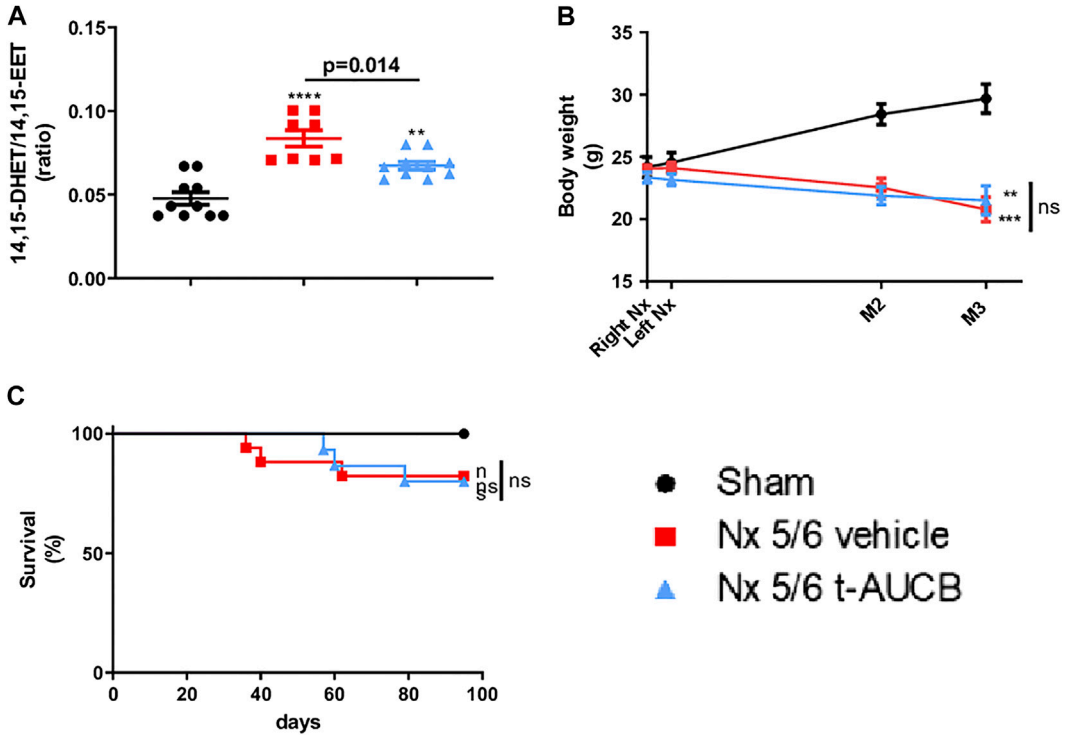

FIGURE 1 | Plasma concentration 14,15-DHET to 14,15-EET ratio **(A)** at sacrifice (n = 8–10 per group). ***$p < 0.001$: Nx 5/6 vehicle vs. sham, **$p < 0.01$: Nx 5/6 *t*-AUCB vs. sham. Body weight evolution **(C)** from right Nx (month 0) to month 3 (n = 12–14 per group). ***$p < 0.001$: Nx 5/6 vehicle vs. sham, **$p < 0.01$: Nx 5/6 *t*-AUCB vs. sham. Survival **(D)** (n = 12–17 per group).

view, allowing to determine peak early (E) and late (A) mitral inflow velocities, and calculation of the E/A ratio, as estimate of diastolic function.

Vascular Function

Flow-mediated dilatation (FMD) was assessed on second mesenteric resistance artery segment. Briefly, the mesentery was removed and placed in cold oxygenated Krebs buffer. A 2–3 mm segment of third mesenteric resistance artery segment was isolated and mounted on an arteriograph (DMT, Denmark). Vessels were pre-constricted using 10^{-5} M phenylephrine (Phe) before assessing the dilatory response to stepwise increase in intraluminal flow (3, 6, 10, 15, 20, 25, 50, 75 and 100 µL/min). FMD was assessed in the absence and in the presence of the NOS inhibitor Nω-nitro-L-arginine (L-NAME; 10–4 M) and the CYP450 epoxygenase inhibitor Fluconazole (10–4 M).

Histology

In 5/6 Nx mice, the remnant kidney was removed at sacrifice. Kidney histological lesions were analysed after Masson's staining as previously described (Guerrot et al., 2011). The slides were independently examined on a blinded basis, using a 0 to four injury scale for the level of interstitial inflammation, interstitial fibrosis and glomerulosclerosis at magnification x20 (0: no damage; 1: <25% of kidney damaged; 2: 25–50% of kidney damaged; 3: 50–75% of kidney damaged; 4: 75–100% of kidney damaged). Tubular lesions were analysed at magnification x10. Vascular thickening and vascular fibrosis were analysed at magnification x40. The upper half of kidney was not analysed since it was ischemic in 5/6 Nx groups.

The heart was harvested, weighed and a section of the left ventricle was snap-frozen for subsequent determination of LV fibrosis, using 8-µm thick histological slices stained with Sirius Red as previously described (Guerrot et al., 2011).

Statistical Analyses

Data were expressed as mean values ± SEM. Comparison between groups was performed by one-way ANOVA, followed by Tukey multiple comparison post-tests, For FMD, analysis was performed by two-way ANOVA with Dunnett's multiple comparisons test. A value of $p < 0.05$ was considered statistically significant. Survival was analysed using Log-rank (Mantel-Cox) test. Statistical tests were performed with Prism software version 8 (8.0.2 263).

RESULTS

sEH Activity

Compared to sham-operated mice, we observed an increase in 14,15-DHET-to-14,15-EET ratio in 5/6 Nx mice treated with the vehicle (**Figures 1A,B**), demonstrating increased sEH activity. As expected, this increase was reduced by the sEH inhibitor *t*-AUCB. The 11,12-DHET-to-11,12-EET ratio followed the same trend as

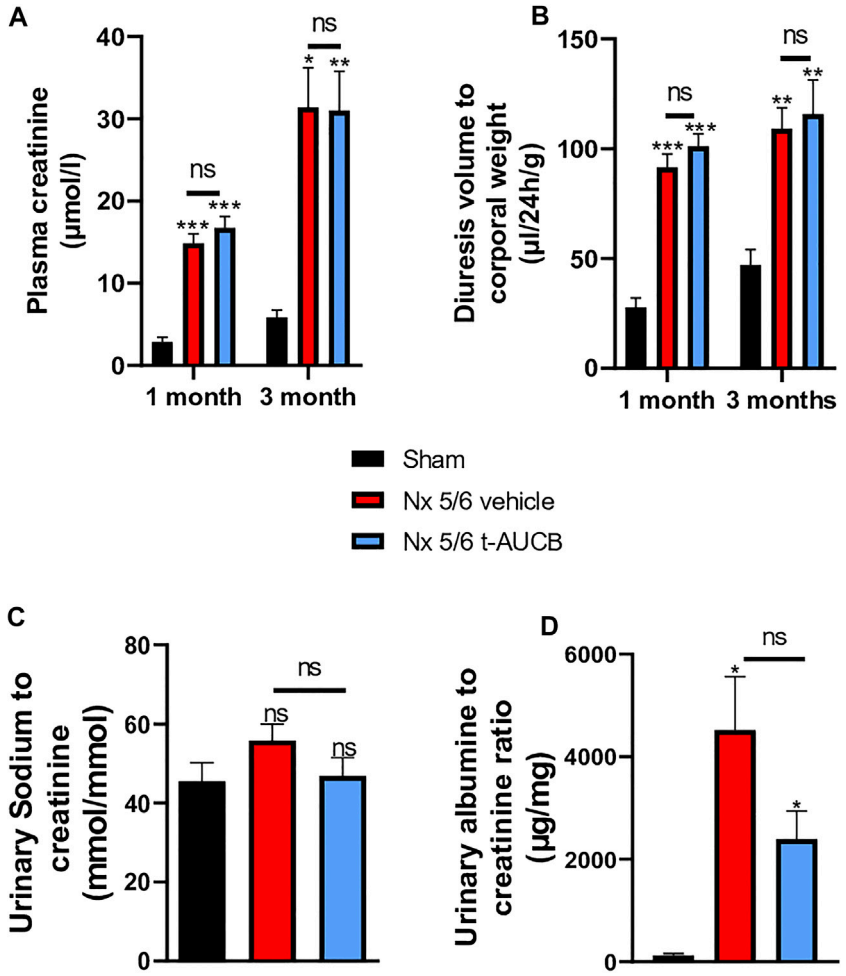

FIGURE 2 | Evolution of plasma **(A)** creatinine 1 and 3 months after 5/6 Nx (n = 7–12 per group). ***$p < 0.001$: Nx 5/6 vehicle vs. Sham, ***$p < 0.001$: Nx 5/6 *t*-AUCB vs. Sham, *$p < 0.05$: Nx 5/6 vehicle vs. Sham, **$p < 0.01$: Nx 5/6 *t*-AUCB vs. Sham, ns: not-significant. Diuresis evolution **(B)** 1 and 3 months after Nx 5/6 (n = 8–12 per group). ***$p < 0.001$: Nx 5/6 vehicle vs. Sham, ***$p < 0.001$: Nx 5/6 *t*-AUCB vs. Sham, **$p < 0.01$: Nx 5/6 vehicle vs. Sham, **$p < 0.01$: Nx 5/6 *t*-AUCB vs. Sham, ns: not-significant. Comparison of urinary albumin to creatinine ratio **(C)** (n = 5-7 per group). *$p < 0.05$: Nx 5/6 vehicle vs. Sham, ***$p < 0.05$: Nx 5/6 *t*-AUCB vs. Sham, ns: not-significant. Urinary sodium to creatinine ratio (n = 8–12 per group). ns: not-significant.

14,15-DHET-to-14,15-EET ratio but the effects was less marked and that there was no change in 8,9-DHET-to-8,9-EET. In addition, 5/6 Nx was associated with an increase in HETE plasma levels that was prevented by *t*-AUCB (**Supplementary Figures S1A–C**).

Body Weight, Survival

Body weight increased in sham-operated mice from surgery to sacrifice but not in 5/6 Nx mice treated with either vehicle or *t*-AUCB (**Figure 1B**), without significant change in survival between groups. (**Figure 1C**).

Kidney Parameters

The onset of CKD was demonstrated by a significant increase in plasma creatinine 1 and 3 months after 5/6 Nx (**Figure 2A**) which was not prevented by *t*-AUCB. In addition, the urine volume 1 and 3 months after surgery and the urine albumin/creatinine ratio at 3 months increased to a similar extent in 5/6 Nx mice treated with vehicle or *t*-AUCB (**Figures 2B,C**). Similarly, the development of glomerulosclerosis, interstitial fibrosis, inflammation, tubular injury and vascular lesions induced by 5/6 Nx was not modified by *t*-AUCB (**Figures 3A–E**, **Supplementary Figure S3**).

Systemic Hemodynamics and Cardiac Parameters

Compared to sham-operated mice, 5/6 Nx mice treated with vehicle or *t*-AUCB followed a similar pattern of increase in systolic arterial pressure after surgery. While systolic arterial pressure was not significantly increased after 1 month, both groups similarly presented a significant increase at 3 months post 5/6 Nx (**Figure 4A**). One month after 5/6 Nx LVEF and E/A ratio were non-significantly altered, while both parameters

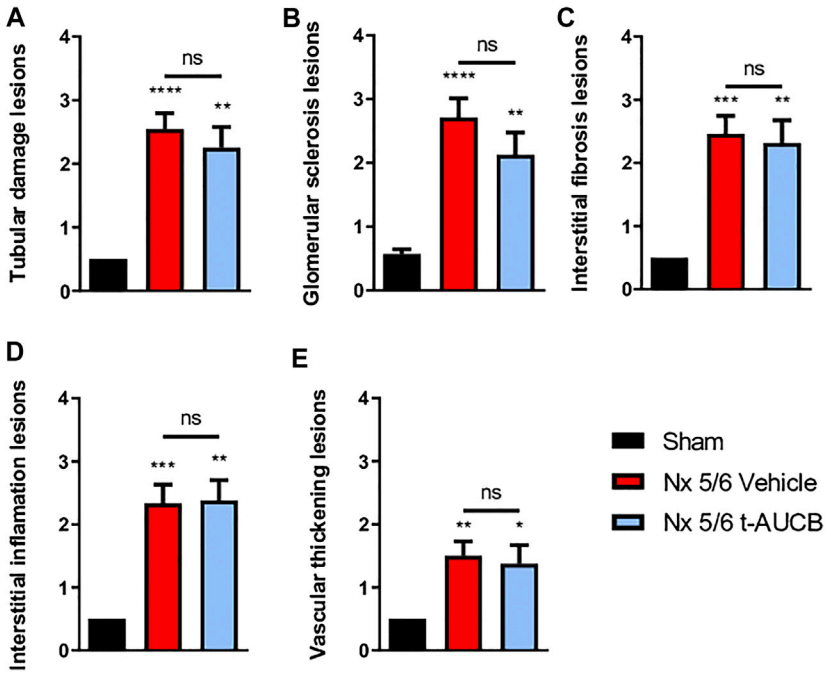

FIGURE 3 | Scoring of kidney lesions at sacrifice (n = 7–12 per group). **(A)** Tubular damage lesions, **(B)** Glomerular sclerosis lesions, **(C)** Interstitial fibrosis lesions, **(D)** Interstitial inflammation lesions, **(E)** Vascular thickening lesions. ****$p < 0.0001$: Nx 5/6 vehicle vs. Sham, **$p < 0.01$: Nx 5/6 *t*-AUCB vs. Sham, ***$p < 0.001$: Nx 5/6 vehicle vs. Sham, **$p < 0.01$: Nx 5/6 vehicle vs. Sham, *$p < 0.05$: Nx 5/6 *t*-AUCB vs. Sham, ns: not-significant.

decreased significantly 3 months after 5/6 Nx in mice treated with vehicle but not in mice treated with *t*-AUCB (**Figures 4B,C**). In addition, *t*-AUCB prevented the increase in heart weight as well as LV fibrosis induced by 5/6 Nx (**Figures 4D,E** and **Supplementary Figure S3**). This was observed while *t*-AUCB was able to prevent the increase in urinary aldosterone, but not in plasma FGF-23 nor heart expression of ICAM-1 and VCAM-1 mRNA (**Supplementary Figures S2A,B**).

Vascular Parameters

FMD was abolished in 5/6 Nx mice treated with vehicle and fully prevented by *t*-AUCB (**Figure 5A**). FMD was decreased by L-NAME in sham-operated mice without significant effect of fluconazole infusion (**Figure 5B**), demonstrating a predominant role of NO in this response. However, FMD restoration in 5/6 Nx mice treated with *t*-AUCB was mainly due to the potentiation of CYP450-dependent pathway, as shown by the significant decrease induced by the CYP450 epoxygenases inhibitor fluconazole but not by L-NAME. In agreement with the improvement in endothelial function, *t*-AUCB prevented the increase in plasma sVCAM-1 (**Figure 5C**).

DISCUSSION

This study provides the first demonstration that pharmacological inhibition of sEH prevents the development of cardiac and vascular disorders due to CKD, independently of kidney function.

The experimental model of 5/6 Nx used here led to a significant and progressive decrease in kidney function, with increased albuminuria and chronic kidney lesions on histology. As is the case in human CKD, this was associated with the onset of hypertension, diastolic and mild systolic dysfunctions, heart hypertrophy, and endothelial dysfunction. These results are in accordance with previously published studies in rodent models of subtotal nephrectomy and provide a reliable experimental setting to analyse the CV consequences of CKD (Ma and Fogo, 2003; Siedlecki et al., 2009; Winterberg et al., 2016; Neuburg et al., 2018; Hamzaoui et al., 2020).

5/6 Nx was associated with an impaired arachidonic acid metabolism, characterized by an increase in 14,15-DHET-to-14,15-EET, and of pro-inflammatory HETEs. Since EETs have potent vasodilator, anti-inflammatory and anti-fibrotic properties, we hypothesized that promoting a more physiological balance with a pharmacological inhibitor of sEH, the key enzyme of EETs degradation, may have beneficial effects on both the heart and the vessels in this setting. As expected, the administration of *t*-AUCB prevented the increase in the DHETs/EETs ratio in 5/6 Nx mice.

Importantly, *t*-AUCB administered for 3 months did not modify the kidney consequences of 5/6 Nx. 5/6 Nx mice treated with *t*-AUCB presented a similar increase in plasma creatinine, albuminuria and kidney lesions compared to mice treated with vehicle. These results were in accordance with a previous study by Jung O et al (Jung et al., 2010), where no difference in kidney histological damage was observed when mice were treated by *c*-AUCB, the *cis*-isomer of *t*-AUCB which

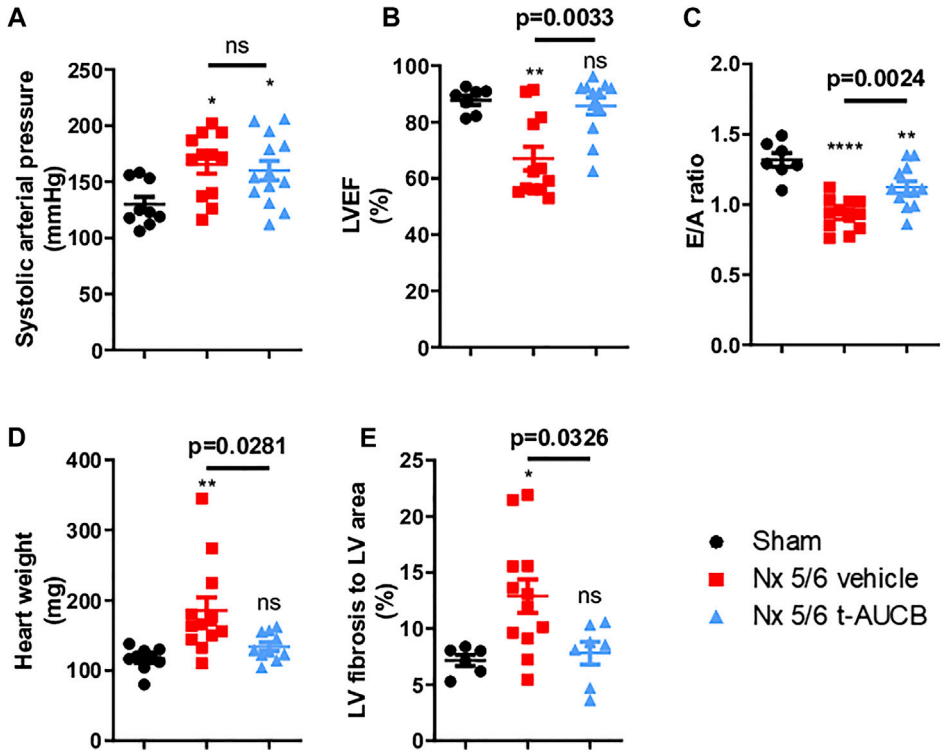

FIGURE 4 | Systolic arterial pressure **(A)** 3 months after surgery (n = 9–12 per group). *$p < 0.05$: Nx 5/6 vehicle vs. Sham, *$p < 0.05$: Nx 5/6 *t*-AUCB vs. Sham, ns: not-significant. Systolic cardiac function **(B)** evaluated by left ventricular ejection fraction (LVEF) in echocardiography ($n = 7–12$ per group). **$p < 0.01$: Nx 5/6 vehicle vs. Sham, ns: not-significant Nx 5/6 *t*-AUCB vs. Sham. Diastolic cardiac function **(C)** evaluated by E to A ratio measured in echocardiography ($n = 7–12$ per group). ****$p < 0.0001$: Nx 5/6 vehicle vs. Sham, **$p < 0.01$: Nx 5/6 *t*-AUCB vs. Sham. Comparison in heart weight after sacrifice **(D)** ($n = 9–12$ per group). **$p < 0.01$: Nx 5/6 vehicle vs. Sham, ns: not-significant Nx 5/6 *t*-AUCB vs. Sham. Comparison of left ventricular (LV) fibrosis area to LV area ($n = 7–11$ per group). *$p < 0.05$: Nx 5/6 vehicle vs. Sham, ns: not-significant Nx 5/6 *t*-AUCB vs. Sham.

possesses similar potency against sEH activity, during 8 weeks. 5/6 Nx mice treated with *t*-AUCB showed no difference in urine output when compared to vehicle, and no difference in sodium excretion. In contrast, previous studies have reported an increase in sodium excretion, related to a decreased reabsorption of sodium as the consequence of tubular effects of EETs (Pavlov et al., 2011; Wang Q. et al., 2013; Wang et al., 2014; Schragenheim et al., 2018). The discrepancy with our results could be explained by the predominant impact of severely decreased glomerular filtration rate, reducing the tubular effects of EETs. After 5/6 Nx, no difference in albuminuria was observed between mice treated with *t*-AUCB and vehicle. On the contrary, Jung O et al (Jung et al., 2010) reported increased albuminuria with *c*-AUCB. This difference could be explained by the longer duration of treatment in our study (8 weeks vs. 3 months) that could allow normalization of arachidonic acid metabolism imbalance induced by short-term inhibition of sEH. In fact, in the previous study (Jung et al., 2010), sEH inhibition was shown to potentiate the formation of pro-inflammatory HETEs while in our study, HETEs were reduced by 3 month *t*-AUCB administration. In addition, given that 14,15-DHET-to-14,15-EET remained elevated compared to sham mice, we could hypothesize that only a partial blockade of sEH occurs, allowing to prevent the shift of arachidonic acid from the CYP450 pathway into the LOX pathway. Accordingly, studies performed in hyperglycaemic overweight mice and mice fed a high-fat diet (Roche et al., 2015b; Luo et al., 2019) even suggest beneficial effects of *t*-AUCB on albuminuria and kidney lesions.

The analysis of direct effects of treatments on CV complications associated with CKD is frequently limited by a parallel impact of the treatment on the kidney disease. In the present study the fact that *t*-AUCB had no significant impact on kidney function and lesions after 5/6 Nx provides an ideal setting to investigate the direct CV impact of sEH inhibition in type 4 cardiorenal syndrome.

Mice treated with *t*-AUCB showed improving systolic and diastolic heart function induced by 5/6 Nx when compared with vehicle. In addition, the increase in heart weight and the onset of LV fibrosis were blunted by *t*-AUCB. In CKD, progressive diffuse myocardial fibrosis and LV hypertrophy contribute to impair the relaxation of the cardiac wall (Zannad Faiez and Rossignol Patrick, 2018). sEH inhibition prevents cardiac hypertrophy in experimental models based on angiotensin II infusion (Ai et al., 2009), aortic banding (Xu et al., 2006), renovascular hypertension (two kidney one clip) (Gao et al., 2011; Wang Z. H. et al., 2013) and metabolic disease related to obesity and insulin resistance (Roche et al., 2015a). This preventive effect was associated with a reduction of myocardial fibrosis, as observed in our study.

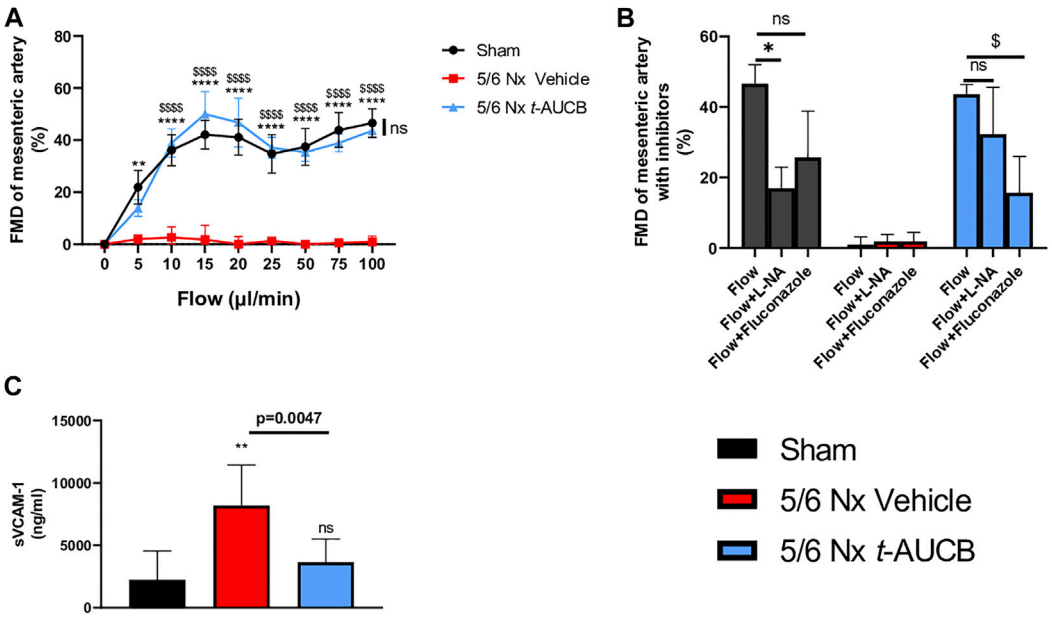

FIGURE 5 | Flow mediated dilatation (FMD) of second mesenteric resistance artery **(A)** at sacrifice (n = 5-8 per group). $^{**}p < 0.01$: Nx 5/6 vehicle vs. Sham, $^{****}p < 0.0001$: Nx 5/6 vehicle vs. Sham, $\$\$\$\$ p < 0.0001$ Nx 5/6 vehicle vs. Nx 5/6 t-AUCB, ns: not-significant Nx 5/6 t-AUCB vs. Sham. FMD in basal condition and after inhibitors (L-NA and Fluconazole) at flow 100 µL/min (n = 5-8 per group). $^{*}p < 0.05$ flow vs. Flow + L-NA, $\$ p < 0.05$ flow vs. Flow + Fluconazole. ns: not-significant. Plasma soluble VCAM1 concentration **(C)** at sacrifice (n = 5–10 per group). $^{**}p < 0.01$: Nx 5/6 vehicle vs. Sham, ns: not-significant Nx 5/6 t-AUCB vs. Sham.

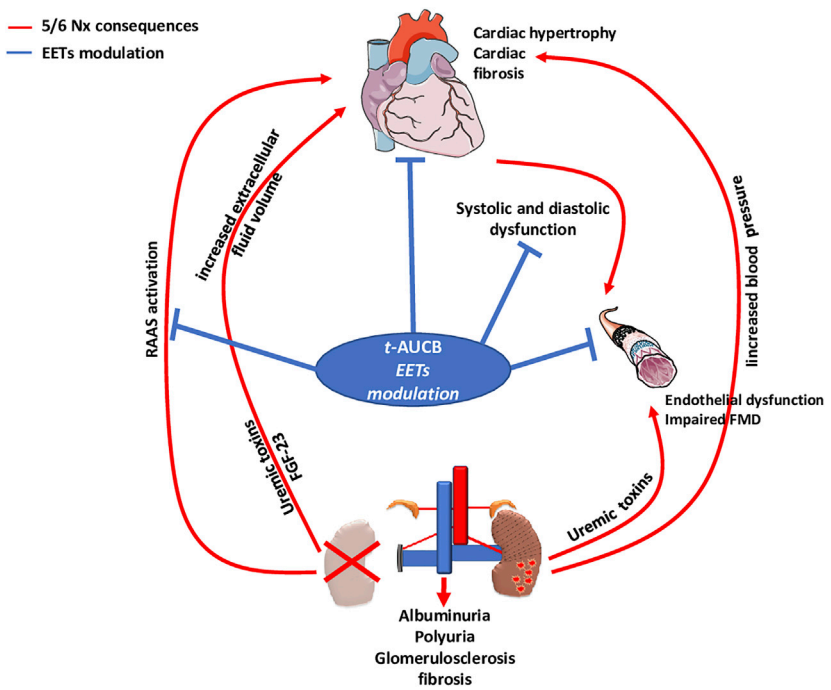

FIGURE 6 | Type 4 cardio-renal syndrome and impact of EETs modulation by t-AUCB.

Experimental and clinical evidences point out a role of FGF-23 in CKD-associated cardiac hypertrophy since FGF-23 increases in patients with CKD and its concentration is correlated to cardiac hypertrophy (Faul et al., 2011; Isakova et al., 2011). In our study, plasma FGF-23 increased after 5/6 Nx without normalization by t-AUCB. This suggests that the beneficial effect of t-AUCB on the

heart is independent of FGF-23. Cardiac hypertrophy can be an adaptive response to the increased afterload related to arterial hypertension. Inhibition of sEH reduced blood pressure in several studies in mice and rats (Yu et al., 2000; Huang et al., 2007; Gao et al., 2011) but *t*-AUCB had no significant effect on the increase of systolic blood pressure after 5/6 Nx, excluding blood pressure as the mediator of *t*-AUCB beneficial effects in this setting. Similarly, Jung O *et al* (Jung et al., 2010) reported no reduction of hypertension with an inhibitor of sEH after subtotal nephrectomy. In fact, the anti-hypertensive effect of sEH inhibition is usually only observed in angiotensin II-dependent hypertension models, which is only partially the case in this setting (Jung et al., 2005).

FMD of resistance arteries is a gold-standard technique to measure the endothelial function in experimental settings. FMD was fully abolished after 5/6 Nx in mice treated with vehicle but was not affected in Nx mice treated with t-AUCB compared to sham-operated mice. Complete dilatation of the mesenteric artery after incubation with SNP, a donor of NO, was observed in all groups showing normal smooth muscle cell function. Together, these results clearly demonstrate that the endothelial dysfunction associated with CKD in our study was prevented by sEH inhibition. Moreover, the improved FMD observed with *t*-AUCB was predominantly mediated by EETs since *ex vivo* inhibition of this pathway with fluconazole blunted FMD. Furthermore, plasma soluble VCAM-1, a surrogate marker for endothelial dysfunction, was sharply increased after 5/6 Nx and *t*-AUCB prevented this increase. Accordingly, similar improvement in endothelial function associated with inhibition of sEH has been observed in animal models of hypertension and insulin resistance (Gao et al., 2011; Zhang et al., 2011; Roche et al., 2015a). In CKD, endothelial dysfunction is multifactorial and considered as an important mediator of CV diseases (Jourde-Chiche et al., 2019). At the organ level, functional and structural alterations of endothelial cells promote inflammation, hypoxia and mesenchymal transition, which are putative mechanisms of cardiac fibrosis in CKD (Yu et al., 2000; Zannad Faiez and Rossignol Patrick, 2018). Together, the protection against microvascular endothelial dysfunction could be a mediator of the cardiac beneficial effects elicited by *t*-AUCB after 5/6 Nx. EETs modulation effects observed in our study were summarized in **Figure 6**.

CONCLUSION

This study provides the first evidence that inhibiting sEH prevents the endothelial dysfunction and cardiac consequences associated with experimental CKD. These beneficial CV effects were independent of both kidney function and hypertension. Preventing EETs degradation by the blockade of sEH therefore appears as a novel and relevant target for the long-term management of type 4 cardiorenal syndrome.

DATA AVAILABILITY STATEMENT

The original contributions presented in the study are included in the article/**Supplementary Material**, further inquiries can be directed to the corresponding author.

ETHICS STATEMENT

The animal study was reviewed and approved by CENOMEXA-Comité National de Réflexion Ethique sur l'EXpérimentation Animale.

AUTHOR CONTRIBUTIONS

MH, DG and JB developed the idea, conducted the research and interpreted the finding. CR and DC investigate cardiac echography. TD and VB conducted biochemical analysis. PM and VR helped to interpreted the finding. All authors have reviewed the manuscript.

SUPPLEMENTARY MATERIAL

The Supplementary Material for this article can be found online at: https://www.frontiersin.org/articles/10.3389/fmolb.2020.604042/full#supplementary-material.

REFERENCES

Ai, D., Pang, W., Li, N., Xu, M., Jones, P. D., Yang, J., et al. (2009). Soluble epoxide hydrolase plays an essential role in angiotensin II-induced cardiac hypertrophy. *Proc. Natl. Acad. Sci. U.S.A.* 106, 564–569. doi:10.1073/pnas.0811022106

Charytan, D. M., Fishbane, S., Malyszko, J., McCullough, P. A., and Goldsmith, D. (2015). Cardiorenal syndrome and the role of the bone-mineral axis and anemia. *Am. J. Kidney Dis.* 66, 196–205. doi:10.1053/j.ajkd.2014.12.016

Duflot, T., Roche, C., Lamoureux, F., Guerrot, D., and Bellien, J. (2014). Design and discovery of soluble epoxide hydrolase inhibitors for the treatment of cardiovascular diseases. *Expert Opin. Drug Discov.* 9, 229–243. doi:10.1517/17460441.2014.881354

Duflot, T., Moreau-Grangé, L., Roche, C., Iacob, M., Wils, J., Rémy-Jouet, I., et al. (2019). Altered bioavailability of epoxyeicosatrienoic acids is associated with conduit artery endothelial dysfunction in type 2 diabetic patients. *Cardiovasc. Diabetol.* 18, 35. doi:10.1186/s12933-019-0843-z

Duflot, T., Pereira, T., Roche, C., Iacob, M., Cardinael, P., Hamza, N. E., et al. (2017). A sensitive LC-MS/MS method for the quantification of regioisomers of epoxyeicosatrienoic and dihydroxyeicosatrienoic acids in human plasma during endothelial stimulation. *Anal. Bioanal. Chem.* 409, 1845–1855. doi:10.1007/s00216-016-0129-1

Faul, C., Amaral, A. P., Oskouei, B., Hu, M. C., Sloan, A., Isakova, T., et al. (2011). FGF23 induces left ventricular hypertrophy. *J. Clin. Invest.* 121, 4393–4408. doi:10.1172/JCI46122

Gao, J., Bellien, J., Gomez, E., Henry, J. P., Dautreaux, B., Bounoure, F., et al. (2011). Soluble epoxide hydrolase inhibition prevents coronary endothelial dysfunction in mice with renovascular hypertension. *J. Hypertens.* 29, 1128–1135. doi:10.1097/HJH.0b013e328345ef7b

Guerrot, D., Kerroch, M., Placier, S., Vandermeersch, S., Trivin, C., Mael-Ainin, M., et al. (2011). Discoidin domain receptor 1 is a major mediator of inflammation and fibrosis in obstructive nephropathy. *Am. J. Pathol.* 179, 83–91. doi:10.1016/j.ajpath.2011.03.023

Hamzaoui, M., Djerada, Z., Brunel, V., Mulder, P., Richard, V., Bellien, J., et al. (2020). 5/6 nephrectomy induces different renal, cardiac and vascular

consequences in 129/Sv and C57BL/6JRj mice. *Sci. Rep.* 10, 1524–1529. doi:10.1038/s41598-020-58393-w

Hatamizadeh, P., Fonarow, G. C., Budoff, M. J., Darabian, S., Kovesdy, C. P., and Kalantar-Zadeh, K. (2013). Cardiorenal syndrome: Pathophysiology and potential targets for clinical management. *Nat. Rev. Nephrol.* 9, 99–111. doi:10.1038/nrneph.2012.279

Hill, N. R., Fatoba, S. T., Oke, J. L., Hirst, J. A., O'Callaghan, C. A., Lasserson, D. S., et al. (2016). Global prevalence of chronic kidney disease - a systematic review and meta-analysis. *PLoS One* 11, e0158765. doi:10.1371/journal.pone.0158765

Huang, H., Morisseau, C., Wang, J., Yang, T., Falck, J. R., Hammock, B. D., et al. (2007). Increasing or stabilizing renal epoxyeicosatrienoic acid production attenuates abnormal renal function and hypertension in obese rats. *Am. J. Physiol. Ren. Physiol.* 293, F342–F349. doi:10.1152/ajprenal.00004.2007

Imig, J. D., Zhao, X., Capdevila, J. H., Morisseau, C., and Hammock, B. D. (2002). Soluble epoxide hydrolase inhibition lowers arterial blood pressure in angiotensin II hypertension. *Hypertension* 39, 690–694. doi:10.1161/hy0202.103788

Isakova, T., Wahl, P., Vargas, G. S., Gutiérrez, O. M., Scialla, J., Xie, H., et al. (2011). Fibroblast growth factor 23 is elevated before parathyroid hormone and phosphate in chronic kidney disease. *Kidney Int.* 79, 1370–1378. doi:10.1038/ki.2011.47

Jourde-Chiche, N., Fakhouri, F., Dou, L., Bellien, J., Burtey, S., Frimat, M., et al. (2019). Endothelium structure and function in kidney health and disease. *Nat. Rev. Nephrol.* 15, 87–108. doi:10.1038/s41581-018-0098-z

Jung, O., Brandes, R. P., Kim, I. H., Schweda, F., Schmidt, R., Hammock, B. D., et al. (2005). Soluble epoxide hydrolase is a main effector of angiotensin II-induced hypertension. *Hypertension* 45, 759–765. doi:10.1161/01.HYP.0000153792.29478.1d

Jung, O., Jansen, F., Mieth, A., Barbosa-Sicard, E., Pliquett, R. U., Babelova, A., et al. (2010). Inhibition of the soluble epoxide hydrolase promotes albuminuria in mice with progressive renal disease. *PLoS One* 5, e11979. doi:10.1371/journal.pone.0011979

Kovesdy, C. P., and Quarles, L. D. (2013). Fibroblast growth factor-23: what we know, what we don't know, and what we need to know. *Nephrol. Dial. Transpl.* 28, 2228–2236. doi:10.1093/ndt/gft065

Kovesdy, C. P., and Quarles, L. D. (2016). FGF23 from bench to bedside. *Am. J. Physiol. Ren. Physiol.* 310, F1168–F1174. doi:10.1152/ajprenal.00606.2015

Lee, C. R., North, K. E., Bray, M. S., Fornage, M., Seubert, J. M., Newman, J. W., et al. (2006). Genetic variation in soluble epoxide hydrolase (EPHX2) and risk of coronary heart disease: the atherosclerosis risk in communities (ARIC) study. *Hum. Mol. Genet.* 15, 1640–1649. doi:10.1093/hmg/ddl085

Lee, C. R., Pretorius, M., Schuck, R. N., Burch, L. H., Bartlett, J., Williams, S. M., et al. (2011). Genetic variation in soluble epoxide hydrolase (EPHX2) is associated with forearm vasodilator responses in humans. *Hypertension* 57, 116–122. doi:10.1161/HYPERTENSIONAHA.110.161695

Liu, J. Y. (2018). Inhibition of soluble epoxide hydrolase for renal health. *Front Pharmacol.* 9, 1551. doi:10.3389/fphar.2018.01551

Luo, Y., Wu, M. Y., Deng, B. Q., Huang, J., Hwang, S. H., Li, M. Y., et al. (2019). Inhibition of soluble epoxide hydrolase attenuates a high-fat diet-mediated renal injury by activating PAX2 and AMPK. *Proc. Natl. Acad. Sci. U S A.* 116, 5154–5159. doi:10.1073/pnas.1815746116

Ma, L. J., and Fogo, A. B. (2003). Model of robust induction of glomerulosclerosis in mice: importance of genetic background. *Kidney Int.* 64, 350–355. doi:10.1046/j.1523-1755.2003.00058.x

Merabet, N., Bellien, J., Glevarec, E., Nicol, L., Lucas, D., Remy-Jouet, I., et al. (2012). Soluble epoxide hydrolase inhibition improves myocardial perfusion and function in experimental heart failure. *J. Mol. Cel. Cardiol.* 52, 660–666. doi:10.1016/j.yjmcc.2011.11.015

Neuburg, S., Dussold, C., Gerber, C., Wang, X., Francis, C., Qi, L., et al. (2018). Genetic background influences cardiac phenotype in murine chronic kidney disease. *Nephrol. Dial. Transplant.* 33, 1129–1137. doi:10.1093/ndt/gfx332

Pavlov, T. S., Ilatovskaya, D. V., Levchenko, V., Mattson, D. L., Roman, R. J., and Staruschenko, A. (2011). Effects of cytochrome P-450 metabolites of arachidonic acid on the epithelial sodium channel (ENaC). *Am. J. Physiol. Ren. Physiol.* 301, F672–F681. doi:10.1152/ajprenal.00597.2010

Rangaswami, J., Bhalla, V., Blair, J. E. A., Chang, T. I., Costa, S., Lentine, K. L., et al. (2019). Cardiorenal syndrome: classification, pathophysiology, diagnosis, and treatment strategies: A scientific statement from the American heart association. *Circulation* 139, e840–e878. doi:10.1161/CIR.0000000000000664

Roche, C., Besnier, M., Cassel, R., Harouki, N., Coquerel, D., Guerrot, D., et al. (2015a). Soluble epoxide hydrolase inhibition improves coronary endothelial function and prevents the development of cardiac alterations in obese insulin-resistant mice. *Am. J. Physiol. Heart Circ. Physiol.* 308, H1020–H1029. doi:10.1152/ajpheart.00465.2014

Roche, C., Guerrot, D., Harouki, N., Duflot, T., Besnier, M., Rémy-Jouet, I., et al. (2015b). Impact of soluble epoxide hydrolase inhibition on early kidney damage in hyperglycemic overweight mice. *Prostaglandins Other Lipid Mediat.* 120, 148–154. doi:10.1016/j.prostaglandins.2015.04.011

Schragenheim, J., Bellner, L., Cao, J., Singh, SP., Bamshad, D., McClung, JA., et al. (2018). EET enhances renal function in obese mice resulting in restoration of HO-1-Mfn1/2 signaling, and decrease in hypertension through inhibition of sodium chloride co-transporter. *Prostaglandins Other Lipid Mediat.* 137, 30–39. doi:10.1016/j.prostaglandins.2018.05.008

Scialla, J. J., Xie, H., Rahman, M., Anderson, A. H., Isakova, T., Ojo, A., et al. (2014). Fibroblast growth factor-23 and cardiovascular events in CKD. *J. Am. Soc. Nephrol.* 25, 349–360. doi:10.1681/ASN.2013050465

Siedlecki, A. M., Jin, X., and Muslin, A. J. (2009). Uremic cardiac hypertrophy is reversed by rapamycin but not by lowering of blood pressure. *Kidney Int.* 75, 800–808. doi:10.1038/ki.2008.690

Ter Maaten, J. M., Damman, K., Verhaar, M. C., Paulus, W. J., Duncker, D. J., Cheng, C., et al. (2016). Connecting heart failure with preserved ejection fraction and renal dysfunction: the role of endothelial dysfunction and inflammation. *Eur. J. Heart Fail.* 18, 588–598. doi:10.1002/ejhf.497

Wang, Q., Pang, W., Cui, Z., Shi, J., Liu, Y., Liu, B., et al. (2013). Upregulation of soluble epoxide hydrolase in proximal tubular cells mediated proteinuria-induced renal damage. *Am. J. Physiol. Ren. Physiol.* 304, F168–F176. doi:10.1152/ajprenal.00129.2012

Wang, Z. H., Davis, B. B., Jiang, D. Q., Zhao, T. T., and Xu, D. Y. (2013). Soluble epoxide hydrolase inhibitors and cardiovascular diseases. *Curr. Vasc. Pharmacol.* 11, 105–111. doi:10.2174/157016113804547593

Wang, W. H., Zhang, C., Lin, D. H., Wang, L., Graves, J. P., Zeldin, D. C., et al. (2014). Cyp2c44 epoxygenase in the collecting duct is essential for the high K+ intake-induced antihypertensive effect. *Am. J. Physiol. Ren. Physiol.* 307, F453–F460. doi:10.1152/ajprenal.00123.2014

Winterberg, P. D., Jiang, R., Maxwell, J. T., Wang, B., and Wagner, M. B. (2016). Myocardial dysfunction occurs prior to changes in ventricular geometry in mice with chronic kidney disease (CKD). *Physiol. Rep.* 4, 12732. doi:10.14814/phy2.12732

Xu, D., Li, N., He, Y., Timofeyev, V., Lu, L., Tsai, H. J., et al. (2006). Prevention and reversal of cardiac hypertrophy by soluble epoxide hydrolase inhibitors. *Proc. Natl. Acad. Sci. U.S.A.* 103, 18733–18738. doi:10.1073/pnas.0609158103

Yu, Z., Xu, F., Huse, L. M., Morisseau, C., Draper, A. J., Newman, J. W., et al. (2000). Soluble epoxide hydrolase regulates hydrolysis of vasoactive epoxyeicosatrienoic acids. *Circ. Res.* 87, 992–998. doi:10.1161/01.res.87.11.992

Zannad, F., and Rossignol, P. (2018). Cardiorenal syndrome revisited. *Circulation* 138, 929–944. doi:10.1161/CIRCULATIONAHA.117.028814

Zhang, L. N., Vincelette, J., Chen, D., Gless, R. D., Anandan, S. K., Rubanyi, G. M., et al. (2011). Inhibition of soluble epoxide hydrolase attenuates endothelial dysfunction in animal models of diabetes, obesity and hypertension. *Eur. J. Pharmacol.* 654, 68–74. doi:10.1016/j.ejphar.2010.12.016

Conflict of Interest: The authors declare that the research was conducted in the absence of any commercial or financial relationships that could be construed as a potential conflict of interest.

frontiers in Cell and Developmental Biology

OPINION
published: 12 March 2021
doi: 10.3389/fcell.2021.658656

A Closure Look at the Pregnancy-Associated Arterial Dissection

Cechuan Deng[1,2], *Han Wang*[1], *Xiangqi Chen*[1] *and Xiaoqiang Tang*[1]*

[1] *Key Laboratory of Birth Defects and Related Diseases of Women and Children of MOE, State Key Laboratory of Biotherapy, West China Second University Hospital, Sichuan University, Chengdu, China,* [2] *Department of Obstetrics and Gynecology, West China Second University Hospital, Sichuan University, Chengdu, China*

Keywords: pregnancy, arterial dissection, risk facors, diabetes, metabolism

INTRODUCTION

Cardiovascular diseases have become the first leading cause of morbidity and mortality (Chen et al., 2020a,b; Tang et al., 2020). Cardiovascular and metabolic syndrome are common in pregnant patients (Li et al., 2017; Timpka et al., 2018). Among cardiovascular diseases, arterial dissection is a severe vascular disease with high-mortality in pregnant patients (Ramlakhan et al., 2020). Arterial dissection is a common cause of arterial disease after atherosclerosis (Adlam et al., 2016). The cause of this arterial disease is not fully understood. Analysis of the risk factors, epidemiology, and mechanisms of pregnancy-associated arterial dissections are important.

RISK FACTORS OF PREGNANCY-ASSOCIATED ARTERIAL DISSECTION

During the past decades, a large number of studies tried to figure out the key risk factors for pregnancy-associated arterial dissection. Hemodynamic and hormone changes during the perinatal period increase the risk factors of arterial dissection (Habashi et al., 2019; Al-Hussaini, 2020). Most previous studies have linked patients with underlying connective tissue diseases such as Marfan and Ehrlers-Danlos syndrome (Al-Hussaini, 2020). With a large population-based database of admissions, Beyer et al. provided a comprehensive analysis of the occurrence and risk factors of dissection within the peripartum period in pregnancy patients (Beyer et al., 2020). Beyer et al. statistically analyzed the occurrence of dissection during the peripartum period and explored the risk factors, time, location, and in-hospital mortality of dissection during the peripartum period. The result showed that 0.005% of pregnancy-related dissections occurred, and the most common diagnosis time point and location were during the postpartum period and coronary, respectively. The mortality of pregnant women with dissections in the hospital was higher than that of pregnant women without dissections, and the mortality of aortic dissection was the highest (8.6%). Most studies before only studied aortic dissection and spontaneous coronary artery dissection (SCAD) in pregnant women, while the relationship between arterial dissections other than aortic dissection and SCAD and pregnancy has been poorly studied. This excellent study has provided timely and comprehensive information but also left some discussion space.

GESTATIONAL DIABETES-THE LEADING RISK FACTOR?

Based on the data of this study, gestational diabetes is the leading risk factor for pregnancy-associated arterial dissections. Interestingly, this study provided new data that gestational diabetes leads to a 65-fold increase in risk for arterial dissections during pregnancy. This

OPEN ACCESS

Edited by:
Venkaiah Betapudi, United States Department of Homeland Security, United States

Reviewed by:
Alberto Maud, Texas Tech University Health Sciences Center El Paso, United States
Hiroaki Tanaka, Mie University, Japan

***Correspondence:**
Xiaoqiang Tang
tangxiaoqiang@scu.edu.cn;
txiaoqiang@yeah.net

Specialty section:
This article was submitted to Cellular Biochemistry, a section of the journal Frontiers in Cell and Developmental Biology

Received: *26 January 2021*
Accepted: *22 February 2021*
Published: *12 March 2021*

Citation:
Deng C, Wang H, Chen X and Tang X (2021) A Closure Look at the Pregnancy-Associated Arterial Dissection. Front. Cell Dev. Biol. 9:658656. doi: 10.3389/fcell.2021.658656

finding highlights the importance of blood glucose control for pregnant patients and leaves the question that whether blood glucose intervention can reduce the risk of arterial dissections. However, previous studies revealed that diabetes mellitus is remarkably uncommon in patients with thoracic aortic dissection (LeMaire and Russell, 2011; Theivacumar et al., 2014). Besides, according to a Japan survey, aortic dissection has not occurred in women with gestational diabetes (Katsuragi et al., 2011). The risk of gestational diabetes to different types of arterial dissections may be different. A further complementary study may include this information.

OTHER CONFOUNDING FACTORS

The authors included many complications/risk factors, and we also suggest analyzing some other risk factors. (**a**) ***Inflammatory reactions***, including systemic lupus erythematosus and multiple nodular arteritis, can increase the risk of arterial dissections in women (Tweet et al., 2018). (**b**) In addition to the Ehlers-Danlos syndrome and Marfan syndrome listed in this article, some ***other connective tissue diseases***, such as the Loeys-Dietz syndrome, are also related to arterial dissections (Ramlakhan et al., 2020). **(c)** Also, ***hereditary arterial disease*** (e.g., hereditary hypertension) is a risk factor for arterial dissections, and about 5% of female arterial dissections patients have hereditary arterial disease (Collet et al., 2020; Ramlakhan et al., 2020). Although the vast majority of the arterial dissection in the supra-aortic arteries is not related to genetic or hereditary, or acquired collagen disease, a genetic mutation in a certain component of the collagen fibers has been demonstrated, and the skin biopsy has shown some dermal dysplastic irregularity of the collagen fibers in concomitant with arterial dissection (Malfait et al., 2020). Thus, hereditary and genetic factors may contribute to arterial dissections in pregnancy patients. (**d**) Furthermore, previous studies have shown that the black race is one of the demographic characteristics and comorbid conditions of pregnancy-associated arterial dissections (Al-Hussaini, 2020; Ramlakhan et al., 2020), so ***ethnics*** can also be included as a confounding factor in the study. (**e**) Oxytocin antagonism can prevent pregnancy-associated aortic dissection in a mouse model of Marfan syndrome (Habashi et al., 2019). As thus, ***oxytocin use*** (and other drug use history) may be induced in the analysis. (**f**) Finally, other confounding factors related to arterial dissections in pregnant women include ***migraine, age at first childbirth, operation history, and infertility treatment*** (Collet et al., 2020). Including these risk factors in the further analysis would provide us more comprehensive information and improve our understanding, prevention, and treatment of pregnancy-associated arterial dissections.

THE INCIDENCE AND MORTALITY TRENDS

The authors discussed the location of arterial dissections during the peripartum period (pregnancy/delivery vs. postpartum), the total incidence and mortality of pregnancy-related arterial dissections, and the respective mortality of dissections at each site (Beyer et al., 2020). We also suggest analyzing the incidence and mortality trends of different types of dissections in pregnancy/delivery and postpartum over the course of the study period, respectively, in further study. Spontaneous cervical arterial dissection is the most common cause of ischemic stroke in North America in people younger than 45 yr (Schievink et al., 1994). The disease has a pendular behavior from mild presentations that do not require further action (like Horner's syndrome) and resolve spontaneously to devastating large hemispheric infarcts (Beletsky et al., 2003). Women with Fibromuscular dysplasia are more predisposed to present with spontaneous cervical arterial dissections and occasionally with spontaneous coronary artery dissection (Hayes et al., 2018; Gornik et al., 2019). Thus, the incidence and mortality trends, as well as risk factor information for different types of arterial dissections, are also important. The complementary analysis may provide warning information, especially for the *Center for Disease Control and Prevention*.

CONCLUSION REMARKS

This study elicited pregnancy and non-pregnancy risk factors that predispose to arterial dissections in all stages of pregnancy and postpartum. Further complementary analysis of detailed risk factors and for different types of pregnancy-associated arterial dissections in different periods of pregnancy would provide some more substantially basic information to this field.

AUTHOR CONTRIBUTIONS

CD and XT prepared and submitted the manuscript. All authors read and approved the final manuscript.

FUNDING

This work was supported by the National Natural Science Foundation of China (grant numbers 81970426 and 81800273); the Young Elite Scientists Sponsorship Program of China Association for Science and Technology (grant number 2018QNRC001); the Scientific and Technological Innovation Talents Program of Sichuan Province (grant number 2020JDRC0017).

REFERENCES

Adlam, D., Maas, A., Vrints, C., and Alfonso, F. (2016). Spontaneous coronary artery dissection. *Eur. Heart J.* 37, 3073–3074. doi: 10.1093/eurheartj/ehw467

Al-Hussaini, A. (2020). Pregnancy and aortic dissections. *Eur. Heart J.* 41, 4243–4244. doi: 10.1093/eurheartj/ehaa754

Beletsky, V., Nadareishvili, Z., Lynch, J., Shuaib, A., Woolfenden, A., and Norris, J. W. (2003). Cervical arterial dissection: time for a therapeutic trial? *Stroke* 34, 2856–2860. doi: 10.1161/01.STR.0000098649.39767.BC

Beyer, S. E., Dicks, A. B., Shainker, S. A., Feinberg, L., Schermerhorn, M. L., Secemsky, E. A., et al. (2020). Pregnancy-associated arterial dissections: a nationwide cohort study. *Eur. Heart J.* 41, 4234–4242. doi: 10.1093/eurheartj/ehaa497

Chen, X.-F., Chen, X., and Tang, X. (2020a). Short-chain fatty acid, acylation and cardiovascular diseases. *Clin. Sci.* 134, 657–676. doi: 10.1042/CS20200128

Chen, X.-F., Yan, L.-J., Lecube, A., and Tang, X. (2020b). Editorial: diabetes and obesity effects on lung function. *Front. Endocrinol.* 11:462. doi: 10.3389/fendo.2020.00462

Collet, J.-P., Thiele, H., Barbato, E., Barthélémy, O., Bauersachs, J., Bhatt, D. L., et al. (2020). 2020 ESC Guidelines for the management of acute coronary syndromes in patients presenting without persistent ST-segment elevation: the task force for the management of acute coronary syndromes in patients presenting without persistent ST-segment elevation of the European Society of Cardiology (ESC). *Eur. Heart J.* doi: 10.1093/eurheartj/ehaa624. [Epub ahead of print].

Gornik, H. L., Persu, A., Adlam, D., Aparicio, L. S., Azizi, M., Boulanger, M., et al. (2019). First international consensus on the diagnosis and management of fibromuscular dysplasia. *Vasc. Med.* 24, 164–189. doi: 10.1177/1358863X18821816

Habashi, J. P., MacFarlane, E. G., Bagirzadeh, R., Bowen, C., Huso, N., Chen, Y., et al. (2019). Oxytocin antagonism prevents pregnancy-associated aortic dissection in a mouse model of Marfan syndrome. *Sci. Transl. Med.* 11:eaat4822. doi: 10.1126/scitranslmed.aat4822

Hayes, S. N., Kim, E. S. H., Saw, J., Adlam, D., Arslanian-Engoren, C., Economy, K. E., et al. (2018). Spontaneous coronary artery dissection: current state of the science: a scientific statement from the American Heart Association. *Circulation* 137, e523–e557. doi: 10.1161/CIR.0000000000000564

Katsuragi, S., Ueda, K., Yamanaka, K., Neki, R., Kamiya, C., Sasaki, Y., et al. (2011). Pregnancy-associated aortic dilatation or dissection in Japanese women with Marfan syndrome. *Circ. J.* 75, 2545–2551. doi: 10.1253/circj.CJ-11-0465

LeMaire, S. A., and Russell, L. (2011). Epidemiology of thoracic aortic dissection. *Nat. Rev. Cardiol.* 8, 103–113. doi: 10.1038/nrcardio.2010.187

Li, W.-P., Neradilek, M. B., Gu, F.-S., Isquith, D. A., Sun, Z.-J., Wu, X., et al. (2017). Pregnancy-associated plasma protein-A is a stronger predictor for adverse cardiovascular outcomes after acute coronary syndrome in type-2 diabetes mellitus. *Cardiovasc. Diabetol.* 16:45. doi: 10.1186/s12933-017-0526-6

Malfait, F., Castori, M., Francomano, C. A., Giunta, C., Kosho, T., and Byers, P. H. (2020). The Ehlers-Danlos syndromes. *Nat. Rev. Dis. Primers* 6:64. doi: 10.1038/s41572-020-0194-9

Ramlakhan, K. P., Johnson, M. R., and Roos-Hesselink, J. W. (2020). Pregnancy and cardiovascular disease. *Nat. Rev. Cardiol.* 17, 718–731. doi: 10.1038/s41569-020-0390-z

Schievink, W. I., Mokri, B., and O'Fallon, W. M. (1994). Recurrent spontaneous cervical-artery dissection. *New. Engl. J. Med.* 330, 393–397. doi: 10.1056/NEJM199402103300604

Tang, X., Li, P.-H., and Chen, H.-Z. (2020). Cardiomyocyte senescence and cellular communications within myocardial microenvironment. *Front. Endocrinol.* 11:280. doi: 10.3389/fendo.2020.00280

Theivacumar, N. S., Stephenson, M. A., Mistry, H., and Valenti, D. (2014). Diabetics are less likely to develop thoracic aortic dissection: a 10-year single-center analysis. *Ann. Vasc. Surg.* 28, 427–432. doi: 10.1016/j.avsg.2013.03.024

Timpka, S., Markovitz, A., Schyman, T., Mogren, I., Fraser, A., Franks, P. W., et al. (2018). Midlife development of type 2 diabetes and hypertension in women by history of hypertensive disorders of pregnancy. *Cardiovasc. Diabetol.* 17:124. doi: 10.1186/s12933-018-0764-2

Tweet, M. S., Kok, S. N., and Hayes, S. N. (2018). Spontaneous coronary artery dissection in women: what is known and what is yet to be understood. *Clin. Cardiol.* 41, 203–210. doi: 10.1002/clc.22909

Conflict of Interest: The authors declare that the research was conducted in the absence of any commercial or financial relationships that could be construed as a potential conflict of interest.

frontiers in Cell and Developmental Biology

MINI REVIEW
published: 01 April 2021
doi: 10.3389/fcell.2021.647631

Mitofusin-2: A New Mediator of Pathological Cell Proliferation

Yanguo Xin[1†], Junli Li[2†], Wenchao Wu[2] and Xiaojing Liu[1,2]*

[1] Department of Cardiology, West China Hospital, Sichuan University, Chengdu, China, [2] Laboratory of Cardiovascular Diseases, Regenerative Medicine Research Center, West China Hospital, Sichuan University, Chengdu, China

Cell proliferation is an important cellular process for physiological tissue homeostasis and remodeling. The mechanisms of cell proliferation in response to pathological stresses are not fully understood. Mitochondria are highly dynamic organelles whose shape, number, and biological functions are modulated by mitochondrial dynamics, including fusion and fission. Mitofusin-2 (Mfn-2) is an essential GTPase-related mitochondrial dynamics protein for maintaining mitochondrial network and bioenergetics. A growing body of evidence indicates that Mfn-2 has a potential role in regulating cell proliferation in various cell types. Here we review these new functions of Mfn-2, highlighting its crucial role in several signaling pathways during the process of pathological cell proliferation. We conclude that Mfn-2 could be a new mediator of pathological cell proliferation and a potential therapeutic target.

Keywords: mitochondria, Mfn-2, cell proliferation, target, apoptosis

OPEN ACCESS

Edited by:
Xiaoqiang Tang,
Sichuan University, China

Reviewed by:
Xiaoqiu Tan,
Southwest Medical University, China
Sichong Ren,
Chengdu Medical College, China

***Correspondence:**
Xiaojing Liu
liuxq@scu.edu.cn

[†] These authors have contributed equally to this work

Specialty section:
This article was submitted to Cellular Biochemistry, a section of the journal Frontiers in Cell and Developmental Biology

Received: *30 December 2020*
Accepted: *02 March 2021*
Published: *01 April 2021*

Citation:
Xin Y, Li J, Wu W and Liu X (2021) Mitofusin-2: A New Mediator of Pathological Cell Proliferation. Front. Cell Dev. Biol. 9:647631. doi: 10.3389/fcell.2021.647631

INTRODUCTION

Cell proliferation is a precision–control process, which is essential for embryonic and postnatal development (Takeuchi and Nakamura, 2014). Under pathological conditions, abnormal cell proliferation is a central mechanism attributing to disease progressions. Abnormal cell proliferation includes both abnormal cell division and abnormal cell differentiation (Fajas, 2003). These processes are common in various diseases. For example, cardiac fibroblast proliferation and fibroblast-to-myofibroblast transition resulted in cardiac fibrosis (Nagpal et al., 2016), a pathological process characterized by the accumulation of extracellular matrix in the cardiac interstitium. Abnormal hepatic stellate cell (HSCs) trans-differentiation, activation, and proliferation of HSCs are the primary driving force to promote chronic cholestatic liver diseases and facilitate the progression of liver fibrosis (Liu et al., 2019). Proliferation is also a main characteristic of cancer cells and the base of metastasis (Carmeliet et al., 1998). Therefore, a thorough understanding of the underlying mechanisms regulating various pathological cell proliferations is the premise for developing new therapeutic strategies.

Previously, mitochondria have been regarded as static and isolated organelles. More recently, they are found to undergo constant changes in morphology, including fission, fusion, and network formation, and they can also relocate to different parts in cells (trafficking); all of these processes are termed mitochondrial dynamics. Mitochondrial dynamics is essential to maintain the normal function of cells such as energy metabolism, calcium homeostasis, and reactive oxygen species generation (Vafai and Mootha, 2012; Tsushima et al., 2018). Mitochondria dynamics (**Figure 1**) is closely related to cell proliferation. Previous evidence has set a link between mitochondria dynamics and cell proliferation; high levels of mitochondrial fission are associated with active proliferation

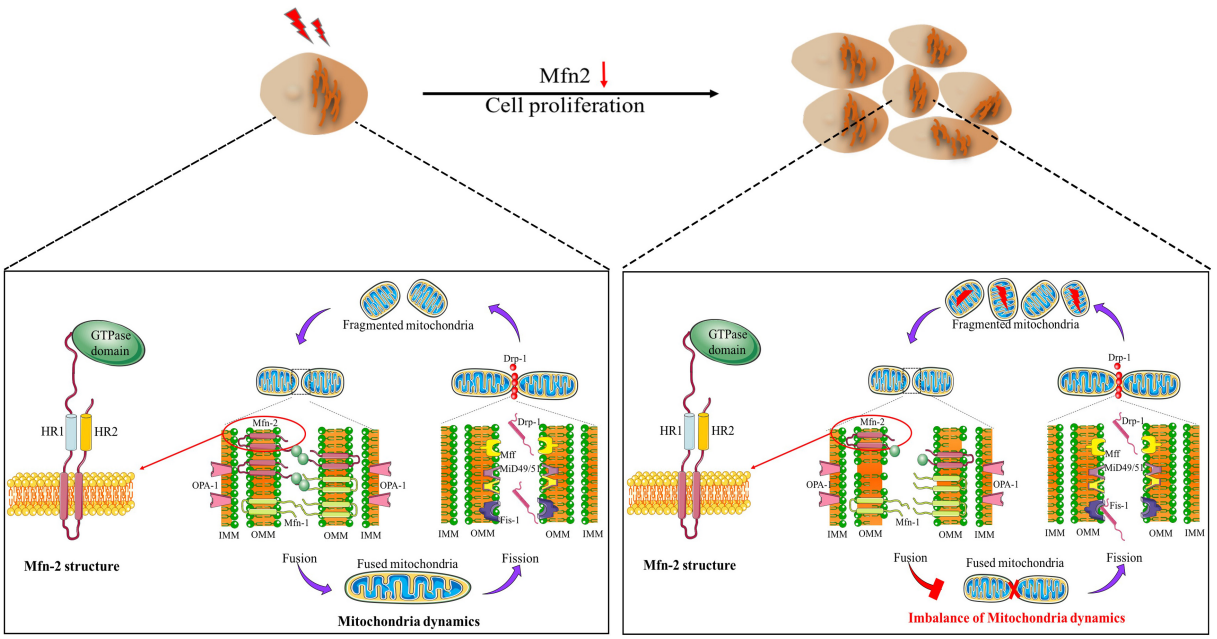

FIGURE 1 | Mitochondria dynamics and Mfn-2 structure. Mfn-2 is one of the main factors regulating mitochondrial fusion. The N-terminal of Mfn-2 is the GTPase domain. There are two HR domains and two transmembrane domains.

(Chen and Chan, 2017). Mitra et al. (2009) reported that maintaining mitochondria in hyperfused morphology could regulate the cell transition from G1 to S phase. In addition, the number of mitochondria throughout the cell cycle is mostly constant, which is attributed to mitochondria dynamics to a great extent (Carlton et al., 2020). Oncocytes could alter mitochondria dynamics to support their proliferation property (Senft and Ronai, 2016).

Research in the past two decades or so have revealed that the mechanisms of mitochondrial dynamics are regulated by a group of highly conserved guanosine triphosphatases (GTPase) (Misaka et al., 2002; Rojo et al., 2002; Son et al., 2017). Mitofusin 1 (Mfn-1) and mitofusin 2 (Mfn-2) control the fusion of the outer mitochondrial membrane (OMM), while optic atrophy 1 (OPA1) regulates the fusion of the inner mitochondrial membrane. Mitochondrial fission is under-controlled by the dynamic-related protein 1 (Drp1), which interacts with several OMM proteins, such as Mid51 and Mid49. Mfns are outer mitochondria membrane proteins, with GTPase domain in the N-terminal, followed by a hydrophobic heptad repeat (HR1), the transmembrane anchor, and HR2. Mfns anchored to OMM by the C-terminal binding domain, and the N-terminal domain extruded to the cytoplasm (Fritz et al., 2001; Rojo et al., 2002; **Figure 1**). Mammalian Mfn-1 and Mfn-2 shared about 80% similarity, consisting of 737 and 757 amino acids, respectively. However, Mfn-1 exhibited higher GTPase activity than Mfn-2, while Mfn-2 exhibited higher GTP affinity. It is reported that Mfn-1 functions in mitochondria tethering, while Mfn-2 has other distinct functions in addition to the fusion reaction (Ishihara et al., 2004). For example, Mfn-2 has been reported to be involved in PINK/Parkin-mediated mitophagy process (Chen and Dorn, 2013). Mfn-2 is one of the first proteins identified to mediate the tethering of endoplasmic reticulum (ER) and mitochondria in mammals (Vance, 1990). This domain, named mitochondria-associated membranes (MAM), has been the new frontiers in bioenergetics and biophysical studies of intracellular organelles. ER lost its physiological morphology, and the ER–mitochondria interaction was disrupted after Mfn-2 ablation (de Brito and Scorrano, 2008). Increasing evidence has indicated that MAM is closely related to cell proliferation in various diseases (Wang et al., 2009; Danese et al., 2017; Yang et al., 2019). Comparing with Mfn-1, Mfn-2 may play a vital role in cell proliferation *via* various pathways.

In this review, we summarized recent advancements in the study of mitochondrial fusion protein Mfn-2. We focus on the link between altered Mfn-2 and pathological cell proliferation.

OVERVIEW OF MITOFUSIN-2 AND CELL PROLIFERATION

Current evidence indicates that Mfn-2 plays various roles in many cellular processes, including cell proliferation and cell death (Chen et al., 2004; Wang et al., 2010; Zhao et al., 2012). Chen et al. (2004) found that Mfn-2 expression decreased in proliferative vascular smooth muscle cells (VSMCs), and overexpression of Mfn-2 could inhibit this proliferation process. Mfn-2 dysfunction has been associated with a variety of pathological conditions, including diabetes mellitus (Hernández-Alvarez et al., 2010), obesity (Bach et al., 2003), Charcot–Marie–Tooth disease (Züchner et al., 2004; Misko et al., 2012), atherosclerosis, hypertension (Chen et al., 2004),

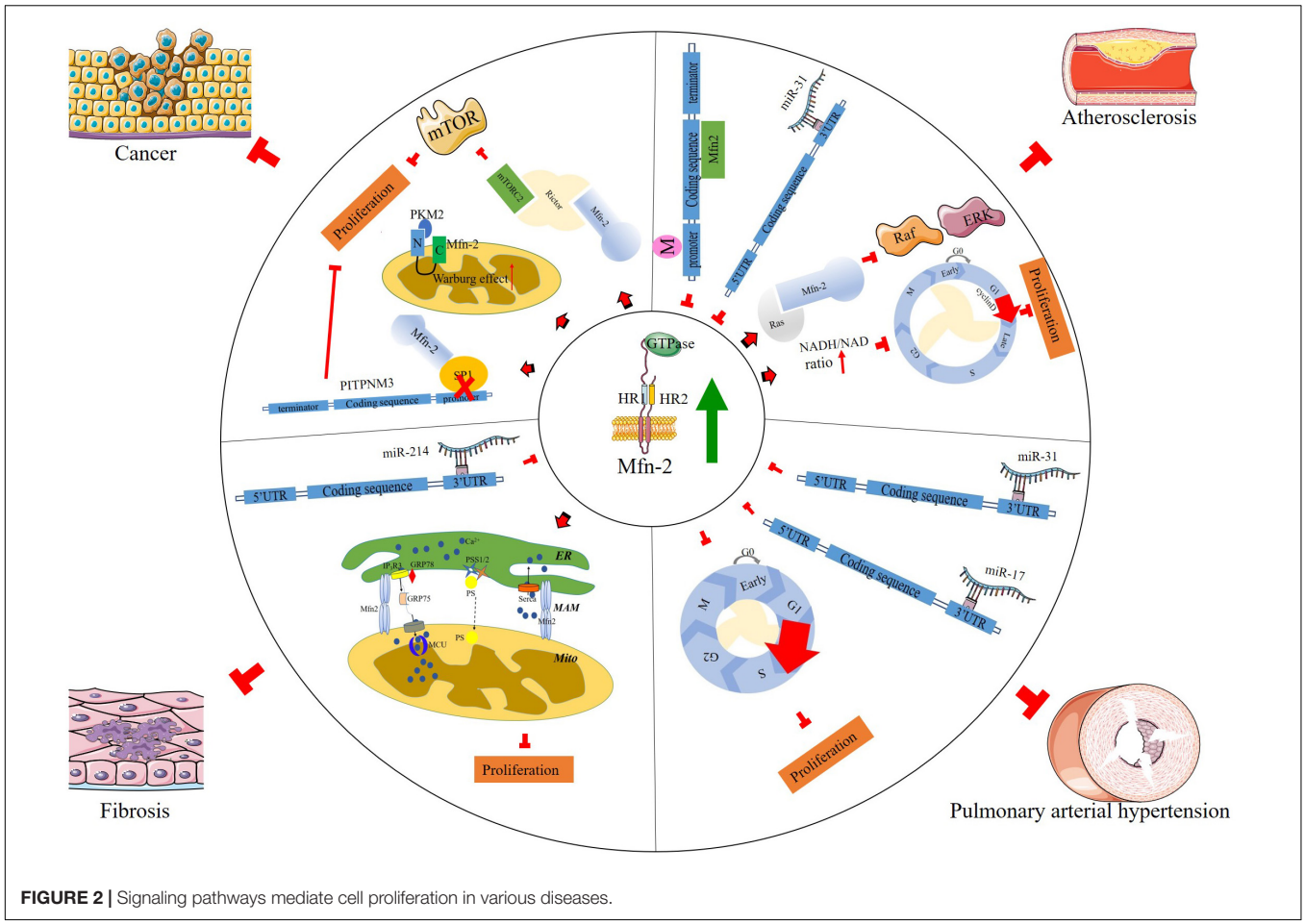

FIGURE 2 | Signaling pathways mediate cell proliferation in various diseases.

and cancer (Zhang et al., 2013; Xu et al., 2017). Collectively, the results of these studies have depicted Mfn-2 as a hyperplasia suppressor gene. In addition, energy is required in cell proliferation; in G1/S phase, mitochondrial elongation requires a higher amount of ATP to sustain cell duplication (Mitra et al., 2009). Mitochondria with intact structure are vital to supply enough ATP in this process, and Mfn-2 is necessary to maintain mitochondrial membrane potential, cellular oxygen consumption, etc. According to Sara's research (Pich et al., 2005), the role of Mfn-2 in mitochondrial nutrient oxidation is a fusion-independent function. Mitochondria fusion is also necessary to maintain the stoichiometry of the protein components of mtDNA replisome. Mfn-2 mutation could cause diseases due to mtDNA depletion, disrupting mouse embryo fibroblast (MEF) proliferation and postnatal heart development (Silva Ramos et al., 2019). Here a more detailed discussion of how Mfn-2 regulates cell proliferation is provided (**Figure 2**).

MITOFUSIN-2 AND ATHEROSCLEROSIS

Atherosclerosis is the main cause of cardiovascular diseases. It has been clearly demonstrated that the development and progression of atherosclerosis involve inflammation, abnormal proliferation of VSMCs, remodeling of the vascular wall, and evolution of occlusive plaques.

It is reported that the antiproliferative effect of Mfn-2 in serum-evoked VSMC proliferation was mediated *via* the inhibition of Erk/mitogen-activated protein kinase (Erk/MAPKs) signaling followed by cell cycle arrest. Cell transition from G0/G1 phase to S phase is one of the important characteristics for proliferation. EdU assay indicated that downregulation of Mfn-2 resulted in a significant decrease of G0/G1 phase cells and a synchronous increase of the percentage of S-phase cells in homocysteine-induced VSMCs, and overexpression of Mfn-2 obtained the contrary results, suggesting that cell cycle arrest at G0/G1 phase is responsible for the anti-proliferation effects of Mfn-2 (Xu et al., 2019). Two related mechanisms involved in this process were reported: one is that Mfn-2 could bind and inhibit the proto-oncogene Ras directly *via* its p21 Ras-binding domain in the N-terminal to control cell proliferation (de Brito and Scorrano, 2009), while Mfn-2 mutant lacking amino acids 77–91 failed to pull down Ras, with no effect on its function in the regulation of mitochondria fusion (de Brito and Scorrano, 2009); the other is that Mfn-2 regulates NAD/NADH ratio to control the transition of cell phase (Li et al., 2015). Infection with Mfn-2 adenovirus could increase NADH level and reduce NAD level, blocking the cell cycle at G0/G1 phase.

The accumulation of cholesterol-containing low-density lipoproteins in the intima and endothelium promotes the recruitment of monocytes, which then differentiate into macrophages and initiate inflammatory activation. Inflammation cells release various cytokines and growth factors, the most powerful factors, such as platelet-derived growth factor (PDGF) and its receptors, inducing VSMCs to transform from quiescent state to secretion and proliferation state *via* many signaling pathways, such as MAPK, PI3K/Akt, etc. (Wang et al., 2018). One remarkable characteristic of this process is migration of VSMCs from the media to the intima, contributing to neo-intima formation. In addition, various inhibitors in the process of inflammation could inhibit VSMC proliferation (Uhrin et al., 2018). In Feng's study, Mfn-2 expression was downregulated in proliferative VSMC primary cells treated with PDGF. Down-regulated Mfn-2 promotes cell proliferation and migration rate not only in PDGF-induced VSMCs but also in arterial smooth muscle cells (ASMCs) mediated by microRNA (miRNA) miR-31 (Huang et al., 2018), which targets the 3′UTR of Mfn-2 and downregulates its expression.

In patients diagnosed with type 2 diabetes, the incidence of atherosclerosis is high, and the expression of Mfn-2 in the muscle decreased; similar results are also observed in high-fat-diet mice. In addition, increasing the level of Mfn-2 could alleviate insulin resistance (Gan et al., 2013) through increasing the phosphorylation levels of PI3K-P85 and AKT2 insulin signaling pathways. Previous studies have identified that nuclear receptor superfamily member peroxisome proliferator-activated receptor-γ (PPARγ) is involved in atheromatous inflammation through the extracellular signal-regulated ERK/MAPKs and p38/MAPK pathways (Chen et al., 2004; Monsalve et al., 2013; Nagy et al., 2013; Yang et al., 2012). Liu et al. (2014) found that Mfn-2 inhibited atherosclerotic plaque formation by increasing PPARγ, and this process may be partially regulated by inactivation of the ERK1/2 and p38/MAPKs pathways. Xu et al. (2019) showed that, in homocysteine (Hcy)-induced atherosclerosis, c-Myc expression was increased, and it bound DNMT1 promoter to cause DNA hypermethylation of the Mfn-2 promoter, resulting in aberrant Mfn-2 transcription that led to VSMC proliferation.

As mentioned above, Mfn-2 is crucial in maintaining MAM structure. MAM is the central platform for the initiation of mitophagy and the formation of autophagosome (Hailey et al., 2010; Hamasaki et al., 2013). Chen and Dorn (2013) has linked Mfn-2 with PINK-Parkin-mediated senescent mitochondria elimination. In their model, PINK phosphorylates Mfn-2 to recruit Parkin to mitochondria, and Parkin, in turn, mediates Mfn-2 ubiquitination and initiates mitophagy. The effects of mitophagy on VSMC survival in response to stimuli in the pathogenesis of vascular disorders have been investigated in numerous studies (Culley and Chan, 2018; Marshall et al., 2018). He et al. (2019) reported that apelin-13 could induce VSMC proliferation and exacerbate atherosclerosis. PINK1/Parkin-mediated mitophagy could promote this process. In addition, a study on miR-145 found that the autophagy level was increased in the carotid intima hyperplasia in C57BL/6J mice (Wang et al., 2020), and activation of autophagy could stimulate aortic VSMC proliferation in metabolic hypertension rats (Wen et al., 2019). Although there is no direct evidence that Mfn-2 regulates cell proliferation *via* autophagy, considering the role of Mfn-2 in the maintenance of MAM, more studies are required to provide evidence linking Mfn-2-mediated autophagy with VSMC proliferation in the future.

MFN-2 AND PULMONARY HYPERTENSION

Pulmonary hypertension is another pathological condition attributed to VSMC proliferation. Pathophysiological changes involve all three layers of pulmonary arteries during vascular remodeling. For instance, endothelial angiogenesis, smooth muscle cell hyperplasia and hypertrophy, adventitial fibroblast proliferation, myofibroblast differentiation, and extracellular matrix deposition have all been reported (Howell et al., 2003; Wilkins et al., 2015). The excessive proliferation and impaired apoptosis of pulmonary artery smooth muscle cells (PASMCs) contribute to vascular obstruction in pulmonary hypertension patients.

The role of Mfn-2 in pulmonary hypertension is complicated. Zhang et al. (2012) reported that hypoxia induced Mfn-2 expression and knock-down Mfn-2 suppressed hypoxia-induced PASMCs proliferation through the PI3K/Akt signaling pathway. However, other studies indicated that the expression of Mfn-2 was decreased in pulmonary hypertension models, and increasing the Mfn-2 level may be a therapeutic strategy (Ryan et al., 2013, 2015; Fang et al., 2016; Lu et al., 2016). Deletion of thrombospondin motifs 8 (ADAMTS8), a secreted protein specifically expressed in the lung and the heart, reduced PASMC proliferation with Mfn-2 upregulation and mitochondrial function improvement (Omura et al., 2019). Downregulation of Mfn-2 may cause more cells to enter the S + G2/M phase of the cell cycle and inhibit the mitochondrial apoptosis pathway. These effects were reversed in PASMCs by Mfn-2 overexpression (Roy et al., 2009), indicating that Mfn-2 could be a therapeutic target in pulmonary hypertension (Ryan et al., 2013). While these discrepancies need to be resolved in future studies, it is clear that Mfn-2 is a critical regulator for pathological pulmonary hypertension.

Recent studies revealed that miRNAs play an important role in the pathogenesis of pulmonary hypertension by regulating ASMC proliferation (Thum et al., 2008; Roy et al., 2009; Bauersachs, 2010; Castoldi et al., 2012; Chen et al., 2014). Several miRNAs have been identified to participate in fibrosis and smooth muscle cell proliferation *via* targeting Mfn-2 directly. Huang et al. (2018) reported that the expression level of miR-31 was increased significantly in the arterial walls of patients with atherosclerosis obliterans. In addition, miR-31 promoted the proliferation and migration of human arterial smooth muscle cells, at least partially, through directly interacting with Mfn-2. In another study, Lu et al. (2016) revealed that miR-17 was upregulated in human PASMCs from patients with pulmonary artery hypertension, and the function of miR-17 in PASMC proliferation and apoptosis was partially mediated by downregulation of Mfn-2.

MITOFUSIN-2 AND FIBROPROLIFERATIVE DISEASES

Fibroblasts are a crucial component of connective tissues in various organs. Fibroblast activation and proliferation is characterized by an excessive accumulation of fibrous connective tissues in response to various stimuli (Kendall and Feghali-Bostwick, 2014). Fibrosis is a key pathological process in the development of various fibroproliferative diseases, such as cardiovascular fibrosis, pulmonary fibrosis, liver cirrhosis, systemic sclerosis, and kidney fibrosis. Fibroblasts produce the structural proteins of extracellular matrix (ECM), such as fibrous collagen (Kendall and Feghali-Bostwick, 2014). Fibroblast activation and proliferation may cause the accumulation of ECM's components, ultimately leading to disruption of the architecture in various tissues and dysfunction of the organs, such as end-stage liver disease and kidney failure. Mfn-2 could inhibit non-alcoholic fatty liver by interacting with phosphatidylserine (PS) directly. Mfn-2 deficiency could reduce PS transfer from the ER to the mitochondria, inducing mitochondrial dysfunction (Hernandez-Alvarez et al., 2019). Knockdown of Mfn-2 could rescue mitochondria Ca^{2+} transfer and inhibit cell proliferation in kidney cysts (Kuo et al., 2019). In addition, overexpressed Mfn-2 could alleviate glomerular mesangial cell proliferation *via* the MAPK/ERK and PI3K/Akt pathways (Wan-Xin et al., 2012; Chen et al., 2019). Mfn-2 regulates mitochondria fusion and intracellular lipid metabolism, which are tightly linked with lung fibrosis (Chung et al., 2019). Prediabetes is a common pathological condition characterized by increased ventricular mass and wall thickness, in which fibroblast proliferation is one of the key factors. Although this is a complicated biological process, Mfn-2 is considered to play a vital role in this process (Koncsos et al., 2016).

Endoplasmic reticulum stress (ERS) is a cellular state in which the protein folding capacity of ER is overwhelmed due to increased protein load or disruption of the protein folding environment (Berridge, 2002). It has been reported that ERS is involved in fibroblast activation and proliferation in many organs such as the liver (Shin et al., 2013), heart (Spitler and Webb, 2014), kidney (Chiang et al., 2011), and lung (Baek et al., 2012). Previous reports also identified the relationship between Mfn-2 and ERS. For example, in cardiac fibrosis, we found that the expression of Mfn-2 was decreased, and upregulating Mfn-2 inhibited fibroblast proliferation *via* the p-PERK/ATF4 pathway but not the IREα/Xbp1s or c-ATF6 signaling pathway (Xin et al., 2019). Ngoh et al. (2012) and Muñoz et al. (2013) also reported that Mfn-2 was an ERS-inducible protein. Philippe and Gary wrote a review discussing the role of Mfn-2 in inflammation-induced ERS (Delmotte and Sieck, 2019). Downregulation of Mfn-2 aggravated ERS, attributing to the proliferation of airway smooth muscle.

A study from Sun et al. (2015) showed that miR-214 mediated ISO-induced proliferation and collagen synthesis in cardiac fibroblasts through directly targeting Mfn-2 and activating the downstream ERK1/2 MAPK signaling pathway.

MITOFUSIN-2 AND CANCER

Abnormal cell proliferation could lead to the destabilization of chromosomal and genetic organization, resulting in the formation of neoplasm. This effect is regulated by a series of genes. Mutation of the genes will drive cells into tumor cells. The increase in glucose uptake and enhanced glycolytic rates indicate that metabolic alteration provides growth advantages for tumor cells (Lunt and Vander Heiden, 2011). In addition, tumor cells may exert different metabolic ways from normal cell proliferation. Warburg noticed that tumor cells exhibit a high rate of glycolysis even in the presence of oxygen (aerobic glycolysis) (Ortega et al., 2009). Some types of cancer, such as bladder cancer, cervical cancer, and breast cancer, are associated with altered mitochondrial morphology and metabolism (Filadi et al., 2018). The expression level of Mfn-2 is usually decreased in various types of cancer, and increasing Mfn-2 expression can suppress cell proliferation (Rehman et al., 2012), indicating that Mfn-2 is a tumor suppressor. One mechanism by which Mfn-2 suppresses cancer cell proliferation is inhibiting the metabolic flux to aerobic glycolysis by interreacting with pyruvate kinase 2 (PKM2) *via* the N-terminus (Li et al., 2009); phosphorylation of Mfn-2 enhances this interaction. Rictor is a subunit of mTORC1; Rictor deletion could block mitochondrial OXPHOS. Xu's recent work showed that Mfn-2 plays a vital role in the inhibition of the mTORC2/Akt signaling pathway through the interaction with Rictor by binding its HR1 domain in breast cancer patients. Mfn-2 knockdown could enhance growth in breast cancer. All these evidence indicated that the mTORC/AKT pathway is closely linked with Mfn-2 in pathological cell proliferation.

Under physiological conditions, mitochondria take up calcium mainly from the ER. Calcium is released through inositol 1,4,5-trisphosphate (IP3) receptors (IP3R) and ryanodine receptors (RyRs) on the ER membrane (Marks, 1997) and enters mitochondria through voltage-dependent anion channels (VDACs). The relationship between calcium signaling pathway and cancer has been discussed in detail in previous reviews (Ivanova et al., 2017; Marchi et al., 2018). In this process, MAM play a vital role (Ivanova et al., 2017) because these harbor key calcium handling proteins such as IP3R, VDACs, and sigma-1 receptors (Hayashi and Su, 2007). In 2008, de Brito and Scorrano (2008) showed that Mfn-2 was required for mitochondrial calcium uptake, and Mfn-2 knockout MEFs exhibited a reduced calcium uptake rate. In addition, translation of the calcium signals is necessary for the regulation of cell death and survival. Lower ER calcium content could arouse the expression of anti-apoptotic protein expression, such as Bcl-2 (Pinton et al., 2001). Mfn-2 could restore calcium homeostasis and downregulate ER stress in mouse neuroblastoma N2a cells.

Besides the regulation of intracellular calcium transportation, Mfn-2 may also regulate other signaling pathways for cell proliferation. Transcription factor SP1 plays an essential role in the expression of PITPNM3 in cancer cells, and Mfn-2 was reported to have anti-tumor activity by interacting with transcription factor SP1 directly (Tang et al., 2020). Pang et al. (2019) found that Mfn-2 inhibited cell proliferation *via* the Wnt/β-catenin pathway in bladder cancer. Mfn-2 knockdown

increased the translocation of β-catenin into the nucleus, resulting in larger tumor volumes and a higher proliferation index. Pharmacological inhibition of the Mfn-2/mTORC2/Akt pathway attenuated tumor growth (Xu et al., 2017). Several other studies also indicated that Mfn-2 interacted with the proapoptotic Bcl-2 family members Bax and Bak (Suen et al., 2008; Li et al., 2020).

FUTURE DIRECTIONS

Despite the significant advancements that deepened our understanding of the structure and functions of Mfn-2, several key questions remain to be elucidated:

(1) Although some evidence indicated that, in addition to fusion reaction, Mfn-2 has been reported to regulate cell proliferation *via* various signaling pathways, there are currently no studies that figured out whether these pathways are related to mitochondria fusion. More studies on this topic may be necessary in the future.
(2) Although there are many evidence about the role of Mfn-2 in neoplastic diseases, the microenvironment may change the impact of Mfn-2 in different types of cancers. In the future, a more detailed analysis of Mfn-2 may be necessary.
(3) Could altered Mfn-2 act as a potential biomarker in pathogenesis?

CONCLUSION

The machineries of mitochondrial fusion/fission and the significance of mitochondrial dynamics in regulating mitochondrial and cellular functions have been established. The mitochondrial fusion protein Mfn-2 regulates mitochondrial morphology, metabolism, calcium homeostasis, and mtDNA stability. Mfn-2 also plays a role *via* MAM formation and mitophagy to regulate cell proliferation and cell survival/death in different tissues. Many important questions await extensive investigation. In the future, studies on the role of Mfn-2 in cell proliferation may lead to the development of new strategies for treating various diseases, such as cancer and cardiovascular diseases.

AUTHOR CONTRIBUTIONS

YX and JL draft the manuscript. WW revised and polished the manuscript. XL supervised the review and established the whole frame. All authors contributed to the article and approved the submitted version.

FUNDING

This study was supported by the National Natural Science Foundation of China (NSFC) projects: 12072215 and 11672197 and the Fundamental Research Funds for the Central Universities: 2020SCU12031.

ACKNOWLEDGMENTS

We thank Wang and Pei Wang for the critical comments.

REFERENCES

Bach, D., Pich, S., Soriano, F. X., Vega, N., Baumgartner, B., and Oriola, J. (2003). Mitofusin-2 determines mitochondrial network architecture and mitochondrial metabolism. a novel regulatory mechanism altered in obesity. *J. Biol. Chem.* 278, 17190–17197. doi: 10.1074/jbc.m212754200

Baek, H. A., Kim, D. S., Park, H. S., Jang, K. Y., Kang, M. J., and Lee, D. G. (2012). Involvement of endoplasmic reticulum stress in myofibroblastic differentiation of lung fibroblasts. *Am. J. Respir. Cell Mol. Biol.* 46, 731–739. doi: 10.1165/rcmb.2011-0121oc

Bauersachs, J. (2010). Regulation of myocardial fibrosis by MicroRNAs. *J. Cardiovasc. Pharmacol.* 56, 454–459. doi: 10.1097/fjc.0b013e3181ee81df

Berridge, M. J. (2002). The endoplasmic reticulum: a multifunctional signaling organelle. *Cell Calcium* 32, 235–249. doi: 10.1016/s0143416002001823

Carlton, J. G., Jones, H., and Eggert, U. S. (2020). Membrane and organelle dynamics during cell division. *Nat. Rev. Mol. Cell Biol.* 21, 151–166. doi: 10.1038/s41580-019-0208-1

Carmeliet, P., Dor, Y., Herbert, J. M., Fukumura, D., Brusselmans, K., and Dewerchin, M. (1998). Role of HIF-1alpha in hypoxia-mediated apoptosis, cell proliferation and tumour angiogenesis. *Nature* 394, 485–490. doi: 10.1038/28867

Castoldi, G., Di Gioia, C. R. T., Bombardi, C., Catalucci, D., Corradi, B., and Gualazzi, M. G. (2012). MiR-133a regulates collagen 1A1: potential role of miR-133a in myocardial fibrosis in angiotensin II-dependent hypertension. *J. Cell. Physiol.* 227, 850–856. doi: 10.1002/jcp.22939

Chen, H., and Chan, D. C. (2017). Mitochondrial dynamics in regulating the unique phenotypes of cancer and stem cells. *Cell Metab.* 26, 39–48. doi: 10.1016/j.cmet.2017.05.016

Chen, H., Du, Y., Li, Y., Zeng, J., Miao, J., and Jiang, X. (2019). Jixuecao (Herba Centellae Asiaticae) alleviates mesangial cell proliferation in IgA nephropathy by inducing mitofusin 2 expression. *J. Tradit. Chin. Med.* 39, 346–355.

Chen, K.-H., Guo, X., Ma, D., Guo, Y., Li, Q., Yang, D., et al. (2004). Dysregulation of HSG triggers vascular proliferative disorders. *Nat. Cell Biol.* 6, 872–883. doi: 10.1038/ncb1161

Chen, S., Puthanveetil, P., Feng, B., Matkovich, S. J., Dorn, G. W., and Chakrabarti, S. (2014). Cardiac miR-133a overexpression prevents early cardiac fibrosis in diabetes. *J. Cell Mol. Med.* 18, 415–421. doi: 10.1111/jcmm.12218

Chen, Y., and Dorn, G. W. (2013). PINK1-phosphorylated mitofusin 2 is a Parkin receptor for culling damaged mitochondria. *Science* 340, 471–475. doi: 10.1126/science.1231031

Chiang, C.-K., Hsu, S.-P., Wu, C.-T., Huang, J.-W., Cheng, H.-T., and Chang, Y.-W. (2011). Endoplasmic reticulum stress implicated in the development of renal fibrosis. *Mol. Med.* 17, 1295–1305. doi: 10.2119/molmed.2011.00131

Chung, K. P., Hsu, C. L., Fan, L. C., Huang, Z., Bhatia, D., and Chen, Y.-J. (2019). Mitofusins regulate lipid metabolism to mediate the development of lung fibrosis. *Nat. Commun.* 10:3390.

Culley, M. K., and Chan, S. Y. (2018). Mitochondrial metabolism in pulmonary hypertension: beyond mountains there are mountains. *J. Clin. Invest.* 128, 3704–3715. doi: 10.1172/jci120847

Danese, A., Patergnani, S., Bonora, M., Wieckowski, M. R., Previati, M., Giorgi, C., et al. (2017). Calcium regulates cell death in cancer: roles of the mitochondria and mitochondria-associated membranes (MAMs). *Biochimica et Biophysica Acta Bioenergetics* 1858, 615–627. doi: 10.1016/j.bbabio.2017.01.003

de Brito, O. M., and Scorrano, L. (2008). Mitofusin 2 tethers endoplasmic reticulum to mitochondria. *Nature* 456, 605–610. doi: 10.1038/nature07534

de Brito, O. M., and Scorrano, L. (2009). Mitofusin-2 regulates mitochondrial and endoplasmic reticulum morphology and tethering: the role of Ras. *Mitochondrion* 3, 222–226. doi: 10.1016/j.mito.2009.02.005

Delmotte, P., and Sieck, G. C. (2019). Endoplasmic reticulum stress and mitochondrial function in airway smooth muscle. *Front. Cell Dev. Biol.* 7:374.

Fajas, L. (2003). Adipogenesis: a cross-talk between cell proliferation and cell differentiation. *Ann. Med.* 35, 79–85. doi: 10.1080/07853890310009999

Fang, X., Chen, X., Zhong, G., Chen, Q., and Hu, C. (2016). Mitofusin 2 downregulation triggers pulmonary artery smooth muscle cell proliferation and apoptosis imbalance in rats with hypoxic pulmonary hypertension Via the PI3K/Akt and mitochondrial apoptosis pathways. *J. Cardiovasc. Pharmacol.* 67, 164–174. doi: 10.1097/fjc.0000000000000333

Filadi, R., Pendin, D., and Pizzo, P. (2018). Mitofusin 2: from functions to disease. *Cell Death Dis.* 9:330.

Fritz, S., Rapaport, D., Klanner, E., Neupert, W., and Westermann, B. (2001). Connection of the mitochondrial outer and inner membranes by Fzo1 is critical for organellar fusion. *J. Cell Biol.* 152, 683–692. doi: 10.1083/jcb.152.4.683

Gan, K.-X., Wang, C., Chen, J.-H., Zhu, C.-J., and Song, G.-Y. (2013). Mitofusin-2 ameliorates high-fat diet-induced insulin resistance in liver of rats. *World Gastroenterol.* 19, 1572–1581. doi: 10.3748/wjg.v19.i10.1572

Hailey, D. W., Rambold, A. S., Satpute-Krishnan, P., Mitra, K., Sougrat, R., Kim, P. K., et al. (2010). Mitochondria supply membranes for autophagosome biogenesis during starvation. *Cell* 141, 656–667. doi: 10.1016/j.cell.2010.04.009

Hamasaki, M., Furuta, N., Matsuda, A., Nezu, A., Yamamoto, A., and Fujita, N. (2013). Autophagosomes form at ER-mitochondria contact sites. *Nature* 495, 389–393. doi: 10.1038/nature11910

Hayashi, T., and Su, T.-P. (2007). Sigma-1 receptor chaperones at the ER-mitochondrion interface regulate Ca(2+) signaling and cell survival. *Cell* 131, 596–610. doi: 10.1016/j.cell.2007.08.036

He, L., Zhou, Q., Huang, Z., Xu, J., Zhou, H., and Lv, D. (2019). PINK1/Parkin-mediated mitophagy promotes apelin-13-induced vascular smooth muscle cell proliferation by AMPKα and exacerbates atherosclerotic lesions. *J. Cell Physiol.* 234, 8668–8682. doi: 10.1002/jcp.27527

Hernandez-Alvarez, M. I., Sebastian, D., Vives, S., Ivanova, S., Bartoccioni, P., and Kakimoto, P. (2019). Deficient endoplasmic reticulum-mitochondrial phosphatidylserine transfer causes liver disease. *Cell* 177, 881–895.e17.

Hernández-Alvarez, M. I., Thabit, H., Burns, N., Shah, S., Brema, I., and Hatunic, M. (2010). Subjects with early-onset type 2 diabetes show defective activation of the skeletal muscle PGC-1{alpha}/Mitofusin-2 regulatory pathway in response to physical activity. *Diabetes Care* 33, 645–651. doi: 10.2337/dc09-1305

Howell, K., Preston, R. J., and McLoughlin, P. (2003). Chronic hypoxia causes angiogenesis in addition to remodelling in the adult rat pulmonary circulation. *J. Physiol.* 547(Pt 1), 133–145. doi: 10.1113/jphysiol.2002.030676

Huang, S., Chen, Z., Wu, W., Wang, M., Wang, R., and Cui, J. (2018). MicroRNA-31 promotes arterial smooth muscle cell proliferation and migration by targeting mitofusin-2 in arteriosclerosis obliterans of the lower extremitie. *Exp. Ther. Med.* 15, 633–640.

Ishihara, N., Eura, Y., and Mihara, K. (2004). Mitofusin 1 and 2 play distinct roles in mitochondrial fusion reactions via GTPase activity. *J. Cell Sci.* 117(Pt 26), 6535–6546. doi: 10.1242/jcs.01565

Ivanova, H., Kerkhofs, M., La Rovere, R. M., and Bultynck, G. (2017). Endoplasmic reticulum-mitochondrial ca fluxes underlying cancer cell survival. *Front. Oncol.* 7:70.

Kendall, R. T., and Feghali-Bostwick, C. A. (2014). Fibroblasts in fibrosis: novel roles and mediators. *Front. Pharmacol.* 5:123.

Koncsos, G., Varga, Z. V., Baranyai, T., Boengler, K., Rohrbach, S., and Li, L. (2016). Diastolic dysfunction in prediabetic male rats: role of mitochondrial oxidative stress. *Am. J. Physiol. Heart Circ. Physiol.* 311, H927–H943.

Kuo, I. Y., Brill, A. L., Lemos, F. O., Jiang, J. Y., Falcone, J. L., and Kimmerling, E. P. (2019). Polycystin 2 regulates mitochondrial Ca 2+ signaling, bioenergetics, and dynamics through mitofusin 2. *Sci. Signal.* 12:eaat7397. doi: 10.1126/scisignal.aat7397

Li, D., Li, X., Guan, Y., and Guo, X. (2015). Mitofusin-2-mediated tethering of mitochondria and endoplasmic eticulum promotes cell cycle arrest of vascular smooth muscle cells in G0/G1 phase. *Acta Biochim. Biophys. Sin.* 47, 441–450. doi: 10.1093/abbs/gmv035

Li, H.-B., Zhang, X.-Z., Sun, Y., Zhou, Q., Song, J.-N., and Hu, Z.-F. (2020). HO-1/PINK1 regulated mitochondrial fusion/fission to inhibit pyroptosis and attenuate septic acute kidney injury. *BioMed. Res. Int.* 2020:2148706.

Li, T., Han, J., Jia, L., Hu, X., Chen, L., and Wang, Y. (2009). PKM2 coordinates glycolysis with mitochondrial fusion and oxidative phosphorylation. *Protein Cell* 10, 583–594. doi: 10.1007/s13238-019-0618-z

Liu, C., Ge, B., He, C., Zhang, Y., Liu, X., Liu, K., et al. (2014). Mitofusin 2 decreases intracellular lipids in macrophages by regulating peroxisome proliferator-activated receptor-γ. *Biochem. Biophys. Res. Commun.* 450, 500–506. doi: 10.1016/j.bbrc.2014.06.005

Liu, R., Li, X., Zhu, W., Wang, Y., Zhao, D., and Wang, X. (2019). Cholangiocyte-derived exosomal long noncoding RNA H19 promotes hepatic stellate cell activation and cholestatic liver fibrosis. *Hepatology* 70, 1317–1335. doi: 10.1002/hep.30662

Lu, Z., Li, S., Zhao, S., and Fa, X. (2016). Upregulated miR-17 regulates hypoxia-mediated human pulmonary artery smooth muscle cell proliferation and apoptosis by targeting Mitofusin 2. *Med. Sci. Monit.* 22, 3301–3308. doi: 10.12659/msm.900487

Lunt, S. Y., and Vander Heiden, M. G. (2011). Aerobic glycolysis: meeting the metabolic requirements of cell proliferation. *Annu. Rev. Cell Dev. Biol.* 27, 441–464. doi: 10.1146/annurev-cellbio-092910-154237

Marchi, S., Patergnani, S., Missiroli, S., Morciano, G., Rimessi, A., Wieckowski, M. R., et al. (2018). Mitochondrial and endoplasmic reticulum calcium homeostasis and cell death. *Cell Calcium* 69, 62–72. doi: 10.1016/j.ceca.2017.05.003

Marks, A. R. (1997). Intracellular calcium-release channels: regulators of cell life and death. *Am. J. Physiol.* 272(2 Pt 2), H597–H605.

Marshall, J. D., Bazan, I., Zhang, Y., Fares, W. H., and Lee, P. J. (2018). Mitochondrial dysfunction and pulmonary hypertension: cause, effect, or both. *Am. J. Physiol. Lung. Cell Mol. Physiol.* 314, L782–L796.

Misaka, T., Miyashita, T., and Kubo, Y. (2002). Primary structure of a dynamin-related mouse mitochondrial GTPase and its distribution in brain, subcellular localization, and effect on mitochondrial morphology. *J. Biol. Chem.* 277, 15834–15842. doi: 10.1074/jbc.m109260200

Misko, A. L., Sasaki, Y., Tuck, E., Milbrandt, J., and Baloh, R. H. (2012). Mitofusin2 mutations disrupt axonal mitochondrial positioning and promote axon degeneration. *J. Neurosci.* 32, 4145–4155. doi: 10.1523/jneurosci.6338-11.2012

Mitra, K., Wunder, C., Roysam, B., Lin, G., and Lippincott-Schwartz, J. (2009). A hyperfused mitochondrial state achieved at G1-S regulates cyclin E buildup and entry into S phase. *Proc. Natl. Acad. Sci. USA* 106, 11960–11965. doi: 10.1073/pnas.0904875106

Monsalve, F. A., Pyarasani, R. D., Delgado-Lopez, F., and Moore-Carrasco, R. (2013). Peroxisome proliferator-activated receptor targets for the treatment of metabolic diseases. *Mediators Inflamm.* 2013:549627.

Muñoz, J. P., Ivanova, S., Sánchez-Wandelmer, J., Martínez-Cristóbal, P., Noguera, E., and Sancho, A. (2013). Mfn2 modulates the UPR and mitochondrial function via repression of PERK. *EMBO J.* 32, 2348–2361. doi: 10.1038/emboj.2013.168

Nagpal, V., Rai, R., Place, A. T., Murphy, S. B., Verma, S. K., and Ghosh, A. K. (2016). MiR-125b is critical for fibroblast-to-myofibroblast transition and cardiac fibrosis. *Circulation* 133, 291–301. doi: 10.1161/circulationaha.115.018174

Nagy, Z. S., Czimmerer, Z., and Nagy, L. (2013). Nuclear receptor mediated mechanisms of macrophage cholesterol metabolism. *Mol. Cell. Endocrinol.* 368, 85–98. doi: 10.1016/j.mce.2012.04.003

Ngoh, G. A., Papanicolaou, K. N., and Walsh, K. (2012). Loss of mitofusin 2 promotes endoplasmic reticulum stress. *J. Biol. Chem.* 287, 20321–20332. doi: 10.1074/jbc.m112.359174

Omura, J., Satoh, K., Kikuchi, N., Satoh, T., Kurosawa, R., and Nogi, M. (2019). ADAMTS8 promotes the development of pulmonary arterial hypertension and right ventricular failure. *Circ. Res.* 125, 884–906.

Ortega, A. D., Sánchez-Aragó, M., Giner-Sánchez, D., Sánchez-Cenizo, L., Willers, I., and Cuezva, J. M. (2009). Glucose avidity of carcinomas. *Cancer Lett.* 276, 125–135. doi: 10.1016/j.canlet.2008.08.007

Pang, G., Xie, Q., and Yao, J. (2019). Mitofusin 2 inhibits bladder cancer cell proliferation and invasion via the Wnt/β-catenin pathway. *Oncol. Lett.* 18, 2434–2442.

Pich, S., Bach, D., Briones, P., Liesa, M., Camps, M., and Testar, X. (2005). The Charcot-Marie-Tooth type 2A gene product, Mfn2, up-regulates fuel oxidation through expression of OXPHOS system. *Hum. Mol. Genet.* 14, 1405–1415. doi: 10.1093/hmg/ddi149

Pinton, P., Ferrari, D., Rapizzi, E., Di Virgilio, F., Pozzan, T., and Rizzuto, R. (2001). The Ca2+ concentration of the endoplasmic reticulum is a key determinant of ceramide-induced apoptosis: significance for the molecular mechanism of Bcl-2 action. *EMBO J.* 20, 2690–2701. doi: 10.1093/emboj/20.11.2690

Rehman, J., Zhang, H. J., Toth, P. T., Zhang, Y., Marsboom, G., Hong, Z., et al. (2012). Inhibition of mitochondrial fission prevents cell cycle progression in lung cancer. *FASEB J.* 26, 2175–2186. doi: 10.1096/fj.11-196543

Rojo, M., Legros, F., Chateau, D., and Lombès, A. (2002). Membrane topology and mitochondrial targeting of mitofusins, ubiquitous mammalian homologs of the transmembrane GTPase Fzo. *J. Cell Sci.* 115(Pt 8), 1663–1674.

Roy, S., Khanna, S., Hussain, S.-R. A., Biswas, S., Azad, A., and Rink, C. (2009). MicroRNA expression in response to murine myocardial infarction: miR-21 regulates fibroblast metalloprotease-2 via phosphatase and tensin homologue. *Cardiovasc. Res.* 82, 21–29. doi: 10.1093/cvr/cvp015

Ryan, J. J., Marsboom, G., Fang, Y.-H., Toth, P. T., Morrow, E., and Luo, N. (2013). PGC1α-mediated mitofusin-2 deficiency in female rats and humans with pulmonary arterial hypertension. *Am. J. Respir. Crit. Care Med.* 187, 865–878. doi: 10.1164/rccm.201209-1687oc

Ryan, J., Dasgupta, A., Huston, J., Chen, K.-H., and Archer, S. L. (2015). Mitochondrial dynamics in pulmonary arterial hypertension. *J. Mol. Med.* 93, 229–242.

Senft, D., and Ronai, Z. A. (2016). Regulators of mitochondrial dynamics in cancer. *Curr. Opin. Cell Biol.* 39, 43–52. doi: 10.1016/j.ceb.2016.02.001

Shin, J., He, M., Liu, Y., Paredes, S., Villanova, L., and Brown, K. (2013). SIRT7 represses Myc activity to suppress ER stress and prevent fatty liver disease. *Cell Rep.* 5, 654–665. doi: 10.1016/j.celrep.2013.10.007

Silva Ramos, E., Motori, E., Brüser, C., Kühl, I., Yeroslaviz, A., and Ruzzenente, B. (2019). Mitochondrial fusion is required for regulation of mitochondrial DNA replication. *PLoS Genet.* 15:e1008085. doi: 10.1371/journal.pgen.1008085

Son, J. M., Sarsour, E. H., Kakkerla, Balaraju, A., Fussell, J., and Kalen, A. L. (2017). Mitofusin 1 and optic atrophy 1 shift metabolism to mitochondrial respiration during aging. *Aging Cell* 16, 1136–1145. doi: 10.1111/acel.12649

Spitler, K. M., and Webb, R. C. (2014). Endoplasmic reticulum stress contributes to aortic stiffening via proapoptotic and fibrotic signaling mechanisms. *Hypertension* 63, e40–e45.

Suen, D.-F., Norris, K. L., and Youle, R. J. (2008). Mitochondrial dynamics and apoptosis. *Genes Dev.* 22, 1577–1590. doi: 10.1101/gad.1658508

Sun, M., Yu, H., Zhang, Y., Li, Z., and Gao, W. (2015). MicroRNA-214 mediates isoproterenol-induced proliferation and collagen synthesis in cardiac fibroblasts. *Sci. Rep.* 5:18351.

Takeuchi, T., and Nakamura, H. (2014). Cell proliferation and development. Preface. *Dev. Growth Differ.* 56:323.

Tang, T., Tao, X., Bao, X., Chen, J., Dai, J., Ye, J., et al. (2020). Mitofusin-2 (Mfn-2) might have anti-cancer effect through interaction with transcriptional factor SP1 and consequent regulation on phosphatidylinositol transfer protein 3 (PITPNM3) expression. *Med. Sci. Monit.* 26:e918599.

Thum, T., Gross, C., Fiedler, J., Fischer, T., Kissler, S., and Bussen, M. (2008). MicroRNA-21 contributes to myocardial disease by stimulating MAP kinase signalling in fibroblasts. *Nature* 456, 980–984. doi: 10.1038/nature07511

Tsushima, K., Bugger, H., Wende, A. R., Soto, J., Jenson, G. A., and Tor, A. R. (2018). Mitochondrial reactive oxygen species in lipotoxic hearts induce post-translational modifications of AKAP121, DRP1, and OPA1 that promote mitochondrial fission. *Circ. Res.* 122, 58–73. doi: 10.1161/circresaha.117.311307

Uhrin, P., Wang, D., Mocan, A., Waltenberger, B., Breuss, J. M., and Tewari, D. (2018). Vascular smooth muscle cell proliferation as a therapeutic target. Part 2: natural products inhibiting proliferation. *Biotechnol. Adv.* 36, 1608–1621. doi: 10.1016/j.biotechadv.2018.04.002

Vafai, S. B., and Mootha, V. K. (2012). Mitochondrial disorders as windows into an ancient organelle. *Nature* 491, 374–383. doi: 10.1038/nature11707

Vance, J. E. (1990). Phospholipid synthesis in a membrane fraction associated with mitochondria. *J. Biol. Chem.* 265, 7248–7256. doi: 10.1016/s0021-9258(19)39106-9

Wang, D., Uhrin, P., Mocan, A., Waltenberger, B., Breuss, J. M., and Tewari, D. (2018). Vascular smooth muscle cell proliferation as a therapeutic target. Part 1: molecular targets and pathways. *Biotechnol. Adv.* 36, 1586–1607. doi: 10.1016/j.biotechadv.2018.04.006

Wang, W., Chen, L., Shang, C., Jin, Z., Yao, F., Bai, L., et al. (2020). miR-145 inhibits the proliferation and migration of vascular smooth muscle cells by regulating autophagy. *J. Cell Mol. Med.* 24, 6658–6669. doi: 10.1111/jcmm.15316

Wang, W., Cheng, X., Lu, J., Wei, J., Fu, G., and Zhu, F. (2010). Mitofusin-2 is a novel direct target of p53. *Biochem. Biophys. Res. Commun.* 400, 587–592. doi: 10.1016/j.bbrc.2010.08.108

Wang, Y., Cao, W., Yu, Z., and Liu, Z. (2009). Downregulation of a mitochondria associated protein SLP-2 inhibits tumor cell motility, proliferation and enhances cell sensitivity to chemotherapeutic reagents. *Cancer Biol. Ther.* 8, 1651–1658. doi: 10.4161/cbt.8.17.9283

Wan-Xin, T., Tian-Lei, C., Ben, W., Wei-Hua, W., and Ping, F. (2012). Effect of mitofusin 2 overexpression on the proliferation and apoptosis of high-glucose-induced rat glomerular mesangial cells. *J. Nephrol.* 25, 1023–1030. doi: 10.5301/jn.5000089

Wen, J., Wang, J., Guo, L., Cai, W., Wu, Y., Chen, W., et al. (2019). Chemerin stimulates aortic smooth muscle cell proliferation and migration via activation of autophagy in VSMCs of metabolic hypertension rats. *Am. J. Transl. Res.* 11, 1327–1342.

Wilkins, M. R., Ghofrani, H.-A., Weissmann, N., Aldashev, A., and Zhao, L. (2015). Pathophysiology and treatment of high-altitude pulmonary vascular disease. *Circulation* 131, 582–590. doi: 10.1161/circulationaha.114.006977

Xin, Y., Wu, W., Qu, J., Wang, X., Lei, S., Yuan, L., et al. (2019). Inhibition of Mitofusin-2 promotes cardiac fibroblast activation via the PERK/ATF4 pathway and reactive oxygen species. *Oxid. Med. Cell. Longev.* 2019:3649808.

Xu, K., Chen, G., Li, X., Wu, X., Chang, Z., and Xu, J. (2017). MFN2 suppresses cancer progression through inhibition of mTORC2/Akt signaling. *Sci. Rep.* 7:41718.

Xu, L., Hao, H., Hao, Y., Wei, G., Li, G., and Ma, P. (2019). Aberrant MFN2 transcription facilitates homocysteine-induced VSMCs proliferation via the increased binding of c-Myc to DNMT1 in atherosclerosis. *J. Cell Mol. Med.* 23, 4611–4626. doi: 10.1111/jcmm.14341

Yang, C.-M., Lu, Y.-L., Chen, H.-Y., and Hu, M.-L. (2012). Lycopene and the LXRα agonist T0901317 synergistically inhibit the proliferation of androgen-independent prostate cancer cells via the PPARγ-LXRα-ABCA1 pathway. *J. Nutr. Biochem.* 23, 1155–1162. doi: 10.1016/j.jnutbio.2011.06.009

Yang, Y.-D., Li, M.-M., Xu, G., Feng, L., Zhang, E.-L., and Chen, J. (2019). Nogo-B receptor directs mitochondria-associated membranes to regulate vascular smooth muscle cell proliferation. *Int. J. Mol. Sci.* 20:2319. doi: 10.3390/ijms20092319

Zhang, D., Ma, C., Li, S., Ran, Y., Chen, J., Lu, P., et al. (2012). Effect of Mitofusin 2 on smooth muscle cells proliferation in hypoxic pulmonary hypertension. *Microvasc. Res.* 84, 286–296. doi: 10.1016/j.mvr.2012.06.010

Zhang, G.-E., Jin, H.-L., Lin, X.-K., Chen, C., Liu, X.-S., Zhang, Q., et al. (2013). Anti-tumor effects of Mfn2 in gastric cancer. *Int. J. Mol. Sci.* 14, 13005–13021. doi: 10.3390/ijms140713005

Zhao, T., Huang, X., Han, L., Wang, X., Cheng, H., and Zhao, Y. (2012). Central role of mitofusin 2 in autophagosome-lysosome fusion in cardiomyocytes. *J. Biol. Chem.* 287, 23615–23625. doi: 10.1074/jbc.m112.379164

Züchner, S., Mersiyanova, I. V., Muglia, M., Bissar-Tadmouri, N., Rochelle, J., and Dadali, E. L. (2004). Mutations in the mitochondrial GTPase mitofusin 2 cause Charcot-Marie-Tooth neuropathy type 2A. *Nat. Genet.* 36, 449–451. doi: 10.1038/ng1341

Conflict of Interest: The authors declare that the research was conducted in the absence of any commercial or financial relationships that could be construed as a potential conflict of interest.

frontiers in Cell and Developmental Biology

BRIEF RESEARCH REPORT
published: 14 May 2021
doi: 10.3389/fcell.2021.664258

Whole-Body Prolyl Hydroxylase Domain (PHD) 3 Deficiency Increased Plasma Lipids and Hematocrit Without Impacting Plaque Size in Low-Density Lipoprotein Receptor Knockout Mice

*Jasper A. F. Demandt[1], Kim van Kuijk[1,2], Thomas L. Theelen[1], Elke Marsch[1], Sean P. Heffron[3], Edward A. Fisher[3], Peter Carmeliet[4,5], Erik A. L. Biessen[1,6] and Judith C. Sluimer[1,7]**

[1] Department of Pathology, Cardiovascular Research Institute Maastricht (CARIM), Maastricht University Medical Center (MUMC), Maastricht, Netherlands, [2] Institute of Experimental Medicine and Systems Biology, RWTH Aachen University, Aachen, Germany, [3] Center for the Prevention of Cardiovascular Disease, Department of Medicine, Grossman School of Medicine, New York University, New York, NY, United States, [4] Laboratory of Angiogenesis and Vascular Metabolism, Department of Oncology, KU Leuven, Leuven, Belgium, [5] Laboratory of Angiogenesis and Vascular Metabolism, VIB Center for Cancer Biology, Leuven, Belgium, [6] Institute for Molecular Cardiovascular Research, RWTH Aachen University, Aachen, Germany, [7] BHF Centre for Cardiovascular Sciences (CVS), University of Edinburgh, Edinburgh, United Kingdom

OPEN ACCESS

Edited by:
Md. Shenuarin Bhuiyan, Louisiana State University Health Sciences Center Shreveport, United States

Reviewed by:
Shunxing Rong, University of Texas Southwestern Medical Center, United States
Kenichi Shimada, Cedars-Sinai Medical Center, United States

***Correspondence:**
Judith C. Sluimer
judith.sluimer@maastrichtuniversity.nl

Specialty section:
This article was submitted to Cellular Biochemistry, a section of the journal Frontiers in Cell and Developmental Biology

Received: 04 February 2021
Accepted: 23 April 2021
Published: 14 May 2021

Citation:
Demandt JAF, van Kuijk K, Theelen TL, Marsch E, Heffron SP, Fisher EA, Carmeliet P, Biessen EAL and Sluimer JC (2021) Whole-Body Prolyl Hydroxylase Domain (PHD) 3 Deficiency Increased Plasma Lipids and Hematocrit Without Impacting Plaque Size in Low-Density Lipoprotein Receptor Knockout Mice. Front. Cell Dev. Biol. 9:664258. doi: 10.3389/fcell.2021.664258

Background and aims: Atherosclerosis is an important cause of clinical cardiovascular events. Atherosclerotic plaques are hypoxic, and reoxygenation improves plaque phenotype. Central players in hypoxia are hypoxia inducible factors (HIF) and their regulators, HIF-prolyl hydroxylase (PHD) isoforms 1, 2, and 3. PHD inhibitors, targeting all three isoforms, are used to alleviate anemia in chronic kidney disease. Likewise, whole-body PHD1 and PHD2ko ameliorate hypercholesterolemia and atherogenesis. As the effect of whole-body PHD3 is unknown, we investigated the effects of germline whole-body PHD3ko on atherosclerosis.

Approach and Results: To initiate hypercholesterolemia and atherosclerosis low-density lipoprotein receptor knockout (LDLrko) and PHD3/LDLr double knockout (PHD3dko), mice were fed a high-cholesterol diet. Atherosclerosis and hypoxia marker pimonidazole were analyzed in aortic roots and brachiocephalic arteries. In contrast to earlier reports on PHD1- and PHD2-deficient mice, a small elevation in the body weight and an increase in the plasma cholesterol and triglyceride levels were observed after 10 weeks of diet. Dyslipidemia might be explained by an increase in hepatic mRNA expression of Cyp7a1 and fatty acid synthase, while lipid efflux of PHD3dko macrophages was comparable to controls. Despite dyslipidemia, plaque size, hypoxia, and phenotype were not altered in the aortic root or in the brachiocephalic artery of

PHD3dko mice. Additionally, PHD3dko mice showed enhanced blood hematocrit levels, but no changes in circulating, splenic or lymphoid immune cell subsets.

Conclusion: Here, we report that whole-body PHD3dko instigated an unfavorable lipid profile and increased hematocrit, in contrast to other PHD isoforms, yet without altering atherosclerotic plaque development.

Keywords: atherosclerosis, triglycerides, prolyl hydroxylase domain protein, hematocrit, hypoxia

INTRODUCTION

Atherosclerosis frequently stands at the origin of cardiovascular disease (CVD). Next to the major risk factors like inflammation (Tabas and Bornfeldt, 2016) and dyslipidemia (Plump et al., 1992; Zhang et al., 1992; Ishibashi et al., 1994), hypoxia contributes to the progression of atherosclerotic plaques (Marsch et al., 2014). Critical in this hypoxic signaling cascade are the hypoxia inducible factor (HIF) family members HIF1α and HIF2α. This master transcription factor family steers multiple cellular adaptations, in order to maintain normal cellular functions during hypoxic conditions. These adaptations include metabolic changes, affecting glucose (Samanta and Semenza, 2018) and lipid (Mylonis et al., 2019) metabolism. Also, inflammatory pathways are affected by HIF signaling, and multiple studies have shown that altered HIF1α signaling interferes with atherosclerotic plaque development (Ben-Shoshan et al., 2009; Christoph et al., 2014; Akhtar et al., 2015; Aarup et al., 2016; Jain et al., 2018). The HIFα subunits are constitutively expressed, but can only exert their functions upon translocation and subsequent dimerization with HIF1β in the nucleus. HIF activity is predominantly regulated in an oxygen-dependent manner by the egl-9 family hypoxia inducible factors (EGLN) family, hereafter referred to as HIF-prolyl hydroxylase enzymes PHD1, 2, and 3 (EGLN2, 1, and 3) (Kaelin and Ratcliffe, 2008). Each of these Fe^{2+} and 2-oxoglutarate-dependent dioxygenases shows a different intracellular localization and affinity for HIF1α and HIF2α (Berra et al., 2003; Appelhoff et al., 2004). Oxygen is used by the PHDs to hydroxylate a proline residue of the HIF1α and HIF2α subunits. Hydroxylated HIF is ubiquitinated by Von Hippel-Lindau proteins, rendering it a target for proteasomal degradation (Appelhoff et al., 2004). PHD2 is considered the most important isoform *in vivo*, as homozygous PHD2 knockout (ko) embryos die between day 12.5 and 14.5 of gestation (Takeda et al., 2006). PHD3 is the most strongly induced isoform in reaction to hypoxia, followed by PHD2 (Appelhoff et al., 2004; Aprelikova et al., 2004). This makes PHD3 an interesting target for further investigation in the hypoxic atherosclerotic plaque.

Recently, our group showed that whole-body PHD1 deficiency in atherosclerosis-prone low-density lipoprotein receptor knockout (LDLR-ko) mice reduced atherosclerotic plaque size and necrotic plaque content as a result of protective effects on extrahepatic lipid metabolism and macrophage oxygen consumption (Marsch et al., 2016). Another group reported reduced plasma lipid levels due to hepatic effects and protective autoantibodies against oxidized lipids in hypomorphic PHD2/LDLR^{C699Y} mutant mice (Rahtu-Korpela et al., 2016). This resulted in ameliorated plaque size, indicating the importance of PHD proteins in metabolism and subsequent plaque development. In line, PHD inhibitors, targeting all three isoforms to alleviate anemia in chronic kidney disease, also ameliorated lipid metabolism in mice and humans, and atherogenesis in mice (Rahtu-Korpela et al., 2016; Chen et al., 2019a,b). Considering that CKD patients are at risk of CVD, plaques are hypoxic, PHDs can interfere with metabolism, and PHD3 is strongly upregulated during hypoxia. PHD3 is an attractive target to study in the context of atherosclerosis. Hence, we set out to study the effects of whole-body PHD3ko on plaque development.

Abbreviations: ABCB5/8, ATP-binding cassette subfamily G member 5/8; BMDM, bone marrow-derived macrophages; CD36, cluster of differentiation 36; CKD, chronic kidney disease; CVD, cardiovascular disease; CYP7a1/8b1, cytochrome P450 7a1/8b1; dko, double knockout; EGLN, egl-9 family hypoxia inducible factors; FAS, fatty acid synthase; HCD, high-cholesterol diet; HIF, hypoxia inducible factor; HMGCR, 3-hydroxy-3-methylglutaryl-CoA reductase; H&E, hematoxylin and eosin; IRS-2, insulin receptor substrate 2; LRLR, low-density lipoprotein receptor; LRP1, low-density lipoprotein receptor-related protein 1; PHD, prolyl hydroxylase; PPARγ, peroxisome proliferator-activated receptor gamma; pVHL, Von Hippel–Lindau protein; SCARB1, scavenger receptor class B type 1; SREBPc1, sterol regulatory element-binding protein; TG, triglycerides.

MATERIALS AND METHODS

Animals and Atherosclerosis Model

All mouse experiments were approved by the regulatory authority of Maastricht University Medical Centre and performed in compliance with the guidelines described in the Directive 2010/63/EU of the European Parliament. All mice were bred at least nine generations on C57/JBl6 background, and male low-density lipoprotein receptor (LDLr) knockout (ko) mice were obtained from an in-house breeding colony, originating from Charles River (Wilmington, MA, United States) and refreshed every 10 generations to avoid genetic drift. All animals were housed in individually ventilated cages (GM500, Tecniplast) in groups of up to five animals per cage, with bedding (corncob, Tecnilab-BMI) and cage enrichment. Cages were changed weekly, reducing handling of the mice to once per week during non-intervention periods. Male PHD3 and LDLr double knockout (PHD3dko) and LDLrko littermates (n = 14 and 22, respectively, 11 weeks old) were fed a high-cholesterol diet (HCD) *ad libitum* (0.25% cholesterol, SDS 824171) for 10 weeks.

Atherosclerosis Quantification and Immunohistochemistry

One hour prior to sacrifice, all mice were intraperitoneally (i.p.) injected with the hypoxia-specific marker pimonidazole (100 mg/kg, hypoxyprobe Omni HP3 kit, Hypoxyprobe Inc., Burlington, MA, United States). Mice were euthanized with a pentobarbital overdose (100 mg/kg i.p.), and blood was withdrawn via the right ventricle for flow cytometry, absolute white and red blood cell counts (Coulter Ac.T diff, Beckman Coulter, United States), and total cholesterol analysis. Mice were perfused via the left cardiac ventricle with PBS containing sodium nitroprusside (0.1 mg/ml; Sigma-Aldrich, Seelze, Germany). Aortic root and all organs were subsequently excised and fixed in 1% PFA overnight, processed, and paraffin-embedded.

Aortic roots and arches were serially sectioned and stained with hematoxylin and eosin (H&E, Sigma) for plaque area and lipid core content quantification. Plaque stage was quantified on plaque characteristics such as foam cells (early), fibrous cap (intermediate), and necrotic core (advanced). Five consecutive H&E sections at 20 μm intervals were analyzed blindly using computerized morphometry (Leica QWin V3, Cambridge, United Kingdom) and averaged per mouse. Sections within this 100 μm interval were used for the remaining immunohistochemical stainings. If appropriate, antigen retrieval was performed at pH6 (Dako REAL target retrieval, Dako). Atherosclerotic plaques were characterized for macrophage content (MAC3 + area/total area, BD Cat# 553322, RRID:AB_394780). Hypoxia was detected in the aortic roots, using a rabbit polyclonal antibody (clone 2627, Cat# HP MAb-1, RRID:AB_2801307) directed against pimonidazole derivates, formed *in vivo* specifically in hypoxic but living cells (% pimonidazole/total plaque area). Liver inflammation was quantified as percentage CD45 + cells/total visible area (BD Cat# 553076, RRID:AB_394606).

Total and Hepatic Cholesterol and Triglycerides

Plasma was separated by centrifugation and stored at −80°C until further use. Standard enzymatic techniques were used to assess plasma cholesterol (cholesterol FS'10; Ref: 1 1300 99 10 021; Diagnostic Systems GmbH, Holzheim, Germany) and plasma triglycerides (TG) (FS5' Ecoline REF 157609990314; DiaSys—Diagnostic Systems GmbH, Holzheim, Germany) automated on the Cobas Fara centrifugal analyzer (Roche). For hepatic cholesterol and TG content, livers were homogenized in SET buffer (250 mM sucrose, 2 mM EDTA, 10 mM Tris, pH 6.8). Upon two freeze-thaw cycles and suction of the homogenate through an insulin syringe, TG and cholesterol were measured in the homogenates using the kits described above. Cholesterol and TG levels were corrected for protein content assessed in the same homogenate using a BCA kit (Thermo Fisher Scientific, Cat. No. 23227).

Flow Cytometry and Blood Variables

Circulating cells were isolated from whole blood and analyzed using flow cytometry (n = 10 per group). Blood was subjected to erythrocyte lysis. The following specific antibodies were used to detect leukocyte subsets: leukocytes (CD45 +, BioLegend Cat# 103129, RRID:AB_893343), T cells (CD3ε +, NK1-1-; Miltenyi, eBioscience Cat# 12-5941-82, RRID:AB_466050), T helper cells (CD4 +, BD Cat# 560246, RRID:AB_1645236), cytotoxic T cells (CD8a +, BD Cat# 560776, RRID:AB_1937317), effector T cells (CD44high CD62low; BD Cat# 560568, RRID:AB_1727481, eBioscience Cat# 25-0621-82, RRID:AB_469633, resp.), B cells (B220 +; BD Cat# 561226, RRID:AB_10563910), NK cells (NK1-1 +, BD Cat# 557391, RRID:AB_396674), eosinophils (SiglecF +; BD Cat# 562681, RRID:AB_2722581), granulocytes (CD11bhigh Ly6Ghigh; BD Cat# 552850, RRID:AB_394491, eBioscience Cat# 12-5931-82, RRID:AB_466045), and monocytes (CD11bhigh Ly6Glow Ly6Chigh/intermediate/low; Miltenyi Cat# 130-093-136, RRID:AB_871571). Data were acquired using a FACS Canto II and analyzed with FACS diva software (BD). For erythropoietic variable analysis, whole blood was diluted 1:10 in Hepes buffer, pH 7.45 (10 mM Hepes, 136 mM NaCl, 2.7 mM KCl, 2 mM MgCl2, 0.1% glucose, 0.1% BSA) and subsequently measured on the XP3000 Sysmex analyzer (Sysmex, Chuo-ku Kobe, Japan).

Cell Culture

Bone marrow was isolated, and cells were cultured for 7 days in RPMI-1640 (Gibco with Glutamax, 2 g/L glucose) supplemented with 10% FCS, 100 U/ml penicillin–streptomycin, and 15% L929-conditioned medium to generate bone marrow-derived macrophages (BMDM).

Real-Time Quantitative PCR

Cells were cultured accordingly, and RNA was isolated and produced as described (Sluimer et al., 2007). qPCR analyses were performed from 10 ng cDNA using SYBR green (Bio-Rad), and gene-specific primer sequences are available on request (Eurogentec, Liege, Belgium). One housekeeping gene (18S) was used to correct for different mRNA quantities between samples.

Insulin ELISA

Insulin was measured in plasma of LDLrko and PHD3dko mice based on the manufacturers' protocol (Mercodia, 10-1247-01).

Bone Marrow-Derived Macrophage Cholesterol Efflux

PHD3dko and LDLrko BMDMs were loaded overnight with acetylated LDL (50 μg/ml, Alfa Aesar J65029) and 1 uCi/mL H^3-cholesterol with or without 2 ug/mL ACAT inhibitor (Sandoz 58-035, Sigma). To increase ABCA1 expression, BMDMs were incubated with 0.3 mmol/L cAMP (Sigma-Aldrich, C3912) for 6 h and were then exposed to purified human HDL 50 ug/mL (Alfa Aesar, Haverhill, MA, United States) in media for 4 h. After these 4 h, the HDL in media was removed, macrophages were lysed, and scintillation counting was used to quantify the amount of ^{3}H-cholesterol in each compartment. We calculated the cholesterol efflux capacity as follows: [microcuries ^{3}H in media containing human HDL/ApoA1—microcuries ^{3}H in serum-free media/(total microcuries ^{3}H in media and cell lysate)] x 100%. This value represents the total cholesterol

efflux capacity. To be able to determine ABCA/G1-mediated cholesterol efflux capacity, we used the same protocol on BMDMs which are not treated with cAMP prior to HDL exposure. The difference between cAMP-induced (global) and non-cAMP-induced cholesterol efflux represents cAMP inducible or ABCA/G1-mediated cholesterol efflux.

Statistical Analysis

All data are presented as mean ± SEM. All variables were analyzed using independent sample tests and were tested for outliers and normal distribution using Grubs test and Shapiro–Wilk normality test, respectively. Variables with two groups were compared with student's *t*-test or Mann–Whitney rank-sum test. In case of more than two groups, variables were analyzed using one-way ANOVA followed by Bonferroni's multiple comparison test. A *p*-value of <0.05 was considered significant ($^{*}p < 0.05$, $^{**}p < 0.01$, $^{***}p < 0.001$).

RESULTS

Vascular Cell Types Expressed PHD3 and PHD3 Deficiency Enhanced Red Blood Cell Count

PHD3 was expressed by all major cell types involved in atherosclerosis (**Figure 1A**) and its deletion might hence change the course of atherogenesis. PHD3 is an important regulator of HIF1α and HIF2α activities, the latter being the main driver of EPO production (Warnecke et al., 2004; Scortegagna et al., 2005; Kapitsinou et al., 2010). As expected, plasma erythrocyte, hematocrit, and hemoglobin were enhanced in PHD3dko compared to controls at the moment of sacrifice (**Figures 1B–F**). White blood cell count and platelets were not significantly different. These results confirm PHD3ko in our mice at functional level.

Whole-Body PHD3dko Increased Murine Body Weight and Circulating Lipids

Before the start of the high-cholesterol diet ($t = 0$) and prior to sacrifice ($t = 10$), body weight was measured. Unexpectedly, PHD3dko mice showed enhanced body weight both before and after the start of the diet (**Figure 2A**). Enhanced body weight at the end of the diet might not only be attributed to enhanced mass prior to the diet, as PHD3dko mice also showed a trend toward more weight gain during the study ($p = 0.08$) (**Figure 2B**). Increased body mass was accompanied by a small increase in circulating total cholesterol (+7.08%) and significantly elevated TG levels (+17.9%) after 10 weeks of diet, while baseline measurements showed no difference (**Figures 2C,D**). Lipid homeostasis is strongly influenced by hepatic uptake, synthesis, and biliary excretion of cholesterol and to a minor extent also by reversed cholesterol transport by macrophages (Afonso et al., 2018; Westerterp et al., 2018). Reversed cholesterol transport probably does not explain circulating lipid levels, as *in vitro* BMDM cholesterol efflux capacity was unchanged (**Figure 2E**). Hence, the hepatic phenotype was studied. Importantly, PHD3 was successfully knocked out in the livers of PHD3dko mice, without compensatory upregulation of other PHD isoforms (**Figures 2F–H**). Liver lipid content, weight, and inflammation were not different between both groups (**Figures 2I–L**). mRNA expression of multiple lipid homeostasis-related genes in PHD3dko and control livers revealed significant changes in fatty acid synthase (FAS) and Cyp7a1 (**Figure 2N**). As alterations in these genes lead to an imbalance in lipid profiles,

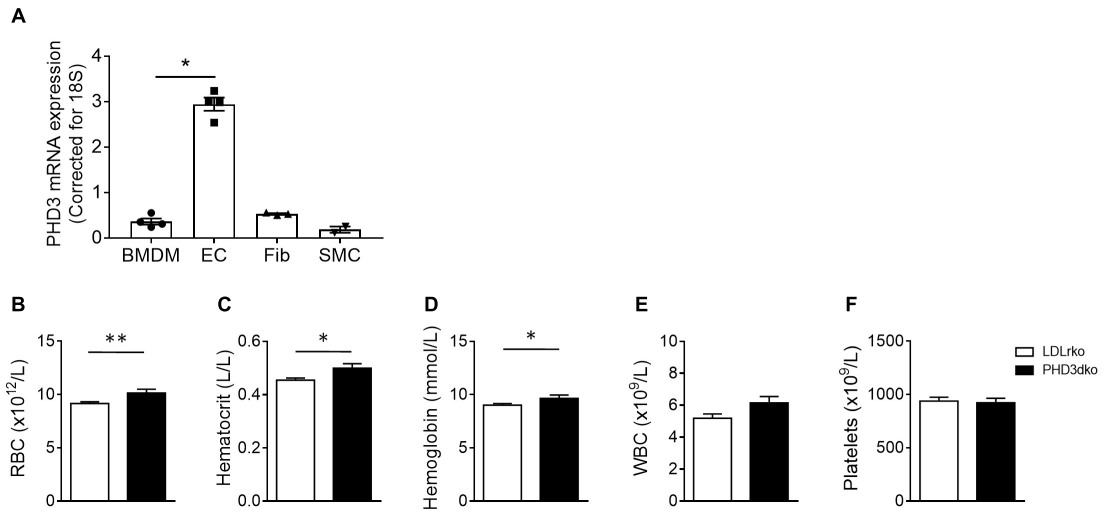

FIGURE 1 | All vascular cells expressed PHD3 and increased Hb and Ht confirmed functional PHD3ko. **(A)** PHD3 mRNA expression in vascular cells involved in atherosclerosis *in vitro* ($n = 4$ replicates per group). Expression is depicted as relative expression, corrected for 18S. **(B–F)** Hematopoietic variables of LDLrko ($n = 21$) and PHD3dko ($n = 14$) mice measured from blood drawn upon sacrifice. **(B)** Red blood cells (RBC), **(C)** Hematocrit, **(D)** Hemoglobin, **(E)** White blood cells (WBC), and **(F)** Platelets. BMDM, bone marrow derived macrophage; SMC, smooth muscle cell; Fib, 3T3 fibroblast; EC, mouse cardiac endothelial cell. All results show mean ± SEM. $^{*}p < 0.05$, $^{**}p < 0.01$.

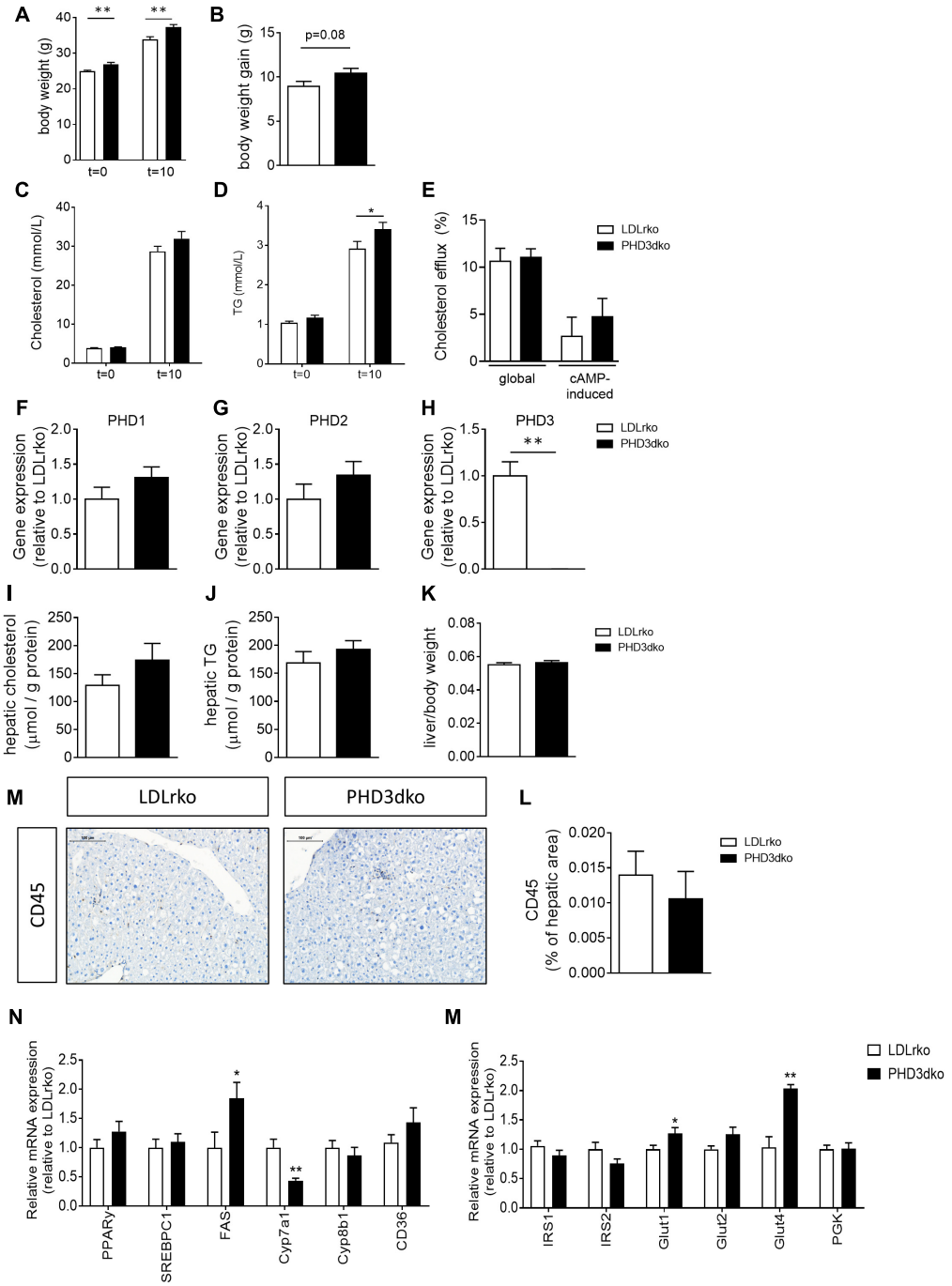

FIGURE 2 | PHD3dko mice showed increased bodyweight and circulating lipids. **(A)** Body weight of PHD3dko and LDLrko mice at start and end of the diet. **(B)** Body weight gain measured after 10 weeks of diet. **(C,D)** Plasma cholesterol and TG levels at start of diet and 10 weeks of diet. **(E)** Global and cAMP-induced cholesterol efflux capacity of LDLrko and PHD3dko BMDMs. **(F)** Gene expression of PHD1, **(G)** PHD2, and **(H)** PHD3 in whole liver tissue of LDLrko and PHD3dko mice (n = 5/group). Expression is relative to LDLrko expression levels of respective gene of interest. **(I,J)** Hepatic cholesterol (PHD3dko n = 20, LDLrko n = 14) and TG (PHD3dko n = 20, LDLrko n = 13) content of mouse livers corrected for total amount of hepatic protein. **(K)** Liver weight corrected for total body weight. **(L)** Representative microphotographs of CD45 stained sections of liver. Scalebar represents 100 µm. **(M)** Hepatic inflammation as measured by CD45 positive cells per visible hepatic area (PHD3dko n = 21, LDLrko n = 14). **(N)** Gene expression of lipid and glucose homeostasis related genes in livers of PHD3dko mice. Expression depicted relative to LDLrko expression levels of respective gene of interest (LDLrko N = 9, PHD3dko N = 7). PPARγ, peroxisome proliferator-activated receptor gamma; SREBPc1, sterol regulatory element-binding protein; FAS, fatty acid synthase; CYP7a1/8b1, cytochrome P450 7a1/8b1; CD36, cluster of differentiation 36; Glut1/2/4, glucose transporter 1, 2, or 4; IRS1/2, insulin receptor substrate 1/2. Sample size n = 14 for PHD3dko and n = 22 for LDLrko groups unless otherwise stated. All results show mean ± SEM. $^{*}p < 0.05$, $^{**}p < 0.01$.

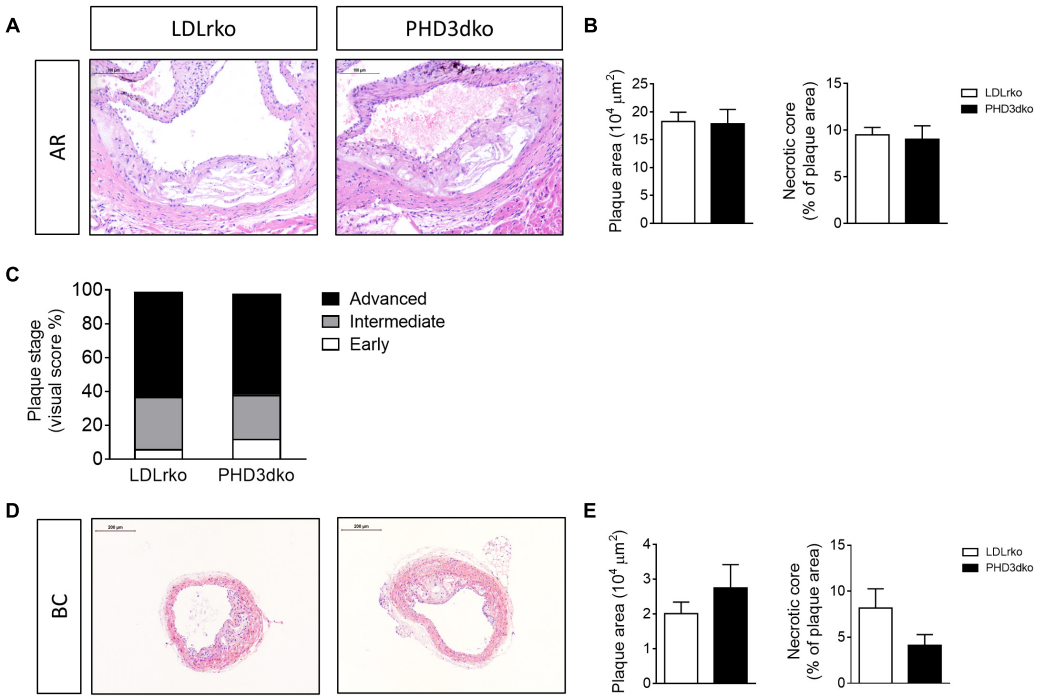

FIGURE 3 | PHD3dko did not change plaque size or necrotic content. **(A)** Representative microphotographs of H&E stained sections of aortic root (AR) (PHD3dko $n = 18$, LDLrko $n = 10$) and **(B)** quantification of plaque size and necrotic plaque content. **(C)** Plaque stage represented as early, intermediate, or advanced. **(D)** Representative microphotographs of H&E stained sections of brachiocephalic artery (BC) (PHD3dko $n = 21$, LDLrko $n = 13$), and **(E)** quantification of plaque size and necrotic plaque content. Scalebar represents 100 µm in AR and 200 µm in BC photographs.

this could be the explanation for our blood lipid phenotype. Next to lipid homeostasis, we also investigated genes related to glucose and insulin signaling in PHD3dko and control livers (**Figure 2M**). We observed an increase in insulin-independent and insulin-dependent glucose transporters, Glut1/Glut2 and Glut4, respectively. Despite the enhanced expression, we were unable to show an increase in insulin levels in the plasma (**Supplementary Figure 1**, data not shown).

PHD3dko Did Not Affect Plaque Size Despite Inducing Hyperlipidemia

Given the increased plasma lipid levels, albeit modest, we expected a small aggravation of atherogenesis in PHD3dko mice. However, the plaque size and the necrotic plaque content in the aortic root were unchanged compared to controls (**Figures 3A,B**). We reasoned that we could not find an effect on atherogenesis, as plaques had progressed to a fulminant stage, where differences might not be observed anymore. This was confirmed in the plaque stage classification, illustrating that the majority of plaques are advanced, irrespective of PHD3 deletion (**Figure 3C**). Hence, we also assessed plaque size at a second location, the brachiocephalic artery, where plaque development starts at a later stage (Nakashima et al., 1994). In line with findings in the aortic root, no differences were observed in plaque size or necrotic core content of the brachiocephalic artery, with less advanced lesions than the aortic root (**Figures 3D,E**). Accordingly, plaque hypoxia, macrophage, and collagen content in the aortic root were not significantly different between both groups (**Figures 4A–F**). Since whole-body PHD1ko on an LDLrko background led to changes in circulating immune cell subsets, we checked whether PHD3dko could lead to similar effects. However, in line with unchanged macrophage content in the plaque, PHD3dko did not lead to changes in circulating leukocyte and lymphocyte subsets between both groups (**Supplementary Figures 2A–L**).

DISCUSSION

In this study, we set out to investigate the effects of whole-body PHD3 deficiency on atherosclerotic plaque development. Despite enhanced lipid and hematocrit levels in whole-body PHD3dko mice, we did not observe an effect on atherogenesis.

Our group and others already showed the significance of PHD proteins in regulating total circulating cholesterol and/or triglyceride levels, which are important contributors to atherogenesis. In our prior study, whole-body PHD1 deficiency was seen to decrease plasma cholesterol and TG levels by ∼30%, subsequently decreasing plaque size and necrotic plaque content in these mice (Marsch et al., 2016). Comparable findings were apparent in hypomorphic PHD2ko mice, with reduced plaque size and advantageous lipid homeostasis (Rahtu-Korpela et al., 2014, 2016). As opposed to PHD1 and PHD2 deficiency, here we report an increase in plasma lipids in PHD3dko mice,

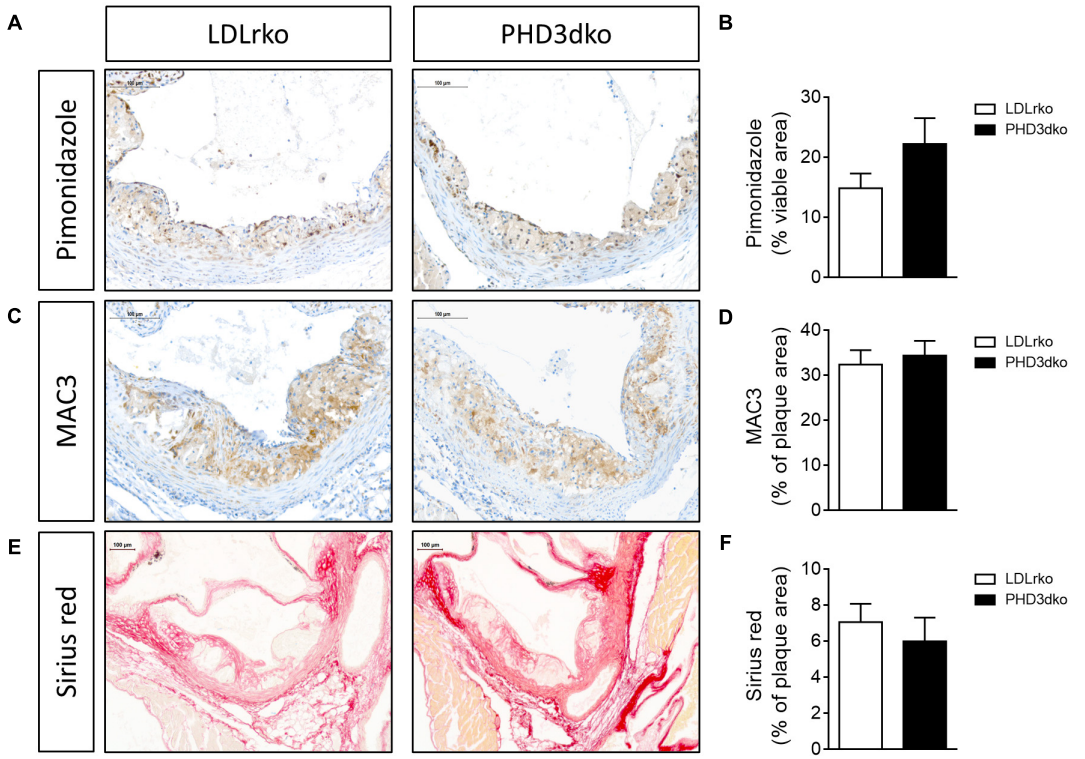

FIGURE 4 | PHD3dko did not affect plaque hypoxia, macrophage or collagen content. **(A)** Representative microphotographs of aortic root sections stained for hypoxia content (pimonidazole), **(B)** quantification (PHD3dko *n* = 18, LDLrko *n* = 10), **(C)** macrophage content (MAC3), and **(D)** quantification (PHD3dko *n* = 16, LDLrko *n* = 10), **(E)** collagen content (Picro sirius red), and **(F)** quantification (PHD3dko *n* = 18, LDLrko *n* = 11). Scalebar represents 100 μm.

albeit only by 10–18%. This may simply be insufficient to alter atherogenesis. The clinical relevance of this moderate increase in cholesterol levels upon high-cholesterol diet feeding is unclear. In a clinical trial testing Vadadustat, a moderately selective PHD3 inhibitor, no changes were found in circulating cholesterol or triglyceride levels (Martin et al., 2017). However, Vadadustat also inhibits PHD2, albeit to a lesser extent. Considering that several PHD2 selective inhibitors reduced lipid levels in humans, the latter study might suggest that potentially harmful effects of PHD3 inhibition may have been masked by the co-inhibition of PHD2. This highlights that PHD3 influences metabolism in an essentially different way than the PHD1 and PHD2 isoforms.

Why whole-body PHD3dko acts hyperlipidemic instead of hypolipidemic, like PHD1 and PHD2, remains elusive. PHD3 deficiency may have led to HIF2α-mediated changes in lipid metabolism, as HIF2α is known to participate in lipid homeostasis. In hepatic PHD3ko mice, glucose tolerance and insulin sensitivity were increased in a HIF2α, but not HIF1α, dependent way by upregulating insulin receptor substrate 2 expression (Taniguchi et al., 2013). Increased insulin sensitivity is, however, expected to promote an advantageous lipid profile, which was not observed in our whole-body PHD3dko model. Moreover, a lack of increase in the plasma insulin and in the hepatic expression of insulin responsive genes suggests that insulin sensitivity was unchanged in whole-body PHD3dko mice. As high-fat diet with 60%kcal from fat, rather than high-cholesterol diet (21%kcal fat), would be needed to induce overt glucose intolerance, the current high-cholesterol study is not suitable to yield conclusions on glucose and/or insulin intolerance. Alternatively, CYP7a1 may underlie the observed effect. Interestingly, liver-specific pVHL knockout mice displayed hypercholesterolemia, an effect that was HIF2α dependent, and presumably involved an inhibition of Cyp7a1-mediated conversion of cholesterol into bile acids (Ramakrishnan et al., 2014). Of note, lack of Von Hippel–Lindau protein (pVHL) can also partly mimic PHD deficiency, since pVHL-deficient mice have a sustained activation of HIF1α and HIF2α, due to disrupted breakdown of HIF proteins. As we observe decreased *Cyp7a1* expression, this may have been the underlying mechanism for enhanced plasma cholesterol in PHD3dko mice. In addition, an increase in fatty acid synthase (FAS) expression could be the cause of the increased triglyceride levels in PHD3dko mice. In cancer, it has been shown that hypoxia can induce FAS expression, possibly via sterol regulatory element-binding protein 1c (SREBP1c). However, the hepatic expression of SREBP1c did not differ between PHD3dko and controls, indicating that the activation of FAS might occur via a different route. One possible pathway could be the induction of Bcl2/adenovirus E1B 19 kDa protein-interacting protein 3 (BNIP3) in hypoxia, leading to the induction of FAS (Lee et al., 2017).

Interestingly, a recent study from Auvinen et al. investigated the relationship between Hb, body mass-index (BMI), and circulating metabolites in two Finnish cohorts: the Northern Finland Birth Cohort 1966 (Rantakallio, 1969; Jarvelin et al., 2004) and Young Finns Study (Raitakari et al., 2008). They found that increased Hb levels were positively associated with BMI (Auvinen et al., 2018). Moreover, Hb levels were positively associated with a unfavorable lipid profile and glucose intolerance, independent of BMI, sex, smoking, and physical activity. However, Mendelian randomization analyses could not establish a causal relationship between Hb and BMI; hence, additional research to address causality is warranted. Nevertheless, experiments in mice that underwent venesection and subsequently showed enhanced Hb levels after 2 weeks also displayed concurrent increase in body weight, circulating glucose and cholesterol levels (Auvinen et al., 2018). The observed increase in Hb with enhanced lipid levels and body weight phenocopied our findings in PHD3dko mice. The mechanistic interplay between Hb, plasma lipid levels and body weight are unfortunately still unchartered. Advancing insights about this relationship might be able to explain our findings in the near future.

The lack of effect on atherogenesis is surprising, considering altered lipid metabolism and the overt phenotypes of the other two isoforms, PHD1 and PHD2 (Rahtu-Korpela et al., 2014; Marsch et al., 2016). Functional effects of PHD3 deficiency in plaque cells may have counteracted the mild, systemic increase in lipids. In addition, cell type-specific effects may have counteracted each other, leaving the net plaque progression unaltered. Cell type-specific knockouts would be needed to convincingly prove this hypothesis. In contrast to our current findings, a study using a short hair-pin approach targeting PHD3 found a beneficial effect on atherogenesis (Liu et al., 2016). The apparent contrasting results may be explained by different methods, i.e., partial KD in adult mice is not similar to complete KO from embryonic stage. In addition, an ApoE knock-out model was used, which manifests in different atherogenic outcome measures compared to LDLrko mice in terms of inflammation, lipid profile, and plaque phenotype (Getz and Reardon, 2016; Oppi et al., 2019).

A third explanation for the lack of effect on atherogenesis may be the potential compensatory upregulation of other PHD isoforms in the arterial wall and other disease-relevant organs following whole-body PHD3 deletion. In our PHD3dko mice, hepatic *Phd1* and *Phd2* mRNA expression was not significantly different compared to controls. According to literature, compensatory upregulation of PHD1 or PHD2 in reaction to PHD3 deficiency and vice versa could occur in other cell types. The extent of these effects is, however, dependent on cell type and the targeted HIF isoform (Appelhoff et al., 2004; Mazzone et al., 2009; Minamishima et al., 2009; Walmsley et al., 2011; Taniguchi et al., 2013). For example, there seems to be an upregulation of PHD1 in MCF7 cells, a breast cancer cell line, treated with PHD3 siRNA (Appelhoff et al., 2004). In contrast, others claim there is no compensatory upregulation of PHD1 or PHD2 in neutrophils isolated from PHD3ko mice (Walmsley et al., 2011). It remains to be studied if this was the case in the arterial wall. Another surprise was that plaque hypoxic content was similar, despite a slight increase in hemoglobin and hematocrit in PHD3dko mice. PHD1 deficiency in atherosclerotic plaques and heart reduced oxygen consumption and tissue hypoxia (Aragones et al., 2008; Marsch et al., 2016). In summary, even though PHD3dko mice are mildly dyslipidemic and polycythemic, PHD3 deficiency does not worsen atherogenesis. These effects are in contrast to effect size and directionality of the other PHD isoforms, suggesting PHD isoform-dependent effects on cardiovascular disease metabolism.

DATA AVAILABILITY STATEMENT

The raw data supporting the conclusion of this article will be made available by the authors, without undue reservation.

ETHICS STATEMENT

The animal study was reviewed and approved by the Animal Welfare Body, Maastricht University Medical Centre.

AUTHOR CONTRIBUTIONS

TT and JS conceived and designed the study. JD, KK, TT, EM, and SH performed the experiments, and analyzed the data. PC generated the mouse model. JD, KK, and JS wrote the main manuscript text. JD, TT, and JS prepared the figures. EF, EB, and PC provided critical input to the manuscript. All authors reviewed and approved the final manuscript.

FUNDING

JS reports grants from the Dutch Organization for scientific research (016.116.017 VENI fellowship, and VIDI fellowship 0.16.186.364), Dekker Senior Postdoc Fellowship of the Dutch Heart Foundation 2016T060, and the Fondation Leducq (15CVD04) during the conduct of the study. PhD-student Fellowships were received from the Cardiovascular Research Institute Maastricht (to TT, and HS BAFTA Fellowship to JD). PC was supported by the long-term structural Methusalem funding by the Flemish Government and grants from Research Foundation Flanders (FWO-Vlaanderen), ERC Proof of Concept, and ERC Advanced Research Grant.

ACKNOWLEDGMENTS

We gratefully acknowledged the excellent technical assistance by Clairy Dinjens, Anique Janssen, and Erwin Wijnands.

SUPPLEMENTARY MATERIAL

The Supplementary Material for this article can be found online at: https://www.frontiersin.org/articles/10.3389/fcell.2021.664258/full#supplementary-material

REFERENCES

Aarup, A., Pedersen, T. X., Junker, N., Bartels, C. E. D., Madsen, M., et al. (2016). Hypoxia-Inducible Factor-1alpha Expression in Macrophages Promotes Development of Atherosclerosis. *Arterioscler. Thromb. Vasc. Biol.* 36, 1782–1790. doi: 10.1161/atvbaha.116.307830

Afonso, M. S., Machado, R. M., Lavrador, M. S., Quintao, E. C. R., Moore, K. J., and Lottenberg, A. M. (2018). Molecular Pathways Underlying Cholesterol Homeostasis. *Nutrients* 10:760. doi: 10.3390/nu10060760

Akhtar, S., Hartmann, P., Karshovska, E., Rinderknecht, F. A., Subramanian, P., Gremse, F., et al. (2015). Endothelial Hypoxia-Inducible Factor-1alpha Promotes Atherosclerosis and Monocyte Recruitment by Upregulating MicroRNA-19a. *Hypertension* 66, 1220–1226. doi: 10.1161/hypertensionaha.115.05886

Appelhoff, R. J., Tian, Y. M., Raval, R. R., Turley, H., Harris, A. L., Pugh, C. W., et al. (2004). Differential function of the prolyl hydroxylases PHD1, PHD2, and PHD3 in the regulation of hypoxia-inducible factor. *J. Biol. Chem.* 279, 38458–38465. doi: 10.1074/jbc.m406026200

Aprelikova, O., Chandramouli, G. V., Wood, M., Vasselli, J. R., Riss, J., Maranchie, J. K., et al. (2004). Regulation of HIF prolyl hydroxylases by hypoxia-inducible factors. *J. Cell Biochem.* 92, 491–501. doi: 10.1002/jcb.20067

Aragones, J., Schneider, M., Van Geyte, K., Fraisl, P., Dresselaers, T., Mazzone, M., et al. (2008). Deficiency or inhibition of oxygen sensor Phd1 induces hypoxia tolerance by reprogramming basal metabolism. *Nat. Genet.* 40, 170–180. doi: 10.1038/ng.2007.62

Auvinen, J., Tapio, J., Karhunen, V., Kettunen, J., Serpi, R., Dimova, E. Y., et al. (2018). Lower hemoglobin levels associate with lower body mass index and healthier metabolic profile. *bioRxiv* 472142 [Preprint]. doi: 10.1101/472142

Ben-Shoshan, J., Afek, A., Maysel-Auslender, S., Barzelay, A., Rubinstein, A., Keren, G., et al. (2009). HIF-1alpha overexpression and experimental murine atherosclerosis. *Arterioscler. Thromb. Vasc. Biol.* 29, 665–670. doi: 10.1161/atvbaha.108.183319

Berra, E., Benizri, E., Ginouves, A., Volmat, V., Roux, D., and Pouyssegur, J. H. I. F. (2003). prolyl-hydroxylase 2 is the key oxygen sensor setting low steady-state levels of HIF-1alpha in normoxia. *EMBO J.* 22, 4082–4090. doi: 10.1093/emboj/cdg392

Chen, N., Hao, C., Liu, B. C., Lin, H., Wang, C., Xing, C., et al. (2019a). Roxadustat Treatment for Anemia in Patients Undergoing Long-Term Dialysis. *N. Engl. J. Med.* 381, 1011–1022. doi: 10.1056/nejmoa1901713

Chen, N., Hao, C., Peng, X., Lin, H., Yin, A., Hao, L., et al. (2019b). Roxadustat for Anemia in Patients with Kidney Disease Not Receiving Dialysis. *N. Engl. J. Med.* 381, 1001–1010.

Christoph, M., Ibrahim, K., Hesse, K., Augstein, A., Schmeisser, A., Braun-Dullaeus, R. C., et al. (2014). Local inhibition of hypoxia-inducible factor reduces neointima formation after arterial injury in ApoE-/- mice. *Atherosclerosis* 233, 641–647. doi: 10.1016/j.atherosclerosis.2014.01.048

Getz, G. S., and Reardon, C. A. (2016). Do the Apoe-/- and Ldlr-/- Mice Yield the Same Insight on Atherogenesis?. *Arterioscler. Thromb. Vasc. Biol.* 36, 1734–1741. doi: 10.1161/atvbaha.116.306874

Ishibashi, S., Goldstein, J. L., Brown, M. S., Herz, J., and Burns, D. K. (1994). Massive xanthomatosis and atherosclerosis in cholesterol-fed low density lipoprotein receptor-negative mice. *J. Clin. Invest.* 93, 1885–1893. doi: 10.1172/jci117179

Jain, T., Nikolopoulou, E. A., Xu, Q., and Qu, A. (2018). Hypoxia inducible factor as a therapeutic target for atherosclerosis. *Pharmacol. Ther.* 183, 22–33. doi: 10.1016/j.pharmthera.2017.09.003

Jarvelin, M. R., Sovio, U., King, V., Lauren, L., Xu, B., McCarthy, M. I., et al. (2004). Early life factors and blood pressure at age 31 years in the 1966 northern Finland birth cohort. *Hypertension* 44, 838–846. doi: 10.1161/01.hyp.0000148304.33869.ee

Kaelin, W. G. Jr., and Ratcliffe, P. J. (2008). Oxygen sensing by metazoans: the central role of the HIF hydroxylase pathway. *Mol. Cell* 30, 393–402. doi: 10.1016/j.molcel.2008.04.009

Kapitsinou, P. P., Liu, Q., Unger, T. L., Rha, J., Davidoff, O., Keith, B., et al. (2010). Hepatic HIF-2 regulates erythropoietic responses to hypoxia in renal anemia. *Blood* 116, 3039–3048. doi: 10.1182/blood-2010-02-270322

Lee, H. J., Jung, Y. H., Choi, G. E., Ko, S. H., Lee, S. J., Lee, S. H., et al. (2017). BNIP3 induction by hypoxia stimulates FASN-dependent free fatty acid production enhancing therapeutic potential of umbilical cord blood-derived human mesenchymal stem cells. *Redox Biol.* 13, 426–443. doi: 10.1016/j.redox.2017.07.004

Liu, H., Xia, Y., Li, B., Pan, J., Lv, M., Wang, X., et al. (2016). Prolyl hydroxylase 3 overexpression accelerates the progression of atherosclerosis in ApoE-/- mice. *Biochem. Biophys. Res. Commun.* 473, 99–106. doi: 10.1016/j.bbrc.2016.03.058

Marsch, E., Demandt, J. A., Theelen, T. L., Tullemans, B. M., Wouters, K., Boon, M. R., et al. (2016). Deficiency of the oxygen sensor prolyl hydroxylase 1 attenuates hypercholesterolaemia, atherosclerosis, and hyperglycaemia. *Eur. Heart J.* 37, 2993–2997. doi: 10.1093/eurheartj/ehw156

Marsch, E., Theelen, T. L., Demandt, J. A., Jeurissen, M., van Gink, M., Verjans, R., et al. (2014). Reversal of hypoxia in murine atherosclerosis prevents necrotic core expansion by enhancing efferocytosis. *Arterioscler. Thromb. Vasc. Biol.* 34, 2545–2553. doi: 10.1161/atvbaha.114.304023

Martin, E. R., Smith, M. T., Maroni, B. J., Zuraw, Q. C., and deGoma, E. M. (2017). Clinical Trial of Vadadustat in Patients with Anemia Secondary to Stage 3 or 4 Chronic Kidney Disease. *Am. J. Nephrol.* 45, 380–388. doi: 10.1159/000464476

Mazzone, M., Dettori, D., de Oliveira, R. L., Loges, S., Schmidt, T., Jonckx, B., et al. (2009). Heterozygous deficiency of PHD2 restores tumor oxygenation and inhibits metastasis via endothelial normalization. *Cell* 136, 839–851. doi: 10.1016/j.cell.2009.01.020

Minamishima, Y. A., Moslehi, J., Padera, R. F., Bronson, R. T., Liao, R., and Kaelin, W. G. Jr. (2009). A feedback loop involving the Phd3 prolyl hydroxylase tunes the mammalian hypoxic response in vivo. *Mol. Cell Biol.* 29, 5729–5741. doi: 10.1128/mcb.00331-09

Mylonis, I., Simos, G., and Paraskeva, E. (2019). Hypoxia-Inducible Factors and the Regulation of Lipid Metabolism. *Cells* 8:214. doi: 10.3390/cells8030214

Nakashima, Y., Plump, A. S., Raines, E. W., Breslow, J. L., and Ross, R. (1994). ApoE-deficient mice develop lesions of all phases of atherosclerosis throughout the arterial tree. *Arterioscler. Thromb.* 14, 133–140. doi: 10.1161/01.atv.14.1.133

Oppi, S., Luscher, T. F., and Stein, S. (2019). Mouse Models for Atherosclerosis Research-Which Is My Line?. *Front. Cardiovasc. Med.* 6:46. doi: 10.3389/fcvm.2019.00046

Plump, A. S., Smith, J. D., Hayek, T., Aalto-Setala, K., Walsh, A., Verstuyft, J. G., et al. (1992). Severe hypercholesterolemia and atherosclerosis in apolipoprotein E-deficient mice created by homologous recombination in ES cells. *Cell* 71, 343–353. doi: 10.1016/0092-8674(92)90362-g

Rahtu-Korpela, L., Karsikas, S., Horkko, S., Blanco Sequeiros, R., Lammentausta, E., Makela, K. A., et al. (2014). HIF prolyl 4-hydroxylase-2 inhibition improves glucose and lipid metabolism and protects against obesity and metabolic dysfunction. *Diabetes* 63, 3324–3333. doi: 10.2337/db14-0472

Rahtu-Korpela, L., Maatta, J., Dimova, E. Y., Horkko, S., Gylling, H., Walkinshaw, G., et al. (2016). Hypoxia-Inducible Factor Prolyl 4-Hydroxylase-2 Inhibition Protects Against Development of Atherosclerosis. *Arterioscler. Thromb. Vasc. Biol.* 36, 608–617. doi: 10.1161/atvbaha.115.307136

Raitakari, O. T., Juonala, M., Ronnemaa, T., Keltikangas-Jarvinen, L., Rasanen, L., Pietikainen, M., et al. (2008). Cohort profile: the cardiovascular risk in Young Finns Study. *Int. J. Epidemiol.* 37, 1220–1226. doi: 10.1093/ije/dym225

Ramakrishnan, S. K., Taylor, M., Qu, A., Ahn, S. H., Suresh, M. V., Raghavendran, K., et al. (2014). Loss of von Hippel-Lindau protein (VHL) increases systemic cholesterol levels through targeting hypoxia-inducible factor 2alpha and regulation of bile acid homeostasis. *Mol. Cell Biol.* 34, 1208–1220. doi: 10.1128/mcb.01441-13

Rantakallio, P. (1969). Groups at risk in low birth weight infants and perinatal mortality. *Acta Paediatr. Scand.* 193:1+.

Samanta, D., and Semenza, G. L. (2018). Metabolic adaptation of cancer and immune cells mediated by hypoxia-inducible factors. *Biochim. Biophys. Acta Rev. Cancer.* 1870, 15–22. doi: 10.1016/j.bbcan.2018.07.002

Scortegagna, M., Ding, K., Zhang, Q., Oktay, Y., Bennett, M. J., Bennett, M., et al. (2005). HIF-2alpha regulates murine hematopoietic development in an erythropoietin-dependent manner. *Blood* 105, 3133–3140. doi: 10.1182/blood-2004-05-1695

Sluimer, J. C., Kisters, N., Cleutjens, K. B., Volger, O. L., Horrevoets, A. J., van den Akker, L. H., et al. (2007). Dead or alive: gene expression profiles of advanced atherosclerotic plaques from autopsy and surgery. *Physiol. Genomics* 30, 335–341. doi: 10.1152/physiolgenomics.00076.2007

Tabas, I., and Bornfeldt, K. E. (2016). Macrophage Phenotype and Function in Different Stages of Atherosclerosis. *Circ. Res.* 118, 653–667. doi: 10.1161/circresaha.115.306256

Takeda, K., Ho, V. C., Takeda, H., Duan, L. J., Nagy, A., and Fong, G. H. (2006). Placental but not heart defects are associated with elevated hypoxia-inducible factor alpha levels in mice lacking prolyl hydroxylase domain protein 2. *Mol. Cell. Biol.* 26, 8336–8346. doi: 10.1128/mcb.00425-06

Taniguchi, C. M., Finger, E. C., Krieg, A. J., Wu, C., Diep, A. N., LaGory, E. L., et al. (2013). Cross-talk between hypoxia and insulin signaling through Phd3 regulates hepatic glucose and lipid metabolism and ameliorates diabetes. *Nat. Med.* 19, 1325–1330. doi: 10.1038/nm.3294

Walmsley, S. R., Chilvers, E. R., Thompson, A. A., Vaughan, K., Marriott, H. M., Parker, L. C., et al. (2011). Prolyl hydroxylase 3 (PHD3) is essential for hypoxic regulation of neutrophilic inflammation in humans and mice. *J. Clin. Invest.* 121, 1053–1063. doi: 10.1172/jci43273

Warnecke, C., Zaborowska, Z., Kurreck, J., Erdmann, V. A., Frei, U., Wiesener, M., et al. (2004). Differentiating the functional role of hypoxia-inducible factor (HIF)-1alpha and HIF-2alpha (EPAS-1) by the use of RNA interference: erythropoietin is a HIF-2alpha target gene in Hep3B and Kelly cells. *FASEB J.* 18, 1462–1464. doi: 10.1096/fj.04-1640fje

Westerterp, M., Fotakis, P., Ouimet, M., Bochem, A. E., Zhang, H., Molusky, M. M., et al. (2018). Cholesterol Efflux Pathways Suppress Inflammasome Activation, NETosis, and Atherogenesis. *Circulation* 138, 898–912. doi: 10.1161/circulationaha.117.032636

Zhang, S. H., Reddick, R. L., Piedrahita, J. A., and Maeda, N. (1992). Spontaneous hypercholesterolemia and arterial lesions in mice lacking apolipoprotein E. *Science* 258, 468–471. doi: 10.1126/science.1411543

Conflict of Interest: The authors declare that the research was conducted in the absence of any commercial or financial relationships that could be construed as a potential conflict of interest.

frontiers in Cell and Developmental Biology

REVIEW
published: 15 July 2021
doi: 10.3389/fcell.2021.691774

Hypoxia-Induced Mitogenic Factor: A Multifunctional Protein Involved in Health and Disease

Moyang Lv[1] *and Wenjuan Liu*[2]*

[1] Department of Gastroenterology, Xinqiao Hospital, Third Military Medical University, Chongqing, China, [2] Department of Pathophysiology, Health Science Center, Shenzhen University, Shenzhen, China

Hypoxia-induced mitogenic factor (HIMF), also known as resistin-like molecule α (RELMα) or found in inflammatory zone 1 (FIZZ1) is a member of the RELM protein family expressed in mice. It is involved in a plethora of physiological processes, including mitogenesis, angiogenesis, inflammation, and vasoconstriction. HIMF expression can be stimulated under pathological conditions and this plays a critical role in pulmonary, cardiovascular and metabolic disorders. The present review summarizes the molecular characteristics, and the physiological and pathological roles of HIMF in normal and diseased conditions. The potential clinical significance of these findings for human is also discussed.

Keywords: hypoxia-induced mitogenic factor, mitogenesis, angiogenesis, proinflammation, vasoconstriction

OPEN ACCESS

Edited by:
Xiaoqiang Tang,
Sichuan University, China

Reviewed by:
Lanlan Zhang,
Sichuan University, China
Claudia Penna,
University of Turin, Italy
Meera G. Nair,
University of California, Riverside, United States

***Correspondence:**
Wenjuan Liu
lwj0320@szu.edu.cn

Specialty section:
This article was submitted to Cellular Biochemistry, a section of the journal Frontiers in Cell and Developmental Biology

Received: *07 April 2021*
Accepted: *23 June 2021*
Published: *15 July 2021*

Citation:
Lv M and Liu W (2021) Hypoxia-Induced Mitogenic Factor: A Multifunctional Protein Involved in Health and Disease. Front. Cell Dev. Biol. 9:691774. doi: 10.3389/fcell.2021.691774

INTRODUCTION

Hypoxia-induced mitogenic factor (HIMF), also known as found in inflammatory zone 1 (FIZZ1) or resistin-like molecule α (RELMα), is a pro-inflammatory cytokine in mice. HIMF expression is markedly increased in the hyperplastic bronchial epithelium of mice with allergic pulmonary inflammation (Holcomb et al., 2000). Three years later, Teng et al. (2003) also reported a novel role for this molecule in the pathogenesis of hypoxia-induced pulmonary hypertension (PH). Hypoxia was found to induce HIMF expression, and the protein was upregulated in a murine chronic hypoxia model of pulmonary hypertension. The authors renamed this gene HIMF, as the recombinant protein stimulated the proliferation of rat pulmonary microvascular smooth muscle cells (PSMCs). Following investigations using a chronic hypoxia-induced PH mouse model uncovered a pluoripotent array of pathological roles played by HIMF, including in angiogenesis, vasoconstriction, inflammation and fibrosis. Together, these properties endow HIMF with a critical function in pulmonary vascular remodeling and, thus, in the development of PH after hypoxia. Notably, HIMF has also been linked to both cell survival and cell death, depending on the dose and cellular context. For example, despite the harmful effects of increased HIMF expression in lung disease, particularly in PH, basal expression of HIMF is required for normal lung development.

In addition to its involvement in pulmonary disease, a number of studies have demonstrated that HIMF also participates in the development of cardiovascular diseases and metabolic disorders in mice. Furthermore, recent studies by our group have uncovered a novel role for HIMF in the pathogenesis of pressure overload-induced cardiac hypertrophy and fibrosis (Kumar et al., 2018, 2019). These findings are of particular note because the two human homologs of HIMF, RELMβ, and resistin (hRETN), are also associated with cardiovascular diseases. For example, there is a positive correlation between resistin plasma levels and the incidence of cardiovascular

events in patients with cardiovascular diseases (Zhang et al., 2011). Furthermore, studies in mice have revealed a causal relationship between the RELMβ expression and the pathogenesis of atherosclerosis (Kushiyama et al., 2013). Therefore, HIMF (and, by extension, its human homologs) may represent potential, clinically significant biomarkers or therapeutic targets for the diagnosis, prognosis and treatment of cardiovascular diseases. The pro-inflammatory properties of HIMF are of particular interest, as these contribute to metabolic complications which are closely associated with chronic low-grade inflammation. Similar to its function in lung tissue, HIMF regulates glucose and energetic metabolism in dose and cell-dependent manners. Increased HIMF expression results in metabolic disturbance, but basal levels of HIMF expression by a certain group of immune cells ($CD301b^+$ mononuclear phagocytes) is required for the maintenance of metabolic homeostasis (Kumamoto et al., 2016).

This review summarizes the molecular characteristics of HIMF, including its molecular structure, tissue-specific distribution, transcription mechanisms and receptors. We primarily focus on the pluripotent physiological and pathological functions of HIMF, particularly in the pathogenesis of pulmonary, cardiovascular and metabolic disorders, alongside, the respective downstream signaling pathways. The potential clinical significance of HIMF is also discussed.

MOLECULAR CHARACTERIZATIONS

Structure

HIMF (RELMα, also known as FIZZ1) is a 9.4 kDa cysteine-rich secretory cytokine that belongs to the FIZZ/RELM family, which also includes RELMβ (FIZZ2) and RELMγ. RELMα, and FIZZ1, as well as RELMβ and FIZZ2 were discovered independently by separate, unrelated labs as different functional proteins, but finally proved to be the same. The RELM proteins share a similar cysteine composition and other signature features with resistin (known as FIZZ3 in mice). The RELM family proteins typically range from 105 to 114 amino acids in length and are composed of three domains: an N-terminal sequence containing a secretory signal peptide, a variable middle portion, and a unique, highly conserved C-terminal signature sequence that contains 10 cysteine residues (Banerjee and Lazar, 2001). Members of the RELM family show strong interspecies and intraspecies homology, especially at this cysteine-rich C-terminus.

Tissue-Specific Distribution

The expression of HIMF, as with other members of the RELM family, is uneven across different types of tissue. For example, expression of HIMF (FIZZ1) is 10-fold higher in murine lung tissue compared with heart tissue or skeletal muscle (Holcomb et al., 2000). Alongside the lung and heart, HIMF is also expressed in the tongue, but its expression is highest in adipose tissue (Steppan et al., 2001). In addition, HIMF has also been found to mediate myeloid cell chemotaxis (Su et al., 2007). Meanwhile, RELMβ (FIZZ2) is exclusively expressed in the gastrointestinal tract, specifically in actively replicating crypt endothelium of the colon and small bowel (Hogan et al., 2006), similar to the findings by Holcomb. RELMγ has been found to be expressed in hematopoietic tissues and lung in rodents (Gerstmayer et al., 2003), and FIZZ3 is expressed in white adipocytes throughout the body (Holcomb et al., 2000).

In addition to these initial findings, RELM proteins may also be expressed in other tissues under pathological conditions or during development. For example, HIMF and other RELM proteins are expressed in the murine liver during helminth-induced Th2-type immune responses (Pesce et al., 2009). HIMF is also expressed by macrophages, and increased HIMF levels can be used as a marker for alternatively activated (M2) macrophages in mice. RELMβb and resistin are homologs of HIMF, and the expression patterns of RELMβ in the human lung are similar to those of HIMF in mice. Human resistin is also expressed in myeloid cells, especially macrophages, with a similar expression pattern to murine HIMF. Advances in protein quantification techniques are also revealing novel expression sites for RELM proteins, with hResistin expression recently being characterized across normal human tissues using a newly developed monoclonal antibody (Lin et al., 2020). hResistin was found to be principally localized in the cytoplasmic granules of macrophages, which are present in the interstitial space of the majority of human tissues. Therefore, the functions of HIMF in rodents may indicate potential roles of human RELMβ and resistin depending on the induction site and the cellular source of the protein.

Transcription Mechanisms

The mechanisms involved in the induction of HIMF transcription remain to be fully characterized, and may vary between physiological and pathological conditions. However, its expression is altered during development. For example, HIMF expression is upregulated in embryonic mouse lung tissue, and is involved in normal lung development. The transcription factor Ets-1, which is also expressed in the developing mouse lung, has been found to contribute to developmental expression of HIMF (Li et al., 2007). In this study, Ets-1 was found to increase HIMF promoter luciferase activity in a heterogenous expression system, and chromatin immunoprecipitation (ChIP) assays revealed that Ets-1 bound to the HIMF promoter region in embryonic day (E) 20 lung tissues. Ets-1 is also known to participate in the transcriptional activation of vascular endothelial growth factor receptor-2 (Flk-1), in coordination with hypoxia-inducible factor 2α (HIF-2α), during vascular development and angiogenesis (Elvert et al., 2003). HIF-2α expression is co-localized with HIMF in the developing airway epithelial cells and alveolar type II cells, suggesting that it may also induce HIMF expression during lung development (Wagner et al., 2004).

Furthermore, signal transducers and activators of transcription 6 (STAT6) and C/EBP have been suggested to mediate HIMF induction during the Th2 inflammatory response (Yamaji-Kegan et al., 2010). Cellular experiments demonstrated that HIMF promoter reporter gene constructs respond to Th2-cytokines, IL-4, and IL-13 stimulation. In addition, the promoter region of the HIMF gene was found to contain functional binding sites for signal transducers and activators of transcription 6 (STAT6) and C/EBP. Point mutations in the STAT6 or the C/EBP

sites led to the loss of cytokine responsiveness, indicating that Th2-related HIMF induction is orchestrated by the coordinated action of STAT6 and C/EBP. The involvement of STAT6 in the mediation of HIMF production has also been confirmed in a murine model of acute pulmonary inflammation, with HIMF found to be upregulated 6 h after antigen challenge. Notably, this effect was abolished by STAT6 gene ablation.

The potential role of hypoxia inducible factor-1α (HIF-1α) in HIMF induction, particularly in hypoxia-induced PH, has also generated a great deal of attention. HIF-1α is also activated during hypoxia, and serves a critical function in both hypoxic inflammation and Th2 immune activation in the lung. Previous experiments in HIF-1α heterozygous null (HIF-1α$^{+/-}$) mice also found that HIMF induced HIF-1α expression, and HIMF-induced PH was significantly diminished in HIF-1α$^{+/-}$ mice (Johns et al., 2016). In addition, recent work by our group revealed that HIMF increases HIF-1α expression and cardiomyocyte hypertrophy, but HIF-1α activation has no impact on HIMF expression (Kumar et al., 2018). Taken together, these results suggest that HIF-1α is a critical downstream mediator of HIMF-induced PH and cardiac hypertrophy, rather than an upstream transcription factor controlling HIMF expression.

Receptors

Although a number of signaling pathways are activated by HIMF, the functional receptors for HIMF, resistin and other RELM proteins, remain unclear. Previous research has determined that HIMF induces the release of intracellular Ca^{2+} in pulmonary artery smooth muscle cells through the PLC-IP3 pathway (Fan et al., 2009). This suggests that HIMF may act as a ligand of G protein coupled receptors (GPCRs), the activation of which stimulates PLC-IP3 signaling. This previous study further revealed that the HIMF-induced Ca^{2+} response was attenuated by the tyrosine kinase inhibitor genistein. In addition, the pattern of Ca^{2+} release was altered by $G\alpha_{q/11}$ knockdown, from sustained oscillatory Ca^{2+} transients with prolonged plateaus to a series of short Ca^{2+} transients. However, this effect was not elicited by $G\alpha_i$ or $G\alpha_s$ knockdown. These results led the authors to conclude that $G\alpha_{q/11}$ protein-coupled receptors and a receptor tyrosine kinase are critical to HIMF-induced Ca^{2+} signaling. A more recent study from the same group demonstrated that Bruton's tyrosine kinase (BTK) is a binding partner for HIMF (Lin et al., 2019a), providing further evidence to suggest that HIMF functions via intracellular receptor tyrosine phosphorylation. However, the exact GPCRs involved remain unknown.

A recent study has reported that extracellular calcium-sensing receptor (CaSR) acts as a receptor for intracellular HIMF (Zeng et al., 2017). Using a yeast 2-hybrid assay, the authors found that HIMF bound to the intracellular domain of CaSR, increasing the activity of the receptor. In turn, this mediated the hypoxia-induced proliferation of PSMCs, pulmonary vascular remodeling, and consequent pulmonary hypertension. However, CaSR appears to be a non-classical receptor for HIMF, mediating intracellular HIMF signaling only. Although the classical HIMF receptor remains to be identified, it is interesting that a synthesized, membrane-permeable peptide targeting the intracellular binding domain of CaSR for HIMF attenuated the development of hypoxia-induced PH.

PLUORIPOTENT EFFECTS AND ASSOCIATED SIGNALING PATHWAYS

Mitogenesis

One of the most prominent functions of HIMF is its involvement in mitogenesis. Indeed, it was initially termed RELMα, but was renamed after it was found to induce PSMC proliferation (Teng et al., 2003). Subsequent studies demonstrated that HIMF can also induce the proliferation of endothelial and fibroblast cells. The activation of the phosphatidylinositol 3-kinase (PI3K)/Akt pathway is critical during PSMC proliferation, with the inhibition of PI3K significantly suppressing Akt phosphorylation and PSMC proliferation. The PI3K/Akt pathway also contributes to the proliferation of HIMF-induced endothelial cells (ECs), by inducing the production of vascular endothelial growth factor (VEGF) through NF–κB (Tong et al., 2006a; Yamaji-Kegan et al., 2006). In addition, the mitogen-activated protein kinase (MAPK) pathway was also found to be involved in HIMF-induced EC proliferation, with the ERK inhibitor U0126 significantly inhibiting EC proliferation. A recent study by our group demonstrated that HIMF also stimulates cardiac fibroblast (CF) proliferation in a dose-dependent manner (Kumar et al., 2019). Here, IL-6 plays a key role, activating the MAPK and calcium/calmodulin-dependent protein kinase II (CaMKII)-STAT3 pathways (**Figure 1**).

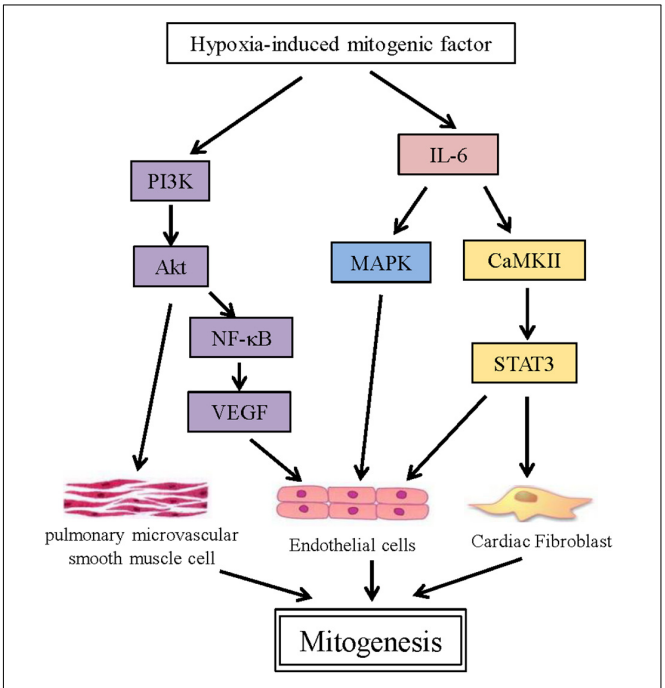

FIGURE 1 | HIMF links multiple mitogenesis-associated pathways. Schematic representing the direct target genes involved in various signaling pathways associated with mitogensis that are induced by HIMF.

Angiogenesis

Angiogenesis involves a cascade of intricately regulated processes, including the dissolvement of the basement membrane and extracellular matrix, EC migration, and subsequent EC proliferation and vascular sprouting (Li et al., 2013). The stimulation of angiogenic growth factors, including VEGFs and fibroblast growth factors (FGFs), plays an important role in this process (Li et al., 2013). HIMF is also strongly associated with angiogenesis. Previous studies have shown that HIMF stimulates VEGF production in vascular ECs, and promotes the proliferation and migration of ECs and vascular sprouting (Tong et al., 2006c; Yamaji-Kegan et al., 2006). Furthermore, suppressing VEGF receptor-2 (VEGFR2) significantly inhibited HIMF-induced angiogenesis. HIMF has also been found to increase the production of Flk-1, which contributes to pulmonary angiogenesis (Tong et al., 2006b). Activation of the PI-3K/Akt-NF-κB signaling pathway has been suggested to mediate the induction of VEGF and Flk-1 expression (Tong et al., 2006a,b). Notably, in addition to targeting endothelial cells directly, HIMF has also been shown to stimulate angiogenesis through the activation of myoblasts (Su et al., 2017). HIMF increases IL-18 production through the PDK1/PI3K/Akt signaling pathway in myoblasts, which in turn promotes tube formation of the endothelial progenitor cells.

Angiogenesis is closely linked to inflammation. Pro-inflammatory cells, particularly macrophages, not only release large quantities of angiogenic factors under pathological conditions, but also indirectly promote angiogenesis through releasing inflammatory factors that recruit endothelial progenitor cells, which also promote vascular formation. HIMF has been found to recruit CD68-positive cells in mouse lungs and to stimulate the production of monocyte chemotactic protein-1 (MCP-1) and stromal cell-derived factor-1 (SDF-1), which are both angiogenesis-related inflammatory factors (Yamaji-Kegan et al., 2006). These effects were suppressed by treatment with a VEGFR2 inhibitor, providing further evidence to support a causal link between HIMF activity and VEGF-associated angiogenesis.

Inflammation

HIMF is a well-known marker of activated M2 anti-inflammatory macrophage. One of the most abundant neuropeptides in lung, calcitonin gene-related peptide (CGRP), has been found to attenuate lipopolysaccharide (LPS)-induced acute lung injury in rats. CGRP significantly reduced LPS-induced NLRP3 activation and increased the expression of HIMF, which was induced by IL-4 in macrophages (Duan et al., 2017). Similar results were reported in the liver of human cholestatic patients and bile duct-ligated mice. The activation of the NLRP3 inflammasome and increased numbers of M2 anti-inflammatory macrophages, as evidenced by increased HIMF expression, aggravated hepatic injury (Cai et al., 2020). Meanwhile, the inhibition of inflammation and induction of M2 macrophage polarization via the miR-223/TRAF6/NF-κB axis alleviated viral myocarditis (Xue et al., 2020).

Previous studies have shown that HIMF induces the production and release of an array of pro-inflammatory factors, including IL-4 (Yamaji-Kegan et al., 2014), IL-6 (Johns et al., 2016), IL-18 (Su et al., 2017), TNF-α (Song et al., 2012), HMGB1 (Lin et al., 2019a,b), vascular adhesion molecule-1 VCAM-1 (Tong et al., 2006d), MCP-1 and SDF-1 (Yamaji-Kegan et al., 2010). A single injection of recombinant HIMF induced IL-4 production and lung injury in mice, while ablation of IL-4 abolished the recruitment of macrophages to the lung and the pulmonary vascular inflammation caused by HIMF (Yamaji-Kegan et al., 2014). In hypoxia-induced PH, HIMF induced the recruitment of macrophages and α-SMA-production cells, and increased IL-6 production via HIF-1α activation (Johns et al., 2016). HIMF also upregulates VCAM-1 expression and mononuclear cell sequestration to the lung parenchyma in bacterial lipopolysaccharide (LPS)-induced acute lung injury, increasing its severity (Tong et al., 2006d). Furthermore, HIMF mediates EC-smooth muscle cell crosstalk, affecting HMGB1-RAGE signaling (Lin et al., 2019a), and induces macrophage-specific HMGB1/RAGE expression. This, in turn, increases the apoptosis-resistant proliferation of human pulmonary artery smooth muscle cells during pulmonary vascular remodeling (Lin et al., 2019b). The induction of the pro-inflammatory factors MCP-1 and SDF-1 by HIMF also results in vascular remodeling in PH. Meanwhile, in the heart, HIMF also stimulates IL-6 production in cardiomyocytes and cardiac fibroblasts via the activation of the MAPK and CaMKII–STAT3 pathways (Kumar et al., 2019).

Interestingly, HIMF appears to regulate T helper type 2 (Th2)-induced inflammation in a different fashion. HIMF expression is induced by the Th2 cytokines IL-4 and IL-13, and serves as a biomarker for the transformation of alternatively activated macrophages (AAMacs). The activation of AAMacs is the hallmark of several inflammatory conditions associated with parasite infection, allergy, diabetes and cancer (Nair et al., 2009). In a *Schistosoma mansoni (Sm)* eggs-induced mouse model of Th2 cytokine-dependent lung inflammation, HIMF suppressed Th2 cytokine-mediated pulmonary inflammation, and ablation of HIMF in mice exacerbated lung inflammation (Nair et al., 2009; Pesce et al., 2009). The effect of HIMF on the suppression of helminth-induced Th2-type immunity also occurs in other organs, such as the liver (Pesce et al., 2009). The underlying mechanism is related to the ability of HIMF inhibiting macrophage and $CD4^+$ cells-mediated Th2 cytokine production in a Bruton's tyrosine kinase-dependent manner (Nair et al., 2009).

Vasoconstriction

In addition to the aforementioned processes, HIMF is also involved in vasoconstriction of the pulmonary artery. For example, intravenous injection of HIMF is known to increase pulmonary arterial pressure and pulmonary vascular resistance in mice. Surprisingly, the constrictive effect of HIMF is even more potent than either endothelin-1 or angiotensin II (Teng et al., 2003). This effect has been attributed to regulation of the Ca^{2+} signal by HIMF, with recombinant murine HIMF increasing the intracellular Ca^{2+} concentration in a sustained, oscillatory manner in human pulmonary artery smooth muscle cells (SMCs). Notably, the Ca^{2+} increase is related to IP_3-mediated intracellular Ca^{2+} release, but not extracellular Ca^{2+}

influx. Inhibition of PLC-IP_3 and tyrosine kinase abolished HIMF-induced Ca^{2+} signaling, while knockdown of $G\alpha_{q/11}$ expression and ryanodine pre-treatment altered the pattern of Ca^{2+} release (Fan et al., 2009). Taken together, this suggests that HIMF stimulates intracellular Ca^{2+} release in human pulmonary artery SMCs through the PLC signaling pathway, in an IP3- and tyrosine phosphorylation-dependent manner. Furthermore, $G\alpha_{q/11}$ protein-coupled receptors and ryanodine receptors are also involved in Ca^{2+} regulation.

However, whether HIMF exerts similar effects on systemic artery SMCs, and the potential roles of HIMF in regulation of blood pressure, remain to be fully elucidated and warrant further study.

HIMF AND DISEASES

Pulmonary Diseases

Pulmonary Hypertension (PH)

The most well-studied disease associated with HIMF is hypoxia-induced PH; a disease characterized by the progressive elevation of hypoxia-induced pulmonary vascular resistance, the development of right ventricular failure, and ultimately death. The elevation of vascular resistance is primarily attributed to pulmonary artery constriction and vascular remodeling in response to hypoxia. Vascular remodeling involves complicated pathological processes that include angiogenesis, muscularization, the thickening of small pulmonary vessels, inflammation, and fibrosis. HIMF is upregulated in the pulmonary vasculature, bronchial epithelial cells, and type II pneumocytes in hypoxia-induced PH (Teng et al., 2003). HIMF is also known to increase pulmonary vasoconstriction, and has a critical role in each pathological process of vascular remodeling. It enhances the angiogenic capacity of pulmonary myoblasts and the tubule formation of progenitor endothelial cells (Su et al., 2017). Furthermore, HIMF also induces the proliferation of pulmonary SMCs and fibroblast (FCs), as well as the differentiation of FCs, leading to muscularization, thickening of small pulmonary vessels, and lung fibrosis (Teng et al., 2003). In addition, HIMF induces lung inflammation, which promotes vascular remodeling and lung fibrosis (Liu et al., 2009; Angelini et al., 2013; **Figure 2**).

The human homolog of HIMF, RELMβ, has been shown to be upregulated in the lung tissue of patients with scleroderma-associated pulmonary hypertension (Angelini et al., 2009). RELMβ is primarily localized in the endothelium and vascular smooth muscle of remodeled vessels and in plexiform lesions, macrophages, T cells, and myofibroblast-like cells; similar to HIMF in hypoxia-induced PH in mice. Thus, clarifying the role of HIMF in the development of PH in mice may aid our understanding of the function of human RELMβ in the development of scleroderma-associated PH.

Allergic Asthma

HIMF was initially described as present in the bronchoalveolar lavage fluid in a murine allergic pulmonary inflammation model (Holcomb et al., 2000). HIMF production in antigen-challenged lungs has been suggested to be driven by either IL-4 or IL-13, involving transcription factors STAT6 and C/EBP (Stutz et al., 2003; Yamaji-Kegan et al., 2010). Since the activation of STAT6 signaling has a critical role in allergic pulmonary inflammation, the STAT6-dependent induction of HIMF in the alveolar epithelium during pulmonary inflammation and fibrosis suggests that HIMF is involved in asthma pathogenesis. Supporting this, HIMF expression has since been found to be increased in OVA-induced inflammation (Fan et al., 2015). Furthermore, another previous study demonstrated that HIMF inhibited the nerve growth factor (NGF)-mediated survival of rat embryonic dorsal root ganglion (DRG) neurons, in addition to suppressing NGF-induced CGRP gene expression in adult rat DRG neurons (Holcomb et al., 2000). HIMF may modulate the function of neurons innervating the bronchial tree, and thus alter the local tissue response to allergic pulmonary inflammation. Further studies to clarify the role of HIMF in the inflammatory response in allergic asthma are clearly warranted.

Cardiovascular Diseases

Cardiac Hypertrophy and Heart Failure

A number of recent studies have demonstrated that HIMF has a critical role in the development of pressure overload-induced cardiac hypertrophy. For example, HIMF is upregulated in both a phenylephrine (PE)-stimulated cell model of cardiomyocyte hypertrophy, and a transverse aortic constriction (TAC)-induced mouse model of cardiac hypertrophy (Kumar et al., 2018). In this study, cardiomyocyte hypertrophy was induced by HIMF overexpression in cardiomyocytes, while knockdown of HIMF expression inhibited this process. In the TAC-induced mouse model, ablation of the HIMF gene attenuated TAC-induced cardiac hypertrophy and fibrosis, and improved cardiac function. The activation of HIF-1α and Ca^{2+}-activated calcineurin (CaN)–nuclear factor of activated T cell (NFAT), as well as the MAPK pathway, contributed to the hypertrophic growth of cardiomyocytes. Interestingly, HIMF is not expressed by cardiac fibroblasts. However, the extracellular application of recombinant HIMF protein and conditioned medium from cultured cardiomyocytes overexpressing HIMF still induced fibroblast proliferation, differentiation, and migration. This indicates that HIMF produced in cardiomyocytes during the development of cardiac hypertrophy activates adjacent cardiac fibroblasts via paracrine signaling, inducing fibrosis (Kumar et al., 2019). Another previous study also demonstrated that serum levels of resistin, the human homolog of HIMF, are positively correlated with the severity of heart failure and the risk of adverse cardiac events in patients with heart failure (Zhang et al., 2011). While HIMF is not expressed in humans, the effects of HIMF on the development of cardiac hypertrophy and deterioration of cardiac function in mice may serve as a model for the function of resistin in the human heart under pathological conditions.

Myocardial Infarction

Recently, HIMF has been found to be involved in inhibiting apoptosis and increasing proliferation in cardiac fibroblasts, which result in cardiac fibrosis in a myocardial infarction (MI) mouse model. Furthermore, HIMF knockout conferred

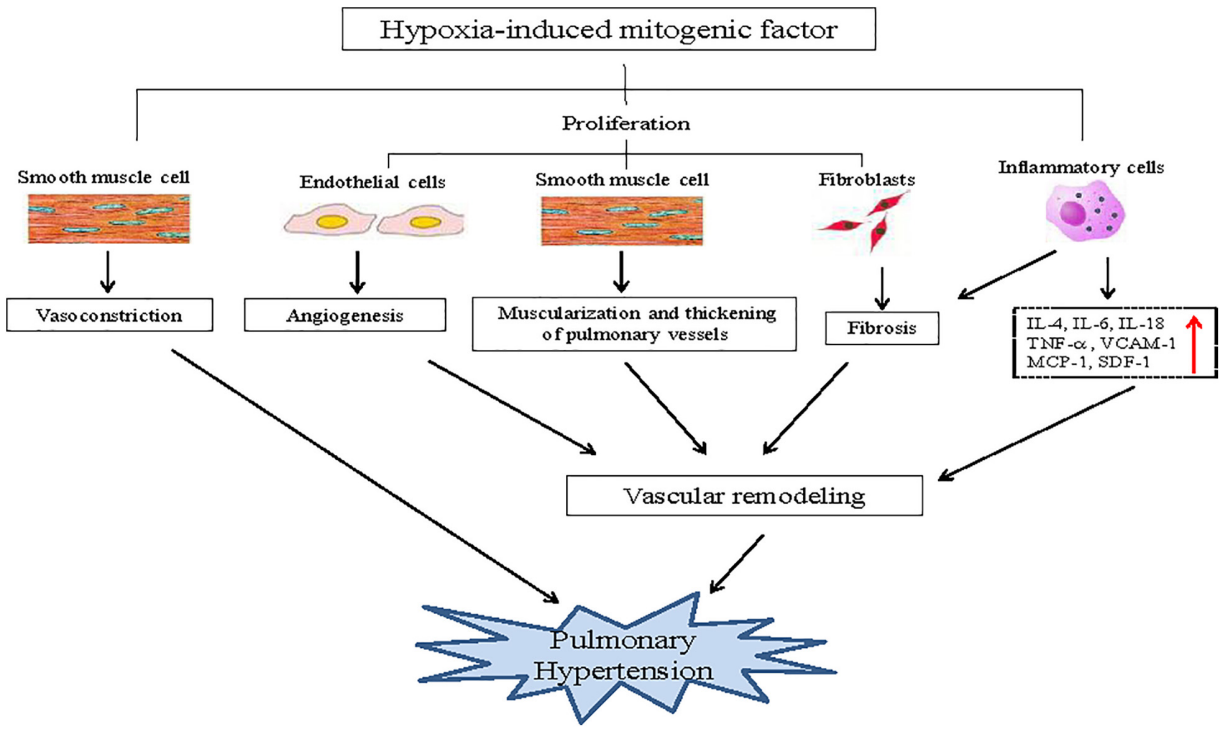

FIGURE 2 | Role of HIMF in hypoxia-induced pulmonary hypertension. HIMF induces pulmonary vasoconstriction, which plays a critical role in pulmonary hypertension. Simultaneously, HIMF also induces the proliferation of pulmonary arterial endothelial cells, smooth muscle cells and fibroblasts, which leads to angiogenesis, muscularization, the thickening of small pulmonary vessels, fibrosis, and subsequent vascular remodeling. Furthermore, HIMF induces inflammation in the lungs, which also promotes vascular remodeling and lung fibrosis, contributing to the pathological process of pulmonary hypertension.

cardioprotective features on mice, with the suppression of cardiomyocyte apoptosis, fibroblast proliferation (Kim et al., 2021). These are contributed by adiponectin-enriched unsorted bone marrow cells (UBCs). Similarly, HIMF deficiency has also been found to reduce myocardial infarct size and improve cardiac function after MI (Li et al., 2021). HIMF overexpression also directly increased CHOP expression in BMDM and RAW264.7 cells, and regulated macrophage polarization (Li et al., 2021). Taken together, these studies suggest a complex role for HIMF during cardiac injury.

Atherosclerosis

HIMF increases EC and VSMC proliferation and, thus, angiogenesis. In addition, HIMF also induces vascular inflammation, which increases vascular permeability and cell adhesion to the endothelium. These functions suggest HIMF may also participate in the development and progression of atherosclerosis, although this has not been confirmed *in vivo*. However, resistin and RELMβ, the two human homologs of HIMF, have been shown to play critical roles in atherosclerosis. Resistin is expressed in atherosclerotic plaque in patients (Jurin et al., 2018; Liberale et al., 2018), and its plasma level is linked to both coronary heart disease (Pourmoghaddas et al., 2020) and future cardiovascular-associated mortality (Park et al., 2017). At the cellular level, resistin upregulates the expression of inflammatory cytokines and adhesion molecules in human ECs (Macdonald et al., 2017), induces SMC proliferation and migration, and promotes foam cell formation (Park et al., 2017). *In vivo* experiments on rabbits have also provided direct evidence that resistin aggravates atherosclerosis by stimulating monocytes, endothelial cells, and vascular smooth muscle cells, inducing vascular inflammation (Cho et al., 2011). Another previous study has also revealed the involvement of RELMβ in atherosclerotic progression (Kushiyama et al., 2013). RELMβ was abundantly expressed in foam cells within plaques from human samples. Furthermore, ablation of RELMβ significantly reduced lipid accumulation in the aortic root and wall in apolipoprotein E-deficient mice, and the inflammatory response of primary cultured peritoneal macrophages. This indicated that RELMβ contributes to atherosclerosis development via lipid accumulation and inflammatory facilitation. RELMβ has also previously been reported to contribute to the regulation of local immune responses in both gut (Ahmed et al., 2019) and bronchial epithelial cells (Fang et al., 2012). The discovery that it is also expressed in foam cells suggests that the tissue-specific distribution of RELM family members may not be particularly strict, and that these proteins can be expressed in unexpected tissues under pathological conditions.

Metabolic Disorders

The prolonged intraperitoneal administration of HIMF has been found to significantly increase insulin resistance in

mice, but the mechanisms remain unknown (Al-Azzawi et al., 2007). Chronic low-grade inflammation is associated with metabolic complications associated during obesity, including insulin resistance. HIMF was readily detected in the serum at baseline, and its level was regulated by energy uptake, strongly suggesting that HIMF has a metabolic role. A previous study in a murine model of dextran sodium sulfate (DSS)-induced colitis and glucose disorder suggested that inflammation may be the mechanism underlying HIMF-induced dysregulation of glucose metabolism and energy balance (Munitz et al., 2009). HIMF serum levels were upregulated in DSS-induced colitis, and ablation of HIMF both decreased inflammation *in situ* and ameliorated DSS-induced colitis. The suppression of the inflammatory response leads to restoration of glucose tolerance, which is impaired in DSS-induced colitis, and protects the mice from hyperglycemia induced by glucose challenge. It support that HIMF contributes to glucose metabolism when it is induced during the setting of specific intestinal inflammatory conditions and the host is exposed to increased pro-inflammatory cytokines and high glucose intake.

While the lack of metabolic phenotype reported in HIMF knockout mice under steady-state conditions, these animals seem to have developed a compensatory mechanism to maintain normal metabolic homeostasis, as they maintain lower leptin concentrations in the sera despite their normal body weight and normal weight gain upon HFD feeding. Leptin plays an important role in regulating energy intake and expenditure, and has a pro-inflammatory role in colitis. The effect of HIMF to regulate leptin levels may also contribute to its overall pro-inflammatory role *in vivo*.

As HIMF serum levels increased in low-density lipoprotein receptor-deficient mice fed a high fat diet, HIMF exerted

TABLE 1 | Presentation of the studied diseases relating to HIMF.

Author/study	Subjects	Pathological condition	Effects
Teng et al. (2003)	Rat pulmonary microvascular smooth muscle cell	Pulmonary hypertension	HIMF has angiogenic and vasoconstrictive properties by upregulating VEGF production and promotes the proliferation and migration of PSMCs.
Su et al. (2017)	Murine myoblastic cell lines (C2C12 and G7); Human circulating EPCs; Male nude mice	Pulmonary hypertension	HIMF increased IL-18 production in myoblasts and promoted tube formation of the endothelial progenitor cells.
Angelini et al. (2013)	Adult C57BL/6 male mice	Pulmonary hypertension	Pulmonary vascular remodeling in mice induced by chronic hypoxia or antigen challenge is associated with marked increases in HIMF expression.
Liu et al. (2009)	Lung fibroblasts; FX knockout C57BL/6 mice	Pulmonary hypertension	Notch1 signaling in response to HIMF plays a significant role in myofibroblast differentiation during lung fibrosis.
Holcomb et al. (2000)	Rat embryonic dorsal root ganglion (DRG) neurons; BALB/c female mice	Allergic asthma	HIMF inhibited the nerve growth factor (NGF)-mediated survival of rat embryonic dorsal root ganglion (DRG) neurons and NGF-induced CGRP gene expression in adult rat DRG neurons. HIMF may modulate the function of neurons innervating the bronchial tree, and thus alter the local tissue response to allergic pulmonary inflammation.
Yamaji-Kegan et al. (2010)	IL-4 and STAT6 knockout C57BL/6 male mice; Mouse pulmonary microvascular endothelial cells (PMVECs)	Lung inflammation	IL-4 signaling may play a significant role in HIMF-induced lung inflammation and vascular remodeling.
Stutz et al. (2003)	BALB/c female mice; BMnot cell line	Allergic asthma	STAT6 directly regulates IL-4- and IL-13-triggered induction of HIMF expression at the transcriptional level by cooperation with C/EBP.
Fan et al. (2015)	RELMa knockout BALB/c male Mice	Allergic asthma	The expression of HIMF increased typically in OVA-induced pulmonary inflammation and vascular remodeling.
Kumar et al. (2018)	HIMF knockout C57BL/6 male mice; Neonatal ratventricular myocytes	Cardiac hypertrophy	HIMF has a critical role in the development of cardiac Hypertrophy via calcium-dependent and HIF-1α Mechanisms.
Kumar et al. (2019)	HIMF knockout C57BL/6 male mice; Neonatal rat ventricular myocytes and Fibroblasts	Cardiac hypertrophy	IL-6 plays a central role in HIMF-induced cardiac hypertrophy and fibrosis that is mediated by activating the MAPK and CaMKII-STAT3 pathways.
Al-Azzawi et al. (2007)	C57BL/6J lean non-diabetic female mice	Metabolic disorders	HIMF increases insulin resistance and reduces gallbladder optimal tension.
Munitz et al. (2009)	*Retnla*$^{-/-}$ male and female mice (backcrossed to C57BL/6 or BALB/c)	DSS-induced colitis	HIMF deficiency reduced the colitis-induced systemic inflammatory response to protect mouse from hyperglycemia induced by glucose injections.
Kumamoto et al. (2016)	Mgl2-DTR (*Mg/2* + ^{eGFP}) C57BL/6 male mice	Metabolic disorders	Reconstituting HIMF in CD301b^{+} MNP-depleted animals restored body weight and normoglycemia.
Lee et al. (2014)	*Ldlr*$^{-/-}$, *Ldlr*$^{-/-}$ *Retnla*$^{-/-}$, *Ldlr*$^{-/-}$ *Retnla-Tg* C57BL/6J male and female mice	Hyperlipidemic and atherosclerosis	HIMF exerts a favorable cholesterol-lowering effect and protects against atherosclerosis by enhancing cholesterol excretion in the form of bile acids in *Ldlr*$^{-/-}$mice.

a favorable cholesterol-lowering effect and conferred protection against atherosclerosis by increasing cholesterol excretion as bile acids (Lee et al., 2014). As demonstrated in a recent study (Kumamoto et al., 2016), a subset of $CD11b^+CD11c^+CD11c^+MHCII^+$ mononuclear phagocytes (MNP) characterized by the expression of CD301b ($CD301b^+$), participate in the maintenance of normal glucose metabolism and energy balance through HIMF secretion. Deletion of $CD301b^+$ MNPs *in vivo* leads to reduced HIMF expression, significant weight loss and increased insulin sensitivity. Reconstitution of HIMF expression in $CD301b^+$ MNP-ablated mice restores body weight and serum glucose level, and maintains the whole body metabolism. How HIMF secreted by $CD301b^+$ MNP controls feeding behavior and energy balance remains to be determined. These results suggest that the beneficial and detrimental roles of HIMF in inflammatory diseases are likely influenced by the type of immune stimulus, the duration of the stimulus exposure and the tissue type. However, the exact mechanisms underlying the involvement of HIMF in metabolic diseases remain to be clarified in full.

CONCLUSION AND PERSPECTIVES

As a secreted protein, HIMF exerts potent pro-inflammatory effects, is enriched at sites of inflammation, and its expression is correlated with markers of inflammatory disease. In recent years, the functional diversity of RELM proteins, such as HIMF, has generated increased attention. Mice are the main animal model used to manipulate the expression of these genes and to study their function. However, this also represents the biggest challenge faced when researching the role of RELM proteins and resistin in the pathogenesis of disease. The expression patterns of these proteins differ between humans and rodents; indeed, humans do not express HIMF at all. However, studies in mice do provide a solid starting point when investigating the function of RELM proteins in humans. HIMF has been suggested to play functional roles similar to those of human resistin, due to their similar expression patterns (Nair et al., 2006). If this is the case, the involvement of HIMF in the development of cardiovascular diseases and metabolic disorders in mice may be comparable to that of resistin in human disease. Using HIMF knockout mice could provide useful data that might indicate the role of resistin in these diseases. However, the situation may be different in the respiratory system. Here, HIMF appears to serve similar roles as human RELM beta: namely, inducing vascular remodeling and pulmonary fibrosis in pulmonary diseases, particularly in PH. Therefore, HIMF data obtained in mice should be cautiously translated to human diseases, depending on the tissue localization and pathological context.

Early research has primarily focused on the involvement of HIMF in pulmonary vasoconstriction, vascular remodeling, pulmonary inflammation and angiogenesis, which are key pathophysiological processes that occur during the development of PH. HIMF has also been reported to be involved in the development of lung maturation, pulmonary fibrosis, acute lung injury and bronchial asthma. The expression and distribution of HIMF could contribute to the initiation of diseases via multiple signaling pathways, which may cross-talk with each other in the development of pulmonary hypertension. A growing body of evidence also indicates a significant role for HIMF in lung disease. However, the underlying molecular mechanisms remain unclear in both pulmonary hypertension and other diseases. Additional studies are required to provide a more definitive account. Alternatively, whether HIMF is involved in other lung diseases, such as lung cancer, pneumonia, or chronic obstructive pulmonary disease (COPD) with emphysema, also warrants further investigation. A more thorough understanding of these mechanisms will be necessary in order to characterize HIMF, and its human homologs, as specific targets for the treatment of lung disease.

More recently, the study of RELM proteins in physiology and disease has expanded to include cardiovascular diseases. Clinical investigations and experimental studies have identified a positive correlation between circulating levels of resistin and the risk of MI. In mice, HIMF deficiency is known to facilitate M2 macrophage transformation and to increase collagen formation and fibrin deposition in the infarct region, preventing the myocardial wall from expansion and rupture. This helps preserve contractility after acute MI (Li et al., 2021). However, HIMF also induces cardiac fibroblast proliferation, migration and differentiation during cardiac hypertrophy and heart failure (Kumar et al., 2019). Additionally, HIMF may serve pathogenic functions in hypercholesterolemia (Lee et al., 2014) and immune-mediated liver injury (Pai and Njoku, 2021). Thus, future studies on the pathogenic functions of HIMF should be extended to other pathological conditions. The main details of the studies focusing on the role of HIMF in diseases are demonstrated in **Table 1**.

At present, the receptors for resistin and RELM proteins are not known. A recent study revealed a non-classical receptor for HIMF, CaSR, which mediates intracellular but not extracellular HIMF signal (Zeng et al., 2017). A synthesized membrane-permeable peptide designed to flank the binding domain of CaSR for HIMF significantly attenuated hypoxia-induced PH progression. The therapeutic effect of this peptide on PH is quite inspiring, and there may be potential for its use to be extended to other HIMF-associated diseases. However, future studies focused on discovering the receptors and associated signaling pathways of RELM proteins will be required to fully understand its translational medical role in human diseases.

AUTHOR CONTRIBUTIONS

ML and WL prepared the figures. WL wrote the manuscript. Both authors contributed to the article and approved the submitted version.

FUNDING

The present study was supported by the National Science Foundation of China (82070340 to WL), the Guangdong Basic

and Applied Basic Research Foundation (2020A1515010259 to WL), the Medical Scientific Research Foundation of Guangdong Province of China (A2016263 to WL), the SZU Top Ranking Project (86000000210 to WL), the Basic Research Foundation of Shenzhen (20200812105703001 to WL), and the SZU Medical Young Scientists Program (71201-000001 to WL).

ACKNOWLEDGMENTS

We appreciate Dr. Jessica Tamanini (Shenzhen University Health Science Center, China and ETediting, United Kingdom) for language editing and critical comments of the article before submission.

REFERENCES

Ahmed, N., Heitlinger, E., Affinass, N., Kuhl, A. A., Xenophontos, N., Jarquin, V. H., et al. (2019). A Novel Non-invasive Method to Detect RELM Beta Transcript in Gut Barrier Related Changes During a Gastrointestinal Nematode Infection. *Front. Immunol.* 10:445. doi: 10.3389/fimmu.2019.00445

Al-Azzawi, H. H., Mathur, A., Lu, D., Swartz-Basile, D. A., Nakeeb, A., and Pitt, H. A. (2007). Resistin-like molecule alpha reduces gallbladder optimal tension. *J. Gastrointest. Surg.* 11, 95–100. doi: 10.1007/s11605-006-0039-1

Angelini, D. J., Su, Q., Yamaji-Kegan, K., Fan, C., Skinner, J. T., Poloczek, A., et al. (2013). Hypoxia-induced mitogenic factor (HIMF/FIZZ1/RELMalpha) in chronic hypoxia- and antigen-mediated pulmonary vascular remodeling. *Respir. Res.* 14:1. doi: 10.1186/1465-9921-14-1

Angelini, D. J., Su, Q., Yamaji-Kegan, K., Fan, C., Teng, X., Hassoun, P. M., et al. (2009). Resistin-like molecule-beta in scleroderma-associated pulmonary hypertension. *Am. J. Respir. Cell Mol. Biol.* 41, 553–561. doi: 10.1165/rcmb.2008-0271OC

Banerjee, R. R., and Lazar, M. A. (2001). Dimerization of resistin and resistin-like molecules is determined by a single cysteine. *J. Biol. Chem.* 276, 25970–25973. doi: 10.1074/jbc.M103109200

Cai, S. Y., Ge, M., Mennone, A., Hoque, R., Ouyang, X., and Boyer, J. L. (2020). Inflammasome Is Activated in the Liver of Cholestatic Patients and Aggravates Hepatic Injury in Bile Duct-Ligated Mouse. *Cell Mol. Gastroenterol. Hepatol.* 9, 679–688. doi: 10.1016/j.jcmgh.2019.12.008

Cho, Y., Lee, S. E., Lee, H. C., Hur, J., Lee, S., Youn, S. W., et al. (2011). Adipokine resistin is a key player to modulate monocytes, endothelial cells, and smooth muscle cells, leading to progression of atherosclerosis in rabbit carotid artery. *J. Am. Coll. Cardiol.* 57, 99–109. doi: 10.1016/j.jacc.2010.07.035

Duan, J. X., Zhou, Y., Zhou, A. Y., Guan, X. X., Liu, T., Yang, H. H., et al. (2017). Calcitonin gene-related peptide exerts anti-inflammatory property through regulating murine macrophages polarization *in vitro*. *Mol. Immunol.* 91, 105–113. doi: 10.1016/j.molimm.2017.08.020

Elvert, G., Kappel, A., Heidenreich, R., Englmeier, U., Lanz, S., Acker, T., et al. (2003). Cooperative interaction of hypoxia-inducible factor-2alpha (HIF-2alpha) and Ets-1 in the transcriptional activation of vascular endothelial growth factor receptor-2 (Flk-1). *J. Biol. Chem.* 278, 7520–7530. doi: 10.1074/jbc.M211298200

Fan, C., Meuchel, L. W., Su, Q., Angelini, D. J., Zhang, A., Cheadle, C., et al. (2015). Resistin-Like Molecule alpha in Allergen-Induced Pulmonary Vascular Remodeling. *Am. J. Respir. Cell Mol. Biol.* 53, 303–313. doi: 10.1165/rcmb.2014-0322OC

Fan, C., Su, Q., Li, Y., Liang, L., Angelini, D. J., Guggino, W. B., et al. (2009). Hypoxia-induced mitogenic factor/FIZZ1 induces intracellular calcium release through the PLC-IP(3) pathway. *Am. J. Physiol. Lung Cell Mol. Physiol.* 297, L263–L270. doi: 10.1152/ajplung.90416.2008

Fang, C., Meng, Q., Wu, H., Eid, G., Zhang, G., Zhang, X., et al. (2012). Resistin-like molecule-beta is a human airway remodelling mediator. *Eur. Respir. J.* 39, 458–466. doi: 10.1183/09031936.00107811

Gerstmayer, B., Kusters, D., Gebel, S., Muller, T., Van Miert, E., Hofmann, K., et al. (2003). Identification of RELMgamma, a novel resistin-like molecule with a distinct expression pattern. *Genomics* 81, 588–595. doi: 10.1016/s0888-7543(03)00070-3

Hogan, S. P., Seidu, L., Blanchard, C., Groschwitz, K., Mishra, A., Karow, M. L., et al. (2006). Resistin-like molecule beta regulates innate colonic function: barrier integrity and inflammation susceptibility. *J. Allergy Clin. Immunol.* 118, 257–268. doi: 10.1016/j.jaci.2006.04.039

Holcomb, I. N., Kabakoff, R. C., Chan, B., Baker, T. W., Gurney, A., Henzel, W., et al. (2000). FIZZ1, a novel cysteine-rich secreted protein associated with pulmonary inflammation, defines a new gene family. *EMBO J.* 19, 4046–4055. doi: 10.1093/emboj/19.15.4046

Johns, R. A., Takimoto, E., Meuchel, L. W., Elsaigh, E., Zhang, A., Heller, N. M., et al. (2016). Hypoxia-Inducible Factor 1alpha Is a Critical Downstream Mediator for Hypoxia-Induced Mitogenic Factor (FIZZ1/RELMalpha)-Induced Pulmonary Hypertension. *Arterioscler. Thromb. Vasc. Biol.* 36, 134–144. doi: 10.1161/ATVBAHA.115.306710

Jurin, I., Paic, F., Bulimbasic, S., Rudez, I., Derek, L., Jurin, H., et al. (2018). Association between Circulatory and Plaque Resistin Levels with Carotid Plaque Instability and Ischemic Stroke Events. *Heart. Surg. Forum* 21, E448–E463. doi: 10.1532/hsf.2071

Kim, Y. S., Cho, H. H., Cho, D. I, Jeong, H. Y., Lim, S. Y., Jun, J. H., et al. (2021). The adipokine Retnla deficiency increases responsiveness to cardiac repair through adiponectin-rich bone marrow cells. *Cell Death Dis.* 12:307. doi: 10.1038/s41419-021-03593-z

Kumamoto, Y., Camporez, J. P. G., Jurczak, M. J., Shanabrough, M., Horvath, T., Shulman, G. I., et al. (2016). CD301b(+) Mononuclear Phagocytes Maintain Positive Energy Balance through Secretion of Resistin-like Molecule Alpha. *Immunity* 45, 583–596. doi: 10.1016/j.immuni.2016.08.002

Kumar, S., Wang, G., Liu, W., Ding, W., Dong, M., Zheng, N., et al. (2018). Hypoxia-Induced Mitogenic Factor Promotes Cardiac Hypertrophy via Calcium-Dependent and Hypoxia-Inducible Factor-1alpha Mechanisms. *Hypertension* 72, 331–342. doi: 10.1161/HYPERTENSIONAHA.118.10845

Kumar, S., Wang, G., Zheng, N., Cheng, W., Ouyang, K., Lin, H., et al. (2019). HIMF (Hypoxia-Induced Mitogenic Factor)-IL (Interleukin)-6 Signaling Mediates Cardiomyocyte-Fibroblast Crosstalk to Promote Cardiac Hypertrophy and Fibrosis. *Hypertension* 73, 1058–1070. doi: 10.1161/HYPERTENSIONAHA.118.12267

Kushiyama, A., Sakoda, H., Oue, N., Okubo, M., Nakatsu, Y., Ono, H., et al. (2013). Resistin-like molecule beta is abundantly expressed in foam cells and is involved in atherosclerosis development. *Arterioscler. Thromb. Vasc. Biol.* 33, 1986–1993. doi: 10.1161/ATVBAHA.113.301546

Lee, M. R., Lim, C. J., Lee, Y. H., Park, J. G., Sonn, S. K., Lee, M. N., et al. (2014). The adipokine Retnla modulates cholesterol homeostasis in hyperlipidemic mice. *Nat. Commun.* 5:4410. doi: 10.1038/ncomms5410

Li, B., Lager, J., Wang, D., and Li, D. (2007). Ets-1 participates in and facilitates developmental expression of hypoxia-induced mitogenic factor in mouse lung. *Front. Biosci.* 12, 2269–2278. doi: 10.2741/2229

Li, X., Yang, Y., Fang, J., and Zhang, H. (2013). FIZZ1 could enhance the angiogenic ability of rat aortic endothelial cells. *Int. J. Clin. Exp. Pathol.* 6, 1847–1853.

Li, Y., Dong, M., Wang, Q., Kumar, S., Zhang, R., Cheng, W., et al. (2021). HIMF deletion ameliorates acute myocardial ischemic injury by promoting macrophage transformation to reparative subtype. *Basic Res. Cardiol.* 116:30. doi: 10.1007/s00395-021-00867-7

Liberale, L., Bertolotto, M., Carbone, F., Contini, P., Wust, P., Spinella, G., et al. (2018). Resistin exerts a beneficial role in atherosclerotic plaque inflammation by inhibiting neutrophil migration. *Int. J. Cardiol.* 272, 13–19. doi: 10.1016/j.ijcard.2018.07.112

Lin, Q., Fan, C., Gomez-Arroyo, J., Van Raemdonck, K., Meuchel, L. W., Skinner, J. T., et al. (2019a). HIMF (Hypoxia-Induced Mitogenic Factor) Signaling Mediates the HMGB1 (High Mobility Group Box 1)-Dependent Endothelial and Smooth Muscle Cell Crosstalk in Pulmonary Hypertension. *Arterioscler. Thromb. Vasc. Biol.* 39, 2505–2519. doi: 10.1161/ATVBAHA.119.312907

Lin, Q., Fan, C., Skinner, J. T., Hunter, E. N., Macdonald, A. A., Illei, P. B., et al. (2019b). RELMalpha Licenses Macrophages for Damage-Associated Molecular Pattern Activation to Instigate Pulmonary Vascular Remodeling. *J. Immunol.* 203, 2862–2871. doi: 10.4049/jimmunol.1900535

Lin, Q., Price, S. A., Skinner, J. T., Hu, B., Fan, C., Yamaji-Kegan, K., et al. (2020). Systemic evaluation and localization of resistin expression in normal human

tissues by a newly developed monoclonal antibody. *PLoS One* 15:e0235546. doi: 10.1371/journal.pone.0235546

Liu, T., Hu, B., Choi, Y. Y., Chung, M., Ullenbruch, M., Yu, H., et al. (2009). Notch1 signaling in FIZZ1 induction of myofibroblast differentiation. *Am. J. Pathol.* 174, 1745–1755. doi: 10.2353/ajpath.2009.080618

Macdonald, S. P. J., Bosio, E., Neil, C., Arendts, G., Burrows, S., Smart, L., et al. (2017). Resistin and NGAL are associated with inflammatory response, endothelial activation and clinical outcomes in sepsis. *Inflamm. Res.* 66, 611–619. doi: 10.1007/s00011-017-1043-5

Munitz, A., Seidu, L., Cole, E. T., Ahrens, R., Hogan, S. P., and Rothenberg, M. E. (2009). Resistin-like molecule alpha decreases glucose tolerance during intestinal inflammation. *J. Immunol.* 182, 2357–2363. doi: 10.4049/jimmunol.0803130

Nair, M. G., Du, Y., Perrigoue, J. G., Zaph, C., Taylor, J. J., Goldschmidt, M., et al. (2009). Alternatively activated macrophage-derived RELM-{alpha} is a negative regulator of type 2 inflammation in the lung. *J. Exp. Med.* 206, 937–952. doi: 10.1084/jem.20082048

Nair, M. G., Guild, K. J., and Artis, D. (2006). Novel effector molecules in type 2 inflammation: lessons drawn from helminth infection and allergy. *J. Immunol.* 177, 1393–1399. doi: 10.4049/jimmunol.177.3.1393

Pai, S., and Njoku, D. B. (2021). The Role of Hypoxia-Induced Mitogenic Factor in Organ-Specific Inflammation in the Lung and Liver: Key Concepts and Gaps in Knowledge Regarding Molecular Mechanisms of Acute or Immune-Mediated Liver Injury. *Int. J. Mol. Sci.* 22:2717. doi: 10.3390/ijms22052717

Park, H. K., Kwak, M. K., Kim, H. J., and Ahima, R. S. (2017). Linking resistin, inflammation, and cardiometabolic diseases. *Korean J. Intern. Med.* 32, 239–247. doi: 10.3904/kjim.2016.229

Pesce, J. T., Ramalingam, T. R., Wilson, M. S., Mentink-Kane, M. M., Thompson, R. W., Cheever, A. W., et al. (2009). Retnla (relmalpha/fizz1) suppresses helminth-induced Th2-type immunity. *PLoS Pathog.* 5:e1000393. doi: 10.1371/journal.ppat.1000393

Pourmoghaddas, A., Elahifar, A., Darabi, F., Movahedian, A., Amirpour, A., and Sarrafzadegan, N. (2020). Resistin and prooxidant-antioxidant balance: markers to discriminate acute coronary syndrome from stable angina. *ARYA Atheroscler.* 16, 46–54. doi: 10.22122/arya.v16i2.1944

Song, L., Xu, J., Qu, J., Sai, Y., Chen, C., Yu, L., et al. (2012). A therapeutic role for mesenchymal stem cells in acute lung injury independent of hypoxia-induced mitogenic factor. *J. Cell Mol. Med.* 16, 376–385. doi: 10.1111/j.1582-4934.2011.01326.x

Steppan, C. M., Brown, E. J., Wright, C. M., Bhat, S., Banerjee, R. R., Dai, C. Y., et al. (2001). A family of tissue-specific resistin-like molecules. *Proc. Natl. Acad. Sci. U. S. A.* 98, 502–506. doi: 10.1073/pnas.98.2.502

Stutz, A. M., Pickart, L. A., Trifilieff, A., Baumruker, T., Prieschl-Strassmayr, E., and Woisetschlager, M. (2003). The Th2 cell cytokines IL-4 and IL-13 regulate found in inflammatory zone 1/resistin-like molecule alpha gene expression by a STAT6 and CCAAT/enhancer-binding protein-dependent mechanism. *J. Immunol.* 170, 1789–1796. doi: 10.4049/jimmunol.170.4.1789

Su, C. M., Wang, I. C., Liu, S. C., Sun, Y., Jin, L., Wang, S. W., et al. (2017). Hypoxia induced mitogenic factor (HIMF) triggers angiogenesis by increasing interleukin-18 production in myoblasts. *Sci. Rep.* 7:7393. doi: 10.1038/s41598-017-07952-9

Su, Q., Zhou, Y., and Johns, R. A. (2007). Bruton's tyrosine kinase (BTK) is a binding partner for hypoxia induced mitogenic factor (HIMF/FIZZ1) and mediates myeloid cell chemotaxis. *FASEB J.* 21, 1376–1382. doi: 10.1096/fj.06-6527com

Teng, X., Li, D., Champion, H. C., and Johns, R. A. (2003). FIZZ1/RELMalpha, a novel hypoxia-induced mitogenic factor in lung with vasoconstrictive and angiogenic properties. *Circ. Res.* 92, 1065–1067. doi: 10.1161/01.RES.0000073999.07698.33

Tong, Q., Zheng, L., Kang, Q., Dodd, O. J., Langer, J., Li, B., et al. (2006d). Upregulation of hypoxia-induced mitogenic factor in bacterial lipopolysaccharide-induced acute lung injury. *FEBS Lett.* 580, 2207–2215. doi: 10.1016/j.febslet.2006.03.027

Tong, Q., Zheng, L., Li, B., Wang, D., Huang, C., Matuschak, G. M., et al. (2006c). Hypoxia-induced mitogenic factor enhances angiogenesis by promoting proliferation and migration of endothelial cells. *Exp. Cell. Res.* 312, 3559–3569. doi: 10.1016/j.yexcr.2006.07.024

Tong, Q., Zheng, L., Lin, L., Li, B., Wang, D., Huang, C., et al. (2006a). VEGF is upregulated by hypoxia-induced mitogenic factor via the PI-3K/Akt-NF-kappaB signaling pathway. *Respir. Res.* 7:37. doi: 10.1186/1465-9921-7-37

Tong, Q., Zheng, L., Lin, L., Li, B., Wang, D., Huang, C., et al. (2006b). Participation of the PI-3K/Akt-NF-kappa B signaling pathways in hypoxia-induced mitogenic factor-stimulated Flk-1 expression in endothelial cells. *Respir. Res.* 7:101. doi: 10.1186/1465-9921-7-101

Wagner, K. F., Hellberg, A. K., Balenger, S., Depping, R., Dodd, O. J., Johns, R. A., et al. (2004). Hypoxia-induced mitogenic factor has antiapoptotic action and is upregulated in the developing lung: coexpression with hypoxia-inducible factor-2alpha. *Am. J. Respir. Cell Mol. Biol.* 31, 276–282. doi: 10.1165/rcmb.2003-0319OC

Xue, Y. L., Zhang, S. X., Zheng, C. F., Li, Y. F., Zhang, L. H., Su, Q. Y., et al. (2020). Long non-coding RNA MEG3 inhibits M2 macrophage polarization by activating TRAF6 via microRNA-223 down-regulation in viral myocarditis. *J. Cell Mol. Med.* 24, 12341–12354. doi: 10.1111/jcmm.15720

Yamaji-Kegan, K., Su, Q., Angelini, D. J., Champion, H. C., and Johns, R. A. (2006). Hypoxia-induced mitogenic factor has proangiogenic and proinflammatory effects in the lung via VEGF and VEGF receptor-2. *Am. J. Physiol. Lung Cell Mol. Physiol.* 291, L1159–L1168. doi: 10.1152/ajplung.00168.2006

Yamaji-Kegan, K., Su, Q., Angelini, D. J., Myers, A. C., Cheadle, C., and Johns, R. A. (2010). Hypoxia-induced mitogenic factor (HIMF/FIZZ1/RELMalpha) increases lung inflammation and activates pulmonary microvascular endothelial cells via an IL-4-dependent mechanism. *J. Immunol.* 185, 5539–5548. doi: 10.4049/jimmunol.0904021

Yamaji-Kegan, K., Takimoto, E., Zhang, A., Weiner, N. C., Meuchel, L. W., Berger, A. E., et al. (2014). Hypoxia-induced mitogenic factor (FIZZ1/RELMalpha) induces endothelial cell apoptosis and subsequent interleukin-4-dependent pulmonary hypertension. *Am. J. Physiol. Lung Cell Mol. Physiol.* 306, L1090–L1103. doi: 10.1152/ajplung.00279.2013

Zeng, X., Zhu, L., Xiao, R., Liu, B., Sun, M., Liu, F., et al. (2017). Hypoxia-Induced Mitogenic Factor Acts as a Non-classical Ligand of Calcium-Sensing Receptor, Therapeutically Exploitable for Intermittent Hypoxia-Induced Pulmonary Hypertension. *Hypertension* 69, 844–854. doi: 10.1161/HYPERTENSIONAHA.116.08743

Zhang, M. H., Na, B., Schiller, N. B., and Whooley, M. A. (2011). Association of resistin with heart failure and mortality in patients with stable coronary heart disease: data from the heart and soul study. *J. Card. Fail.* 17, 24–30. doi: 10.1016/j.cardfail.2010.08.007

Conflict of Interest: The authors declare that the research was conducted in the absence of any commercial or financial relationships that could be construed as a potential conflict of interest.

frontiers in Cell and Developmental Biology

ORIGINAL RESEARCH
published: 26 July 2021
doi: 10.3389/fcell.2021.698254

A GSK3-SRF Axis Mediates Angiotensin II Induced Endothelin Transcription in Vascular Endothelial Cells

Yuyu Yang[1,2], Huidi Wang[3], Hongwei Zhao[1], Xiulian Miao[2,4], Yan Guo[2,4], Lili Zhuo[5] and Yong Xu[2,3]*

[1] Jiangsu Key Laboratory for Medical Biotechnology, College of Life Sciences, Nanjing Normal University, Nanjing, China, [2] Institute of Biomedical Research, Liaocheng University, Liaocheng, China, [3] Key Laboratory of Targeted Intervention of Cardiovascular Disease and Collaborative Innovation Center for Cardiovascular Translational Medicine, Department of Pathophysiology, Nanjing Medical University, Nanjing, China, [4] College of Life Sciences, Liaocheng University, Liaocheng, China, [5] Department of Geriatrics, The Second Affiliated Hospital of Nanjing Medical University, Nanjing, China

Endothelin, encoded by *ET1*, is a vasoactive substance primarily synthesized in vascular endothelial cells (VECs). Elevation of endothelin levels, due to transcriptional hyperactivation, has been observed in a host of cardiovascular diseases. We have previously shown that serum response factor (SRF) is a regulator of *ET1* transcription in VECs. Here we report that angiotensin II (Ang II) induced *ET1* transcription paralleled activation of glycogen synthase kinase 3 (GSK3) in cultured VECs. GSK3 knockdown or pharmaceutical inhibition attenuated Ang II induced endothelin expression. Of interest, the effect of GSK3 on endothelin transcription relied on the conserved SRF motif within the *ET1* promoter. Further analysis revealed that GSK3 interacted with and phosphorylated SRF at serine 224. Phosphorylation of SRF by GSK3 did not influence its recruitment to the *ET1* promoter. Instead, GSK3-mediated SRF phosphorylation potentiated its interaction with MRTF-A, a key co-factor for SRF, which helped recruit the chromatin remodeling protein BRG1 to the *ET1* promoter resulting in augmented histone H3 acetylation/H3K4 trimethylation. Consistently, over-expression of a constitutively active GSK enhanced Ang II-induced *ET1* transcription and knockdown of either MRTF-A or BRG1 abrogated the enhancement of *ET1* transcription. In conclusion, our data highlight a previously unrecognized mechanism that contributes to the transcriptional regulation of endothelin. Targeting this GSK3-SRF axis may yield novel approaches in the intervention of cardiovascular diseases.

Keywords: transcriptional regulation, vascular endothelial cell, post-translational modification, phosphorylation, serum response factor

OPEN ACCESS

Edited by:
Prasun K. Datta, Tulane University, United States

Reviewed by:
Francesca Di Sole, Des Moines University, United States
Manish Kumar Gupta, University of Central Florida, United States

****Correspondence:***
Lili Zhuo
zhuolili@njmu.edu.cn

Specialty section:
This article was submitted to Cellular Biochemistry, a section of the journal Frontiers in Cell and Developmental Biology

Received: *21 April 2021*
Accepted: *09 July 2021*
Published: *26 July 2021*

Citation:
Yang Y, Wang H, Zhao H, Miao X, Guo Y, Zhuo L and Xu Y (2021) A GSK3-SRF Axis Mediates Angiotensin II Induced Endothelin Transcription in Vascular Endothelial Cells. Front. Cell Dev. Biol. 9:698254. doi: 10.3389/fcell.2021.698254

INTRODUCTION

The vascular endothelium not only functions as a physical barrier separating the circulation from the basal lamina but synthesizes and secretes a host of substances contributing to the maintenance and regulation of internal microenvironment either locally (via paracrine) or systemically (via endocrine) (Rafii et al., 2016). Endothelin, encoded by *ET1*, is a polypeptide derived from

endothelial cells (Yanagisawa et al., 1988). Endothelin primarily signals through one of the two cognate receptors, ETRA and ETRB. Whereas binding of endothelin to ETRA leads to contraction of vascular smooth muscle cells, the endothelin-ETRB interaction is thought to trigger endothelin clearance and vasorelaxation (Abman, 2009). Elevated plasma endothelin levels have been observed in patients with hypertension (Letizia et al., 1997), pulmonary hypertension (Rubens et al., 2001), atherosclerosis (Hasdai et al., 1997), diabetes (Cardillo et al., 2002), and heart failure (Wei et al., 1994). Concordantly, ETR antagonists have been demonstrated to be effective in the intervention of a host of cardiovascular and metabolic diseases (Enevoldsen et al., 2020).

Increased production of endothelin is primarily achieved through transcriptional activation of the *ET1* gene, which is localized on chromosome 6 in the human genome (Stow et al., 2011). The proximal *ET1* promoter is responsive to a number of stimuli including angiotensin II (Ang II), hypoxia, transforming growth factor (TGF), thrombin, and tumor necrosis factor (TNF) (Imai et al., 1992; Delerive et al., 1999; Yamashita et al., 2001; Castanares et al., 2007; Wort et al., 2009). The stimulatory effects of these humoral factors on *ET1* transcription are mediated by different sequence-specific transcription factors. For instance, we and others have shown that activator protein 1 (AP-1) is recruited to the -115/-108 region of the *ET1* promoter in response to Ang II and mediates *ET1* trans-activation in endothelial cells (Lee et al., 1991; Imai et al., 1992; Weng et al., 2015a). Hypoxia-induced ET1 trans-activation can be mediated by, according to Yamashita et al. (2001), a complex that contains HIF-1α, AP-1, and GATA-2. Alternatively, we have previously shown that serum response factor (SRF) can be detected on the proximal *ET1* promoter and mediates hypoxia induced *ET1* trans-activation (Yang et al., 2013).

In the vasculature, SRF is known to regulate the transcription of contractile genes in vascular smooth muscle cells by recognizing the so-called CArG box [$CC(A/T)_6GG$] located on its target promoters (Miano, 2010). The role of SRF in the regulation of endothelial function is relatively less well defined. It has been demonstrated independently by Franco et al. (2008) and by Holtz et al. (Holtz and Misra, 2008) that endothelium-specific deletion of SRF in mice results in embryonic lethality owing to defective angiogenesis/vasculogenesis and hemorrhaging. Transcrptionally, SRF is essential for the activation of E-Cadherin (*CDH5*) and β-actin (*ACTAB*) to maintain endothelial homeostasis. The transcriptional activity of SRF is subject to multiple layers of modulation including post-translational modifications (PTMs). Matsuzaki et al. (2003), for instance, have discovered that lysine residue 147 of SRF can be SUMOylated, which suppresses its transcriptional activity likely by interfering with its DNA binding potential. More recently, Kwon et al. (2021) have reported that lysine residue 165 of SRF can be methylated by SET7 and de-methylated by KDM2B; dynamic SRF methylation is proposed to regulate its affinity for target promotes and contribute to muscle differentiation. By far, phosphorylation represents the most extensively characterized PTM for SRF. There is evidence to support a host of kinases, including MK2 (Heidenreich et al., 1999), PKA (Blaker et al., 2009), CaMKII (Ely et al., 2011), GSK3β (Li et al., 2014), and PKC (Iyer et al., 2006), using SRF as a substrate. Whether or not SRF phosphorylation can contribute to *ET1* transcription is yet to be examined. Here we report that GSK3β mediated SRF phosphorylation facilitates its interaction with key co-factors to mediate Ang II induced endothelin expression in endothelial cells.

MATERIALS AND METHODS

Cell Culture

Immortalized human endothelial cells (EAhy926) were maintained in DMEM supplemented with 10% FBS as previously described (Chen et al., 2020c). ET1 promoter-luciferase constructs (Yang et al., 2013), SRF expression constructs (Li et al., 2014; Kong et al., 2019a,b) have been previously described. Constitutively active GSK3β, in which serine 9 was substituted by alanine (S9A), dominant negative GSK3β, in which arginine 96 was substituted by alanine (R96A), phosphorylation-defective SRF, in which serine 224 was substituted by alanine (S224A), and phosphorylation mimetic SRF in which serine 224 was substituted by aspartic acid (S224D), were generated by a QuikChange kit (Thermo Fisher Scientific, Waltham, MA, United States) and verified by direct sequencing as previously described (Bechard and Dalton, 2009). Angiotensin II was purchased from Sigma (St. Louis, MO, United States). LY2090314 were purchased from Selleck (Houston, TX, United States). Small interfering RNAs were purchased from Dharmacon (Lafayette, CO, United States): siGSK3B#1, AAGTAATCCACCTCTGGCTAC; siGSK3B#2, GUAAUCCACCUCUGGCUAC; siMRTFA#1, GUG UCUUGGUGUAGUGU; siMRTFA#2, CUGCGUGCAU AUCAAGAAC; siBRG1#1, AACATGCACCAGATGCAC AAG; siBRG1#2, GCCCATGGAGTCCATGCAT. Transient transfections were performed with Lipofectamine 2000 (for DNA plasmids, Thermo Fisher Scientific, Waltham, MA, United States) or Lipofectamine RNAiMax (for siRNAs, Thermo Fisher Scientific, Waltham, MA, United States). Cells were harvested 48 h after transfection and reporter activity was measured using a luciferase reporter assay system (Promega, Madison, WI, United States) as previously described (Wu X. et al., 2020; Hong et al., 2021).

Protein Extraction, Immunoprecipitation, and Western Blotting

Whole cell lysates were obtained by re-suspending cell pellets in RIPA buffer (50 mM Tris pH7.4, 150 mM NaCl, 1% Triton X-100) with freshly added protease inhibitor (Roche, Basel, Switzerland) as previously described (Chen et al., 2020a,b,c, 2021; Dong et al., 2020, 2021; Fan et al., 2020; Li N. et al., 2020; Li et al., 2020a,b; Lv et al., 2020; Mao et al., 2020; Sun et al., 2020; Wu T. et al., 2020; Wu X. et al., 2020; Yang et al., 2020; Hong et al., 2021; Kong et al., 2021; Zhang et al., 2021). Specific antibodies were added to and incubated with cell lysates overnight before being absorbed by Protein A/G-plus Agarose beads (Santa Cruz, Santa Cruz, CA, United States).

Precipitated immune complex was released by boiling with 1X SDS electrophoresis sample buffer. Proteins were separated by 8% polyacrylamide gel electrophoresis with pre-stained markers (Bio-Rad, Hercules, CA, United States) for estimating molecular weight and efficiency of transfer to blots. Proteins were transferred to nitrocellulose membranes (Bio-Rad, Hercules, CA, United States) in a Mini-Trans-Blot Cell (Bio-Rad, Hercules, CA, United States). The membranes were blocked with 5% milk powder in Tris-buffered saline buffer (0.05% Tween 20, 150 mM NaCl, 100 mM Tris-HCl pH7.4) at 4°C overnight. Western blot analyses were performed with anti-GFP (Proteintech, 50430-2, Wuhan, China), anti-FLAG (Sigma, F3165, St. Louis, MO, United States), anti-GSK3β (Cell Signaling Tech, 12456, Danvers, MA, United States), anti-phospho-Ser9-GSK3β (Cell Signaling Tech, 5558), anti-GSK3α (Proteintech, 13419-1, Wuhan, China), anti-phospho-Ser21-GSK3α (Cell Signaling Tech, 9316, Danvers, MA, United States), anti-phospho-(S/T)F (Cell Signaling Tech, 9631, Danvers, MA, United States), anti-SRF (Cell Signaling Tech, 5147, Danvers, MA, United States), and anti-β-actin (Sigma, A2228, St. Louis, MO, United States) antibodies. For densitometrical quantification, densities of target proteins were normalized to those of β-actin as previously described (Sun et al., 2020; Wu T. et al., 2020). Data are expressed as relative protein levels compared to the control group which is arbitrarily set as 1.

RNA Isolation and Real-Time PCR

RNA was extracted with the RNeasy RNA isolation kit (Qiagen, Hilden, Germany). Reverse transcriptase reactions were performed using a SuperScript First-strand Synthesis System (Invitrogen, Waltham, MA, United States) as previously described (Zhang et al., 2020; Liu et al., 2021). Real-time PCR reactions were performed on an ABI Prism 7500 system with the following primers: *ET1*, 5′-AGAGTGTGTCTACTTCTGCCA-3′ and 5′-CTTCCAAGTCCATACGGAACAA-3′; GSK3B, 5′-GG CAGCATGAAAGTTAGCAGA-3′ and 5′-GGCGACCAGT TCTCCTGAATC-3′. Ct values of target genes were normalized to the Ct values of housekeeping control gene (18s, 5′-CGCGGTTCTATTTTGTTGGT-3′ and 5′-TCGTCTTCGAAACTCCGACT-3′ for both human and mouse genes) using the ΔΔCt method and expressed as relative mRNA expression levels compared to the control group which is arbitrarily set as 1.

Chromatin Immunoprecipitation (ChIP)

Chromatin immunoprecipitation (ChIP) assays were performed essentially as described before. In brief, chromatin in control and treated cells were cross-linked with 1% formaldehyde. Cells were incubated in lysis buffer (150 mM NaCl, 25 mM Tris pH 7.5, 1% Triton X-100, 0.1% SDS, 0.5% deoxycholate) supplemented with protease inhibitor tablet and PMSF. DNA was fragmented into ∼200 bp pieces using a Branson 250 sonicator (Brookfield, CT, United States). Aliquots of lysates containing 200 μg of protein were used for each immunoprecipitation reaction with anti-MRTF-A (Santa Cruz, sc-10768), anti-SRF (Cell Signaling Tech, 5147, Danvers, MA, United States), anti-BRG1 (Abcam, ab110641, Cambridge, United Kingdom), anti-acetyl histone H3 (Millipore, 06-599, Burlington, MA, United States), and anti-trimethyl H3K4 (Millipore, 07-442, Burlington, MA, United States). Precipitated genomic DNA was amplified by real-time PCR with the following primers: *ET1* proximal promoter, 5′-GGCGTCTGCCTCTGAAGT-3′ and 5′-GGGTAAACAGCTCCGACTT-3′. A total of 10% of the starting material is also included as the input. Data are then normalized to the input and expressed as% recovery relative the input as previously described (Chen et al., 2020b,c). All experiments were performed in triplicate wells and repeated three times.

Enzyme-Linked Immunosorbent Assay (ELISA)

Secreted endothelin in the culture media was measured by ELISA using a commercially available kit (R&D, DET100, Minneapolis, MN, United States) per vendor recommendations.

Statistical Analysis

Sample sizes reflected the minimal number needed for statistical significance based on power analysis and prior experience. Two-tailed Student's *t*-test was performed using an SPSS package. Unless otherwise specified, *p*-values smaller than 0.05 were considered statistically significant.

RESULTS

Ang II Induced Endothelin Expression Parallels GSK3 Activation

When cultured endothelial cells were exposed to Ang II treatment, ET1 expression levels were significantly up-regulated as measured by qPCR (**Figure 1A**) and ELISA (**Figure 1B**) in keeping with previous findings (Weng et al., 2015a,b; Yu et al., 2015). Of note, although GSK3β expression levels were not altered by Ang II treatment, GSK3β activity, as measured by loss of serine 9 phosphorylation, was up-regulated by Ang II treatment (**Figures 1A,C**). GSK3α is the other GSK3 isoform that shares similar structure with GSK3β but possesses distinct functions (Liang and Chuang, 2006). By comparison, neither expression nor activity of GSK3α was altered by Ang II treatment (**Figures 1A,C**).

GSK3 Is Essential for Ang II Induced Endothelin Expression

We asked whether GSK3 activation and endothelin expression was correlative or causative. In the first set of experiments, endogenous GSK3 was depleted with two separate pairs of siRNAs; GSK3 knockdown markedly attenuated Ang II induced endothelin expression (**Figures 2A,B**). In the second set of experiments, a specific GSK3 inhibitor (LY2090314) was added to the cells in the presence of Ang II; GSK3 inhibition by LY2090314 ameliorated endothelin induction in a dose-dependently manner (**Figures 2C,D**).

Next, we asked whether regulation of endothelin expression by GSK3 occurred at the transcriptional level. To this end, an *ET1* promoter-luciferase construct was transfected into EAhy926 cells with or without a constitutively active (CA) GSK3β (S9A) or a

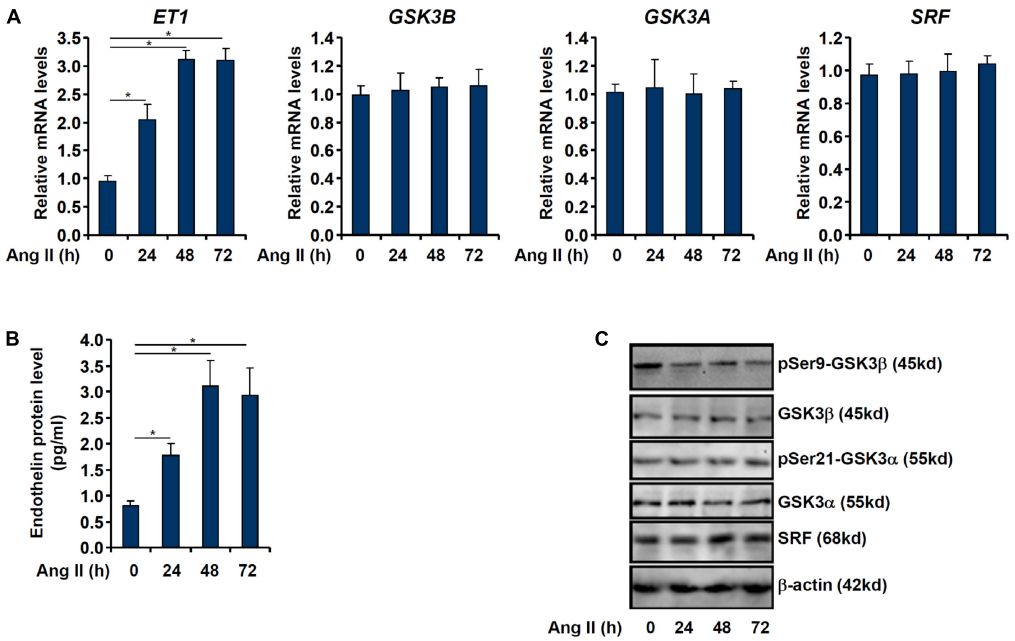

FIGURE 1 | Ang II induced endothelin expression parallels GSK3 activation. EAhy926 cells were treated with Ang II (0.1 μM) and harvested at indicated time points. Endothelin expression levels were examined by qPCR **(A)** and ELISA **(B)**. GSK3 phosphorylation was examined by Western **(C)**. Error bars represent SD (*$p < 0.05$, two-way Student's *t*-test). All experiments were repeated three times and one representative experiment is shown.

dominant negative (DN) GSK3β (S9D). As shown in **Figure 2E**, over-expression of GSK3β CA enhanced the activation of the *ET1* promoter whereas over-expression of GSK3β DN dampened the activation of the *ET1* promoter. Interestingly, the effect of GSK3β on the *ET1* promoter seemed to rely on the SRF site located between −48 and −41 relative to the transcription start site (Yang et al., 2013) as mutagenesis of this site completely abrogated the response of the *ET1* promoter to GSK3β over-expression (**Figure 2F**).

GSK3 Interacts With and Phosphorylates SRF in Endothelial Cells

Previously, Li et al. (2014) have reported that SRF can be phosphorylated by GSK3β in neurons to promote axonal growth. Immunoprecipitation assay was performed to verify GSK3β could interact with SRF in endothelial cells. EAhy926 cells were transduced with adenovirus carrying FLAG-tagged SRF and/or GFP-tagged GSK3β. An anti-FLAG could precipitate both SRF and GSK3β only when both were over-expressed thus confirming that SRF and GSK3β could interact with each other in endothelial cells (**Figure 3A**). Although Ang II treatment did not affect SRF expression levels in endothelial cells (**Figures 1A,C**), it significantly up-regulated SRF phosphorylation levels (**Figure 3B**). Based on these observations, we hypothesized that GSK3β might phosphorylate SRF to participate in ET1 transcription. As shown in **Figure 3C**, over-expression of GFP-tagged GSK3β CA alone was sufficient to augment SRF phosphorylation in the absence of Ang II whereas over-expression of GFP-tagged GSK3β DN suppressed Ang II-induced SRF phosphorylation. In addition, knockdown of endogenous GSK3β by siRNAs or GSK3β inhibition by a small-molecule compound (LY2090314) comparably attenuated SRF phosphorylation by Ang II treatment (**Figures 3D,E**).

Phosphorylation of SRF by GSK3 Is Essential for Ang II Induced Endothelin Expression

Next, we evaluated the relevance of GSK3β-mediated SRF phosphorylation in ET1 transcription. In the reporter assay, it was observed that over-expression of a phosphomimetic SRF (S234D) enhanced trans-activation of the ET1 promoter by Ang II whereas over-expression of a phosphor-defective SRF (S234A) weakened ET1 trans-activation (**Figure 4A**). Next, endogenous SRF in endothelial cells was depleted by siRNAs followed by re-introduction of ectopic SRF via adenviral transduction (**Figure 4B**). As shown in **Figures 4C,D**, whereas SRF depletion attenuated Ang II induced ET1 expression, introduction of SRF S234D more than compensated for the loss of endogenous SRF by restoring ET1 induction; SRF S234A, however, failed to recover the reduction of ET1 expression. In the next set of experiments, wild type (WT) or the phosphomimetic (S234D) SRF was over-expressed in SRF-depleted endothelial cells followed by GSK3β knockdown or inhibition. Whereas GSK3β knockdown or inhibition completely deprived the ability of WT SRF to rescue ET1 expression in SRF-depleted endothelial cells, the phosphomimetic SRF was refractory to the manipulation of GSK3β expression/activity (**Figures 4E–H**). Taken together, these data point to an interplay between

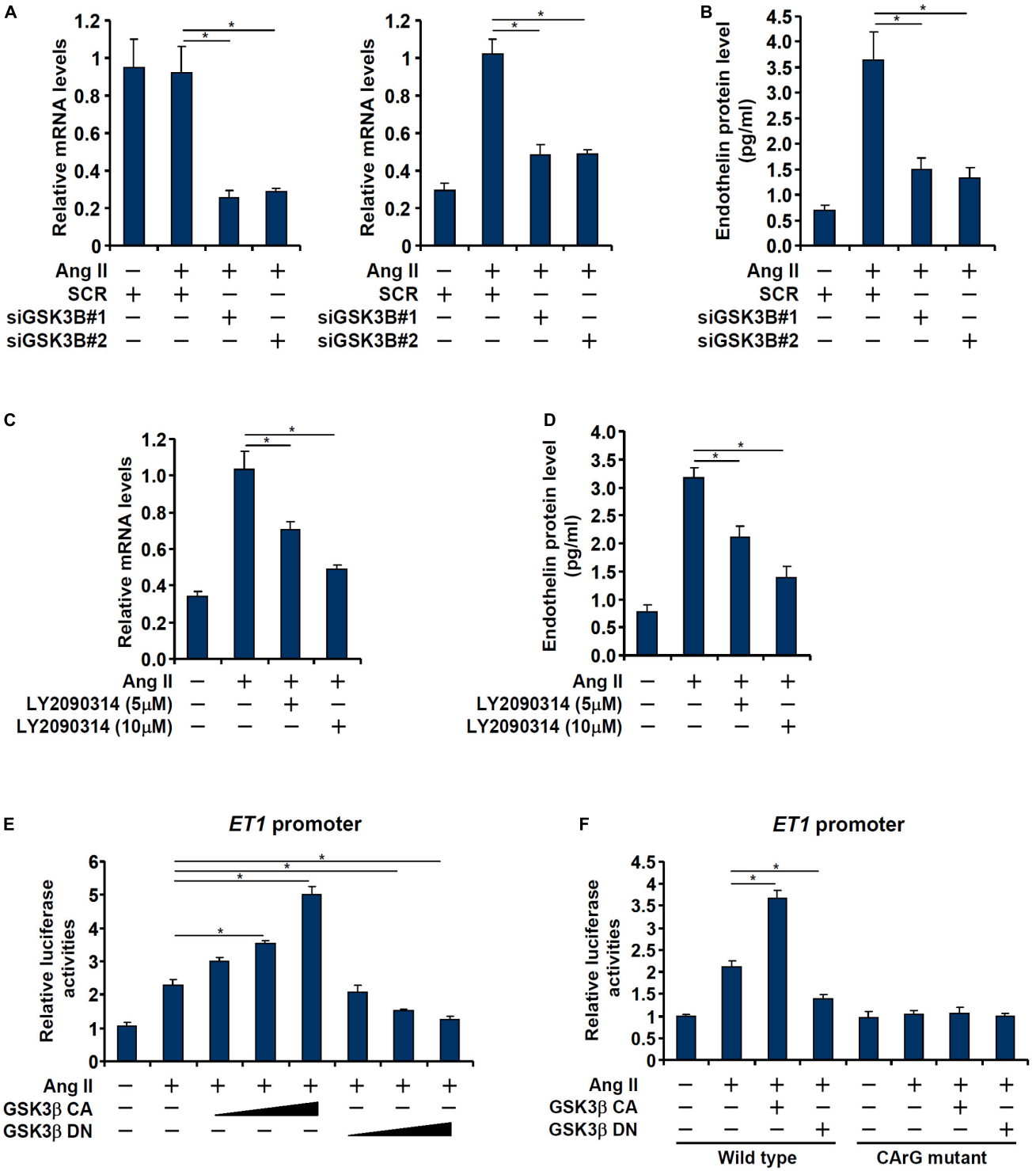

FIGURE 2 | GSK3 is essential for Ang II induced endothelin expression. **(A,B)** EAhy926 cells were transfected with siRNAs targeting GSK3β or scrambled siRNA (SCR) followed by treatment with Ang II (0.1 μM) for 48 h. Endothelin expression was examined by qPCR and ELISA. **(C,D)** EAhy926 cells were treated with Ang II (0.1 μM) with or without LY2090314 for 48 h. Endothelin expression was examined by qPCR and ELISA. **(E)** An *ET1* promoter-luciferase construct was transfected into EAhy926 cells with indicated GSK3 expression constructs followed by treatment with Ang II (0.1 μM) for 48 h. Luciferase activities were normalized by protein concentration and GFP fluorescence. **(F)** Wild type or mutant *ET1* promoter-luciferase construct was transfected into EAhy926 cells with indicated GSK3 expression constructs followed by treatment with Ang II (0.1 μM) for 48 h. Luciferase activities were normalized by protein concentration and GFP fluorescence. Error bars represent SD (*$p < 0.05$, two-way Student's *t*-test). All experiments were repeated three times and one representative experiment is shown.

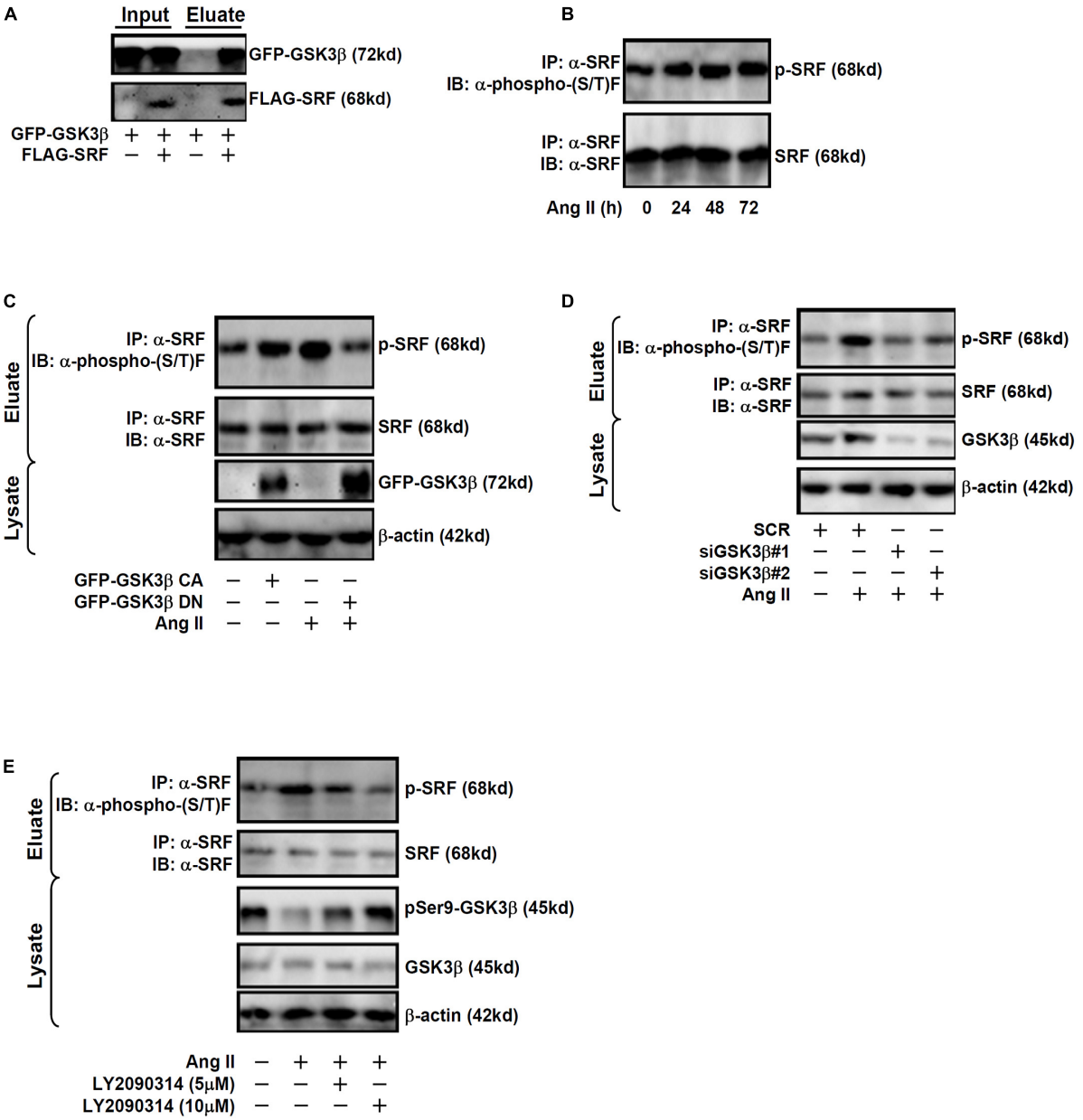

FIGURE 3 | GSK3 interacts with and phosphorylates SRF in endothelial cells. **(A)** EAhy926 cells were transduced with FLAG-tagged SRF and GFP-tagged GSK3β followed by treatment with Ang II (0.1 μM). Immunoprecipitation was performed with anti-FLAG. **(B)** EAhy926 cells were treated with Ang II (0.1 μM) and harvested at indicated time points. Immunoprecipitation was performed with anti-SRF. **(C)** EAhy926 cells were transduced with adenovirus carrying GFP-tagged GSK3β CA or GSK3β DN followed by treatment with Ang II (0.1 μM). Immunoprecipitation was performed with anti-SRF. **(D)** EAhy926 cells were transfected with siRNAs targeting GSK3β or scrambled siRNA (SCR) followed by treatment with Ang II (0.1 μM) for 48 h. Immunoprecipitation was performed with anti-SRF. **(E)** EAhy926 cells were treated with Ang II (0.1 μM) with or without LY2090314 for 48 h. Immunoprecipitation was performed with anti-SRF.

SRF and GSK3β that contributes to Ang II induced ET1 transactivation.

Phosphorylation of SRF by GSK3 Is Essential for Co-factor Recruitment

Consistent with our prior observation (Yang et al., 2013), chromatin immunoprecipitation (ChIP) assay showed that Ang II treatment significantly enhanced the occupancies of SRF (**Figure 5A**) and MRTF-A (**Figure 5B**), a key co-activator of SRF, on the ET1 promoter. GSK3β depletion did not affect SRF binding (**Figure 5A**) but markedly dampened the binding of MRTF-A (**Figure 5B**). Typically, active transcription is associated with enrichment of trimethylated H3K4 (H3K4Me3) on the gene promoters (Shilatifard, 2012). On the contrary, transcriptional repression can be measured by enrichment

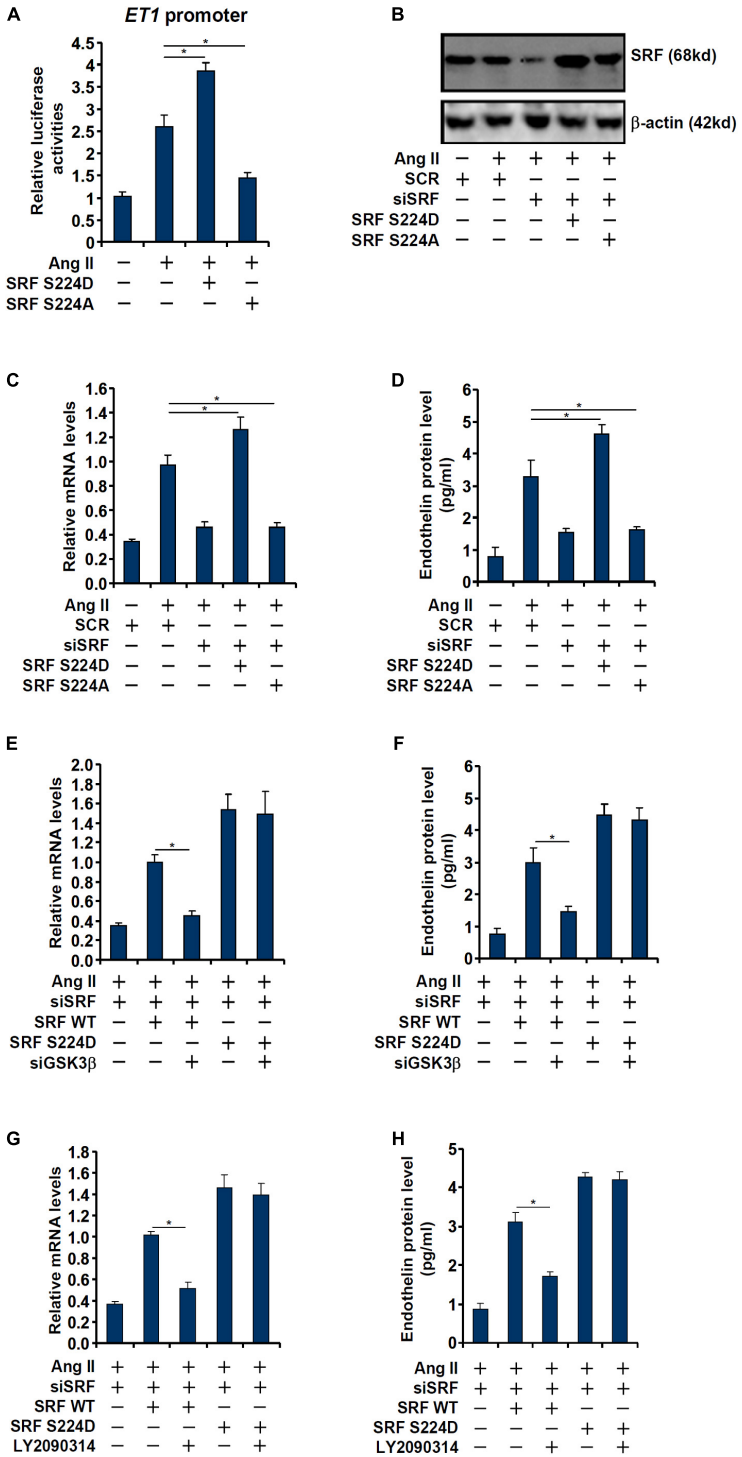

FIGURE 4 | Phosphorylation of SRF by GSK3 is essential for Ang II induced endothelin expression. **(A)** An *ET1* promoter-luciferase construct was transfected into EAhy926 cells with indicated SRF expression constructs (S224A or S224D) followed by treatment with Ang II (0.1 μM) for 48 h. Luciferase activities were normalized by protein concentration and GFP fluorescence. **(B–D)** EAhy926 cells were transfected with siRNA targeting SRF followed by transduction with adenoviral SRF expression constructs (S224A or S224D) and treatment with Ang II (0.1 μM) for 48 h. SRF expression was examined by Western. Endothelin expression was examined by qPCR and ELISA. **(E,F)** EAhy926 cells were transfected with siRNA targeting SRF/GSK3β followed by transduction with adenoviral SRF expression constructs (WT or S224D) and treatment with Ang II (0.1 μM) for 48 h. Endothelin expression was examined by qPCR and ELISA. **(G,H)** EAhy926 cells were transfected with siRNA targeting SRF followed by transduction with adenoviral SRF expression constructs (WT or S224D) and treatment with Ang II (0.1 μM) and LY2090314 for 48 h. Endothelin expression was examined by qPCR and ELISA. Error bars represent SD (*$p < 0.05$, two-way Student's *t*-test). All experiments were repeated three times and one representative experiment is shown.

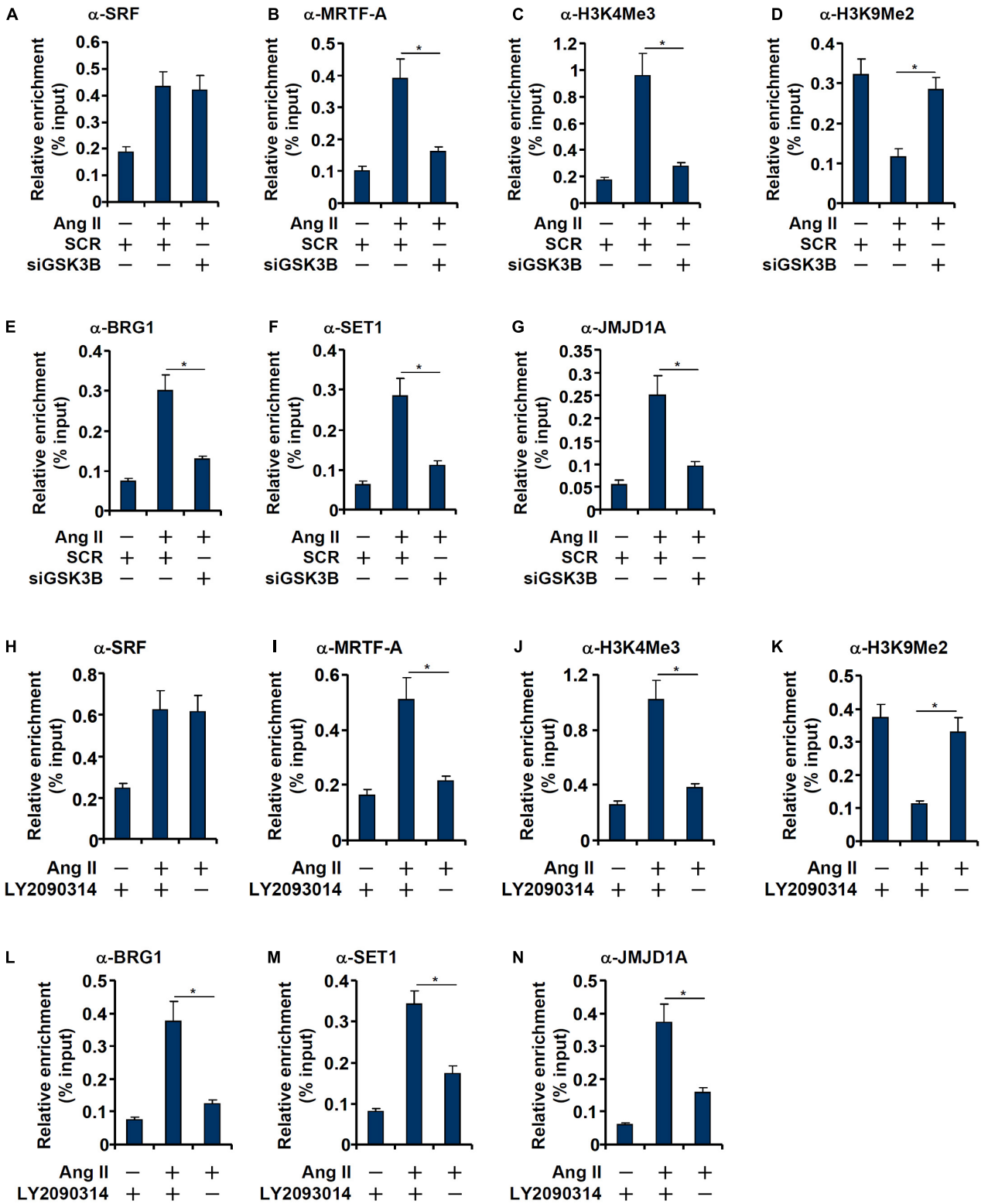

FIGURE 5 | GSK3 knockdown or inhibition attenuates recruitment of co-factors to the ET1 promoter. **(A–G)** EAhy926 cells were transfected with siRNAs targeting GSK3β or scrambled siRNA (SCR) followed by treatment with Ang II (0.1 μM) for 48 h. ChIP assays were performed with anti-SRF, anti-MRTF-A, anti-H3K4Me3, anti-H3K9Me2, anti-BRG1, anti-SET1, and anti-JMJD1A. **(H–N)** EAhy926 cells were treated with Ang II (0.1 μM) with or without LY2090314. ChIP assays were performed with anti-SRF, anti-MRTF-A, anti-H3K4Me3, anti-H3K9Me2, anti-BRG1, anti-SET1, and anti-JMJD1A. Error bars represent SD (*$p < 0.05$, two-way Student's *t*-test). All experiments were repeated three times and one representative experiment is shown.

of dimethylated H3K9 (H3K9Me2) on the gene promoters (Piunti and Shilatifard, 2021). Previous studies have shown that SRF interacts with MRTF-A to regulate transcription by differentially modulating histone methylation levels (Kong et al., 2019a,b). ChIP assays showed that Ang II treatment triggered an increase in H3K4Me3 (**Figure 5C**) and a simultaneous decrease in H3K9Me2 (**Figure 5D**) on the ET1 promoter, both of which were reversed by GSK3β depletion. Consistently, the epigenetic factors involved in catalyzing these characteristic histone modifications, namely BRG1 (**Figure 5E**), SET1 (**Figure 5F**), and JMJD1A (**Figure 5G**), were similarly recruited to the ET1 promoter upon Ang II treatment but disrupted by GSK3β knockdown. In the second set of experiments, LY2090314 was added to the endothelial cells to inhibit GSK3β activity: GSK3b inhibition similarly led to dampened recruitment of MRTF-A (**Figure 5I**), BRG1 (**Figure 5L**), SET1 (**Figure 5M**), and JMJD1A (**Figure 5N**), erasure of trimethyl H3K4 (**Figure 5J**), and accumulation of dimethyl H3K9 (**Figure 5K**) without influencing SRF binding (**Figure 5H**) to the ET1 promoter.

Next, we performed Re-ChIP assay to evaluate whether GSK3-mediated SRF phosphorylation might be necessary for the assembly of a transcriptional complex on the ET1 promoter. As shown in **Figure 6A**, in the presence of WT SRF, Ang

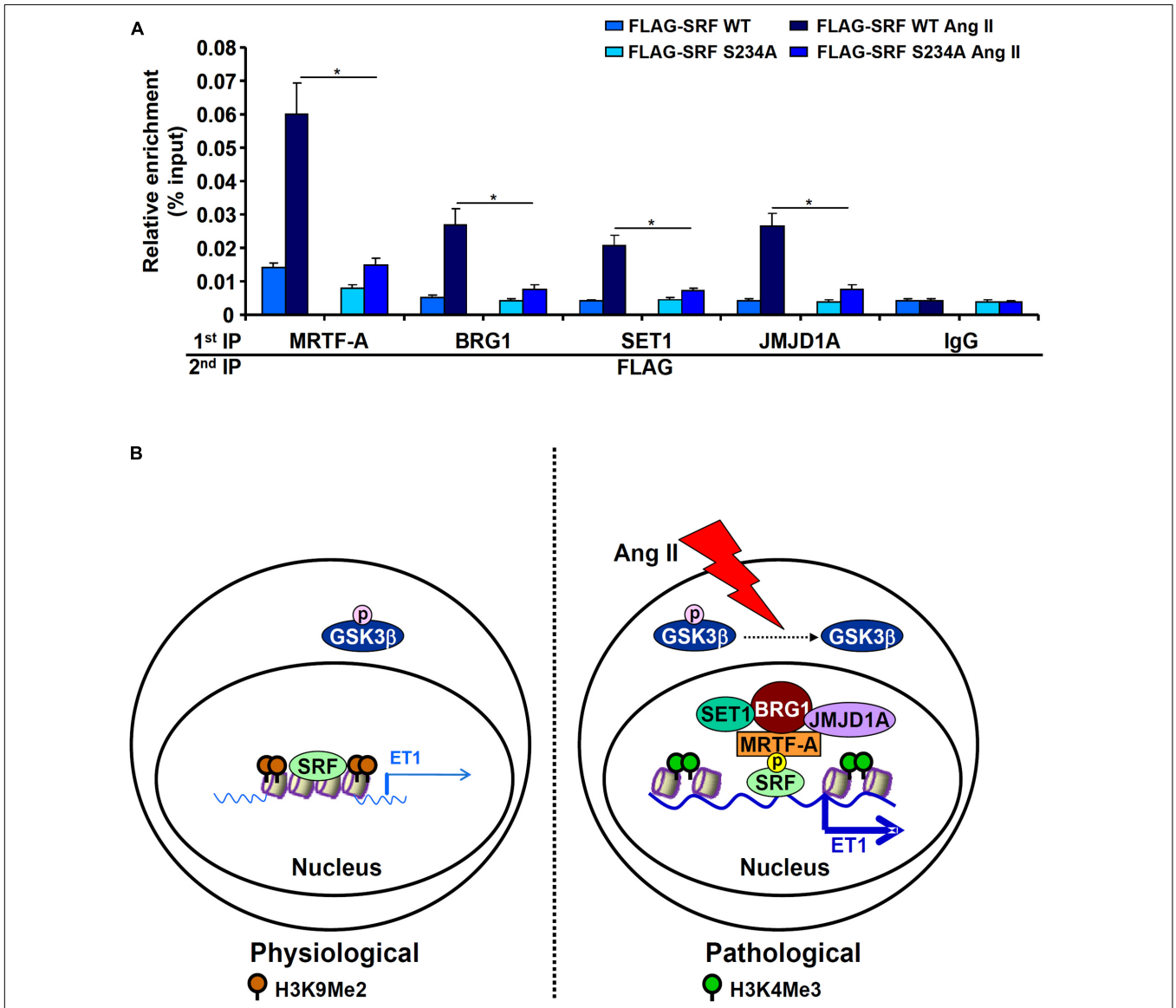

FIGURE 6 | GSK3-mediated SRF phosphorylation licenses the assembly a transcriptional complex to activate endothelin expression. **(A)** EAhy926 cells were transfected with siRNA targeting SRF followed by transduction with adenoviral SRF expression constructs and treatment with Ang II (0.1 μM) for 48 h. Re-ChIP assays were performed with indicated antibodies. Error bars represent SD (*$p < 0.05$, two-way Student's *t*-test). All experiments were repeated three times and one representative experiment is shown. **(B)** A schematic model.

II treatment stimulated the assembly of an SRF-centered complex that contained MRTF-A, BRG1, SET1, and JMJD1A. When replaced by a phosphorylation-defective SRF (S234A), incorporation of co-factors into this transcriptional complex was severely compromised. Taken together, these data support a model wherein GSK3-mediated SRF phosphorylation licenses the assembly of a transcriptional complex to activate endothelin expression (**Figure 6B**).

DISCUSSION

Post-translational modifications play a key role in the regulation of cardiovascular diseases (Smith and White, 2014; Gajjala et al., 2015; Fert-Bober et al., 2018). Alteration of SRF activity contributes to the disruption of cardiovascular homeostasis and is associated with a wide range of cardiovascular diseases (Miano, 2010). SRF relies on its interaction with co-factors to orchestrate specific transcriptional events and participate in disease pathogenesis (Onuh and Qiu, 2020). Based on our findings here, we propose a model in which phosphorylation of SRF by GSK3β mediates Ang II induced *ET1* transcription (**Figure 6B**).

We show here that GSK3β is activated by Ang II treatment in endothelial cells. This observation is consistent with a previous report by Zhang et al. (2017) showing that Ang II treatment activates GSK3β in human primary umbilical endothelial cells. Similarly, blockade of Ang II signaling by a specific angiotensin II receptor antagonist Telmisartan inhibits GSK3β activity in endothelial cells (Song et al., 2017). On the contrary, Ang II infusion seems to have an inhibitory effect on GSK3β in cardiomyocytes (Li et al., 2005) and smooth muscle cells (Cuevas et al., 2015). One possible explanation could be that differential expression levels of angiotensin receptor 1 (AT1) and 2 (AT2) in these cells because AT1 and AT2 often exert opposing roles once engaged by angiotensin II (Kaschina et al., 2017).

Our data suggest that GSK3β may contribute to ET1 transcription via SRF phosphorylation. These data, however, leave the door open to alternative interpretations. First, SRF phosphorylation status is influenced by multiple kinases other than GSK3β. For instance, SRF can be phosphorylated by MK2 at serine residue 103, which enhances its DNA binding activity (Heidenreich et al., 1999). Because MK2 can be placed downstream of Ang II and MK2 completely abrogates Ang II induced organ damage *in vivo* (Bao et al., 2007), it is plausible that Ang II may induce ET1 transcription through MK2-mediated SRF phosphorylation. Alternatively, phosphorylation of SRF at threonine residue 160 by CaMKII potentiates its DNA binding (Fluck et al., 2000). Mounting evidences suggests that CaMKII signaling plays an essential role mediating the pathophysiological effects of Ang II (Li et al., 2010; Prasad et al., 2015; Basu et al., 2019). It is reasonable to speculate that the ability of SRF to trans-activate ET1 expression may be attributable, at least in part, to CaMKII-catalyzed T160 phosphorylation. Second, other components of the SRF-centered transcriptional complex may be subject to GSK3β mediated phosphorylation. The Treisman laboratory has previously systemically profiled the phosphorylation status of MRTF-A in MEF cells with the finding that several serine/threonine residues may be targeted by GSK3β; collective mutation of these sites blocks nuclear translocation of MRTF-A (Panayiotou et al., 2016). BRG1, SET1, and JMJD1A all have been demonstrated to be phosphorylated under specific circumstances (Cheng et al., 2014; Padilla-Benavides et al., 2017) although it remains to be determined whether GSK3β makes a contribution.

There are a few unsolved issues that warrant further investigation. First, we focused in the present study on the effect of SRF S234 phosphorylation on ET1 transcription. It is not clear how genomewide gene expression levels would be affected by this specific modification. A recent study by Li et al. have shown that dynamic regulation of SRF serine 103 phosphorylation by RSK3 and PP2A significantly impacts phenylephrine-induced gene transcription in cardiomyocytes. Specifically, the authors demonstrate, using ChIP-seq and PRO-seq, that the phosphomimetic SRF S103D appears to promote the association of SRF with enhancers, facilitate the recruitment of the basal transcription machinery, and preferentially augment the expression of early response and hypertrophic genes (Li J. et al., 2020). Similar strategies could exploited to determine how the SRF S234D mutant influence the endothelial transcriptome. Second, the functional relevance of the present study is not entirely clear. Global deletion of GSK3β exacerbates myocardial hypertrophy possibly due to hyperproliferation of cardiomyoblast (Kerkela et al., 2008). On the other hand, GSK3β hypomorphic mice are protected from dilated cardiomyopathy and heart failure (Mohamed et al., 2016). Endothelial-specific role for GSK3β is yet to be determined. Third, although our model suggests that SRF is a primary substrate for GSK3β, it does not rule out the possibility that GSK3β may indirectly regulate SRF activity. Both SRF and its most importantly cofactor MRTF-A are modulated by cytoskeletal remodeling (Olson and Nordheim, 2010). GSK3β, by targeting multiple components of cytoskeleton, is considered a key mechanosensor in endothelial cells (Gaetani et al., 2020). Therefore, it is conceivable that GSK3β may contribute to ET1 transcription by relaying the mechanic signal to the SRF complex. Finally, although we focused the effect of SRF phosphorylation on its interaction with histone methyltransferase/demethylase, the potential involvement of histone acetyltransferases/deacetylase cannot be excluded. Several histone acetyltransferases with distinct substrate specificities including PCAF (Puttagunta et al., 2014), p300 (Kong et al., 2019b), CBP (Qiu and Li, 2002), and KAT8 (Kong et al., 2019a), have been shown to interact with SRF and participate in SRF-mediated transcriptional events. Previous studies have implicated p300 and CBP in the regulation of ET1 transcription in endothelial cells (Yamashita et al., 2001; Cianfrocca et al., 2016). It would be of interest to determine whether recruitment of CBP and/or p300 might be affected by SRF phosphorylation.

CONCLUSION

In conclusion, our data portray GSK3β as a regulator of Ang II-induced ET1 transcription in endothelial cells by licensing

the assembly of an phospho-SRF-MRTF-A-BRG1-SET1-JMJD1A complex. Further investigations are needed to solidify the role of this complex in regulating endothelial function and eventually devise novel therapeutic strategies by targeting this complex.

DATA AVAILABILITY STATEMENT

The original contributions presented in the study are included in the article/**Supplementary Material**, further inquiries can be directed to the corresponding author/s.

AUTHOR CONTRIBUTIONS

LZ conceived the project. YY, HW, HZ, XM, and YG designed and performed the experiments, and collected and analyzed the data. YX wrote the manuscript. YY and LZ secured funding and provided supervision. All authors contributed to the article and approved the submitted version.

FUNDING

This work was supported by grants from the National Natural Science Foundation of China (81870302), the Priority Academic Program Development of Jiangsu Higher Education Institutions (PAPD), and the Six Talent Peaks Project in Jiangsu Province.

SUPPLEMENTARY MATERIAL

The Supplementary Material for this article can be found online at: https://www.frontiersin.org/articles/10.3389/fcell.2021.698254/full#supplementary-material

REFERENCES

Abman, S. H. (2009). Role of endothelin receptor antagonists in the treatment of pulmonary arterial hypertension. *Annu. Rev. Med.* 60, 13–23. doi: 10.1146/annurev.med.59.110106.212434

Bao, W., Behm, D. J., Nerurkar, S. S., Ao, Z., Bentley, R., Mirabile, R. C., et al. (2007). Effects of p38 MAPK Inhibitor on angiotensin II-dependent hypertension, organ damage, and superoxide anion production. *J. Cardiovasc. Pharmacol.* 49, 362–368. doi: 10.1097/FJC.0b013e318046f34a

Basu, U., Case, A. J., Liu, J., Tian, J., Li, Y. L., and Zimmerman, M. C. (2019). Redox-sensitive calcium/calmodulin-dependent protein kinase IIalpha in angiotensin II intra-neuronal signaling and hypertension. *Redox Biol.* 27:101230. doi: 10.1016/j.redox.2019.101230

Bechard, M., and Dalton, S. (2009). Subcellular localization of glycogen synthase kinase 3beta controls embryonic stem cell self-renewal. *Mol. Cell. Biol.* 29, 2092–2104. doi: 10.1128/MCB.01405-08

Blaker, A. L., Taylor, J. M., and Mack, C. P. (2009). PKA-dependent phosphorylation of serum response factor inhibits smooth muscle-specific gene expression. *Arterioscler. Thromb. Vasc. Biol.* 29, 2153–2160. doi: 10.1161/ATVBAHA.109.197285

Cardillo, C., Campia, U., Bryant, M. B., and Panza, J. A. (2002). Increased activity of endogenous endothelin in patients with type II diabetes mellitus. *Circulation* 106, 1783–1787. doi: 10.1161/01.cir.0000032260.01569.64

Castanares, C., Redondo-Horcajo, M., Magan-Marchal, N., ten Dijke, P., Lamas, S., and Rodriguez-Pascual, F. (2007). Signaling by ALK5 mediates TGF-beta-induced ET-1 expression in endothelial cells: a role for migration and proliferation. *J. Cell Sci.* 120, 1256–1266. doi: 10.1242/jcs.03419

Chen, B., Fan, Z., Sun, L., Chen, J., Feng, Y., Fan, X., et al. (2020a). Epigenetic activation of the small GTPase TCL contributes to colorectal cancer cell migration and invasion. *Oncogenesis* 9:86. doi: 10.1038/s41389-020-00269-9

Chen, B., Yuan, Y., Sun, L., Chen, J., Yang, M., Yin, Y., et al. (2020b). MKL1 Mediates TGF-β Induced RhoJ Transcription to Promote Breast Cancer Cell Migration and Invasion. *Front. Cell Dev. Biol.* 8:832. doi: 10.3389/fcell.2020.00832

Chen, B., Zhao, Q., Xu, T., Yu, L., Zhuo, L., Yang, Y., et al. (2020c). BRG1 activates PR65A transcription to regulate NO bioavailability in vascular endothelial cell. *Front. Cell Dev. Biol.* 8:774. doi: 10.3389/fcell.2020.00774

Chen, B., Zhu, Y., Chen, J., Feng, Y., and Xu, Y. (2021). Activation of TC10-Like transcription by lysine demethylase KDM4B in colorectal cancer cells. *Front. Cell Dev. Biol.* 9:617549. doi: 10.3389/fcell.2021.617549

Cheng, M. B., Zhang, Y., Cao, C. Y., Zhang, W. L., and Shen, Y. F. (2014). Specific phosphorylation of histone demethylase KDM3A determines target gene expression in response to heat shock. *PLoS Biol.* 12:e1002026. doi: 10.1371/journal.pbio.1002026

Cianfrocca, R., Tocci, P., Rosano, L., Caprara, V., Sestito, R., Di Castro, V., et al. (2016). Nuclear beta-arrestin1 is a critical cofactor of hypoxia-inducible factor-1alpha signaling in endothelin-1-induced ovarian tumor progression. *Oncotarget* 7, 17790–17804. doi: 10.18632/oncotarget.7461

Cuevas, C. A., Gonzalez, A. A., Inestrosa, N. C., Vio, C. P., and Prieto, M. C. (2015). Angiotensin II increases fibronectin and collagen I through the beta-catenin-dependent signaling in mouse collecting duct cells. *Am. J. Physiol. Renal Physiol.* 308, F358–F365. doi: 10.1152/ajprenal.00429.2014

Delerive, P., Martin-Nizard, F., Chinetti, G., Trottein, F., Fruchart, J. C., Najib, J., et al. (1999). Peroxisome proliferator-activated receptor activators inhibit thrombin-induced endothelin-1 production in human vascular endothelial cells by inhibiting the activator protein-1 signaling pathway. *Circ. Res.* 85, 394–402. doi: 10.1161/01.res.85.5.394

Dong, W., Kong, M., Zhu, Y., Shao, Y., Wu, D., Lu, J., et al. (2020). Activation of TWIST Transcription by Chromatin Remodeling Protein BRG1 Contributes to Liver Fibrosis in Mice. *Front. Cell Dev. Biol.* 8:340. doi: 10.3389/fcell.2020.00340

Dong, W., Zhu, Y., Zhang, Y., Fan, Z., Zhang, Z., Fan, X., et al. (2021). BRG1 Links TLR4 Trans-Activation to LPS-Induced SREBP1a Expression and Liver Injury. *Front. Cell Dev. Biol.* 9:617073. doi: 10.3389/fcell.2021.617073

Ely, H. A., Mellon, P. L., and Coss, D. (2011). GnRH induces the c-Fos gene via phosphorylation of SRF by the calcium/calmodulin kinase II pathway. *Mol. Endocrinol.* 25, 669–680. doi: 10.1210/me.2010-0437

Enevoldsen, F. C., Sahana, J., Wehland, M., Grimm, D., Infanger, M., and Kruger, M. (2020). Endothelin Receptor Antagonists: status Quo and Future Perspectives for Targeted Therapy. *J. Clin. Med.* 9:824. doi: 10.3390/jcm9030824

Fan, Z., Kong, M., Li, M., Hong, W., Fan, X., and Xu, Y. (2020). Brahma Related Gene 1 (Brg1) Regulates Cellular Cholesterol Synthesis by Acting as a Co-factor for SREBP2. *Front. Cell Dev. Biol.* 8:259. doi: 10.3389/fcell.2020.00259

Fert-Bober, J., Murray, C. I., Parker, S. J., and Van Eyk, J. E. (2018). Precision Profiling of the Cardiovascular Post-Translationally Modified Proteome: where There Is a Will, There Is a Way. *Circ. Res.* 122, 1221–1237. doi: 10.1161/CIRCRESAHA.118.310966

Fluck, M., Booth, F. W., and Waxham, M. N. (2000). Skeletal muscle CaMKII enriches in nuclei and phosphorylates myogenic factor SRF at multiple sites. *Biochem. Biophys. Res. Commun.* 270, 488–494. doi: 10.1006/bbrc.2000.2457

Franco, C. A., Mericskay, M., Parlakian, A., Gary-Bobo, G., Gao-Li, J., Paulin, D., et al. (2008). Serum response factor is required for sprouting angiogenesis and vascular integrity. *Dev. Cell* 15, 448–461. doi: 10.1016/j.devcel.2008.07.019

Gaetani, R., Zizzi, E. A., Deriu, M. A., Morbiducci, U., Pesce, M., and Messina, E. (2020). When Stiffness Matters: mechanosensing in Heart Development and Disease. *Front. Cell Dev. Biol.* 8:334. doi: 10.3389/fcell.2020.00334

Gajjala, P. R., Fliser, D., Speer, T., Jankowski, V., and Jankowski, J. (2015). Emerging role of post-translational modifications in chronic kidney disease and

cardiovascular disease. *Nephrol. Dial. Transplant.* 30, 1814–1824. doi: 10.1093/ndt/gfv048

Hasdai, D., Holmes, D. R. Jr., Garratt, K. N., Edwards, W. D., and Lerman, A. (1997). Mechanical pressure and stretch release endothelin-1 from human atherosclerotic coronary arteries in vivo. *Circulation* 95, 357–362. doi: 10.1161/01.cir.95.2.357

Heidenreich, O., Neininger, A., Schratt, G., Zinck, R., Cahill, M. A., Engel, K., et al. (1999). MAPKAP kinase 2 phosphorylates serum response factor in vitro and in vivo. *J. Biol. Chem.* 274, 14434–14443. doi: 10.1074/jbc.274.20.14434

Holtz, M. L., and Misra, R. P. (2008). Endothelial-specific ablation of serum response factor causes hemorrhaging, yolk sac vascular failure, and embryonic lethality. *BMC Dev. Biol.* 8:65. doi: 10.1186/1471-213X-8-65

Hong, W., Kong, M., Qi, M., Bai, H., Fan, Z., Zhang, Z., et al. (2021). BRG1 mediates nephronectin activation in hepatocytes to promote T lymphocyte infiltration in ConA-induced hepatitis. *Front. Cell Dev. Biol.* 8:587502. doi: 10.3389/fcell.2020.587502

Imai, T., Hirata, Y., Emori, T., Yanagisawa, M., Masaki, T., and Marumo, F. (1992). Induction of endothelin-1 gene by angiotensin and vasopressin in endothelial cells. *Hypertension* 19, 753–757. doi: 10.1161/01.hyp.19.6.753

Iyer, D., Chang, D., Marx, J., Wei, L., Olson, E. N., Parmacek, M. S., et al. (2006). Serum response factor MADS box serine-162 phosphorylation switches proliferation and myogenic gene programs. *Proc. Natl. Acad. Sci. U. S. A.* 103, 4516–4521. doi: 10.1073/pnas.0505338103

Kaschina, E., Namsolleck, P., and Unger, T. (2017). AT2 receptors in cardiovascular and renal diseases. *Pharmacol. Res.* 125, 39–47. doi: 10.1016/j.phrs.2017.07.008

Kerkela, R., Kockeritz, L., Macaulay, K., Zhou, J., Doble, B. W., Beahm, C., et al. (2008). Deletion of GSK-3beta in mice leads to hypertrophic cardiomyopathy secondary to cardiomyoblast hyperproliferation. *J. Clin. Invest.* 118, 3609–3618. doi: 10.1172/JCI36245

Kong, M., Chen, X., Lv, F., Ren, H., Fan, Z., Qin, H., et al. (2019a). Serum response factor (SRF) promotes ROS generation and hepatic stellate cell activation by epigenetically stimulating NCF1/2 transcription. *Redox Biol.* 26:101302. doi: 10.1016/j.redox.2019.101302

Kong, M., Hong, W., Shao, Y., Lv, F., Fan, Z., Li, P., et al. (2019b). Ablation of serum response factor in hepatic stellate cells attenuates liver fibrosis. *J. Mol. Med.* 97, 1521–1533. doi: 10.1007/s00109-019-01831-8

Kong, M., Zhu, Y., Shao, J., Fan, Z., and Xu, Y. (2021). The Chromatin Remodeling Protein BRG1 Regulates SREBP Maturation by Activating SCAP Transcription in Hepatocytes. *Front. Cell Dev. Biol.* 9:622866. doi: 10.3389/fcell.2021.622866

Kwon, D. H., Kang, J. Y., Joung, H., Kim, J. Y., Jeong, A., Min, H. K., et al. (2021). SRF is a nonhistone methylation target of KDM2B and SET7 in the regulation of skeletal muscle differentiation. *Exp. Mol. Med.* 53, 250–263. doi: 10.1038/s12276-021-00564-4

Lee, M. E., Dhadly, M. S., Temizer, D. H., Clifford, J. A., Yoshizumi, M., and Quertermous, T. (1991). Regulation of endothelin-1 gene expression by Fos and Jun. *J. Biol. Chem.* 266, 19034–19039.

Letizia, C., Cerci, S., De Toma, G., D'Ambrosio, C., De Ciocchis, A., Coassin, S., et al. (1997). High plasma endothelin-1 levels in hypertensive patients with low-renin essential hypertension. *J. Hum. Hypertens.* 11, 447–451. doi: 10.1038/sj.jhh.1000454

Li, C. L., Sathyamurthy, A., Oldenborg, A., Tank, D., and Ramanan, N. (2014). SRF phosphorylation by glycogen synthase kinase-3 promotes axon growth in hippocampal neurons. *J. Neurosci.* 34, 4027–4042. doi: 10.1523/JNEUROSCI.4677-12.2014

Li, H., Li, W., Gupta, A. K., Mohler, P. J., Anderson, M. E., and Grumbach, I. M. (2010). Calmodulin kinase II is required for angiotensin II-mediated vascular smooth muscle hypertrophy. *Am. J. Physiol. Heart Circ. Physiol.* 298, H688–H698. doi: 10.1152/ajpheart.01014.2009

Li, H. L., Wang, A. B., Huang, Y., Liu, D. P., Wei, C., Williams, G. M., et al. (2005). Isorhapontigenin, a new resveratrol analog, attenuates cardiac hypertrophy via blocking signaling transduction pathways. *Free Radic. Biol. Med.* 38, 243–257. doi: 10.1016/j.freeradbiomed.2004.10.020

Li, J., Tan, Y., Passariello, C. L., Martinez, E. C., Kritzer, M. D., Li, X., et al. (2020). Signalosome-Regulated Serum Response Factor Phosphorylation Determining Myocyte Growth in Width Versus Length as a Therapeutic Target for Heart Failure. *Circulation* 142, 2138–2154. doi: 10.1161/CIRCULATIONAHA.119.044805

Li, N., Liu, S., Zhang, Y., Yu, L., Hu, Y., Wu, T., et al. (2020). Transcriptional activation of matricellular protein Spondin2 (SPON2) by BRG1 in vascular endothelial cells promotes macrophage chemotaxis. *Front. Cell Dev. Biol.* 8:794. doi: 10.3389/fcell.2020.00794

Li, Z., Kong, X., Zhang, Y., Yu, L., Guo, J., and Xu, Y. (2020a). Dual roles of chromatin remodeling protein BRG1 in angiotensin II-induced endothelial-mesenchymal transition. *Cell Death Dis.* 11:549. doi: 10.1038/s41419-020-02744-y

Li, Z., Zhang, Y., Yu, L., Xiao, B., Li, T., Kong, X., et al. (2020b). BRG1 Stimulates Endothelial Derived Alarmin MRP8 to Promote Macrophage Infiltration in an Animal Model of Cardiac Hypertrophy. *Front. Cell Dev. Biol.* 8:569. doi: 10.3389/fcell.2020.00569

Liang, M. H., and Chuang, D. M. (2006). Differential roles of glycogen synthase kinase-3 isoforms in the regulation of transcriptional activation. *J. Biol. Chem.* 281, 30479–30484. doi: 10.1074/jbc.M607468200

Liu, L., Zhao, Q., Lin, L., Yang, G., Yu, L., Zhuo, L., et al. (2021). Myeloid MKL1 Disseminates Cues to Promote Cardiac Hypertrophy in Mice. *Front. Cell Dev. Biol.* 9:583492. doi: 10.3389/fcell.2021.583492

Lv, F., Li, N., Kong, M., Wu, J., Fan, Z., Miao, D., et al. (2020). CDKN2a/p16 Antagonizes Hepatic Stellate Cell Activation and Liver Fibrosis by Modulating ROS Levels. *Front. Cell Dev. Biol.* 8:176. doi: 10.3389/fcell.2020.00176

Mao, L., Liu, L., Zhang, T., Qin, H., Wu, X., and Xu, Y. (2020). Histone Deacetylase 11 Contributes to Renal Fibrosis by Repressing KLF15 Transcription. *Front. Cell Dev. Biol.* 8:235. doi: 10.3389/fcell.2020.00235

Matsuzaki, K., Minami, T., Tojo, M., Honda, Y., Uchimura, Y., Saitoh, H., et al. (2003). Serum response factor is modulated by the SUMO-1 conjugation system. *Biochem. Biophys. Res. Commun.* 306, 32–38. doi: 10.1016/s0006-291x(03)00910-0

Miano, J. M. (2010). Role of serum response factor in the pathogenesis of disease. *Lab. Invest.* 90, 1274–1284. doi: 10.1038/labinvest.2010.104

Mohamed, R. M., Morimoto, S., Ibrahim, I. A., Zhan, D. Y., Du, C. K., Arioka, M., et al. (2016). GSK-3beta heterozygous knockout is cardioprotective in a knockin mouse model of familial dilated cardiomyopathy. *Am. J. Physiol. Heart Circ. Physiol.* 310, H1808–H1815. doi: 10.1152/ajpheart.00771.2015

Olson, E. N., and Nordheim, A. (2010). Linking actin dynamics and gene transcription to drive cellular motile functions. *Nat. Rev. Mol. Cell Biol.* 11, 353–365. doi: 10.1038/nrm2890

Onuh, J. O., and Qiu, H. (2020). Serum response factor-cofactor interactions and their implications in disease. *FEBS J.* 288, 3120–3134. doi: 10.1111/febs.15544

Padilla-Benavides, T., Nasipak, B. T., Paskavitz, A. L., Haokip, D. T., Schnabl, J. M., Nickerson, J. A., et al. (2017). Casein kinase 2-mediated phosphorylation of Brahma-related gene 1 controls myoblast proliferation and contributes to SWI/SNF complex composition. *J. Biol. Chem.* 292, 18592–18607. doi: 10.1074/jbc.M117.799676

Panayiotou, R., Miralles, F., Pawlowski, R., Diring, J., Flynn, H. R., Skehel, M., et al. (2016). Phosphorylation acts positively and negatively to regulate MRTF-A subcellular localisation and activity. *Elife* 5:e15460. doi: 10.7554/eLife.15460

Piunti, A., and Shilatifard, A. (2021). The roles of Polycomb repressive complexes in mammalian development and cancer. *Nat. Rev. Mol. Cell Biol.* 22, 326–345. doi: 10.1038/s41580-021-00341-1

Prasad, A. M., Morgan, D. A., Nuno, D. W., Ketsawatsomkron, P., Bair, T. B., Venema, A. N., et al. (2015). Calcium/calmodulin-dependent kinase II inhibition in smooth muscle reduces angiotensin II-induced hypertension by controlling aortic remodeling and baroreceptor function. *J. Am. Heart Assoc.* 4:e001949. doi: 10.1161/JAHA.115.001949

Puttagunta, R., Tedeschi, A., Soria, M. G., Hervera, A., Lindner, R., Rathore, K. I., et al. (2014). PCAF-dependent epigenetic changes promote axonal regeneration in the central nervous system. *Nat. Commun.* 5:3527. doi: 10.1038/ncomms4527

Qiu, P., and Li, L. (2002). Histone acetylation and recruitment of serum responsive factor and CREB-binding protein onto SM22 promoter during SM22 gene expression. *Circ. Res.* 90, 858–865. doi: 10.1161/01.res.0000016504.08608.b9

Rafii, S., Butler, J. M., and Ding, B. S. (2016). Angiocrine functions of organ-specific endothelial cells. *Nature* 529, 316–325. doi: 10.1038/nature17040

Rubens, C., Ewert, R., Halank, M., Wensel, R., Orzechowski, H. D., Schultheiss, H. P., et al. (2001). Big endothelin-1 and endothelin-1 plasma levels are correlated with the severity of primary pulmonary hypertension. *Chest* 120, 1562–1569. doi: 10.1378/chest.120.5.1562

Shilatifard, A. (2012). The COMPASS family of histone H3K4 methylases: mechanisms of regulation in development and disease pathogenesis. *Annu. Rev. Biochem.* 81, 65–95. doi: 10.1146/annurev-biochem-051710-134100

Smith, L. E., and White, M. Y. (2014). The role of post-translational modifications in acute and chronic cardiovascular disease. *Proteomics Clin. Appl.* 8, 506–521. doi: 10.1002/prca.201400052

Song, K. H., Bae, S. J., Chang, J., Park, J. H., Jo, I., Cho, K. W., et al. (2017). Telmisartan mitigates hyperglycemia-induced vascular inflammation by increasing GSK3beta-Ser(9) phosphorylation in endothelial cells and mouse aortas. *Biochem. Biophys. Res. Commun.* 491, 903–911. doi: 10.1016/j.bbrc.2017.07.134

Stow, L. R., Jacobs, M. E., Wingo, C. S., and Cain, B. D. (2011). Endothelin-1 gene regulation. *FASEB J.* 25, 16–28. doi: 10.1096/fj.10-161612

Sun, L., Chen, B., Wu, J., Jiang, C., Fan, Z., Feng, Y., et al. (2020). Epigenetic regulation of a disintegrin and metalloproteinase (ADAM) promotes colorectal cancer cell migration and invasion. *Front. Cell Dev. Biol.* 8:581692. doi: 10.3389/fcell.2020.581692

Wei, C. M., Lerman, A., Rodeheffer, R. J., McGregor, C. G., Brandt, R. R., Wright, S., et al. (1994). Endothelin in human congestive heart failure. *Circulation* 89, 1580–1586. doi: 10.1161/01.cir.89.4.1580

Weng, X., Yu, L., Liang, P., Chen, D., Cheng, X., Yang, Y., et al. (2015a). Endothelial MRTF-A mediates angiotensin II induced cardiac hypertrophy. *J. Mol. Cell. Cardiol.* 80, 23–33. doi: 10.1016/j.yjmcc.2014.11.009

Weng, X., Yu, L., Liang, P., Li, L., Dai, X., Zhou, B., et al. (2015b). A crosstalk between chromatin remodeling and histone H3K4 methyltransferase complexes in endothelial cells regulates angiotensin II-induced cardiac hypertrophy. *J. Mol. Cell. Cardiol.* 82, 48–58. doi: 10.1016/j.yjmcc.2015.02.010

Wort, S. J., Ito, M., Chou, P. C., Mc Master, S. K., Badiger, R., Jazrawi, E., et al. (2009). Synergistic induction of endothelin-1 by tumor necrosis factor alpha and interferon gamma is due to enhanced NF-kappaB binding and histone acetylation at specific kappaB sites. *J. Biol. Chem.* 284, 24297–24305. doi: 10.1074/jbc.M109.032524

Wu, T., Wang, H., Xin, X., Yang, J., Hou, Y., Fang, M., et al. (2020). An MRTF-A-Sp1-PDE5 Axis Mediates Angiotensin-II-Induced Cardiomyocyte Hypertrophy. *Front. Cell Dev. Biol.* 8:839. doi: 10.3389/fcell.2020.00839

Wu, X., Dong, W., Zhang, T., Ren, H., Wang, J., Shang, L., et al. (2020). Epiregulin (EREG) and Myocardin Related Transcription Factor A (MRTF-A) Form a Feedforward Loop to Drive Hepatic Stellate Cell Activation. *Front. Cell Dev. Biol.* 8:591246. doi: 10.3389/fcell.2020.591246

Yamashita, K., Discher, D. J., Hu, J., Bishopric, N. H., and Webster, K. A. (2001). Molecular regulation of the endothelin-1 gene by hypoxia. Contributions of hypoxia-inducible factor-1, activator protein-1, GATA-2, AND p300/CBP. *J. Biol. Chem.* 276, 12645–12653. doi: 10.1074/jbc.M011344200

Yanagisawa, M., Kurihara, H., Kimura, S., Tomobe, Y., Kobayashi, M., Mitsui, Y., et al. (1988). A novel potent vasoconstrictor peptide produced by vascular endothelial cells. *Nature* 332, 411–415. doi: 10.1038/332411a0

Yang, Y., Chen, D., Yuan, Z., Fang, F., Cheng, X., Xia, J., et al. (2013). Megakaryocytic leukemia 1 (MKL1) ties the epigenetic machinery to hypoxia-induced transactivation of endothelin-1. *Nucleic Acids Res.* 41, 6005–6017. doi: 10.1093/nar/gkt311

Yang, Y., Yang, G., Yu, L., Lin, L., Liu, L., Fang, M., et al. (2020). An Interplay Between MRTF-A and the Histone Acetyltransferase TIP60 Mediates Hypoxia-Reoxygenation Induced iNOS Transcription in Macrophages. *Front. Cell Dev. Biol.* 8:484. doi: 10.3389/fcell.2020.00484

Yu, L., Yang, G., Weng, X., Liang, P., Li, L., Li, J., et al. (2015). Histone Methyltransferase SET1 Mediates Angiotensin II-Induced Endothelin-1 Transcription and Cardiac Hypertrophy in Mice. *Arterioscler. Thromb. Vasc. Biol.* 35, 1207–1217. doi: 10.1161/ATVBAHA.115.305230

Zhang, W., Yang, R., Feng, Y., Hu, B., Zhang, J., Zhang, Q., et al. (2017). Angiotensin II degrades myeloid cell leukemia 1 in human umbilical vein endothelial cells. *IUBMB Life* 69, 321–327. doi: 10.1002/iub.1607

Zhang, Y., Wang, H., Song, M., Xu, T., Chen, X., Li, T., et al. (2020). Brahma-Related Gene 1 Deficiency in Endothelial Cells Ameliorates Vascular Inflammatory Responses in Mice. *Front. Cell Dev. Biol.* 8:578790. doi: 10.3389/fcell.2020.578790

Zhang, Z., Chen, B., Zhu, Y., Zhang, T., Zhang, X., Yuan, Y., et al. (2021). The Jumonji domain-containing histone demethylase homolog 1D/lysine demethylase 7A (JHDM1D/KDM7A) is an epigenetic activator of RHOJ transcription in breast cancer cells. *Front. Cell Dev. Biol.* 9:664375.

Conflict of Interest: The authors declare that the research was conducted in the absence of any commercial or financial relationships that could be construed as a potential conflict of interest.

Publisher's Note: All claims expressed in this article are solely those of the authors and do not necessarily represent those of their affiliated organizations, or those of the publisher, the editors and the reviewers. Any product that may be evaluated in this article, or claim that may be made by its manufacturer, is not guaranteed or endorsed by the publisher.

frontiers in Cell and Developmental Biology

BRIEF RESEARCH REPORT
published: 12 August 2021
doi: 10.3389/fcell.2021.695684

Partial Inhibition of the 6-Phosphofructo-2-Kinase/Fructose-2,6-Bisphosphatase-3 (PFKFB3) Enzyme in Myeloid Cells Does Not Affect Atherosclerosis

*Renée J. H. A. Tillie[1], Jenny De Bruijn[1], Javier Perales-Patón[2,3], Lieve Temmerman[1], Yanal Ghosheh[4], Kim Van Kuijk[1], Marion J. Gijbels[1,5,6], Peter Carmeliet[7,8,9], Klaus Ley[4,10], Julio Saez-Rodriguez[2,3] and Judith C. Sluimer[1,11]**

[1] Department of Pathology, Cardiovascular Research Institute Maastricht (CARIM), Maastricht University Medical Center, Maastricht, Netherlands, [2] Faculty of Medicine, Institute for Computational Biomedicine, Heidelberg University Hospital, Heidelberg University, Heidelberg, Germany, [3] Institute of Experimental Medicine and Systems Biology, Rheinisch-Westfälische Technische Hochschule (RWTH) Aachen University, Aachen, Germany, [4] La Jolla Institute for Immunology, San Diego, CA, United States, [5] Department of Pathology, GROW-School for Oncology and Developmental Biology, Maastricht University Medical Center, Maastricht, Netherlands, [6] Department of Medical Biochemistry, Experimental Vascular Biology, Amsterdam UMC, University of Amsterdam, Amsterdam, Netherlands, [7] Laboratory of Angiogenesis and Vascular Metabolism, Department of Oncology, Center for Cancer Biology, Vlaams Instituut voor Biotechnologie (VIB), Leuven Cancer Institute, KU Leuven, Leuven, Belgium, [8] State Key Laboratory of Ophthalmology, Zhongshan Opthalmic Center, Sun Yat-sen University, Guangzhou, China, [9] Department of Biomedicine, Aarhus University, Aarhus, Denmark, [10] Department of Bioengineering, University of California, San Diego, San Diego, CA, United States, [11] British Heart Foundation (BHF) Centre for Cardiovascular Sciences (CVS), University of Edinburgh, Edinburgh, United Kingdom

OPEN ACCESS

Edited by:
Xiaoqiang Tang,
Sichuan University, China

Reviewed by:
Mingzhi Luo,
Changzhou University, China
Dwijendra K. Gupta,
Jai Prakash Vishwavidyalaya, India

***Correspondence:**
Judith C. Sluimer
judith.sluimer@maastrichtuniversity.nl

Specialty section:
This article was submitted to Cellular Biochemistry, a section of the journal Frontiers in Cell and Developmental Biology

Received: 15 April 2021
Accepted: 26 July 2021
Published: 12 August 2021

Citation:
Tillie RJHA, De Bruijn J, Perales-Patón J, Temmerman L, Ghosheh Y, Van Kuijk K, Gijbels MJ, Carmeliet P, Ley K, Saez-Rodriguez J and Sluimer JC (2021) Partial Inhibition of the 6-Phosphofructo-2-Kinase/Fructose-2,6-Bisphosphatase-3 (PFKFB3) Enzyme in Myeloid Cells Does Not Affect Atherosclerosis. Front. Cell Dev. Biol. 9:695684. doi: 10.3389/fcell.2021.695684

Background: The protein 6-phosphofructo-2-kinase/fructose-2,6-bisphosphatase-3 (PFKFB3) is a key stimulator of glycolytic flux. Systemic, partial PFKFB3 inhibition previously decreased total plaque burden and increased plaque stability. However, it is unclear which cell type conferred these positive effects. Myeloid cells play an important role in atherogenesis, and mainly rely on glycolysis for energy supply. Thus, we studied whether myeloid inhibition of PFKFB3-mediated glycolysis in $Ldlr^{-/-}LysMCre^{+/-}Pfkfb3^{fl/fl}$ ($Pfkfb3^{fl/fl}$) mice confers beneficial effects on plaque stability and alleviates cardiovascular disease burden compared to $Ldlr^{-/-}LysMCre^{+/-}Pfkfb3^{wt/wt}$ control mice ($Pfkfb3^{wt/wt}$).

Methods and Results: Analysis of atherosclerotic human and murine single-cell populations confirmed *PFKFB3/Pfkfb3* expression in myeloid cells, but also in lymphocytes, endothelial cells, fibroblasts and smooth muscle cells. $Pfkfb3^{wt/wt}$ and $Pfkfb3^{fl/fl}$ mice were fed a 0.25% cholesterol diet for 12 weeks. $Pfkfb3^{fl/fl}$ bone marrow-derived macrophages (BMDMs) showed 50% knockdown of *Pfkfb3* mRNA. As expected based on partial glycolysis inhibition, extracellular acidification rate as a measure of glycolysis was partially reduced in $Pfkfb3^{fl/fl}$ compared to $Pfkfb3^{wt/wt}$ BMDMs. Unexpectedly, plaque and necrotic core size, as well as macrophage (MAC3), neutrophil (Ly6G) and collagen (Sirius Red) content were unchanged in advanced $Pfkfb3^{fl/fl}$ lesions. Similarly, early lesion plaque and necrotic core size and total plaque burden were unaffected.

Conclusion: Partial myeloid knockdown of PFKFB3 did not affect atherosclerosis development in advanced or early lesions. Previously reported positive effects of systemic, partial PFKFB3 inhibition on lesion stabilization, do not seem conferred by monocytes, macrophages or neutrophils. Instead, other *Pfkfb3*-expressing cells in atherosclerosis might be responsible, such as DCs, smooth muscle cells or fibroblasts.

Keywords: myeloid cells, PFKFB3, macrophage, dendritic cell, glycolysis, atherosclerosis, neutrophil, glycolysis inhibition

INTRODUCTION

Myeloid cells [i.e., monocytes, macrophages, neutrophils and dendritic cells (DCs)] play an active role in atherogenesis. Early pathogenesis of atherosclerotic plaques is characterized by activation of intimal endothelial cells (ECs) in arteries, followed by extravasation of low-density lipoprotein (LDL) cholesterol (Tabas et al., 2007). In the subendothelial space, LDL is oxidized (oxLDL) by reactive oxygen species (ROS) and enzymes (Tabas et al., 2007). This results in a pro-inflammatory response that triggers myeloid cell recruitment (Moore and Tabas, 2011; Silvestre-Roig et al., 2020). Recruited myeloid cells act in parallel to stimulate inflammation through cytokine secretion and other mechanisms. Recruited, activated neutrophils further stimulate monocyte recruitment and macrophage activation. Furthermore, neutrophils contribute to the pro-inflammatory environment by secretion of ROS and neutrophil extracellular traps (NETs), and to LDL oxidation by secreting myeloperoxidase (Silvestre-Roig et al., 2020). DCs modulate T cell responses in atherosclerosis. Additionally, recruited monocytes can differentiate into macrophages or monocyte-derived DCs (moDCs), which ingest oxLDL and become lipid-laden foam cells (Moore and Tabas, 2011; Subramanian and Tabas, 2014; Zernecke, 2015). Excess uptake of oxLDL can result in leukocyte apoptosis. In advanced disease stages, accumulation of apoptotic leukocytes in combination with decreased phagocytic clearance contributes to formation of a detrimental necrotic core (Moore and Tabas, 2011). Moreover, during atherogenesis, smooth muscle cells (SMCs) migrate into the plaque and synthesize collagen, forming a stabilizing fibrous cap. Secretion of matrix metalloproteinases, serine proteases and NETs by macrophages and neutrophils can cause fibrous cap thinning (Moore and Tabas, 2011; Silvestre-Roig et al., 2020). This increases the risk of plaque rupture, which can have detrimental consequences.

Activated neutrophils, DCs and pro-inflammatory macrophages highly depend on glycolysis for their energy production and function (Galván-Peña and O'Neill, 2014; Kumar and Dikshit, 2019; Wculek et al., 2019). During glycolysis, glucose is metabolized to pyruvate, yielding ATP and NADH (Lunt and Heiden, 2011). A rate-limiting step of glycolysis is the conversion of fructose-6-phosphate into fructose-1,6-bisphosphate, catalyzed by phosphofructokinase-1 (PFK-1). Another enzyme, 6-phosphofructo-2-kinase/fructose-2,6-bisphosphatase-3 (PFKFB3), catalyzes the conversion of fructose-6-phosphate into fructose-2,6-bisphosphate, which is an allosteric activator of PFK-1. Thus, PFKFB3 is a potent stimulator of glycolytic rate (Lunt and Heiden, 2011), and possibly an attractive target to interfere with myeloid cell function in atherogenesis.

A few studies have indeed assessed the effect of systemic administration of 3-(3-pyridinyl)-1-(4-pyridinyl)-2-propen-1-one (3PO) or derivatives to partially inhibit PFKFB3 in atherosclerosis. These studies reported decreased total plaque burden (Perrotta et al., 2020) and increased plaque stabilization, respectively (Beldman et al., 2019; Poels et al., 2020). However, as these studies entailed systemic pharmacological PFKFB3 inhibition, it is unclear which cell type confers these positive effects. Although *Pfkfb3* expression in atherosclerotic DCs and neutrophils remains to be assessed, Tawakol et al. (2015) reported increased *Pfkfb3* expression in macrophages incubated with atherosclerosis-relevant stimuli *in vitro*. This effect was exacerbated by hypoxia. Still, the *in vivo* effect of partial inhibition of PFKFB3-mediated glycolysis, specifically in myeloid cells, on atherogenesis has not been studied. Thus, we studied the hypothesis that myeloid inhibition of PFKFB3-mediated glycolysis in $Ldlr^{-/-}LysMCre^{+/-}Pfkfb3^{fl/fl}$ ($Pfkfb3^{fl/fl}$) mice confers beneficial effects on plaque stability and alleviates cardiovascular disease burden compared to $Ldlr^{-/-}LysMCre^{+/-}Pfkfb3^{wt/wt}$ control mice ($Pfkfb3^{wt/wt}$).

MATERIALS AND METHODS

Single-Cell Gene Expression Analysis

Single-cell RNA-sequencing (scRNA-seq) datasets from atherosclerotic plaques were collected from Gene Expression Omnibus (GEO) database or requested to corresponding authors: Wirka et al., 2019 (4 human specimens, GSE131780), Zernecke et al., 2020 (meta-analysis from 9 mice datasets), and van Kuijk et al., 2021 (11 pooled $Ldlr^{-/-}$ $LysMCre^{+/-}$ mice, GSE150089). Seurat R package (v3.0.1) was used as toolbox for analysis (Stuart et al., 2019) in R (v3.6.1). Single-cell

Abbreviations: 3PO, 3-(3-pyridinyl)-1-(4-pyridinyl)-2-propen-1-one; ApoE, apolipoprotein E; BMDM, bone marrow-derived macrophages; CD, cluster of differentiation; cDC, conventional dendritic cell; DAB, diaminobenzidine; DC, dendritic cell; EC, endothelial cell; ECAR, extracellular acidification rate; H&E, haematoxylin and eosin; HCD, high cholesterol diet; HIF, hypoxia inducible factor; IFN, interferon; LCM, L929-conditioned medium; LDLr, low density lipoprotein receptor; Ly6G, lymphocyte antigen 6 complex locus G6D; LysM, lysozyme M; (ox)LDL, oxidized low density lipoprotein; moDC, monocyte-derived dendritic cell; NET, neutrophil extracellular trap; pDC, plasmacytoid dendritic cell; PFK-1, phosphofructokinase-1; PFKFB, 6-phosphofructo-2-kinase/fructose-2;6-biphosphatase; ROS, reactive oxygen species; scRNA-seq, single-cell RNA sequencing; SMC, smooth muscle cell; TREM2, triggering receptor expressed on myeloid cells 2.

gene expression was normalized by library size, multiplied by a scaling factor of 10,000 and log-transformed. Original cell cluster annotations were used for analysis. *HIF1α/Hif1α* (hypoxia-inducible factor 1-alpha) transcription factor (TF) activity was estimated using DoRothEA[1] (Garcia-Alonso et al., 2019), using the TF regulons of A, B, and C confidence classes as previously described (Holland et al., 2020). For 2-group comparison between cells undergoing and not undergoing hypoxia response, cells were stratified by the third quartile (Q3) of *HIF1A/Hif1a* TF activity within each cell cluster (high > Q3, low ≤ Q3). Differential *PFKFB3/Pfkfb3* expression was performed using Wilcoxon Rank Sum test. No test was performed when the sample size of any condition was lower than 5 observations. *P*-values were adjusted for multiple testing using the Benjamini and Hochberg method. R effect sizes from Wilcoxon Rank-Sum test were calculated as Z divided by the square root of total observations. The greater the absolute r value, the greater the effect size, with positive values for an effect in cells with High *HIF1A/Hif1a* activity. Dot plots show the percentage of cells within cell clusters that express the gene (size), and average expression of each cluster scaled across clusters. Violin plots show the normalized gene expression level of each cell cluster with individual observations (each cell) as data points, 50th percentile of the distribution as a horizontal line, and sample sizes (number of cells) at the bottom. For 2-group comparisons, violin plots are split by hypoxia response stratification, with Wilcoxon test statistics of FDR-adjusted *p*-values and r effect sizes at the top. Analysis code is available at https://github.com/saezlab/Myeloid_PFKFB3_atherosclerosis.

Experimental Animals

Mouse experiments were approved by regulatory authorities of Maastricht University Medical Centre and performed in compliance with Dutch governmental guidelines and European Parliament Directive 2010/63/EU on protection of animals used for scientific purposes. Mice with a loxP-flanked *Pfkfb3* gene ($Pfkfb3^{lox/lox}$) (De Bock et al., 2013) were crossed to mice with both a LDL receptor knockout ($Ldlr^{-/-}$) to ensure atherosclerosis susceptibility, and hemizygous Cre-recombinase expression under control of the *Lyz2* gene promoter ($LysMCre^{+/-}$). *Lyz2* is highly expressed in macrophages, monocytes and neutrophils, and to a lower extent in DCs (**Supplementary Figure 1A**; Faust et al., 2000). Thus, myeloid-specific Cre-mediated excision of the *Pfkfb3* gene could be ensured. Resulting mice ($Ldlr^{-/-}LysMCre^{+/-}Pfkfb3^{fl/fl}$) are referred to as $Pfkfb3^{fl/fl}$. $Ldlr^{-/-}LysMCre^{+/-}Pfkfb3^{wt/wt}$ mice were used as controls ($Pfkfb3^{wt/wt}$). Mice were housed in the Maastricht University laboratory animal facility under standard conditions, in individually ventilated cages (GM500, Techniplast) with up to 5 animals per cage, with bedding (corncob, Technilab-BMI) and cage enrichment. Cages were changed weekly, reducing handling of mice during non-intervention periods.

[1]https://saezlab.github.io/dorothea/

Induction of Atherosclerosis and Tissue Collection

To induce atherosclerosis, 11-week-old male $Pfkfb3^{wt/wt}$ and $Pfkfb3^{fl/fl}$ mice were fed a high cholesterol diet (HCD) for 12 weeks *ad libitum*, containing 0.25% cholesterol (824171, Special Diet Services). Mice were euthanized by intraperitoneal pentobarbital injection (100 mg/kg). Blood was withdrawn from the right ventricle and centrifuged (2,100 rpm, 10 min, 4°C). Plasma aliquots were stored at −80°C. Brachiocephalic arteries (BCAs) and hearts were dissected, fixed in 1% PFA overnight and paraffin-embedded.

Plasma Cholesterol and Triglyceride Levels

Plasma cholesterol (Cholesterol FS Ecoline, 113009990314; DiaSys Diagnostic Systems GmbH) and triglyceride (FS5' Ecoline, 157609990314; DiaSys Diagnostic Systems GmbH) levels were assessed by standard enzymatic techniques, automated on the Cobas Fara centrifugal analyzer (Roche).

Histology and Immunohistochemistry

Paraffin-embedded BCA and aortic root (AR) were serially sectioned (4 μm) and stained with hematoxylin and eosin (H&E) to quantify plaque size and necrotic core content. For ARs, five consecutive H&E sections with 20 μm intervals were blinded and analyzed using computerized morphometry (Leica QWin V3, Cambridge, United Kingdom). The sum of plaque within three valves was averaged per mouse. Total plaque burden was quantified in BCA (Σ total plaque length/Σ total vessel length). Furthermore, AR atherosclerotic plaques were analyzed for macrophage content (MAC3+ area/plaque area, 553322, BD), collagen content (Sirius Red+ area/plaque area, 09400, Polyscience) and neutrophil content (Ly6G+ cells/plaque area, 551459, BD). Antigen retrieval was performed with pepsin digestion (Ly6G) or at pH 6 (MAC3, Target Retrieval Solution, S2031, DAKO). Stainings were analyzed using Leica Qwin software (V3, Cambridge United Kingdom) or QuPath V0.2.3 (Bankhead et al., 2017).

Isolation and Differentiation of Bone Marrow Cells

Femur and tibia of $Pfkfb3^{wt/wt}$ and $Pfkfb3^{fl/fl}$ mice on standard laboratory diet were dissected. Bones were flushed with PBS and cells passed through a 70 μm cell strainer.

To obtain bone marrow-derived macrophages, bone marrow cells were cultured in RPMI 1640 medium (72400047, Gibco), with 15% L929-conditioned medium, 10% fetal calf serum (FCS, FBS-12A, Capricorn Scientific) and 1% penicillin-streptomycin (15070-063, Gibco). After 7-day differentiation, BMDMs were detached with lidocaine and plated for downstream assays. For pro-inflammatory polarization of BMDMs, cells were incubated with LPS (10 ng/ml, L2880, Sigma) and IFN-γ (100 units/ml, HC1020, Hycult Biotech) for 24 h after overnight attachment.

To obtain bone marrow-derived DCs, bone marrow cells were cultured in IMDM medium (21980032, Thermo Fisher Scientific), with 5% FCS, 0.029 mM 2-mercaptoethanol, 150

ng/ml Flt3 ligand (472-FL, R&D Systems) and 1% penicillin-streptomycin for 8 days. After differentiation, DCs were detached by rinsing.

Quantitative PCR

RNA was isolated with TRIzol reagent (15596026, Thermo Fisher Scientific) according to manufacturer's protocol. RNA concentrations were determined by NanoDrop 2000 (Thermo Fisher Scientific) and reverse transcription performed following manufacturer's protocol (1708890, Bio-Rad and 04379012001, Roche). Real-time qPCR was performed using 10 ng cDNA, SYBR Green Supermix (1708885, Bio-Rad) and specific primer sets (**Supplementary Table 1**). One housekeeping gene (18s rRNA) was used to correct for different mRNA quantities between samples.

Lactate and Glucose Levels

Lactate and glucose levels in *Pfkfb3*$^{wt/wt}$ and *Pfkfb3*$^{fl/fl}$ BMDM cell culture medium were assessed after 26 h of conditioning, using a GEM Premier 4000 Analyzer and the manufacturer's protocol (Instrumentation Laboratory).

Seahorse

BMDMs were plated onto XF96 tissue culture microplates. Growth medium was replaced with glucose-free assay medium (RPMI-1640 (R1383, Sigma), 143 mM NaCl, 3 mg/L Phenol Red, 2 mM L-glutamine, in dH_2O, pH 7.35) and cells were incubated in a non-CO_2 incubator for 1 h. Thereafter, the assay was performed according to manufacturer's protocol (103020-100, Agilent), using a 10 mM glucose stimulus, with a Seahorse XF96 Analyzer (Agilent).

Statistical Analyses

Data are represented as mean ± SEM. For results besides single-cell analysis, ROUT outlier analysis was performed and subsequently, normality (Shapiro-Wilk) and equal variances (*F*-test) analysis and corresponding parametric or non-parametric testing were performed for two-independent groups. $^{*}p < 0.05$, $^{**}p < 0.01$, and $^{***}p < 0.001$.

RESULTS

Expression of *PFKFB3*/*Pfkfb3* in Human and Murine Plaques in Both Immune and Stromal Cells

We first sought to assess *PFKFB3/Pfkfb3* expression patterns in human and murine atherosclerotic plaques. The scRNA-seq dataset from human atherosclerotic coronary arteries by Wirka et al. (2019) showed *PFKFB3* expression mainly in macrophages, but also in ECs, fibroblasts and other leukocytes such as T cells (**Figure 1A**). This confirms PFKFB3 expression in human atherosclerosis, and particularly in macrophages.

Next, we analyzed murine *Pfkfb3* expression in myeloid cells specifically, from the scRNA-seq meta-analysis by Zernecke et al. (2020) including data from 9 atherosclerosis studies of murine aorta. Traditionally, macrophages were classified into pro-inflammatory M1 and anti-inflammatory M2 macrophages (Mantovani et al., 2009). However, the rise of single-cell techniques has shown that macrophage phenotypes are diverse and has led to identification of 5 main macrophage subsets in atherosclerosis: resident-like macrophages, inflammatory macrophages, foamy "triggering receptor expressed on myeloid cells" (TREM2^{hi}) macrophages, interferon (IFN)-inducible macrophages, and so-called cavity macrophages, whose transcriptome resembles that of peritoneal macrophages (Willemsen and de Winther, 2020; Zernecke et al., 2020). Furthermore, DCs can be broadly classified into moDCs, plasmacytoid DCs (pDCs) and conventional DCs (cDCs) (Eisenbarth, 2019). Interestingly, of all myeloid cells, *Pfkfb3* expression was highest in mature DCs and pDCs. Furthermore, *Pfkfb3* was expressed across the 5 main macrophage subsets, albeit by a low percentage of cells (**Figure 1B**). Aside from the aforementioned DC and macrophage subsets, *Pfkfb3* expression was confirmed in monocytes, neutrophils, cluster of differentiation (CD) 209a + moDCs and cDCs.

The meta-analysis dataset contains only myeloid data from several murine atherosclerosis models. Considering the use of *Ldlr*$^{-/-}$*LysMCre*$^{+/-}$ mice in the current study, we confirmed *Pfkfb3* expression in a scRNA-seq dataset from *Ldlr*$^{-/-}$*LysMCre*$^{+/-}$ aortic arch lesions by van Kuijk et al. (2021). Although the number of cells in this *Ldlr*$^{-/-}$*LysMCre*$^{+/-}$ dataset is low, in accordance with the meta-analysis and human datasets, *Pfkfb3* was expressed in a wide range of plaque cells, including macrophage subsets, monocytes, neutrophils, DCs and lymphocytes, but also ECs, SMCs and fibroblasts (**Figure 1C**).

In line with *in vitro* analysis of HIF1α-dependent expression of *PFKFB3* (Tawakol et al., 2015), *in vivo PFKFB3/Pfkfb3* expression was significantly increased in both human and murine atherosclerotic macrophages with high *HIF1α/Hif1α* signatures (**Figures 1D,E**). However, next to macrophages, a high *HIF1α/Hif1α* signature was associated with increased *PFKFB3/Pfkfb3* expression in human ECs, fibroblasts, B cells, neurons, NK cells, pericytes and plasma cells, and in murine CD209a+ moDCs and cDCs. Although cell number is low in some populations, these data suggest that hypoxia regulates *PFKFB3/Pfkfb3* expression *in vivo*, both in humans and mice, in a wide range of cell types.

Decreased Glycolysis and Pro-inflammatory Profile in *Pfkfb3*$^{fl/fl}$ Macrophages

To study if myeloid cells were indeed responsible for the observed effects of systemic PFKFB3 inhibition, we generated *Ldlr*$^{-/-}$ *LysMCre*$^{+/-}$*Pfkfb3*$^{fl/fl}$ (*Pfkfb3*$^{fl/fl}$) mice, using *Ldlr*$^{-/-}$ *LysMCre*$^{+/-}$*Pfkfb3*$^{wt/wt}$ mice as controls (*Pfkfb3*$^{wt/wt}$). Partial myeloid *Pfkfb3* knockdown was confirmed in *Pfkfb3*$^{fl/fl}$ versus *Pfkfb3*$^{wt/wt}$ BMDMs (50%, **Figure 2A**). As available antibodies are non-specific, confirmation of PFKFB3 knockdown on a protein level was prevented. Therefore, we further sought to obtain functional confirmation of *Pfkfb3* knockdown. The (near-)complete inhibition of glycolysis (≥ 80%) induces cell

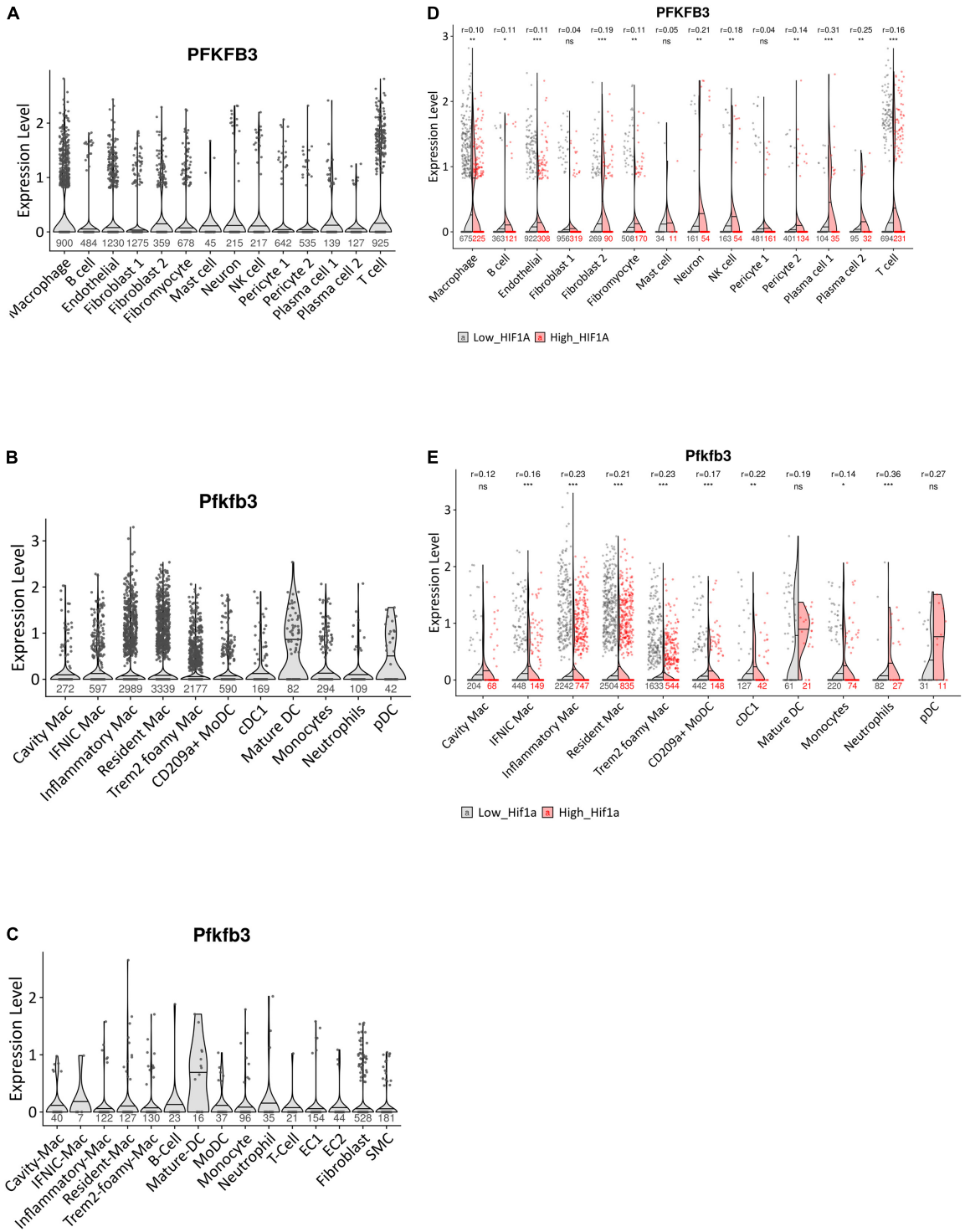

FIGURE 1 | Expression pattern of *PFKFB3/Pfkfb3* in human and murine atherosclerosis. **(A)** Violin plot of *PFKFB3* expression in single-cell populations of human atherosclerotic coronary arteries (Wirka et al., 2019). **(B)** Violin plot of *Pfkfb3* expression in single-cell populations of murine atherosclerotic myeloid cells (Zernecke et al., 2020). **(C)** Violin plot of *Pfkfb3* expression in single-cell populations of murine *Ldlr*$^{-/-}$ *LysMCre*$^{+/-}$ aortic arch lesions (van Kuijk et al., 2021). **(D)** Split violin plot of *PFKFB3* expression in cells with high versus low *HIF1*α signature from human atherosclerotic coronary arteries (Wirka et al., 2019). **(E)** Split violin plot of *Pfkfb3* expression in murine atherosclerotic myeloid cells, with high versus low *Hif1*α signature (Zernecke et al., 2020). In **(D,E)**, Wilcoxon test statistics of FDR-adjusted *p*-values and r effect sizes are indicated at the top. Sample sizes per cell type indicated under (split) violin plots. CD, cluster of differentiation; cDC, conventional dendritic cell; EC, endothelial cell; HIF1α, hypoxia-inducible factor 1-alpha; IFNIC, interferon-inducible; Mac, macrophage; moDC, monocyte-derived dendritic cell; NK cell, natural killer cell; pDC, plasmacytoid DC; SMC, smooth muscle cell; TREM2, triggering receptor expressed on myeloid cells 2. *$p < 0.05$, **$p < 0.01$, ***$p < 0.001$.

death (Schoors et al., 2014). Thus, partial glycolysis inhibition is desirable to affect cell function, without compromising cell viability. Seahorse analysis after glucose dosing revealed decreased basal extracellular acidification rate (ECAR) in *Pfkfb3*$^{fl/fl}$ BMDMs compared to controls (**Figure 2B**), indicating partially decreased glycolytic rates. During glycolysis, glucose is metabolized into pyruvate. Pyruvate can either be utilized in the tricarboxylic acid cycle to generate ATP, or metabolized into organic acids such as lactate (Lunt and Heiden, 2011). As expected based on glycolysis disruption, residual glucose levels were increased, whereas lactate levels were decreased in *Pfkfb3*$^{fl/fl}$ BMDM-conditioned medium (**Figures 2C,D**).

We previously mentioned that pro-inflammatory macrophages rely on glycolysis for their energy supply (Galván-Peña and O'Neill, 2014). As *PFKFB3* silencing using siRNA previously reduced glycolysis and pro-inflammatory activation of human macrophages (Tawakol et al., 2015), we studied the effect of *Pfkfb3* knockdown on BMDM cytokine gene expression. Indeed, already in unstimulated *Pfkfb3*$^{fl/fl}$ BMDMs, we observed increased expression of anti-inflammatory *Il10* (**Figure 2E**). Thereafter, we stimulated *Pfkfb3*$^{fl/fl}$ and *Pfkfb3*$^{wt/wt}$ BMDMs with LPS and IFN-γ to mimic the plaque pro-inflammatory phenotype of these cells and showed that partial *Pfkfb3* knockdown was maintained (60%, **Figure 2F**). Moreover, pro-inflammatory *Il6* and *Il12b* expression were decreased in *Pfkfb3*$^{fl/fl}$ versus *Pfkfb3*$^{wt/wt}$ BMDMs after pro-inflammatory stimulation (**Figures 2G,H**). These results indicate a decreased pro-inflammatory profile in *Pfkfb3*$^{fl/fl}$ macrophages, and thus confirm a role of *Pfkfb3* in pro-inflammatory macrophage polarization.

In our mouse model, Cre-recombinase expression is under control of the *Lyz2* promoter. Compared to macrophages, monocytes and neutrophils, *Lyz2* gene expression is low in DCs (**Supplementary Figure 1A**). Nevertheless, we assessed if DCs were targeted by our model, as *Pfkfb3* expression was abundant in this cell type (**Figures 1B,C**). We differentiated DCs from bone marrow cells and confirmed protein expression of the DC marker CD11c by flow cytometry (**Supplementary Figure 1B**). As expected based on lower *Lyz2* gene expression, DCs were not targeted in our model, as *Pfkfb3* expression was unchanged between *Pfkfb3*$^{fl/fl}$ and *Pfkfb3*$^{wt/wt}$ DCs (**Figure 2I**).

No Effect of Partial Myeloid *Pfkfb3* Disruption on Atherosclerosis

After confirming partial *Pfkfb3* knockdown, functional disruption of glycolysis and a decreased pro-inflammatory profile in macrophages *in vitro*, we studied the effects of myeloid *Pfkfb3* disruption on atherosclerosis. Therefore, *Pfkfb3*$^{fl/fl}$ and *Pfkfb3*$^{wt/wt}$ mice were fed a HCD for 12 weeks. We observed advanced atherosclerotic plaques in ARs with a necrotic core and fibrous cap (**Figure 3A**). Body weight and plasma cholesterol and triglyceride levels were similar between *Pfkfb3*$^{fl/fl}$ and *Pfkfb3*$^{wt/wt}$ mice after HCD (**Figures 3B–D**).

Unexpectedly, plaque and necrotic core size, as well as plaque macrophage and collagen content were unaffected in *Pfkfb3*$^{fl/fl}$ advanced AR lesions compared to controls (**Figures 3E–G**). Moreover, Ly6G+ neutrophil content was also unchanged between *Pfkfb3*$^{wt/wt}$ and *Pfkfb3*$^{fl/fl}$ AR lesions (**Figure 3H**). Similarly, no changes in plaque or necrotic core size were observed in early lesions without or with very little necrosis in BCA (**Supplementary Figure 2A**). Besides plaque size, total plaque burden, as measured by plaque index (Perrotta et al., 2020), was also unaffected in *Pfkfb3*$^{fl/fl}$ BCA (**Supplementary Figure 2B**).

Pfkfb Isoenzyme Expression in Plaque Myeloid Cells

To study potential genetic compensation by other *Pfkfb* isoenzymes keeping glycolytic rate above a certain threshold, we assessed expression of these isoenzymes in murine plaque myeloid cells. Expression of *Pfkfb1* and *Pfkfb2* was minimal in myeloid cells of the meta-analysis (**Figures 4A,B**) and *Ldlr*$^{-/-}$ *LysMCre*$^{+/-}$ datasets (**Supplementary Figures 3A,B**). Similarly to *Pfkfb3*, *Pfkfb4* was expressed in macrophage and DC subsets, monocytes and neutrophils, albeit in a small proportion of cells (**Figure 4C** and **Supplementary Figure 3C**). To assess possible genetic compensation, we determined expression of *Pfkfb1, Pfkfb2,* and *Pfkfb4* in *Pfkfb3*$^{fl/fl}$ versus *Pfkfb3*$^{wt/wt}$ BMDMs, which was unaffected (**Figure 4D**). Thus, genetic compensation by other *Pfkfb* isoenzymes seems absent in BMDMs.

DISCUSSION

The current study assessed the effect of partial myeloid *Pfkfb3* disruption on atherosclerosis *in vivo*, after 12 weeks of HCD. Collectively, our findings suggest that although myeloid *Pfkfb3* disruption decreases the pro-inflammatory macrophage profile *in vitro*, it does not affect atherosclerosis development *in vivo*, neither in advanced, nor early lesions. No effects on circulating lipids, plaque size and composition, or total plaque burden were observed.

A few studies have looked into partial pharmacological inhibition of glycolysis in atherosclerosis by targeting PFKFB3, using 3PO(-derivatives). Similar to the current study, no effect on plaque size was reported (Beldman et al., 2019; Perrotta et al., 2020; Poels et al., 2020). Although plaque size was unchanged, total plaque burden over the aorta length was reduced in 3PO-treated *ApoE*$^{-/-}$ and *ApoE*$^{-/-}$ *Fbn1*$^{C1039G\pm}$ mice (Perrotta et al., 2020). This decreased plaque occurrence was independent of changes in plaque composition, such as macrophage content, necrosis, fibrosis or angiogenesis.

In contrast, other studies did report effects of 3PO treatment on plaque composition. Plaque stability was increased, as indicated by decreased necrotic core area and a thicker fibrous cap, in *Ldlr*$^{-/-}$ mice treated with 3PO-derivative PFK158 (Poels et al., 2020). While Perrotta et al. (2020), hypothesized that decreased plaque burden after 3PO treatment was linked to decreased expression of EC adhesion molecules during early lesion development, no changes in EC adhesion molecules were observed in PFK158-treated *Ldlr*$^{-/-}$ mice (Poels et al., 2020). It was suggested that glycolysis inhibition

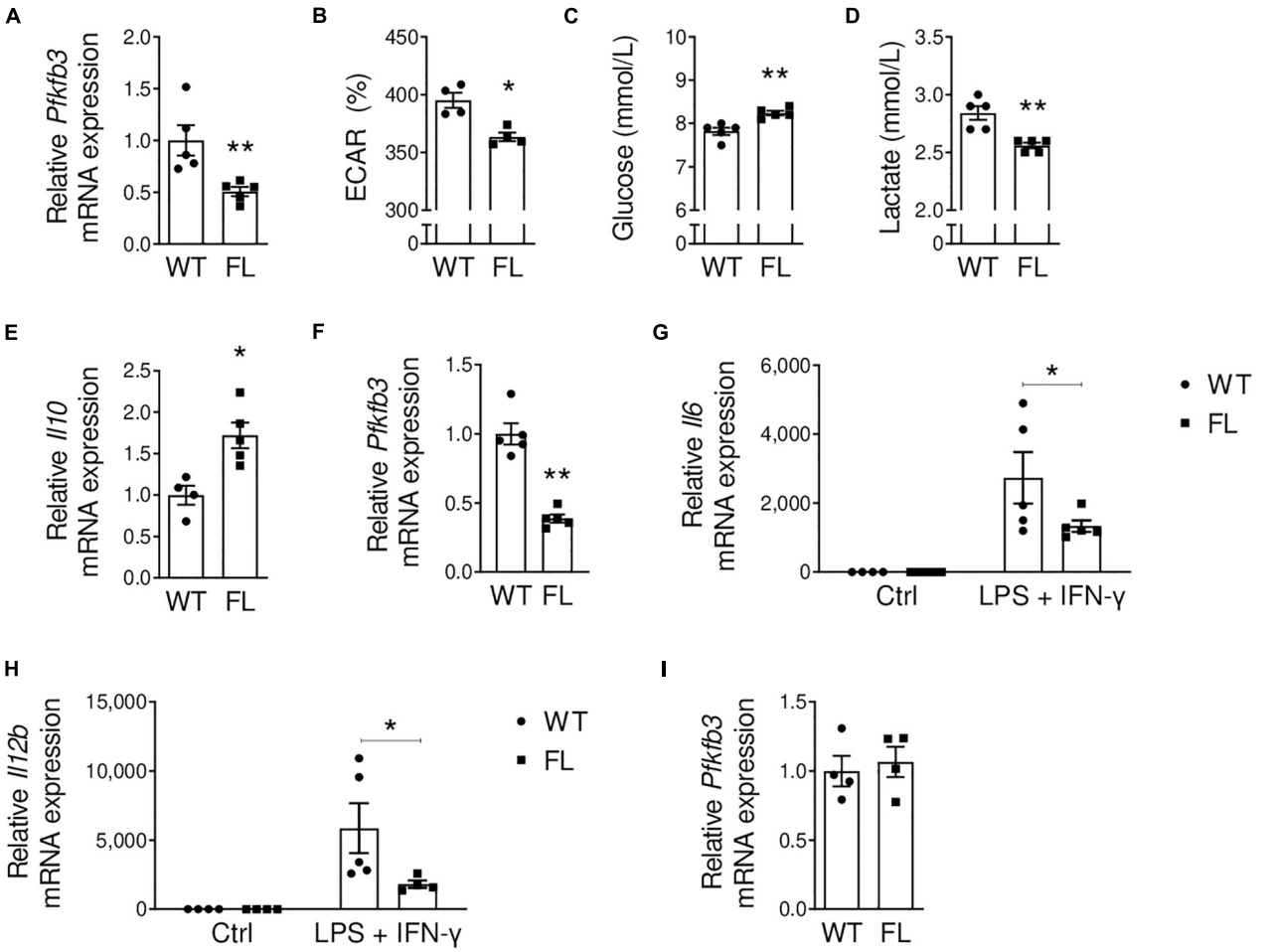

FIGURE 2 | Decreased *Pfkfb3* expression and decreased glycolysis in *Pfkfb3*$^{fl/fl}$ bone marrow-derived macrophages. **(A)** *Pfkfb3* mRNA expression in *Pfkfb3*$^{fl/fl}$ (FL) relative to *Pfkfb3*$^{wt/wt}$ (WT) bone marrow-derived macrophages (BMDM). **(B)** Extracellular acidification rate (ECAR, percentage of baseline) of *Pfkfb3*$^{fl/fl}$ and *Pfkfb3*$^{wt/wt}$ BMDMs after 10 mM glucose stimulus, as assessed with a Seahorse XF Analyzer. **(C)** Glucose and **(D)** lactate levels in *Pfkfb3*$^{fl/fl}$ and *Pfkfb3*$^{wt/wt}$ BMDM culture media after 26 h of culture. **(E)** *Il10* mRNA expression in unstimulated *Pfkfb3*$^{fl/fl}$ relative to *Pfkfb3*$^{wt/wt}$ BMDMs. **(F)** *Pfkfb3* mRNA expression in *Pfkfb3*$^{fl/fl}$ relative to *Pfkfb3*$^{wt/wt}$ BMDMs after pro-inflammatory stimulation with LPS and IFN-γ. **(G)** *Il6* and **(H)** *Il12b* mRNA expression in *Pfkfb3*$^{fl/fl}$ and *Pfkfb3*$^{wt/wt}$ BMDMs cultured without additions (ctrl; control) or stimulated with LPS and IFN-γ. Expression is relative to unstimulated *Pfkfb3*$^{wt/wt}$ BMDMs. **(I)** *Pfkfb3* mRNA expression in *Pfkfb3*$^{fl/fl}$ relative to *Pfkfb3*$^{wt/wt}$ bone marrow-derived dendritic cells. The graphs represent mean ± SEM. * $p < 0.05$, ** $p < 0.01$. Data were analyzed using Mann-Whitney U test. ECAR; extracellular acidification rate.

in macrophages and monocytes could be responsible for the observed plaque stabilization.

On the contrary, here, we show that partially decreased PFKFB3-mediated glycolysis in monocytes, macrophages and granulocytes does not affect atherogenesis. Possibly, opposing effects of *Pfkfb3* knockdown within myeloid cells and subsets, result in an absence of net effect. However, we did not observe changes in neutrophil and macrophage numbers. Thus, positive effects reported after systemic 3PO treatment are likely conferred by other myeloid or stromal cell types, that are affected by inhibition of PFKFB3-mediated glycolysis and are important in atherogenesis, such as DCs, SMCs and fibroblasts. Indeed, we show that our model does not induce *Pfkfb3* knockdown in DCs. However, *Pfkfb3* expression is high in atherosclerotic DCs, and DCs play a fundamental role in atherogenesis by contributing to activation of adaptive immunity, foam cell formation and pro-inflammatory cytokine secretion (Zhao et al., 2021). Next to DCs and other myeloid cells, through analysis of scRNA-seq datasets, we showed that fibroblasts and SMCs, but also ECs and lymphocytes express *PFKFB3/Pfkfb3* in human and murine atherosclerosis. Importantly, increased αSMA + cells, i.e., SMCs and fibroblasts, were observed upon PFK158-treatment in *Ldlr*$^{-/-}$ and upon 3PO-treatment in *ApoE*$^{-/-}$ mice (Beldman et al., 2019; Poels et al., 2020). Additionally, EC activation and dysfunction are at the center of atherogenesis, while ECs also highly depend on glycolysis (De Bock et al., 2013; Eelen et al., 2015). Both specific *PFKFB3/Pfkfb3* knockdown in ECs and 3PO treatment reduced EC sprouting *in vivo* and *in vitro,* by affecting EC migration and proliferation (De Bock et al., 2013; Schoors et al., 2014). Moreover, 3PO decreased EC activation

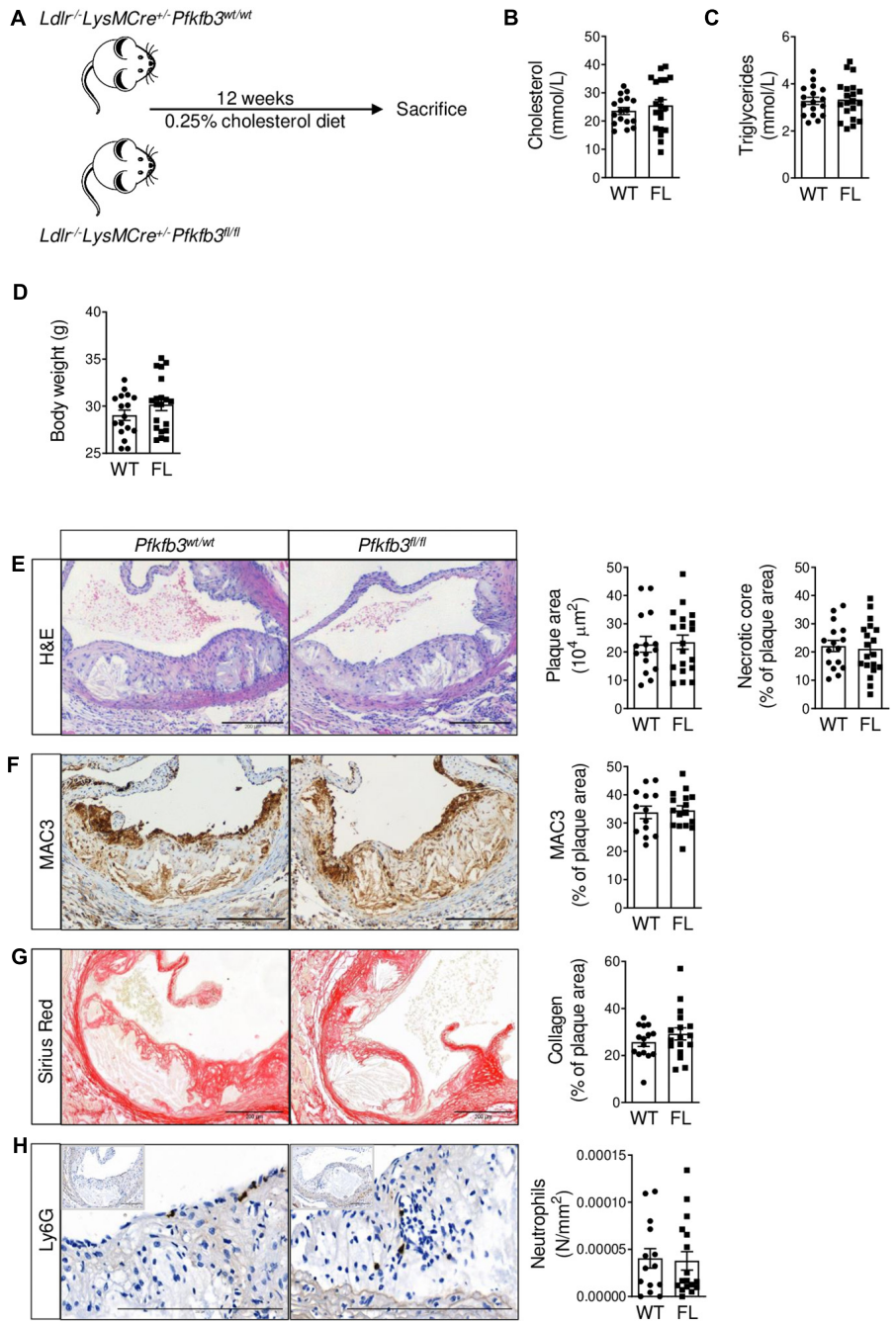

FIGURE 3 | No effect of partial myeloid *Pfkfb3* disruption on advanced atherosclerotic lesions in aortic roots. **(A)** Setup of mouse experiment using *Ldlr*$^{-/-}$ *LysMCre*$^{+/-}$*Pfkfb3*$^{fl/fl}$ (*Pfkfb3*$^{fl/fl}$, $n = 20$) and *Ldlr*$^{-/-}$ *LysMCre*$^{+/-}$*Pfkfb3*$^{wt/wt}$ (*Pfkfb3*$^{wt/wt}$, $n = 17$) mice. **(B)** Cholesterol and **(C)** triglyceride levels in *Pfkfb3*$^{wt/wt}$ (WT) and *Pfkfb3*$^{fl/fl}$ (FL) plasma. **(D)** Body weight of *Pfkfb3*$^{wt/wt}$ and *Pfkfb3*$^{fl/fl}$ mice after 12 weeks of high cholesterol diet. **(E)** H&E, **(F)** MAC3, **(G)** Sirius Red and **(H)** Ly6G staining in *Pfkfb3*$^{wt/wt}$ and *Pfkfb3*$^{fl/fl}$ AR lesions and corresponding quantifications. The graphs represent mean ± SEM. Scale bars 200 µm. Data in B and H were analyzed using Mann-Whitney U test. Data in C–G were analyzed using Student's *t*-test.

and increased endothelial barrier stability *in vitro*. However, while increasing plaque stability, 3PO treatment in *ApoE*$^{-/-}$ mice did not affect plaque endothelial barrier function (Beldman et al., 2019). Except for myeloid-specific *Pfkfb3* knockdown in the current study, effects of other cell-specific *Pfkfb3* knockdowns in atherosclerosis have not been studied yet. This could shine additional light on cell-specific effects of disrupted PFKFB3-mediated glycolysis on atherogenesis.

Another factor that might explain the lack of effect on atherosclerosis compared to studies utilizing 3PO treatment,

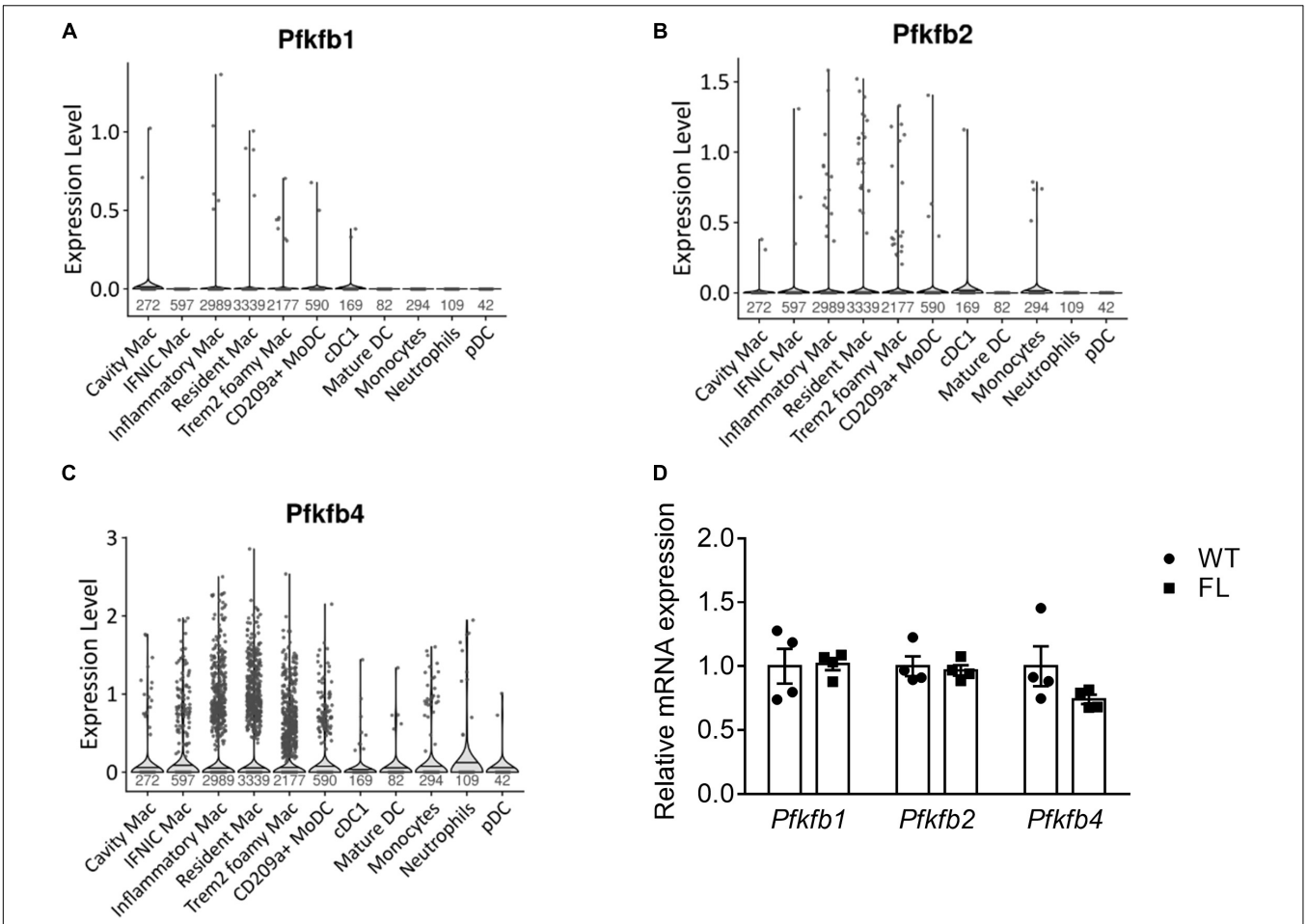

FIGURE 4 | Expression of *Pfkfb* isoenzymes in plaque cells. Violin plot of **(A)** *Pfkfb1*, **(B)** *Pfkfb2,* and **(C)** *Pfkfb4* expression in murine atherosclerotic myeloid cells (Zernecke et al., 2020). **(D)** *Pfkfb1, Pfkfb2,* and *Pfkfb4* mRNA expression in $Pfkfb3^{fl/fl}$ (FL) relative to $Pfkfb3^{wt/wt}$ (WT) BMDMs. Data in **(D)** were analyzed using Two-way ANOVA. Sample sizes per cell type indicated under violin plots. CD, cluster of differentiation; cDC, conventional dendritic cell; IFNIC, interferon-inducible; Mac, macrophage; moDC, monocyte-derived dendritic cell; pDC, plasmacytoid DC; TREM2, triggering receptor expressed on myeloid cells 2.

is recent evidence that 3PO inhibits glycolysis through intracellular acidification, rather than specific PFKFB3 inhibition (Burmistrova et al., 2019; Emini Veseli et al., 2020). Thus, one should take possible unintended off-target effects of intracellular acidification into consideration when using 3PO(-derivatives). Small molecule AZ67 does bind to PFKFB3 specifically (Boyd et al., 2015; Emini Veseli et al., 2020) and might be an interesting pharmacological inhibitor for future *in vivo* atherosclerosis studies, while keeping in mind that effects are likely not mediated by monocytes, macrophages or neutrophils.

In addition to greater relevance of PFKFB3-mediated glycolysis in other cell types in atherosclerosis, or off-target effects of reported inhibitors, other factors may explain the observed lack of effect of myeloid *Pfkfb3* inhibition on atherosclerosis.

Firstly, *Pfkfb3* knockdown in $Pfkfb3^{fl/fl}$ BMDMs is only partial (∼50–60%). The LysMCre-loxP system often results in ≥ 70% deletion efficiency in myeloid cells (Clausen et al., 1999). Efficiency of the Cre-lox system in our model could be complicated by *Pfkfb3* gene locus (Murray and Wynn, 2011). Moreover, it should be noted that although we report expression of *Pfkfb3* in atherosclerotic myeloid cells, the percentage of monocytes, neutrophils and macrophages that express *Pfkfb3* is low (∼10–20%, **Supplementary Figure 4A**). Furthermore, as PFKFB3 is merely one of several stimulators of glycolytic flux (Mor et al., 2011), *Pfkfb3* inhibition reduces glycolysis only partially, in line with previous studies that targeted PFKFB3-mediated glycolysis (De Bock et al., 2013; Schoors et al., 2014; Yetkin-Arik et al., 2019). Nevertheless, glycolysis inhibition by 3PO treatment *in vivo* is also partial (Schoors et al., 2014; Poels et al., 2020), and a similar, partial approach was very successful to change EC function *in vivo* (De Bock et al., 2013; Beldman et al., 2019).

Indeed, we focus only on PFKFB3-mediated glycolysis in the current study. Atherosclerotic plaques are associated with increased glycolytic activity (Ali et al., 2018). As glycolysis is controlled at different levels, other glycolytic regulators than PFKFB3 might be involved in this association, such as hexokinase

2, glucose transporter 1 or enolase 2, which should be studied in the future (Berg et al., 2002; Ali et al., 2018).

Another factor that could explain the lack of effect, is the possible role of other PFKFB isoenzymes. Although we showed that *Pfkfb1*, *Pfkfb2,* and *Pfkfb4* expression was unaffected in *Pfkfb3*$^{fl/fl}$ BMDMs, PFKFB isoenzyme activity could still be increased, independent of expression (Macut et al., 2019).

Finally, differences in experimental setup, gender, HCD length and composition, and vascular sites assessed may cause differences in observed effects between the current and previous studies (**Supplementary Table 2**; VanderLaan et al., 2004; Getz and Reardon, 2006; Man et al., 2020). Moreover, glycolysis inhibition using chronic gene silencing by LysMCre from embryonic stage versus acute pharmacological protein inhibition or siRNA silencing in adult mice may result in different functional outcomes and may also explain a lack of effect in the current study (Knight and Shokat, 2007). As mentioned, the selectivity of pharmacological agents is often not entirely clear.

In conclusion, we showed that partial myeloid knockdown of PFKFB3 does not affect atherosclerosis development. Positive effects of systemic, partial glycolysis inhibition on lesion stabilization or total plaque burden that were previously reported, might be conferred by other *Pfkfb3*-expressing cells such as DCs, fibroblasts, SMCs and lymphocytes. Possibly, more severe reduction of myeloid glycolysis may be needed.

DATA AVAILABILITY STATEMENT

The datasets presented in this study can be found in online repositories. The names of the repository/repositories and accession number(s) can be found in the article/ **Supplementary Material**.

ETHICS STATEMENT

The animal study was reviewed and approved by the regulatory authority of the Maastricht University Medical Centre.

AUTHOR CONTRIBUTIONS

JS, JDB, LT, and RT devised and planned the experiments. JDB, KVK, and RT carried out the experiments. JDB, KVK, MG, and RT performed the data analysis. JP-P, JS-R, YG, and KL were responsible for single-cell sequencing data analysis. PC kindly provided *Pfkfb3*$^{lox/lox}$ mice for the experiments and provided critical input to the manuscript. RT and JS wrote the manuscript. All authors reviewed and approved the manuscript.

FUNDING

JS report grants from the Dutch Organization for Scientific Research (016.116.017 VENI fellowship, and VIDI fellowship 0.16.186.364), grants from Dekker senior postdoc fellowship of the Dutch Heart Foundation 2016T060, and the Fondation Leducq (15CVD04) during the conduct of the study. JS-R report grants from JRC for Computational Biomedicine partially funded by Bayer AG., during the conduct of the study; and grants from GSK, grants from Sanofi, personal fees from Travere Therapeutics, outside the submitted work. PC report grants from Methusalem funding (Flemish government) and an ERC Advanced Research Grant (EU- ERC743074).

ACKNOWLEDGMENTS

We gratefully acknowledge excellent technical assistance by Clairy Dinjens and Jacques Debets. We would like to thank Mieke Dewerchin and Guy Eelen for reading the manuscript and providing input.

SUPPLEMENTARY MATERIAL

The Supplementary Material for this article can be found online at: https://www.frontiersin.org/articles/10.3389/fcell.2021.695684/full#supplementary-material

REFERENCES

Ali, L., Schnitzler, J. G., and Kroon, J. (2018). Metabolism: the road to inflammation and atherosclerosis. *Curr. Opin. Lipidol.* 29, 474–480. doi: 10.1097/mol.0000000000000550

Bankhead, P., Loughrey, M. B., Fernández, J. A., Dombrowski, Y., McArt, D. G., Dunne, P. D., et al. (2017). QuPath: open source software for digital pathology image analysis. *Sci. Rep.* 7:16878. doi: 10.1038/s41598-017-17204-5

Beldman, T. J., Malinova, T. S., Desclos, E., Grootemaat, A. E., Misiak, A. L. S., van der Velden, S., et al. (2019). Nanoparticle-Aided Characterization of Arterial Endothelial Architecture during Atherosclerosis Progression and Metabolic Therapy. *ACS Nano* 13, 13759–13774. doi: 10.1021/acsnano.8b08875

Berg, J. M., Tymoczko, J. L., and Stryer, L. (2002). *Biochemistry*, 5th Edn. New York: W H Freeman.

Boyd, S., Brookfield, J. L., Critchlow, S. E., Cumming, I. A., Curtis, N. J., Debreczeni, J., et al. (2015). Structure-Based Design of Potent and Selective Inhibitors of the Metabolic Kinase PFKFB3. *J. Med. Chem.* 58, 3611–3625. doi: 10.1021/acs.jmedchem.5b00352

Burmistrova, O., Olias-Arjona, A., Lapresa, R., Jimenez-Blasco, D., Eremeeva, T., Shishov, D., et al. (2019). Targeting PFKFB3 alleviates cerebral ischemia-reperfusion injury in mice. *Sci. Rep.* 9:11670. doi: 10.1038/s41598-019-48196-z

Clausen, B. E., Burkhardt, C., Reith, W., Renkawitz, R., and Förster, I. (1999). Conditional gene targeting in macrophages and granulocytes using LysMcre mice. *Transgenic Res.* 8, 265–277. doi: 10.1023/a:1008942828960

De Bock, K., Georgiadou, M., Schoors, S., Kuchnio, A., Wong, B. W., Cantelmo, A. R., et al. (2013). Role of PFKFB3-Driven Glycolysis in Vessel Sprouting. *Cell* 154, 651–663. doi: 10.1016/j.cell.2013.06.037

Eelen, G., de Zeeuw, P., Simons, M., and Carmeliet, P. (2015). Endothelial cell metabolism in normal and diseased vasculature. *Circ. Res.* 116, 1231–1244. doi: 10.1161/CIRCRESAHA.116.302855

Eisenbarth, S. C. (2019). Dendritic cell subsets in T cell programming: location dictates function. *Nat. Rev. Immunol.* 19, 89–103. doi: 10.1038/s41577-018-0088-1

Emini Veseli, B., Perrotta, P., Van Wielendaele, P., Lambeir, A. M., Abdali, A., Bellosta, S., et al. (2020). Small molecule 3PO inhibits glycolysis but does not

bind to 6-phosphofructo-2-kinase/fructose-2,6-bisphosphatase-3 (PFKFB3). *FEBS Lett.* 594, 3067–3075. doi: 10.1002/1873-3468.13878

Faust, N., Varas, F., Kelly, L. M., Heck, S., and Graf, T. (2000). Insertion of enhanced green fluorescent protein into the lysozyme gene creates mice with green fluorescent granulocytes and macrophages. *Blood* 96, 719–726.

Galván-Peña, S., and O'Neill, L. A. J. (2014). Metabolic reprograming in macrophage polarization. *Front. Immunol.* 5:420. doi: 10.3389/fimmu.2014.00420

Garcia-Alonso, L., Holland, C. H., Ibrahim, M. M., Turei, D., and Saez-Rodriguez, J. (2019). Benchmark and integration of resources for the estimation of human transcription factor activities. *Genome Res.* 29, 1363–1375. doi: 10.1101/gr.240663.118

Getz, G. S., and Reardon, C. A. (2006). Diet and Murine Atherosclerosis. *Arterioscler. Thromb. Vasc. Biol.* 26, 242–249. doi: 10.1161/01.ATV.0000201071.49029.17

Holland, C. H., Tanevski, J., Perales-Patón, J., Gleixner, J., Kumar, M. P., Mereu, E., et al. (2020). Robustness and applicability of transcription factor and pathway analysis tools on single-cell RNA-seq data. *Genome Biol.* 21:36. doi: 10.1186/s13059-020-1949-z

Knight, Z. A., and Shokat, K. M. (2007). Chemical Genetics: where Genetics and Pharmacology Meet. *Cell* 128, 425–430. doi: 10.1016/j.cell.2007.01.021

Kumar, S., and Dikshit, M. (2019). Metabolic Insight of Neutrophils in Health and Disease. *Front. Immunol.* 10:2099. doi: 10.3389/fimmu.2019.02099

Lunt, S. Y., and Heiden, M. G. V. (2011). Aerobic Glycolysis: meeting the Metabolic Requirements of Cell Proliferation. *Annu. Rev. Cell Dev. Biol.* 27, 441–464. doi: 10.1146/annurev-cellbio-092910-154237

Macut, H., Hu, X., Tarantino, D., Gilardoni, E., Clerici, F., Regazzoni, L., et al. (2019). Tuning PFKFB3 Bisphosphatase Activity Through Allosteric Interference. *Sci. Rep.* 9:20333. doi: 10.1038/s41598-019-56708-0

Man, J. J., Beckman, J. A., and Jaffe, I. Z. (2020). Sex as a Biological Variable in Atherosclerosis. *Circ. Res.* 126, 1297–1319. doi: 10.1161/CIRCRESAHA.120.315930

Mantovani, A., Garlanda, C., and Locati, M. (2009). Macrophage Diversity and Polarization in Atherosclerosis. *Arterioscler. Thromb. Vasc. Biol.* 29, 1419–1423. doi: 10.1161/ATVBAHA.108.180497

Moore, K. J., and Tabas, I. (2011). Macrophages in the pathogenesis of atherosclerosis. *Cell* 145, 341–355. doi: 10.1016/j.cell.2011.04.005

Mor, I., Cheung, E. C., and Vousden, K. H. (2011). Control of Glycolysis through Regulation of PFK1: old Friends and Recent Additions. *Cold Spring Harb. Symp. Quant. Biol.* 76, 211–216. doi: 10.1101/sqb.2011.76.010868

Murray, P. J., and Wynn, T. A. (2011). Obstacles and opportunities for understanding macrophage polarization. *J. Leukoc. Biol.* 89, 557–563. doi: 10.1189/jlb.0710409

Perrotta, P., Veken, B. V. D., Veken, P. V. D., Pintelon, I., Roosens, L., Adriaenssens, E., et al. (2020). Partial Inhibition of Glycolysis Reduces Atherogenesis Independent of Intraplaque Neovascularization in Mice. *Arterioscler. Thromb. Vasc. Biol.* 40, 1168–1181.

Poels, K., Schnitzler, J. G., Waissi, F., Levels, J. H. M., Stroes, E. S. G., Daemen, M., et al. (2020). Inhibition of PFKFB3 Hampers the Progression of Atherosclerosis and Promotes Plaque Stability. *Front. Cell Dev. Biol.* 8:581641. doi: 10.3389/fcell.2020.581641

Schoors, S., De Bock, K., Cantelmo, A. R., Georgiadou, M., Ghesquière, B., Cauwenberghs, S., et al. (2014). Partial and transient reduction of glycolysis by PFKFB3 blockade reduces pathological angiogenesis. *Cell Metab.* 19, 37–48. doi: 10.1016/j.cmet.2013.11.008

Silvestre-Roig, C., Braster, Q., Ortega-Gomez, A., and Soehnlein, O. (2020). Neutrophils as regulators of cardiovascular inflammation. *Nat. Rev. Cardiol.* 17, 327–340. doi: 10.1038/s41569-019-0326-7

Stuart, T., Butler, A., Hoffman, P., Hafemeister, C., Papalexi, E., Mauck, W. M. III, et al. (2019). Comprehensive Integration of Single-Cell Data. *Cell* 177, 1888–1902.e21. doi: 10.1016/j.cell.2019.05.031

Subramanian, M., and Tabas, I. (2014). Dendritic cells in atherosclerosis. *Semin. Immunopathol.* 36, 93–102. doi: 10.1007/s00281-013-0400-x

Tabas, I., Williams, K. J., and Borén, J. (2007). Subendothelial Lipoprotein Retention as the Initiating Process in Atherosclerosis. *Circulation* 116, 1832–1844. doi: 10.1161/CIRCULATIONAHA.106.676890

Tawakol, A., Singh, P., Mojena, M., Pimentel-Santillana, M., Emami, H., MacNabb, M., et al. (2015). HIF-1α and PFKFB3 Mediate a Tight Relationship Between Proinflammatory Activation and Anerobic Metabolism in Atherosclerotic Macrophages. *Arterioscler. Thromb. Vasc. Biol.* 35, 1463–1471. doi: 10.1161/atvbaha.115.305551

van Kuijk, K., Demandt, J. A. F., Perales-Patón, J., Theelen, T. L., Kuppe, C., Marsch, E., et al. (2021). Deficiency of myeloid PHD proteins aggravates atherogenesis via macrophage apoptosis and paracrine fibrotic signalling: atherogenic effects of myeloid PHD knockdown. *Cardiovasc. Res.* [Epub Online ahead of print]. doi: 10.1093/cvr/cvab152

VanderLaan, P. A., Reardon, C. A., and Getz, G. S. (2004). Site Specificity of Atherosclerosis. *Arterioscler. Thromb. Vasc. Biol.* 24, 12–22. doi: 10.1161/01.ATV.0000105054.43931.f0

Wculek, S. K., Khouili, S. C., Priego, E., Heras-Murillo, I., and Sancho, D. (2019). Metabolic Control of Dendritic Cell Functions: digesting Information. *Front. Immunol.* 10:775. doi: 10.3389/fimmu.2019.00775

Willemsen, L., and de Winther, M. P. (2020). Macrophage subsets in atherosclerosis as defined by single-cell technologies. *J. Pathol.* 250, 705–714. doi: 10.1002/path.5392

Wirka, R. C., Wagh, D., Paik, D. T., Pjanic, M., Nguyen, T., Miller, C. L., et al. (2019). Atheroprotective roles of smooth muscle cell phenotypic modulation and the TCF21 disease gene as revealed by single-cell analysis. *Nat. Med.* 25, 1280–1289. doi: 10.1038/s41591-019-0512-5

Yetkin-Arik, B., Vogels, I. M. C., Nowak-Sliwinska, P., Weiss, A., Houtkooper, R. H., Van Noorden, C. J. F., et al. (2019). The role of glycolysis and mitochondrial respiration in the formation and functioning of endothelial tip cells during angiogenesis. *Sci. Rep.* 9:12608. doi: 10.1038/s41598-019-48676-2

Zernecke, A. (2015). Dendritic Cells in Atherosclerosis. *Arterioscler. Thromb. Vasc. Biol.* 35, 763–770. doi: 10.1161/ATVBAHA.114.303566

Zernecke, A., Winkels, H., Cochain, C., Williams, J. W., Wolf, D., Soehnlein, O., et al. (2020). Meta-Analysis of Leukocyte Diversity in Atherosclerotic Mouse Aortas. *Circ. Res.* 127, 402–426. doi: 10.1161/circresaha.120.316903

Zhao, Y., Zhang, J., Zhang, W., and Xu, Y. (2021). A myriad of roles of dendritic cells in atherosclerosis. *Clin. Exp. Immunol.* [Epub Online ahead of print]. doi: 10.1111/cei.13634

Conflict of Interest: The authors declare that the research was conducted in the absence of any commercial or financial relationships that could be construed as a potential conflict of interest.

Publisher's Note: All claims expressed in this article are solely those of the authors and do not necessarily represent those of their affiliated organizations, or those of the publisher, the editors and the reviewers. Any product that may be evaluated in this article, or claim that may be made by its manufacturer, is not guaranteed or endorsed by the publisher.

frontiers in Cell and Developmental Biology

OPINION
published: 18 August 2021
doi: 10.3389/fcell.2021.701672

Endothelial Cell: Lactate Metabolic Player in Organ Regeneration

Lanlan Zhang[1], Xuezhen Gui[1], Xin Zhang[2], Yujing Dai[3], Xiangjun Wang[3], Xia Tong[2] and Shasha Li[4]*

[1] State Key Laboratory of Biotherapy of China, Division of Pulmonary Diseases, West China Hospital of Sichuan University, Chengdu, China, [2] Department of Gastroenterology, West China Hospital of Sichuan University, Chengdu, China, [3] First Affiliated Hospital of Sun Yat-sen University, Guangzhou, China, [4] Athinoula A. Martinos Center for Biomedical Imaging, Department of Radiology, Massachusetts General Hospital, Harvard Medical School, Boston, MA, United States

Keywords: endothelial cell, metabolism, regeneration, angiogenesis, lactate

OPEN ACCESS

Edited by:
Md. Shenuarin Bhuiyan, Louisiana State University Health Shreveport, United States

Reviewed by:
Xiao-Feng Chen, Chengdu University of Traditional Chinese Medicine, China
Jia-Hua Qu, National Institute on Aging, National Institutes of Health (NIH), United States

****Correspondence:***
Lanlan Zhang
lanlanzhangsc@gmail.com

Specialty section:
This article was submitted to Cellular Biochemistry, a section of the journal Frontiers in Cell and Developmental Biology

Received: *28 April 2021*
Accepted: *27 May 2021*
Published: *18 August 2021*

Citation:
Zhang L, Gui X, Zhang X, Dai Y, Wang X, Tong X and Li S (2021) Endothelial Cell: Lactate Metabolic Player in Organ Regeneration. Front. Cell Dev. Biol. 9:701672. doi: 10.3389/fcell.2021.701672

INTRODUCTION

Endothelial cells (ECs), as the "gatekeeper" by controlling the extravasation of circulating cells into tissues, play an essential role in regulating tissue homeostasis (Eelen et al., 2018). By altering their production of cytokines, chemokines, and adhesion molecules, endothelial cells control the traffic of immune cells into injury sites (Gerhardt and Ley, 2015). Injury or dysfunction of ECs is known to contribute to many pathologies, including metabolism-related disease, in which loss of the glycolytic activator phosphofructokinase-2/fructose-2,6-bisphosphatase isoform 3 in ECs impairs vessel formation (Li et al., 2019). Besides, ECs also contribute to homeostasis and regeneration *via* "angiocrine" signaling (Ding et al., 2014; Cao et al., 2016; Rafii et al., 2016), which secretes "angiocrine" cytokines for tissue regeneration.

Lactate (2-hydroxypropanoic acid) is divided into two types, L-lactate and D-lactate. The former is the focus of this review; L-lactate means lactate. Lactate is stored in the body and is the terminal product of anaerobic metabolism, considered a metabolic waste. In recent years, it has been discovered that lactate is not simply waste but fertilizer. However, EC's function on lactate metabolism for peripheral tissue regeneration remains to be fully elucidated.

This paper focuses on the role of endothelial–lactate interactions in regulating metabolic microenvironment on tissue regeneration and propose that endothelial–lactate interactions affect the microenvironment through two pathways except for the classical angiogenesis pathway; (1) lactate uses endothelium as a gatekeeper to regulate the microenvironment through immune cells, affecting the regeneration of the damaged tissues; (2) ECs secrete lactate to repair the organ regeneration caused by the damaged tissues.

ENDOTHELIAL CELLS "GATEKEEPER" FUNCTION FOR TISSUE REGENERATION

The role of "gatekeeper" is a vital role for ECs. ECs play an essential role in the chemotaxis of neutrophils by inflammation and the recruitment of macrophages for homeostasis. Former studies focused on the classical hypothesis that cancer cells ensure sufficient oxygen and nutrient supply for proliferation through lactate-induced secretion of vascular endothelial growth factor (VEGF), forming the new vessels (form a barrier for "gatekeeper") (Kumar et al., 2007; Longchamp et al., 2018). Lactate uses the "lactate shuttle" in ECs to shuttle between cells and affect cell differentiation in cancers (de la Cruz-López et al., 2019). Even under quiescent conditions, ECs can use glycolysis to convert glucose into lactate (De Bock et al., 2013). Simultaneously, lactate as a metabolizable

anion may lead to Cl^- egress from ECs, giving rise to ECs swelling and functional barrier changes (Hoffmann et al., 2009).

In recent years, that lactate promotes organ regeneration through ECs and that the classic lactate enhances ECs angiogenesis have been put on the agenda. ECs and lactate transporter play an essential role in lactate-induced tissue regeneration. The brain is an excellent example of lactate going through ECs for tissue regeneration for the "gatekeeper" role. Exercise can increase lactate production from skeleton muscle and promote lactate penetration through the blood–brain barrier. Morland et al. (2017) reported that high-intensity exercise induces the release of lactate from the muscle strains through the vascular endothelial lactate receptor (hydroxycarboxylic acid receptor 1) receptor. Previous studies have also suggested that cerebral vascular ECs highly express monocarboxylate transporter (MCT), a lactate transporter, allowing lactate to shuttle through the ECs' cell membrane, which works as a path for the lactate-induced metabolism of the entire brain (Zhang et al., 2014). Lactate in the blood can be transferred into ECs through MCT1 and then transported to the brain. After lipopolysaccharide stimulation, MCT-1 of the ECs decreased, and interleukin 1β accumulates in the brain, followed by a rise in lactate content (Boitsova et al., 2018). Lev-Vachnish et al. (2019) blocked the expression of MCT2 in ECs *in vivo*, which transports lactate to the brain, and finally found that mouse brain neuron regeneration was enhanced. Therefore, the lactate transporter plays a "gatekeeper" role in transporting lactate through the endothelial barrier to the damaged organ.

The mechanism of how the "gatekeeper" function of ECs on lactate affects the brain's cognitive function through supporting tissue regeneration is also worth discussing. Wang et al. (2019) illustrated how the brain ECs maintained lactate homeostasis and contributed to adult hippocampal neurogenesis and cognitive functions. Conditional phosphatase and tensin homolog (PTEN) knockout in ECs increased the outflow of lactate from the blood through ECs to nearby tissue, and administering lactate to wild-type animals impaired adult hippocampal neurogenesis. Thus, the brain lactate was upregulated, suggesting that ECs can maintain the lactate-induced metabolic homeostasis. Simultaneously, the expression of MCT1 decreased with the knockout of PTEN in ECs, and neurocognitive function also declined in the hippocampus of mice, indicating that PTEN of ECs regulates the metabolism of lactate in the brain by upregulating the expression of MCT1. Moreover, deletion of Akt1 in ECs restored MCT1 expression, decreased lactate levels, and normalized hippocampal neurogenesis and cognitive function in PTEN mutant mice. As a virtual channel of "gatekeeper," lactate transporter carries lactate in the blood to neurons through critical signal transduction pathways of ECs to improve neurogenesis and cognitive functions.

Therefore, based on these particular steps of metabolism, ECs can reprogram the lactate and promote the regeneration of the damaged tissue. Finally, lactate is released and transported through the lactate transporter on ECs, passing through the endothelial barrier to the damaged tissues for tissue repair (**Figure 1A**).

LACTATE "ANGIOCRINE" FUNCTION IN ENDOTHELIAL CELLS FOR TISSUE REGENERATION

ECs act as a "gatekeeper," controlling lactate secretion for organ-like brain regeneration in previous reports. ECs also can maintain lactate homeostasis and facilitate tissue repair and regeneration *via* "angiocrine" signaling. For instance, Jag1 derived from lung ECs ensures control of the lung regeneration after bleomycin injection (Cao et al., 2016); in the mouse brain, quiescence of neural stem cells can be sustained by neurotrophin-3 released from the brain endothelium (Ottone et al., 2014).

ECs relied on glycolysis rather than on oxidative phosphorylation for adenosine triphosphate production, and the loss of the glycolytic activator phosphofructokinase-2/fructose-2,6-bisphosphatase isoform 3 (PFKFB3) in ECs impaired vessel formation. EC's activation enhanced the glycolytic regulator PFKFB3 when along with glucose, it was oxidized during glycolysis. Deletion of PFKFB3 in ECs prevents revascularization and lactate reprogramming, and the addition of the lactate to PFKFB3-knockdown cells rescued the suppression of EC proliferation and migration (De Bock et al., 2013; Schoors et al., 2014; Xu et al., 2014). Dual inhibition of PFKFB3 and VEGF normalized tumor vasculature, reduced lactate production, and improved chemotherapy in glioblastoma (Zhang et al., 2020b). Moreover, the lactate promoted EC proliferation and migration in PFKFB3-knockdown cells. Eventually, PFKFB3 can control lactate secretion in ECs. However, whether the ECs acted as a "reservoir" for lactate through PFKFB3 is rarely reported.

The function of macrophages to promote fibrosis and regeneration has been well-studied (Cui et al., 2021). However, few studies on ECs regulate macrophages by releasing lactate and macrophages as mediators for tissue regeneration and repair. Zhang et al. (2020a) exploited lactate–EC metabolic communication that contributes to tissue regeneration uniquely. They found that endothelial PFKFB3 is required for ischemia-induced muscle revascularization and regeneration and that knocking PFKFB3 in muscle ECs impairs muscle function upon ischemia. Loss of endothelial PFKFB3 in ECs increased monocyte recruitment during ischemia but dampened M2 macrophage polarization. Muscle ECs use lactate as a signal of sprouting within the muscle microenvironment, promoting M2-like macrophage functional polarization and augmentation VEGF secretion from macrophages. Eventually, macrophages create a positive feedback loop that can stimulate EC's angiogenesis further.

It is novel that ECs metabolically collaborate with macrophages to repair muscle, efficiently sharing the energetic substrate glucose *via* the glycolysis to lactate. Finally, ECs are no longer a simple barrier but are activated by tissue damage and activated ECs, which become a reservoir of metabolites such as lactate. ECs with a large amount of lactate are used as raw material and fuel to combine with the lactic acid transporter of immune cells to promote the release of cytokines, amplifying the repairing effect of immune cells in damaged tissues (**Figure 1B**).

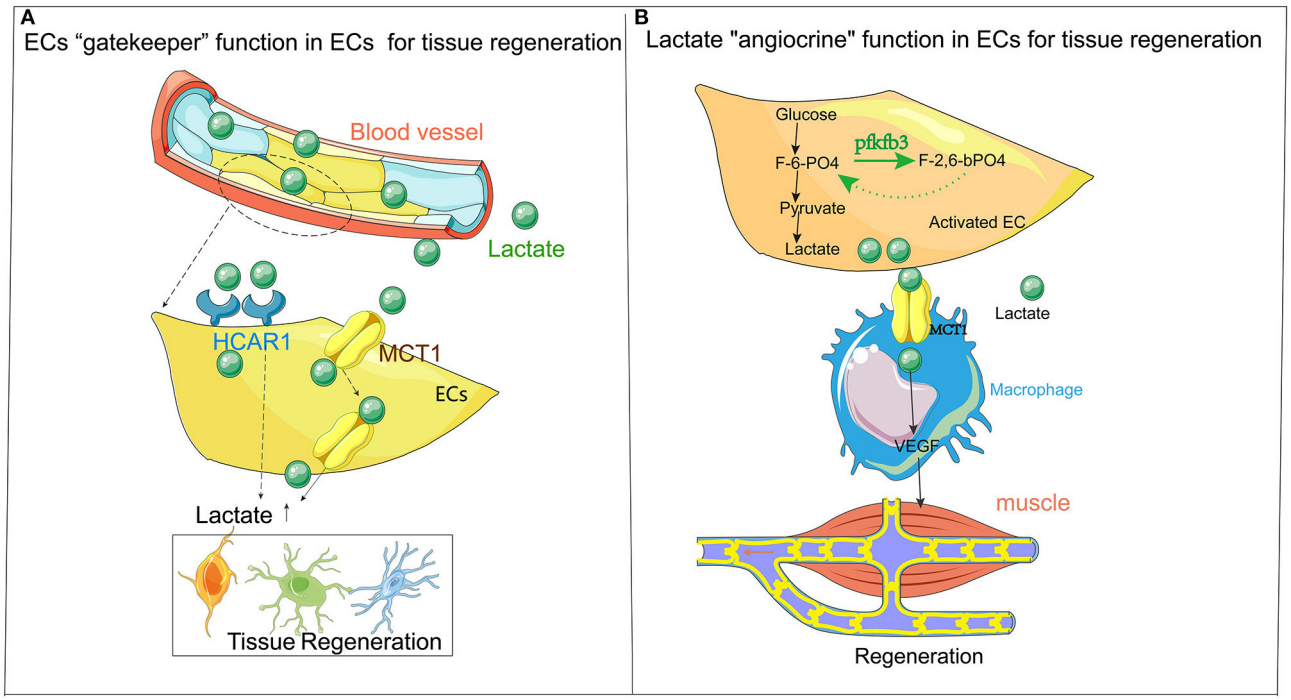

FIGURE 1 | (A) ECs are the "gatekeepers" of lactate. Lactate metabolism plays a vital role in the regeneration of tissues (especially in the nervous system). The accumulation of lactate often leads to neurodegenerative diseases. The primary mechanism of action is the "gatekeeper" function of ECs as a metabolite, allowing lactate to be carried through the bloodstream to the site that needs damage and repair with the transporter (HCAR1 and MCT1) on ECs, thereby affect the damage and repair of tissues. **(B)** Flow chart describing "classical" ECs release lactate for local metabolism and tissue regeneration. The endothelium itself is a high-metabolic organ, causes lactate accumulation through endothelial activation, which affects the regeneration and repair of surrounding tissues. The primary mechanism is that lactate (after exercise) undergoes anaerobic metabolism in ECs and finally changes from glucose to lactate, following an amount of lactate accumulated in ECs. Through ECs' transporter, such as MCT1, the lactate is released from ECs to recruit immune cells such as macrophages. The macrophages release VEGF and other cytokines to the surrounding ischemic tissues (such as muscle tissue), producing regeneration and repair. HCAR1, lactate receptor Vascular endothelial growth factor; MCT1, monocarboxylate transporter 1; ECs, endothelial cell.

Traditionally, ECs are the blood barrier in which oxygen, nutrients, and metabolites can be transported and exchanged with the blood flow, among which lactate is a vital metabolite shuttled through the "switch" action of ECs. Lactate passes through the transporter of ECs, allowing the lactate produced by other tissues (such as muscles) to be carried through the blood to the targeted organs (such as neurons), promoting tissue regeneration. However, ECs can also serve as a "reservoir" for the release of lactate, allowing the lactate with "angiocrine" function to be released from ECs, and the damaged tissue can be repaired with lactate. Therefore, the "gatekeeper" role of ECs can allow activated ECs to act as a gated channel to release lactate when repairing other tissues. However, the angiocrine function of ECs is achieved by endothelial activation. Then, lactate is released, and immune cells are recruited, which are undergoing tissue regeneration and repair.

CONCLUSION AND FUTURE PROSPECTS

Here, in addition to the angiogenesis effect of lactate on ECs, this paper further discusses the "gatekeeper" function effect of ECs on the metabolism of lactate for tissue regeneration and how lactate penetrates ECs to affect the surrounding tissues of blood vessels, such as the formation of brain nerves. More interestingly, we also discuss the ECs as a "reservoir" of lactate, which can secrete lactate from ECs, thus affecting the regeneration of nearby tissues.

In EC microenvironment, lactate contributes metabolic crosslinks between immune cells and stromal cells, acting as a "lactate-shuttle" in the damaged tissue. Lactate is no longer a waste product derived from anaerobic metabolism; instead, it is a powerful molecule tool that contributes to EC's angiocrine function, favoring tissue regeneration. Thus, new tools, including tracing lactate location and consumption and transporting lactate to damaged tissue, deserve further study.

Although several profoundly illustrated mechanisms have been identified as causes of organ regeneration in lactate-related microenvironments, limited evidence supports metabolic cross talk between immune cells or supportive tissues and ECs, which is obviously another challenge for future research in the EC metabolism field. Despite the scarcity of researches related to ECs' molecular function of regulating lactate, translational research on lactate

metabolism in ECs has transferred some fundamental aspects of the regeneration-related disease to the clinical aspects. Clinical researchers working in regeneration disease are encouraged to utilize lactate metabolism to treat ischemia or neuron degeneration.

In summary, ECs can promote blood vessel formation in an environment with high lactate levels and act as a gate of lactate, controlling lactate secretion and affecting tissue regeneration. Finally, activated ECs also serve as a storehouse of lactate, and the activated ECs can secrete lactate to promote the regeneration of surrounding tissues.

AUTHOR CONTRIBUTIONS

LZ: conception or design of the work and critical revision of the article. XG: drafting the article and data collection. XZ and XT: drafting the manuscript and revision of the article. YD: drafting the article. XW: drafting the manuscript. SL: critical revision of the article.

FUNDING

Project supported by the National Science Foundation for Young Scientists of China (81900065).

REFERENCES

Boitsova, E. B., Morgun, A. V., Osipova, E. D., Pozhilenkova, E. A., Martinova, G. P., Frolova, O. V., et al. (2018). The inhibitory effect of LPS on the expression of GPR81 lactate receptor in blood-brain barrier model *in vitro*. *J. Neuroinflam.* 15:196. doi: 10.1186/s12974-018-1233-2

Cao, Z., Lis, R., Ginsberg, M., Chavez, D., Shido, K., Rabbany, S. Y., et al. (2016). Targeting of the pulmonary capillary vascular niche promotes lung alveolar repair and ameliorates fibrosis. *Nat. Med.* 22, 154–162. doi: 10.1038/nm.4035

Cui, H., Xie, N., Banerjee, S., Ge, J., Jiang, D., Dey, T., et al. (2021). Lung myofibroblasts promote macrophage profibrotic activity through lactate-induced histone lactylation. *Am. J. Res. Cell Mol. Biol.* 64, 115–125. doi: 10.1165/rcmb.2020-0360OC

De Bock, K., Georgiadou, M., Schoors, S., Kuchnio, A., Wong, B. W., Cantelmo, A. R., et al. (2013). Role of PFKFB3-driven glycolysis in vessel sprouting. *Cell* 154, 651–663. doi: 10.1016/j.cell.2013.06.037

de la Cruz-López, K. G., Castro-Muñoz, L. J., Reyes-Hernández, D. O., García-Carranc,á, A., and Manzo-Merino, J. (2019). Lactate in the regulation of tumor microenvironment and therapeutic approaches. *Front. Oncol.* 9:1143. doi: 10.3389/fonc.2019.01143

Ding, B.-S., Cao, Z., Lis, R., Nolan, D. J., Guo, P., Simons, M., et al. (2014). Divergent angiocrine signals from vascular niche balance liver regeneration and fibrosis. *Nature* 505, 97–102. doi: 10.1038/nature12681

Eelen, G., de Zeeuw, P., Treps, L., Harjes, U., Wong, B. W., and Carmeliet, P. (2018). Endothelial cell metabolism. *Physiol. Rev.* 98, 3–58. doi: 10.1152/physrev.00001.2017

Gerhardt, T., and Ley, K. (2015). Monocyte trafficking across the vessel wall. *Cardiovasc. Res.* 107, 321–330. doi: 10.1093/cvr/cvv147

Hoffmann, E. K., Lambert, I. H., and Pedersen, S. F. (2009). Physiology of cell volume regulation in vertebrates. *Physiol. Rev.* 89, 193–277. doi: 10.1152/physrev.00037.2007

Kumar, V. B., Viji, R. I., Kiran, M. S., and Sudhakaran, P. R. (2007). Endothelial cell response to lactate: implication of PAR modification of VEGF. *J. Cell. Physiol.* 211, 477–485. doi: 10.1002/jcp.20955

Lev-Vachnish, Y., Cadury, S., Rotter-Maskowitz, A., Feldman, N., Roichman, A., Illouz, T., et al. (2019). L-Lactate promotes adult hippocampal neurogenesis. *Front. Neurosci.* 13:403. doi: 10.3389/fnins.2019.00403

Li, X., Sun, X., and Carmeliet, P. (2019). Hallmarks of endothelial cell metabolism in health and disease. *Cell Metab.* 30, 414–433. doi: 10.1016/j.cmet.2019.08.011

Longchamp, A., Mirabella, T., Arduini, A., MacArthur, M. R., Das, A., Treviño-Villarreal, J. H., et al. (2018). Amino Acid restriction triggers angiogenesis via GCN2/ATF4 regulation of VEGF and H(2)S production. *Cell* 173, 117–129.e114. doi: 10.1016/j.cell.2018.03.001

Morland, C., Andersson, K. A., Haugen, Ø., P., Hadzic, A., Kleppa, L., et al. (2017). Exercise induces cerebral VEGF and angiogenesis via the lactate receptor HCAR1. *Nat. Commun.* 8:15557. doi: 10.1038/ncomms15557

Ottone, C., Krusche, B., Whitby, A., Clements, M., Quadrato, G., Pitulescu, M. E., et al. (2014). Direct cell-cell contact with the vascular niche maintains quiescent neural stem cells. *Nat. Cell Biol.* 16, 1045–1056. doi: 10.1038/ncb3045

Rafii, S., Butler, J. M., and Ding, B.-S. (2016). Angiocrine functions of organ-specific endothelial cells. *Nature* 529, 316–325. doi: 10.1038/nature17040

Schoors, S., De Bock, K., Cantelmo, A. R., Georgiadou, M., Ghesquière, B., Cauwenberghs, S., et al. (2014). Partial and transient reduction of glycolysis by PFKFB3 blockade reduces pathological angiogenesis. *Cell Metab.* 19, 37–48. doi: 10.1016/j.cmet.2013.11.008

Wang, J., Cui, Y., Yu, Z., Wang, W., Cheng, X., Ji, W., et al. (2019). Brain Endothelial cells maintain lactate homeostasis and control adult hippocampal neurogenesis. *Cell Stem Cell* 25, 754–767.e759. doi: 10.1016/j.stem.2019.09.009

Xu, Y., An, X., Guo, X., Habtetsion, T. G., Wang, Y., Xu, X., et al. (2014). Endothelial PFKFB3 plays a critical role in angiogenesis. *Arterioscler. Thromb. Vasc. Biol.* 34, 1231–1239. doi: 10.1161/atvbaha.113.303041

Zhang, J., Muri, J., Fitzgerald, G., Gorski, T., Gianni-Barrera, R., Masschelein, E., et al. (2020a). Endothelial lactate controls muscle regeneration from ischemia by inducing M2-like macrophage polarization. *Cell Metab.* 31, 1136–1153.e1137. doi: 10.1016/j.cmet.2020.05.004

Zhang, J., Xue, W., Xu, K., Yi, L., Guo, Y., Xie, T., et al. (2020b). Dual inhibition of PFKFB3 and VEGF normalizes tumor vasculature, reduces lactate production, and improves chemotherapy in glioblastoma: insights from protein expression profiling and MRI. *Theranostics* 10, 7245–7259. doi: 10.7150/thno.44427

Zhang, Y., Chen, K., Sloan, S. A., Bennett, M. L., Scholze, A. R., O'Keeffe, S., et al. (2014). An RNA-sequencing transcriptome and splicing database of glia, neurons, and vascular cells of the cerebral cortex. *J. Neurosci.* 34, 11929–11947. doi: 10.1523/jneurosci.1860-14.2014

Conflict of Interest: The authors declare that the research was conducted in the absence of any commercial or financial relationships that could be construed as a potential conflict of interest.

Publisher's Note: All claims expressed in this article are solely those of the authors and do not necessarily represent those of their affiliated organizations, or those of the publisher, the editors and the reviewers. Any product that may be evaluated in this article, or claim that may be made by its manufacturer, is not guaranteed or endorsed by the publisher.

frontiers in Cell and Developmental Biology

REVIEW
published: 19 August 2021
doi: 10.3389/fcell.2021.686548

The Roles of CCR9/CCL25 in Inflammation and Inflammation-Associated Diseases

Xue Wu[1,2†], Meng Sun[3†], Zhi Yang[1,2†], Chenxi Lu[1,2†], Qiang Wang[1], Haiying Wang[1], Chao Deng[4], Yonglin Liu[1] and Yang Yang[1,2*†]*

[1] Department of Paediatrics, Shenmu Hospital, School of Life Sciences and Medicine, Northwest University, Shenmu, China, [2] Key Laboratory of Resource Biology and Biotechnology in Western China, Ministry of Education, Faculty of Life Sciences, Northwest University, Xi'an, China, [3] Department of Cardiology, The First Hospital of Shanxi Medical University, Taiyuan, China, [4] Department of Cardiovascular Surgery, The First Affiliated Hospital of Xi'an Jiaotong University, Xi'an, China

OPEN ACCESS

Edited by:
InKyeom Kim, Kyungpook National University, South Korea

Reviewed by:
Dwijendra K. Gupta, Jai Prakash Vishwavidyalaya, India
Olga Scudiero, University of Naples Federico II, Italy

***Correspondence:**
Yonglin Liu
yonglinliusm@163.com
Yang Yang
yang200214yy@163.com

† These authors have contributed equally to this work

Specialty section:
This article was submitted to Cellular Biochemistry, a section of the journal Frontiers in Cell and Developmental Biology

Received: *12 April 2021*
Accepted: *23 July 2021*
Published: *19 August 2021*

Citation:
Wu X, Sun M, Yang Z, Lu C, Wang Q, Wang H, Deng C, Liu Y and Yang Y (2021) The Roles of CCR9/CCL25 in Inflammation and Inflammation-Associated Diseases. Front. Cell Dev. Biol. 9:686548. doi: 10.3389/fcell.2021.686548

Chemokine is a structure-related protein with a relatively small molecular weight, which can target cells to chemotaxis and promote inflammatory response. Inflammation plays an important role in aging. C-C chemokine receptor 9 (CCR9) and its ligand C-C chemokine ligand 25 (CCL25) are involved in the regulating the occurrence and development of various diseases, which has become a research hotspot. Early research analysis of CCR9-deficient mouse models also confirmed various physiological functions of this chemokine in inflammatory responses. Moreover, CCR9/CCL25 has been shown to play an important role in a variety of inflammation-related diseases, such as cardiovascular disease (CVD), rheumatoid arthritis, hepatitis, inflammatory bowel disease, asthma, etc. Therefore, the purpose of this review gives an overview of the recent advances in understanding the roles of CCR9/CCL25 in inflammation and inflammation-associated diseases, which will contribute to the design of future experimental studies on the potential of CCR9/CCL25 and advance the research of CCR9/CCL25 as pharmacological inflammatory targets.

Keywords: chemokine, CCR9, CCL25, autoimmune, inflammatory disease

INTRODUCTION

Chemokines are a large family of small cytokines and generally have low molecular weight ranging from 7 to 15 kDa (Palomino and Marti, 2015). Chemokines can interact with different chemokine receptors that control the residence and migration of immune cells. When the body is stimulated by antigen, chemokines can be secreted by various cells such as endothelial and dendritic cells (DCs) (Vassilatis et al., 2003). Currently, more than 50 chemokines have been discovered, which can be divided into four categories according to the position of two cysteines at the N-terminus: C subfamily, CC subfamily, CXC subfamily, and CX3C subfamily (**Figure 1**; Bleul et al., 1996). Moreover, according to the expression of chemokines and their functions in the immune system, chemokines can be also divided into homeostatic and inflammatory chemokines (**Table 1**; Moser et al., 2004). Chemokines expression is regulated via a variety of factors such as interleukin (IL)-10 and glucocorticoids, which can inhibit the secretion of chemokines, while IL-1 and tumor necrosis factor (TNF)-α can increase chemokines expression (Cocchi et al., 1995; Oberlin et al., 1996;

Zlotnik and Yoshie, 2012). The chemokine receptor is a G-protein coupled receptor of the seven-transmembrane receptor family, which contains seven transmembrane segments and is widely expressed on white blood cells surface derived from bone marrow such as neutrophils and macrophages (Schulz et al., 2016). In addition, chemokine receptors have also been shown to be expressed in epithelial cells, vascular endothelial cells, and other tissue cells. The combination of chemokines and their corresponding receptors can involve in normal body development, and also participate in various pathological and physiological processes such as leukocyte activation, angiogenesis, aging, breast cancer resistance, and autoimmune diseases (Zhong et al., 2015).

C-C chemokine ligand 25 (CCL25) is also considered a thymus expressed chemokine, and the gene is located on chromosome 19p13.2 (**Figure 1**; Qiuping et al., 2004). Tu et al. (2016) confirmed that CCL25 is mainly expressed in the thymus and intestinal epithelium, and also produced by vascular endothelial cells and other parenchymal cells, which can migrate immature T cells into the thymus to mature and release (**Table 1**). C-C chemokine receptor 9 (CCR9) was discovered in 1996 as a G protein-coupled receptors expressed on the cell membrane of dendritic cell, neutrophils, lymphocytes, monocyte macrophages, and vascular endothelial cells (Yu and Stamenkovic, 2000). However, in the 3 years after the discovery of CCR9, its ligand has not been found, so it was once called "orphan receptor." It was not until 1999 that CCL25 was found to be one-to-one combined with CCR9 (Zaballos et al., 1999). CCR9 belongs to the β-chemokine receptor family, and its gene is located on chromosome 3 p21.31 (Tu et al., 2016). CCR9 is mainly distributed in immature T lymphocytes and intestinal cells surface, and after binding to its specific ligands, plays a key role in T lymphocyte development and tissue-specific homing (Wermers et al., 2011; Wu et al., 2014). Further study found that CCL25 promoted proliferation and chemotaxis of inflammatory cells that expressed its specific receptor CCR9 (Igaki et al., 2018).

CCR9 and CCL25 are members of the CC subfamily of chemokines that are involved in a variety of inflammatory diseases and promote inflammatory responses. Over the years, the role of CCR9/CCL25 in inflammation and related diseases has become increasingly clearness, including cardiovascular disease (CVD), hepatitis, arthritis (Yokoyama et al., 2014), inflammatory bowel disease (Kalindjian et al., 2016), and asthma. This study provides abundant evidence that CCR9/CCL25 can be a potential target for a variety of inflammatory diseases. Therefore, the focus of this review is to evaluate the latest findings on the role of CCR9/CCL25 in inflammatory disease. The structure and physiological function of CCR9/CCL25 were briefly introduced. The various roles of CCR9/CCL25 in the development of inflammatory disease were described (**Figure 2**), and some different insights were put forward concerning the CCR9/CCL25 pathway.

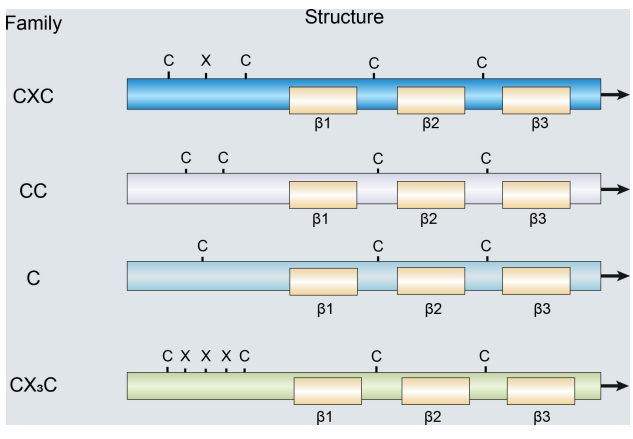

FIGURE 1 | Structure of members of the chemokine family.

CCR9 AND CCL25 EXPRESSION IN TISSUE

Vicari et al. (1997) isolated CCL25 cDNA from the thymus of recombinase activation gene-1 (RAG-1) deficient mice and were designated thymus-expressed chemokine (TECK). Moreover, they also found that CCL25 appeared weak sequence homology to other members of the CC chemokine family and located on mouse chromosome 8 (Vicari et al., 1997). Besides the thymus, mRNA encoding CCL25 was detected at substantial levels in the small intestine and at low levels in the liver (Vicari et al., 1997; Zabel et al., 1999; Kunkel et al., 2000). However, studies found that CCL25 is highly expressed in the small intestinal epithelium and thymus, which can regulate trafficking of gut-specific memory/effector T cells via upregulation of the integrin homing receptor α47 and CCR9 (Stenstad et al., 2006; Wurbel et al., 2000, 2007). Meanwhile, the source of CCL25 in the thymus was determined to be thymic dendritic cells; in contrast, bone marrow-derived dendritic cells do not express CCL25. The murine CCL25 recombinant protein showed chemotactic activity for activated macrophages, dendritic cells, and thymocytes. These research results fully demonstrated that CCL25 represents a novel thymic dendritic cell-specific CC chemokine that is possibly involved in T cell development. Within the intestines of normal mice, CCL25 expression was highest in the proximal small intestine, lowest in the distal small bowel, and no or almost no expression in the colon (Svensson et al., 2002; Rivera-Nieves et al., 2006; Stenstad et al., 2007; Wermers et al., 2011; Wurbel et al., 2011).

In circulating white blood cells, CCR9 expression is limited to activated B cells and a certain proportion of CD4 and CD8 T cells (Zabel et al., 1999; Kunkel et al., 2000; Papadakis et al., 2000, 2001, 2003). CCR9 has been identified in plasmacytoid dendritic cells in mice, but there is a lack of relevant data in humans (Wendland et al., 2007; Hadeiba et al., 2012). Similarly, despite the fact that a few papers describe the expression of CCR9 on mouse macrophages, there is a lack of human data (Nakamoto et al., 2012). In the peripheral tissues, $CCR9^{+}$ cells are mostly concentrated in colon, thymus, and small intestine (Zabel et al., 1999; Kunkel et al., 2000; Papadakis et al., 2000). Intraepithelial

TABLE 1 | Classification, structural features, function, and location of the chemokine family members.

Family	Structural features	Function	Location	Chemokines
CXC	The CXC family has a single amino acid residue in between the first two cysteines.	CXC chemokines have the highest ability to attract neutrophils and monocytes.	4q12-13 4q21.21 10q11.1 4q21 5p31 17p13	CXCL1-8 CXCL9-11 CXCL12 CXCL13 CXCL14 CXCL1
CC	The CC chemokine family has the first two cysteine residues adjacent to each other.	CC chemokines are mainly responsible for the recruitment of lymphocytes.	17q11.2 7q11.23 16q13 17q11.2 9q13 2q33-3 9q13 16q13 11q11.2 7q11.23 19p13.2 7q11.23 9q13 5q	CCL1-15 CCL16 CCL17 CCL18 CCL19 CCL20 CCL21 CCL22 CCL23 CCL24 CCL25 CCL26 CCL27 CCL28
C	The C family there is only one cysteine residue and only one disulfide chain.	C chemokine has chemotactic activity for lymphocytes, $CD4^+$ and $CD8^+$ T cells, and NK cells.	1q23	XCL1-2
CX3C	The CX3C chemokine family three amino acid residues separate the first two cysteines.	CX3C chemokines can induce chemotaxis of monocytes and cytotoxic T cells.	16q13	CX3CL1

The spacing of two conserved cysteine residues at the N-terminus determines the nomenclature and classification of the chemokine family members; in CXC, CC, C, and CX3C chemokines. Moreover, according to the classification of chemokines, these four types also have different functions and localizations.

lymphocytes are mainly $CD8^+$, most of which express CCR9 surface (Zabel et al., 1999; Kunkel et al., 2000).

THE ROLE OF CCR9/CCL25 IN INFLAMMATORY DISEASES

Inflammation underlies many physiological and pathological processes. In particular, chronic inflammation is attributed to the pathophysiological basis of various modern diseases. Of note, inflammatory diseases are characterized by wide coverage, complex pathogenesis, and large difference in prognosis (Guo et al., 2015). Therefore, we mainly focus on the effect of CCR9/CCL25 in inflammatory diseases as well as elaborate on their mechanism of action in related diseases.

Cardiovascular Disease

Cardiovascular disease, also known as circulatory disease, is a series of diseases involving the circulatory system, including the heart and blood vessels, which have always been at the forefront of human major causes of death (Jokinen, 2015). Heart failure, cardiac hypertrophy, and atherosclerosis are belong to CVD and are also a chronic vascular inflammatory disease, which have high morbidity, high mortality, and high disability rate, and thus, seriously threaten human health (Van Camp, 2014).

In CCR9 knockout $CCR9^{+/+}$ mice, surgical ligation of the left anterior descending coronary artery caused myocardial infarction (MI), and found that the expression of CCR9 in the heart of mice was significantly up-regulated after MI. Down-regulation of CCR9 expression can improve survival rate and left ventricular dysfunction, reduce infarct size, and improve cardiac function after MI. In addition, abolish of CCR9 in the mouse MI heart significantly increased Bcl-2 expression, while the expression of Bax and cleaved caspase 3 was remarkably reduced, thereby attenuating the apoptosis of cardiomyocytes. Inflammation is considered the most vital pathological response to damage and repair, and abolish of CCR9 can decrease pro-inflammatory cytokines mRNA levels (IL-6, IL-1β, and TNF-α) and suppress the inflammatory response after MI. In addition, CCR9 is involved in structural remodeling mainly by interfering with NF-κB and MAPK signaling pathways (**Figure 2**). These results confirmed that CCR9/CCL25 may exert a positive role in MI (Huang et al., 2016).

Heart failure is the leading cause of death in many countries, particularly in an aging population (Kumarswamy and Thum, 2013). Currently, heart failure is widely recognized as a clinical syndrome caused by cardiac hypertrophy and remodeling that involves changes of structural and functional in the left ventricle (Zhang et al., 2014). Study found that CCR9 protein levels have significantly increased in failing human hearts and mice or cardiomyocyte hypertrophy model. The loss of CCR9 in mice can reduce the hypertrophy caused by pressure overload. The results show that heart weight/body weight, lung weight, and heart weight/tibia length ratios of CCR9-deficient mice are significantly lower than those of the control group. And aortic banding treated CCR9-deficient mice were characterized by decreased Left ventricular (LV) end diastolic and systolic diameters and increased fractional shortening, demonstrating smaller LV dimensions and elevated systolic function. Moreover, the hypertrophic response of the CCR9-deficient mice was

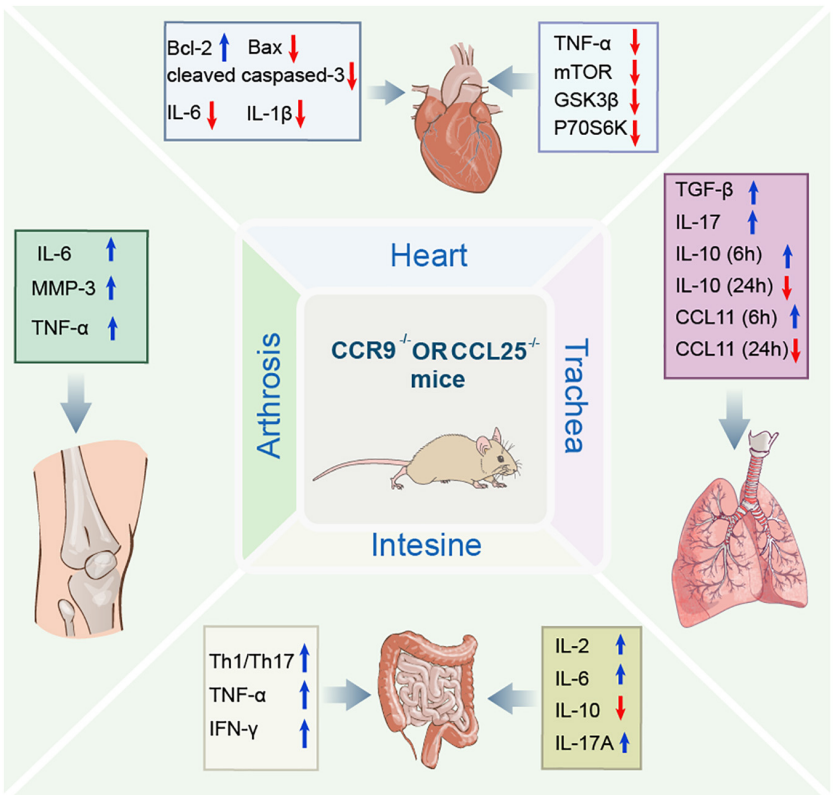

FIGURE 2 | Schematic diagram illustrating the regulation of molecular mechanisms of CCR9/CCL25 in inflammatory diseases. CCR9/CCL25 exerts multiple effects in a variety of inflammatory diseases by regulating molecular mechanisms, such as molecules associated with apoptosis and inflammation. CCR9, C-C chemokine receptor 9; CCL25, C-C chemokine ligand 25; Bcl-2, B-cell lyumphoma-2; Bax, Bcl-2 Associated X-protein; IL-6, interleukin-6; IL-1β, interleukin-1β; TNF-α, tumor necrosis factor-α; mTOR, mechanistic target of rapamycin; GSK3β, glycogen synthase kinase 3-beta; p70S6K, p70 S6 kinase; IL-10, interleukin-10; MMP3, matrix metalloproteinase-3; TNF-β, tumor necrosis factor-β; IL-17, interleukin-17; CCL11, C-C chemokine ligand 11; Th1/Th17, helper T1/helper T17; IFN-γ, interferon-gamma; IL-2, interleukin-2; IL-17A, interleukin-17A.

remarkably attenuated compared with controls, and these animals manifested decreased heart size and cardiomyocyte cross sectional area as well as alleviation of interstitial fibrosis. The mRNA levels of hypertrophic and fibrotic markers were also reduced significantly in the CCR9 deficient mice. Notably, overexpression of CCR9 in mice reversed the result of the appeal (Xu et al., 2016). In terms of mechanism, they further found that the expression levels of MAPK lack difference between the two groups, while the phosphorylation levels of AKT/protein kinase B and downstream effectors (mTOR, GSK3b, and p70S6K) were remarkably reduced in CCR9 knockout mice and increased in CCR9 transgenic mice after aortic surgery (**Figure 2**). These results suggested that CCR9 could promote hypertrophy mainly due to the protein kinase B mammalian target of the rapamycin GSK-3β signaling cascade, rather than through the MAPK signaling pathway, which indicates that CCR9 can be used as a new regulator of myocardial hypertrophy and may provide a novel therapeutic target for suppressing myocardial hypertrophy in the future (Xu et al., 2016).

In conclusion, the knockout of CCR9/CCL25 serves as a novel modulator of pathological progression for inhibiting the development of MI and heart failure (**Table 2**). However, the role of CCR9/CCL25 in other CVD has not been reported, so further research is needed.

Hepatitis

Hepatitis usually refers to various pathogenic factors, including parasites, viruses, drugs, bacteria, and autoimmune factors, which cause damage to liver cells and functions, thereby causing a series of uncomfortable symptoms of the body and abnormal liver function indicators (Crispe, 2003; Thomson and Knolle, 2010; Linder and Malani, 2017).

As well known, various immune cells in the liver involve in the pathogenesis of liver diseases. Inflammatory macrophages play a key role in liver injury and then liver fibrosis and canceration. Nakamoto et al. (2012) previous research suggests that $CCR9^{+}$ inflammatory macrophage triggers acute liver injury by interacting with helper T 1 (Th1) cells in the inflamed liver. Subsequently, they found that macrophages expressing $CCR9^{+}CD11b^{+}$ aggravated liver damage through production of inflammatory cytokines and the promotion of Th1 cell development during the concanavalin A-induced murine acute liver injury and human acute hepatitis (Nakamoto, 2016). Further analysis using liver-shielded radiation and

TABLE 2 | The role of CCR9/CCL25 in inflammatory-associated diseases.

Inflammation disease	Expression of CCR9 or CCL25	Model	Effect of CCR9/CCL25	Outcome	References
Myocardial infarction	Increased CCR9	Model of myocardial infarction induced by ligation of left anterior descending coronary artery of $CCR9^{-/-}$ and $CCR9^{+/+}$ mice	Down-regulation of CCR9 expression can improve survival rate, left ventricular dysfunction, cardiac function, reduce infarct size, meanwhile, significantly attenuate the apoptosis of cardiomyocytes, and inhibit the inflammatory response after myocardial infarction.	CCR9/CCL25 axis may play an important role in inflammatory cell infiltration and cardiac remodeling after myocardial infarction.	Huang et al., 2016
Hepatitis	–	Concanavalin A-induced murine acute liver injury and human acute hepatitis	Macrophages expressing $CCR9^{+}CD11b^{+}$ aggravated liver damage through production of inflammatory cytokines and the promotion of Th1 cell development.	Inflammatory macrophages originated from bone marrow and became locally differentiated and proliferated by interaction with hepatic stellate cells via knocking out CCR9 gene during acute liver injury.	Amiya et al., 2016; Nakamoto, 2016
Rheumatoid arthritis	Increased CCR9 and CCL25	In the synovium of RA and non-RA patients	Stimulation with CCL25 increased IL-6 and MMP-3 production from RA fibroblast-like synoviocytes, and also increased IL-6 and TNF-α production from peripheral blood monocytes. Collagen-induced arthritis was suppressed in CCR9-deficient mice.	The interaction between CCL25 and CCR9 may promote cell infiltration and production of inflammatory mediator in RA synovial tissues.	Yokoyama et al., 2014
Inflammatory bowel disease	Increased CCR9 and CCL25	DSS-induced acute colitis	$CCR9^{-/-}$ mice are more susceptible to DSS colitis than WT littermate controls as shown by higher mortality, increased IBD score, and delayed recovery. During recovery, the $CCR9^{-/-}$ colonic mucosa is characterized by the accumulation of activated macrophages and elevated levels of Th1/Th17 inflammatory cytokines.	CCR9/CCL25 interaction regulates the inflammatory immune response of the intestinal mucosa by balancing different dendritic cell subsets.	Wurbel et al., 2011
Inflammatory bowel disease	Increased CCR9 and CCL25	DSS-induced acute colitis	The mice lacking the interaction of CCR9/CCL25 showed enhanced adhesion promoting ability of coli after the transfer of naive T cells, and regulated the pro-inflammatory and anti-inflammatory subgroups of cDC.	CCR9/CCL25 interactions have protection against large intestinal inflammation in chronic colitis.	Wurbel et al., 2014
Asthma	Increased CCL25	OVA-induced model of allergic inflammation within CCR9 deficient mice	In challenged CCR9-deficient mice, cell recruitment was impaired at peribronchial and perivenular levels. OVA administration in CCR9-deficient mice leads to a less inflammatory cell recruitment, which modifies the expression of IL-10, CCL11, and CCL25 after OVA challenge.	CCR9 and CCL25 expressions are induced in the early stages of airway inflammation and they have an important role in modulating eosinophils and lymphocytes recruitment at the first stages of inflammatory process.	Lopez-Pacheco et al., 2016
Asthma	Increased CCR9	NKT cells	In patients with allergic asthma, the CCR9/CCL25 binding method selectively induces chemotaxis of NKT cells. And NKT cells may be in direct contact with $CD3^{+}$ T cells, polarizing them to a Th2 bias.	CCR9/CCL25 signal can interact with CD226 signaling to activate asthmatic NKT cells, leading to airway hyperresponsiveness and inflammation, aggravating asthma.	Sen et al., 2005

Compelling evidence has indicated that alterations of CCR9 or CCL25 expression are also involved in inflammatory-associated diseases, including myocardial infarction, hepatitis, rheumatoid arthritis, inflammatory bowel disease, and asthma.

CCR9, C-C chemokine receptor 9; CCL25, C-C chemokine ligand 25; RA, rheumatoid arthritis; IBD, inflammatory bowel disease; DSS, dextran sulfate sodium; DCs, dendritic cells; IL-6, interleukin-6; IL-10, interleukin-10; MMP3, matrix metalloproteinase-3; TNF-α, tumor necrosis factor-α; NKT, natural killer T; DCs, dendritic cells; Th, helper T.

bone marrow transplantation mouse models revealed that these $CCR9^{+}CD11b^{+}$ macrophages were originated from bone marrow-derived monocytes, but not liver resident macrophages. In addition, in contact with hepatic stellate cells, these $CD11b^{+}$ inflammatory macrophages participated in the pathogenesis of experimental liver fibrosis by knocking out CCR9 gene. The results with further verification in human samples clarified the pathogenic role of CCR9/CCL25 axis as therapeutic target of a variety of liver diseases (Nakamoto, 2016). Similarly, Amiya et al. (2016) also demonstrated that in acute liver injury, inflammatory macrophages originated from bone marrow and became locally differentiated and proliferation through interaction with hepatic stellate cells by knocking out CCR9 gene (**Figure 2**).

Primary sclerosing cholangitis (PSC), as a chronic inflammatory liver disease, is characterized by progressive bile duct destruction and is also a parenteral complication of inflammatory bowel disease (IBD). In addition, PSC is a non-suppurative autoimmune granulomatous inflammation of the small bile ducts in the liver that can lead to chronic progressive cholestasis and eventually cirrhosis and liver failure (Chapman, 1991). In the healthy liver, the expression of CCL25 is very low or even undetected (Vicari et al., 1997; Zabel et al., 1999; Eksteen et al., 2004). However, in PSC, the expression of CCL25 was increased in the liver, mainly through hepatic sinusoidal endothelial cells and portal DCs expression (Eksteen et al., 2004). The hepatic inflammation in PSC was related to the increase

of CCR9 positive T cells. Other study proposed that long-lived memory gut homing cells that expressed CCR9 and $\alpha_4\beta_7$ and were early activated during episodes of IBD could exacerbate PSC through interactions with hepatic endothelial that ectopically expressed CCL25 (Eksteen et al., 2004). Notably, they also demonstrated for the first time that T cells activated in the intestine can be recruited to extra-intestinal site of disease in humans and provide basic research to explain the pathogenesis of extra-intestinal complications of IBD (Eksteen et al., 2004; **Table 2**).

Rheumatoid Arthritis

Rheumatoid arthritis (RA) is a chronic inflammatory disease that can cause a large number of macrophages, T cells, and B cells to accumulate in the synovium (Firestein, 1991; Kinne et al., 2000), and the accumulation of these cells can further participate in the development of inflammation, joint destruction, and pain. However, biological agents (TNF blockers and IL-6 receptor antagonists) are effective in RA patients (Feldmann, 2002; Nishimoto et al., 2004; Smolen et al., 2010).

A large number of mononuclear/macrophages accumulate in the rheumatoid synovium, which play a promotive role in inflammation and joint destruction. Identifying the molecules involved in its accumulation and differentiation is essential for the development of therapeutic strategies (Mulherin et al., 1996; Haringman et al., 2005; Nishimoto and Takagi, 2010). Cluster of differentiation (CD) 14 and CD68 co-localize with CCR9 or CCL25 to identify macrophages. Other studies have confirmed that the augment $CD68^+$ cells in the substratum of RA are one of the characteristic pathological changes of synovial membrane in early RA (Singh et al., 2004). Other study demonstrated that CCR9 was expressed by PB monocytes/macrophages in RA and healthy donors, and increased in RA. Moreover, in the synovium of RA and non-RA patients, CCR9 colocates with $CD14^+$ and $CD68^+$ macrophages and was more abundant in RA synovium. Therefore, the percentage of $CCR9^+$ monocytes in the synovium of RA (81%) is increased compared to that in blood (40%), and the percentage of $CCR9^+$ monocytes in the synovium of non-RA (66%) is greater than that in blood (16%). Meanwhile, CCL25 could be detected in both RA and non-RA synovia, which can be co-localized within $CD14^+$ and $CD68^+$ cells (Schmutz et al., 2010). Furthermore, CCL25 induced stronger monocyte differentiation in RA. CCL25 induced significant chemotaxis of peripheral blood monocytes, however, which was inconsistent between different individuals. These results indicate that monocyte-induced CCR9/CCL25 expression is significantly increased in RA. CCL25 may be involved in the differentiation of monocytes to macrophages particularly in RA (Haringman et al., 2005). Moreover, CCR9 and CCL25 are expressed at higher levels in RA synovial tissues compared to osteoarthritis synovial tissues. Most $CD68^+$ macrophages in RA synovial tissue express CCR9 and CCL25 revealed by immunohistochemical. CCR9 was expressed in macrophage, fibroblast-like synoviocytes, and DCs of synovial tissues. CCL25 stimulated the production of IL-6 and MMP-3 in RA fibroblast-like synoviocytes, and also increased the production of IL-6 and TNF-α in peripheral blood monocytes (**Figure 2**). Collagen-induced arthritis was inhibited in $CCR9^{-/-}$ mice. CCR9 antagonist (CCX8037) also suppressed collagen-induced arthritis and decreased the migration of $CD11b^+$ splenic cells to synovial tissues. These results suggested that the interaction between CCL25 and CCR9 may promote cell infiltration and production of inflammatory mediator in RA synovial tissues. Blocking CCL25 or CCR9 may represent a strange new safety therapy for RA, and provide theoretical basis for further research a novel safe therapy for RA (Yokoyama et al., 2014; **Table 2**).

Inflammatory Bowel Disease

Inflammatory bowel disease is a group of chronic, non-specific inflammatory bowel diseases whose etiology has not yet been clarified, mainly including ulcerative colitis (UC) and Crohn's disease (CD). UC is a continuous inflammation of the colonic mucosa and submucosa that first affects the rectum and gradually spreads to the entire colon. CD can affect the entire digestive tract and is a discontinuous full-layer inflammation, most commonly involving terminal ileum, colon, and perianal (Loftus, 2004; Molodecky et al., 2012).

Wurbel et al. (2011) study the acute inflammation and recovery in WT and $CCR9^{-/-}$ mice in a model of dextran sulfate sodium (DSS)-induced colitis. The results show that CCL25 and CCR9 are both expressed in the large intestine and are upregulated during DSS colitis. $CCR9^{-/-}$ mice are more susceptible to DSS colitis than WT littermate controls as shown by higher mortality, increased IBD score, and delayed recovery. During recovery, the $CCR9^{-/-}$ colonic mucosa is characterized by the accumulation of activated macrophages and added Th1/Th17 inflammatory cytokines levels. Activated plasmacytoid dendritic cells (pDC) accumulate in the mesenteric lymph nodes of $CCR9^{-/-}$ animals, changing the local proportion of DC subsets. The T cells separate from these mesenteric lymph nodes were stimulated again, which were significantly higher levels of TNF-α, IFN-γ, IL-2, IL-6, and IL-17A while down-regulating IL-10 production (**Figure 2**). These results suggest that the CCR9/CCL25 interaction regulates the inflammatory immune response of the intestinal mucosa by balancing different dendritic cell subsets (Wurbel et al., 2011).

As mentioned before, $CCR9^{-/-}$ and $CCL25^{-/-}$ mice are more susceptible to acute DSS colitis than WT controls. As human ulcerative colitis is associated with signs of chronic colonic inflammation, they investigated whether the increased susceptibility to acute inflammation associated with defective CCL25/CCR9 interactions would also translate into increased susceptibility to chronic inflammation, and found that chronic DSS exposure results in exacerbated colitis in mice deficient for either CCR9 or CCL25 when compared with WT control mice. Although $CCR9^{-/-}$ T cells traffic to the colon and induce severe colitis similar to WT T cells, naive WT T cells induce more severe disease in recipient animals devoid of CCL25 expression. Moreover, compared with WT control mice, there was no significant difference in the total number of pDC and conventional dendritic cells (cDC), and the pro-inflammatory and anti-inflammatory subgroups of cDC were regulated by the CCR9/CCL25 interaction. In the end, the

CCR9/CCL25-dependent innate immune cell lineage specificity and lineage-dependent function will be remarkably assisted via targeting the loss of CCR9/CCL25 in innate immune cell and/or epithelial compartment. These results suggested that CCR9/CCL25 interactions have protection against large intestinal inflammation in chronic colitis (Wurbel et al., 2014). Moreover, Papadakis et al. (2001) demonstrated that the proportion of peripheral blood $CCR9^+$ $CD4^+$ cells rose remarkably in active small bowel CD compared with normal groups, but not in patients with purely colonic Crohn's. It is worth noting that GSK/Chemocentryx has advanced its CCR9 antagonist CCX282-B (also known as vercirnon) to a pivotal phase III clinical trial. It was unfortunate that due to poor efficacy of IBD, the clinical project was terminated at the end of 2013 (Zhang et al., 2015).

The pathophysiological characteristics of necrotizing enterocolitis (NEC) include excessive inflammation and necrosis, which can affect any part of the gastrointestinal tract (especially the small intestine) (Neu and Walker, 2011; Nino et al., 2016). The imbalance caused by the decrease in tolerogenic Foxp3+ regulatory T (Treg) cells and the increase in the production of Th17 cells in the lamina propria pro-inflammatory il-17 leads to the NEC-induced excessive inflammatory response (Weitkamp et al., 2013; Liu et al., 2014; Egan et al., 2016). Moreover, another study has shown that in the peripheral blood of NEC patients and mice, the proportion of $CCR9^+$ $CD4^+$ T cells was significantly elevated. Increased $CCR9^+$ $CD4^+$ T cells were mainly $CCR9^+$ IL-17-producing Treg cells, which are characteristic of common Treg cells, but their inhibitory activities were seriously damaged and passively correlated with the serious of intestinal tissue injury. Treg cells that produce $CCR9^+$ IL-17 may be an important biomarker, improving NEC by regulating the balance of lymphocytes (Ma et al., 2019). In summary, these results demonstrated that $CCR9^+$ IL-17-producing Treg cells could be an important biomarker, but further research is needed for clinical use (**Table 2**).

Asthma

Asthma, as a lung disease, is characterized by reversible airway obstruction, airway inflammation, and increased airway responsiveness to a variety of stimuli (Hahn, 2009; Mims, 2015). Chemokine receptors have been confirmed to be involved in leukocyte recruitment, and are closely related to asthma pathology (DeKruyff et al., 2014; Griffith et al., 2014). An ovalbumin (OVA)-induced allergic inflammation model was established in $CCR9^{-/-}$ mice, and the expression of CCR9 and CCL25 in eosinophils and T lymphocytes was found 6 h post-OVA challenge. Meanwhile, compared with wild-type mice, the peribronchial infiltration in CCR9-deficient mice was significantly reduced (nearly 50%), while the total number of eosinophils recruited in bronchoalveolar fluid (BALF) was decreased (30%). Moreover, in $CCR9^{-/-}$ mice, OVA administration can reduce the recruitment of inflammatory cell, which modifies IL-10, CCL11, and CCL25 expression at 24 h after OVA (Lopez-Pacheco et al., 2016). Interestingly, expression of TGF-β and IL-17 was elevated in OVA-stimulated CCR9-deficient mice compared to WT mice, whereas IL-10, as an anti-inflammatory chemokine, was significantly reduced (more than 60%). In addition, there was an increase in the expression of CCL25 in the WT mice as early as 6 h after ova-challenge. Meanwhile, CCL25 expression was decreased at all time test in $CCR9^{-/-}$ mice (**Figure 2**). The above results confirm that CCR9 deficiency has a positive regulatory effect on eosinophils and lymphocytes in the early stage of inflammation induction, suggesting that they may be potential targets for regulating asthma inflammation in asthma (Lopez-Pacheco et al., 2016).

Natural killer T (NKT) cells are the main operators in the development of asthma. Multiple NKT cells migrate and aggregate in the airway, producing a Th2 bias effect that directly or indirectly promotes asthma. Studies have found that the recruitment of NKT cells depends on the high expression of CCR9 and the connection of CCR9/CCL25 (DeKruyff et al., 2014; Griffith et al., 2014). In patients with allergic asthma, the CCR9/CCL25 binding method selectively induces chemotaxis of NKT cells, whereas in healthy volunteers, normal NKT cells are not able to induce. Further studies have confirmed that the pathways for NKT cells regulate the development of asthma. In the process of migrating from blood vessels to airway bronchial mucosa, NKT cells may directly contact $CD3^+$ T cells, making them polarized toward Th2. This regulatory function depends on DC participation and CCR9/CD226 coordinated activation. The adhesion molecule CD226 is overexpressed in asthmatic NKT cells. The CCR9/CCL25 linkage can directly phosphorylate CD226, and the lack of CD226 can block the Th2 bias effect induced by NKT cells. These results indicate that CCR9/CCL25 signaling pathway could interact with CD226 signals to activate asthmatic NKT cells, leading to airway hyperresponsiveness and inflammation, aggravating asthma (Sen et al., 2005). In addition, Castan et al. (2018) demonstrated that CCR9 knock-out mice eliminated the aggravation of lung symptoms in consecutive food and respiratory allergies, which were featured by a rose in lung resistance and a higher Th17/Treg ratio in solely asthmatic-like mice. Moreover, to better understand the mechanism underlying the food allergy-induced aggravation of asthma and the role of CCR9, they performed adoptive transfer of $CD4^+$ T cells from food-allergic mice into naïve mice, which were subsequently sensitized to house dust mites. They found that asthmatic mice received food-sensitized $CD4^+$ T cells and had more severe inflammation than asthmatic mice that received non-sensitized $CD4^+$ T cells. Interestingly, when mice received food allergen-sensitized lymphocytes from $CCR9^{-/-}$ mice, the exacerbation of asthma caused by food allergen $CD4^+$ lymphocytes was eliminated. These results show that CCR9 is a driving factor for the worsening of lung inflammation in food allergic mice (Castan et al., 2018), and confirm its application potential in the development of treatment strategies for allergic diseases (**Table 2**).

Autoimmune Diseases

Toll-like receptor 4 (TLR4) is an important part of innate immunity and has been linked to central nervous system (CNS) inflammatory diseases (Ureña-Peralta et al., 2020). Zhang et al. (2019) have shown that $TLR4^{-/-}$ mice were inadequate to induce experimental autoimmune encephalomyelitis (EAE),

which is featured by reducing low clinic score, weight loss, demyelinating, and spinal cord inflammatory cell infiltration. The deletion of TLR4 in the lesion area of EAE mice can decrease inflammatory cytokines and CCL25 secretion. After transformation, CCR9 expression is reduced in TLR4$^{-/-}$ Th17 cells, and the chemotaxis and migration ability are weakened. In summary, TLR4 may play an important role in the infiltration of Th17 during the pathogenesis of EAE by CCL25/CCR9 signaling pathway (Zhang et al., 2019). Kadowaki et al. (2019) also demonstrate that in the mice model of experimental autoimmune encephalomyelitis, CCR9^{+} memory T cells preferentially infiltrate the inflammatory CNS and express lymphocyte activation 3 gene (LAG3) in the late stage. Antibiotic treatment can alleviate the symptoms of experimental autoimmune encephalomyelitis, which is supported by a significant rise in peripheral blood CCR9^{+} memory T cells. Generally speaking, they postulate that the alterations in CCR9^{+} memory T cells observed, caused by either the gut microbiota changes or ageing, may lead to the development of secondary progressive multiple sclerosis (Kadowaki et al., 2019). Moreover, the CCL25/CCR9 was also powerful to authorize effector/memory T cells to access anatomic sites (Evans-Marin et al., 2015). Binding of CCR9 to CCL25 inhibits CD4 T cells differentiating to Tregs. In autoimmunity, CCR9^{+} T helper cells induce diabetes by secreting IL-21 and promote the expansion and survival of CD8t cells (McGuire et al., 2011).

Omenn syndrome is resulted from a mild rag mutation, which is featured by severe immunodeficiency and similar manifestations of autoimmunity (Villa et al., 1998; Khiong et al., 2007). Rigoni et al. (2016) confirmed that long-term use of broad-spectrum antibiotics in Rag2 (R229Q) mice can ameliorate intestinal and systemic autoimmunity by reducing mucosal and circulating gut-tropic CCR9(+) Th1 and Th17 T cells frequency. In addition, during the allergic reaction, CCL25 drives the mobilization of IL-17^{+} γδ T cells to inflamed tissues through α4β7 integrin, and regulates the level of IL-17 (Costa et al., 2012). The above studies have proved that CCR9/CCL25 plays an important role in autoimmune diseases.

Cancer

In microenvironment, tumor formation and immune system are mutually restricted, and chemokines also play an important role between tumor formation and immune system (Fan et al., 2019; Rossi et al., 2019; Lei et al., 2020). T cells are one of the main functional cells of the anti-cancer immune response. CD4^{+} T cells have an important regulatory effect, and CD8^{+} T cell stem cell-like subgroups have the potential to self-proliferate and differentiate toward effector cells, which can produce durable anti-tumor immune response and specifically kill tumor cells (Borst et al., 2018; Farhood et al., 2019; He et al., 2019; Brightman et al., 2020).

Studies have found that T cell function depends on the expression of CCR9. CD4^{+} CCR9^{+} T helper cells express high amounts of interleukin 21 and induce T cell costimulatory factor, transcription factor B cell CLL/lymphoma 6 (Bcl-6), and Maf, which are local features of autoimmune diseases that affect the accessory organs of the digestive system (McGuire et al., 2011). The CCR9 signal transmitted during the startup of naïve T cells promotes the differentiation of memory CD4^{+} T cells that produce α 4 β + 7 IFN-γ, increasing the immune microenvironment in gastrointestinal tissues, thereby affecting effector immunity in infections and cancer (Fu et al., 2019). Notably, Chen et al. (2020) used tumor acidity-responsive nanoparticle delivery system (NP-siCD47/CCL25) to discharge CCL25 protein and CD47 siRNA in tumors to enhance CD47 targeted immunotherapy.

In the study, NP-siCD47/CCL25 remarkably increased the invasiveness of CCR9^{+}CD8^{+} T cells, inhibited the expression of CD47 in tumor cells, and inhibited tumor cells metastasis and growth by T-cell-dependent immunity (Chen et al., 2020). In addition, Khandelwal et al. (2015) pointed out that CCR9 regulates the STAT signal in T cells and inhibits the secretion and cytotoxicity of T lymphocytes type 1 cytokines. This study shows that inhibiting CCR9 expression may promote tumor-specific T cell immunotherapy (Khandelwal et al., 2015). In conclusion, targeting CCR9/CCL25 is expected to be a new approach for treating tumors, by suppressing or treating tumor patients with an autoimmune system that produces a lasting antitumor response.

CONCLUSION AND POTENTIAL FUTURE DIRECTIONS

Inflammatory diseases have become a serious threat to the health of the global population. Inflammatory diseases involve lesions of multiple tissues and organs in the body, which are characterized by tissue damage caused by excessive or persistent inflammation, such as CVD, hepatitis, asthma, RA, and inflammatory bowel diseases. However, the common features of these diseases are abnormal regulation of inflammatory response and imbalance of immune pathways. Chemokines are a family of small molecule cytokines whose receptors are seven-transmembrane glycoproteins, mainly expressed on the surface of inflammatory cells. Previous studies have shown that as members of the chemokine CC subfamily, CCR9 and CCL25 have been related to various inflammatory diseases as well as could promote inflammatory responses. Recently, the roles of CCR9/CCL25 in inflammation and related diseases have become clearer. CCR9/CCL25 is participated in many inflammatory diseases, including CVD, hepatitis, RA, IBD, and asthma (**Table 2**). Although the functional studies regarding CCR9/CCL25 in inflammatory diseases have gradually deepened, the understanding of CCR9/CCL25 has become more comprehensive. However, studies on the mechanisms of CCR9/CCL25 underlying inflammatory diseases are mostly restricted to the theoretical basic, and their clinical application is few.

Although several lines of evidence have clarified the specific mechanism of CCR9/CCL25 signaling in inflammation-associated diseases, the development of successful treatment of CCR9/CCL25 is still in further study stage.

CCX282-B is bioavailable in the circulation following oral administration, and which has high specificity for CCR9 with negligible binding to any other chemokine receptor, have been evaluated in murine models of IBD as well as in clinical trials. Meanwhile, related studies have confirmed that the use of an oral antagonist for CCR9 (CCX282-B) was also evaluated in phase II and phase III clinical trials with mixed results, but the results were not as expected. Therefore, to make further progress in delineating the potential clinical role of CCR9 in human disease, detailed mechanistic studies and well-designed proof-of-concept human trials are now required. Further investigation is likely to focus on (1) studying the effects of blocking CCR9 on the activation state of circulating and tissue-infiltrating lymphocytes, (2) investigating disease remission in CD remains a strong indication for CCR9 antagonist treatment, and any future clinical trials should include patients with UC and with PSC, (3) investigating whether the clinical application of CCR9 antagonism has any suboptimum efficacy, and (4) continuing to study CCR9/CCL25 upstream and downstream molecules, which are possible future potential therapeutic targets for inflammatory diseases. In conclusion, this review presents a comprehensive picture of the role of CCR9/CCL25 in inflammatory diseases and proposes a new underlying therapeutic mechanisms and target for the future treatment of inflammatory diseases.

AUTHOR CONTRIBUTIONS

XW and MS: conceptualization, literature search, and original draft writing and editing. ZY, CL, QW, HW, and CD: original draft writing and editing. YL and YY: conceptualization, original draft writing and editing, supervision, and funding acquisition. All authors contributed to the article and approved the submitted version.

FUNDING

This work was supported by the Key R&D Plans of Shaanxi Province (2021SF-317 and 2021SF-075), Science and Technology Plan Project of Yulin City (YF-2020-191 and CXY-2020-098), National Natural Science Foundation of China (81871607, 82070422, and 81700236), and Natural Science Foundation of Shaanxi Province (2020JM-386 and 2018JM3042).

REFERENCES

Amiya, T., Nakamoto, N., Chu, P. S., Teratani, T., Nakajima, H., and Fukuchi, Y. (2016). Bone marrow-derived macrophages distinct from tissue-resident macrophages play a pivotal role in Concanavalin A-induced murine liver injury via CCR9 axis. *Sci Rep.* 6, 35146.

Bleul, C. C., Farzan, M., Choe, H., Parolin, C., Clark-Lewis, I., Sodroski, J., et al. (1996). The lymphocyte chemoattractant SDF-1 is a ligand for LESTR/fusin and blocks HIV-1 entry. *Nature.* 382, 829–833. doi: 10.1038/382829a0

Borst, J., Ahrends, T., Bąbała, N., Melief, C. J. M., and Kastenmüller, W. (2018). CD4(+) T cell help in cancer immunology and immunotherapy. *Nat Rev. Immunol.* 18, 635–647. doi: 10.1038/s41577-018-0044-0

Brightman, S. E., Naradikian, M. S., Miller, A. M., and Schoenberger, S. P. (2020). Harnessing neoantigen specific CD4 T cells for cancer immunotherapy. *J Leukoc. Biol.* 107, 625–633. doi: 10.1002/jlb.5ri0220-603rr

Castan, L., Cheminant, M. A., Colas, L., Brouard, S., Magnan, A., and Bouchaud, G. (2018). Food allergen-sensitized CCR9(+) lymphocytes enhance airways allergic inflammation in mice. *Allergy* 73, 1505–1514. doi: 10.1111/all.13386

Chapman, R. W. (1991). Aetiology and natural history of primary sclerosing cholangitis–a decade of progress? *Gut.* 32, 1433–1435. doi: 10.1136/gut.32.12.1433

Chen, H., Cong, X., Wu, C., Wu, X., Wang, J., Mao, K., et al. (2020). Intratumoral delivery of CCL25 enhances immunotherapy against triple-negative breast cancer by recruiting CCR9(+) T cells. *Science Advances* 6, 4690.

Cocchi, F., DeVico, A. L., Garzino-Demo, A., Arya, S. K., Gallo, R. C., and Lusso, P. (1995). Identification of RANTES, MIP-1 alpha, and MIP-1 beta as the major HIV-suppressive factors produced by CD8+ T cells. *Science.* 270, 1811–1815. doi: 10.1126/science.270.5243.1811

Costa, M. F., Bornstein, V. U., Candéa, A. L., Henriques-Pons, A., Henriques, M. G., and Penido, C. (2012). CCL25 induces α4β7 integrin-dependent migration of IL-17^{+} γδ T lymphocytes during an allergic reaction. *Eur J. Immunol.* 42, 1250–1260. doi: 10.1002/eji.201142021

Crispe, I. N. (2003). Hepatic T cells and liver tolerance. *Nat Rev. Immunol.* 3, 51–62. doi: 10.1038/nri981

DeKruyff, R. H., Yu, S., Kim, H. Y., and Umetsu, D. T. (2014). Innate immunity in the lung regulates the development of asthma. *Immunol. Rev.* 260, 235–248. doi: 10.1111/imr.12187

Egan, C. E., Sodhi, C. P., Good, M., Lin, J., Jia, H., and Yamaguchi, Y. (2016). Toll-like receptor 4-mediated lymphocyte influx induces neonatal necrotizing enterocolitis. *J Clin. Invest.* 126, 495–508. doi: 10.1172/jci83356

Eksteen, B., Grant, A. J., Miles, A., Curbishley, S. M., Lalor, P. F., and Hubscher, S. G. (2004). Hepatic endothelial CCL25 mediates the recruitment of CCR9+ gut-homing lymphocytes to the liver in primary sclerosing cholangitis. *J Exp. Med.* 200, 1511–1517. doi: 10.1084/jem.20041035

Evans-Marin, H. L., Cao, A. T., Yao, S., Chen, F., He, C., and Liu, H. (2015). Unexpected Regulatory Role of CCR9 in Regulatory T Cell Development. *PLoS One.* 10:e0134100. doi: 10.1371/journal.pone.0134100

Fan, L., Li, Y., Chen, J. Y., Zheng, Y. F., and Xu, X. M. (2019). Immune checkpoint modulators in cancer immunotherapy: Recent advances and combination rationales. *Cancer Lett.* 456, 23–28. doi: 10.1016/j.canlet.2019.03.050

Farhood, B., Najafi, M., and Mortezaee, K. (2019). CD8(+) cytotoxic T lymphocytes in cancer immunotherapy: A review. *J Cell Physiol.* 234, 8509–8521. doi: 10.1002/jcp.27782

Feldmann, M. (2002). Development of anti-TNF therapy for rheumatoid arthritis. *Nat Rev. Immunol.* 2, 364–371. doi: 10.1038/nri802

Firestein, G. S. (1991). The immunopathogenesis of rheumatoid arthritis. *Curr Opin. Rheumatol.* 3, 398–406. doi: 10.1097/00002281-199106000-00012

Fu, H., Jangani, M., Parmar, A., Wang, G., Coe, D., and Spear, S. (2019). A Subset of CCL25-Induced Gut-Homing T Cells Affects Intestinal Immunity to Infection and Cancer. *Front Immunol.* 10:271.

Griffith, J. W., Sokol, C. L., and Luster, A. D. (2014). Chemokines and chemokine receptors: positioning cells for host defense and immunity. *Annu Rev. Immunol.* 32, 659–702. doi: 10.1146/annurev-immunol-032713-120145

Guo, H., Callaway, J. B., and Ting, J. P. (2015). Inflammasomes: mechanism of action, role in disease, and therapeutics. *Nat. Med.* 21, 677–687. doi: 10.1038/nm.3893

Hadeiba, H., Lahl, K., Edalati, A., Oderup, C., Habtezion, A., and Pachynski, R. (2012). Plasmacytoid dendritic cells transport peripheral antigens to the thymus to promote central tolerance. *Immunity.* 36, 438–450. doi: 10.1016/j.immuni.2012.01.017

Hahn, D. L. (2009). Importance of evidence grading for guideline implementation: the example of asthma. *Ann. Fam Med.* 7, 364–369. doi: 10.1370/afm.995

Haringman, J. J., Gerlag, D. M., Zwinderman, A. H., Smeets, T. J., Kraan, M. C., and Baeten, D. (2005). Synovial tissue macrophages: a sensitive biomarker for

response to treatment in patients with rheumatoid arthritis. *Ann Rheum. Dis.* 64, 834–838. doi: 10.1136/ard.2004.029751

He, Q. F., Xu, Y., Li, J., Huang, Z. M., Li, X. H., and Wang, X. (2019). CD8+ T-cell exhaustion in cancer: mechanisms and new area for cancer immunotherapy. *Brief. Funct Genomics.* 18, 99–106. doi: 10.1093/bfgp/ely006

Huang, Y., Wang, D., Wang, X., Zhang, Y., Liu, T., and Chen, Y. (2016). Abrogation of CC chemokine receptor 9 ameliorates ventricular remodeling in mice after myocardial infarction. *Sci Rep.* 6, 32660.

Igaki, K., Komoike, Y., Nakamura, Y., Watanabe, T., Yamasaki, M., and Fleming, P. (2018). MLN3126, an antagonist of the chemokine receptor CCR9, ameliorates inflammation in a T cell mediated mouse colitis model. *Int. Immunopharmacol.* 60, 160–169. doi: 10.1016/j.intimp.2018.04.049

Jokinen, E. (2015). Obesity and cardiovascular disease. *Minerva. Pediatr.* 67, 25–32.

Kadowaki, A., Saga, R., Lin, Y., Sato, W., and Yamamura, T. (2019). Gut microbiota-dependent CCR9+CD4+ T cells are altered in secondary progressive multiple sclerosis. *Brain.* 142, 916–931. doi: 10.1093/brain/awz012

Kalindjian, S. B., Kadnur, S. V., Hewson, C. A., Venkateshappa, C., Juluri, S., and Kristam, R. (2016). A New Series of Orally Bioavailable Chemokine Receptor 9 (CCR9) Antagonists; Possible Agents for the Treatment of Inflammatory Bowel Disease. *J Med. Chem.* 59, 3098–3111. doi: 10.1021/acs.jmedchem.5b01840

Khandelwal, N., Breinig, M., Speck, T., Michels, T., Kreutzer, C., and Sorrentino, A. (2015). A high-throughput RNAi screen for detection of immune-checkpoint molecules that mediate tumor resistance to cytotoxic T lymphocytes. *EMBO. Mol. Med.* 7, 450–463. doi: 10.15252/emmm.201404414

Khiong, K., Murakami, M., Kitabayashi, C., Ueda, N., Sawa, S., and Sakamoto, A. (2007). Homeostatically proliferating CD4 T cells are involved in the pathogenesis of an Omenn syndrome murine model. *J Clin. Invest.* 117, 1270–1281. doi: 10.1172/jci30513

Kinne, R. W., Brauer, R., Stuhlmuller, B., Palombo-Kinne, E., and Burmester, G. R. (2000). Macrophages in rheumatoid arthritis. *Arthritis. Res.* 2, 189–202.

Kunkel, E. J., Campbell, J. J., Haraldsen, G., Pan, J., Boisvert, J., and Roberts, A. I. (2000). Lymphocyte CC chemokine receptor 9 and epithelial thymus-expressed chemokine (TECK) expression distinguish the small intestinal immune compartment: Epithelial expression of tissue-specific chemokines as an organizing principle in regional immunity. *J Exp. Med.* 192, 761–768. doi: 10.1084/jem.192.5.761

Lei, X., Lei, Y., Li, J. K., Du, W. X., Li, R. G., and Yang, J. (2020). Immune cells within the tumor microenvironment: Biological functions and roles in cancer immunotherapy. *Cancer. Lett.* 470, 126–133. doi: 10.1016/j.canlet.2019.11.009

Liu, Y., Tran, D. Q., Fatheree, N. Y., and Marc Rhoads, J. (2014). Lactobacillus reuteri DSM 17938 differentially modulates effector memory T cells and Foxp3+ regulatory T cells in a mouse model of necrotizing enterocolitis. *Am J. Physiol. Gastrointest. Liver Physiol.* 307, G177–G186.

Loftus, E. V. Jr. (2004). Clinical epidemiology of inflammatory bowel disease: Incidence, prevalence, and environmental influences. *Gastroenterology.* 126, 1504–1517. doi: 10.1053/j.gastro.2004.01.063

Lopez-Pacheco, C., Soldevila, G., Du Pont, G., Hernandez-Pando, R., and Garcia-Zepeda, E. A. (2016). CCR9 Is a Key Regulator of Early Phases of Allergic Airway Inflammation. *Mediators Inflamm* 2016, 3635809.

Ma, F., Li, S., Gao, X., Zhou, J., Zhu, X., and Wang, D. (2019). Interleukin-6-mediated CCR9(+) interleukin-17-producing regulatory T cells polarization increases the severity of necrotizing enterocolitis. *EBioMedicine.* 44, 71–85. doi: 10.1016/j.ebiom.2019.05.042

Malani, P. N. (2017). Hepatitis A. *JAMA.* 318, 2393.

Marti, L. C. (2015). Chemokines and immunity. *Einstein (São Paulo).* 13, 469–473.

McGuire, H. M., Vogelzang, A., Ma, C. S., Hughes, W. E., Silveira, P. A., and Tangye, S. G. (2011). A subset of interleukin-21+ chemokine receptor CCR9+ T helper cells target accessory organs of the digestive system in autoimmunity. *Immunity.* 34, 602–615. doi: 10.1016/j.immuni.2011.01.021

Mims, J. W. (2015). Asthma: definitions and pathophysiology. *Int Forum. Allergy Rhinol.* 5 Suppl 1, S2–S6.

Molodecky, N. A., Soon, I. S., Rabi, D. M., Ghali, W. A., Ferris, M., and Chernoff, G. (2012). Increasing incidence and prevalence of the inflammatory bowel diseases with time, based on systematic review. *Gastroenterology* 142, 46–54.e42;quiz e30.

Moser, B., Wolf, M., Walz, A., and Loetscher, P. (2004). Chemokines: multiple levels of leukocyte migration control. *Trends. Immunol.* 25, 75–84. doi: 10.1016/j.it.2003.12.005

Mulherin, D., Fitzgerald, O., and Bresnihan, B. (1996). Synovial tissue macrophage populations and articular damage in rheumatoid arthritis. *Arthritis. Rheum.* 39, 115–124. doi: 10.1002/art.1780390116

Nakamoto, N. (2016). Role of inflammatory macrophages and CCR9/CCL25 chemokine axis in the pathogenesis of liver injury as a therapeutic target. *Nihon Rinsho. Meneki. Gakkai Kaishi.* 39, 460–467. doi: 10.2177/jsci.39.460

Nakamoto, N., Ebinuma, H., Kanai, T., Chu, P. S., Ono, Y., and Mikami, Y. (2012). CCR9+ macrophages are required for acute liver inflammation in mouse models of hepatitis. *Gastroenterology.* 142, 366–376. doi: 10.1053/j.gastro.2011.10.039

Nino, D. F., Sodhi, C. P., and Hackam, D. J. (2016). Necrotizing enterocolitis: new insights into pathogenesis and mechanisms. *Nat Rev Gastroenterol Hepatol.* 13, 590–600. doi: 10.1038/nrgastro.2016.119

Nishimoto, N., and Takagi, N. (2010). Safety and efficacy profiles of tocilizumab monotherapy in Japanese patients with rheumatoid arthritis: meta-analysis of six initial trials and five long-term extensions. *Mod Rheumatol.* 20, 222–232. doi: 10.3109/s10165-010-0279-5

Nishimoto, N., Yoshizaki, K., Miyasaka, N., Yamamoto, K., Kawai, S., and Takeuchi, T. (2004). Treatment of rheumatoid arthritis with humanized anti-interleukin-6 receptor antibody: a multicenter, double-blind, placebo-controlled trial. *Arthritis Rheum.* 50, 1761–1769. doi: 10.1002/art.20303

Oberlin, E., Amara, A., Bachelerie, F., Bessia, C., Virelizier, J. L., and Arenzana-Seisdedos, F. (1996). The CXC chemokine SDF-1 is the ligand for LESTR/fusin and prevents infection by T-cell-line-adapted HIV-1. *Nature.* 382, 833–835. doi: 10.1038/382833a0

Papadakis, K. A., Landers, C., Prehn, J., Kouroumalis, E. A., Moreno, S. T., and Gutierrez-Ramos, J. C. (2003). CC chemokine receptor 9 expression defines a subset of peripheral blood lymphocytes with mucosal T cell phenotype and Th1 or T-regulatory 1 cytokine profile. *J. Immunol.* 171, 159–165. doi: 10.4049/jimmunol.171.1.159

Papadakis, K. A., Prehn, J., Moreno, S. T., Cheng, L., Kouroumalis, E. A., and Deem, R. (2001). CCR9-positive lymphocytes and thymus-expressed chemokine distinguish small bowel from colonic Crohn's disease. *Gastroenterology.* 121, 246–254. doi: 10.1053/gast.2001.27154

Papadakis, K. A., Prehn, J., Nelson, V., Cheng, L., Binder, S. W., and Ponath, P. D. (2000). The role of thymus-expressed chemokine and its receptor CCR9 on lymphocytes in the regional specialization of the mucosal immune system. *J. Immunol.* 165, 5069–5076. doi: 10.4049/jimmunol.165.9.5069

Qiuping, Z., Jei, X., Youxin, J., Wei, J., Chun, L., and Jin, W. (2004). CC chemokine ligand 25 enhances resistance to apoptosis in CD4+ T cells from patients with T-cell lineage acute and chronic lymphocytic leukemia by means of livin activation. *Cancer Res.* 64, 7579–7587. doi: 10.1158/0008-5472.can-04-0641

Rigoni, R., Fontana, E., Guglielmetti, S., Fosso, B., D'Erchia, A. M., and Maina, V. (2016). Intestinal microbiota sustains inflammation and autoimmunity induced by hypomorphic RAG defects. *J Exp. Med.* 213, 355–375. doi: 10.1084/jem.20151116

Rivera-Nieves, J., Ho, J., Bamias, G., Ivashkina, N., Ley, K., Oppermann, M., et al. (2006). Antibody blockade of CCL25/CCR9 ameliorates early but not late chronic murine ileitis. *Gastroenterology.* 131, 1518–1529. doi: 10.1053/j.gastro.2006.08.031

Rossi, J. F., Céballos, P., and Lu, Z. Y. (2019). Immune precision medicine for cancer: a novel insight based on the efficiency of immune effector cells. *Cancer Commun. (Lond).* 39, 34. doi: 10.1186/s40880-019-0379-3

Schmutz, C., Cartwright, A., Williams, H., Haworth, O., Williams, J. H., and Filer, A. (2010). Monocytes/macrophages express chemokine receptor CCR9 in rheumatoid arthritis and CCL25 stimulates their differentiation. *Arthritis Res. Ther.* 12, R161.

Schulz, O., Hammerschmidt, S. I., Moschovakis, and Forster, R. (2016). Chemokines and Chemokine Receptors in Lymphoid Tissue Dynamics. *Annu Rev. Immunol.* 34, 203–242. doi: 10.1146/annurev-immunol-041015-055649

Sen, Y., Yongyi, B., Yuling, H., Luokun, X., Li, H., and Jie, X. (2005). V alpha 24-invariant NKT cells from patients with allergic asthma express CCR9 at high frequency and induce Th2 bias of CD3+ T cells upon CD226 engagement. *J. Immunol.* 175, 4914–4926. doi: 10.4049/jimmunol.175.8.4914

Singh, J. A., Pando, J. A., Tomaszewski, J., and Schumacher, H. R. (2004). Quantitative analysis of immunohistologic features of very early rheumatoid synovitis in disease modifying antirheumatic drug- and corticosteroid-naive patients. *J. Rheumatol.* 31, 1281–1285.

Smolen, J. S., Landewe, R., Breedveld, F. C., Dougados, M., Emery, P., and Gaujoux-Viala, C. (2010). EULAR recommendations for the management of rheumatoid arthritis with synthetic and biological disease-modifying antirheumatic drugs. *Ann Rheum, Dis.* 69, 964–975.

Yu, Q., and Stamenkovic, I. (2000). Cell surface-localized matrix metalloproteinase-9 proteolytically activates TGF-beta and promotes tumor invasion and angiogenesis. *Genes. Dev.* 14, 163–176.

Stenstad, H., Ericsson, A., Johansson-Lindbom, B., Svensson, M., Marsal, J., and Mack, M. (2006). Gut-associated lymphoid tissue-primed CD4+ T cells display CCR9-dependent and -independent homing to the small intestine. *Blood.* 107, 3447–3454. doi: 10.1182/blood-2005-07-2860

Stenstad, H., Svensson, M., Cucak, H., Kotarsky, K., and Agace, W. W. (2007). Differential homing mechanisms regulate regionalized effector CD8alphabeta+ T cell accumulation within the small intestine. *Proc Natl Acad Sci U S A.* 104, 10122–10127. doi: 10.1073/pnas.0700269104

Svensson, M., Marsal, J., Ericsson, A., Carramolino, L., Broden, T., Marquez, G., et al. (2002). CCL25 mediates the localization of recently activated CD8alphabeta(+) lymphocytes to the small-intestinal mucosa. *J Clin. Invest.* 110, 1113–1121. doi: 10.1172/jci0215988

Thomson, A. W., and Knolle, P. A. (2010). Antigen-presenting cell function in the tolerogenic liver environment. *Nat. Rev. Immunol.* 10, 753–766. doi: 10.1038/nri2858

Thum, T. (2013). Non-coding RNAs in cardiac remodeling and heart failure. *Circ. Res.* 113, 676–689. doi: 10.1161/circresaha.113.300226

Tu, Z., Xiao, R., Xiong, J., Tembo, K. M., Deng, X., and Xiong, M. (2016). CCR9 in cancer: oncogenic role and therapeutic targeting. *J Hematol. Oncol.* 9, 10.

Ureña-Peralta, J. R., Pérez-Moraga, R., and García-García, F. (2020). Lack of TLR4 modifies the miRNAs profile and attenuates inflammatory signaling pathways. *PLoS One* 15:e0237066. doi: 10.1371/journal.pone.0237066

Van Camp, G. (2014). Cardiovascular disease prevention. *Acta Clin. Belg.* 69, 407–411.

Vassilatis, D. K., Hohmann, J. G., Zeng, H., Li, F., Ranchalis, J. E., and Mortrud, M. T. (2003). The G protein-coupled receptor repertoires of human and mouse. *Proc Natl Acad Sci U S A.* 100, 4903–4908.

Vicari, A. P., Figueroa, D. J., Hedrick, J. A., Foster, J. S., Singh, K. P., and Menon, S. (1997). TECK: a novel CC chemokine specifically expressed by thymic dendritic cells and potentially involved in T cell development. *Immunity.* 7, 291–301. doi: 10.1016/s1074-7613(00)80531-2

Villa, A., Santagata, S., Bozzi, F., Giliani, S., Frattini, A., and Imberti, L. (1998). Partial V(D)J recombination activity leads to Omenn syndrome. *Cell.* 93, 885–896. doi: 10.1016/s0092-8674(00)81448-8

Walker, W. A. (2011). Necrotizing enterocolitis. *N Engl. J. Med.* 364, 255–264.

Weitkamp, J. H., Koyama, T., Rock, M. T., Correa, H., Goettel, J. A., and Matta, P. (2013). Necrotising enterocolitis is characterised by disrupted immune regulation and diminished mucosal regulatory (FOXP3)/effector (CD4, CD8) T cell ratios. *Gut.* 62, 73–82. doi: 10.1136/gutjnl-2011-301551

Wendland, M., Czeloth, N., Mach, N., Malissen, B., Kremmer, E., Pabst, O., et al. (2007). CCR9 is a homing receptor for plasmacytoid dendritic cells to the small intestine. *Proc Natl Acad Sci U S A.* 104, 6347–6352. doi: 10.1073/pnas.0609180104

Wermers, J. D., McNamee, E. N., Wurbel, M. A., Jedlicka, P., and Rivera-Nieves, J. (2011). The chemokine receptor CCR9 is required for the T-cell-mediated regulation of chronic ileitis in mice. *Gastroenterology* 140, 1526–1535.e1523.

Wu, W., Doan, N., Said, J., and Pullarkat, S. T. (2014). Strong expression of chemokine receptor CCR9 in diffuse large B-cell lymphoma and follicular lymphoma strongly correlates with gastrointestinal involvement. *Hum Pathol.* 45, 1451–1458. doi: 10.1016/j.humpath.2014.02.021

Wurbel, M. A., Le Bras, S., Ibourk, M., Pardo, M., McIntire, M. G., and Coco, D. (2014). CCL25/CCR9 interactions are not essential for colitis development but are required for innate immune cell protection from chronic experimental murine colitis. *Inflamm Bowel. Dis.* 20, 1165–1176. doi: 10.1097/mib.0000000000000059

Wurbel, M. A., Malissen, M., Guy-Grand, D., Malissen, B., and Campbell, J. J. (2007). Impaired accumulation of antigen-specific CD8 lymphocytes in chemokine CCL25-deficient intestinal epithelium and lamina propria. *J Immunol.* 178, 7598–7606. doi: 10.4049/jimmunol.178.12.7598

Wurbel, M. A., McIntire, M. G., Dwyer, P., and Fiebiger, E. (2011). CCL25/CCR9 interactions regulate large intestinal inflammation in a murine model of acute colitis. *PLoS One.* 6:e16442. doi: 10.1371/journal.pone.0016442

Wurbel, M. A., Philippe, J. M., Nguyen, C., Victorero, G., Freeman, T., and Wooding, P. (2000). The chemokine TECK is expressed by thymic and intestinal epithelial cells and attracts double- and single-positive thymocytes expressing the TECK receptor CCR9. *Eur J. Immunol.* 30, 262–271. doi: 10.1002/1521-4141(200001)30:1<262::aid-immu262>3.0.co;2-0

Xu, Z., Mei, F., Liu, H., Sun, C., and Zheng, Z. (2016). C-C Motif Chemokine Receptor 9 Exacerbates Pressure Overload-Induced Cardiac Hypertrophy and Dysfunction. *J Am. Heart Assoc* 5, e003342.

Yokoyama, W., Kohsaka, H., Kaneko, K., Walters, M., Takayasu, A., and Fukuda, S. (2014). Abrogation of CC chemokine receptor 9 ameliorates collagen-induced arthritis of mice. *Arthritis. Res. Ther.* 16, 445.

Zaballos, A., Gutierrez, J., Varona, R., Ardavin, C., and Marquez, G. (1999). Cutting edge: identification of the orphan chemokine receptor GPR-9-6 as CCR9, the receptor for the chemokine TECK. *J. Immunol.* 162, 5671–5675.

Zabel, B. A., Agace, W. W., Campbell, J. J., Heath, H. M., Parent, D., and Roberts, A. I. (1999). Human G protein-coupled receptor GPR-9-6/CC chemokine receptor 9 is selectively expressed on intestinal homing T lymphocytes, mucosal lymphocytes, and thymocytes and is required for thymus-expressed chemokine-mediated chemotaxis. *J Exp. Med.* 190, 1241–1256. doi: 10.1084/jem.190.9.1241

Zhang, J., Romero, J., Chan, A., Goss, J., Stucka, S., and Cross, J. (2015). Biarylsulfonamide CCR9 inhibitors for inflammatory bowel disease. *Bioorg Med Chem Lett.* 25, 3661–3664. doi: 10.1016/j.bmcl.2015.06.046

Zhang, Y., Han, J., Wu, M., Xu, L., Wang, Y., and Yuan, W. (2019). Toll-Like Receptor 4 Promotes Th17 Lymphocyte Infiltration Via CCL25/CCR9 in Pathogenesis of Experimental Autoimmune Encephalomyelitis. *J Neuroimmune Pharmacol* 14, 493–502. doi: 10.1007/s11481-019-09854-1

Zhang, Y., Liu, Y., Zhu, X. H., Zhang, X. D., Jiang, D. S., and Bian, Z. Y. (2014). Dickkopf-3 attenuates pressure overload-induced cardiac remodelling. *Cardiovasc Res.* 102, 35–45. doi: 10.1093/cvr/cvu004

Zhong, Y., Jiang, L., Lin, H., Li, B., Lan, J., and Liang, S. (2015). Expression of CC chemokine receptor 9 predicts poor prognosis in patients with lung adenocarcinoma. *Diagn. Pathol.* 10, 101.

Zlotnik, A., and Yoshie, O. (2012). The chemokine superfamily revisited. *Immunity.* 36, 705–716. doi: 10.1016/j.immuni.2012.05.008

Conflict of Interest: The authors declare that the research was conducted in the absence of any commercial or financial relationships that could be construed as a potential conflict of interest.

Publisher's Note: All claims expressed in this article are solely those of the authors and do not necessarily represent those of their affiliated organizations, or those of the publisher, the editors and the reviewers. Any product that may be evaluated in this article, or claim that may be made by its manufacturer, is not guaranteed or endorsed by the publisher.

Advantages of publishing in Frontiers

OPEN ACCESS
Articles are free to read for greatest visibility and readership

FAST PUBLICATION
Around 90 days from submission to decision

HIGH QUALITY PEER-REVIEW
Rigorous, collaborative, and constructive peer-review

TRANSPARENT PEER-REVIEW
Editors and reviewers acknowledged by name on published articles

Frontiers
Avenue du Tribunal-Fédéral 34
1005 Lausanne | Switzerland

Visit us: www.frontiersin.org
Contact us: frontiersin.org/about/contact

REPRODUCIBILITY OF RESEARCH
Support open data and methods to enhance research reproducibility

DIGITAL PUBLISHING
Articles designed for optimal readership across devices

FOLLOW US
@frontiersin

IMPACT METRICS
Advanced article metrics track visibility across digital media

EXTENSIVE PROMOTION
Marketing and promotion of impactful research

LOOP RESEARCH NETWORK
Our network increases your article's readership